

CRANFIELD UNIVERSITY



ADEYEMI JOSEPH OSHO

**EFFECTS OF PIPE ORIENTATION  
ON SAND TRANSPORTATION**

SCHOOL OF ENGINEERING

PHD THESIS  
Academic Year: 2012 - 2013

Supervisor: PROFESSOR HOI YEUNG  
NOVEMBER, 2013

SCHOOL OF ENGINEERING  
DEPARTMENT OF OFFSHORE, PROCESS AND ENERGY  
ENGINEERING

PHD THESIS  
Academic Year 2012 - 2013

ADEYEMI JOSEPH OSHO

**EFFECTS OF PIPE ORIENTATION  
IN ON SAND TRANSPORTATION**

Supervisor: PROFESSOR HOI YEUNG  
NOVEMBER, 2013

This thesis is submitted in partial fulfilment of the requirements for  
the degree of Doctor of Philosophy

© Cranfield University 2013. All rights reserved. No part of this  
publication may be reproduced without the written permission of the  
copyright owner.

## ABSTRACT

Sand transport in hilly terrain geometry is different and complex to understand compared to horizontal pipeline, due to the influence of the geometry that greatly affect multiphase flow and sand behaviour at the dip. The overall aim of this research work is to use experimental method to investigate the effects of multiphase flow behaviour on sand transport in a dip configuration.

Experimental work was carried out to understand the complex dynamic mechanisms that exist during sand multiphase flow using 2" inch dip test facility with different inclination angles of  $\pm 24^\circ$  and  $\pm 12^\circ$  configurations. In order determine the multiphase flow parameters and sand flow regimes, extensive data were collected and analysed from continuous local measurement of instantaneous liquid hold up and sand hold up using conductivity rings.

Significant observations were made during this study from which several conclusions were made. In the air-water test, three slug behaviours were observed at the dip: complete stratified flow downhill with slug initiation at dip; stratified flow (with energetic ripple) downhill with slug initiation and slug growth upward dip; and aerated slug downhill and slug growth at the dip. These behaviours are different from published work on this subject with low angle of inclination. The data analysis revealed that the two types of slug initiation mechanisms (wave growth and wave coalescence) observed are geometry specifics. The slug translational velocities (at the dip and uphill section) were used as criterion to determine the flow condition for each slug initiation mechanism at the dip.

Five sand-water flow regimes (full suspension, streak, saltation, sand dune, and sand bed) were established by physical observation and data analysis. It was also observed that sand streaks were denser towards the central line of pipe bottom in the downhill pipe than that in uphill pipe. At downhill pipe section, there were sand gathering toward the central line of the pipe bottom. The characteristics of sand transportation at the dip section were found slightly different from downhill and uphill pipe for higher sand concentrations. When dense streak occurred at the downhill, the sand particles become dispersed at the dip. The minimum transport conditions (MTC) were determined at different sand concentration. The sand minimum transport condition in the dip section was found to be slightly lower than those in the downhill and uphill section. The minimum transport condition for a single phase water flow for the  $24^\circ$  dip

test section was slightly higher (with difference of about 0.1m/s) than that of the 12° at the downward and upward of the dip section at low sand concentration. In addition, local sand measurements using conductivity time series results at the downhill and uphill section showed the influence of sand concentration and flow condition on sand flow patterns.

The air-water-sand results showed that sand deposits occurred in uphill section after sand transport at the downhill and dip sections. This was due to different flow regimes exhibited at the different pipe sections. The stratified (wavy) flow was the dominant flow in downhill pipe; therefore sand was observed transporting within the liquid film as thin streak for most of test conditions. The slug initiation at the dip section was observed to be a major factor that influences the sand behaviour. Sand particles in the slug unit (at the dip and uphill of the pipe) were observed to be entrained in the slug body once slug is initiated, thereby changing the force vector generating turbulence flow at the front of slug body. Once the sand particles entered the film zone of the slug unit, they immediately stopped moving forward due to the film velocity significantly lower than the slug body coupled with gravity effect. . Sand particles were found to be falling back while travelling with the water film at some conditions, until they were picked up by the next slug body.

The results of this work provide a better understanding to the study of multiphase flow for pipeline design and most especially sand behaviour at the dip. The sand dune regime is identified distinctively using conductivity ring technique which would assist in determining the operating conditions that allow sand dune formation. The knowledge of flow condition at full suspension of sand is an important parameter to determine the erosion rate over the life span of the pipeline. Also, the quantity of sand bed and flow condition of sand settling at the dip is useful information for production chemist in order to determine the effectiveness of corrosion inhibitor at the bottom of the pipe.

In conclusion, sand transport characteristics and MTC were strongly dependent on the gas-liquid flow regime and pipe geometry; and cannot be generalised on the superficial liquid and gas velocities of the transport fluid.

Keywords: Multiphase Flow, Flow Regime, Slug Mechanism, Conductivity Ring.

## ACKNOWLEDGEMENTS

This thesis would not have been possible without the valuable contributions of a number of people over the past three years. Therefore it is an honour for me to acknowledge the support of the following people.

Firstly, I want to express my sincere gratitude to my supervisor, Prof Hoi Yeung for his guidance support and ideas throughout the duration of this work. The enthusiastic and fruitful discussions with him had always inspired me. Also, the financial support provided by the Department of Process System Engineering is gratefully appreciated.

The assistance received from Dr. Wei Yan during the preliminary work and setting up of the rig is gratefully appreciated. I also wish to express my appreciation to my colleague Mr. Nonso Okeke for his assistance and corporation during his MSc project when we both shared the rig together.

I wish to express my appreciation to the entire staff and students of Process Systems Engineering group; with special mention of Dr. Yi Cao, Dr. Liyun Lao and most especially, I wish to thank Mrs. Sam Skears for always being there whenever I needed help and advice. Also indebted to David Whittington, Kelvin White, Clive Wood, Stan Collins and John Knopp for their help with the construction and installation of the test rigs and LABVIEW Programme. All of you have been very helpful.

I wish to thank my family, friends and colleagues among them are: Ayorinde Solademi, Callistus Okhasie, Ayo Akinwande, Dr. Edith Ejikeme, Dr. Tesi Arubi, Dr Daramola Michael, Solomon Alagbe, Leshi Semiu for their prayers, motivation and encouragement.

I want to express my deepest gratitude to my mum, my dear wife and my children for their love, understanding and encouragement.

Above all, I thank Almighty God for keeping me and my family. I remain grateful Lord for your divine favour, provision and protection. *There is absolutely nothing impossible for God to do!!!!*



# TABLE OF CONTENTS

ABSTRACT.....	i
ACKNOWLEDGEMENTS .....	iii
TABLE OF CONTENTS .....	v
LIST OF FIGURES .....	viii
LIST OF TABLES .....	xii
<b>1 INTRODUCTION</b> .....	<b>1</b>
1.1 Background.....	1
1.2 Study of Sand Transportation in Hilly Terrain Pipeline .....	4
1.3 Research Objectives .....	5
1.4 Thesis Structure .....	6
<b>2 LITERATURE REVIEW</b> .....	<b>9</b>
2.1 Multiphase Flow Gas-Liquid System.....	9
2.1.1 Flow Regime in Gas-Liquid Flow System .....	9
2.1.2 Horizontal Flow Regime .....	10
2.1.3 Inclined Pipeline Flow Regime .....	12
2.1.4 Hilly Terrain Flow Behaviour .....	13
2.1.5 Slug Flow Behaviour in Hilly-Terrain Pipelines.....	14
2.1.6 Liquid Holdup in Pipe .....	16
2.1.7 Slug Flow Parameters.....	19
2.1.8 Slug Characteristics Correlation .....	20
2.2 Bifurcation Analysis .....	26
2.3 Study of Sand Transport in Pipeline .....	27
2.3.1 Single Phase Liquid-Sand Transport .....	28
2.3.2 Liquid- Sand Flow Patterns in Horizontal Pipeline: .....	30
2.3.3 Factors Affecting Sand Transportation .....	32
2.3.4 Sand Transport Models in Liquid Flow System .....	35
2.3.5 Liquid-Solid Transport in Inclined Pipeline .....	45
2.3.6 Study of Liquid-Solid Transport at the Dip.....	46
2.4 Sand Transport in Two Phase Air-Water Flow .....	46
2.4.1 Sand Transport in Stratified Flow.....	48
2.4.2 Sand Transport in Intermittent Flow.....	48
2.4.3 Sand Transport in Air-Water Flow of Inclined Pipeline .....	50
2.4.4 Sand Transport Models in Gas-Liquid Flow System .....	51
2.5 Studies of Sand Dunes in Pipes.....	56
2.6 Challenges:.....	56
<b>3 EXPERIMENTAL SET UP</b> .....	<b>59</b>
3.1 The Test Sections.....	59
3.1.1 The 24° Dip Pipeline .....	61
3.1.2 The 12° Dip Pipeline .....	61
3.1.3 Liquid Supply System.....	62
3.1.4 Air Supply System .....	62
3.1.5 Sand Injection System .....	62
3.2 Instrumentation .....	63
3.2.1 Flow Meters .....	63
3.2.2 Absolute Pressure Transducers.....	64
3.2.3 Temperature Transducer .....	65
3.2.4 Conductivity Rings.....	65

3.2.5	Flow Data Acquisition System .....	69
3.3	Description of Experimental Programme .....	70
3.3.1	Experimental Procedure for Sand Test.....	71
3.4	Sand Holdup Measurement.....	73
3.4.1	Velocity Measurement Using Cross Correlation.....	75
3.5	Measurement Error.....	77
3.6	Chapter Summary .....	78
4	AIR-WATER EXPERIMENTAL RESULT AND ANALYSIS .....	81
4.1	Results of 24° Dip Pipeline Air-Water Experiment.....	83
4.1.1	Flow Regime in 2-inch 24° Dip Pipeline.....	83
4.1.2	Data Analysis (Flow Regime).....	89
4.1.3	Air-Water Flow Behaviour at the Dip in 2-inch 24° Test Section.....	91
4.1.4	Slug Initiation Mechanism at the Dip in 2-inch 24° Test Section.....	92
4.1.5	Liquid Holdup in 2-inch 24° Dip Pipeline .....	94
4.1.6	Slug Flow Characteristics in Air-Water for 2-inch 24° Dip Pipe .....	100
4.1.7	Bifurcation Map of Air-Water Flow in 2-inch +24° Configuration.....	114
4.1.8	Criteria for Slug Flow Mechanism in 2-inch 24° Test Section .....	119
4.2	Results of 12° Dip Pipeline Air-Water Experiment.....	121
4.2.1	Air-Water Flow Regime in 2-inch +12° Dip Pipeline .....	121
4.2.2	Liquid Holdup in 2-inch 12° Dip Pipeline .....	124
4.2.3	Bifurcation Map of Multiphase flow 2-inch 12° Configuration.....	125
4.2.4	Slug Flow Characteristics in 2-inch 12° Dip Pipeline.....	130
4.2.5	Criteria for Slug Flow Mechanism in 2-inch 12° Test Section .....	135
4.3	Chapter Summary .....	136
5	RESULTS AND DISCUSSION OF SAND-WATER TEST .....	139
5.1	Sand-Water Settling Test Result.....	139
5.1.1	Sand-Water Transport Characteristics .....	139
5.1.2	Sand-Water Settling Test Result in +24° Inclined Section .....	141
5.1.3	Sand-Water Settling Test Result in +24° Dip Section .....	145
5.1.4	Sand-Water Settling Test Result in +12° Dip Configuration.....	149
5.1.5	Comparison of Sand Flow Regime with Published Work.....	151
5.2	Identification of Sand-Water Flow Regime Using Conductivity Ring Signals....	152
5.2.1	Limitation of Conductivity Ring in Sand Measurement.....	159
5.2.2	Sand Holdup Measurement Conductivity Ring.....	159
5.3	Sand-Water Entrainment Test Result .....	161
5.4	Sand Dune Mechanism .....	161
5.5	Sand Dune Measurement .....	165
5.5.1	Sand Hold up Calculation.....	167
5.6	Sand Dune Analysis .....	167
5.7	Sand Minimum Transport Condition in Dip Pipelines .....	172
5.7.1	Sand Minimum Transport Velocities in Sand-Water Flow in +24° Dip Pipeline .....	172
5.7.2	Sand Minimum Transport Velocities in Sand-Water Flow in +12° Dip Pipeline .....	175
5.7.3	Comparison of Sand Minimum Transport Condition with Published Work .....	175
5.8	Chapter Summary .....	178
6	RESULTS AND DISCUSSION OF SAND-AIR-WATER TEST .....	181
6.1	Sand Transport Characteristics in Air-Water Flow Regime.....	181
6.1.1	Sand Transport Characteristics in Segregated Flow.....	181
6.1.2	Sand Transport Characteristics in Intermittent Flow .....	182
6.2	Sand-Air-Water Entrainment Test Result.....	185
6.3	Sand Minimum Transport Condition in Sand-Air-Water Flow in +24° and +12° Dip Pipeline .....	187



6.3.2 Comparison of MTC in Sand-Air-Water Flow .....	199
6.4 Chapter Summary .....	201
7 Conclusions and Recommendation for Future Work.....	203
7.1 Conclusions .....	203
7.2 Recommendation for Future Work.....	205
REFERENCES.....	209
APPENDICES.....	219

## LIST OF FIGURES

Figure 2-1: Horizontal flow pattern map (Mandhane et al., 1973)).....	12
Figure 2-2: Schematic showing flow through the bed.....	14
Figure 2-3: In-situ liquid volume fraction correlation ( Guzhov et al., 1967).....	18
Figure 2-4: An idealised slug unit.....	19
Figure 2-5: Schematic presentation of flow patterns and concentration distributions in normal direction to flow adapted from Perker, 2008.....	29
Figure 2-6 Liquid-sand flow regimes in horizontal pipelines (Yan, 2010) .....	31
Figure 2-7: Chart for estimating the critical velocities (Multiphase flow handbook -Cowe, 2006).....	39
Figure 2-8 Sand/Liquid/Gas multiphase flow system (Yan, 2010) .....	47
Figure 2-9 Schematic sand behaviour in slug flow, (Al-lababidi et al., 2008).....	50
Figure 2-10: Locus of transportation of sand particles (King et al., 2000) .....	52
Figure 2-11: 6-inch dip experiment (King et al., 2000) .....	54
Figure 3-1: Schematic drawing of 2-inch dip facility .....	60
Figure 3-2: Dimensional configuration for 2 inch dip section.....	61
Figure 3-3: Sand size distribution used in the test.....	63
Figure 3-4: Calibration of single pressure transducer (absolute) in the gas line.....	64
Figure 3-5: Calibration of single pressure transducer (gauge) in the horizontal inlet line .....	65
Figure 3-6: Conductivity ring .....	67
Figure 3-7: Probe electronics diagram (Fossa, 1998) .....	68
Figure 3-8: Sand Injection calculation model.....	71
Figure 3-9: Time delay cross correlation flow measurement.....	76
Figure 3-10: Generated signals.....	77
Figure 4-1: Instrument and rig nomenclature.....	82
Figure 4-2: Air-water flow regime map for downhill 24° test section .....	84
Figure 4-3: Air pocket downhill section at $V_{sl} = 0.55$ m/s, $V_{sg} = 0.05$ m/s .....	84
Figure 4-4: Flow pattern map, 30° downward inclination, 5.1 cm pipe (Barnea et al., 1982).....	85
Figure 4-5: Air-water flow regime map for downward dip 24° test section .....	86
Figure 4-6: Liquid accumulation at the dip section at $V_{sl} = 0.55$ m/s, $V_{sg} = 0.05$ m/s ...	86
Figure 4-7: Slug generates position as $V_{sg} = 0.5$ m/s, $V_{sl} = 0.15$ m/s & 0.35 m/s.....	87
Figure 4-8: Air-water flow regime map for upward dip 24° test section .....	87
Figure 4-9: Air-water flow regime map for uphill section .....	88
Figure 4-10: Aerated slug at the uphill section, $V_{sl} = 0.55$ m/s and $V_{sg} = 1.0$ m/s .....	88
Figure 4-11: Flow pattern map, 20° downward inclination, 5.1 cm pipe (Barnea et al, 1985).....	89
Figure 4-12: Typical time traces of the liquid holdup .....	90
Figure 4-13: Air-water flow behaviour at dip-on downhill section, 24° test section.....	92
Figure 4-14: Slug initiation due to wave growth mechanism at $V_{sl} = 0.07$ m/s, and $V_{sg} = 0.6$ m/s.....	93
Figure 4-15: Wave coalescence initiation at $V_{sl} = 0.07$ m/s, $V_{sg} = 1.5$ m/s .....	94
Figure 4-16: Overall-average liquid hold at CR-1, 24° downhill test section.....	95
Figure 4-17: Overall-average liquid hold at CR-7, 24° uphill test section.....	96
Figure 4-18: Comparison of measured overall liquid holdup and predicted by Greskovisch, 1972 for CR-1, downhill test section .....	97
Figure 4-19: Comparison of measured overall liquid holdup and predicted by Greskovisch, 1972 for CR-7, uphill test section.....	97

Figure 4-20: Comparison of measured overall liquid holdup and predicted by Beggs and Brill, 1973 for CR-5, upward dip test section .....	98
Figure 4-21: Comparison of measured overall liquid holdup and predicted by Beggs and Brill, 1973 for CR-7, uphill test section.....	98
Figure 4-22: Comparison of measured overall liquid holdup and predicted by Mattr and Gregory, 1974 for CR-5, upward dip test section .....	99
Figure 4-23: Comparison of measured overall liquid holdup and predicted by Mattr and Gregory, 1974 for CR-7, uphill test section.....	99
Figure 4-24: Slug liquid holdup for uphill section at CR-5 .....	101
Figure 4-25: Slug liquid holdup for uphill section at CR-7 .....	102
Figure 4-26: Slug frequency in the slug body for uphill section (CR-5).....	103
Figure 4-27: Slug frequency in the slug body for uphill section (CR-7).....	103
Figure 4-28: Liquid holdup signal from two conductivity ring uphill section (CR-7 and CR-8), +24° Inclination, $V_{sl}=0.15\text{m/s}$ and $V_{sg}=1.5\text{m/s}$ .....	104
Figure 4-29: Cross correlation coefficient for the two liquid holdup signals of Figure 4-28.....	105
Figure 4-30: Cross correlation coefficient extract from Figure 4-29.....	105
Figure 4-31: Slug velocity for uphill section at CR-5/CR-6 .....	107
Figure 4-32: Slug velocity for uphill section at CR-7/CR-8 .....	107
Figure 4-33: Dimensionless slug velocity for uphill section at CR-5/CR-6.....	108
Figure 4-34: Dimensionless slug velocity for uphill section at CR-7/CR-8.....	108
Figure 4-35: Slug translational velocity against mixture velocity for uphill section .....	109
Figure 4-36: Comparison of measured slug translational velocity in the slug body and predicted by Bendiksen 1984 correlation and for uphill section .....	110
Figure 4-37: Type A, dimensionless slug length distribution along uphill section at ( $V_{sg}=0.2\text{-}1.5\text{m/s}$ , $V_{sl}=0.07\text{m/s}$ ).....	111
Figure 4-38: Type B, dimensionless slug length distribution along uphill section at ( $V_{sg}=2.0\text{-}4.0\text{m/s}$ , $V_{sl}=0.07\text{m/s}$ ).....	112
Figure 4-39: Type C, Dimensionless slug length distribution along uphill section, ( $V_{sg}=4\text{-}5\text{m/s}$ $V_{sl}=0.35\text{m/s}$ ).....	112
Figure 4-40: Bifurcation map of 24° downhill section (CR-1), $V_{sl}=0.07\text{m/s}$ .....	115
Figure 4-41: Bifurcation map of 24° downhill section (CR-1), $V_{sl}=0.35\text{m/s}$ .....	116
Figure 4-42: Bifurcation map of 24° uphill section (CR-7), $V_{sl}=0.07\text{m/s}$ .....	116
Figure 4-43: Bifurcation map of 24° uphill section (CR-7), $V_{sl}=0.35\text{m/s}$ .....	117
Figure 4-44: Bifurcation map across 24° dip geometry pipe, $V_{sl}=0.07\text{m/s}$ and $V_{sg}=0.7\text{m/s}$ .....	117
Figure 4-45: Bifurcation map across 24° dip geometry pipe, $V_{sl}=0.15\text{m/s}$ and $V_{sg}=0.7\text{m/s}$ .....	118
Figure 4-46: Bifurcation map across 24° dip geometry pipe, $V_{sl}=0.35\text{m/s}$ and $V_{sg}=0.7\text{m/s}$ .....	118
Figure 4-47: Bifurcation map across 24° dip geometry pipe, $V_{sl}=0.55\text{m/s}$ and $V_{sg}=0.7\text{m/s}$ .....	119
Figure 4-48: Initiation slugs translational to mixture velocities ratio trend (present work) .....	120
Figure 4-49: Initiation slugs translational to mixture velocities ratio trend (Al-safran, 2004).....	120
Figure 4-50: Air-water flow regime map for downhill 12° test Section.....	122
Figure 4-51: Air-water flow regime map for downward dip 12° test section .....	122
Figure 4-52: Air-water flow regime map for upward dip 12° test section.....	123
Figure 4-53: Air-water flow regime map for uphill 12° test section.....	123
Figure 4-54: Overall-average liquid hold up for 12° downhill test section (CR-1) .....	124
Figure 4-55: Overall-average liquid hold up for 12° Uphill test section (CR-8) .....	125

Figure 4-56: Bifurcation map of 12° configuration at downhill section (CR-1), Vsl=0.07m/s.....	126
Figure 4-57: Bifurcation map of 12° configuration at downhill section (CR-1), Vsl =0.35m/s.....	127
Figure 4-58: Bifurcation map of 12° configuration at uphill section (CR-7), Vsl =0.07m/s .....	127
Figure 4-59: Bifurcation map of 12° configuration at uphill section (CR-7), Vsl =0.35m/s .....	128
Figure 4-60: Bifurcation map across the 12° dip geometry pipe, Vsl=0.07m/s and Vsg =0.7m/s.....	128
Figure 4-61: Bifurcation map across the 12° dip geometry pipe, Vsl=0.15m/s and Vsg =0.7m/s.....	129
Figure 4-62: Bifurcation map across the 12° dip geometry pipe, Vsl=0.35m/s and Vsg =0.7m/s.....	129
Figure 4-63: Bifurcation map across the 12° dip geometry pipe, Vsl=0.55m/s and Vsg =0.7m/s.....	130
Figure 4-64: Slug liquid holdup in the slug body for uphill 12° test section (CR-5) .....	131
Figure 4-65: Slug liquid holdup in the slug body for uphill 12° test section (CR-7) .....	132
Figure 4-66: Slug frequency for uphill 12° test section (CR-5) .....	133
Figure 4-67: Slug frequency for uphill 12° test section (CR-7) .....	133
Figure 4-68: Slug translational velocity for upward-dip, 12° test section (CR-5 &CR-6) .....	134
Figure 4-69: Slug translational velocity for uphill, 12° test section (CR-7 &CR-8) .....	135
Figure 4-70: Initiation slugs translational to mixture velocities ratio for 12° test section .....	135
Figure 5-1: Sand streaks transition to saltation in downhill section.....	141
Figure 5-2: Sand characteristics in downhill and uphill pipe (50lb/1000bbl, VL=0.3m/s) .....	143
Figure 5-3: Downhill sand-water flow regime map for +24° inclined section.....	144
Figure 5-4: Uphill sand-water flow regime map for +24° inclined section .....	145
Figure 5-5: Terrain effect on sand characteristics at the dip (VL=0.7m/s, 200lb/1000bbl) .....	146
Figure 5-6: Terrain effect on sand characteristics at the dip (VL=0.7m/s, 200lb/1000bbl) .....	147
Figure 5-7: Terrain effect on sand characteristics at the dip (VL=0.6m/s, 500lb/1000bbl) .....	147
Figure 5-8: Dip section sand-water flow regime at the dip .....	148
Figure 5-9: Downhill sand-water flow regime map for +12° dip pipeline .....	149
Figure 5-10: Uphill sand-water flow regime Map for +12° dip pipeline.....	150
Figure 5-11: Dip section sand-water flow regime map for +12° dip pipeline .....	150
Figure 5-12: Full suspension from conductivity ring, (50lb/1000bbl, Vsl=1.0m/s) .....	153
Figure 5-13: Streak regime from conductivity ring, (50lb/1000bbl, Vsl=0.8m/s) .....	154
Figure 5-14: Saltation regime from conductivity ring, (50lb/1000bbl, Vsl=0.6m/s) .....	154
Figure 5-15: Sand dune regime from conductivity ring, (50lb/1000bbl, Vsl=0.4m/s) ..	155
Figure 5-16: Sand bed regime from conductivity ring, (200lb/1000bbl, Vsl=0.3m/s) ..	156
Figure 5-17: Average normalised voltage vs. liquid velocity (downhill,(CR-1)).....	157
Figure 5-18: Average normalised voltage vs. liquid velocity (downward- dip, (CR-3))	157
Figure 5-19: Average normalised voltage vs. liquid velocity (upward dip, (CR-5)) ....	158
Figure 5-20: Average normalised voltage vs. liquid velocity (uphill section, (CR-7))..	158
Figure 5-21: Static sand bed, sand bed layer =0.29D .....	162
Figure 5-22: Sand dune Initiation at water velocity =0.18m/s .....	162
Figure 5-23: Sand bed forming Ripple at water velocity =0.18m/s.....	162
Figure 5-24: Unstable sand dune at water velocity =0.18m/s .....	163

Figure 5-25: Sand dune reach stability at water velocity =0.18m/s.....	163
Figure 5-26: Sand dune evolution at water velocity =0.21m/s .....	165
Figure 5-27: 0.44D sand bed layer ( $V_L = 0$ to 0.20m/s).....	168
Figure 5-28: Sand dune formation at ( $V_L = 0.30$ m/s).....	169
Figure 5-29: Sand dune development.....	169
Figure 5-30: Average sand dune velocity with sand dune geometry .....	169
Figure 5-31: Comparison of sand dune parameter in this work and Thomas (1964) result .....	170
Figure 5-32: Stable sand dunes developed from sand bed height = 0.29D and water velocity =0.18m/s.....	171
Figure 5-33: Stable sand dunes developed from sand bed height = 0.37D and water velocity =0.15m/s.....	171
Figure 5-34: sand characteristics at MTC in downhill and uphill pipe, 500lb/1000bbl ( $V_{MTC}=0.8$ m/s).....	173
Figure 5-35: Comparison between downhill and dip section (50lb/1000bbl, $V_L = 0.5$ m/s).....	174
Figure 5-36 MTC comparison with other published correlations for 12° and 24° configuration bend.....	176
Figure 6-1: Sand streaks transporting on the bottom of the pipe sand concentration = 200 lb/1000bbl, $V_L = 0.35$ m/s .....	182
Figure 6-2: sand transport characteristics in plug flow ( $V_{sl}=0.55$ m/s, $V_{sg}=0.2$ for 500lb/1000bbl).....	182
Figure 6-3: Sand transport characteristics in slug flow, (50/1000bbl, $V_{sl}= 0.15$ m/s, $V_{sg}=$ 0.3m/s).....	183
Figure 6-4: Sand transports in aerated slug (50 lb/1000bbl, $V_{sl} = 0.08$ m/s $V_{sg} = 2.0$ m/s).....	184
Figure 6-5: Sand transports in aerated slug (500lb/1000bbl, $V_{sl} = 0.15$ m/s, $V_{sg} = 2.0$ m/s).....	185
Figure 6-6: Sand transport characteristics in air/water flow in dip pipeline .....	186
Figure 6-7: Sand streaks transporting on the bottom of the pipe .....	187
Figure 6-8: Sand behaviour around MTC (50 lb/1000bbl, $V_{sl} = 0.08$ m/s).....	188
Figure 6-9: Sand transport behaviour before MTC (500lb/1000bbl, $V_{sl}=0.08$ m/s, $V_{sg}=$ 6.0 m/s).....	189
Figure 6-10: Sand behaviour around MTC (50 lb/1000bbl, $V_{sl} = 0.15$ m/s) .....	190
Figure 6-11: Sand behaviour around MTC (500lb/1000bbl, $V_{sl} = 0.15$ m/s) .....	190
Figure 6-12: Illustration of energetic ripples' effect (500lb/1000bbl, $V_{sl}= 0.15$ m/s, $V_{sg} \geq$ 3.0 m/s).....	191
Figure 6-13: Sand behaviour around MTC (50lb/1000bbl, $V_{sl} = 0.35$ m/s).....	191
Figure 6-14: Sand behaviour around MTC (500 lb/1000bbl, $V_{sl} = 0.35$ m/s) .....	192
Figure 6-15: Sand behaviour around MTC, 500 lb/1000bbl $V_{sl} = 0.55$ m/s).....	193
Figure 6-16: MTC for sand-air-water on +24° dip (uphill section).....	194
Figure 6-17: Sand MTC in sand-air-water multiphase flow on flow regime map (+24° dip, uphill section).....	195
Figure 6-18 MTC for Sand-Air-Water on +12° dip (uphill section) .....	197
Figure 6-19: Sand MTC in sand-air-water multiphase flow on flow regime map (+12° dip, uphill section).....	198
Figure 6-20: Comparison of MTC in sand-air-water flow between + 24° and +12° dip section, and Yan, 2010 work, sand concentration 50 lb/1000bbl.....	200
Figure 6-21: Comparison of MTC in sand-air-water flow between + 24° and +12° dip section, and Yan, 2010, sand concentration 500 lb/1000bbl.....	200

## LIST OF TABLES

Table 2-1: King et al., 2000 Sand-air-water test result .....	53
Table 3-1: Sand concentration Test Matrix .....	70
Table 3-2: Measurement parameter errors .....	78
Table 5-1: Velocity range of various sand flow regimes at 24 <sup>0</sup> downhill .....	143
Table 5-2: Velocity range of various sand flow regimes at 24 <sup>0</sup> uphill .....	144
Table 5-3: Velocity range for different flow regime of 24 <sup>0</sup> downstream-dip section....	148
Table 5-4: Comparison of measured velocity range for sand flow regime of inclined section and Yan, 2010 result.....	151
Table 5-5: Flow behaviour from conductivity ring sand hold up measurement.....	160
Table 5-6: Threshold velocity of sand entrainment.....	164
Table 5-7: Sand (MTC) in sand-water flow for +24 <sup>0</sup> dip pipeline.....	174
Table 5-8: Sand-water MTC for + 12 dip pipeline .....	175
Table 5-9: Comparison of MTC in single phase flow between +24 <sup>0</sup> and previous work .....	177
Table 5-10: Comparison of MTC in single phase flow between +12 <sup>0</sup> and previous work .....	177
Table 6-1: Sand MTC in Sand-air-water multiphase flow for +24 <sup>0</sup> dip (uphill section)	194
Table 6-2: Sand MTC in sand-air-water multiphase flow for +12 <sup>0</sup> dip (uphill section)	196

# NOMENCLATURE

## A. Symbols

<i>Symbol</i>	<i>Units</i>	<i>Description</i>
$A$	[m <sup>2</sup> ]	Pipe Cross Section Area
$C_D$	[-]	Drag Coefficient
$C_g$	[-]	Gas Volume Fraction
$C_v$	[-]	Volumetric Sand Concentration
$C_o$	[-]	Distribution Coefficient
$D$	[m]	Pipe Internal Diameter
$d_e$	[m]	Bubble Diameter
$d_p$	[m]	Sand Diameter (Particle size)
$d_w$	[m]	Weighted Mean Diameter
$E_g$	[-]	In-situ Gas Volume Fraction
$E_l$	[-]	In-situ Liquid Volume Fraction
$E_T$	[Jm <sup>-3</sup> ]	Turbulent Energy per Unit volume
$F_d, N_l$	[-]	Constant
$Fr$	[-]	Froude Number
$F_L$	[-]	Lift Force
$f_s$	[s <sup>-1</sup> ]	Slug Frequency
$g$	[ms <sup>-2</sup> ]	Acceleration due to Gravity
$H_h$	[-]	Homogenous Liquid Holdup
$H_l$	[-]	Average Liquid Holdup
$H_{ls}$	[-]	Slug Liquid Holdup
$H_o$	[-]	Horizontal Pipe Liquid Holdup
$H_\beta$	[-]	Inclination Pipe Liquid Holdup
$i_m$	[Pa/m]	Pressure Gradient of Slurry

$L_1, L_2$	[-]	Dimensionless Number
$L_u$	[m]	Slug Unit Length
$L_s$	[m]	Slug Body Length
$L_f$	[m]	Liquid Film Length
$N_{Re}$	[-]	Reynolds's Number
$P$	[bar]	Pressure
$\Delta P$	[bar]	Differential Pressure
$R_{xy}, R_{y0y1}$	[-]	Cross-correlation Function
$s$	[-]	Density Ratio of Solid to Liquid
$u_b$	[ms <sup>-1</sup> ]	Slug Tail Velocity
$u_d$	[ms <sup>-1</sup> ]	Drift Velocity
$u_l$	[m/s]	Liquid Film Velocity
$u_s$	[ms <sup>-1</sup> ]	Solid Liquid Body Velocity
$u_m$	[ms <sup>-1</sup> ]	Mixture Velocity
$u_s$	[ms <sup>-1</sup> ]	Bubble Velocity
$u_{sg}, V_{sg}$	[ms <sup>-1</sup> ]	Superficial Gas Velocity
$u_{sl}, V_{sl}$	[ms <sup>-1</sup> ]	Superficial Liquid Velocity
$u^*_o$	[ms <sup>-1</sup> ]	friction Velocity at Minimum Transport Velocity
$u_t$	[ms <sup>-1</sup> ]	Slug Front Velocity
$u_y$	[m/s]	mixture Velocity in y-direction
$u_z$	[ms <sup>-1</sup> ]	mixture Velocity in z-direction
$u_l$	[ms <sup>-1</sup> ]	Mean Liquid Velocity
$V$	[ms <sup>-1</sup> ]	Velocity
$V_c$	[ms <sup>-1</sup> ]	Critical Sand Velocity
$W$	[ms <sup>-1</sup> ]	Particle Terminal Velocity



## B. Greek Symbols

<i>Symbol</i>	<i>Units</i>	<i>Description</i>
$\alpha_g$	[-]	Gas Volume Fraction
$\alpha_l$	[-]	Liquid Volume Fraction
$\beta$	[-]	Inclination
$\delta$	[m]	Laminar Sub-layer
$\Delta$	[-]	Change
$\eta$	[-]	Constant
$\theta$	[-]	Angle
$\lambda_g$	[-]	Gas Hold-up
$\lambda_l$	[-]	Liquid Hold-up
$\mu_g$	[Pa-s]	Dynamic Gas Viscosity
$\mu_l$	[Pa-s]	Dynamic Liquid Viscosity
$\nu_l$	[m <sup>2</sup> s <sup>-1</sup> ]	Kinematic Liquid Viscosity
$\rho_g$	[kgm <sup>-3</sup> ]	Gas Density
$\rho_l$	[kgm <sup>-3</sup> ]	Liquid Density
$\rho_m$	[kgm <sup>-3</sup> ]	Mixture Density
$\rho_o$	[kgm <sup>-3</sup> ]	Oil Density
$\rho_w$	[kgm <sup>-3</sup> ]	Water Density
$\rho_{TP}$	[kgm <sup>-3</sup> ]	Two Phase Density
$\Delta\rho$	[kgm <sup>-3</sup> ]	Density Difference between the Two Phases
$\sigma$	[Nm <sup>-1</sup> ]	Surface Tension



# 1 INTRODUCTION

## 1.1 Background

Sand production is a natural consequence of fluid flow into a well bore from the reservoir. It is the migration of sand grains from formation rocks into the well bore and is transported to the surface by reservoir fluid. The process may be divided into three stages; the loss of mechanical integrity of the rocks surrounding an open hole or perforation (cavity), separation of solid particles from the rocks due to hydrodynamic forces and solid transportation of the particles to the surface by reservoir fluids. The key to sand production in weakly-consolidated and unconsolidated formations is the loss of mechanical integrity of the rocks surrounding the cavity.

Sand Production is a persistent problem in the petroleum industry for many years, especially in poorly consolidated reservoir of relatively low strength (<2000 psi) or where hydrocarbon is in the increasing demand. Many reservoirs from major oil producing regions (such as Gulf of Mexico, North Sea, Middle East) are prone to sand production due to their unconsolidated formations and high sand production potential during the life of the well.

Sand production is a concern for field development and the conventional approach of sand management strategy is to install a down-hole sand exclusion system (such as gravel packing, chemical consolidated, screen/slotted liners, frac-pack, etc.). This could be efficient though with additional completion cost in the early stage of production when sand influx is not large enough to cause impairment to productivity or damage to pipeline and surface equipment. However, this approach has not only proved too costly but also causes difficulties in subsequent recompletion due to completion complexities involved. Moreover, once sand production increase at later stage of reservoir life above the threshold, the integrity of the completion tubing would be compromised, where blockage and erosion could occur. In addition, it is quite impossible to produce a sand free hydrocarbon even with a sand exclusion system in place.

With these limitations faced by conventional sand management strategies, the need to produce sand along with the hydrocarbon is inevitable. However, this does not go without its own challenges such as reduction in throughput, pigging problems and pipe bottom erosion. Furthermore, presence of solid phase with the multiphase flow of gas

and liquid; and the operating window to optimize production within integrity limit are considered during pipeline design.

The world's demand for oil and gas has continuously increased with the increasing demand of energy requirements. Oil and gas industry continues to advance in technologies to exploit reserve and produced the unprocessed hydrocarbon fluid along with sand particles through multiphase pipeline to the topside facilities. The economic benefits of this "assured" option in the ever increasing demand of oil and gas is more pronounced in offshore environment coupled with problems associated with formation damage and impaired productivity.

In the advent of subsea wells with long-distance multiphase export line, tie-back to onshore production platform is the alternative solution to produce from deep water and ultra-deep water field development. Therefore, produced hydrocarbon and sand have to be transported from the wellhead through a long-distance multiphase export line, tie-back to floating or onshore production platforms. These pipelines could sometimes run through some tough terrains such as hills and valleys; and the pipe layout in such scenarios result in complex flow mechanism within the pipeline.

However, it is generally recognized that one of the major issues of sand management technology yet to be addressed in the petroleum industry is the effective transport of particles in oil-gas multiphase flow from sand face to surface processing facilities (Bello, 2008). Therefore, sand particle transport is one of the major flow assurance concerns during gas-oil-sand multiphase flows through wellbore, flow line and subsea tieback systems which if not addressed may be a setback in sand management technology.

Sand particle transport in gas-liquid multiphase flow requires accurate multiphase flow prediction tools for efficient design and performance assessment. Accurate prediction of flow condition, sand velocity, sand holdup and minimum transport condition in sand-liquid-gas flow systems are important parameters to solve the problems of sand management (Bello, 2008).

The difficulties are aggravated once the pipelines exhibit undulating patterns. In typical hydrocarbon transportation, pipeline follows the undulating topography of the offshore seafloors or onshore mountains, known as hilly terrain geometry. These pipelines

comprise downhill/uphill sections and also elbows. The elbow is normally described as dip. Due to the complex pipe geometry, air-liquid multiphase flow regimes will be strongly affected and different from those in horizontal pipeline under same flow conditions, hence affect sand transport characteristics. Therefore, it is vital to understand both air-liquid multiphase flow regime and sand transport characteristics in dip geometry for an efficient pipeline design.

Furthermore, the flow behaviour of sand in hilly terrain pipeline geometry will be quite different from other pipe geometry due to their distinct flow behaviour of multiphase flow. Many questions such as: what happens to sand particles that settle at the dip; and what physical phenomenon should be used to describe the flow pattern existing in this region have not been answered. Also, there is no established prediction of minimum sand transport condition at the dip. There is little detailed work in the literature that addresses these issues. The hydrodynamic parameters such as friction losses, pressure gradient along the pipe and mixture velocity all depend strongly on the pattern formation developed in the pipe. In addition, solids may be transported in fluids both under conditions where they are totally suspended and where they are partially or wholly settled out and move as bed. Again, below minimum condition of flow in a pipeline, solid transport at low concentration will form a bed on the bottom of the pipe. Thus, knowledge of the flow condition leading to deposition of solid particles is of vital interest in all fluid-solid conveying systems.

In multiphase flow, flow regime is strongly dependent on the pipe orientation (Mukherjee and Brill, 1983; Taiter and Dukler, 1976; Zheng et al., 1994; Al-safran et al., 2004). Therefore, the existing study of sand in horizontal/inclined cannot be generalised for undulating pipe. The studies of sand transport in multiphase flow at the bend are not readily available in the literature. Trippets and Priestman, 1997 and King et al., 2000 studied sand transport in multiphase undulating pipe flow where the downward-and-upward pipe were approximately  $1^\circ$  of arc representing a typical grade line on the sea bed.

On a wider application of designing a hydraulic system, solid-liquid-gas flows are commonly encountered in industries such as chemical processing plants, sewage systems, and mining industry. Over the years, long distance hydraulic transport of solids has received increasing attention (Durand, 1953; Thomas, 1961, 1962 and 1964; Oroskar and Turian, 1980; Newitt et al., 1995; Kokpinar and Gogus, 2001; Bello, 2008;

Smart, 2009). The general behaviour of mixtures of liquid-solid and gas-liquid-solid in horizontal and inclined pipelines have been subjected to continuous investigation for decades (Angelson et al., 1989; Oudemans, 1993; Danielson, 2007).

During shutdown of sand transport systems or at low flow rate, there is possibility of partial blockage of the pipe by sand /or solid materials and sand may deposit at the dip. In order to flush out the sand particle, a minimum velocity will be required for sand entrainment at the dip. Therefore, the behaviour of the particles at low velocities has to be fully investigated in order to prevent pipe blockages and also to transport particles securely and reliably.

It is important to predict the sand behaviour in multiphase flows for pipeline design. It is desirable to understand and predict the behaviour of sand in slug flow so that these problems can be avoided at the design stages.

The immediate application of this work is to solve problem of sand transportation at low loading of sand concentration in an undulating pipeline for water-sand and air-water multiphase flow.

## **1.2 Study of Sand Transportation in Hilly Terrain Pipeline**

In typical hydrocarbon pipeline transportation, flowline follows through the undulating topography of the seafloor that resulted to complex flow mechanism within the pipeline.

Undulating pipelines such as hilly terrain pipelines consist of interconnected, downhill elbow and uphill sections. They are inevitable in field operations. Both offshore seafloor and onshore land exhibit hilly-terrain configurations. The flow characteristics changes along the hilly-terrain pipelines and such changes must be considered during pipeline and downstream facility designs. Accurate prediction of pressure drop, liquid holdup and flow pattern along the pipeline are not only essential to enhance pipeline design, sizing and routing; but also for the design of downstream separation and processing facilities.

The erratic behaviour as a result of the undulating pipeline has adverse impact on downstream processing facilities. Many researchers have studied the terrain slugging in multiphase flow (gas-liquid), Taitel and Barnea, 2000; Zheng et al., 1994; Al-Safran

et al., 2004. Slug flow in a separate pipeline of each of the three configurations (horizontal, downhill and uphill pipes) is relatively well understood. It has been established that at the dip; there are two types of slug initiation mechanism (wave growth mechanism and wave coalescence mechanism) based on the flow conditions and pipe geometry. The slug mechanism at the dip may affect sand transport characteristics and efficiency.

However, the study of sand movement or behaviour in the multiphase system in an undulating pipe has not been thoroughly considered. The undulating pipeline faces different flow assurance problems especially in sand transport systems if not managed properly. It is not practically possible to have a distinct straight horizontal pipeline for long distance pipeline transportation. Therefore, the study of sand behaviour in different section (horizontal and inclined pipelines) is not the ideal situation in the oil and gas industry. It has been established experimentally that inclined plane (downhill and uphill) slope will play an important role in sand transportation, Yan, 2010. Furthermore, there is no adequate information on the effect of sand transport at the dip with interconnected inclined pipe.

In addition, empirical models to calculate sand bed and the bed layer height in relation to fluid stream velocity at the dip are not extensively studied in the literature. It is also important to mention that prediction of the minimum transport condition with wide range of parameters, providing the operating window to prevent sand accumulation in a pipeline is essential to the oil and gas industry.

In gas-liquid-sand multiphase flow, sand transport efficiency is strongly dependent on the flow regime. While downward flow is dominated by stratified flow, effect of sand concentration in stratified flow (outside the minimum transport condition) has not been fully investigated. In uphill section, sand transport is dominated by slug flow that required further investigation.

### **1.3 Research Objectives**

The fundamental aim of this research work is to carry out experimental study of sand transport in liquid-solid and gas-liquid-solid for various dip configurations. Based on this aim, multiphase flow loops capable of inclined ( $\pm 24^\circ$  and  $\pm 12^\circ$ ) were built to investigate

sand transport at various sections of the pipeline and for various flow regimes, geometry and operating conditions. The specific objectives are as follows:

- Review the literature of the multiphase (gas-liquid-solid) flows in hilly terrain pipeline and sand transport in hydraulic and multiphase system.
- Design and build a three-phase gas-liquid-solid dip facility and its instrumentation to study the pipeline sand transportation.
- Compare the current experimental data for air-water with other experimental studies where appropriate.
- Study sand flow behaviour appearing in water-sand and air-water-sand phase flow in an undulating pipeline. Develop sand pattern for individual pipe geometries. Determine the influence of gas and liquid flow on sand transport such as moving bed, sand dunes and sand entrainment (entrainment test).
- Investigate minimum transport condition of water-sand and air-water-sand for  $\pm 24^\circ$  and  $\pm 12^\circ$  dip configuration.

## **1.4 Thesis Structure**

### **Chapter 2: Review of Sand Transport in Multiphase flow systems**

The first part of this chapter provides review of literature relevant to the subject matter as follows: fundamentals of multiphase flow, flow regimes and flow map in horizontal pipes, inclined pipes and hilly terrain pipelines; and slug flow characteristics. The second part of this chapter review previous research findings on solid transportation in single phase liquid flow and two phase gas-liquid flow, with discussion on the parameters which affect solid transportation.

### **Chapter 3: Experimental Set-up**

This chapter describes flow loop design and also outlines the instrumentation used, data acquisition and processing, installation and calibration of the experimental facilities of  $\pm 24^\circ$  and  $\pm 12^\circ$  dip configuration. It also discusses the experimental procedure and measurement.



The second part of this chapter detailed the conductivity ring design and its calibration process, and data processing techniques. While the final part of this section discussed the sand distribution used and the test methodology used in this work.

#### **Chapter 4: Air-Water Experimental Results and Analysis**

This chapter presents the experimental findings obtained in the laboratory-scale air-water multiphase flow loop in  $\pm 24^\circ$  and  $\pm 12^\circ$  dip configuration. The slug initiation mechanisms are detailed in this chapter.

#### **Chapter 5: Results and Discussion of Sand-Water Test**

Chapter 5 presents the experimental results obtained in water-sand tests. The sand characteristics observed in  $\pm 24^\circ$  and  $\pm 12^\circ$  dip configuration are described under different flow condition and develop sand regime maps. The dynamics of sand dune geometry are investigated experimentally and the conditions of sand dune formation are determined. The minimum transport conditions, MTC of sand-water test are reported in this chapter.

#### **Chapter 6: Results and Discussion of Sand-Air-Water Test**

This chapter presents the experimental findings obtained in sand-air-water test. The sand characteristics observed in stratified and slug flow in  $\pm 24^\circ$  and  $\pm 12^\circ$  dip pipeline are described under different flow conditions. Part of this work predicts MTC to account for various sand concentrations at various sections of undulating pipeline in air-water flows.

#### **Chapter 7: Conclusions and Future work**

This final chapter brings the key conclusions from this research work and outlines the recommendations for future research work.



## **2 LITERATURE REVIEW**

Sand transport in multiphase flow gas-liquid system is strongly dependent on the flow behaviour of the gas-liquid system. In certain flow regime, sand behaviours are serious concern to flow assurance (especially, at relatively low flow rates). In addition, the pipe geometry like hilly terrain is considered to exhibit complex and difficult flow behaviour. Therefore, the first section aims to cover literature review on gas-liquid multiphase flow in general and also hilly terrain in particular. The remaining section will cover literature review on liquid-sand and gas-liquid-sand system.

### **2.1 Multiphase Flow Gas-Liquid System**

Gas-liquid multiphase flow is the simultaneous flow of two phases in a pipe. It is a complex phenomenon and difficult to understand, predict and model. Gas-liquid multiphase flow phase distribution result to different flow regime even in the same pipe depending on the local conditions in the pipe. This section will discuss flow regime and the gas-liquid multiphase flow parameters such as liquid holdup and slug parameters relevant to sand transport.

#### **2.1.1 Flow Regime in Gas-Liquid Flow System**

When gas and liquid flow co-currently in a pipe, the phases will distribute themselves in a variety of combinations; this physical distribution of the fluid phases in a pipe section results in the formation of various flow pattern called flow regimes (Mandhane et al., 1973; Taitel and Dukler, 1976). The phase distribution of the fluids differs for various flow regimes. The configuration of the flow regime is determined by the operating conditions, fluid properties, flow rates, pipe geometry and pipe orientation through which the fluids are flowing. The flow regimes are mapped out using flow parameters like superficial velocities of the two fluids.

The early researchers of multiphase flow (Dukler and Hubbard, 1966) determined their flow regimes based on spectra distribution of wall pressure fluctuations. They classified flow regimes into dispersed, separated, and intermittent flows. However, the concept does not discriminate between stratified, annular flow, or dispersed liquid and dispersed gas flow regimes.

The flow regimes in two phase flow have been extensively studied and reported in many literatures (Barnea, 1986; Lee, 1993; Oddie et al., 2003; Barnea et al., 1985; Taitel et al., 1990). These maps have been developed for the prediction of flow patterns under various flow conditions.

In spite of the amount of work treated on this subject in the literature, there is no perfect general model capable of representing vertical, horizontal and inclined flow. The reliability of available correlations is limited to the particular flow regime or certain ranges of geometry and physical properties. This is due to inability to account for the coexistence of several flow regimes along the pipe for a given set of operating conditions. Review of flow regimes in this work is limited to horizontal and inclined pipeline that are relevant to hilly terrain pipeline. Thus individual pipe orientation (horizontal and inclined) will be discussed in brief.

### **2.1.2 Horizontal Flow Regime**

This is the type of flow structure that occurs in horizontal or near horizontal pipes. It is common in pipeline transportation of multiphase flow. The flow regime is classified into the following:

- **Dispersed Bubble:** This occurs at very low gas velocity, and high liquid velocity, the gas flows as small bubbles inside a continuous liquid flows. The gas bubbles are not uniform and mostly flow at the upper portion of the pipe due to buoyancy effect. The relative velocity of the bubbles is due to the difference in density between the two fluids.
- **Stratified Smooth Flow:** This occurs at low gas and liquid velocities. The gas and liquid segregates completely from each other in the flowline by gravitational force. The lighter fluid (in this case-gas) flows at the top of the heavier fluid (liquid flow) and creates a smooth gas-liquid interface.
- **Stratified Wavy Flow:** As the gas increases, gas-liquid interface of the stratified smooth flow becomes wavy such that there may be occasional splashing of liquid on the upper walls and some liquid entrainment into the gas phase.
- **Plug Flow:** This is an intermittent flow at moderate liquid rate and low gas flow rate. Most of the gas moves as large bubbles dispersed within continuous liquid. The liquid plugs are nearly free of entrained gas bubbles and separated by zones of

elongated bubbles. Plug flow resembles slug flow but the bubbles are generally smaller and move more slowly.

- **Slug Flow:** As the gas rate increases, the interface will grow even larger and will cover the cross section of the pipe. The liquid plug becomes aerated by small entrained bubbles in the liquid. The small bubbles within the liquid coalesce to form large bubbles which intermittently bridge some of the pipe length. The flow geometry is complex and chaotic.
- **Annual Flow:** At very high gas flow rate and low liquid flow rate, the gas flows as a core in the centre of the pipe and the liquid flows as a film along the circumference of the pipe. The liquid film is thicker at the bottom of the pipe. Some liquid droplets can also flow with the gas core as dispersed liquid.

There are various two-phase flow regime maps developed by many researchers based on experimental data and theoretical analyses. Mandhane et al., 1973 developed a flow regime map using superficial gas and liquid velocities as coordinates for horizontal pipe air-water system. This map as shown in Figure 2-1 was based on experimental results of about 6,000 data points from pipelines of diameter between 1.27 cm and 16.51 cm, at given flow condition (pressure, temperature). However, there is lack of precision in describing the visual observation and numerous classification of flow regimes being reported; such as smooth stratified, wavy, semi annular, bubble, annular, froth, dispersed bubble, dispersed liquid, plug, annular, froth and slug flow.

Another more complex flow regime map for horizontal gas-liquid two phase flow was developed by Taitel and Dukler, 1976. The map was based upon mechanistic model, and the flow regime transitions are governed by different flow parameters in dimensionless form.

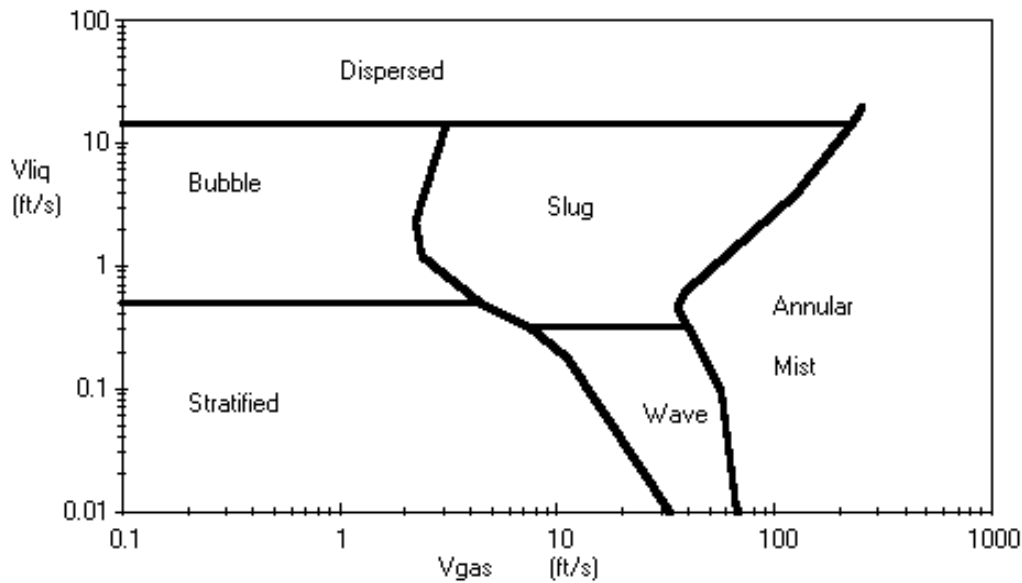


Figure 2-1: Horizontal flow pattern map (Mandhane et al., 1973))

### 2.1.3 Inclined Pipeline Flow Regime

The physical phenomenon of flow behaviour in inclined pipes can be explained by considering the effects of gravity and viscosity of liquid phase. This section is important since hilly terrain is formed based on the combination of downward and upward inclined flow.

Barnea et al. (1985) gave extensive models for predicting flow pattern transitions in inclined gas-liquid flows. They published method on how to determine flow patterns that covers the whole range of upward inclinations from horizontal to vertical.

#### 2.1.3.1 Inclined Downward (Downhill)

The effect of small degrees of inclination was reported by Taitel and Dukler, 1976 and 1981. it was reported that the downward inclinations causes the liquid to move more rapidly to a lower level due to the downward gravity force.

Barnea, 1982 explained that the transition from smooth to wavy interface depends only on the liquid rate and is independent on the gas flow rate. Increasing the negative angle between  $10^\circ$  to  $70^\circ$ , stratified flow region remains the same. Barnea, 1982 showed in her work that downward inclination has a major effect on the stratified flow regime; the liquid moves more rapidly than in the horizontal case and has a lower level in the pipe due to the downward gravity force. As a result, higher gas and liquid flow

rates are required to cause transition from stratified flow. Her flow regime map showed that the stratified flow region is considerably expanded as the angle of inclination increases. However, as from 70° downward inclination, stratified flow shrinks (reduces) and the flow changes to annular flow.

#### **2.1.3.2 Inclined Upward (Uphill):**

The study of inclined pipes was first investigated by Singh and Griffith, 1970 for small upward inclination to study the behaviour of slug flow. This was followed by Bonnacase, 1971 who further extended the angle to 10° from Horizontal.

Extensive work was carried out by Beggs and Brill, 1973. They developed a model to predict pressure drop and liquid hold up. However, their investigation did not report flow patterns but reported that segregated flow was not observed at any angle greater than +3° from horizontal. More of the liquid is in contact with the pipe surface, and viscous drag causes a decrease in liquid velocity and increase in liquid hold up. Though, Gould et al., 1974 established that bubble and annular flow pattern do not vary significant with inclination but this claim does not cover wide range of angles.

Barnea et al., 1985 carried out experimental study on the behaviour of upward flow pattern of air-water in pipes inclination from 0°- 90°. They reported that stratified flow to intermittent flow is very sensitive to pipe inclination and takes place over a wide range of angles.

In summary, within the angles of 10° - 60° to the horizontal and depending on the flow rate; downward inclined pipe is typically dominated by stratified flow while upward inclined pipe is typically dominated by slug flow.

#### **2.1.4 Hilly Terrain Flow Behaviour**

The flow behaviour in hilly terrain pipelines is gravity dominated and complex due to unsteady conditions that develop in both the downward and upward inclined sections. This transient behaviour of the flow is due to pipe geometry and the compressible nature of the gas phase. The result is occurrence of induced terrain slugging which can cause operational problems. In hilly terrain geometry, slug flow is dominant at the dip and upward section such that liquid production rate fluctuates with time intermittently and leads to a unsteady hydrodynamic behaviour.

### 2.1.5 Slug Flow Behaviour in Hilly-Terrain Pipelines

The studies of slug flow in horizontal and inclined pipelines are mostly based on the assumption that there is no slug growth or slug decay along the pipe once slug formed is stable. This steady state assumption cannot be used at the dip of a hilly terrain pipeline. As shown in Figure 2-2 the slug flow behaviour can be described as follows: initially at the dip, liquid accumulate by the in-coming flow from downward section and liquid fall back from the upward section. This accumulated liquid continues to form long slugs (and grow in length) until the upstream pressure overcomes the hydrostatic head provided by the liquid. Then, gas will penetrate into the dip, this triggers slug initiation. Once the aeration of the upward inclined section is completed, the pressure decrease and the gas flow in the upward inclined section decreases. This leads to increase in upward inclined section liquid hold up and liquid blockage occurs while the gas flow in the upward inclined section ceases. This is followed by liquid accumulation at the dip section and the next cycle begins.

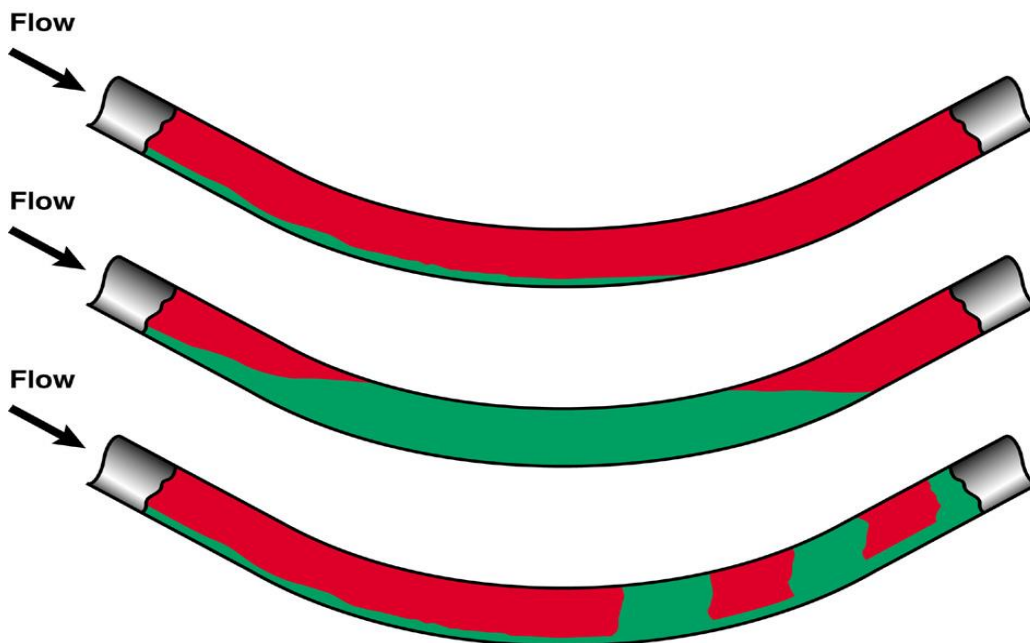


Figure 2-2: Schematic showing flow through the bed

Scott and Kouba, 1990 propose a model for change in slug length as slugs pass a bottom elbow (dip) assuming no change in the liquid holdup in the slug and an equilibrium film thickness. Their result shows a significant change in slug length for a



fully-developed slug from horizontal pipeline segment with different angle. The slug initiation or dissipation mechanism was not considered in their model.

Zheng et al., 1993, 1994 & 1995 studied the effects of hilly terrain pipeline configuration on flow characteristics. Zheng et al., 1994 & 1995 proposed slug tracking model that follows the behaviour of all individual slugs for geometry consisting of single hilly terrain unit. Zheng et al., 1995 conducted a detailed experimental study on the behaviour of slug flow in a hilly terrain pipeline. It consist of air-kerosene two phase flow loop with a pipeline diameter of 7.79cm ID and a total length of 420.3m having an inclination of  $-1^\circ$  to  $+5^\circ$  from horizontal. The experimental data was compared with the model to demonstrate its applicability. The comparison demonstrates the main physical behaviour of slugs in hilly terrain pipelines. However, the model considered films of constant thickness and does not take account of change in the film thickness with relative distance from the back of the slug.

Henau and Raithby, 1995 carried out experimental study and model validation on induced terrain slugging in multiple hills and valleys. They introduced a new correlation for drag coefficient and virtual mass force to improve the transient two-phase flow model to account for the frictional force coefficient.

Zhang et al., 2000 predicts the average slug length and slug frequency at any location along a hilly-terrain pipeline, given the average slug length or slug frequency at the entrance. They model slug dissipation and growth along a hilly terrain pipeline by using a steady state approach with the liquid film as the control volume to solve the mechanistic equations.

Al-Safran et al., 2004 carried out detailed experimental study of slug characteristics using air and paraffinic mineral oil in an hilly terrain multiphase flow loop. The test section was made of 50.8mm diameter smooth transparent acrylic pipe of 21.34m downhill section and uphill sections. The range of inclination investigated was  $+0.915^\circ$  and  $+1.93^\circ$  valley configuration. He categorised the flow behaviour into five possible flow behaviour based on superficial gas and liquid velocities:

1. Complete slug dissipation downhill section with slug initiation at the elbow
2. No hilly-terrain effect on slug characteristics

3. Partial slug dissipation in downhill section with slug initiation and slug growth at the elbow
4. No slug dissipation in downhill section with slug initiation and slug growth at elbow
5. No slug dissipation in downhill section with slug growth at elbow.

They developed a flow regime based on the flow mechanism and also superimposed it on steady state flow pattern maps for the upstream downhill section. He was able to relate quantitative flow behaviour at the dip to the flow pattern maps through the flow behaviour in the downhill section.

Considering low liquid flow rates in hilly terrain or induced terrain, the downward flow is stratified flow but getting down to the dip (lower elbow) it transit to slug flow.

The literature review confirms there is significant effect of hilly-terrain pipe geometry on slug flow characteristics. However, the literature review showed that slug behaviour in a hilly terrain pipe has not been fully investigated. There was no attempt to investigate the slug initiation mechanisms for other pipe inclination.

### **2.1.6 Liquid Holdup in Pipe**

The liquid hold is defined as the ratio of the liquid volume in a pipeline segment to the whole volume of the pipeline. It is an important parameter in the study of two-phase mixture. The in-situ volume fraction along the pipe is different from that at the inlet of the pipe.

Baker, 1957 defined the relation between average liquid holdup,  $H_l$  and superficial gas velocity  $u_{sg}$  as:

$$H_l = 1.61u_{sg}^{-0.70} \quad \mathbf{2-1}$$

Guzhov et al., 1967 determined in-situ liquid volume fraction,  $E_l$ , from the knowledge of the input liquid volume fraction,  $C_l$  and the Froude number based on the mixture velocity,  $u_m$ .

They proposed the following expressions:

$$E_g = 0.81C_g \left(1 - \exp(-2.2\sqrt{Fr_m})\right) \quad \mathbf{2-2}$$

$$E_l = 1 - 0.81(1 - C_l) \left(1 - \exp(-2.2\sqrt{Fr_m})\right) \quad \mathbf{2-3}$$

Their result is said to be applicable for pipe inclinations up to  $90^\circ$  from the horizontal.

Equation (2-3) shows that Guzhov et al., 1967 correlation predicts small value for in-situ liquid holdup for pipe inclination of up to  $9^\circ$  to be equal to 0.19.

Greskvoich, 1972 modified the Guzhaov et al., 1967 procedure based on the straight line obtained by Guzhaov et al., 1967 for a given mixture Froude number in Figure 2-3. Since at  $C_l=1$ , all these lines converge at  $E_l=1$ ; Greskvoich, 1972 suggested that only the intercept corresponding to  $C_l=0$  needed to be measured in order to establish the whole line for a given Froude number. Hence, the entire line for a mixture Froude number equal to the particular Froude number based on the gas velocity through the straight line of  $E_l$  at  $C_l = 0$  and the point  $E_l = C_l = 1$ . This gave a significant effect of inclination on the measured hold up.

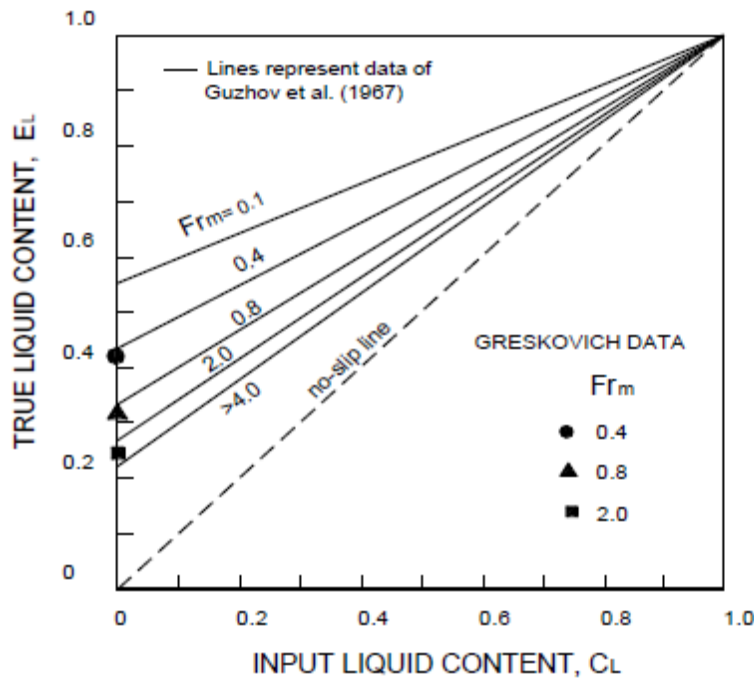


Figure 2-3: In-situ liquid volume fraction correlation (Guzhov et al., 1967)

Mattar and Gregory, 1974 studied variation of  $0^{\circ}$ - $10^{\circ}$  inclination using air-oil with superficial liquid velocity,  $u_{sl}$ , of 0.09m/s – 1.5m/s and superficial gas velocity,  $u_{sg}$ , of 0.3m/s – 7.6m/s. They proposed liquid holdup relationship as follows:

$$H_l = 1 - \frac{u_{sg}}{1.3(u_{sg} + u_{sl}) + 0.7} \quad \mathbf{2-4}$$

There are a number of liquid hold up that took account of the spatial distribution of the liquid and gas within the pipe (Beggs and Brill, 1973; Mukherjee and Brill, 1983; Kokal and Stanislav, 1989b and Abduvayt et al., 2003).

Beggs and Brill, 1973 developed flow pattern-specific correlations for the liquid holdup,  $H_l$  and the two-phase friction factor,  $f_{TP}$ , which they used to calculate the pressure gradient. The applicable inclination ranges from  $-90^{\circ}$  to  $+90^{\circ}$

The liquid holdup at any pipe inclination  $H_\beta$  is calculated as follows:

$$H_\beta = H_o \left[ 1 + c \left( \sin 1.8\beta - \frac{\sin^3(1.8\beta)}{3} \right) \right] \quad \text{2-5}$$

Where ( $\beta$ ) is the pipe inclination from the horizontal, in radians and parameter,  $c$  is determined based on the flow regime determinant.  $H_o$  is the liquid holdup for the horizontal pipe(i.e.  $\beta = 0$ ).

### 2.1.7 Slug Flow Parameters

Slug flow consist of complex geometry and the need to understand the terminology and parameters used is important in order to study slug characteristics at various flow conditions.

Considering a slug unit in a pipe; consist of two region, 1. a liquid slug region of ( $L_s$ )-slug body section, and 2. a film region-(liquid film region ( $L_f$ ) section and gas bubble section above the film layer) as shown in Figure 2-4.

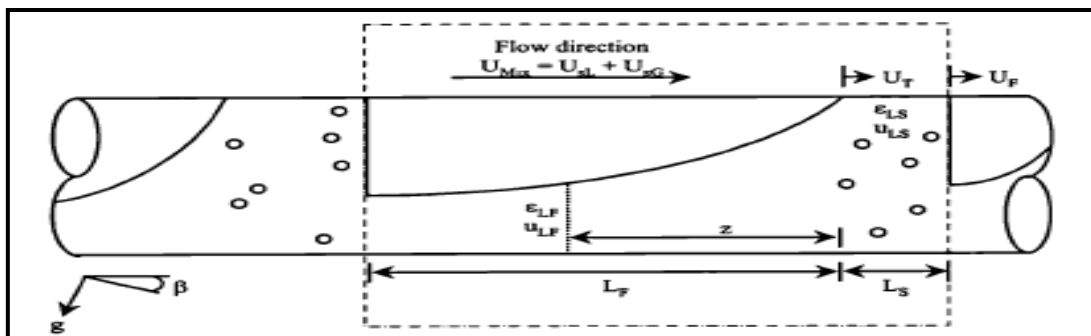


Figure 2-4: An idealised slug unit

The slug unit  $L_u$  length is defined by:

$$L_u = L_s + L_f \quad \text{2-6}$$

The front of the slug moves along the pipe at a velocity ( $u_t$ ) and the tail at a velocity ( $u_b$ ). At equilibrium state, the propagation velocities of the tail and front must be the same,  $u_t$ .

The slug frequency is the number of slugs passing through a stationary point per unit time, defined by:

$$f_s = \frac{u_t}{L_u} \quad 2-7$$

In steady state flow with a control volume at any point along the pipe, the overall volumetric flow rate (assuming incompressible flow) at any cross section of the pipe must be the same, therefore continuity equation is given as:

$$A(u_m) = A(u_{sl} + u_{sg}) \quad 2-8$$

where  $u_{sl}$  and  $u_{sg}$ , represent the liquid and gas superficial velocity respectively, subscripts  $l$  and  $g$  stand for the liquid and the gas phase respectively. If the terms in equation (2-8) are divided by the area of the pipe ( $A$ ), then:

$$u_m = u_{sl} + u_{sg} \quad 2-9$$

## 2.1.8 Slug Characteristics Correlation

### 2.1.8.1 Slug Holdup

The slug liquid holdup is important parameters that determine the frictional pressure gradient during the passing of a slug. The following empirical correlations available in the literature to evaluate the slug liquid holdup are as follows:

Gregory et al., 1978 correlation is widely used for estimation of gas fraction in slugs as a function of superficial mixture flow rate, given as:

$$H_{ls} = \frac{1}{1 + \left(\frac{u_m}{8.66}\right)^{1.39}} \quad \mathbf{2-10}$$

However, this correlation is limited to case of  $u_m$  less than 10m/s in order to reduce the possibility of entering the transitional zone between slug annular flows where the correlation is not applicable. Also, this correlation does not take into account the effect of fluids properties although air-liquid oil mixture was used as test fluids.

Malnes,1983 improved on Gregory et al., 1978 by including fluid properties from the experimental data. This proposed correlation is given as:

$$H_{ls} = 1 - \frac{u_m}{\left[83 \left(\frac{g\sigma_{gl}}{\rho_l}\right)^{1/4} + u_m\right]} \quad \mathbf{2-11}$$

Andreussi and Bendiksen, 1989 carried out experiment to investigate the effect of inclination angle and pipe diameter on the slug void fraction. Their work was performed with 0.048m and 0.089m diameter pipes in air-water mixture at atmospheric conditions. The result was based on balance equation involving the net entrainment rate at the slug front and the net loss rate of small bubbles at the slug tail, given as:

$$u_m > u_o \quad H_{ls} = 1 - \frac{u_m - u_y}{(u_m + u_z)^n} \quad \mathbf{2-12}$$

$$u_m < u_o \quad H_{ls} = 0$$

Where

$$u_y = 2.6 \left[1 - 2 \left(\frac{d_e}{D}\right)^2\right] \left(\sqrt{gD \left(\frac{\rho_l - \rho_g}{\rho_l}\right)}\right) \quad \mathbf{2-13}$$

Where  $d_e = 0.025\text{m}$

$$u_z = 24000 \left(1 - \frac{\sin\theta}{3}\right) \left(\frac{gD^2\rho_l}{\sigma}\right)^{-3/4} \left(\sqrt{\frac{gD(\rho_l - \rho_g)}{\rho_l}}\right) \quad 2-14$$

The effect of gas density was taken into account through the  $n$  exponent as:

$$n = 1 - 3 \left(\frac{\rho_g}{\rho_l}\right) \quad 2-15$$

Gomez et al., 2000 slug liquid holdup was performed as a function of upward inclination. Data from six authors with pressure from 1.5 to 20bar with pipe diameters from 51 to 203mm, and pipe inclination range from 0 - 90°. The data indicated a clear dependency between pipe angle, Reynolds number and slug void fraction. A correlation was suggested as:

$$H_{ls} = e^{-(0.45\theta + cRe)} \quad 2-16$$

$$0 \leq \theta_R \leq \pi/2$$

Where the pipe angle  $\theta$  is in radian, the coefficient  $c$  is  $2.48 \times 10^{-6}$ , and the Reynolds number is defined as:

$$N_{Re(l)} = \frac{\rho_l u_m D}{\mu} \quad 2-17$$

The correlation predicted the data sets on which it was based within an error of 30%.

### 2.1.8.2 Slug Translational Velocity

This is the velocity at which the bubble nose (or slug tail) travels along the pipe. The slug translational velocity of elongated bubble in continuous flow ( $u_t$ ) was expressed for the first time by Nicklin et. al., 1962 for the case of upward vertical flow as:



$$u_t = cu_m + u_d \quad \mathbf{2-18}$$

Where  $u_d$  is the drift velocity, namely, the velocity of propagation of a large bubble in a stagnant liquid. The coefficient,  $c$  represents the ratio between the maximum and average velocities at the tail of the slug, around 2 and 1.2 for laminar and fully turbulent flow respectively.

$$c = u_{max}/u_m \quad \mathbf{2-19}$$

However, Nicholson et al., 1978; Bendiksen, 1984 and others showed that a drift velocity exists also for the horizontal flow.

The correlation for elongated (Taylor) transitional velocity in incline tubes is based on Bendiksen, 1984:

$$u_t = cu_s + 0.35\sqrt{gD\sin\theta} + 0.54\sqrt{gD\cos\theta} \quad \mathbf{2-20}$$

Where  $c = 1.2$  for turbulent flow and  $c = 2.0$  for laminar flow

The velocity of dispersed bubbles in the slug body is govern by

$$u_b = 1.2u_m + 1.53 \left[ \frac{\sigma_g(\rho_l - \rho_g)}{\rho_l^2} \right] H_s^{0.1} \sin\theta \quad \mathbf{2-21}$$

Cook & Behnia, 2000 investigated the rate of collapse of short slugs as a function of their length. They arrived at the conclusion that the ratio between the slug tail and front velocities must satisfy the following relationship:

$$\frac{u_b}{u_t} = 1.0 + 0.56 \exp\left(-0.46 \frac{l_s}{D}\right) \quad \mathbf{2-22}$$

In the limit of very long slugs, the ratio  $l_s/D$  tends to a large value and the exponential in equation (2-22) almost vanishes. In that case, the slug tail and front velocities would be equal.

Gregory & Scott, 1969 measured the slug velocity for a carbon dioxide-water system in a pipe of 300 diameters long. They correlated the slug velocity to the mixture velocity  $u_m$ , as:

$$u_t = 1.35u_m \quad \mathbf{2-23}$$

### 2.1.8.3 Slug Frequency

The slug frequency is the average number of slug units passing per unit time, at a specific location in the pipe (Hubbard, 1965; Gregory and Scott, 1969). It represents the reciprocal of the average passage time of slugs.

$$f_s = \frac{u_t}{l_s} \quad \mathbf{2-24}$$

Most of the empirical correlations for slug frequency relate to strictly developed slugs downstream (Gregory and Scott, 1969; Heywood and Richardson, 1979).

Gregory and Scott, 1969 developed correlation based on comparison made between their experiment and Hubbard, 1965 data. Their studies showed that slug frequency is dependent on pipe diameter. The relation obtained by Gregory and Scott, 1969 is:

$$f_s = 0.0434 \left[ \frac{u_{sl}}{gD} \left( \frac{19.75}{u_m} + u_m \right) \right]^{1.2} \quad \mathbf{2-25}$$

Nydal, 1992 compare the correlation with experimental data and found a good fit within the original range ( $u_{sg} < 10\text{m/s}$  and  $u_{sl} < 1.3\text{ m/s}$ ). The relation obtained by Nydal, 1991 is:

$$f_s = 0.0226 \left[ \frac{u_{sl}}{gD} \left( \frac{19.75}{u_m} + u_m \right) \right]^{1.2} \quad \mathbf{2-26}$$

Heywood and Richardson, 1979 estimated the average slug frequency by calculating the probability density function and power spectral density of the hold-up. They proposed the following relation for the slug frequency using a much larger amount of experimental data:

$$f_s = 0.0434 \left[ \alpha' \left( \frac{2.02}{D} + \frac{u_m^2}{gD} \right) \right]^{1.02} \quad \mathbf{2-27}$$

Where  $H_h$  represents non-slip holdup

$$H_h' = \frac{u_l}{u_l + u_g} \quad \mathbf{2-28}$$

Al-Safran, 2008 work centres on slug initiation mechanism at the pipe entrance and to develop an empirical correlation for slug frequency. The slug frequency was analysed to observe entrance effects and pipe length effects for hydrodynamic slugging at horizontal test section and terrain slugging in hilly terrain pipeline section respectively. The result showed that there is significant effect of slugging mechanism on developed slug which was characterised by mixture Froude number for horizontal test section.

Analysing the slug frequency variations with pipe length showed mixed result while constant slug frequency was obtained for some cases. Al-Safran correlation equation (2-29) was obtained by using the coefficients from the statistical confidence interval.

$$\ln(f_s) = 0.77 + 0.288\ln(u_l) + 0.37 \frac{u_s}{u_m} + 1.56(D) \quad \mathbf{2-29}$$

Hanyang and Liejin, 2008 carried out experimental study of slug development on horizontal two-phase flow. Slug initiation and evolution along 10 different axial positions along 5.0 cm ID, 16m long horizontal pipe, are measured using 20pairs of parallel-wire conductivity probes. The experiment carried out described the transient characteristics of interfacial structures as a replenishment and depletion of liquid. The liquid re-builds from the level of necessary conditions for slug stability to the critical level of stratified to slug flow transition. The sensors signal shows that increase in superficial liquid velocity result to a pronounced peak of slug frequency within the first 50D of the pipe and drops to almost constant value sharply as some slug collapse back into waves. However, the increase of superficial gas velocity leads to decrease in peak frequency near the inlet and in fully developed slug frequency.

It was reported that the slug is initiated by a deterministic process with replenishment and depletion of liquid near the inlet for the superficial gas velocity  $u_{sg} < 3.0 \text{ m}\cdot\text{s}^{-1}$  and by a stochastic process with wave coalescence along the pipe for  $u_{sg} > 3.0 \text{ m}\cdot\text{s}^{-1}$ . The evolution of the slugs is strongly affected by superficial gas and liquid velocities for  $u_{sg} < 3.0 \text{ m}\cdot\text{s}^{-1}$  but weakly affected by the superficial gas velocity for  $u_{sg} > 3.0 \text{ m}\cdot\text{s}^{-1}$ .

## **2.2 Bifurcation Analysis**

One of the subjects of dynamic systems is to identify the changes of stability properties with the system parameters, to determine the stable operating point /or point of acceptable fluctuations. This phenomenon is called bifurcation. Bifurcation theory is commonly applied to the mathematical study of dynamic systems. It is a mathematical study of changes in the qualitative or topological structure due to changes in the system parameters. Bifurcations occur in both continuous systems and discrete systems. It was first introduced by Henri Poincare in 1885.

Application of bifurcation covers diverse scientific fields such as fluid mechanics, electronics, chemistry and theoretical ecology. Performing a bifurcation analysis is

often a powerful way to analyse the properties of dynamic systems. This bifurcation changes can be presented as a bifurcation diagram.

A straight forward approach in continuous multiphase flow is simply plotting maximum/minimum value in order to show degree of fluctuations.

Karima et al., 2012 applied bifurcation map in the use of gas injection to mitigate for hydrodynamic slug with different control strategies. The bifurcation of differential pressure against gas flow rates and at constant gas valve opening are used to determine the stability of the flow for different control strategies.

Hyllestad, 2010 applied bifurcation map in his work on stabilization of two-phase flow in riser from reservoirs (anti-slug control). The aim was to see how a dynamic feedback controller could increase the production rate and extend the lifetime of a reservoir. The experimental facility consists of air-water mini flow loop with an inner diameter of 20mm and was made of transparent silicon-rubber.

The controlled variable was the inlet pressure and the manipulated variable is the top side valve opening. The dynamic controller was compared to choking the valve manually in bifurcation map. The maximum and minimum inlet pressure was plotted with varying gas flow rate. The flow regimes transition to hydrodynamic slugging and severe slugging were determined.

The purpose of bifurcation analysis is to describe the flow structure in an experimental work. Its application is concerned primarily for validation of flow regime in multiphase flow. The mathematical theories are not discussed in this work but can be found in McCracken and Marsden, 1976.

## **2.3 Study of Sand Transport in Pipeline**

The study of solid transportation can be categorised as single phase flow of solid (gas-solid, liquid-solid), or two phase multiphase solid mixture (gas-liquid-solid). This research work is limited to liquid-sand and gas-liquid-sand mixtures.

### 2.3.1 Single Phase Liquid-Sand Transport

Studies have shown that sand production characteristics and behaviour depends on the distinction between settling particles and non-settling particles. The settling particle differs significantly from the flow of non-settling particles in the following ways:

- i. Average value of flow parameters
- ii. The flow pattern formation
- iii. The concept of interface differs

Categorising sand-liquid single phase based on sand **concentration /or particle sizes** in the carrier fluids as shown in Figure 2-5 are:

#### a. Homogenous flow

The homogenous flow is characterised by a uniform distribution of solid particles throughout the fluid. Homogenous flow is common when the sand particle is a fine particle or dilute phase with low concentration. The volume fraction of the phases across the pipe sections remains constant through the pipeline. Homogenous flow can also behave like a slurry with high concentration ( $>40\mu\text{m}$ ) which exhibit viscous behaviour with rheological properties that are mostly non-Newtonian (Perker, 2008). It occurs mostly at high fluid velocity, turbulent flow or low solid density/concentration.

#### b. Heterogeneous flow

Particles are all suspended when they are large and dense enough to form a different layer and are no longer uniformly distributed. It can be assumed that solid particle is the most important parameters in categorizing the heterogeneous flow and homogenous flow because fine particles have the tendency to form homogenous flow while coarse particle form heterogeneous flow. There are situation where the system contains wide range of sand particle sizes and densities, which result to mixed homogenous-heterogeneous system. The heterogeneous flow is more complicated than the homogenous flow because the analyses of heterogeneous flow consider the particle-particle interaction, and particle-fluid interaction in each layer. At this stage, the critical velocity and pressure losses are important.

#### c. Heterogeneous with moving bed (Two layer flow)

This has a characteristic behaviour of combination of solid-liquid suspension flow and a distribution of particle volume fraction both along the cross sectional area and in the flow direction. This flow regime exhibit accumulation of solid particles at the bottom of

the pipe while heterogeneous mixture flows at the upper section. In this case the particle in the bed is moving or sliding as a result of shear stress of the upper heterogeneous fluid on the solid particle bed. A moving bed causes pipe wear at the bottom of the pipe.

**d. Flow with stationary bed ( Three layer flow)**

This is observed at a very low flow rate. Sand bed is formed at the bottom of the pipe. There is distinct moving layer on the top of the bed. There is formation of dune like shape on the surface of the bed. It is regarded as three-layer flow because of existence of heterogeneous suspension flow with more evident of solid bed concentration profile with moving bed. The concentration of the three layer flow with stationary bed in Figure 2-5 is adjusted to represent the different sand concentration.

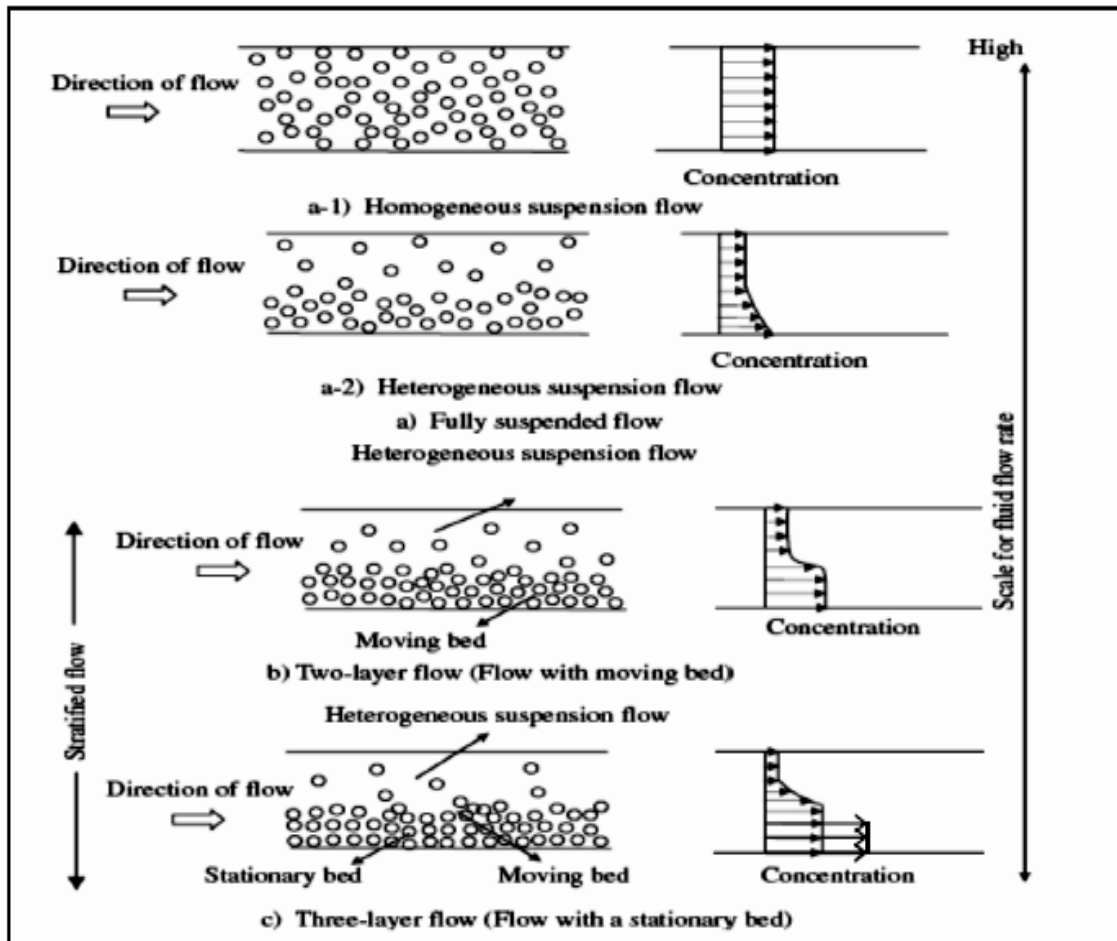


Figure 2-5: Schematic presentation of flow patterns and concentration distributions in normal direction to flow adapted from Perker, 2008

### **2.3.2 Liquid- Sand Flow Patterns in Horizontal Pipeline:**

The description generally categorised the sand-liquid flow pattern **based on pipe geometry** is reported for horizontal pipeline according to Yan, 2010. The following are the four main types of liquid-sand flow pattern in horizontal pipeline:

#### **1. Stationary bed**

This flow behaviour exist at a very low liquid flowing velocities in which sand particles formed stationary bed at the bottom and there is no movement of particles. The upper surface of the bed is flat at very low flow rates but becomes wavy as the flow rate increases; further increase in flow rate result to decrease in the height of the stationary bed. Thus an equilibrium point is reached where the rate of sand deposition is equal to the rate of sand entrainment. This flow regime reduces the surface area and lead to pipe blockage. This regime is very important concern to flow assurance and design of pipeline facilities and carrying capacity consideration.

#### **2. Moving dunes**

Increasing the liquid flow rates further, the sand particles form moving dunes such that the upper surface of the dune are rolled along from back to front. The instability in the sand movement resulted to different sizes of dunes formed with smaller dunes faster than the larger ones.

#### **3. Scouring**

As the flow rate further increases, the particles start to roll along the top of the dunes with sufficient momentum that they escape and separate away as individual scouring grains.

#### **4. Dispersed**

At high liquid flow rates, the dunes are dispersed. The sand particles move in the produced fluid in an erratic pattern.

It is important to note that the pressure drop and fluid velocity are different from one flow regime to another; a variety of parameters are important in determine the pressure drop and fluid velocity of the flow regime.



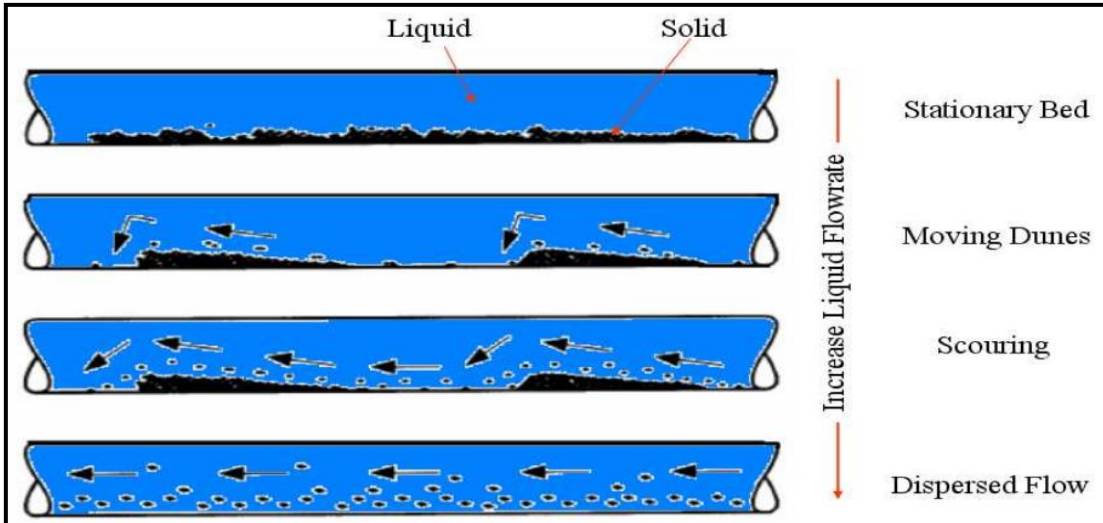


Figure 2-6 Liquid-sand flow regimes in horizontal pipelines (Yan, 2010)

The transitions between flow patterns are commonly determined by visual observations. There are two definitions of transition velocities, limit deposit and suspending velocity. Limit deposit velocity condition in slurry flow comprise stationary bed flow with a stagnant lower zone. While suspending deposit velocity (otherwise called minimum transport condition) is the threshold velocity required for a fully suspended flow. Prevention of this limit deposit velocity is essential for the avoidance of the partial blockage of the pipes that reduces the efficiency of the pipelines, enhancing pipe wear in industrial applications.

Therefore, the only way to get the sand flowing without accumulation or deposition in a pipeline is to maintain sand in suspension or in a moving bed flow pattern. Solid particles can be transported without depositing at the bottom of the pipe provided the mean stream velocity is greater than the minimum transport velocity. Conversely, solids deposition occurs and leads to blockage when the minimum transport velocity is less than the mean stream velocity.

The mechanics of flow of solids suspended in multiphase flow is very important; especially in the determination of the friction loss characteristics; i.e. frictional pressure drop as a function of flow rate. For sand transportation by gas-liquid mixture in horizontal pipes, Scott et al., 1971 stated two key issues to consider in order for the sand to flow:

- The energy consumption per unit mass of carrier or solid transported at the flow condition
- The effect of various flow regime of multiphase (gas/liquid) and single phase (liquid) phase on solid behaviour.

The design limit of sand transportation is based on the mean velocity of the fluid flow. Various definition have been used by different researchers like sliding bed velocity, saltation velocity, suspending velocity and deposition velocity, critical velocity or homogenous velocity. Yan, 2010 clarified the definition of each of them, and reported a comprehensive report on different models in sand transportation. The design of a system that will keep the sand moving required the prediction of the critical velocity below which sand settles or the minimum velocity below which the particle start to deposit. The liquid velocity in the system must stay high above the critical velocity in order to prevent the stationary bed from forming.

### **2.3.3 Factors Affecting Sand Transportation**

Sand transportation through pipelines is a complex physical phenomenon which identify basic flow pattern based on a number of variables.

The key parameters required to predict sand behaviour in a multiphase systems are:

1. Sand concentration
2. Transporting medium properties: viscosity and density
3. Pipeline properties: length, diameter, inclination
4. Fluid flow rate, multiphase flow regime
5. Sand properties: size, shape, size distribution, density

The complexity in multiphase flow transportation is the inability and difficulty to accurately measure sand transport phenomena characteristics. In hydraulic slurry transport study, the wide range of fluid and particle properties (particle size, fluid viscosity etc.) in different size of pipe has been studied (Durand, 1953; Durand and Condolio, 1952, Smith, 1955; Oroskar and Turian, 1980; Kokpiar and Gogus, 2001; Yan, 2010 and Al-lababidi et al., 2012).

## **Sand Concentration**

The energy consumption per unit mass of solid transported at the flow condition is a function of sand concentration. There has been a lot of study in the literature in hydraulic slurry transport on effect of sand concentration (Durand, 1953; Newitt et al, 1955; Kokpiar and Gogus, 2001; and Yan, 2010). Increase in sand concentration will require higher energy consumption and also result to increase in frictional pressure loss. Effect of sand concentration is still an on-going research in oil and gas industry. Very few models look at the effect of concentration of solids in the multiphase flow system. For the purpose of this study, the solid particles categorised as low concentration is of range 0.000005 to 0.00005 by volume fraction, v/v (i.e. 5lb/1000bbl to 50lb/1000bbl). According to Stevenson et al., 2001, this sand concentration is typical of sand particles produced in the oil industry. However during shutdown or maintenance, sand concentration could get to a range of 200lb/1000bl to 500lb/1000bbl maximum.

## **Fluid Viscosity**

The study of viscosity effect in sand transport is limited. Yan, 2010 found that the sand minimum transport condition (MTC) increased slightly as the fluid viscosity (water, oil 7 and 20cP) increased due to turbulent flow observed. However, when the bulk flow became laminar and viscosity higher than 105cP, the MTC decreased as the fluid viscosity increased. There is increase in shear force acting on the sand particles from the liquid and decrease in settling velocity of sand particles due to the high viscous fluid. Fairhurst and Baker, 1983 studied the viscosity effect up to around 3cP. There appeared to be no effect of the increased viscosity compared to an air-water-sand system. Oudeman, 1993 also looked at a greater change in viscosity up to 7cP. He developed a plot of solid-fluid flow regime on gas-liquid flow pattern map co-ordinates. The test section was slightly less likely to form a stationary bed and was slightly more likely to form a suspension. Oudeman attributed the slight difference to the fact that the fluid is less likely to erode the sand bed despite the fact that it is more likely to carry the particles.

Similar work was done using water (1cP) and oil (78cP) by Gillies et al., 1997. The sand transport velocity was found lower in oil flow (78cP) than that in water flow at the same sand concentration.

### **Multiphase Flow Regime**

Sand transport is greatly influenced by multiphase flow due to the flow regime. In plug flow, the bubbles of gas will flow along the top of the pipe and will have little effect on the solids flow. Slug flow enhances solids transport. While literature review of multiphase flow of gas-liquid has been reported in the previous section, further review of multiphase flow effect in sand transport is discussed in section 2.4 below.

### **Pipeline Orientation**

The critical velocity increased slightly (of the order of 10%) for uphill flows at angles below about +15 degrees in slurry system (Shook and Roco, 1991; Angelsen et al., 1989 and Danielson, 2007). However, in Yan, 2010 experimental study, there was no clear difference between the horizontal and incline flow. He suggested it could be because the sand concentration tested in his work was very low compared to the previous work on slurry system. His result shows that in sand-water flow, there was little effect observed on sand behaviours and MTC from pipeline orientation in 2 inch and 4 inch pipeline. In sand-air-water flow, the sand transport characteristics in slug body were similar to those in horizontal pipeline. However, the sand particles were observed moving backward with the liquid film until they are transported by another slug.

### **Particle Diameter**

Sand particle size has significant impact on the transport velocity; uniform diameter is often assumed rather than have a size distribution. According to Durand and Condolios, 1952 result, the critical velocity steeply increases with increasing sand particle diameter until 600 microns. Further increasing the sand particle diameter, the critical velocity for 0.02 sand v/v was found gently increasing. However, the critical velocity for 0.05 - 0.15 sand v/v slightly decreased and then flattened as the sand particle increases.

There is limited data regarding to the particle diameter effect on sand transport for multiphase system. Angelsen et al., 1989 studied the sand transport in stratified wavy flow for 100, 200 and 400 microns particle diameter in 4 inch pipe and found that more energy was required to transport bigger sand particle diameter.

Yan, 2010 studied particle size effect on MTC in water flow with two different average sizes of 200 microns and 750 microns. It was found that, for 5lb/1000bbl, less water velocity was required to transport bigger sand particles. Fewer particles were observed for 750 microns sand than 200 microns sand at the same concentration. For 50lb/1000bbl, the water velocity at MTC for 750 microns sand was found to be close to that for 200 microns.

### **2.3.4 Sand Transport Models in Liquid Flow System**

The prediction of deposit velocity for any given set of operational conditions is very important for design because it is not desirable to operate a partially blocked pipeline. There are many correlations available in the literature to determine deposit velocity in hydraulic slurry transport. These correlations were developed based on different definitions of minimum fluid velocity required to prevent bed formation. The term limit deposit velocity also called deposit velocity was used by some researchers (Durand, 1953; Wailson, 1970; Kazanskji, 1979). This is the velocity at which particles settle out as the flow rate is reduced. This is identified by the appearance of a deposit regime. Critical velocity is defined as the velocity solid particles settled out of suspension and form stationary bed (Oroskar and Turian, 1980; Turian et al., 1987). Bain and Bonnington, 1970 defined critical velocity as the velocity at minimal pressure gradient.

Thomas, 1962 definition of minimum transport condition (MTC) as ***“the mean stream velocity required to prevent the accumulation of a layer of sliding particles on the bottom of horizontal pipe”***. Thomas definition of MTC is based on theoretical expression relating terminal settling velocity to friction velocity; since settling tendency is a function of turbulent fluctuation that keep the particle in suspension.

Hydrodynamic forces on single particle are also used to predict minimum transport velocity, Stevenson et al. 2002, Bello, 2007.

Their works were based on the theoretical technique of hydraulic modelling of solid particle to calculate the velocity required to transport solid particles in solid-liquid pipeline transportation.

Solid particles transporting in a homogenous suspension liquid flow is as a result of the several forces acting on the solid particles but the commonly considered forces due to the small sand particles sizes are; gravity, buoyancy, drag, lift, particle–particle

interaction, and particle–liquid (turbulent) forces. The hydraulic modelling based on conservation equation of mass and momentum governing solid phase in liquid-solid phase flow in a pipe was used to develop the model (Bello, 2008).

Smart, 2009 also calculate the minimum velocity required to lift particle from a bed of loose particle and transport it down in oil and gas pipelines based on hydraulic model. This analysis also known as wick's model (Zandi, 1971) was developed considering several forces such as gravity, buoyancy, lift and drag forces. While gravity and buoyancy forces are constant, lift and drag forces vary with flow. At low flow rates, gravity and buoyancy predominate and particles settle to the bottom and form layer of sediment. The condition for solid particle to move is such that the forces acting on the particle to move (i.e. the sum of buoyancy, drift and drag forces) must be greater than the gravity force.

The solution of the basic equation of the governing equation cannot be solved by simple linear analytical solution but rather solved by numerical solution or trial error (Bello, 2008; Zandi, 1971),

### **Durand's Correlation (1953)**

This work studied the screening of solids sizes. It is regarded as the most expensive experimental work in hydraulic transport. He defined the critical velocity as the velocity at which particles can be transported without forming a stationary bed with minimum head loss. Durand conducted a series of tests with sand, coal and gravel covering particle sizes from 0.05 mm to 25 mm and pipe diameters from 0.0381 m (1.5 inch) to 0.7112 m (28 inch) with a maximum sand concentration v/v of 0.15. The effect of concentration, pipe diameter, particle size, solid density and liquid density were considered in this work.

The correlation for a given particle size, specific gravity, concentration and pipe size is given as:

$$V_c = F_L \sqrt{2gD(s - 1)} \quad \mathbf{2-30}$$

### **Hughmark's Correlation (1961)**

Hughmark dimensionless correlation was developed to predict the mean velocity of flow at which all the particles are in suspension; by using the data from literature. He

correlated the experimental data with particle diameter, pipe size, liquid density, solid density, and solid concentration as variables and mean velocity of flow as the dependent variable. The correlation developed is given as

$$\frac{V_c}{\sqrt{gD}} = \varphi C_v \left( \frac{\rho_p - \rho_l}{\rho_l} \right) F_d \quad \mathbf{2-31}$$

Where:

$\varphi$  is unknown function

$F_d$  is the correction factor for particle diameter ( $F_d$  is 1 for  $0.0145\text{inch} < d_p < 0.09\text{inch}$ ). With given particle size, the value of  $F_d$  is obtained from Hugh mark chart, the value  $C_v(s - 1)F_d$  are determined, then a corresponding value of  $\frac{V_c}{\sqrt{gD}}$  is obtained from Hugh mark correlation to give  $V_c$ .

#### **Condolios and Chapus Correlation (1963)**

They developed a critical velocity correlation for sand concentration  $v/v$  less than 0.02 as:

$$V_c = 3.0 C_v^{0.148} \sqrt{gD} \quad \mathbf{2-32}$$

#### **Thomas's Correlation (1964)**

Thomas developed different correlations for particles sizes below and above thickness of the laminar sub layer which he takes as:

$$\delta = \frac{5\mu}{\rho u_{ow}^*} \quad \mathbf{2-33}$$

Where:

$$u_{ow}^* = \sqrt{\tau_w / \rho} \quad \mathbf{2-34}$$

For,

$$(\delta/d) < 1, \quad \frac{V_o}{(u_{ow}^*)_o} = 0.010 \left[ \frac{d(u_{ow}^*)_o \rho}{\mu} \right]^{2.71} \quad \mathbf{2-35}$$

$$(\delta/d) > 1, \quad \frac{V_o}{(u_{ow}^*)_o} = 4.90 \left[ \frac{d(u_{ow}^*)_o \rho}{\mu} \right] \left[ \frac{\mu}{D(u_{ow}^*)_o \rho} \right]^{0.60} (s - 1)^{0.23} \quad \mathbf{2-36}$$

$(u_{ow}^*)_o$  is the friction velocity corresponding to velocity with zero sand concentration

#### **Wilson's Correlation (1970)**

Wilson developed a chart (Figure 2-7) by considering the effect of pipe diameter, particle diameter and relative density on critical velocity. This is a simple and easy method to estimate the conditions to determine the velocity when stationary deposition begins. Also the viscosity is not included in the chart because it was generated for viscosity of about 1cp. The pipe inclination was not included.



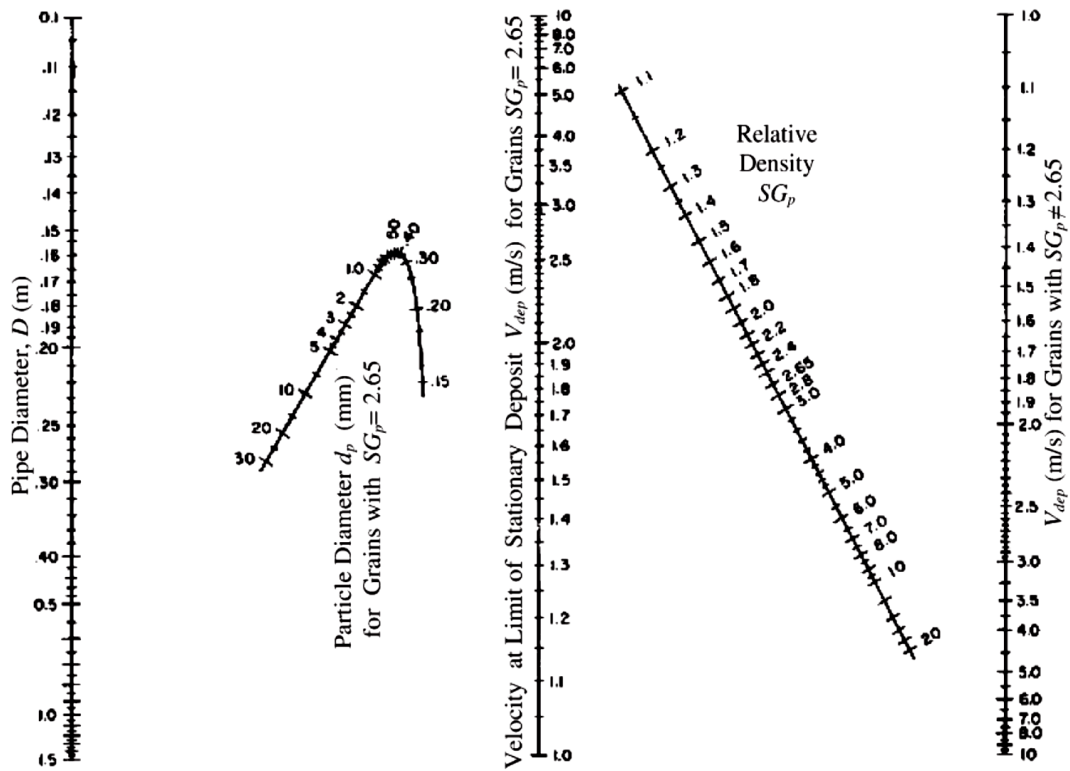


Figure 2-7: Chart for estimating the critical velocities (Multiphase flow handbook -Cowe, 2006)

### Charles' Correlation (1970)

Charles defined critical velocity as the velocity at which solid particles are deposited on the bottom of the pipe. Charles developed an equation to predict pressure gradients starting with Durand and Condolios' (1952) equation. By differentiating mixture pressure gradients with respect to the average velocity, he proposed the correlation to predict mean critical velocity  $V_c$  as:

$$V_c = \frac{4.80 C_v^{1/3} (gD(s-1))^{1/2}}{C_D^{1/4} (C_v(s-1) + 1)^{1/3}} \quad \text{2-37}$$

### **Wicks' Correlation (1971)**

Wicks performed experiments of low sand concentration ( $C_V = 1.00 \times 10^{-2}$ ) in 0.0025m and 0.15m pipes with two different liquid; water and kerosene. He proposed a mathematical model derived from the analysis of lift, drag, gravity and buoyancy forces acting on the particles on the surface of sand bed. He defined critical velocity of sand transport (i.e. when sand starts to move) as the condition when the drag, lift, and buoyant forces which tend to cause rotation of the particle exceed the gravity force which tends to hold the particle in place. Two dimensionless terms,  $S^1$  and  $\Psi$  (Wicks' dimensionless groups), were proposed to predict the possibilities for the formation of sand bed as:

$$S^1 = \frac{1}{8} (f_1 + S f_2) \phi^2 \quad \mathbf{2-38}$$

$$\Psi = \rho_L^3 d_p V_C^4 / [(\rho_P - \rho_L) g \mu_L^2] \quad \mathbf{2-39}$$

The parameter group  $\Psi$  can be calculated directly from the known solid and liquid properties and the average flow velocity. The parameter group  $S^1$  contains drag and lift coefficient ( $f_1$  and  $f_2$ ) wall shear stress ( $\phi$ ) which was dependent on the Reynolds number.

### **Oroskar and Turian's Correlation (1980)**

They defined critical velocity as the minimum velocity demarcating flows between solids from a bed at the bottom of the pipe and from a fully suspended flow. The analytical model was based on force balance and turbulence theory. Their correlation uses a hindered settling velocity of the particles, estimate from expression:

$$v_s = v_{\infty} (1 - C_v)^2 \quad \mathbf{2-40}$$

$$\frac{V_c}{\sqrt{gd_p(s-1)}} = \left\{ 5C_v(1 - C_v)^{2n-1} \left( \frac{D}{d_p} \right) \left( \frac{D\rho_l\sqrt{gd_p(s-1)}}{\mu_l} \right)^{1/8} \frac{1}{x} \right\}^{8/15} \quad \mathbf{2-41}$$

They modify their original equation with 357 data points collected from the literature as follows:

$$\frac{V_c}{\sqrt{gd_p(s-1)}} = 1.85C_v^{0.1536}(1 - C_v)^{0.3564} \left( \frac{D}{d_p} \right)^{0.378} (Re_p)^{0.09} x^{0.3} \quad \mathbf{2-42}$$

$$Re_p = \frac{D\rho_l\sqrt{gd_p(s-1)}}{\mu_l} \quad \mathbf{2-43}$$

Where  $x = V_s/V_c$  and  $s = \rho_p/\rho_l$

However, their correlation is less reliable for large particles in large pipes and is best used for particles of diameter below 0.5mm limit.

### **Wani's Correlation (1982)**

Wani et al., 1982 investigated the critical velocity of multi size particle transport in pipes. They developed a correlation to account for particle size distribution by using weighted mean diameter, ( $d_w$ ) and the standard deviation of the particle size distribution. They collected a wide range of data from literature and classified them into Stoke range and intermediate range based on their particle settling velocity. They developed equations to predict critical velocities in the Stokes range and intermediate range assuming that the Froude number of the particles is a function of the Reynolds number of the slurry at critical velocity, size distribution of solids, concentration of solids, and roughness of the pipe surface. They further developed a correlation to account for particle size distribution. The prediction uses weighted mean diameter,  $d_w$ . Two of their correlations reported to give better results are:

$$V_c = \left[ 2.3 \times 10^{-4} g d_w (s - 1) Re_p^{0.27} \left( \frac{100\sigma}{d_w} \right) \alpha^{0.307} \epsilon^{1.67} \right]^{0.5} \quad \mathbf{2-44}$$

and

$$V_c = \left[ 7.7 \times 10^{-6} g d_w (s - 1) Re_p^{0.0014} \left( \frac{100\sigma}{d_w} \right)^{-1.25} \alpha^{0.272} \epsilon^{4.77} \right]^{0.5} \quad \mathbf{2-45}$$

### **Turian's Correlation (1987)**

This empirical correlation was developed from 864 experimental data with 0.5m pipe diameter and wide range of sand particles of range of about 19mm. This particle size will be higher than the range of sand particle size considered in this work. Five different forms of empirical correlation of equation (2-46) were developed by adjusting the constant ( $x_1, x_2, x_3, x_4, x_5$ ) to identify the different form.

The correlation is given as:

$$\frac{V_c}{\{2gD(s-1)\}^{0.5}} = x_1 \alpha_s^{x_2} (1 - \alpha) x_3 \left\{ \frac{D\rho_l [gD(s-1)]}{\mu_l} \right\}^{x_4} \left( \frac{d_p}{D} \right)^{x_5} \quad \mathbf{2-46}$$

However, Turian correlations did not account for the effect of the width of particle size distribution.

### **Dorand and Barnea (1987)**

They applied fluid layer model for the prediction of slurry in pipe flow of slurries containing relative coarse particles. They model two layer model and three layer model. They considered that at low velocity the flow consists of three layers; stationary bed, followed by a moving bed on the layer, then a heterogeneous suspended mixture on the top layer. They argue that the critical velocity is the stream velocity when the stationary bed height is zero. They claimed that their critical velocity is better than other predicted correlation.

### Davies' Correlation (1987)

Davies, 1987 approach is a theoretical equation based on simple turbulence theory of force balance between sedimentation force and eddy fluctuation force.

Sedimentation force is given as:

$$\frac{\pi}{6} d_p^3 \Delta \rho g (1 - C_v)^n = \rho_l (v')^2 \left( \frac{\pi d_p^2}{4} \right) \quad \text{2-47}$$

While the eddy fluctuation velocity necessary to suspend particles is derived as:

$$v' = 0.82 (1 - C_v)^{n/2} d_p^{1/2} \left[ \frac{\Delta \rho g}{\rho_l} \right]^{1/2} \quad \text{2-48}$$

He considered that the sedimentation force was equal to the eddy fluctuation force when all the particles are suspended in the flow by eddies.

$$\frac{\pi}{6} d_p^3 \Delta \rho g (1 - C_v)^n = \rho_l (v')^2 \left( \frac{\pi d_p^2}{4} \right) \quad \text{2-49}$$

Davies calculated eddy fluctuation velocity as a function of eddy length and the power dissipated per unit mass of fluid. This is based on the assumption that only the eddies which are of the particle size are active in suspending the particles; smaller eddies will not be able to lift the particles while larger eddies cannot be present close to the bottom of the pipe.

Davies introduced turbulence correction factor to obtain minimum mean flow velocity to suspend particles as:

$$V_c = V_m = 1.08 (1 + 3.64 C_v)^{1.09} (1 - C_v)^{0.55 n_v - 0.09} d_p^{0.18} \left[ 2g \frac{\Delta \rho}{\rho_l} \right]^{0.54} D^{0.46} \quad \text{2-50}$$

### Gillies and Shook's Correlation (1991)

Gillies and Shook, 1991 uses 0.5m in diameter in aqueous slurry with viscosity of 0.5 and 5cp. it contains more coarse particles and large pipe diameter than Orskar and Turian, 1980. This correlation uses an equivalent fluid density defined as:

$$\rho = \frac{\rho_s \alpha_f + \rho_l (1 - \alpha_r)}{1 - \alpha_r - \alpha_f} \quad \text{2-51}$$

Where  $\alpha_r$  is the mean in situ total solids concentration and

$$\alpha_f = \alpha_r * (\text{volume of less than } 74 \mu \text{ m solids or total volume of solids})$$

$$\frac{V}{\left[ gD \frac{(\rho_s - \rho_f)}{\rho_f} \right]^{-0.5}} = F \quad \text{2-52}$$

$$F = \exp(0.51 - 0.0073C_D - 12.5k_2)$$

$$k_2 = (k_1 - 0.14)^2 \quad \text{2-53}$$

$$k_1 = \frac{(\mu/\rho_l)^{2/3}}{g^{1/3}d_{50}}$$

$C_D$  is the drag coefficient of the median diameter ( $d_{50}$ ) of the +74micron fraction, it is recommended as a guide. Orskar–Turian correlation is less reliable for large particles in large pipes whereas Wilson chart shows that critical velocity does not continue to increase with  $d_{50}$ . Gillies' correlation is not applicable at this high viscosity.

### Kokpinar and Gogus' Correlation (2001)

Kokpinar and Gogus, 2001 proposed an empirical equation to predict critical velocity based on experimental data from different published work. They defined critical velocity as the velocity below which deposits will occur but above which no deposits in the pipeline will be encountered. Critical velocity as a function of solid density  $\rho_s$ , particle

diameter,  $d_p$ , fluid density,  $\rho_l$ , dynamic viscosity,  $\mu_l$ , volumetric concentration of solid particles,  $C_v$ , pipe diameter,  $D$ , particle settling velocity in mixture flow,  $V_c$ , and gravitational acceleration,  $g$ . The empirical correlation developed is given as:

$$\frac{V_c}{\sqrt{gD}} = 0.055 \left( \frac{d_p}{D} \right)^{-0.6} C_v^{0.27} (s - 1)^{0.07} \left[ \frac{\rho_l u_t d_p}{\mu_l} \right]^{0.3} \quad \mathbf{2-54}$$

### Al-Mutahar's Correlation (2006)

Al-Mutahar, 2006 mechanistic model for critical deposition velocity based on a force balance and turbulent theory, similar to Davies, 1987 and Oroskar and Turian, 1980 approach. Al-Mutahar model of critical deposition velocity,  $V_c$ , was given as:

$$V_c = 5.66 \left[ f(C_v) \sqrt{g d_p (s - 1)} \right]^{8/7} \left( \frac{D \rho_l}{\mu_l} \right)^{1/7} \left( \frac{1}{\Omega} \right)^{8/7} \quad \mathbf{2-55}$$

Where

$$\Omega = \frac{1}{1+3.64C_v}, \text{ for higher concentration } (>>1\%) \text{ (proposed by Davies), and}$$

$$\Omega = \frac{1}{0.5(1+3.64C_v)}, \text{ for concentration } (\leq 1\%) \text{ (proposed by Al-Mutahar).}$$

### 2.3.5 Liquid-Solid Transport in Inclined Pipeline

Inclined pipes create more difficult problems in establishing deposition velocity. Pipe inclination can be expected to affect both head loss and critical velocity. There are disturbances produced by bends and these disturbances need to decay before representative measurements are made. Otherwise, this effect must be taken into account. Roco and shoko, 1977 reported that minimum transport velocity can be measured as a function of inclination and pipe diameter for fine intermediate and coarse particles slurries. They reported that upward slope deposition velocity increase

slightly by 10% (angle  $<15^\circ$ ) while for angle  $>15^\circ$ , the deposit velocity decrease slowly with increase angle. A more rapid decrease was observed for downward slope pipes due to gravity effect.

### 2.3.6 Study of Liquid-Solid Transport at the Dip

The study of solids suspended in liquid is very important, especially to determine the frictional loss characteristics of the suspension in the turbulent flow. Sand settling at the dip (lower elbow) would require turbulent energy to flush out completely the sand particles in order to prevent partial or complete blockage. In such case entrainment test of sand will be required. These sand particles can only be lifted out when the turbulent energy from the fluid is sufficient to suspend the particles.

Analysis based on balancing the energy required to suspend the particles with that derived from dissipation of an appropriate fraction of the turbulent eddies could be used to develop a correlation for prediction of the critical velocity (Oroskar and Turian 1980; and Davies, 1987).

At full suspension flow when the mean velocity is very high, the sand particles exhibit random movement similar to the fluid eddies. However, the turbulent energy from the fluid usually exceeds the corresponding turbulent energy required to keep the sand particles in suspension.

The sand deposit will occur in liquid-sand systems when the mean stream velocity is less than the fluid velocity at the dip.

## 2.4 Sand Transport in Two Phase Air-Water Flow

The behaviour of sand in multiphase depends on the flow pattern existing in the flow line. For stratified flow, it is similar to the single phase sand/liquid described in section 2.3.2 because the liquid always flows at the bottom of the pipe. However, the sand behaviour is different in the following multiphase flow regime:

**Plug Flow:** Gas bubbles move along the pipe and liquid below. The gas bubbles have no effect on the sand flow.

**Slug Flow:** Sand behaviour is a complex phenomenon due to the flow structure of flow regime. The sand exhibit two different distinct behaviours with the slug unit (slug



section and the film section). Sand attempts to settle at the film region and get transported at the slug body.

**Low Hold up Wavy Flow:** This is common in wet gas pipelines, when the liquid flow holdup is very low. The sand concentration invariably becomes high at the liquid film section.

**Annular Flow:** The liquid film at the wall and the gas at the core of the pipe. The annular flow regime exist at high gas rate and liquid flow rate, therefore the streamline velocity will be above the critical velocity condition for sand to deposit and this makes sand accumulation less concern in this flow regime.

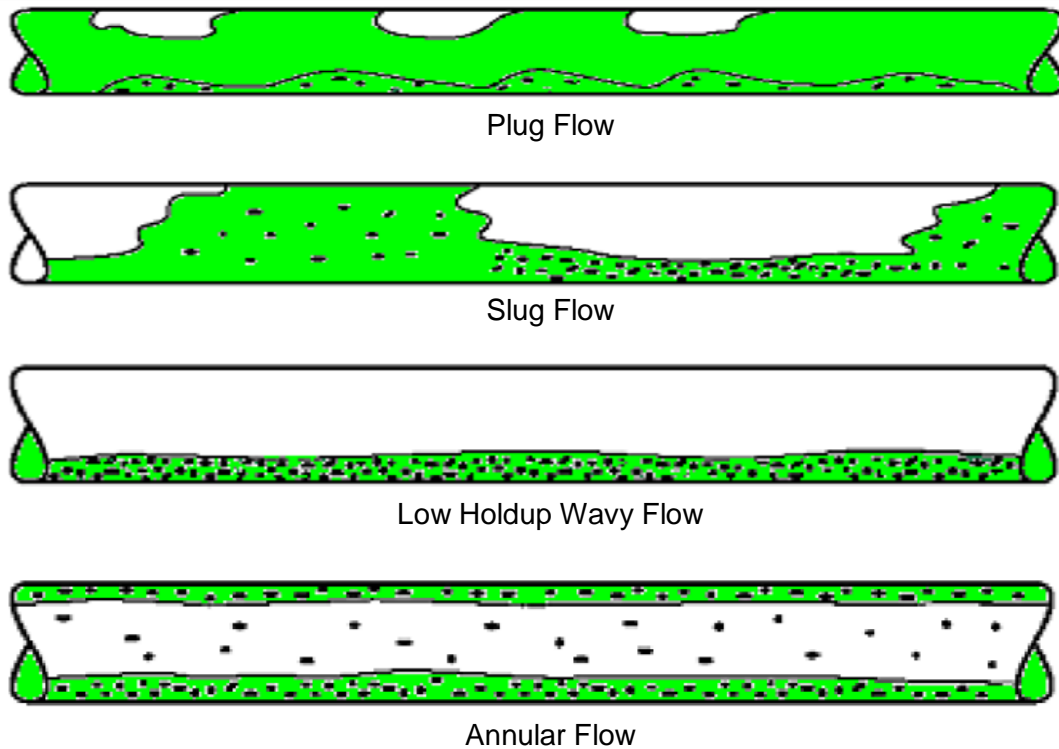


Figure 2-8 Sand/Liquid/Gas multiphase flow system (Yan, 2010)

### **2.4.1 Sand Transport in Stratified Flow**

Sand behaviour and characteristics in multiphase horizontal flow was extensively studied using the 2-inch and 4-inch flow loop at PASE Cranfield University, in order to determine the minimum transport condition (MTC) of sand particles Yan, 2010.

It was observed that sand transport also increases with higher gas flow rate in stratified wavy; and this enhances the transportation of sand into two phase flow systems.

### **2.4.2 Sand Transport in Intermittent Flow**

The transport of sand in slug flow is a complex phenomenon which depends on many parameters such as the characteristics of the slug flow (the turbulent energy, slug body, and film length), pipe inclination, fluid properties, pipe diameter, and pipe roughness. Slug flow mechanism is affected differently with pipe orientation and this distinct behaviour has greater impact on sand transport.

Angelsen et al., 1989 reported that higher gas flow rates leads to slugging which leads to more solids transport. Oudemans, 1993 also noted that the transport of a moving bed is enhanced by the turbulence created by slug flow. Danielson, 2007 suggested that liquid velocity was the dominant part affecting the sand transport. Sand bed formation was strongly influenced by two-phase air-water flow regimes

The behaviour of sand transport in slug flow mechanism according to Al-lababidi et al., 2008 involving the picking up process and the shedding process are described below:

#### **Pick up process**

This is due to turbulent diffusion and the effect of kinetic energy: Turbulence is generated at the slug front, where the pick-up process occurs. The slowly moving liquid film penetrates into the highly turbulent fluid in slug body. Turbulence is diffused along the direction of the penetrating film. When the turbulent eddies reach the sand particles which are settled on the pipe wall they are lifted into the slug body after the slug front has travelled a distance between 0.5~1.5 pipe diameters.

Once the sand particles start to move, they become very energetic due to the kinetic energy imparted on them. Some of the particles are picked up from the pipe bottom into the turbulent core of the slug while others begin to saltate along the bottom of the pipe wall, depending on the sand size distribution.

### **Shedding Process**

It was reported that at the slug tail, the sand particles began to shed into the film zone along with the water (Al-lababidi et al., 2008). As the sand particles enter the film zone, its velocity begins to decelerate partially due to the counter-current flow in the film zone. The active sand particles rolled or bounced at the beginning of the film zone due to kinetic energy that they obtained in the slug body. Energy is continuously consumed by the drag, the active sand particles become less energetic and eventually settled on the bottom of the pipe unless they are picked up by another slug body. Sand is picked up by the slug body and shed in the film. The process repeats for each passing slug. The process of sand transport in slug flow is illustrated in Figure 2-9.

### **Effect of gas superficial velocity**

Increasing the gas superficial velocity causes two effects that counter balance each other.

1. The length of the film zone increased due to increase in the gas pocket. As a result, more sand would deposit in this zone, (Al-lababidi et al., 2008).
2. In contrast, increasing the gas superficial velocity at constant water superficial velocity; the number of gas bubble and chaotic behaviour at the front of the slug body increases: this generates gradual turbulence at the slug front.

### **Effect of liquid superficial velocity**

Increasing the liquid superficial velocity will increase the liquid slug body and invariably increase the turbulence energy generated at the front of the slug. This promotes the sand particles entrainment in the slug body. Experimental evidence shows that increasing water superficial velocity promotes the efficiency of sand transportation.

Based on this experimental observation, Al-lababidi et al, 2008 re-defined minimum transport condition for the sand particle under slug flow regime as: **“the condition at which the sand particles will continue to be energetic enough to keep moving and not deposit in the slug body”**.

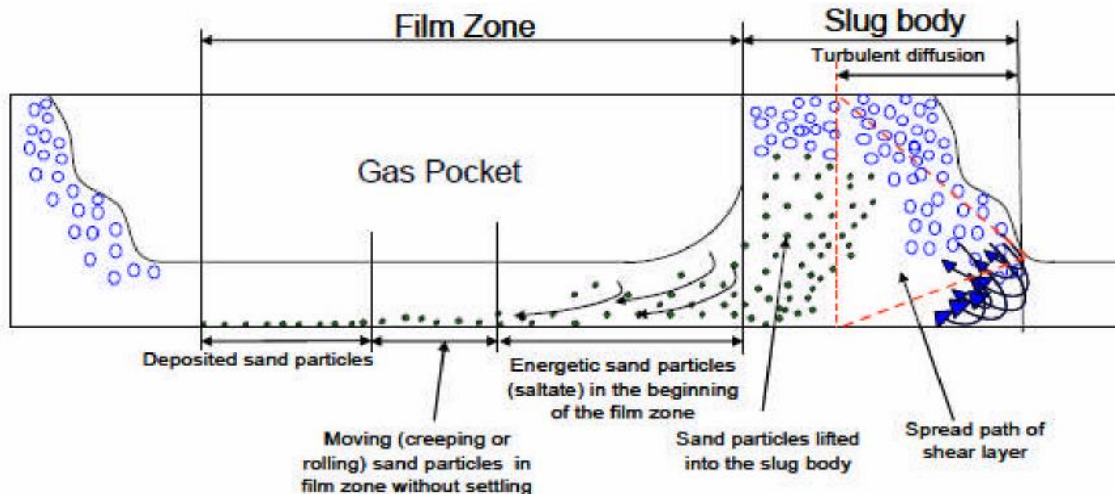


Figure 2-9 Schematic sand behaviour in slug flow, (Al-lababidi et al., 2008)

## 2.4.3 Sand Transport in Air-Water Flow of Inclined Pipeline

### 2.4.3.1 Sand Transport Characteristics in Air-Liquid Flow of Uphill Pipe

In slightly inclined pipe, at certain gas flow rate, the flow pattern exhibits slug behaviour where the surface wave occasionally bridges the top of the pipe. Once, sand particles entered the film zone of the slug unit, they immediately stopped moving forward due to two effects; the shedding process, and the effect of gravity caused by the inclination. Due to these two effects the sand particles tends to move backward with the backflow rather than settled. Meanwhile, due to the difference of the sand size distribution, some of the sand particles began to fall down towards the centreline of the bottom of the pipe while travelling with the water film until they were picked up by the next slug body.

### 2.4.3.2 Sand Transport Characteristics in Air-Liquid Flow of Downhill Pipe

Sand behaviour in downhill behaviour is gravity dominated when sand behaviour is based mostly on the stratified flow regime. The upstream of the pipeline that is above  $5^\circ$  is stratified wavy dominated. A downward inclination causes the liquid to move more rapidly than in the horizontal case and has a lower level in the pipe due to the downward gravity force. There is no reverse flow during sand transportation.

## 2.4.4 Sand Transport Models in Gas-Liquid Flow System

### Salama, 2000 Model

**Salam** developed a correlation to predict sand settling in single and two-phase flows using two main approaches: Modified Wicks model; and Oroskar and Turian models. He proposed the model as follows:

$$V_m = \left[ 1.3 \left( \frac{V_{sl}}{V_m} \right)^{0.53} \right] d^{0.17} v^{0.09} \left( \frac{\Delta\rho}{\rho_f} \right)^{0.55} D^{0.47} \quad \mathbf{2-56}$$

For single phase flow, ratio  $\left( \frac{V_{sl}}{V_m} \right)$  is equal to 1.

He uses sand diameter of 100 microns to 500 microns, and also gas, water and oil fluid properties.

### King, Fairhurst and Hill 2000 Model

King et al., 2000 developed a model, namely “minimum transport pressure drop model”. This is an extension of Thomas’ solid/liquid equations for predicting minimum transport conditions. Thomas named a “lower model” that assumed the particle size,  $d_p$ , is smaller than the laminar sub-layer,  $\delta$  and an “upper model” that assumed the particle size is greater than the laminar sub-layer. The frictional velocities can be calculated using Thomas, 1962 equations as follows:

Lower Model

$$u_0^* = \left[ 100u_t \left( \frac{v}{d_p} \right)^{2.71} \right]^{0.269} \quad \mathbf{2-57}$$

Upper Model

$$u_0^* = \left[ 0.204u_t \left( \frac{v}{d_p} \right) \left( \frac{v}{d_p} \right)^{-0.6} \left( \frac{\rho_P - \rho_l}{\rho_l} \right)^{-0.23} \right]^{0.269} \quad \mathbf{2-58}$$

From the friction velocity, King et al., 2000 calculated the associated friction pressure drop at MTC in the fluid instead of the minimum transport velocity. The frictional pressure drop can be calculated based on the definition of the friction velocity as given by the equation:

$$\left| \frac{\Delta P}{\Delta X} \right|_{mtc} = \frac{4\rho_l(u_0^*)^2}{g_c D} \quad \text{2-59}$$

Where the pressure gradient is given as (psi/ft)

If the actual pressure drop (ACPD) is greater than the pressure drop at the minimum transport condition (MTC), then the solids will be transported.

This series of points can be used as a design guide, where any gas/liquid superficial velocity above the boundary should allow transport of the solids along the pipeline, as shown in Figure 2-10.

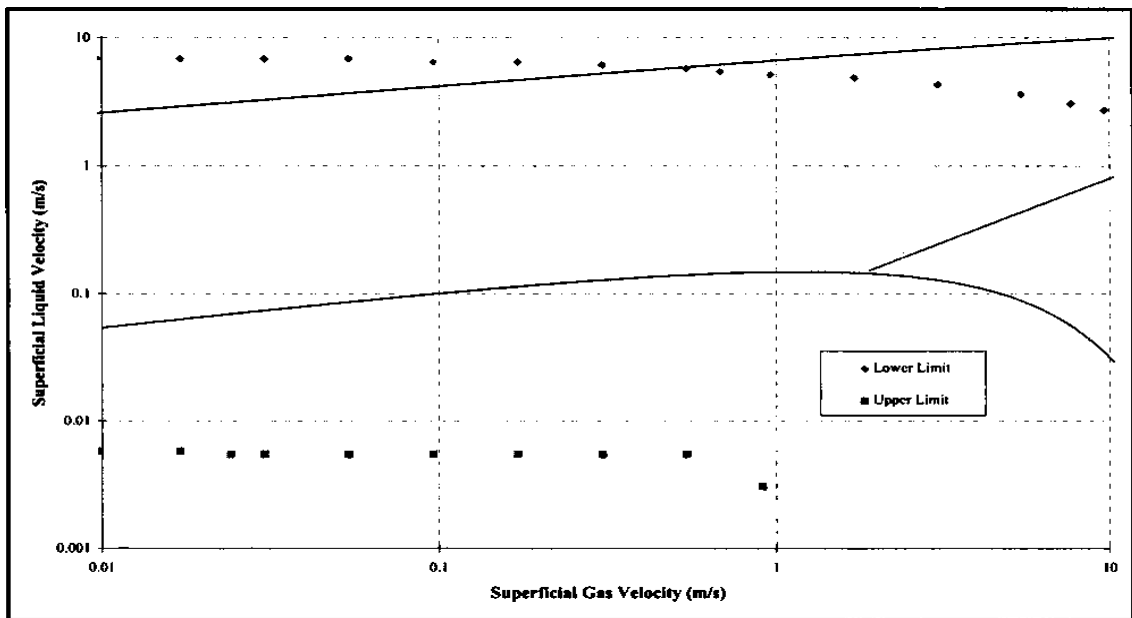


Figure 2-10: Locus of transportation of sand particles (King et al., 2000)

They also carried out three types of entrainment tests for both single and multiphase tests. In the single phase test, water was first transported around the loop and sand was placed at the dip itself to provide a bench mark for the test. Then the sand was placed on the dip itself, increasing the flow rate. The result is shown below in Table 2-1.

There are two tests carried out on multiphase flow test:

Air/flowing water/sand: where by the sand was located at 5m away from the dip and set air at 0.85 m/s, then increased water flow rate from 0.1-0.17 m/s, the sand begins to move at 0.23.

Air/static water/ sand: With 100 litres of water placed at the dip in order to bring the liquid level to 1" of the top of the pipe. The gas velocity was set at 0.85m/s, the sand placed at the dip was stationary. The position of the sand was changed and placed 5m away from the dip; the slug formed at the dip transported the solid. This implies that the turbulence associated with the front of the slug was unable to transport the solids when placed at the dip; but when the solids was placed downstream of the slug formation point, uphill section, the turbulence could act on the particles themselves and transport of sand particles occurred.

Table 2-1: King et al., 2000 Sand-air-water test result

Experiment	$V_{sL}$ (m/s)	$V_{sg}$ (m/s)
MTC sand /liquid	0.72	-
MTC in air /flowing water /sand	0.23	0.85
*MTC in air/static water /sand (sand placed 5m downstream of the dip)	static water =100litres (1" to cover the top of the dip)	0.85

\* The sand was stationary when placed at the dip for superficial gas velocity set at 0.85m/s

King et al., 2000 explains sand transport behaviour at the dip. However their work was not in detail about the mechanism of various flow conditions on the sand transport at the dip and the effect of various angles were not considered.

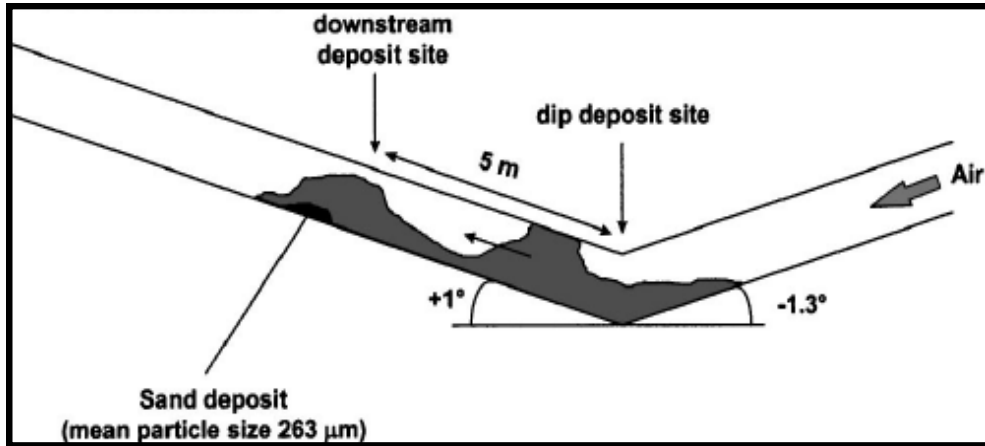


Figure 2-11: 6-inch dip experiment (King et al., 2000)

### Stevenson's Model (2001)

Stevenson et al., 2000 and 2001 centred their work on oil and gas industry, where the sand particles are low concentration ( $<0.01v/v$ ) compared to the hydraulic conveyance. They studied the behaviour of isolated grains of very small amount in multiphase flow (stratified and intermittent flow regime).

He carried out experiment by introducing ten particles in the test pipeline (two different pipes of 40mm and 70mm diameter of 12m long each, water and solution of Rheovis CR2 as the fluid). They developed a correlation based on dimensional analysis between particle velocity and the fluid superficial velocity, given as:

$$\frac{V_p}{u_{sl}} = 0.95 \left[ 1 + \frac{u_{sg}}{u_{sl}} \right] - \left[ 1.38 \frac{u_{sg}}{u_{sl}} + 0.88 \sqrt{Fr_f} \right] * \left[ N_{Re(f)_f} \sqrt{Fr_f} \left( \frac{d}{D} \right)^{1.5} \right]^{-0.180} \quad \mathbf{2-60}$$

The threshold of critical velocity did not yield accurate results for low concentration transport of sand due to enhanced turbulence at the slug nose.



They noted that the particle did not move immediately on arrival of the slug nose, that the nose passes about 3-4 pipe diameters before it was picked up from the bottom of the pipe. The pickup of sand grains by diffusing shear layer is more energetic than the subsequent saltation in the slug section. They suggested that the zone of enhanced energy dissipation which picks up the particles determines the critical transport velocity for the sand. The enhanced ability to pick up particles due to extra energy dissipation has been quantified as the slug nose enhancement factor.

### **Danielson's Model (2007)**

Danielson, 2007 developed correlation for liquid–solid transport using SINTEF data. Sand height and pressure drop models were developed based on the assumption that the critical slip velocity between sand and liquid were relatively constant over a wide range of flow velocities. He observed that in the gas-liquid–solid experiment, gas rate had no direct influence on the critical slip velocity. He observed also that in gas-liquid-sand model, the liquid is a strong function of the angle. Therefore sand bed formation would also be strongly correlated with pipe angle. This is a critical difference between liquid-solid and where pipe angle had negligible influence on sand bed formation and gas-liquid-solid systems. He presented the critical velocity as:

$$V_c = kv^{-1/9}d^{1/9}[gD(s-1)]^{5/9} \quad \mathbf{2-61}$$

Where  $k$  is derived experimentally as 0.23 based on SINTEF data.

### **Bello's Model (2008)**

Bello, 2008 developed a phenomenological model and computational algorithm for estimating optimal transport velocity, particle velocity, particle holdup and critical velocity in three-phase flow. The mathematical model involves balance equations deduced from macroscopic mass and momentum conservation laws, constitutive models and hydrodynamic force. The governing equations are numerically solved using fourth order Runge-Kutta method on discretized pipeline systems. Local and axial distributions of particle velocity and hold-up were determined

The experimental results using non-invasive high speed camera showed that the flow behaviour of the particles through the three-phase gas-liquid-sand pipe flow systems is

changing with various operating conditions. The sand particle velocity in slug flow is significantly higher than that in bubble, dispersed and liquid pipe flows. The sand particle with an equivalent particle diameter of the order of 0.0006m and pipe diameter of 0.04m was used for this study. The ratio of particle velocity to gas–liquid velocity mixture increases with decreasing particle diameter. The proposed model was validated with experimental data obtained from literature. The model predictions show good agreement with the experimental data.

## **2.5 Studies of Sand Dunes in Pipes**

The hydraulic transport of solid particles in pipelines has an important application in oil and gas industries for conveying the sand and solid aggregate through the pipes. Previous studies have shown that sand deposits occurred when the stream velocity is below certain critical velocity (Salama, 2000; Danielson, 2007; Oroskar and Turian, 1980), none of these studies ever considered the saltation for dip geometry.

Saltation is characterised by the formation of dunes with specific length and velocity travelling inside the pipe. One of the typical characteristics of solid-liquid mixture at low velocity is to form dunes. These dunes move slowly in the direction of flow. The saltation mode can be characterised using dune wavelength, height, and velocity which strongly influence the dynamics of sand transportation and blockage process. Furthermore, lack of fundamental understanding of sand transport mechanism can be attributed to the limitation of measurement techniques to characterise the complex interaction between the solid and liquid phases.

## **2.6 Challenges:**

Terrain slugging is a transient two-phase flow associated with low gas and liquid flow rates. Liquid and sand accumulate at low points in the line when the internal drag between the phases becomes too low to balance the gravity effects. Sand particle will be deposited at the bottom of the pipe since there is tendency for liquid accumulation to increase at the point where the terrain slugging is initiated. The inflow liquid and sand particles accumulate at the dip causes local environment conducive to electrochemical corrosion of the pipe wall. Therefore, it is expected that the lowest part of the elbow is prone to corrosion.

While the gas flow builds up the upstream pressure until it is high enough to blow the slug out of the uphill pipe. Two things could occur; part of the liquid could be blown out leaving sand particle behind depending on the accumulation of sand bed formation at the dip. At high gas flow rate, both sand and the liquid get blow out. This requires high pressure to completely remove the sand particle at the bottom of the dip. As the liquid move with sand, more energy dissipation is required from the fluid uphill of the terrain due to gravity effect on the particles and liquid, also the sand loading.

Most correlations developed in multiphase flow in sand transportation are limited due to the complexity of the phenomenon parameters being considered which does not apply to the oil and gas industry; such as high solids loading, wide range of sand concentration and sand particles sizes.

There is little or no information (experimental data and models) relating to solids transport across hilly terrain in undulating pipelines, especially at the dip. The correlations and models that can account for the unique interactions which take place between the sand, gas and liquid phases at the dip has not been investigated. The existing models and correlations have been based on horizontal pipe line.

There are detailed studies of hilly terrain behaviour in the literature of low angles ( $+5^\circ$ ) for gas-liquid flow Zheng et al., 1994 & 1995 and Al safran et al., 2004 & 2005. Sand transport has been studied for inclined pipeline of about  $+5^\circ$ , Yan, 2010. However, in hydrocarbon pipeline design and multiphase flow studies in the literature; the various field bathymetries in long distance pipe layouts and subsea systems showed that there are complex hilly terrains of very steep angles far outside the range of low angles (Hill et al, 1996; Alvarez and Al-Awwami, 1999, Utvik, 2005). Therefore, multiphase flow in sand transport known to be influenced by the pipe inclination, the study of  $\pm 12^\circ$  and  $\pm 24^\circ$  considered in this study are more relevant and applicable to steep angles and complex hilly terrain geometries.

Therefore, this research work will carry out the following tasks in other to achieve the objectives mention in section 1.3:

- Experimental study of the complex dynamic mechanism in a dip using  $\pm 24^\circ$  and  $\pm 12^\circ$  dip configurations. To determine various flow regime and multiphase flow

parameters and investigate the slug behaviour mechanism existing in  $\pm 24^\circ$  and  $\pm 12^\circ$  dip configurations for various flow conditions

- Experimental study of liquid-sand behaviour in  $\pm 24^\circ$  and  $\pm 12^\circ$  configurations. Measurement of local sand concentration to describe the sand behaviour for various sand concentrations using conductivity rings
- Experimental study of sand transport in gas-liquid flow in  $\pm 24^\circ$  and  $\pm 12^\circ$  dip configurations. The sand behaviour for stratified and intermittent flow will be investigated
- Determine the minimum transport condition for sand-water and sand-air-water for  $\pm 24^\circ$  and  $\pm 12^\circ$  dip configurations.

## **3 EXPERIMENTAL SET UP**

The objective of the experimental work was to investigate air-water and sand transport in multiphase flow systems for dip configuration. This chapter describes the general features of the newly constructed experimental facility used in this work. It also outlines the instrumentation, calibration, data acquisition and processing techniques employed.

The design details of the test facility are described in the following sections, including water and air supply, other devices and measuring instruments. Finally, the details of the experimental campaign are presented.

### **3.1 The Test Sections**

The test section was designed and constructed using Perspex pipe to conduct multiphase flow experiments including air-water and air-water-sand tests at the Department of Process and Systems Engineering (PASE) Flow Laboratory, Cranfield University. The facility is used to investigate the flow regime, liquid hold up and other slug parameters and sand behaviour along the downhill as well as the dip and uphill section. Figure 3-1 illustrates the general schematic of dip test facility; a 2-inch (inner diameter of 50.24 mm) dip rig, designed and constructed using Perspex pipe to conduct multiphase flow experiments of air/water and air/water/sand tests.

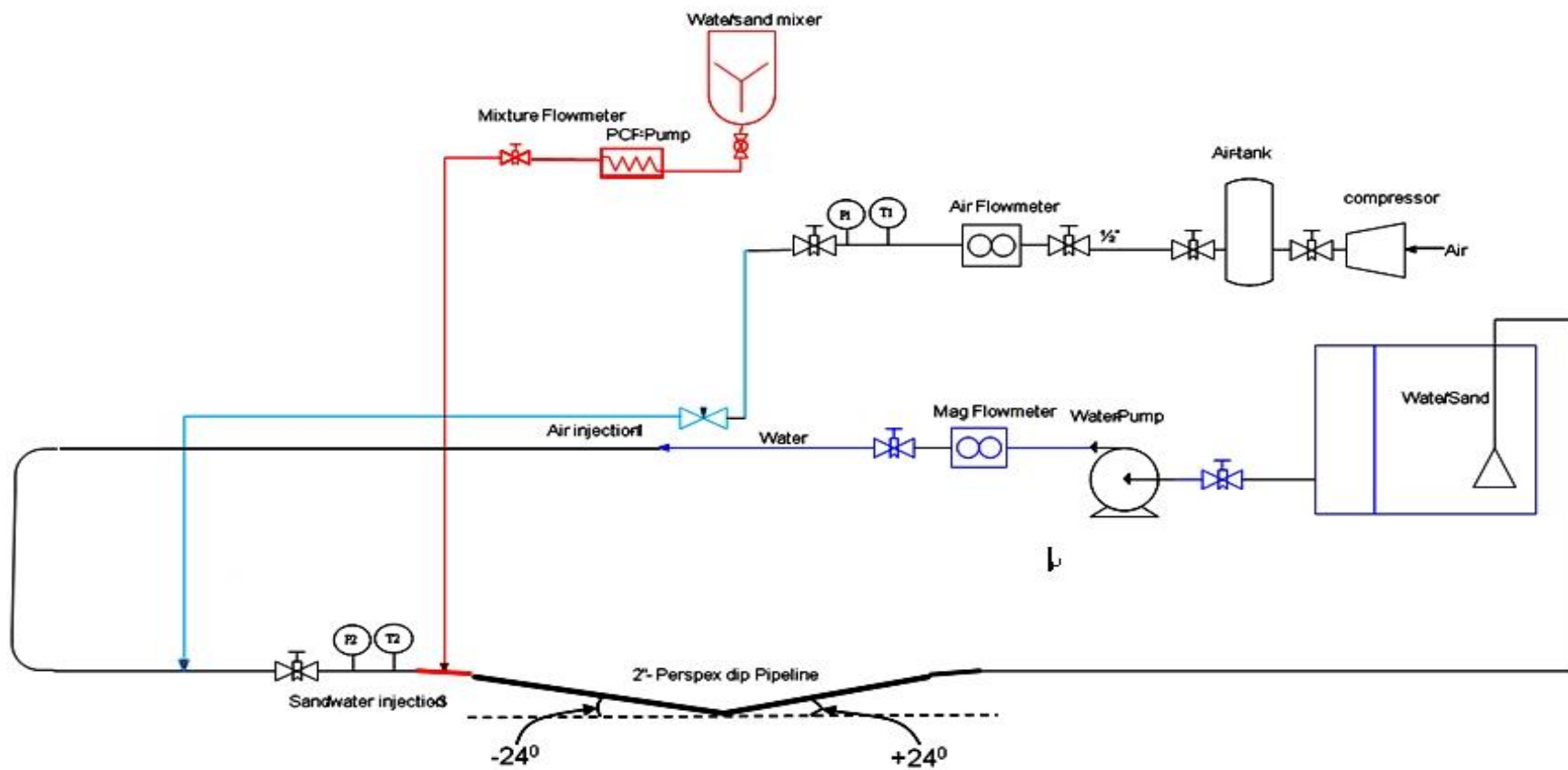


Figure 3-1: Schematic drawing of 2-inch dip facility

### 3.1.1 The 24° Dip Pipeline

The 24° test rig comprises a Perspex dip pipeline of 1.4m high and 6.5m in length, a horizontal inlet line (2.1m of PVC pipe, 2m of Perspex pipe) and a 2-inch PVC pipe with the length of 10.5m as the water supply line.

Figure 3-2 indicates the specific dimension of the 24° dip test facility. The downward and upward pipes were joined together by a smooth bend with the radius of 132°. The total length of the arc is 1.26m, bend radius of 0.55m. Four conductivity sensors were installed at the downhill and uphill pipeline with a differential pressure transducers coupled at each test section (downward, dip and upward section).

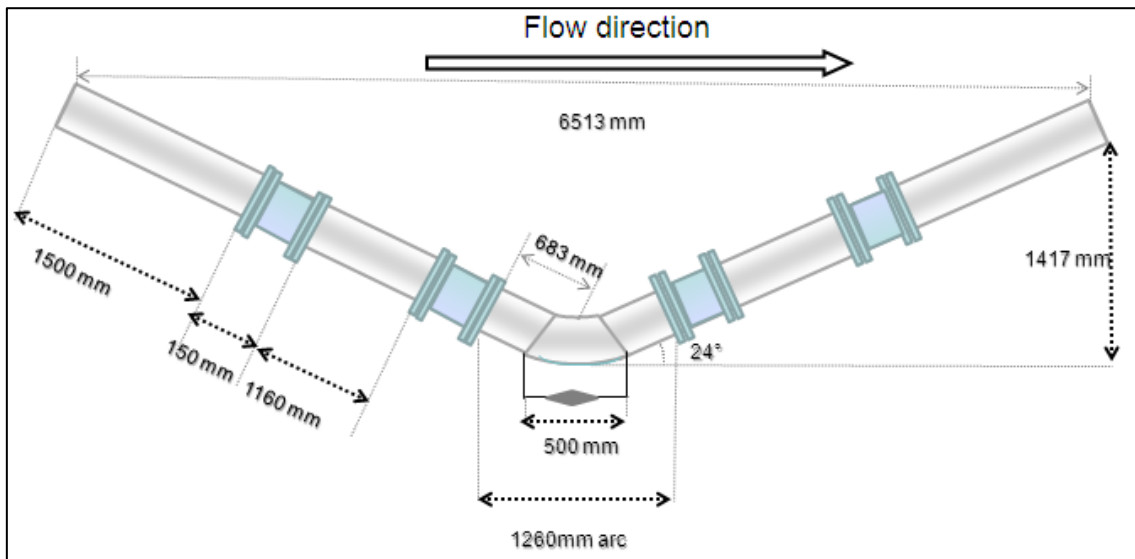


Figure 3-2: Dimensional configuration for 2 inch dip section

### 3.1.2 The 12° Dip Pipeline

The 12° dip test facility designed similar to 24° dip test facility with the following specification; a Perspex dip pipeline of 1.97m high and 7.2m in length, a horizontal inlet line (2.1m of PVC pipe, 2m of Perspex pipe) and a 2 inch PVC pipe with the length of 10.5m as the water supply line. The downward and upward pipes were joined together by a smooth bend with the radius of 156°. The total length of the arc is 0.78m, bend radius of 0.29m. Four conductivity rings were also installed in downhill and uphill

pipeline with a differential pressure transducers coupled at each test section (downward, dip and upward section).

### **3.1.3 Liquid Supply System**

Water was used as the carrier fluid, supplied from, and returned to, the water tank with capacity of 1.7m<sup>3</sup> and opened to the atmosphere with the base resting on the floor. The water tank was divided into two chambers by a baffle (with a sieve) between the return chamber and suction chamber in order to prevent sand particle being sucked by the pump. A centrifugal pump positioned at the suction side of the tank was connected: 20cm above the bottom of the tank to allow sand in the tank to settle, rather than being sucked by the pump. The centrifugal pump has a capacity of 40m<sup>3</sup>/h. The water flow rate was measured by an electromagnetic flow meter, ABB K280/0 AS model having a range of 0 to 20m<sup>3</sup>/h, placed upstream of the air/water mixing point. The flow rate of water was controlled by means of a throttling valve downstream of the pump.

### **3.1.4 Air Supply System**

Compressed air was supplied to the test rig by screw compressor unit. This compressor has a maximum supply capacity of 400 m<sup>3</sup>/ h free air delivery and a maximum discharge pressure of 10 barg. Air was metered by a 0.5-inch thermal flow meter ranging from 0 to 70m<sup>3</sup>/h. The flow meter Endress + Hauser, Proline t-mass flanged 65 F 15PMP 1400 with the range of 6 barg was connected into the 12.5mm (0.5") airline. Gas was injected at the entrance of the horizontal pipeline; 4m upstream to the downhill section. Pressure transducer and thermocouple were installed at the exit of the flow meter as shown in Figure 3-1. The gas flow meter had a 4-20mA HART analogue with 0-10volts DC which was connected to the data acquisition system. The different superficial velocities of liquid and gas ( $V_{sl}$  and  $V_{sg}$ ) were controlled by throttling valves upstream of the flow meters.

### **3.1.5 Sand Injection System**

Sand injection unit was constructed and connected prior to the entrance of the downhill pipe injection point through a ¼ inch line. The sand unit is permitted to support a wide range of continuous sand concentration experiment. It comprises of sand slurry hopper of 800 mm in diameter and 800 mm in height, with a 200 mm diameter axial flow



impeller, and a variable speed pump with an impeller. A 1-inch OPTIFLUX 23000C Krohne magnetic flow meter was installed downstream of the injection pump. The sand injection volumetric flow rate is a constant flow rate of  $0.16 \times 10^{-3} \text{ m}^3/\text{s}$ . Sand used in this study was Congelton HST 50 with an average particle diameter of 270 micron and density of  $2650 \text{ kg/ m}^3$ . Figure 3-3 represents sand size distribution.

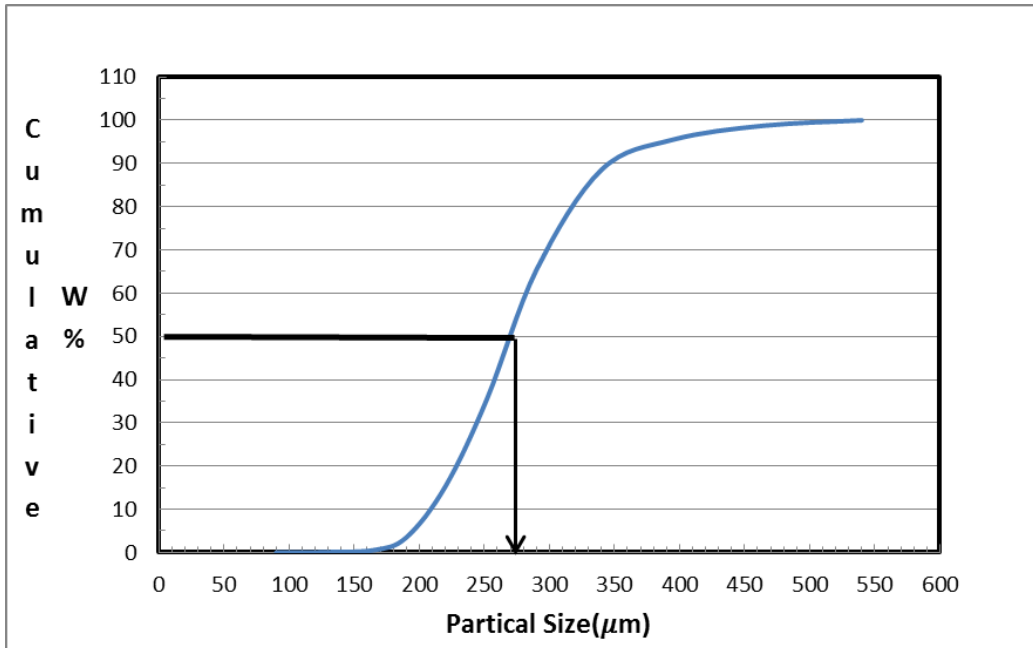


Figure 3-3: Sand size distribution used in the test

## 3.2 Instrumentation

This section outlines the details of the instrumentation used to carry out the experimental work.

### 3.2.1 Flow Meters

The ABB K280/0 AS model electromagnetic flow meter was used to measure the water flow rate downstream of the centrifugal pump. It has an accuracy of  $\pm 0.5\%$  with range of  $0\text{-}2\text{m}^3/\text{h}$  at 9 bar. The flow meter was connected with serial port of the PC using serial communication RS 232 protocol to serially communicate with the data acquisition system.

The gas flow meter Endress + Hauser, Proline t-mass flanged 65 F 15PMP 1400 with the range of 6 bar measures the gas flow rate entering into the ½-inch pipeline from the screw compressor. Flow metering, temperature and pressure of gas were measured at the downstream immediately after gas flow meter.

The slurry flow meter OPTIFLUX 23000C Krohne magnetic flow meter connected from the downstream of the injection pump to ¼ -inch injection line. It has an accuracy of  $\pm 0.2\%$  with range of 0 - 20l/min at 10barg.

### 3.2.2 Absolute Pressure Transducers

Two single PMP 14000 model pressure transducers made by Druck, with silicon diaphragm type, were installed in the test section. The pressure transducers were installed in the gas-line and on the horizontal test section. The pressure transducers were flush mounted, so they do not interfere with the flow. The measurement ranges from 0 to 6barg and an output voltage of 0 to 5voltage D.C. It was installed at the flow meter outlet of the 1-inch gas line and also at the entrance of the downward test section. Figure 3-4 and Figure 3-5 below are the calibration of the pressure transducers.

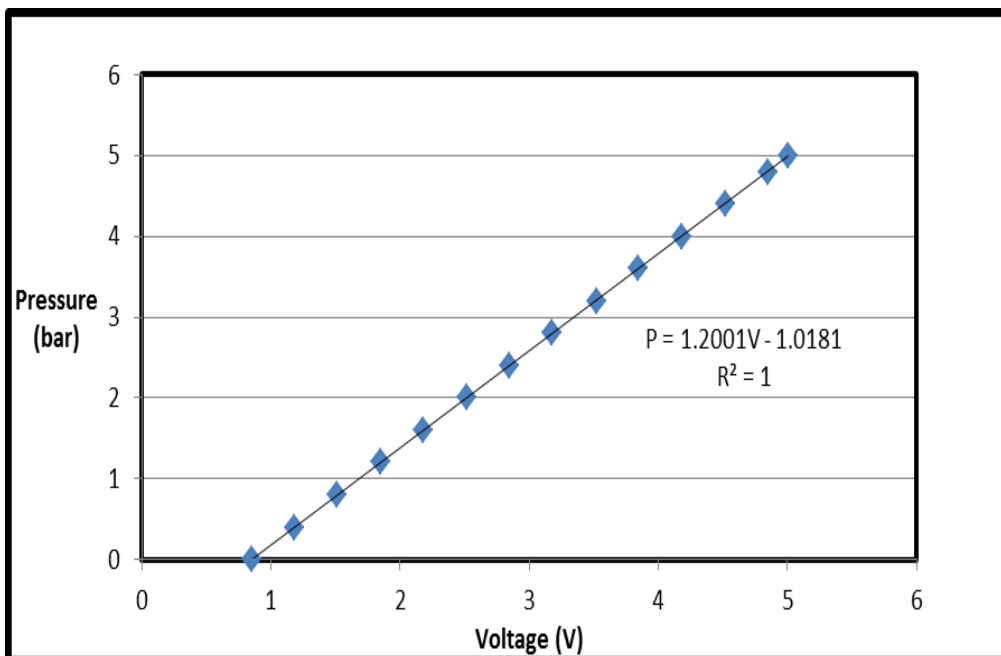


Figure 3-4: Calibration of single pressure transducer (absolute) in the gas line

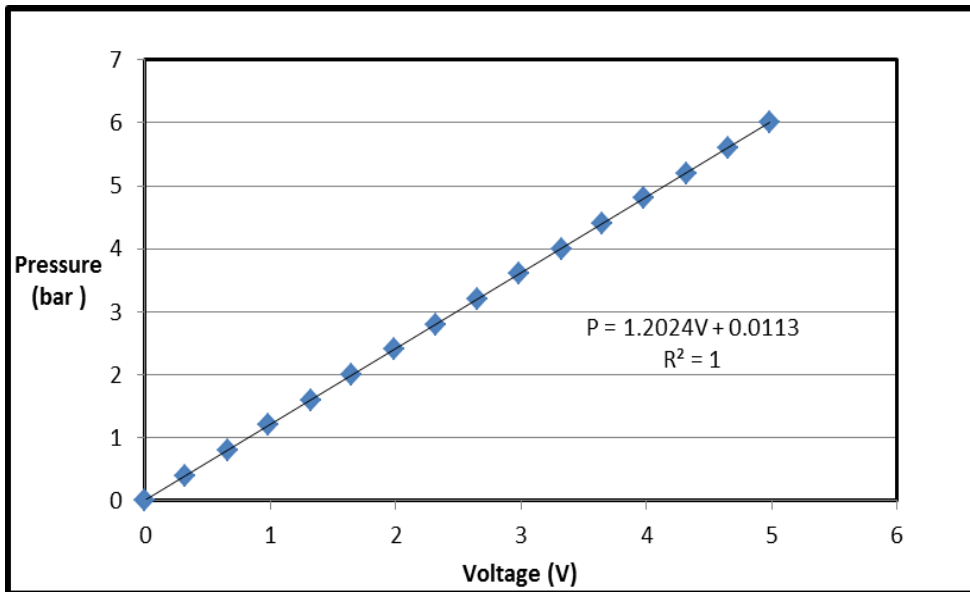


Figure 3-5: Calibration of single pressure transducer (gauge) in the horizontal inlet line

### 3.2.3 Temperature Transducer

The T-type thermocouple temperature transducer was installed to measure the temperature of the fluid. It had a range of -200 to 400°C. Its signal response was of the order of 1 Hz. The temperature of air was monitored before entering into the test section and also on test section.

### 3.2.4 Conductivity Rings

The conductivity rings uses the electrical conductivity technique to measure the liquid fraction across a pipe section. The conductivity ring uses the contact electrode (ring shape) to determine the electrical conductance of the fluid across the pipe diameter.

Electrical conductivity technique is one of the most common multiphase flow measurements in conducting (as a continuous phase) and non-conducting medium.

The advantages of impedance technique are as follows:

1. The impedance technique is non-intrusive, so does not disturb flow field or interference to flow
2. Provide continuous recording of the in-situ liquid volume fraction
3. Relatively simple to design and cost effective

The instrument determines the relationship between the electrical impedance of the medium and the phase distribution; and consequently determines the average cross section void fraction. For conducting liquid like tap water, the electrode pair is essentially resistive when the frequency excitation signal is about (10 - 100 kHz). For these experiments (air/water, sand/water, air/water/sand), the conductance method is applicable. Conductivity rings provide a continuous measure of liquid holdup and can be used to determine the slug characteristics (Fossa et al. 2003). The probes discussed here are of twin-ring electrodes type.

#### **3.2.4.1 Design & Construction Aspect of Conductivity Ring**

The design and geometry of the conductivity is important for accurate measurement of multiphase flow system. There are several complicated designs of the electrical conductivity probe in the literature (Andreussi et al.,1988; Merilo M et al.,1977). However, the limitation of these conductivity probes is the inability to account for the various flow patterns in two-phase flow.

A simple non-intrusive probe made of two rings electrodes mounted to the tube wall is reported to be very effective for measuring mean liquid hold up under different flow conditions due to the following reasons (Andreussi et al.,1988; Fossa,1998).

1. Good repeatability of ring electrodes was confirmed on condition that the measured conductance must be normalised to a reference situation (i.e. when the conductance of the pipe is full of liquid). This will avoid having to monitor the electrical conductivity of the liquid during the operation.
2. Ring probes are more suitable applications for evaluation of the mean void fraction.

In this work, the ring shaped electrical conductivity as shown in Figure 3-6 was designed and constructed at the Department of Process and Systems Engineering (PASE), Cranfield University; to study continuous air-water flow, sand-water and air-water-sand flow in a dip pipeline.

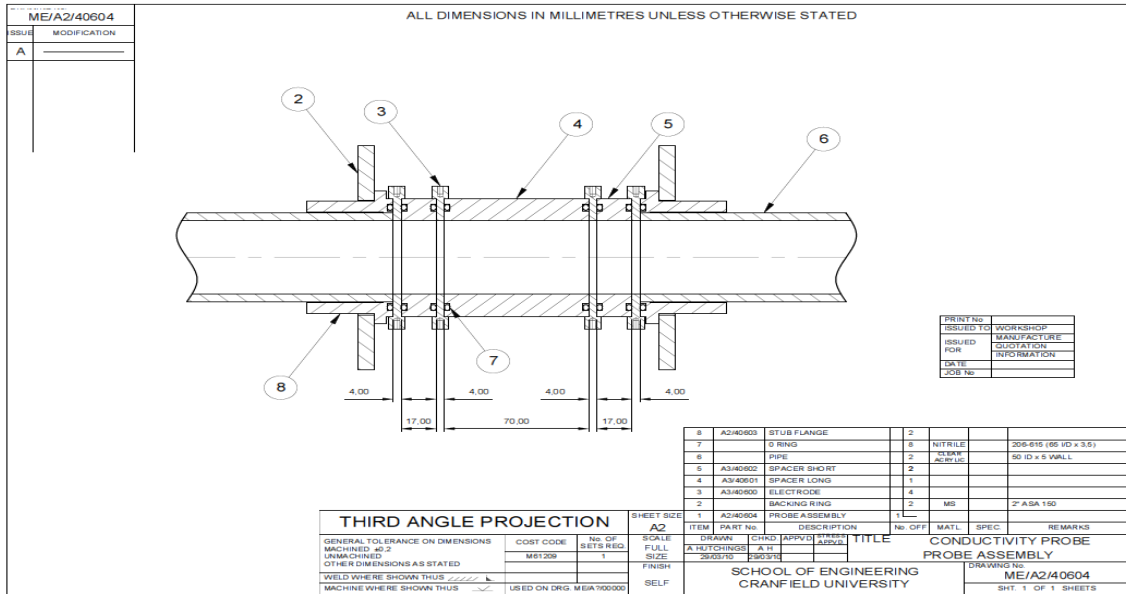


Figure 3-6: Conductivity ring

The effects of the probe geometry upon the response of the measuring devices have been investigated with reference to stratified, bubble and annular flow by Coney, 1973 and Fossa, 1998. Based on their studies, the response of the conductivity probe is affected by the probe geometry and even more by the flow pattern. Consequently, the mixture impedance changes with the phase distribution at the same mean void fraction. To overcome this problem, the conductivity probe geometry was chosen to produce a probe response that is relatively insensitive to the changes between the uniformly dispersed (bubble) regime and the stratified regime (Fossa et al., 2003).

Fossa et al., 2003 suggested that the probe geometry aspect ratios:

$$(D_e / D) < 0.4$$

$$(S/D) < 0.08$$

Where

$D_e$  is the distance between conductivity ring pair,

S is the thickness of each ring, and

D is the pipe internal diameter

Following recommended design guidelines, the two stainless steel rings electrodes with a width of ( $S=4$  mm) and spaced at ( $D_e = 17$  mm) apart were constructed for this experimental work.

### 3.2.4.2 Electronics Instrument Design

An electronic circuit was used to measure the electrical impedance between the electrodes. The electronic instrument provides a primary voltage output proportional to the conductance of the probe. An electronics metering device described by (Fossa, 1998) was adopted for this research work as shown in Figure 3-7. It supplies a carrier 22 kHz A.C signal to the measuring electrodes. At this frequency, measurements of both signal amplitude and phase shift demonstrated that the liquid (tap water) behaves as a resistive medium. The key elements of the electronics are an a.c. Wheatstone bridge, an instrumentation amplifier and a precision rectifier with cut-off frequency of 100Hz. The D.C output from the electronic box was read by a precision voltmeter and stored as raw voltage in data acquisition system.

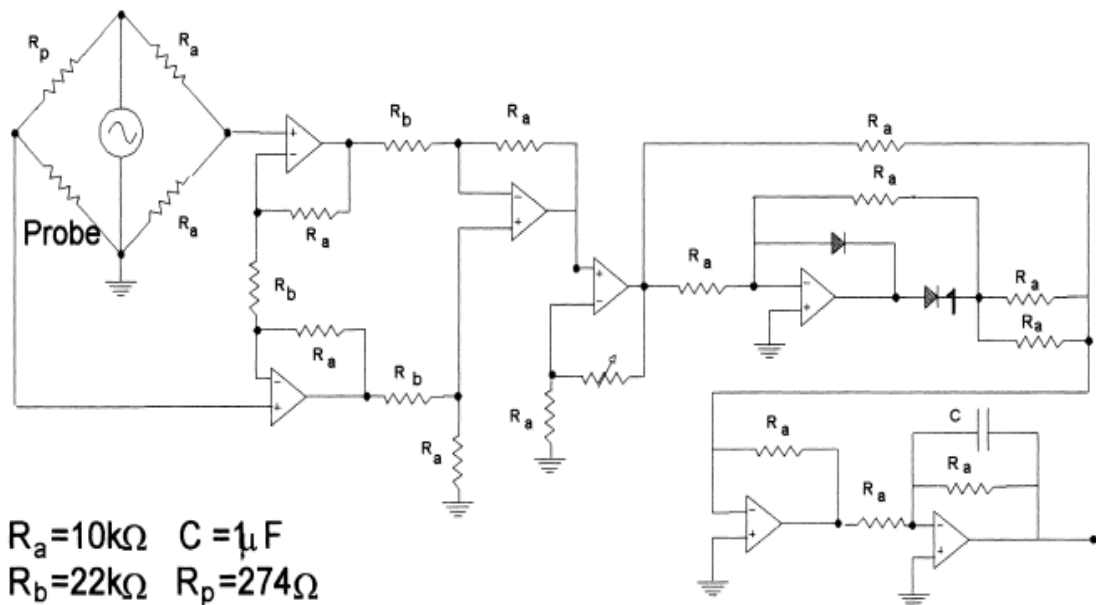


Figure 3-7: Probe electronics diagram (Fossa, 1998)

### 3.2.4.3 Calibration of Conductivity Rings

Calibration of the instrument is important in calculating the required parameters (holdup or void fraction) from impedance readings of the dynamic test. Calibration is also useful

to ensure the output signal from the conductivity sensors remains within a fixed voltage range. The calibration was carried out using tap water, the same liquid used in the experiment.

Calibrations of the rings were performed by connecting the electrode pairs to a conductivity electronic box that supplied a 22 kHz A.C. carrier signal.

The procedures of conductivity sensor calibration for air-water experiment are described as follows:

- When the sensor is clean and dry, adjust the conductivity box to set the in-situ value for air. In this case, the in-situ value is set as 1.5 volts for box 1 and 0.5 volts for box 2.
- Fill up the conductivity unit with water and measure the voltage output
- Dry and clean the conductivity unit, ensure there is no water droplet in the conductivity ring.
- Start filling the conductivity ring gradually with constant step weight of water.
- Record the voltage output of both two sensors at each step.

Every calibration for each conductivity sensor has been repeated 3 times. The diagram was plotted using “normalized voltage ratio” against “hold-up”, and calibration curves was obtained by applying 5<sup>th</sup> order polynomial fit on plots. The calibration curves of four conductivity sensors are shown in Figure A 3 to Figure A 10.

### **3.2.5 Flow Data Acquisition System**

All measured data from the flow meters, pressure transducers, thermocouples and conductivity rings were acquired using a 12 channel PC based Data Acquisition System (DAS). This system consists of a series of custom-built signal conditioning units. The signal was then fed to the PC via a 32 channels parallel port multiplexer (SCB-68) after being converted to an appropriate digital signal. A runtime 6.2 version of LABVIEW was used to gather these data in real time and display the results on a computer monitor, after being converted to engineering units for the corresponding instruments, for example volt to bar, in the case of pressure measurement. The PC system runs with a Windows XP operating system and 2.8GHz Pentium processor, with a hard disc capacity of 100 GB.

### 3.3 Description of Experimental Programme

Table 3-1 presents the test matrix for the sand test. The experimental work was performed in three stages.

1. The experiment for air-water test at given superficial velocities, aimed to cover a wide range of flow regime existing in the dip pipeline. The superficial liquid velocities were 0.07m/s, 0.15m/s, 0.35m/s and 0.55m/s. The superficial gas velocities range from 0.05m/s to 6m/s)
2. The experiment for single phase water-sand settling test and entrainment test for range of entire sand flow regime
3. Air-water-sand experiments were conducted for settling and entrainment tests within stratified and slug flow regime.

Table 3-1: Sand concentration Test Matrix

Sand Concentration (lb/1000bbl)	Volume Fraction (v/v)
50	5.38E-05
100	1.075E-04
200	2.15E-04
500	5.38E-04

The sand was injected from the sand hopper as sand-liquid homogenous mixture prior to the entrance of the downhill pipe injection point through a ¼ inch line. The amount of sand injected into the test section was calculated based on material balance model shown in Figure 3-8.



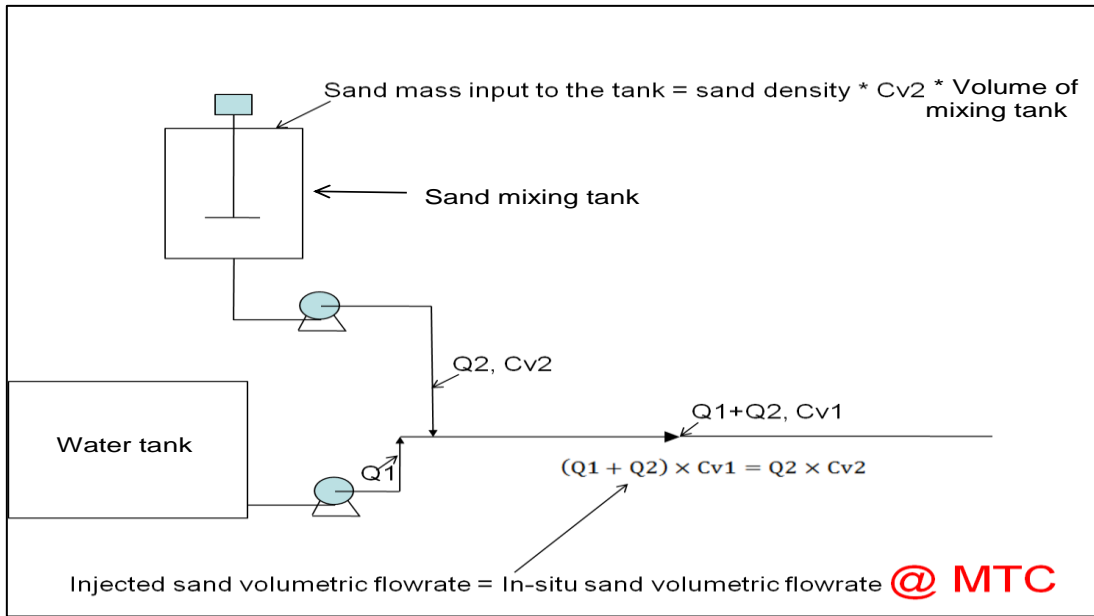


Figure 3-8: Sand Injection calculation model

where

Cv1 is the concentration Vol/Vol given (or required) in the test section as stated in Table 3-1. Cv2 is the sand hopper concentration Vol/Vol, back calculated from test section (in order to achieve the given sand concentration (Cv1) and flow rate at the test section). Q2 is a fixed flow rate of homogenous sand–water, set at  $0.16 \times 10^{-3} \text{ m}^3/\text{s}$  for all test carried out. Q1 is the calculated flow rate based on the given (or required) liquid flow rates at the test section.

The amount of sand added was based on the sand concentration of the sand hopper calculated from the test section concentration. Test for each sand concentration was carried out individually for each flow rate in order to control injected sand from the sand hopper.

### 3.3.1 Experimental Procedure for Sand Test

#### 3.3.1.1 Sand Settling Test

##### Test 1: Single Phase Water-Sand Settling Test

- Prepared sand mixture of required concentration in the slurry hopper
- Start the water pump and maintain the mixture velocity with the required value

- Inject sand slurry into the dip rig with continuous stirring
- Start reducing the water till it reach next given flow rate and establish a stable flow
- During the time the desired flow rate is stabilized, collect the data, observe the sand pattern and the MTC using video camera
- Flush the remaining sand particles or air bubble out of the test section and ensure the transmission tubes of differential pressure transducers are full of water
- Repeat the experiment for another given sand concentration.

### **Test 2: Sand-Air-Water Multiphase Flow Test**

- Prepare sand mixture of required concentration in the slurry hopper
- Start the water pump and maintain the mixture velocity in the required value by throttling the valve downstream of the flow meter. Then open the air valve and keep the gas velocity at a constant value
- Inject sand slurry into the dip rig; ensure homogeneous mixing of the slurry by continuous stirring of the sand hopper while it is being injected into the dip rig
- Start reducing the gas flow rate at interval of 5mins and maintain a steady flow rate
- During the time the desired flow rate is established, collect the data, observe the sand pattern and the MTC using video camera
- Flush the remaining sand particles or air bubble out of the dip section and ensure the transmission tubes of differential pressure transducers are full of water
- Decrease the water velocity to the next test point and repeat the experiment
- Repeat the experiment for another given sand concentration.

#### **3.3.1.2 Sand Entrainment Test**

##### **Test 1: Single phase Sand-Water Entrainment Test**

To study the movement of sand deposit at the dip

1. Place sand bed at the dip with water filled to the top of the dip pipe section
2. Take measurement of the sand bed layer with a tape rule at test section

3. Open the water-line starting from the minimum flow rate
4. Gradually increase the water supply into the pipeline and video the sand behaviour at the dip up to the allowable maximum flow rate that the sand get flushed out

Repeat the experiment using different level of sand bed layer

### **Test 2: Sand-Air-Water Entrainment Test**

To study the movement of sand bed deposited at the dip with flowing air and static water.

1. Place sand bed at the dip with water filled close to the top of the dip pipe section
2. Take measurement of the sand bed layer with a tape rule at test section
3. Open the air-line starting from the minimum superficial velocity
4. Gradually increase the air supply into the pipeline and video the sand behaviour at the dip up to the allowable maximum flow rate that the sand get flushed out

Repeat the experiment using different level of sand bed layer.

## **3.4 Sand Holdup Measurement**

Sand holdup is an important parameter that is needed for design, operation and control of liquid-gas-sand multiphase production and pipeline transportation systems. In this present work, the sand holdup was determined by converting the normalised voltage values (from the sensor signals) to sand fraction using the calibrated curves. The calibration of conductivity rings in homogenous condition and sand bed layer condition are important in this work.

The procedure of conductivity sensor calibration is as follows:

1. The pipe spool carrying conductivity sensors is blinded on both ends with flanges and bolted tight to prevent leakages
2. Place the sensor on a workbench- flat and horizontal surface
3. Connect the sensor to two. Channels in the conductivity box (e.g. Channel 1 and Channel 2)

4. Connect two multi-meters to the corresponding channel output of the conductivity box and set to an appropriate voltage range
5. Tune the conductivity box to achieve a zero setting of 1.5 volts on the multi-meter when the conductivity is empty and dry. This fixes the lower range value of the sensor. Adjusting the output voltage to a value different from 0 volts to confirm its functionality and when the conductivity section is empty and dry. This gives the voltage value for air
6. Fill the conductivity sensor with water to obtain the maximum range value of the sensor. This enables the conductivity box to maintain a linear behaviour of the calibration curve
7. Empty the pipe spool of water and clean the inside thoroughly to dry out any water left in the pipe
8. Start adding a determined weight of the calibration sand into the conductivity ring (displacing the water in the conductivity ring) at intervals of equal weight. Take the voltage output at each interval
9. For sand bed layer static test, ensure the sand is evenly laid at the bottom of pipe before taking the reading
10. For sand homogenous test, ensure the sand is evenly mixed in the pipe while taking the reading
11. Continue this process until the pipe is full of sand. Take the voltage output for the wetted sand

The result of the sand calibration is reported in Appendix A.

In addition, flow pattern observations were made through clear Perspex sections in the whole pipeline during the experimental runs. A high-speed digital video camera of 256 x 256 pixels was used to record video and images in order to visualise the flow patterns and measure the sand bed layer and to further determine sand dune characteristics. The sand bed layer geometry was determined and reported in Appendix A by assuming the sand bed is flat. The pixel coordinates is converted to millimetres. As a result, all screen resolutions (magnification) in the video is scaled to real unit values. Also, the porosity of the sand particles was determined to give 0.36.

### 3.4.1 Velocity Measurement Using Cross Correlation

Slug transitional velocity measurement along the flow direction is calculated based on the cross correlation of signals from two similar sensors detecting slugs. There are various sensors that can detect the signal generated by slug e.g. ultrasound, optical, capacitance, impedance etc.

Cross correlation techniques have been widely used in both laboratory and industry for pipeline flow velocity measurement. The cross-correlation technique has been used for processing a variety of measurement results for multi-phase flow (Beck, 1987).

There are two types of cross-correlation application; time delayed-cross correlation and spatial cross correlation. Also, cross-correlation can be carried out either by direct cross correlation or by using discrete Fast Fourier Transformation (FFT) which has less computational time. This study will further briefly discuss the time delay cross correlation because of its application in this research work to determine slug velocity.

**Time Delay-Cross Correlation:** Bubble, solid or liquid flow distribution in a pipeline produce random disturbance signals. These signals are collected from two sensors separated by axial distance (L). Assuming the signal distribution remains the same as it travels from A to B, and then the output signal of sensor A will be time delayed replica of sensor B. The time delay of the flow patterns between the upstream sensor and a downstream sensor as shown in Figure 3-9 is determined using the cross correlation function of the two random signals. The cross correlation function for flow rate measurement in Figure 3-10 can be calculated from the two sets of signals as follows:

$$R_{V_A V_B}(\Delta) = \frac{1}{T} \int_0^T V_A(t) V_B(t + \Delta) dt \quad 3-1$$

Time delay cross correlation shown in equation 3-1 is a common result of two sensors positioned with considerable distance that will be sufficient enough to capture the same quantity of fluid or particle pattern e.g. slug holdup.

where

$V_A(t)$  and  $V_B(t)$  are the upstream and downstream disturbance signals respectively (analogues to characteristic input signals of the flow probes)  $\Delta$  is the cross correlation

lag (time delay), and  $T$  is the sampling (integration) time. The cross correlation function  $R_{V_A V_B}(\Delta)$  reaches its maximum when the cross correlation lag  $\Delta$  is equal to the transit time  $t_0$  of the tagging signals.

The flow velocity is given by

$$V = \frac{L}{\tau} \quad \text{3-2}$$

where

$L$  is the spacing between the upstream and downstream sensors and  $\tau$  is the time delay ( $\Delta$ )

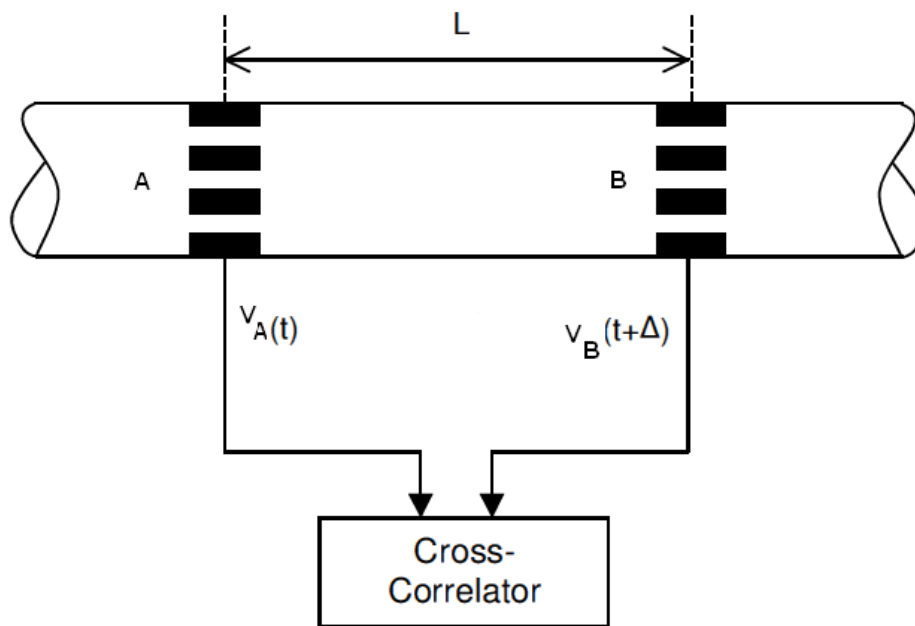


Figure 3-9: Time delay cross correlation flow measurement

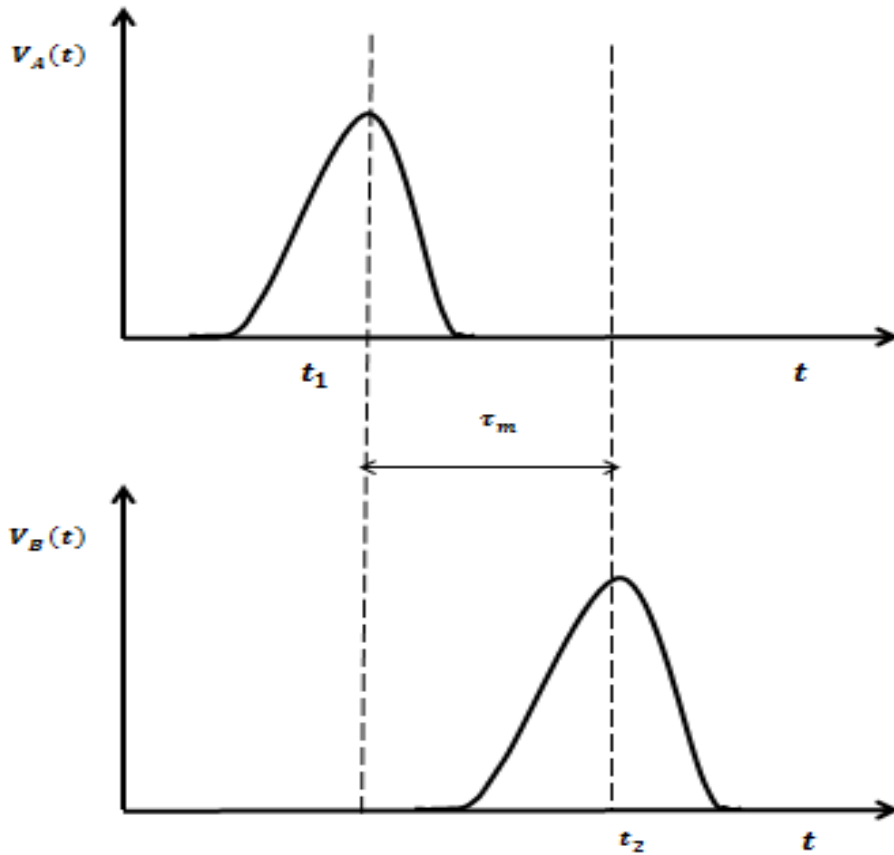


Figure 3-10: Generated signals

### 3.5 Measurement Error

Experimental results are very important in the analysis of physical process. Every measurement inherits error by nature. A number of different instruments are available for use on the 2-Inch dip facility to measure both “gross flow” characteristics such as pressures, inlet flow rates, and “local” data such as liquid holdup at various points along the test section.

The measurement errors used for the present work are summarized in Table 3-2 below

Table 3-2: Measurement parameter errors

Measured Parameter	Range	Error in Full Range Measurement	Instrument
Superficial gas velocity	0 -6m/s	$\pm 0.2\%$	Electromagnetic flow meter
Superficial liquid velocity (water)	0-1m/s	$\pm 0.5\%$	Magnetic flow meter
Liquid Holdup	0 - 1	1%	Conductivity ring
Sand Holdup	0 – 0.69	$\pm 15\%$	Conductivity ring

At the start of each experimental run, the electrical connections from the sensors were checked along with inspection of pressure tapping and temperature probes. For each experimental run, a waiting time of 5 minutes was established in order to obtain readings after stable flow was established before taking readings. All the parameters were continuously logged for a specified time period of 5 minutes which is considered sufficient for data analysis. However the repeatability of the runs was also performed frequently during the tests and they are in good agreement with the initial runs. The measurement error was reduced by averaging three times measurement of liquid holdup for a given flowing conditions.

### 3.6 Chapter Summary

This chapter presented the detailed experimental set up for two-phase air-water; sand-water and air-water-sand tests. The facilities were designed to perform investigations of sand behaviour in single and multiphase flow.

Section 3.1 described the supply for air, water and sand to the test facilities, and the instrumentation specification for air and water flow rate measurements, Section 3.2 described the measuring section. In this section the design aspects of the conductivity probe and the calibration process were presented. Section 3.3 presented the data acquisition system (DAS) deployed to extract the experimental data from the tests which were conducted at atmospheric pressure and with different air and water flow



rates. It also described the experimental measurement methods used; the signals from the instrumentation installed at various locations on the rig were acquired through dedicated LABVIEW software for further analysis using Microsoft excel spread sheet and MATLAB software.

Lastly in Section 3.3 methodology adopted to perform experiments were discussed in detail, operating ranges were defined and various parameter deduction techniques used in later chapters were summarized.

The results of the series of experiments mentioned in this chapter are discussed in chapter 4 for air-water experiment, while chapter 5 and 6 discussed water-sand and air-water-sand results respectively.



## 4 AIR-WATER EXPERIMENTAL RESULT AND ANALYSIS

This chapter describes the result of the experiments conducted using 2-inch (ID=50.24 mm) dip facility of  $\pm 24^\circ$  and  $\pm 12^\circ$  configuration test rigs respectively; which consists of a downhill pipe, a smooth bend (dip) and an uphill pipe. The experimental arrangement was described in chapter 3. The main aim of this chapter is to develop a flow regime mapping for the three sections of each test rigs; and to study the flow behaviour and slug initiation mechanisms at the dip.

In order to achieve the set objectives, liquid holdup was measured from the conductivity rings because it has a major influence on the type of pattern that occur in a pipeline. The time series analysis was performed on the holdup time traces and average and distribution of the flow characteristics are reported (e.g., liquid holdup in the slug body, slug length and slug frequency). Moreover, the slug translational velocities were calculated using measured liquid holdup to evaluate the influence of air/water flow regimes at the dip. Comparison of results with literature was made in relationship with flow regime, liquid hold up and slug parameters.

Prior to this analysis, the nomenclature of the rig for discussion is presented in Figure 4-1. There are eight (8) conductivity rings on the experimental rig: the CR-1 & CR-2 are downhill section, CR-3 & CR-4 are downward-dip (entrance to the dip), CR-5 & CR-6 are upward-dip section (exist of the dip), CR-7 & CR-8 are uphill section. The DP-1, DP-2 and Dp-3 are the differential pressure transducers for downhill, dip and uphill sections respectively.

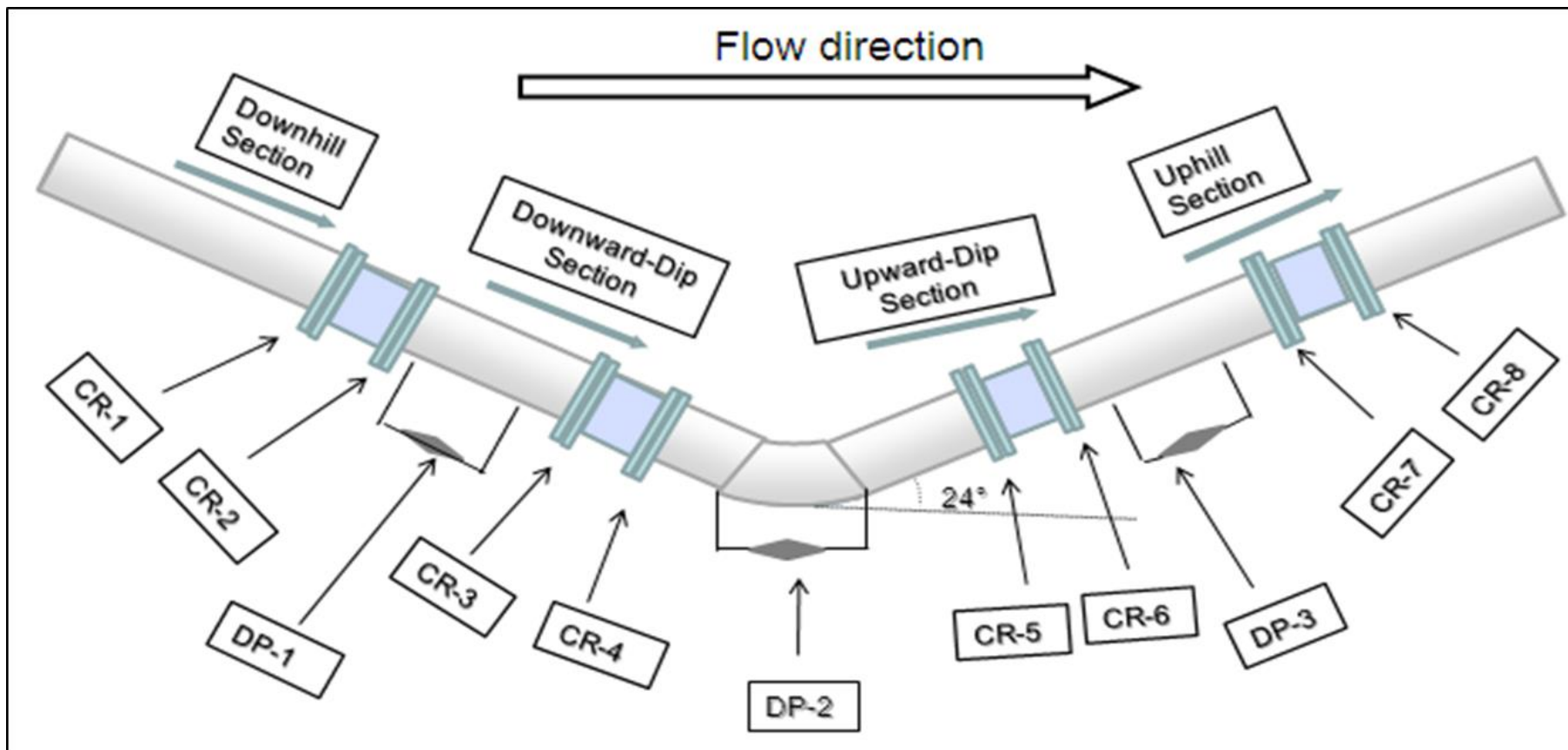


Figure 4-1: Instrument and rig nomenclature

## **4.1 Results of 24° Dip Pipeline Air-Water Experiment**

This section examined the various flow regime maps, liquid hold up and slug flow parameters (slug body hold up, slug velocity, average slug length, and slug frequency). Also, the flow interaction in 2-inch  $\pm 24^\circ$  dip pipeline and the slug initiation mechanism were investigated.

### **4.1.1 Flow Regime in 2-inch 24° Dip Pipeline**

The flow regime was assessed both by direct visual observation and analysis of conductivity ring time series data. The flow maps for different section of the dip pipeline were developed. Since different flow mechanisms are dominant in different flow patterns, correct identification of various flow patterns are basis for the prediction of liquid holdup.

#### **4.1.1.1 Air-Water Flow Regime for Downhill Section in 2-inch 24° Dip Pipeline**

Figure 4-2 shows the flow regime map in downhill section. Four different flow regimes were observed during the experiment: stationary air pocket, stratified flow, stratified with energetic ripples and aerated slug flow.

At low superficial liquid velocity, ( $V_{sl} = 0.07\text{m/s}$ ) and low superficial gas velocity ( $V_{sg} = 0.05\text{m/s}-0.1\text{m/s}$ ), a low liquid layer was observed flowing at the bottom of the pipe. Increasing  $V_{sg}$  did not change the level of the liquid thickness at this low  $V_{sl}$ .

At  $V_{sl} = 0.15\text{m/s}$  and  $V_{sg} = 2\text{m/s}$ , stratified flow with long energetic ripple of high liquid hold up was observed. Increasing the  $V_{sg}$  at this given  $V_{sl}$ , slugs were about to be initiated at the horizontal pipeline which got dissipated in the downhill section. This leads to increase in liquid hold up seen as energetic ripples.

At higher  $V_{sl}$  of  $0.55\text{m/s}$  and low  $V_{sg}$  ( $0.05\text{m/s}$ ); long air pockets were observed along the pipe as shown in Figure 4-3. As the  $V_{sg}$  increases higher than  $3\text{m/s}$ ; the slug coming from horizontal pipeline persisted and does not dissipates in downhill section.

The flow regime was dominated by stratified flow whereby the liquid flows along the bottom, of the pipe and air flow over it due to downward gravity force. Therefore, higher gas and liquid flow rate are required to cause a transition from stratified flow to other

flow regime. Within the range of the flow condition of this experiment, the transition occurred from the stratified flow (energetic ripple) to aerated flow at high liquid and gas velocities.

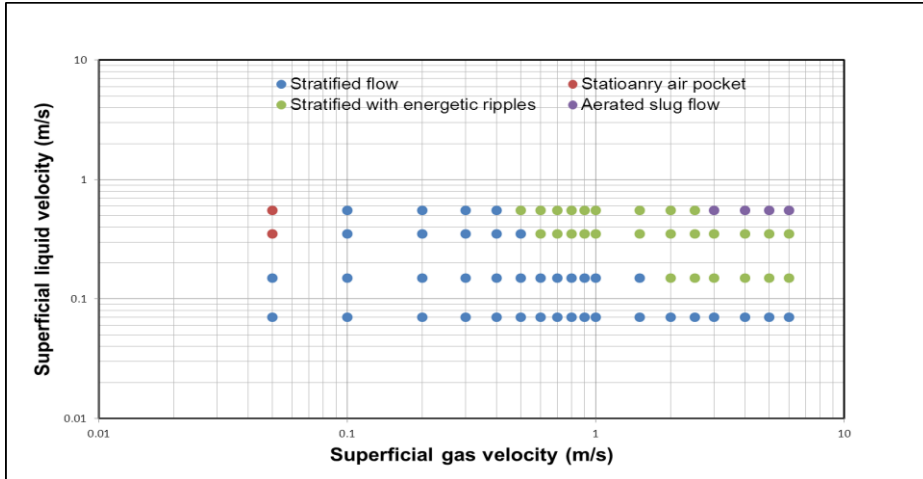


Figure 4-2: Air-water flow regime map for downhill 24° test section

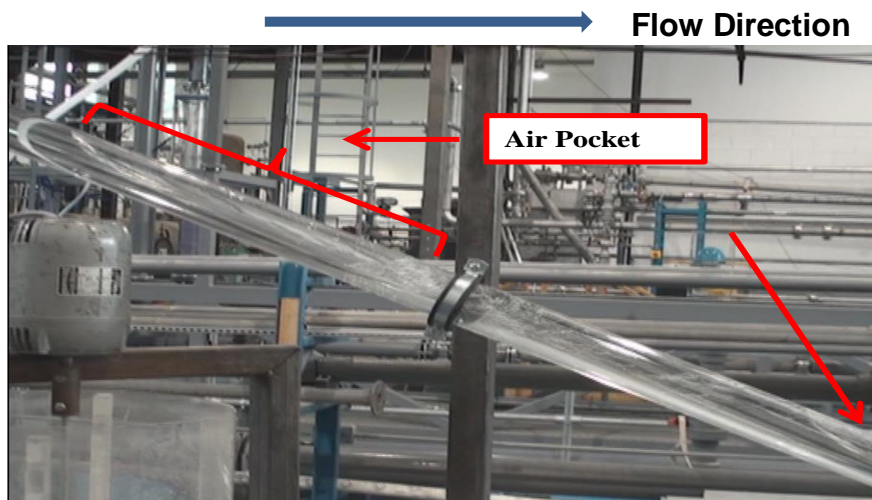
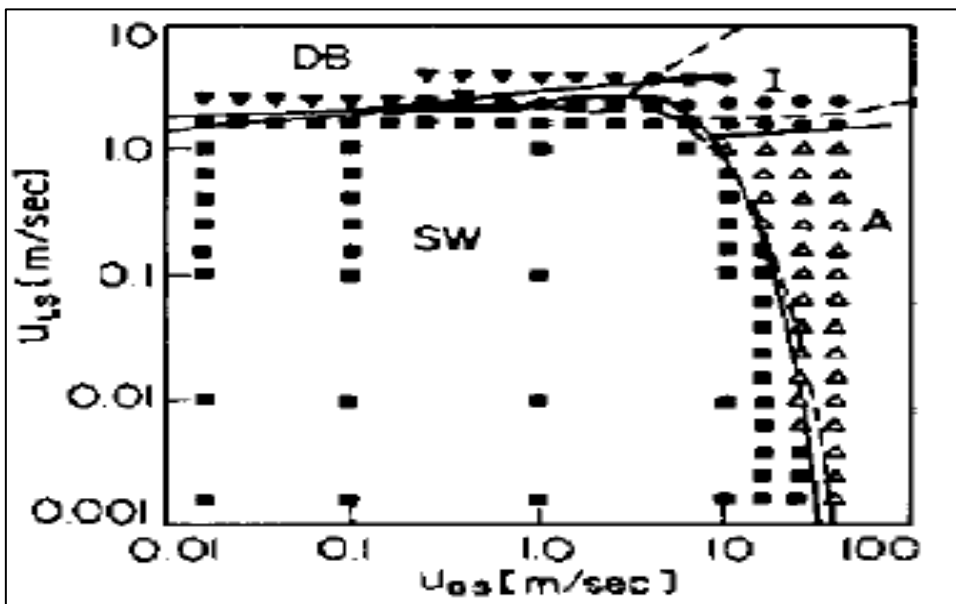


Figure 4-3: Air pocket downhill section at  $V_{sl} = 0.55$  m/s,  $V_{sg} = 0.05$  m/s

Comparison with Published Work: The downhill flow regime was compared with the experimental work carried out by Barnea et al., 1982, within 30° inclined pipes as shown in Figure 4-4. Their downhill flow regime result was defined as stratified wavy flow. There was no information about the stratified flow with energetic ripple in their

work. Their work reported that the stratified smooth flow was only observed for downward inclination less than  $10^\circ$ . The reason for their generalised result was based on their visual observation which is subjective to the observer. The stationary air pocket observed at  $V_{sg} = 0.05\text{m/s}$  and  $V_{sl} = 0.55\text{m/s}$  shown in Figure 4-3 was not reported, this may be subjective to rig design and pipe geometry. The aerated slug was not reported in their work. Comparing the two maps, the aerated slug flow condition was close to the transition to annular flow reported in their work. The deviation in the result could be as a result of the entrance effect, the change in geometry from the horizontal to inclined, and the length of the inclined pipe sections.



■ = Stratified Wavy Flow, ▼ = Dispersed Bubble Flow; Δ = Annular Flow; ● = Slug Flow

Figure 4-4: Flow pattern map,  $30^\circ$  downward inclination, 5.1 cm pipe (Barnea et al., 1982)

#### 4.1.1.2 Air-Water Flow Regime for Dip Section in 2-inch $24^\circ$ Dip Pipeline

##### Downward Dip Section:

The flow was mostly dominated by smooth stratified flow at the downhill section as illustrated in the flow regime in Figure 4-5 below. However, at low  $V_{sg} = 0.05\text{m/s}$ , the gas could not penetrate the liquid, thereby caused liquid accumulation. As the flow

rates increases, the flow regime changes to stratified flow similar to Barnea et al., 1982 work.

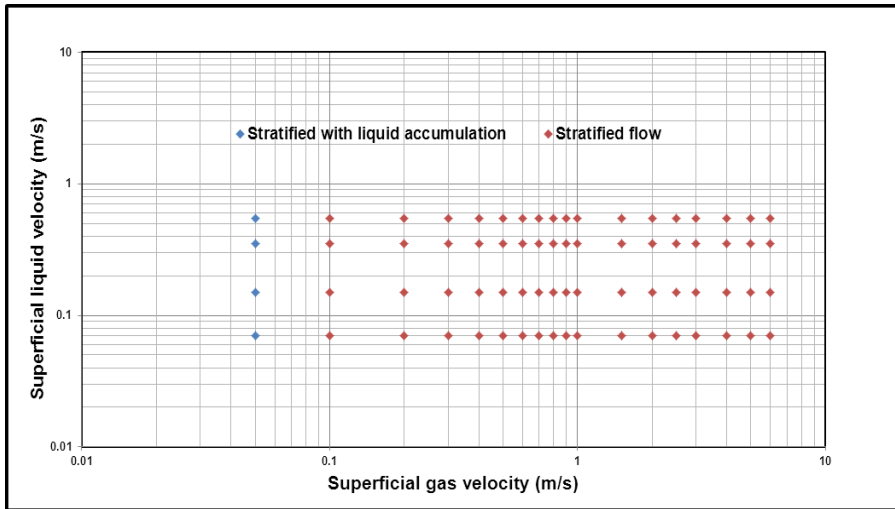


Figure 4-5: Air-water flow regime map for downward dip  $24^{\circ}$  test section

At very low gas flow rate, there was liquid accumulation due to gravity and no sufficient compressed gas to push the accumulated liquid down the dip. There was also back flow effect due to the accumulated liquid from the dip. Comparing the two maps in Figure 4-2 and Figure 4-5 (downhill and downward dip respectively); the stationary pocket in Figure 4-3 changed to stratified with liquid accumulation due to the critical flow condition of this section. Moreover, increase in the superficial gas velocity provides the much needed energy required by the hydrostatic head at the dip to flush the accumulated liquid out of the dip, consequently reduces the liquid holdup at the dip.

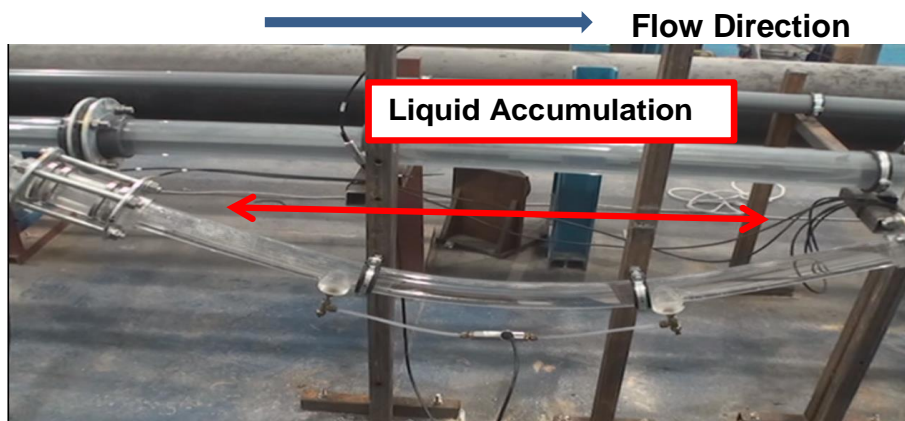


Figure 4-6: Liquid accumulation at the dip section at  $V_{sl} = 0.55$  m/s,  $V_{sg} = 0.05$  m/s



### Upward Dip Section

The flow characteristics in this section were different from the downward section with new definition of the flow pattern. This section experienced a film blockage due to the accumulated liquid; slug generation took place in this segment. It was also observed that at a given  $V_{sg}$  when slug is initiated (e.g.  $V_{sg} = 0.5\text{m/s}$ ), the slug generation position moved forward as the  $V_{sl}$  increases from  $0.15\text{-}0.35\text{m/s}$  as shown in Figure 4-7. This is due to the presence of more liquid capable of flushing liquid forward and prevents accumulation at the dip. The observation at this section is basically used to define the flow regime as shown in Figure 4-8.

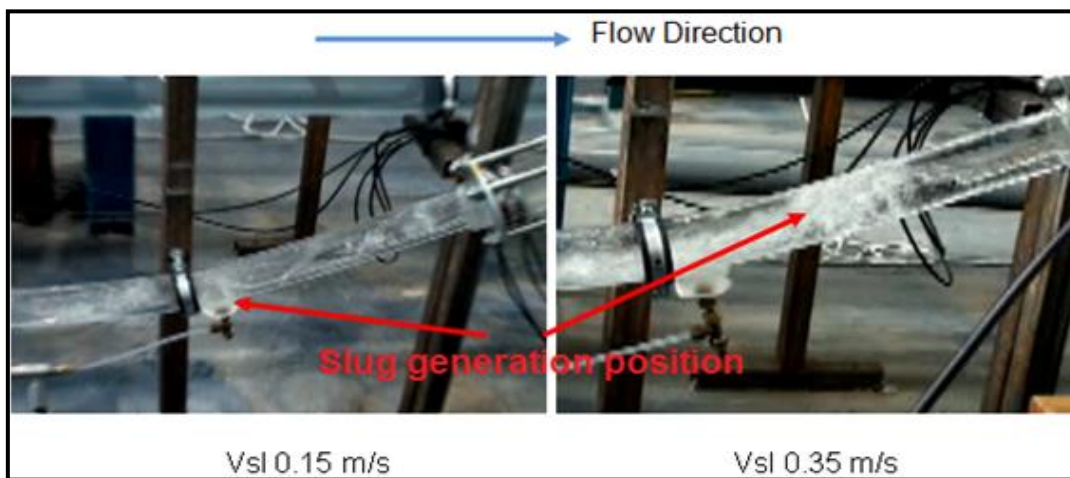


Figure 4-7: Slug generates position as  $V_{sg} = 0.5\text{ m/s}$ ,  $V_{sl} = 0.15\text{m/s}$  &  $0.35\text{m/s}$

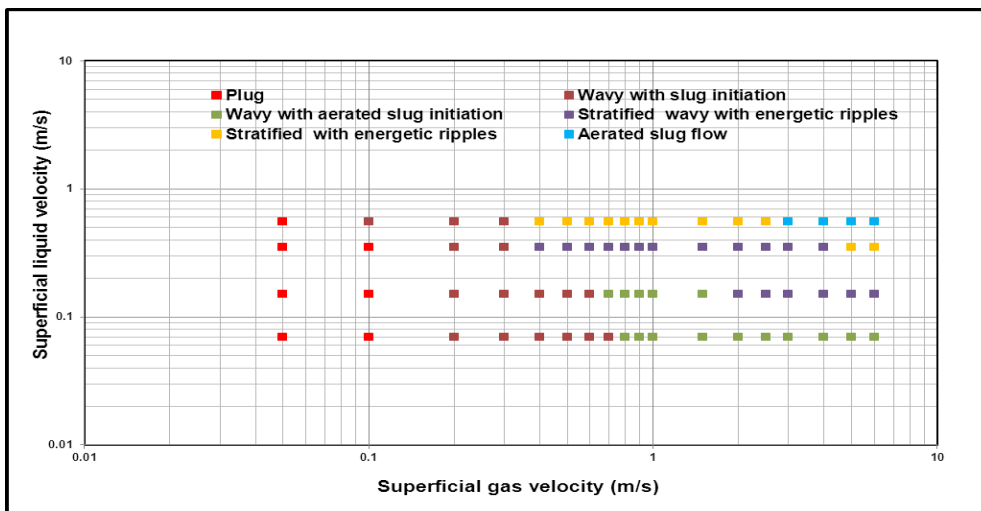


Figure 4-8: Air-water flow regime map for upward dip  $24^\circ$  test section

#### 4.1.1.3 Air-Water Flow Regime for Uphill Section in 2-inch 24° Dip Pipeline

Figure 4-9 shows the flow regimes map at this section. At low  $V_{sg}$  ( $=0.05\text{m/s}$ - $0.1\text{m/s}$ ), plug flow was observed with continuous gas bubbles travelling at the top of the pipe. Further increasing  $V_{sg}$ , the gas bubble tend to coalesce with each other to form slug. At a higher  $V_{sg}$  above  $0.7\text{m/s}$ , air bubble entrained and penetrates the liquid body. It forms a sequence of aerated slugs in the direction of flow.

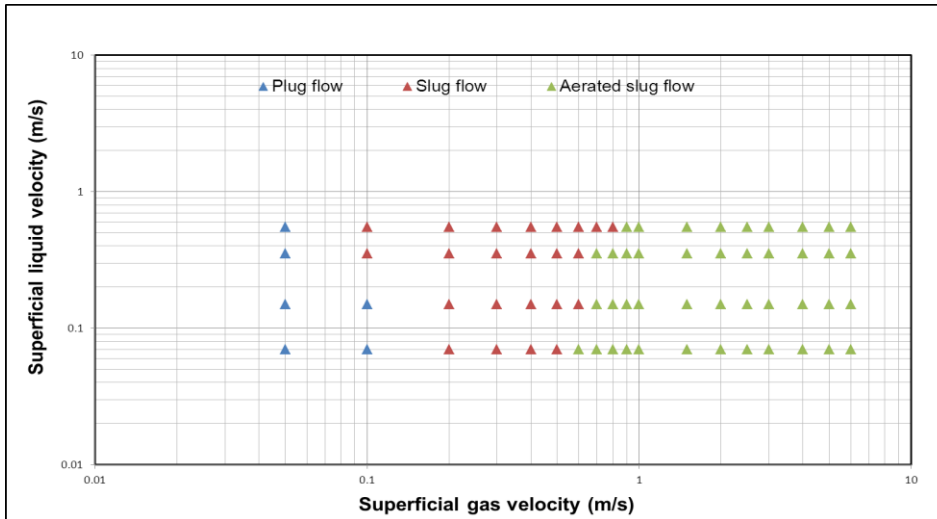


Figure 4-9: Air-water flow regime map for uphill section

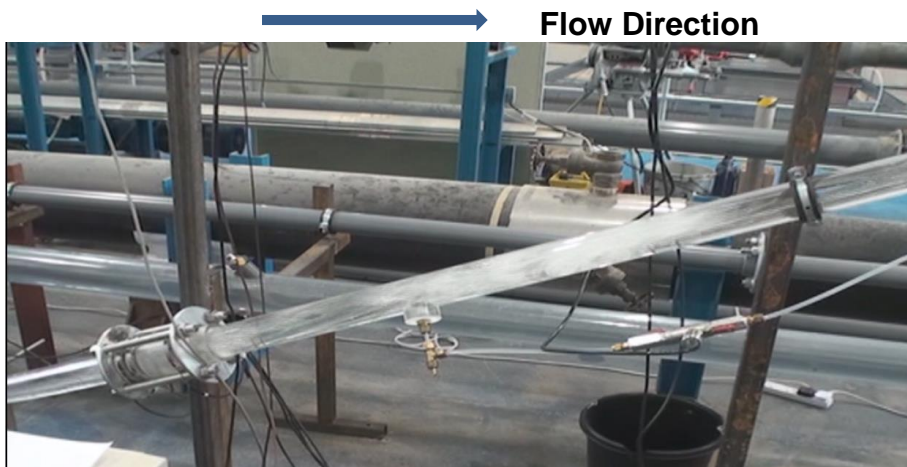
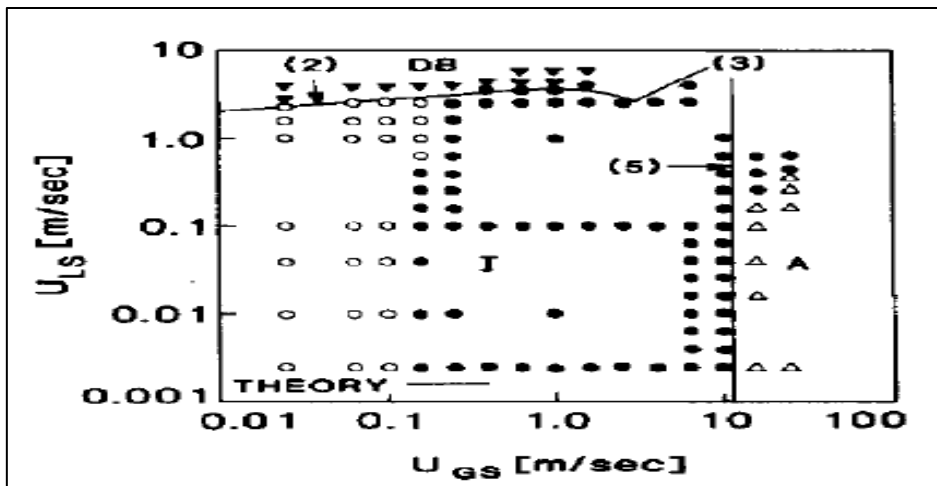


Figure 4-10: Aerated slug at the uphill section,  $V_{sl}=0.55\text{m/s}$  and  $V_{sg}=1.0\text{m/s}$

Comparison with published work: The flow regime was compared with the experimental work carried out by Barnea et al., 1980, with 20 degree upward inclined pipes.

Figure 4-11 shows the Barnea et al., 1980 flow regime with plug flow and slug flow within the flow regime that this experiment was carried out. However, their work could not distinguish between aerated slug and slug flow, rather generalised the whole section as slug flow. The reason for their generalised result was based on their classification of slug flow. The aerated slug was not reported in Barnea et al., 1980 work. Comparing the two maps, the aerated slug flow condition was close to the transition to annular flow reported in their work which could be as a result of flow interaction.



○ =Elongated Bubble, ▼= Dispersed Bubble Flow; △=Annular Flow; ●=Slug Flow

Figure 4-11: Flow pattern map, 20° downward inclination, 5.1cm pipe (Barnea et al, 1985)

In addition to visual observation discussed in this work; time traces was also used to identify and categorise the flow pattern.

#### 4.1.2 Data Analysis (Flow Regime)

The flow regime present in each of the flow cases was determined from visual analysis of video recordings and the time series of the collected data itself. The response of conductivity rings output voltage signal were converted to liquid hold up using the

normalized voltage and the calibrated curve of the individual signals of the conductivity rings. The time traces of liquid holdup detected the essential component of the series. (See Appendix B for the whole results).

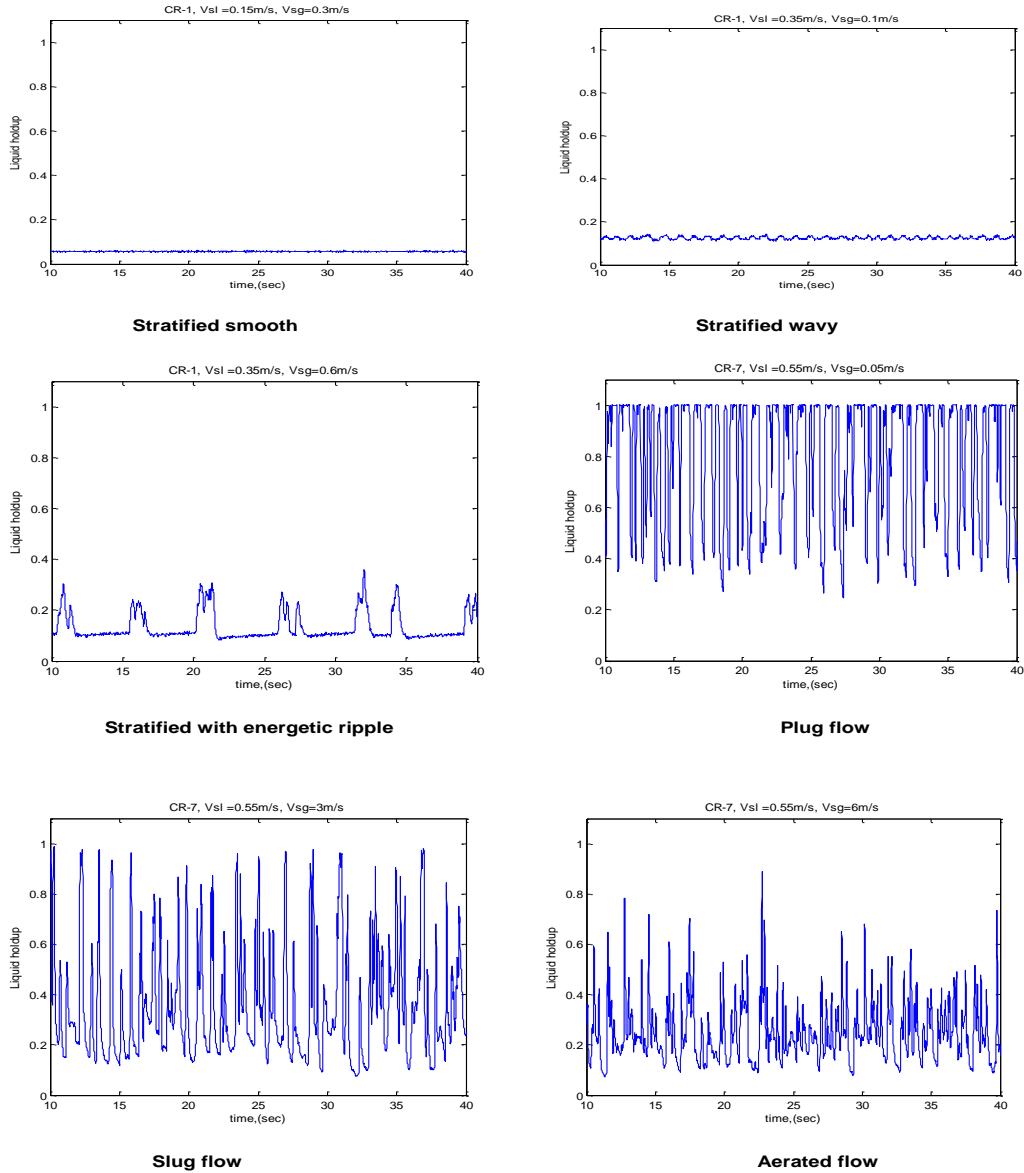


Figure 4-12: Typical time traces of the liquid holdup

### 4.1.3 Air-Water Flow Behaviour at the Dip in 2-inch 24° Test Section

The flow behaviour at the dip is a function of the  $V_{sl}$  and  $V_{sg}$ . The liquid accumulation at the dip was as a result of liquid coming from the downhill section, and the liquid falling- back from uphill section. Therefore, the flow behaviour at the dip is coupled with the flow conditions of the upstream downhill section and the downstream uphill section. The flow behaviour at the dip is qualitatively described as slug initiation or slug growth. Thus, three categories of slug behaviour observed in the experiment are:

1. **Complete Stratified flow downhill with slug initiation at dip:** The horizontal slug flow get completely dissipated as it enters downhill. This occurs at low and moderate  $V_{sg}$  where the stratified flow was not energetic enough to prevent liquid getting accumulated at the dip. This behaviour favours high inclination that resulted to liquid accumulation and slug initiation. As the velocity increases, there was a shift of slug initiation upward dip.
2. **Stratified flow with energetic ripple downhill with slug initiation and slug growth upward dip:** This occurred at moderate and high  $V_{sg}$  when the stratified flow was energetic enough to prevent the liquid accumulation at the dip, rather the ripple waves coalesce to form a pseudo-slug upward the dip. The occurrence of this behaviour was at high  $V_{sg}$  when the stratified flow was sufficiently energetic enough to pick up the liquid at the dip.
3. **Aerated slug downhill and slug growth at the dip:** It was observed that at very high  $V_{sg}$  (4-6m/s), the gas was blowing through the pipe and slug persist from horizontal into the downhill section. This occurred at a very high  $V_{sl}$  and  $V_{sg}$  when the downhill aerated slugs persist and slug growth occurred at the dip. This behaviour only occurred for few data points.

The flow behaviour described above is superimposed with the flow regime map for downhill section in Figure 4-13. The result shows that when the downhill is dominated as stratified flow, the condition at the dip is wavy with slug initiation which becomes aerated as  $V_{sg}$  increases. The stratified flow with energetic ripple persisted from downhill through the dip at high  $V_{sl}$  and  $V_{sg}$ . Aerated slug at the downhill also persisted through the dip. Plug flow was experienced at the dip at a very low  $V_{sg}$  (less than 0.1).

Comparing this work with Al-Safran et al., 2005 discussed in section 2.1.5, the different flow behaviour categories based on the visual observation was due to different inclination that was used.

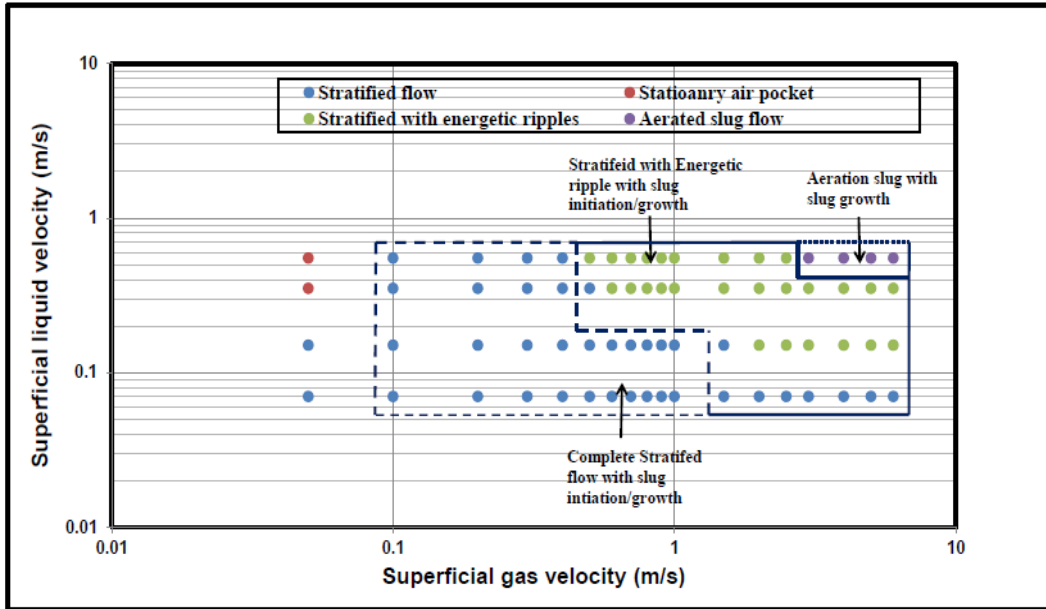


Figure 4-13: Air-water flow behaviour at dip-on downhill section, 24° test section

#### 4.1.4 Slug Initiation Mechanism at the Dip in 2-inch 24° Test Section

Slug flow mechanism at the dip depends relatively on flow conditions and pipe geometry. While the slug flow mechanism at the dip can be linked with the behaviour in the downhill section; it can also be characterised by investigating the slug parameters such as mean slug length, slug frequency and slug translation velocity at the dip and the uphill section.

There are basically two types of slug initiation mechanism at the dip, each producing totally different slug characteristics.

**Wave Growth Initiation Mechanism:** When liquid phase slowly accumulates at the dip from downstream and upstream under the effect of gravity. Consequently the gas flowing area at the dip section is reduced, leading to a local increase in gas velocity.

Velocities of slugs initiated are expected to fall and maintain high slug frequency and high liquid hold up (Nicklin et al., 1962). At the uphill section, wave growth initiation mechanism was peculiar with the smooth and relatively high liquid film in the bubble region.

**Wave Coalescence Initiation Mechanism:** This slug initiation mechanism was usually observed to be related to the coalescence of the very small waves initiated at the dip: which partially block the dip. The tiny waves move by the presence of high gas velocity along the uphill section where they coalesce to form slug. There was low frequency and low liquid holdup for slug coalescence. The slug flow structured are not fully slug but nevertheless could not be observed as waves. Visual observation shows that there was gas blowing through the slug body to form aerated slug, this distinguish them from waves.

This initiation mechanism is commonly observed at relatively high superficial gas velocity and low superficial liquid velocity (Al-Safran et al., 2005). This range of flow rates also depends on the inclination.

Relating these definitions to experimental observation, wave growth mechanism could only be achieved at the bottom of the dip section or when the liquid film was able to bridge the top surface of the pipe originally. Figure 4-14 illustrates the blockage effect and slug initiation at the bottom of the dip.

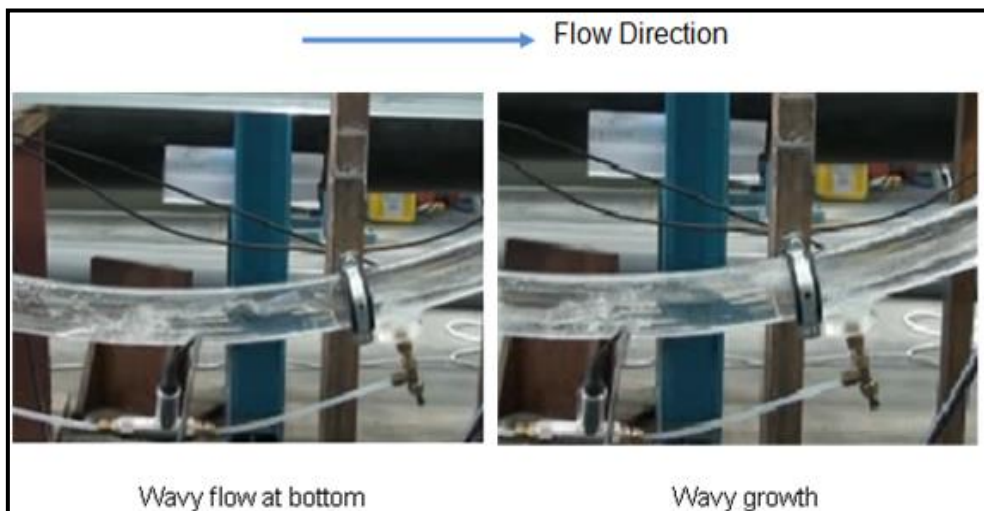


Figure 4-14: Slug initiation due to wave growth mechanism at  $V_{sl}=0.07\text{m/s}$ , and  $V_{sg}=0.6\text{m/s}$

Wave coalescence mechanism start to occur as the liquid velocity increases and the slug generated position moved out of the bottom section. At moderate gas velocity (e.g.  $V_{sl} = 0.15 \text{ m/s}$ ,  $V_{sg} = 1.0 \text{ m/s}$ ), as shown in Figure 4-15, wave flow was not able to block the pipe at the beginning. Then, another wave fell back from uphill section and merged with the former wave and bridged the top of the pipe. Slug was generated and transported immediately, as far as possible to coalesce with the next wave.

With reference to Al-Safran's investigation, wave growth initiation and wave coalescence initiation were observed at the dip section of this work. However, these two slug initiation mechanisms are only partially executable in this work. The reason is due to the difference in the inclination ( $\pm 24^\circ$ ) in this work compared to  $\pm 0.915^\circ$  and  $\pm 1.93^\circ$  in Al-Safran's work.

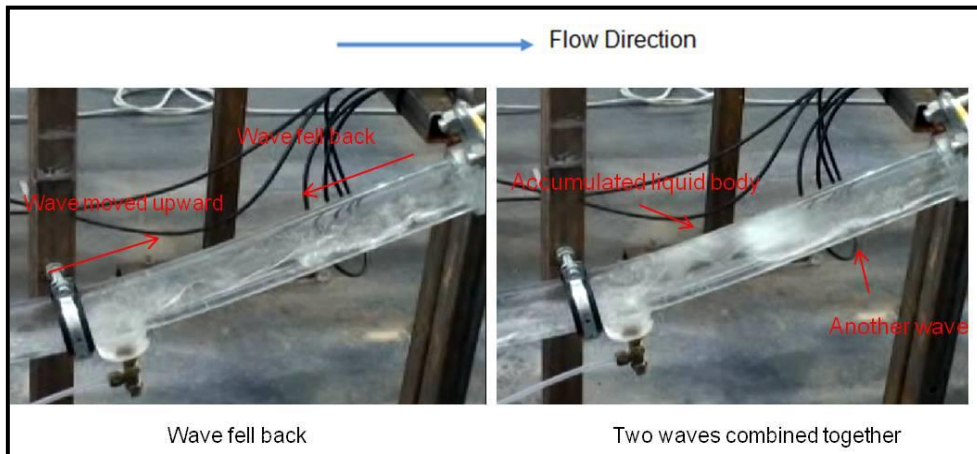


Figure 4-15: Wave coalescence initiation at  $V_{sl} = 0.07 \text{ m/s}$ ,  $V_{sg} = 1.5 \text{ m/s}$

#### 4.1.5 Liquid Holdup in 2-inch 24° Dip Pipeline

The liquid hold was measured using conductivity rings at various section of the pipe in form of time series. This was used to determine the average liquid hold.

Figure 4-16 showed that the average liquid holdup was generally low for downhill flow. The liquid hold up for downward inclined flow is independent on the superficial gas velocity, while upward flow in Figure 4-17 is dominated by intermittent flow. There is significant effect of superficial gas velocity on liquid hold up for uphill section. This was expected and can be explained as follows: for downhill flow, the liquid moves faster



due to the gravity effect resulting in lower liquid holdups; for uphill flow there is an increase in gas flow rate that promote formation of slug which sweeps down the liquid with higher driving velocity behind it.

In addition, the slope of the curves in Figure 4-17 is very steep at low velocity and a small change in gas velocity causes a substantial change in liquid holdup. However, at high gas velocities, the liquid hold is becoming almost constant, this could be as a result of the aerated slug flow approaching.

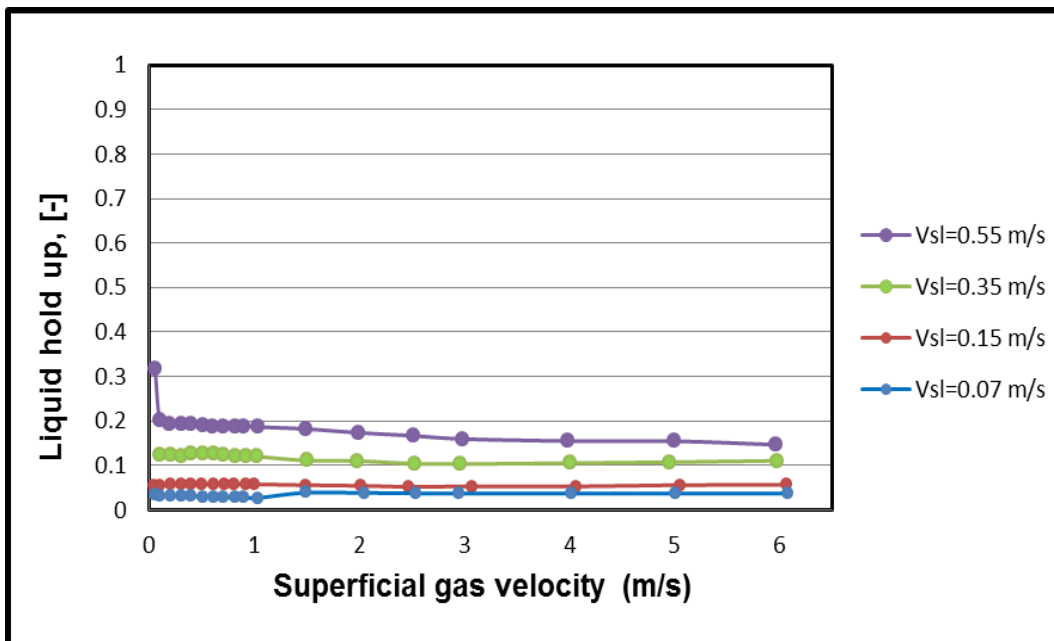


Figure 4-16: Overall-average liquid hold at CR-1, 24° downhill test section

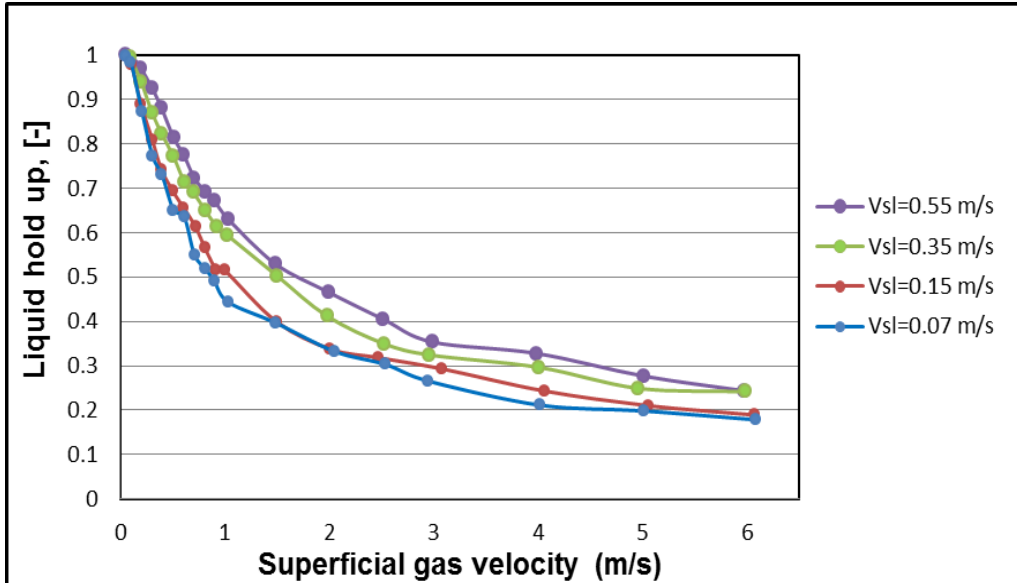


Figure 4-17: Overall-average liquid hold at CR-7, 24<sup>o</sup> uphill test section

Comparison with published work: Correlations from the literature similar to the present work are used to calculate liquid holdup, and are compared (based on the flow condition) with the liquid holdup data obtained in the present work.

Greskovich, 1972 describes liquid hold correlation using in-situ volume fraction and input liquid content. In this work, the measured or calculated liquid hold up (i.e. In-situ volume fraction) is different from the inlet of the pipe liquid content (also known as - Input liquid content given as  $(V_{sl} / V_{sm})$ ). At the downhill section (Figure 4-18), liquid holdup is less than the input liquid content. Conversely for the uphill (Figure 4-19), the liquid holdup is higher than the input liquid content. This is expected as liquid move faster due to gravity in downhill section while the gas phase slip faster at the uphill section.

Beggs and Brill, 1973 correlation under predict the result for the uphill section of the pipe as shown in Figure 4-20 and Figure 4-21. The reasons for these discrepancies could be as a result of difference in pipe diameter and the measurement techniques. Moreover, the correlation is based on the modification for horizontal systems and the influence of dip configuration; Moreover, Beggs and Brills, 1973 correlation has been reported to be less reliable at low flow rates (Minami and Brill, 1987).

Mattar and Gregory 1974 proposed correlation for liquid holdup was developed specifically for slug flow at inclination angles less than  $10^\circ$ . This correlation (Figure 4-22 and Figure 4-23) is in a better agreement with the experimental result.

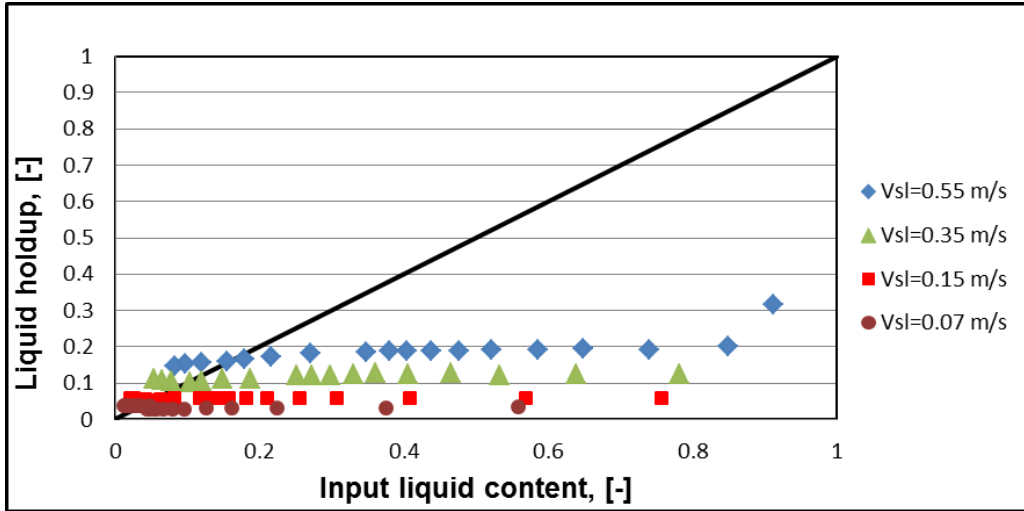


Figure 4-18: Comparison of measured overall liquid holdup and predicted by Greskovisch, 1972 for CR-1, downhill test section

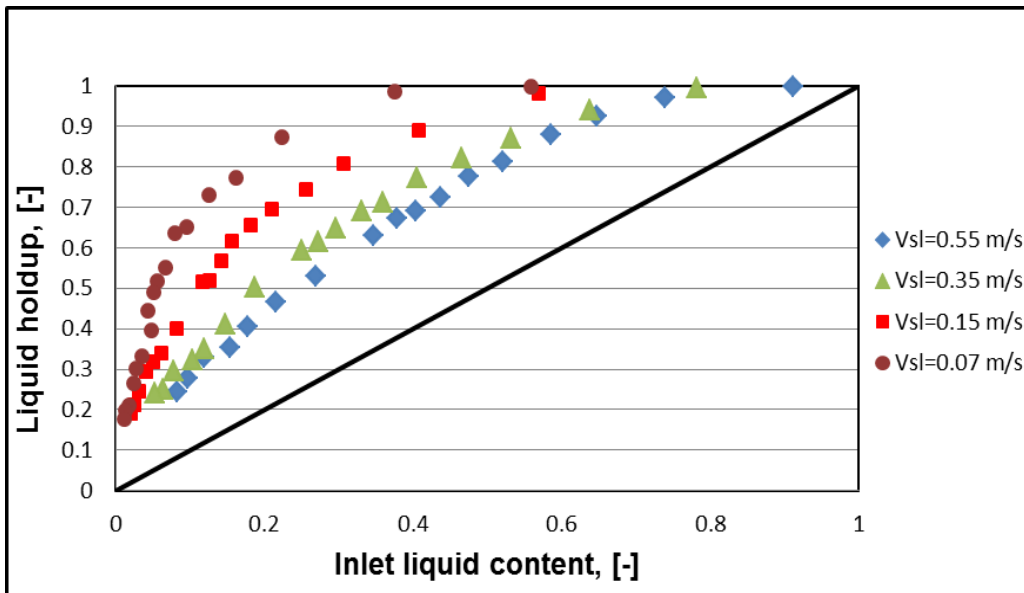


Figure 4-19: Comparison of measured overall liquid holdup and predicted by Greskovisch, 1972 for CR-7, uphill test section

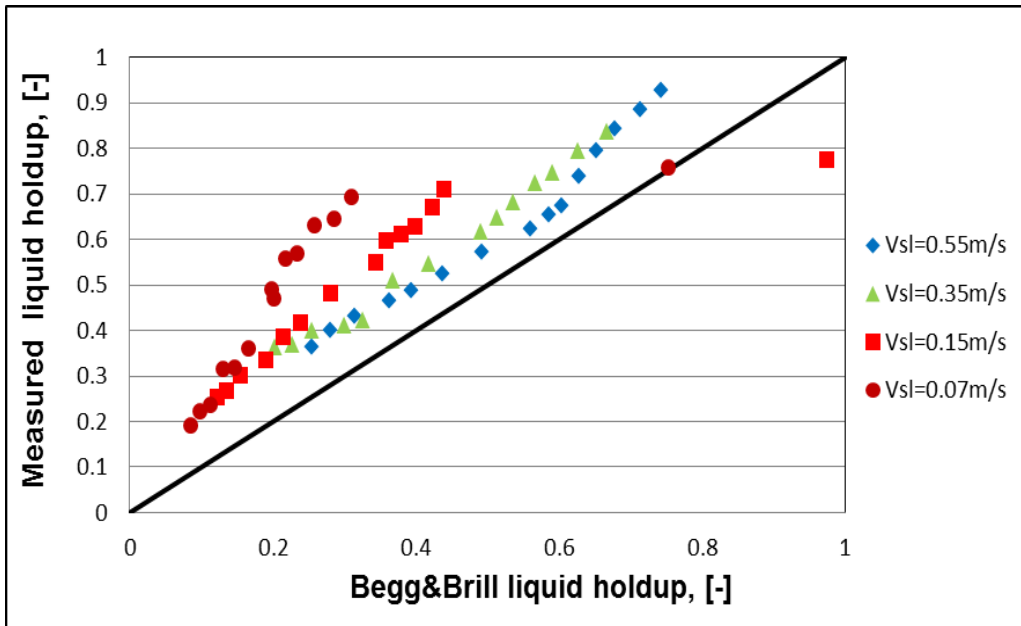


Figure 4-20: Comparison of measured overall liquid holdup and predicted by Beggs and Brill, 1973 for CR-5, upward dip test section

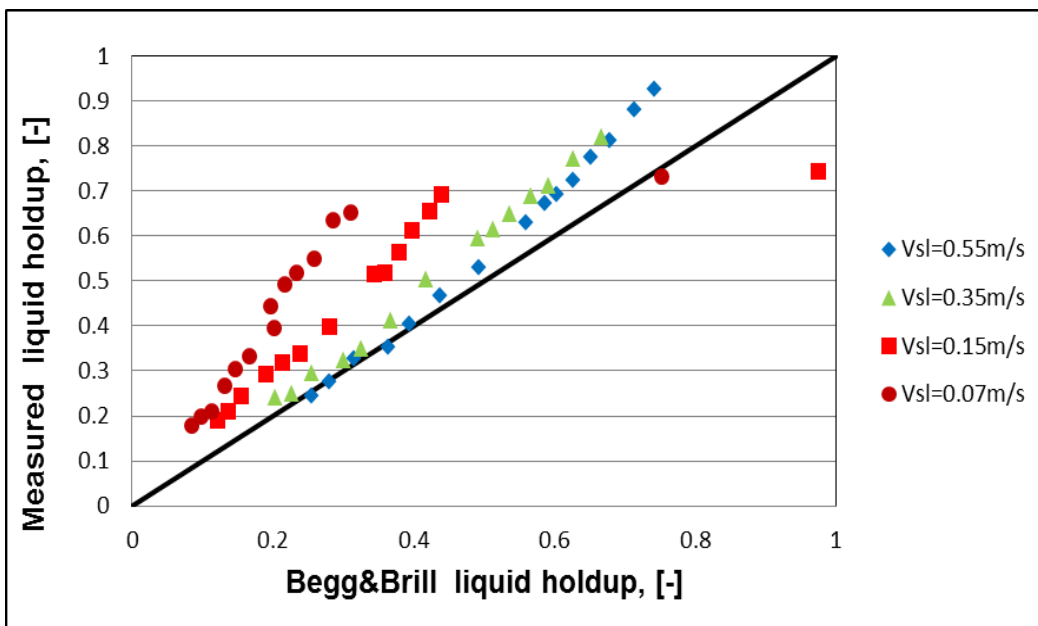


Figure 4-21: Comparison of measured overall liquid holdup and predicted by Beggs and Brill, 1973 for CR-7, uphill test section

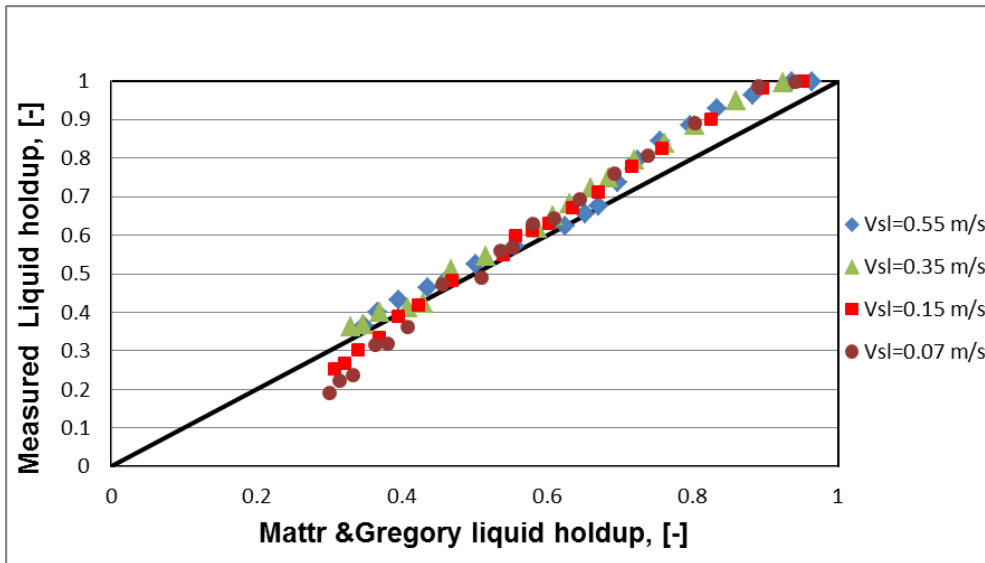


Figure 4-22: Comparison of measured overall liquid holdup and predicted by Mattr and Gregory, 1974 for CR-5, upward dip test section

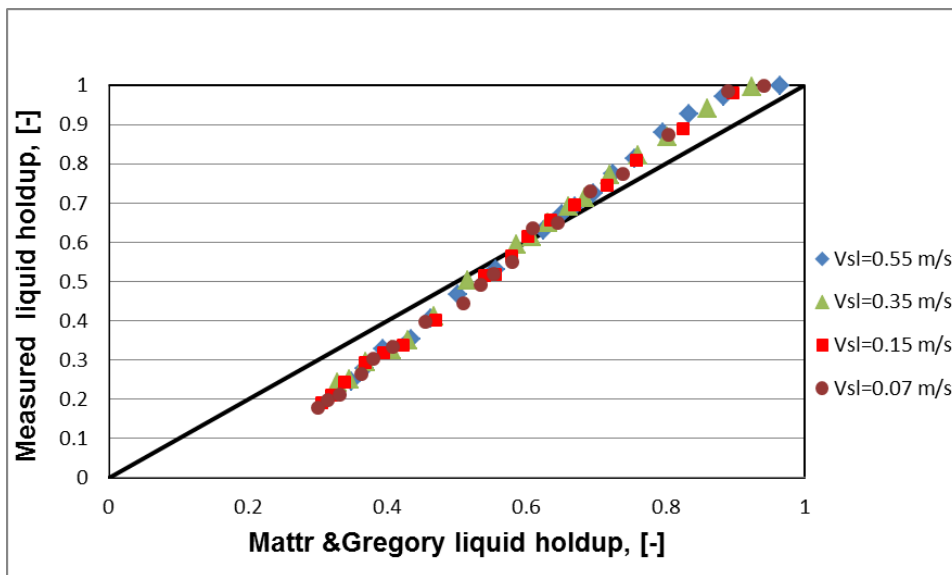


Figure 4-23: Comparison of measured overall liquid holdup and predicted by Mattr and Gregory, 1974 for CR-7, uphill test section

#### **4.1.6 Slug Flow Characteristics in Air-Water for 2-inch 24° Dip Pipe**

Slug flow is one of the most prevalent flow patterns encountered during production and transportation of oil and gas. It exists over a wider range of gas and liquid flow rate; and pipe geometry.

Typical time series of slugs from conductivity rings and physical observation determine two major types of slugs along the uphill section:

Regular slugs are fully structured slug with distinct slug body and film section while aerated slugs are slugs that bridge pipe wall but with gas blowing through the slug body. Aerated slugs are shorter and more aerated than regular slug. According to Nydal et al. (1992), they are regarded as non-developed slugs.

In addition, there is another stratified wavy behaviour which occasionally blocked the pipe and travel at a lower velocity. It is necessary but difficult to distinguish between wave and slug that are present in the inclined section (Hanyang and Liejin, 2008).

The common procedure is to consider a trigger level such that slug which does not achieve the threshold level ( $T_{L,slug}$ ) is considered travelling waves. However, defining the optimal threshold value is subjective to the investigator.

In order to distinguish regular slug flow from other flow behaviour, a statistical analysis of slug flow was carried out whereby liquid holdup time traces were subjected to various thresholds (0.4, 0.5, 0.6, 0.7 and 0.8) for all position in the uphill section. The result presented in Appendix C.3 show that threshold of 0.7 fairly accounts for the slug in the pipe.

##### **4.1.6.1 Slug Liquid Holdup in 2-inch 24° Dip Pipeline**

The slug liquid holdup was measured by applying threshold level processed from the time series liquid holdup as presented in Appendix C.3. The variation of liquid hold up in the slug body with superficial gas velocity is given in Figure 4-24 and Figure 4-25 below for two of the conductivity rings at the uphill section for discussion. For all the results, liquid holdup approaches unity as the superficial gas velocity approaches zero.

The results showed that for a given  $V_{sl}$ , the slug liquid holdup decreases as  $V_{sg}$  increases for uphill section of the pipe. This explains the fact that as the gas increases, it swept more liquid away and prevented the liquid to bridge up the pipe easily.

At low  $V_{sg}$ , the slug liquid hold up at upward section of the dip is greater than the downstream of the uphill. Further increasing the gas velocity causes the coalescence of waves with slugs. Merging of the waves and slugs occurred as indicated in Figure 4-24 & Figure 4-25 with slug liquid holdup of CR-5 greater than CR-7 at low  $V_{sg}$  and the reverse is the case at high  $V_{sg}$ . The reason could be as a result of the type of slug flow initiation mechanism at this flow conditions.

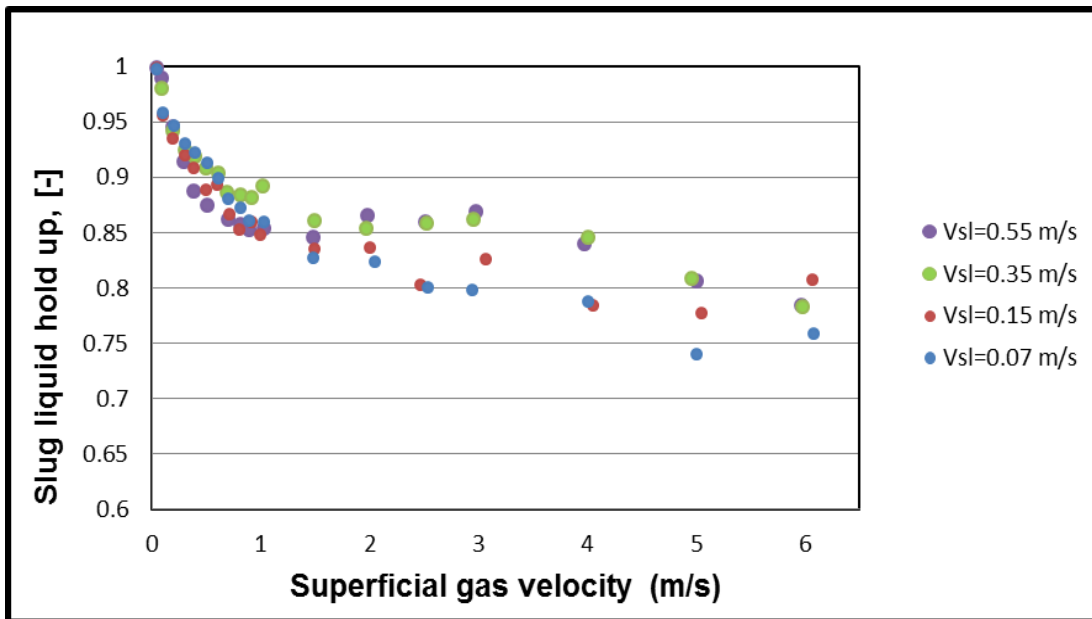


Figure 4-24: Slug liquid holdup for uphill section at CR-5

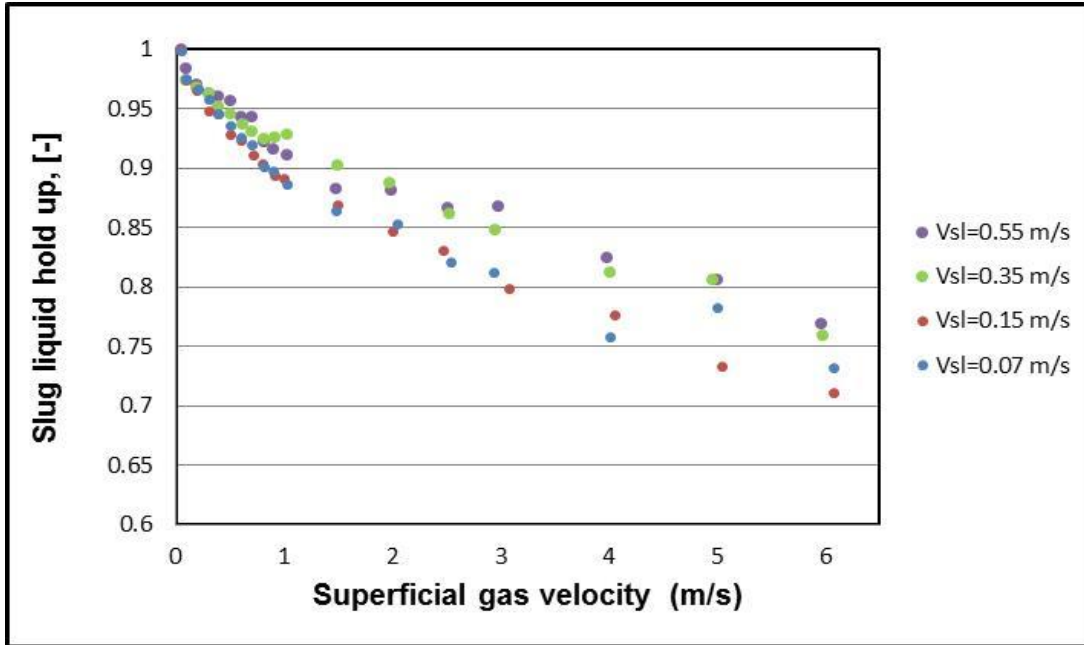


Figure 4-25 Slug liquid holdup for uphill section at CR-7

#### 4.1.6.2 Slug Frequency in 2-inch 24° Dip Pipeline

Slug frequency is the number of slug passing through per unit time at a specific location in the pipe. This work investigate the effect of the superficial gas velocities on slug frequency at the dip section for a given superficial liquid velocities.

The frequency of each conductivity ring was determined by counting the number of slugs (peaks) above the threshold of 0.7 in the time series plot for a given Vsl and Vsg.

Figure 4-26 shows that at a given superficial liquid velocity, the slug frequency decreases as the superficial gas increases. At a given gas velocity, the slug frequency decreases as the superficial liquid decreases.

Figure 4-27 shows an overlapping (relative constant) of the slug frequency result for all the conductivity rings uphill, this is more obvious at high flow rates. This is similar to Zheng et al., 1993 observation where the slug frequency is constant through the hilly terrain at high liquid flow rates. Also comparing the slug frequency upstream dip (CR-5 and CR-6) to the downstream dip (CR-7 & CR-8) in Figure 4-27; at low Vsl, the slug



frequency is higher for CR-5/6 than CR-7/8 at low Vsg. This is because some of the slug decay along this section and only few of them survive through the entire pipe.

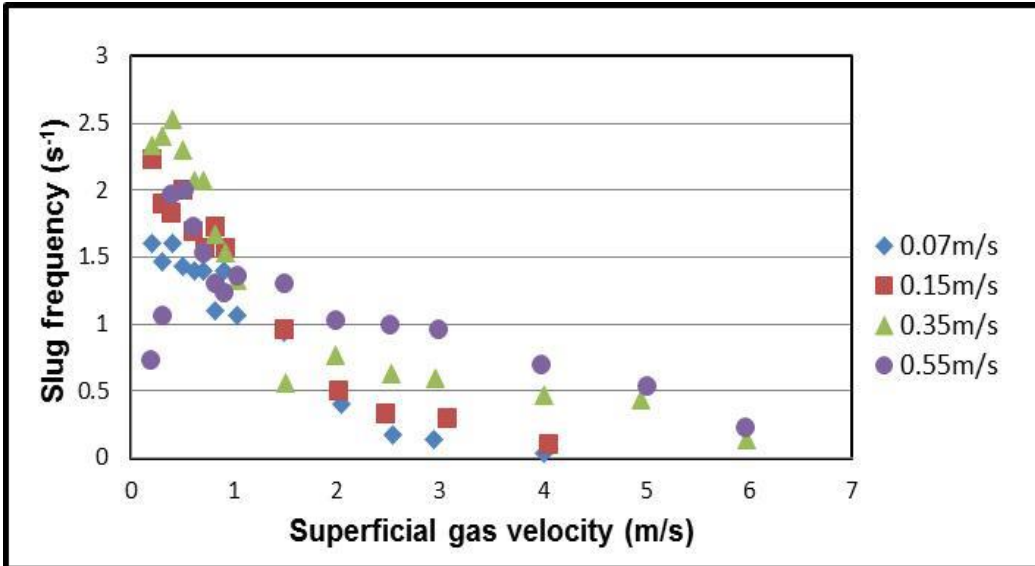


Figure 4-26: Slug frequency in the slug body for uphill section (CR-5)

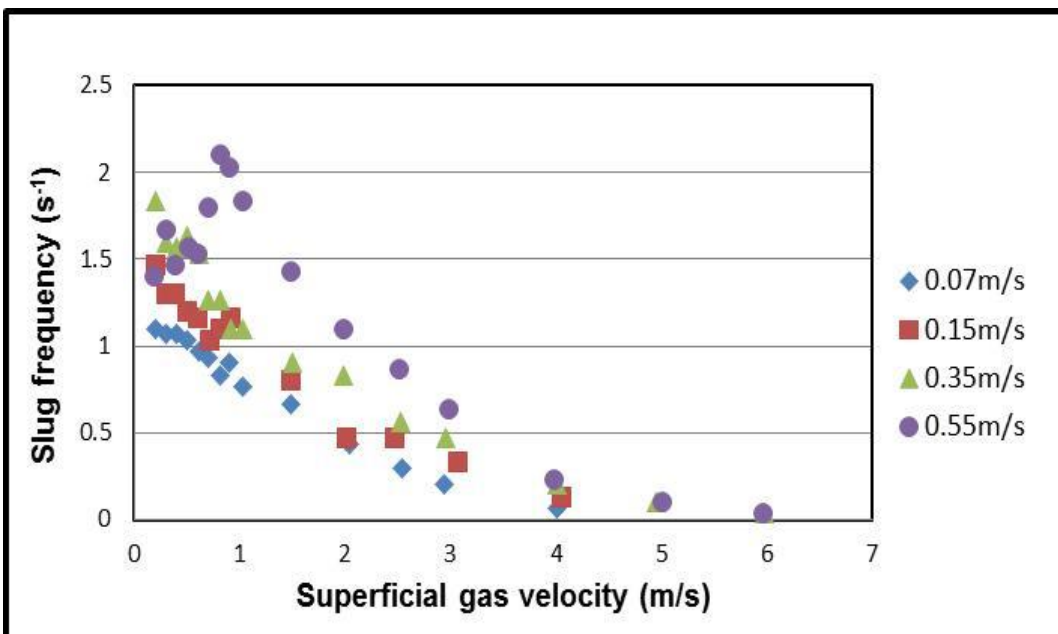


Figure 4-27: Slug frequency in the slug body for uphill section (CR-7)

#### 4.1.6.3 Slug Translational Velocity in 2-inch 24° Dip Pipeline

The slug translational velocity is calculated using the cross correlation techniques of two signals from a pair of conductivity ring installed apart.

Cross-correlation of the liquid holdup time series produced by the two conductivity rings upward the dip section (CR-5 and CR-6) and uphill section (CR-7 and CR-8) allows the translational velocity of periodical structures such as slugs to be determined. A plot of time series for the two conductivity rings is shown in Figure 4-28.

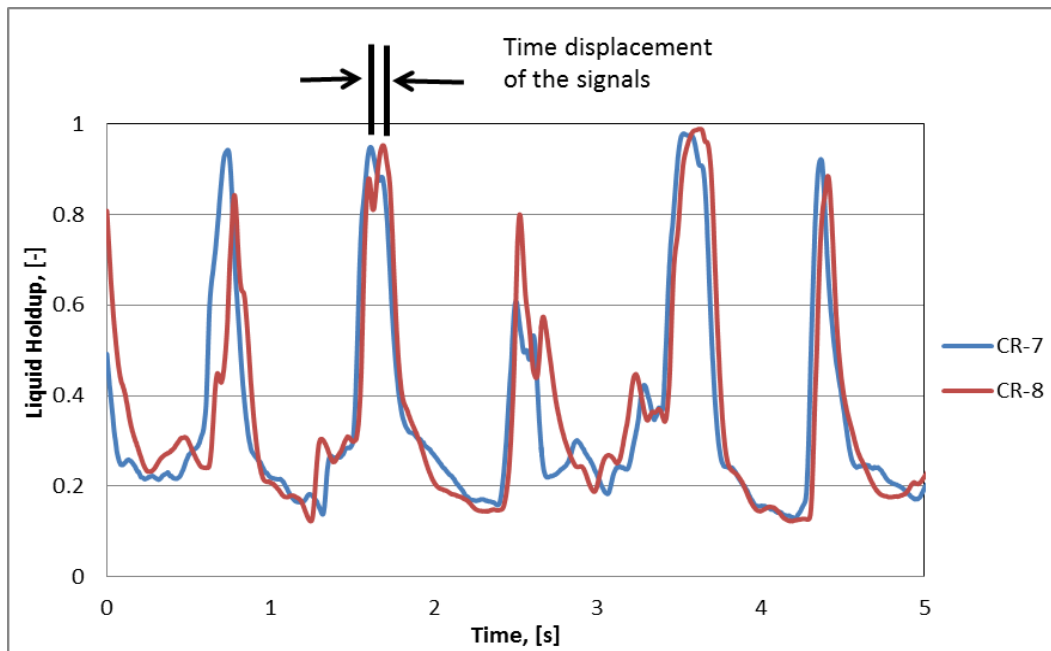


Figure 4-28: Liquid holdup signal from two conductivity ring uphill section (CR-7 and CR-8), +24° Inclination,  $V_{sl}=0.15\text{m/s}$  and  $V_{sg}=1.5\text{m/s}$

The character of each signal is distinguished by only two variables, the amplitude of the fluctuations and their frequency. In the general theory of harmonic analysis, an expression of considerable importance and interest is periodic functions described in section 3.4.1.

The cross correlation is a measure of the similarity between any two different signals and is a function of the relative time between the signals, sometimes called the sliding dot product. Figure 4-30 shows the cross correlation plot corresponding to the pair of

liquid holdup signals in Figure 4-28. This is a typical cross correlation plot is similar for the rest of the experiments performed.

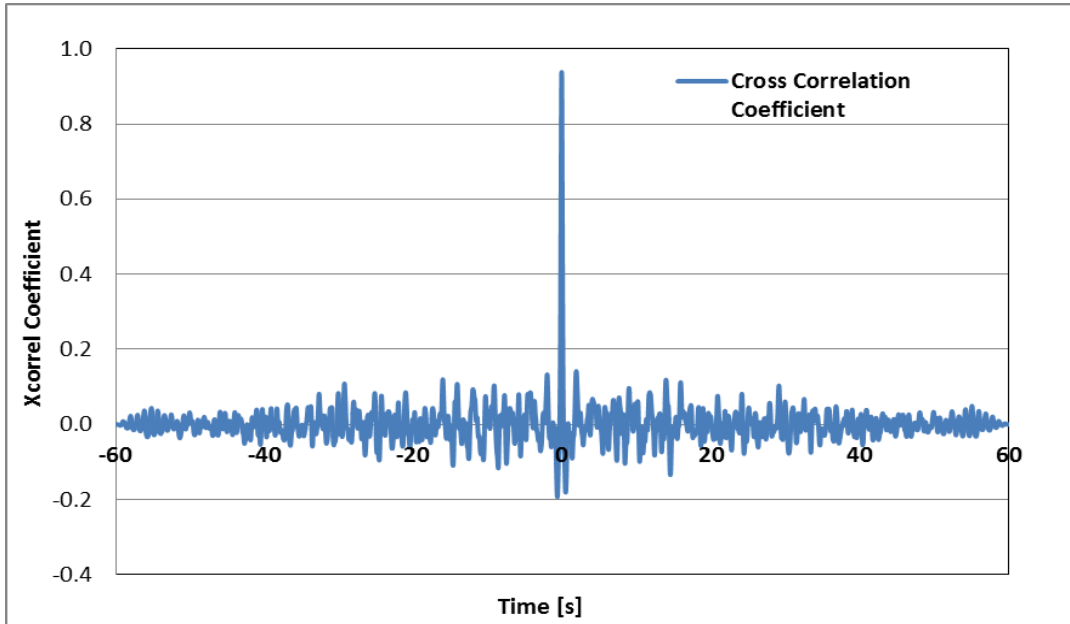


Figure 4-29: Cross correlation coefficient for the two liquid holdup signals of Figure 4-28

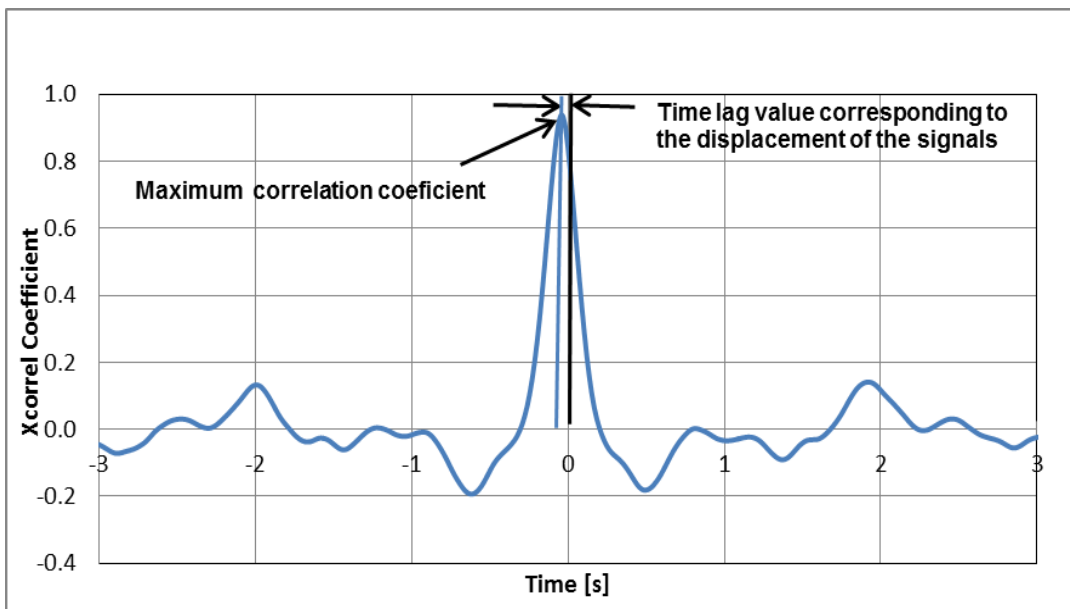


Figure 4-30: Cross correlation coefficient extract from Figure 4-29

Correlation is computed into what is known as the correlation coefficient, which ranges between -1 and +1. Following the procedure explained above, the slug translational velocity was calculated for all the slug flow and the results are presented below in Figure 4-31 and Figure 4-32.

The slug translational velocity result presented in Figure 4-31 & Figure 4-32 below, appears that the slug translational velocity increases linearly with superficial velocity up to certain point and then remain relatively constant from  $V_{sg}=3\text{m/s}$ . The transition from linearity to constant at  $V_{sg} =3\text{m/s}$  is due to the slug flow structure of aerated slug present at this flow condition (Nicklin et al., 1962; Bendiksen, 1984; Nicholson et al., 1978).

Many researchers of multiphase flow considered slug translational velocity to be linearly dependent on the mixture slug velocity (Nicklin et al., 1962; Bendiksen, 1984; Nicholson et al., 1978). This subject has been treated extensively both for vertical case with elongated bubbles, horizontal and upward inclined case. Bendiksen, 1984 proposed a practical formula for the drift velocity.

Similarly, Figure 4-36 presented the correlating linear line for the different uphill sections (CR5/6 and CR7/8) with their relationships and regression coefficient. However, the conditions that the intermittent flow data deviate from these linear lines are considered to distinguish regular slug from aerated slug; and to determine the transition to other flow regime. Figure 4-36 shows that none of the linear plot intercepts at the origin but rather intercept at the y-axis. This indicates there is presence of drift velocity component. The reason for the different linearity is due to the dynamics of slug initiation that changes along the pipe.

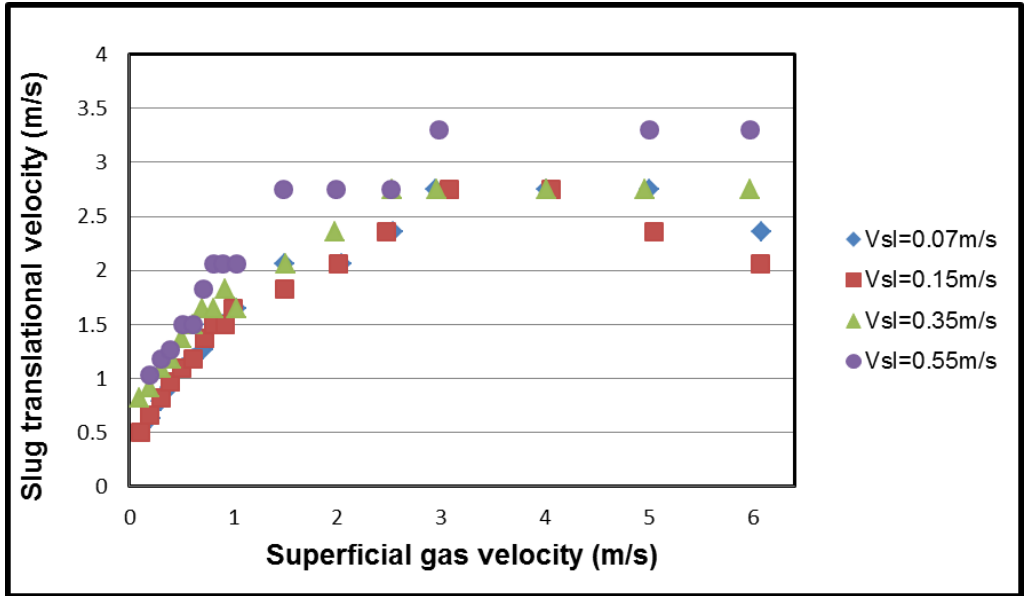


Figure 4-31: Slug velocity for uphill section at CR-5/CR-6

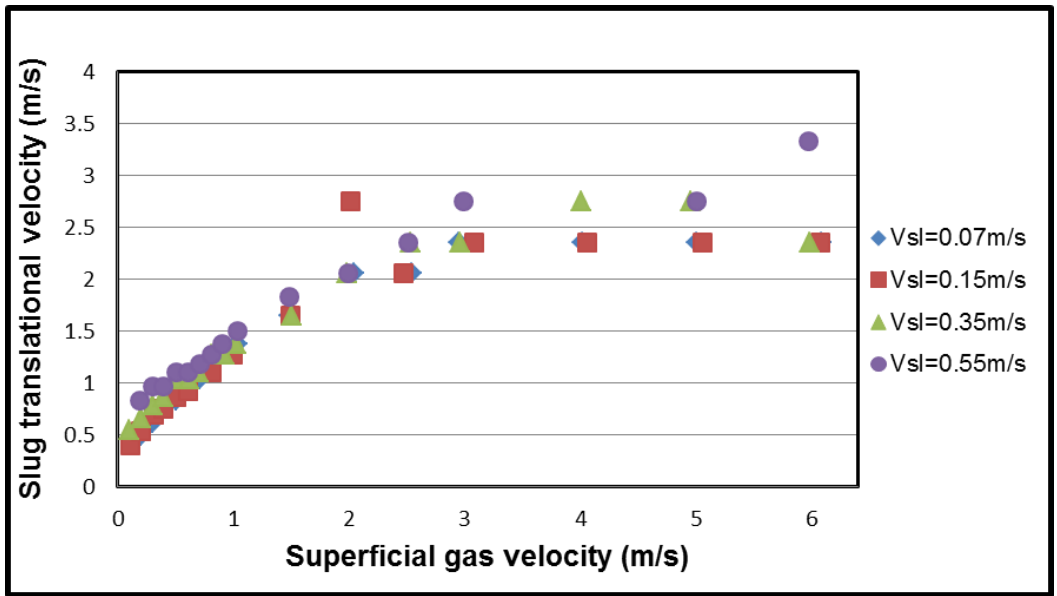


Figure 4-32: Slug velocity for uphill section at CR-7/CR-8

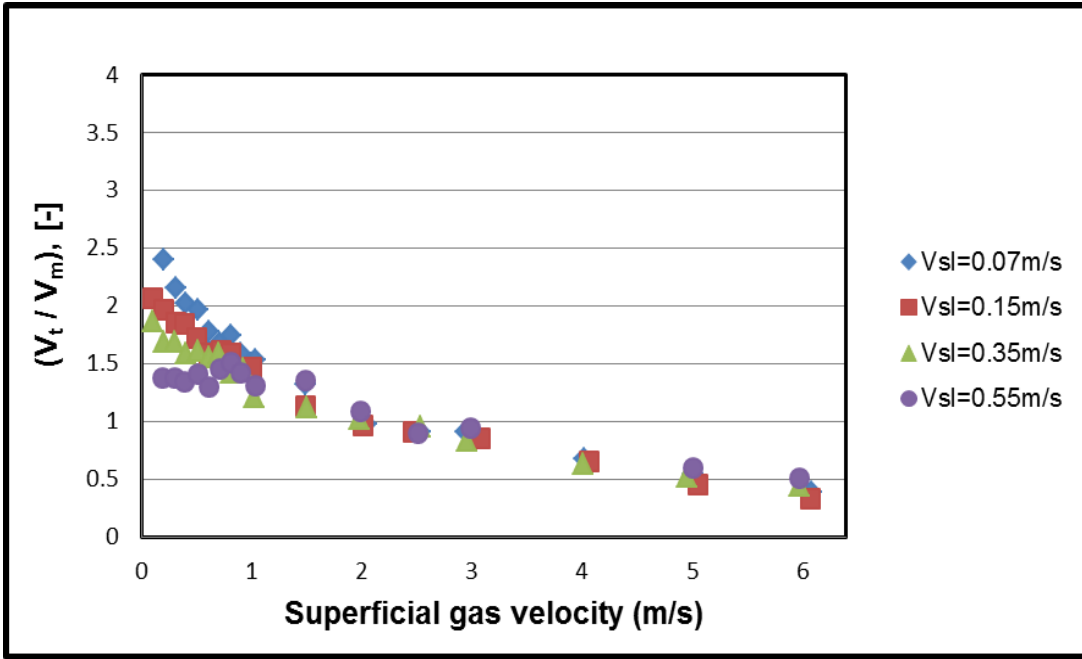


Figure 4-33: Dimensionless slug velocity for uphill section at CR-5/CR-6

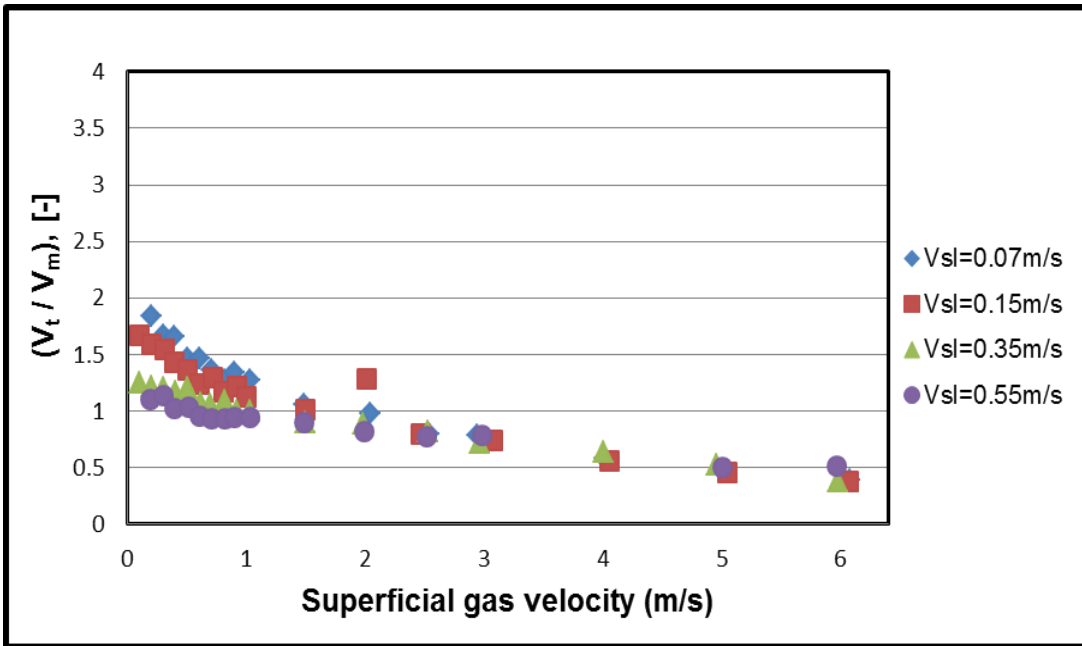


Figure 4-34: Dimensionless slug velocity for uphill section at CR-7/CR-8

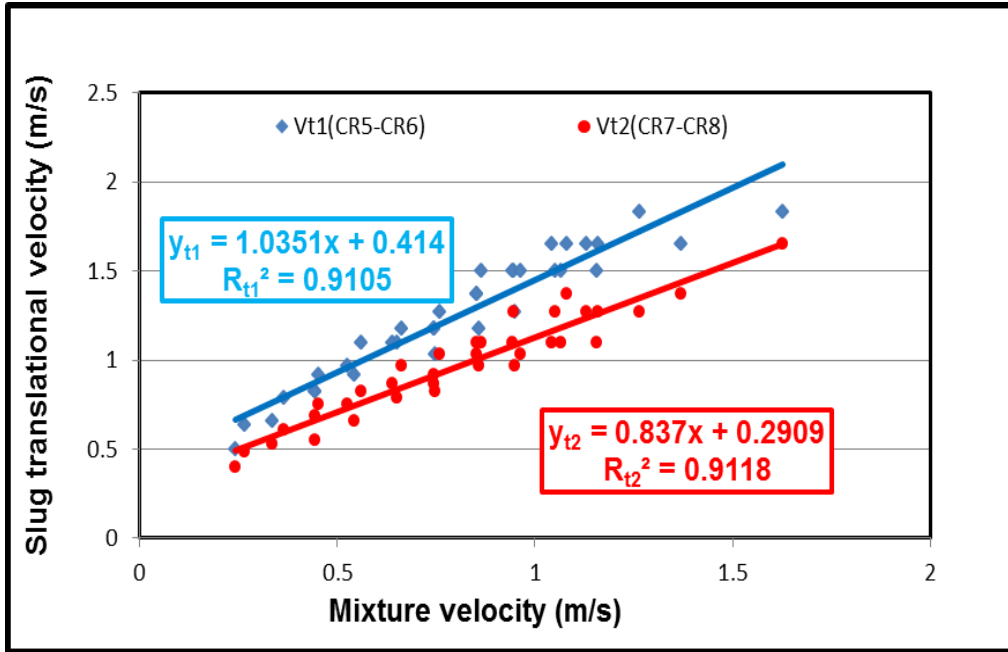


Figure 4-35: Slug translational velocity against mixture velocity for uphill section

Comparison with published work: It was observed in Figure 4-36 below that the drift velocities in this work is higher than the values predicted by Bendiksen, 1984 which is a weighted interpolation between the horizontal and vertical cases. This may be due the different liquid velocity profile that exists in the aerated slug and also due to the influence of the dip.

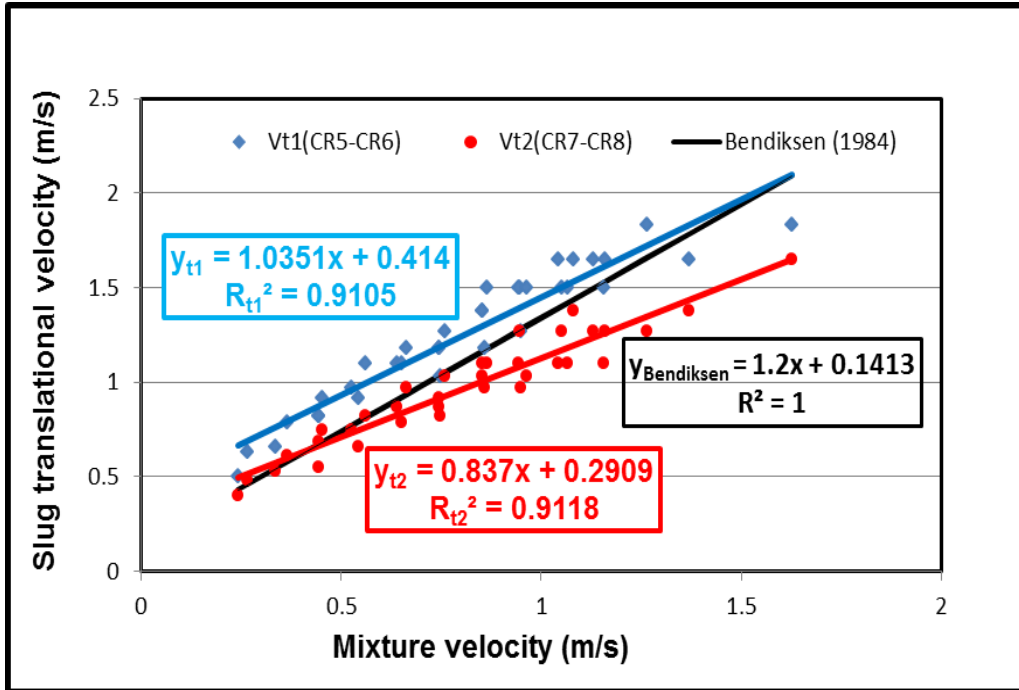


Figure 4-36: Comparison of measured slug translational velocity in the slug body and predicted by Bendiksen 1984 correlation and for uphill section

#### 4.1.6.4 Mean Slug Length in 2-inch 24° Dip Pipeline

This section investigates the characteristics of slug initiation at the dip calculating the mean slug length along the uphill section of the dip. The slug length is defined as dimensionless slug length (ratio of slug length to pipe diameter). For each category in section 4.1.4, three different categories of mean slug length were used to describe the specific hilly terrain effect at the dip.

The average slug length in Figure 4-37 and Figure 4-38 below can be deduced from the equation 4-1 below. The result is presented as dimensionless slug length as a ratio of the slug length and pipe diameter for convenience of discussion with other published work.



$$\bar{l}_{slug} = \bar{\tau}_{slug} * \bar{V}_t$$

4-1

$\bar{l}_{slug}$  = the average slug length;  $\bar{\tau}_{slug}$  = the average slug body passing time (average residence time);  $\bar{V}_t$  = the average slug translational velocity

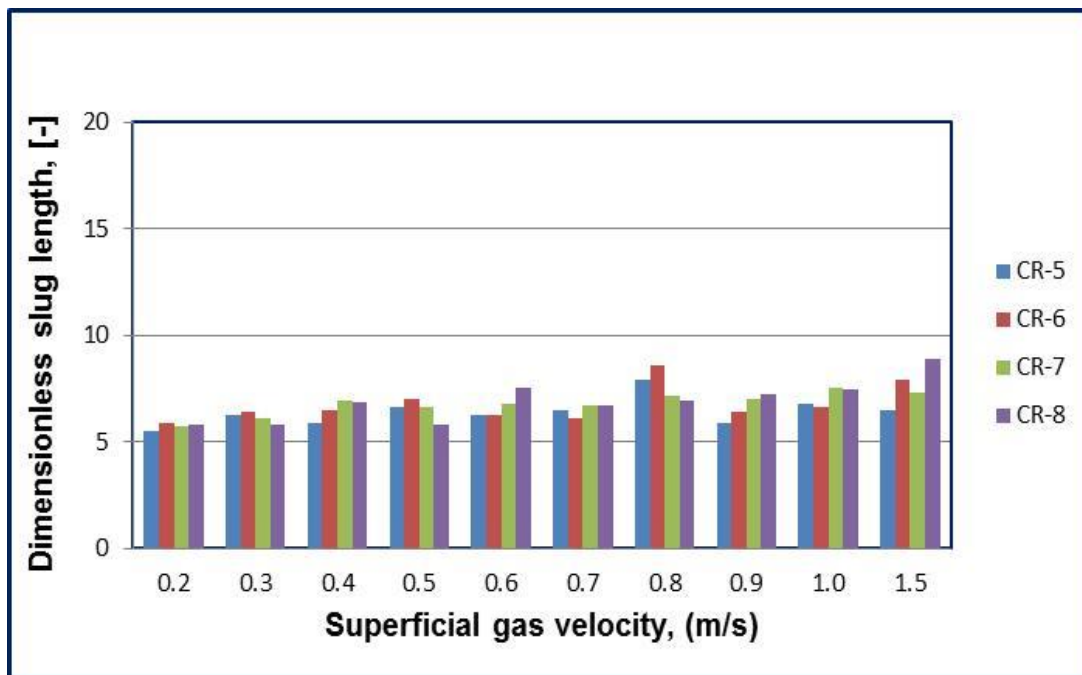


Figure 4-37: Type A, dimensionless slug length distribution along uphill section at (Vsg=0.2-1.5m/s, Vsl=0.07m/s)

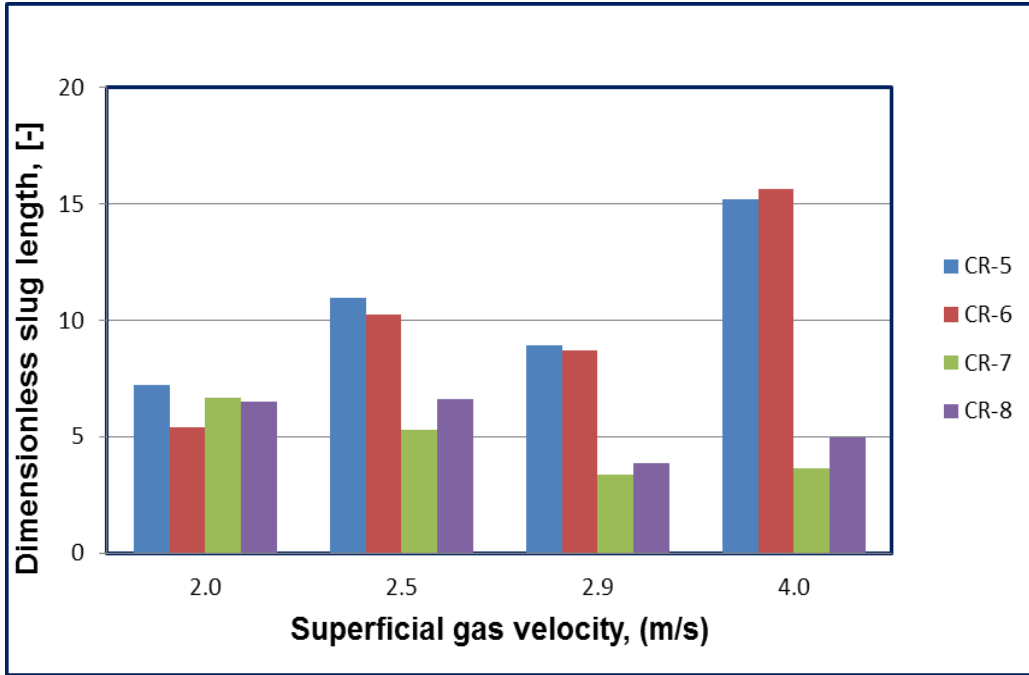


Figure 4-38: Type B, dimensionless slug length distribution along uphill section at ( $V_{sg}=2.0-4.0\text{m/s}$ ,  $V_{sl}=0.07\text{m/s}$ )

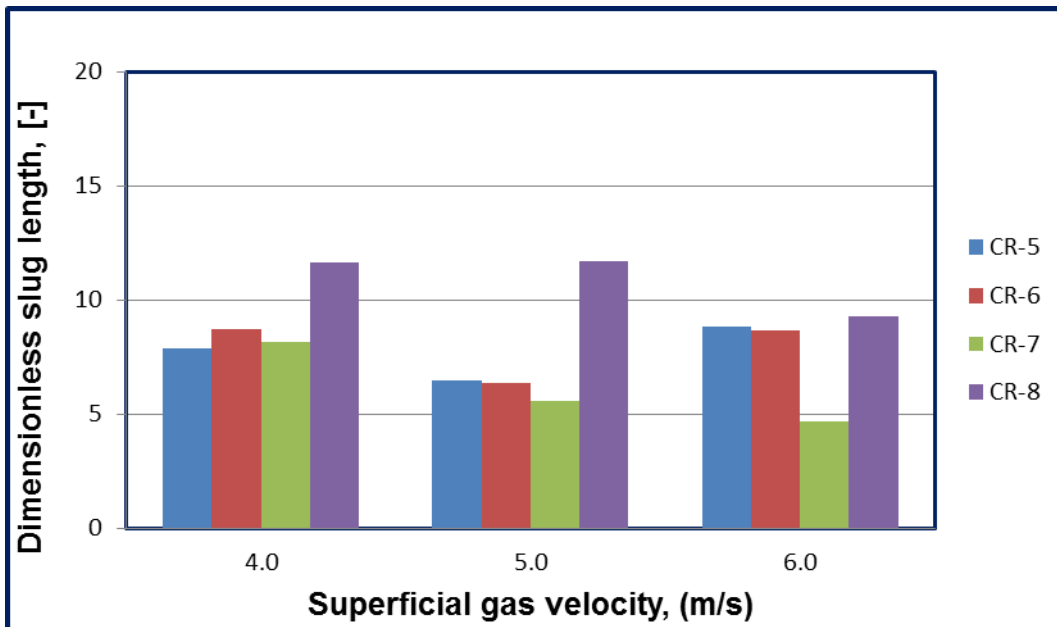


Figure 4-39: Type C, Dimensionless slug length distribution along uphill section, ( $V_{sg}=4-5\text{m/s}$ ,  $V_{sl}=0.35\text{m/s}$ )

The method of using flow pattern to qualitatively predict the flow mechanism in the dip in section 4.1.1 is extended to predict the hilly terrain effect on slug flow parameters. The trends of mean slug distribution at the dip and along the uphill section with respect to flow behaviour at the downhill section are used to classify the category of each hilly terrain effect.

Type A= Stratified flow with slug initiation

Type B= Energetic ripple with slug initiation /growth at the dip

Type C= Aerated slug with slug growth along the pipe.

Figure 4-37 shows that at low superficial gas velocity and low superficial liquid velocity, the slug length is fairly constant for type A, with a slight increase at the upstream section. At this flow condition, the downhill section is stratified and wavy while slug initiation occurs at the dip and survives through the hilly terrain pipeline. This indicates that the stratified flow could compensate slug growth (due to high inclination, and low  $V_{sg}$ ) at the dip, but does not result to increase in slug length along the uphill section.

Figure 4-38 shows that at high  $V_{sg}$ , and low and moderate  $V_{sl}$ ; the mean slug distribution is type B; where the mean slug length decreases along uphill section. At this condition, the slug initiated at the dip gets dissipated and could not survive through the uphill section which resulted to decrease along the pipe line. The low liquid flow rate with high gas velocity prevents accumulation of liquid at the dip. The mean slug length and slug frequency results showed that there are no regular slugs at the exit (CR-7 & CR-8) when  $V_{sg}$  is greater than 5m/s.

Figure 4-39 show that at high  $V_{sl}$  &  $V_{sg}$ , the slug initiation survives at the exits of the pipe (type C) because the persistent slugs from the downhill section override the initiated slug at the dip to form longer slugs at the exit. For high inclination, it can only occur at high gas and liquid flow rate.

Comparing this work with Al-safran work, the trend of mean slug length is different mostly at low flow rate where there is complete slug dissipation downhill section. It was reported that the mean slug length decrease from the entrance to the exit of the hilly terrain section. This is due to pipe inclination used in his work. Generally, the deviation

of the two investigators shows that the induced terrain slugging effect on slug initiation is different due to geometry of the flow line.

#### **4.1.7 Bifurcation Map of Air-Water Flow in 2-inch $\pm 24^\circ$ Configuration**

The objective is to develop bifurcation map to characterize changes in the qualitative dynamic behaviour of flow behaviour as key parameters (flow rates) are varied. The experimental data analysed in terms of liquid holdup exhibit changes in qualitative dynamic behaviour. Bifurcation analysis provides complete picture of the flow behaviour in the form of a bifurcation diagram. This diagram is used to determine the flow regime observed experimentally.

In order to view and determine the flow regime at a glance for a given flow condition (i.e.  $V_{sl}$  and  $V_{sg}$ ) across the pipeline; a bifurcation map for each sensor (conductivity ring) is plotted using the maximum and minimum liquid holdup time series data. The downhill and uphill section CR-1 and CR-7 result for 0.07m/s and 0.35m/s will be used for discussion for individual sensor, while Appendix C.1 presents the complete result.

Also, a profile plot is developed using a bifurcation map across the given sensor position. Results of  $V_{sl}$  0.07m/s to 0.55 m/s for a given  $V_{sg}$  of 0.7m/s will be used for discussion. This bifurcation map is developed to describe the flow pattern exhibited at various pipeline sections and for various flow conditions.

Slug flow results generally show a large difference between the maximum and minimum liquid holdup representing slug body and liquid film respectively. However, this difference start reducing once the slug flow becomes aerated at high  $V_{sg}$ .

While in stratified flow, there is little difference between the maximum and minimum liquid hold up with maximum value very close to minimum value. In bubble flow, there is also little difference between maximum and minimum liquid hold up with minimum value close to maximum value, due to less void fraction.

Based on the description of the rig in Figure 4-1, the result of downhill is presented in Figure 4-40 and Figure 4-41, At  $V_{sl}$  0.07m/s, stratified flow occurs all through the given

$V_{sg}$  with little difference between maximum and minimum liquid holdups. At  $V_{sl}$  0.35m/s, pseudo slug behaviour is exhibited at moderate  $V_{sg}$  because the maximum liquid hold up is not close to one. Above 4m/s  $V_{sg}$ , the difference between maximum and minimum liquid holdups start to decrease, this is due to the aerated slug flow behaviour occurring at high  $V_{sg}$ .

Figure 4-42 and Figure 4-43 are results from the uphill section result. At  $V_{sg}$  0.05-0.1, the flow behaviour is a bubble flow because the minimum liquid holdups are very high and with little difference from the maximum value. However, there is significant drop of this behaviour as the flow behaviour changes to slug flow from  $V_{sg}$  of 0.2m/s. Also the maximum value begins to drop as the slug flow changes to aerated flow.

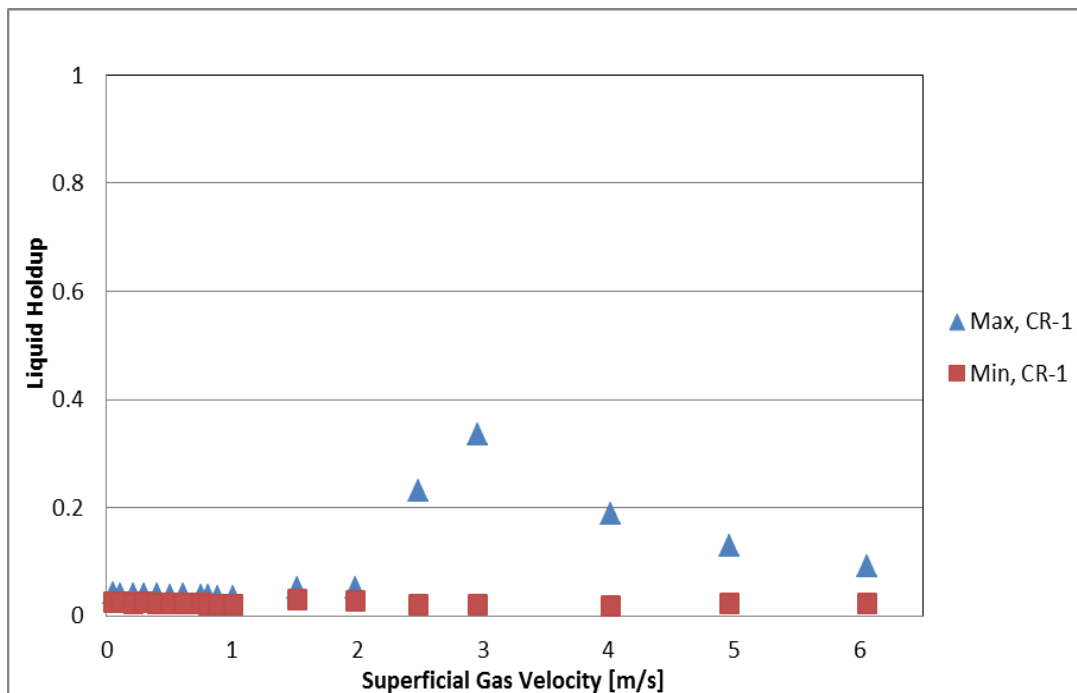


Figure 4-40: Bifurcation map of 24° downhill section (CR-1),  $V_{sl}=0.07\text{m/s}$

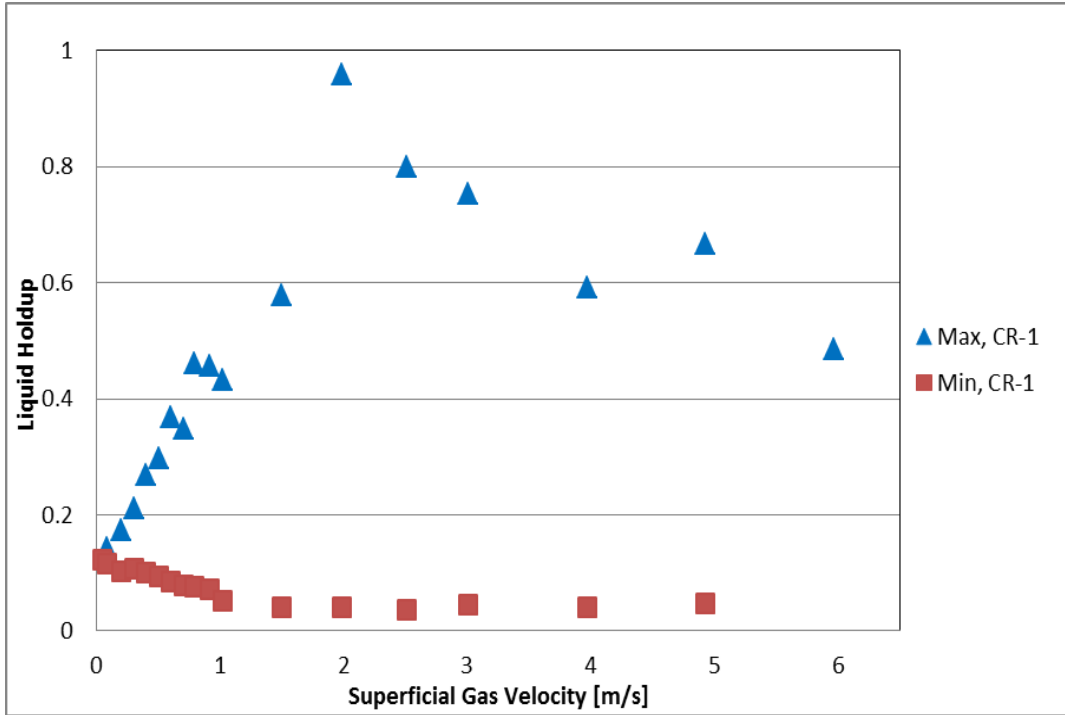


Figure 4-41: Bifurcation map of 24° downhill section (CR-1),  $V_{sl} = 0.35\text{m/s}$

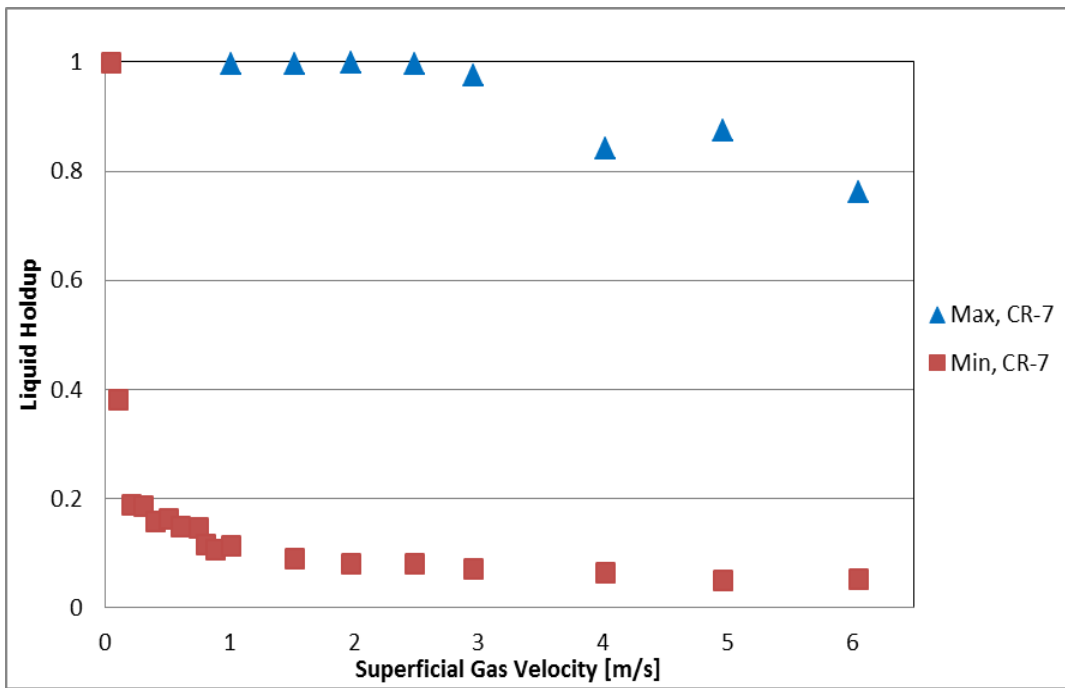


Figure 4-42: Bifurcation map of 24° uphill section (CR-7),  $V_{sl} = 0.07\text{m/s}$

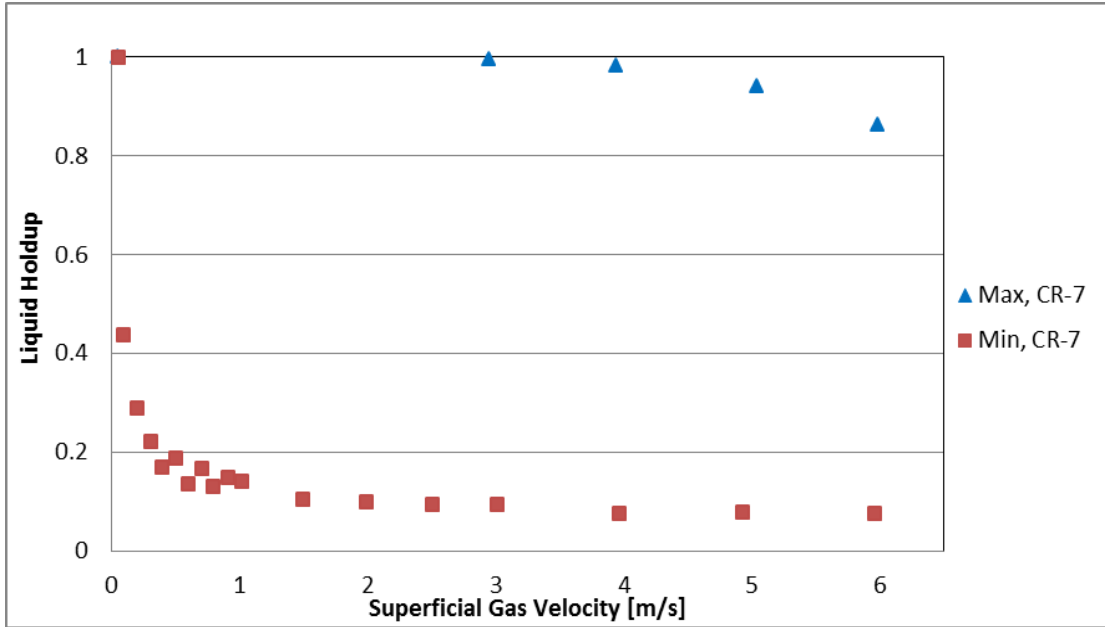


Figure 4-43: Bifurcation map of 24° uphill section (CR-7),  $V_{sl} = 0.35 \text{ m/s}$

Figure 4-44 to Figure 4-47 represent a profile plot across the pipeline, It can be seen that CR1 to CR4 in Figure 4-44 to Figure 4-47 are stratified flow but the trend changes as it get to CR5 through to CR7 indicating slug behaviour. The rest of the bifurcation map shows this similar interpretation.

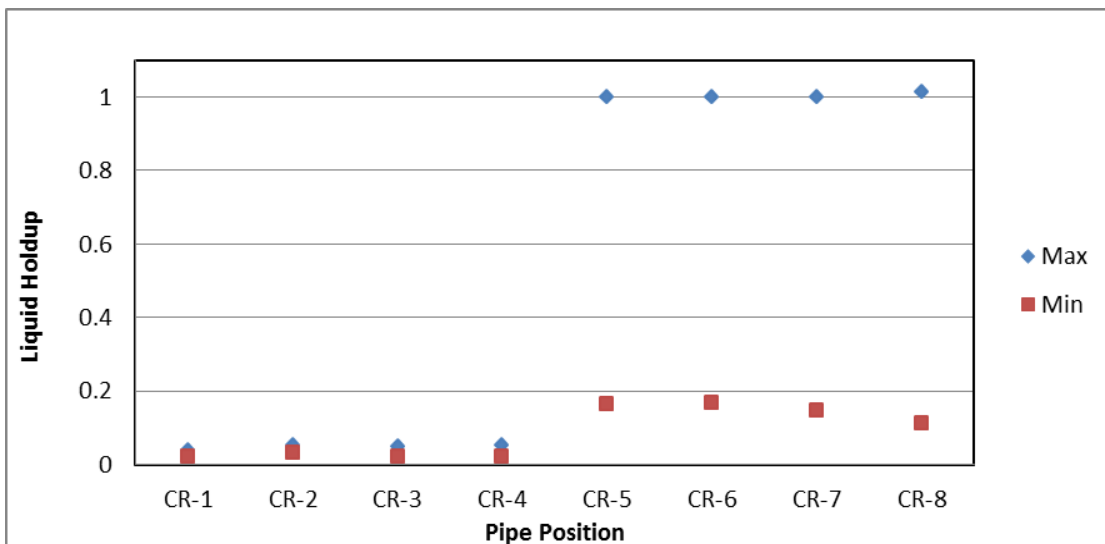


Figure 4-44: Bifurcation map across 24° dip geometry pipe,  $V_{sl} = 0.07 \text{ m/s}$  and  $V_{sg} = 0.7 \text{ m/s}$

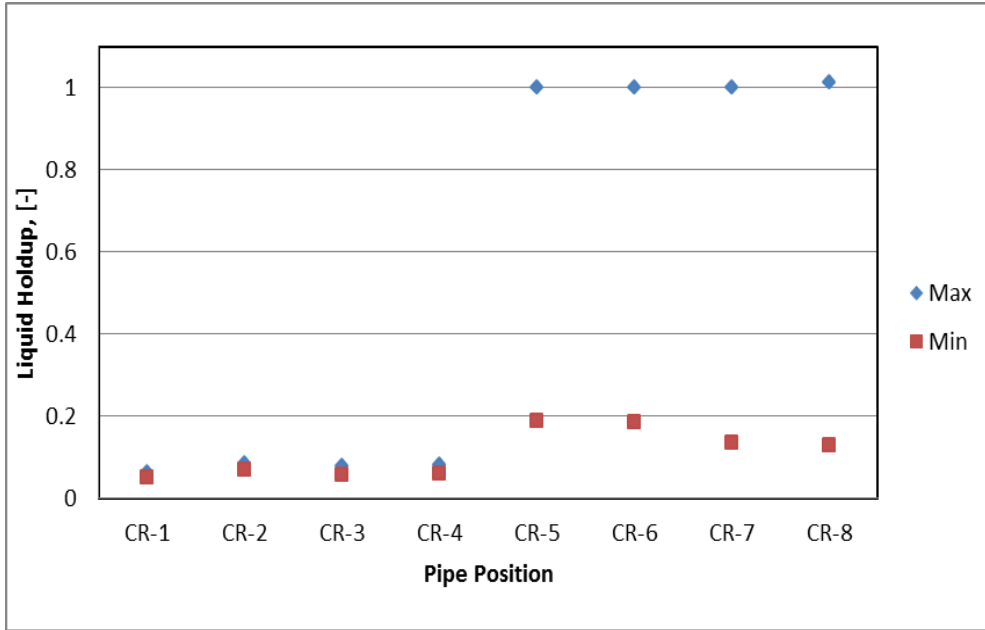


Figure 4-45: Bifurcation map across 24° dip geometry pipe,  $V_{sl}=0.15\text{m/s}$  and  $V_{sg}=0.7\text{m/s}$

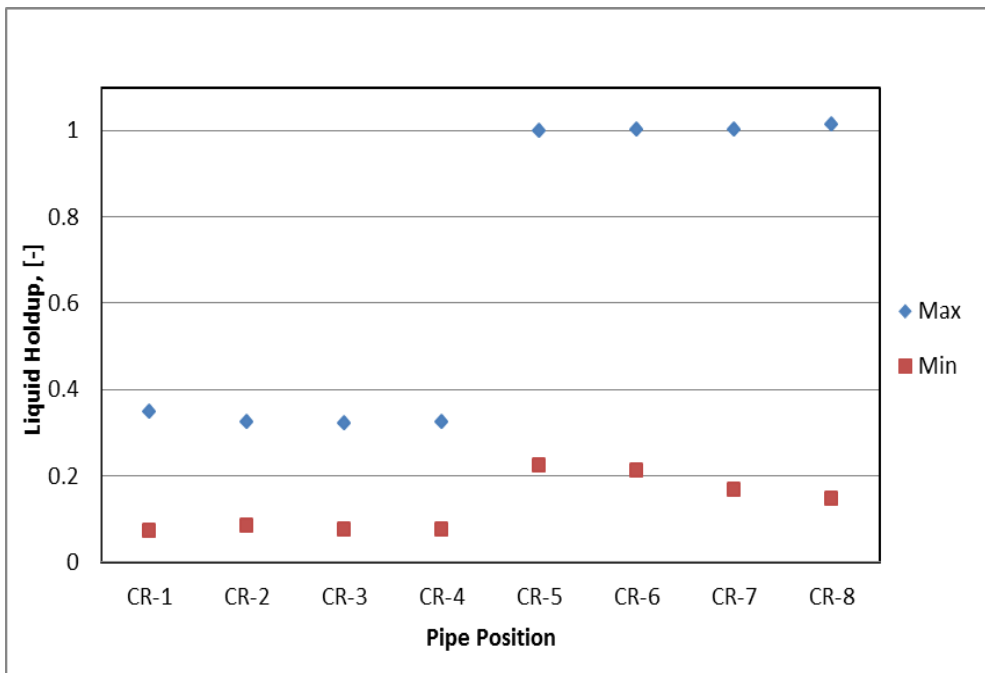


Figure 4-46: Bifurcation map across 24° dip geometry pipe,  $V_{sl}=0.35\text{m/s}$  and  $V_{sg}=0.7\text{m/s}$



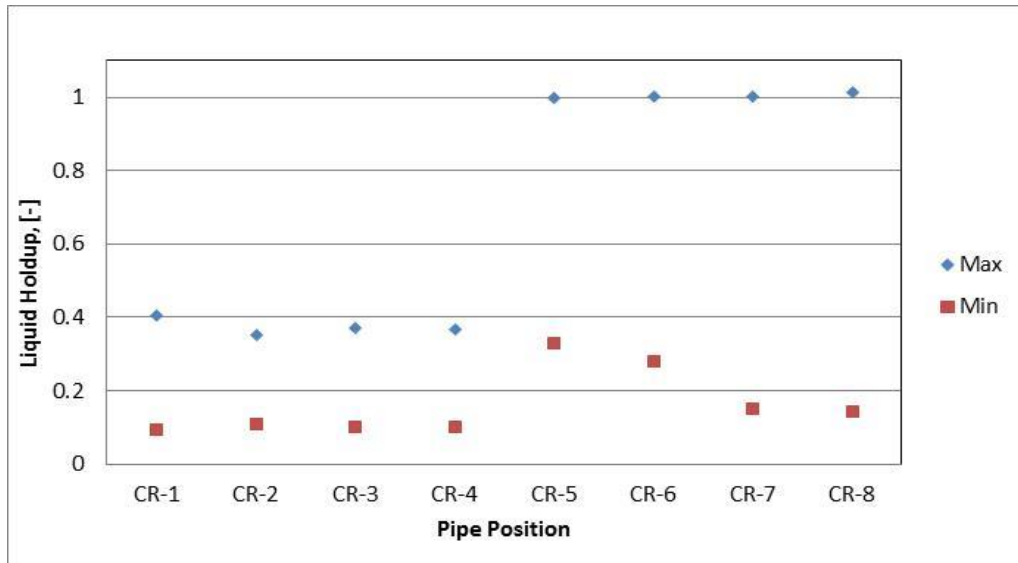


Figure 4-47: Bifurcation map across 24° dip geometry pipe,  $V_{sl}=0.55\text{m/s}$  and  $V_{sg}=0.7\text{m/s}$

#### 4.1.8 Criteria for Slug Flow Mechanism in 2-inch 24° Test Section

It has been reported that certain slug characteristics can be used to determine the flow condition for each slug initiation mechanism to occur. According to Al-Safran et al., 2005, the slug growth mechanism can be determined when the slug translational velocity is greater than the mixture velocity. Conversely, the wave coalescence initiation mechanism exists when the slug translational velocity is less than mixture velocity. The normalised slug translational velocity result in Figure 4-48 shows the region where this flow initiation mechanism exists in this present work. It is interesting to note that it is in agreement with Al-safran result shown in Figure 4-49.

The reason for the slug translation velocity to be less than mixture velocity in wave coalescence is attributed to the fact that it violates a major assumption of fully developed flow in the slug body.

Another criterion being considered in the literature is using the slug frequency. It is not considered in this report because the use of threshold to determine the slug body is subjective and would not give common or generalised conclusion.

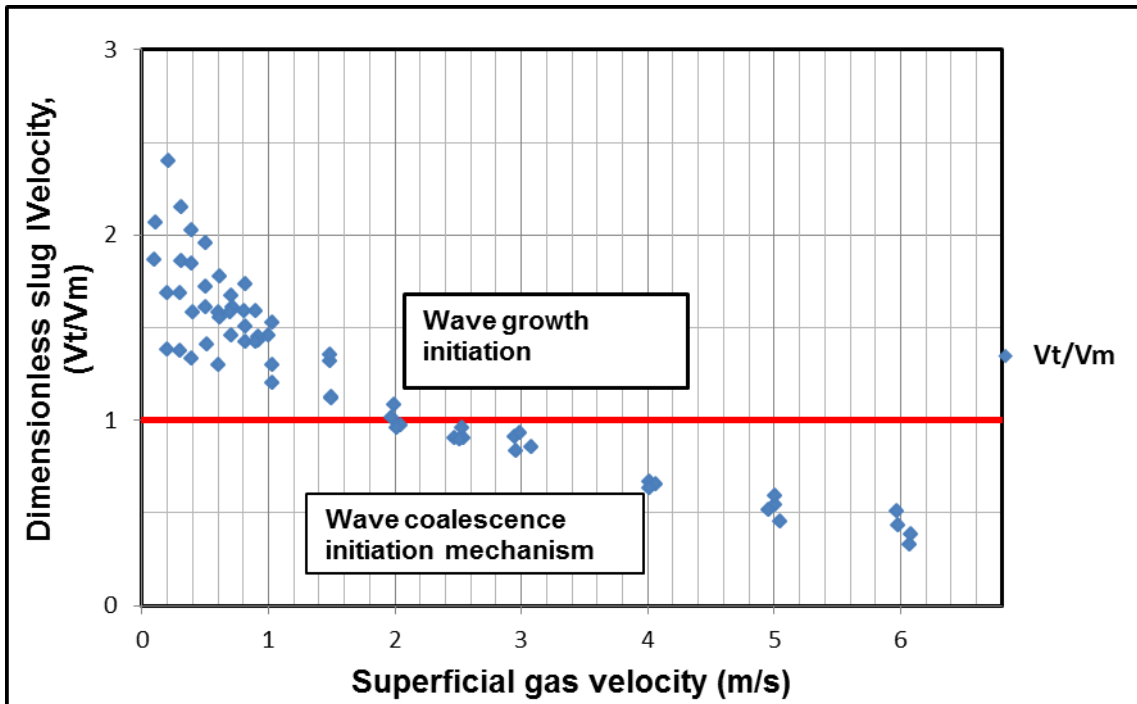


Figure 4-48: Initiation slugs translational to mixture velocities ratio trend (present work)

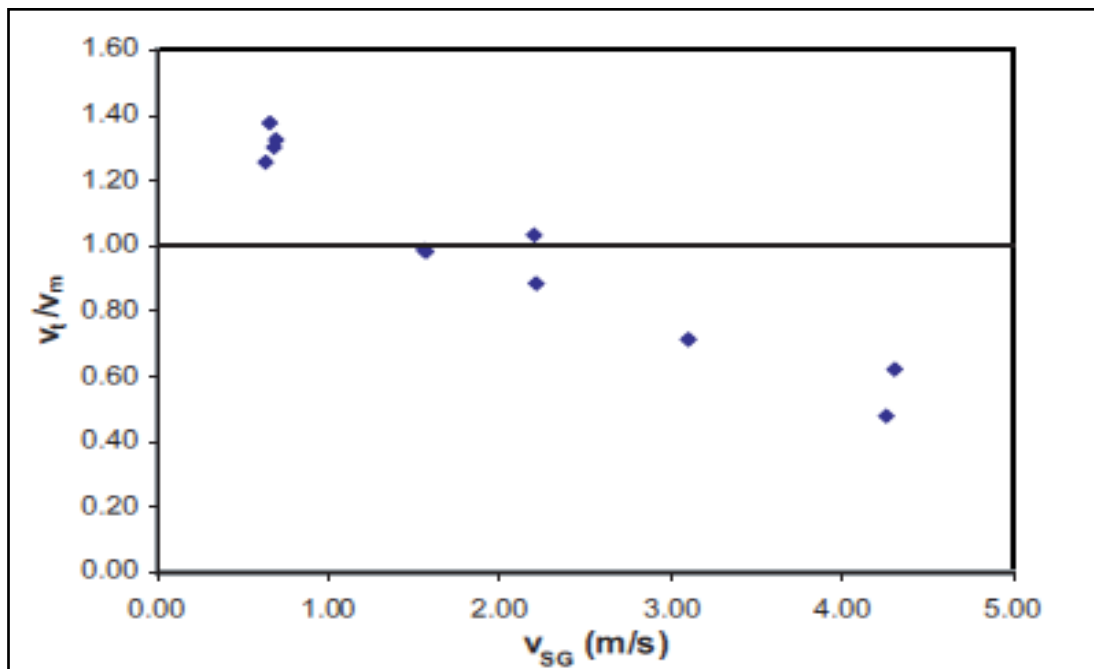


Figure 4-49 Initiation slugs translational to mixture velocities ratio trend (Al-safran, 2004)

## 4.2 Results of 12° Dip Pipeline Air-Water Experiment

Air-water experiments in 12° exhibited the same flow behaviour and slug flow phenomenon but at different test condition. Therefore, 12° results would be summarised in brevity for various flow regime maps, liquid hold up and slug flow parameters. The influence of the configurations (12°) in multiphase flow and slug initiation mechanism shall be discussed.

### 4.2.1 Air-Water Flow Regime in 2-inch $\pm 12^\circ$ Dip Pipeline

The flow regimes in 2inch of  $\pm 12^\circ$  dip configuration are presented in Figure 4-50 to Figure 4-53 for the four sections of the pipe. The downhill section of 12° in Figure 4-50 exhibited stratified flow at low to moderate  $V_{sg}$  and low to high  $V_{sl}$ . Aerated slug flow is prominent at high  $V_{sg}$  of 1.5 m/s to 6m/s and very high  $V_{sl}$  of 0.35m/s to 0.55m/s. In comparison with 24° downhill in Section 4.1.1.1., aerated slug starts to occur in 24° downhill at  $V_{sl}$  of 0.55m/s and very high  $V_{sg}$  from 3m/s to 6m/s. There is no stationary air pocket in 12° downhill test section.

At the downward dip, Figure 4-51 shows that it is well dominated with stratified flow for all the flow conditions. Unlike the  $\pm 24^\circ$  dip flow regime, there is no liquid accumulation at the dip. This is due to change in geometry.

Figure 4-52 presented the uphill dip section; it exhibited similar flow regime and slug initiation mechanism as mentioned in Section 4.1.1.2. However, due to the difference in geometry, the flow conditions for slug initiation are different. Flow condition for plug flow remains the same for both dip sections of the various dip configurations (i.e. 12° and 24°). Also, other flow behaviour such slug flow and aerated slug flow similar to the 24° uphill section also occurred at different flow conditions for 12° test section as shown in Figure 4-53.

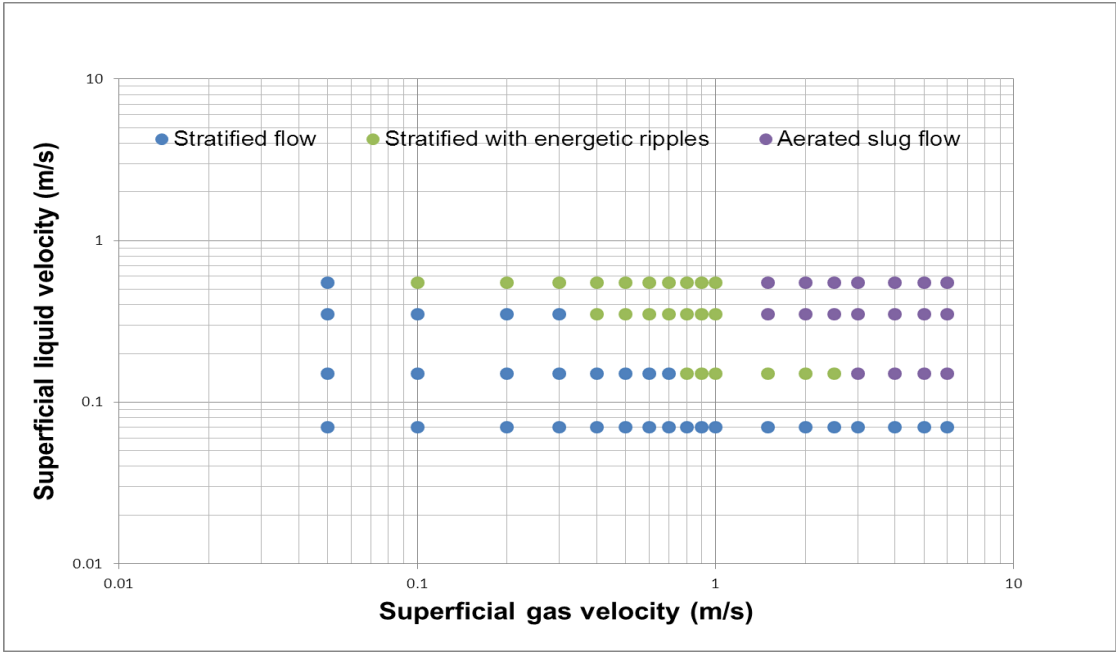


Figure 4-50: Air-water flow regime map for downhill 12° test Section

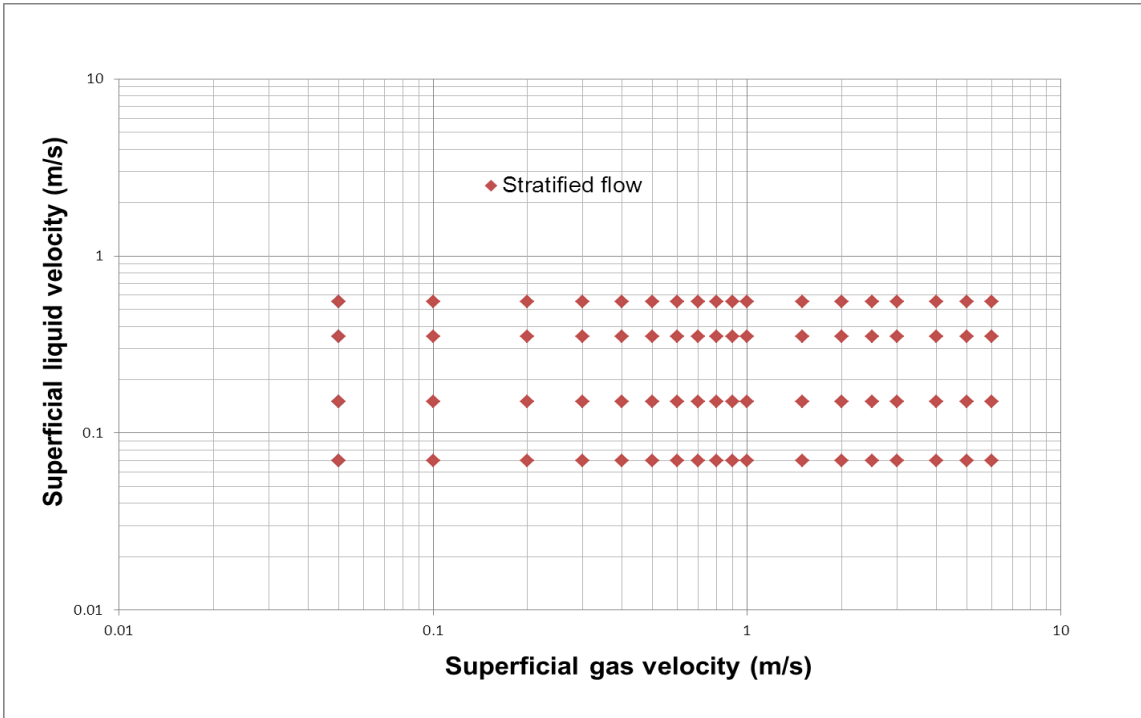


Figure 4-51: Air-water flow regime map for downward dip 12° test section

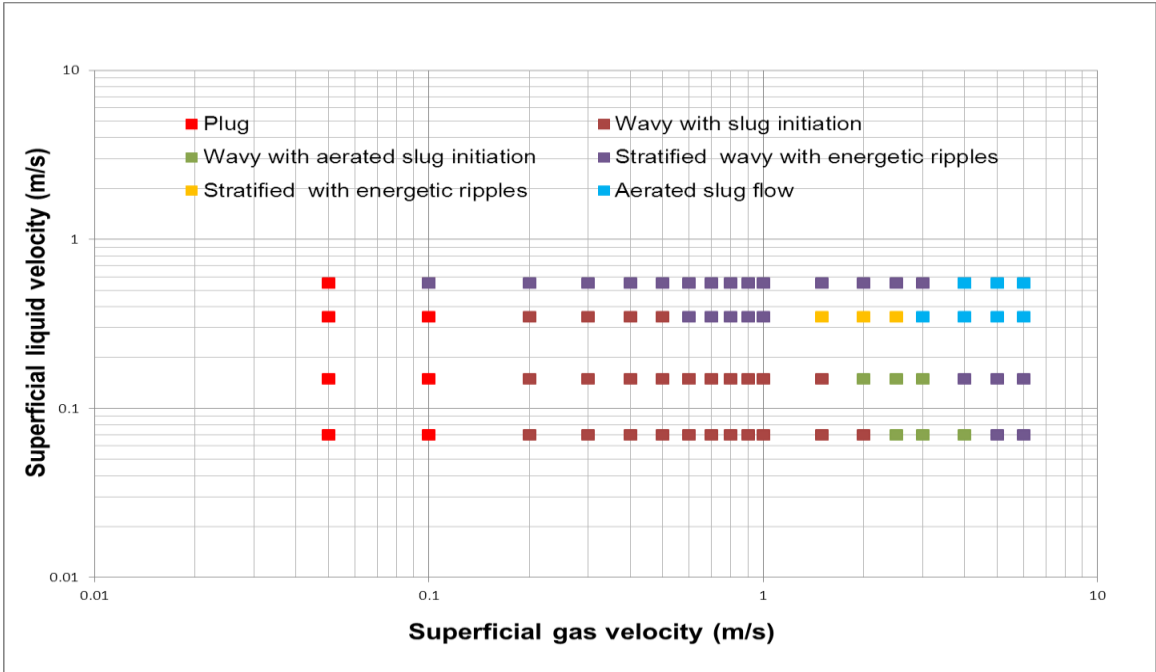


Figure 4-52: Air-water flow regime map for upward dip 12° test section

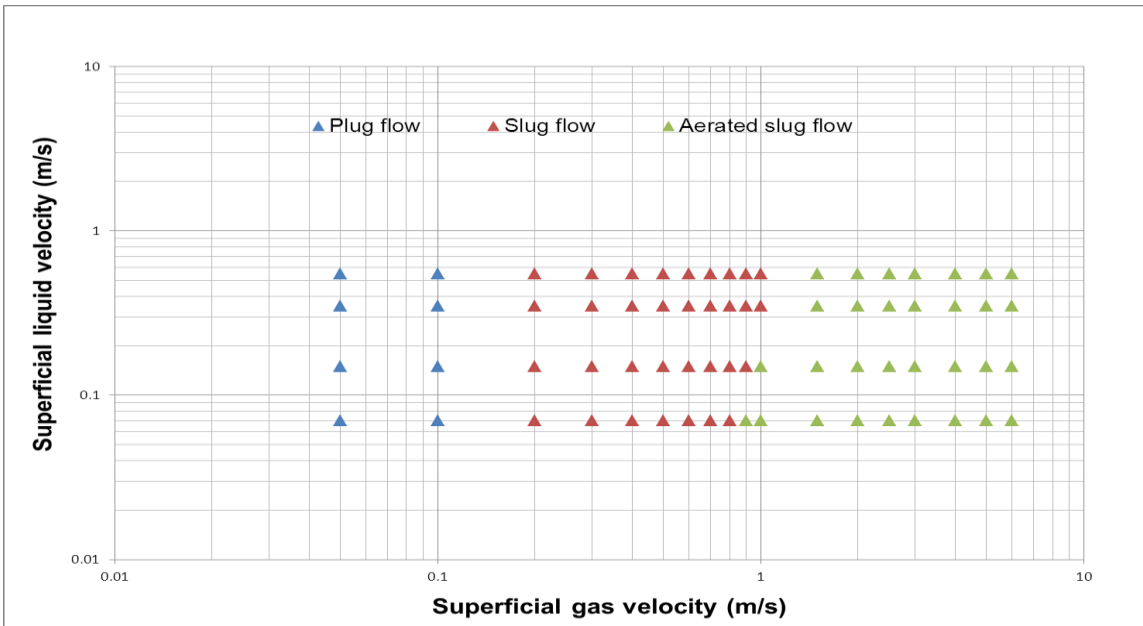


Figure 4-53: Air-water flow regime map for uphill 12° test section

## 4.2.2 Liquid Holdup in 2-inch 12° Dip Pipeline

The liquid hold was also measured using conductivity rings at various section of the pipe in form of time series. This was used to determine the overall average liquid hold up. Figure 4-54 showed that the average liquid holdup is generally low for downhill flow. The liquid hold up for downward inclined flow is independent on the superficial gas velocity. While upward flow in Figure 4-55 is dominated by intermittent flow. There is significant effect of superficial gas velocity on liquid hold up. This was expected as explained in section 4.1.5.

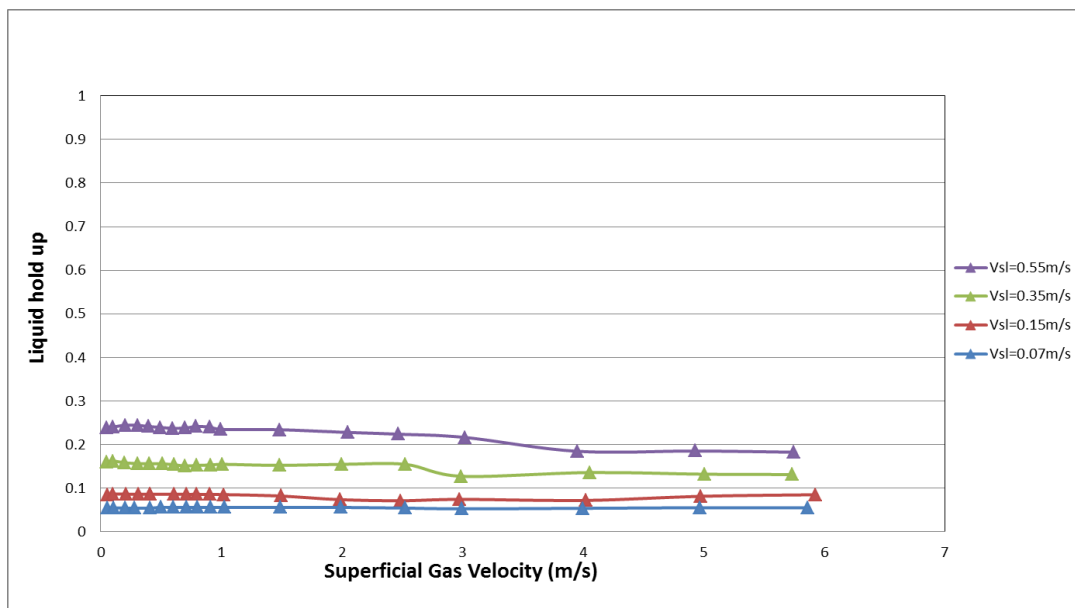


Figure 4-54: Overall-average liquid hold up for 12° downhill test section (CR-1)

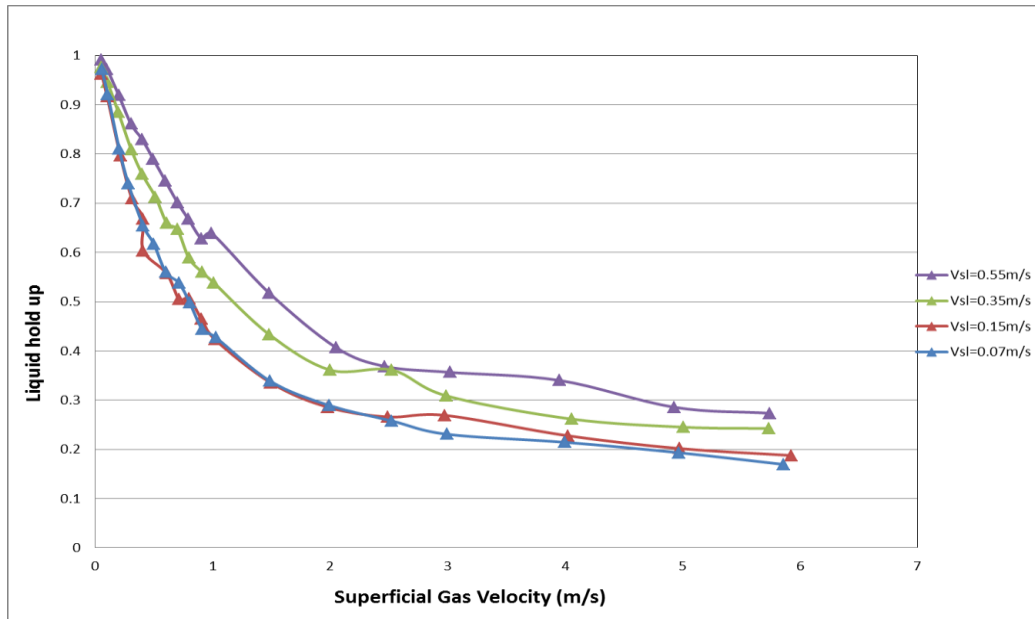


Figure 4-55: Overall-average liquid hold up for 12° Uphill test section (CR-8)

### 4.2.3 Bifurcation Map of Multiphase flow 2-inch 12° Configuration

Similarly as in Section 4.1.7 the flow regime at a glance for a given flow condition (i.e. Vsl and Vsg) across the pipeline was also determined using bifurcation map. The maximum and minimum liquid holdup time series for each flow condition is determined for each sensor position and the profile plot is also developed using the bifurcation map across the given sensor position.

The downhill and uphill section CR-1 and CR-7 result for 0.07m/s and 0.35m/s will be used for discussion for individual sensor, while Appendix C.2 presents the complete result. Based on the description in Section 4.1.7, the result of downhill is presented in Figure 4-56 and Figure 4-57. At Vsl 0.07m/s, stratified flow occurs all through the given Vsg with little difference between maximum value and minimum liquid hold ups. At Vsl 0.35m/s, pseudo slug behaviour is exhibited at moderate Vsg because the maximum liquid hold up is not close to one. Above 3m/s Vsg, the difference between maximum and minimum liquid hold ups start to decrease, this is due to the aerated slug flow behaviour occurring at high Vsg.

Figure 4-58 and Figure 4-59 presented the uphill section maps. At  $V_{sg}$  0.05-0.1, the flow behaviour is a bubble flow because the minimum liquid hold up is very high and with little difference from the maximum liquid hold up. However, there is significant drop of this behaviour as the flow behaviour changes to slug flow from  $V_{sg}$  of 0.2m/s. Also the maximum liquid hold up begins to drop as the slug flow changes to aerated flow.

Figure 4-60 and Figure 4-63 present the profile plot across the pipeline, At low  $V_{sl}$  (0.07m/s and 0.15m/s), CR-1 to CR-4 in Figure 4-61 and Figure 4-62 are stratified flow but the trend changes as it get to CR-5 through to CR-8 indicating slug behaviour. While at high  $V_{sl}$  (0.35m/s and 0.55m/s), stratified wavy is exhibited at CR-1 to CR-4 in Figure 4-62 and Figure 4-63 , this then changes to slug flow at CR-5 to CR-8.

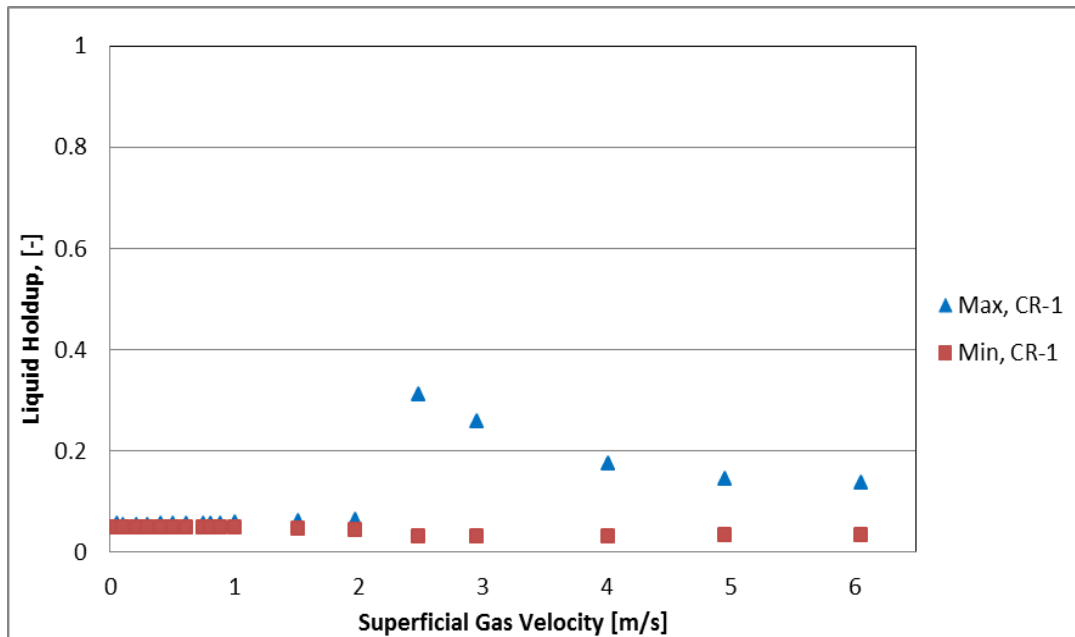


Figure 4-56: Bifurcation map of 12° configuration at downhill section (CR-1),  $V_{sl}=0.07\text{m/s}$



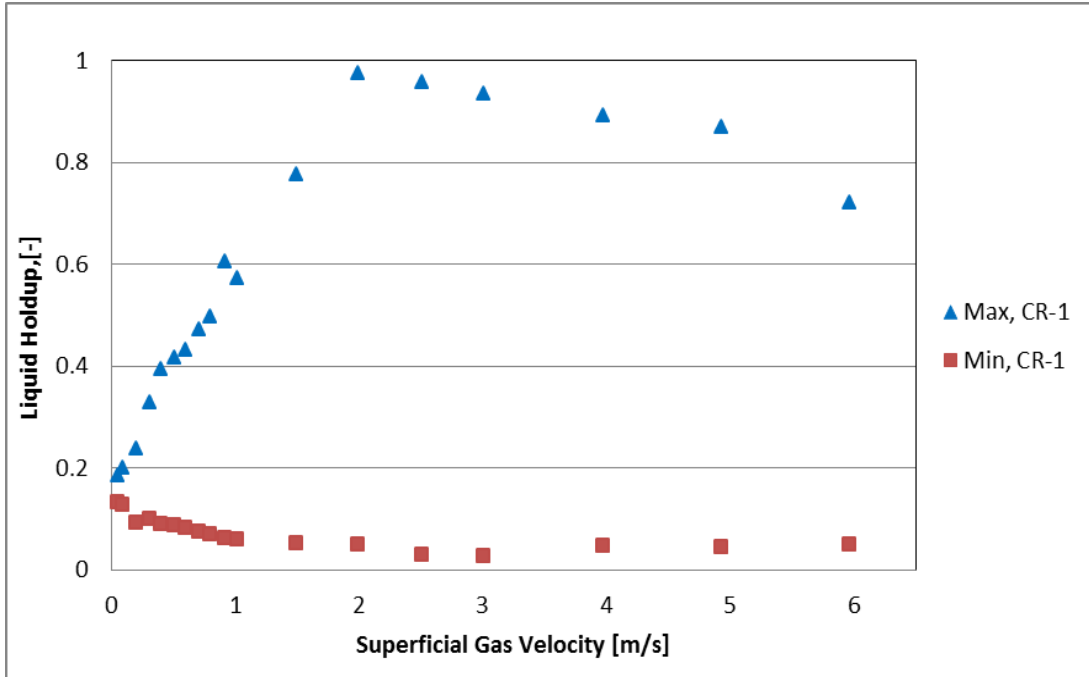


Figure 4-57: Bifurcation map of 12° configuration at downhill section (CR-1),  $V_{sl} = 0.35\text{m/s}$

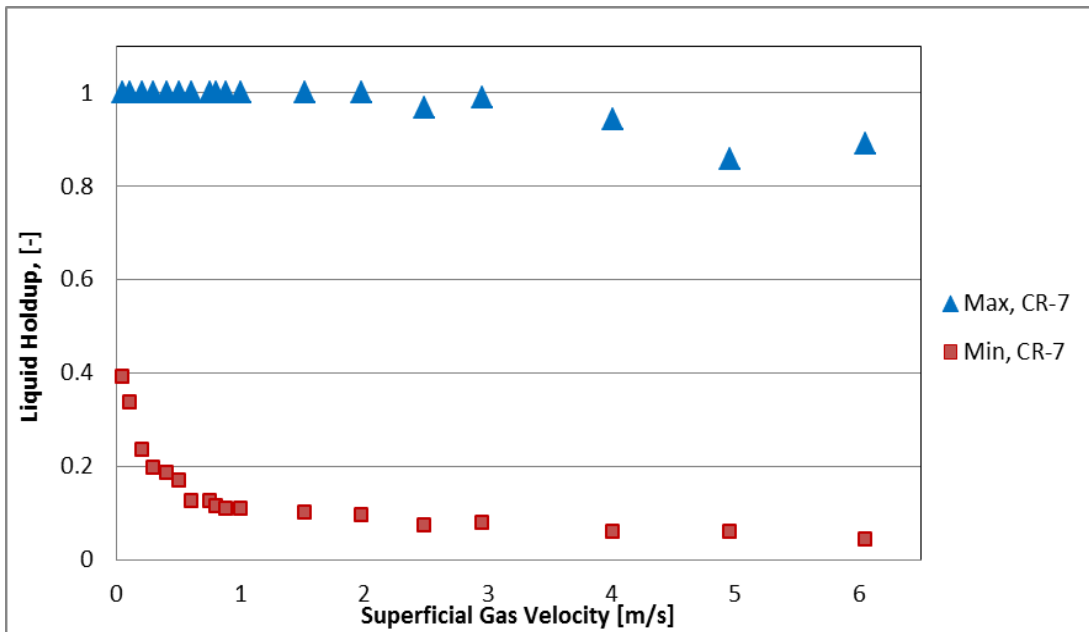


Figure 4-58: Bifurcation map of 12° configuration at uphill section (CR-7),  $V_{sl} = 0.07\text{m/s}$

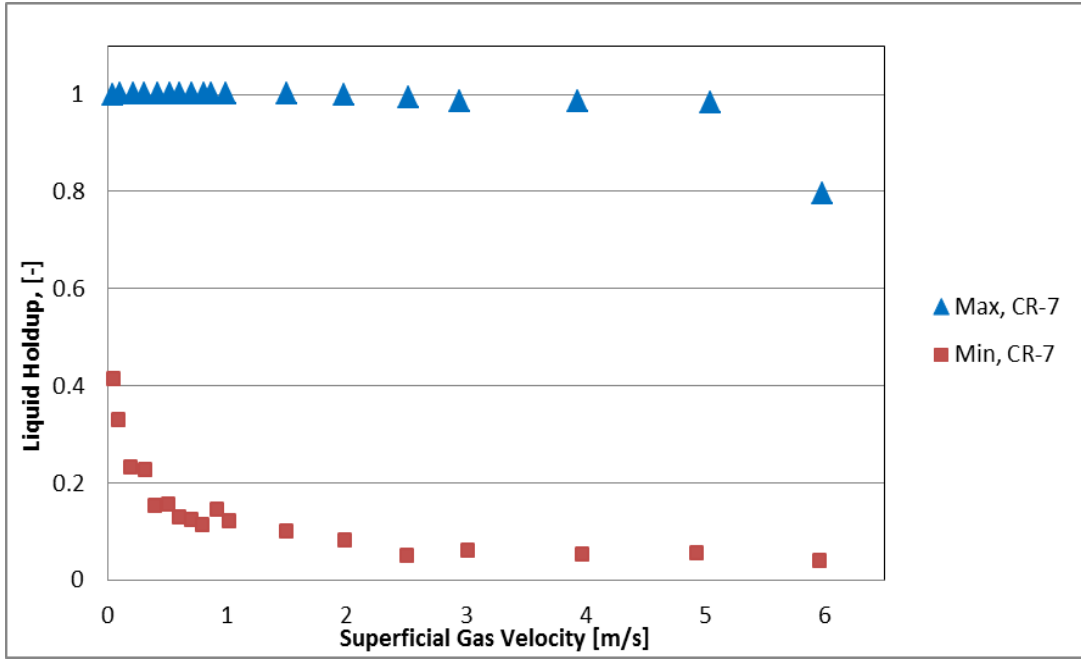


Figure 4-59: Bifurcation map of 12° configuration at uphill section (CR-7),  $V_{sl}=0.35\text{m/s}$

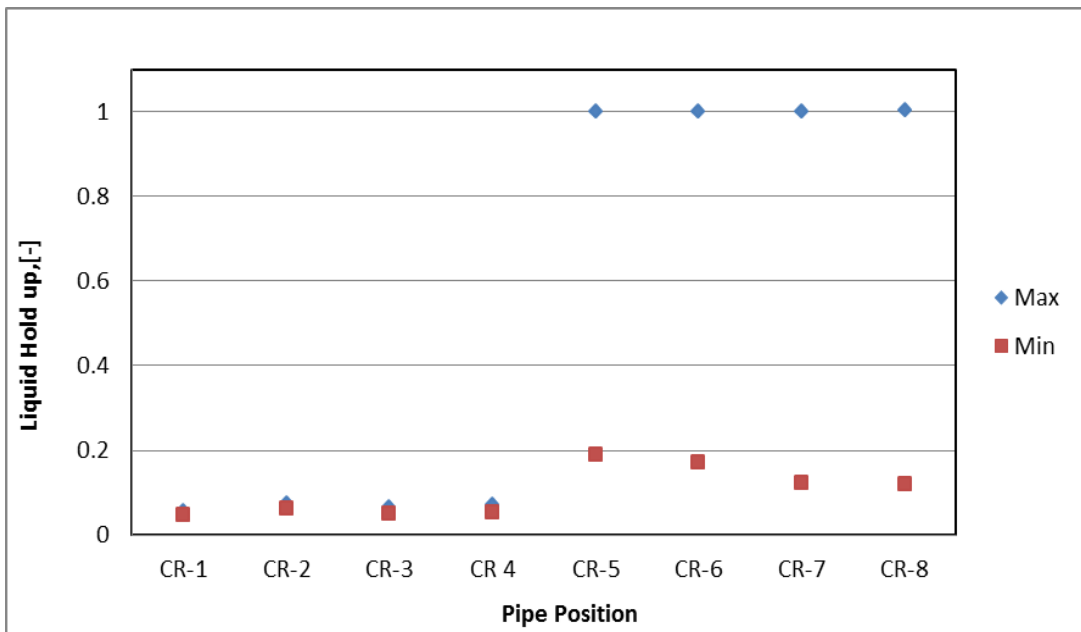


Figure 4-60: Bifurcation map across the 12° dip geometry pipe,  $V_{sl}=0.07\text{m/s}$  and  $V_{sg}=0.7\text{m/s}$

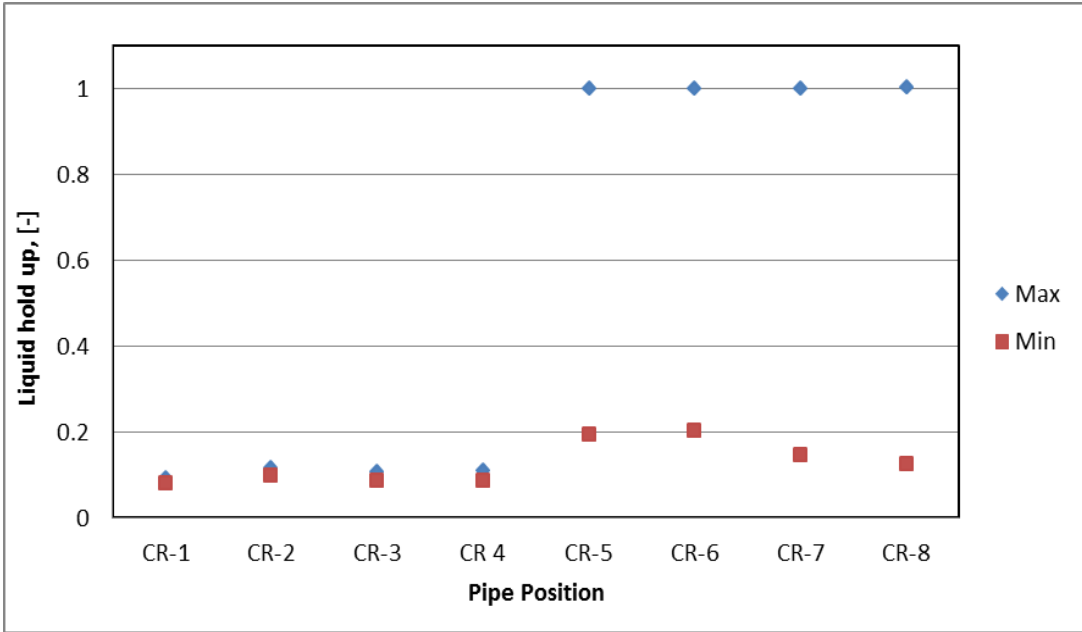


Figure 4-61: Bifurcation map across the 12° dip geometry pipe,  $V_{sl}=0.15\text{m/s}$  and  $V_{sg}=0.7\text{m/s}$

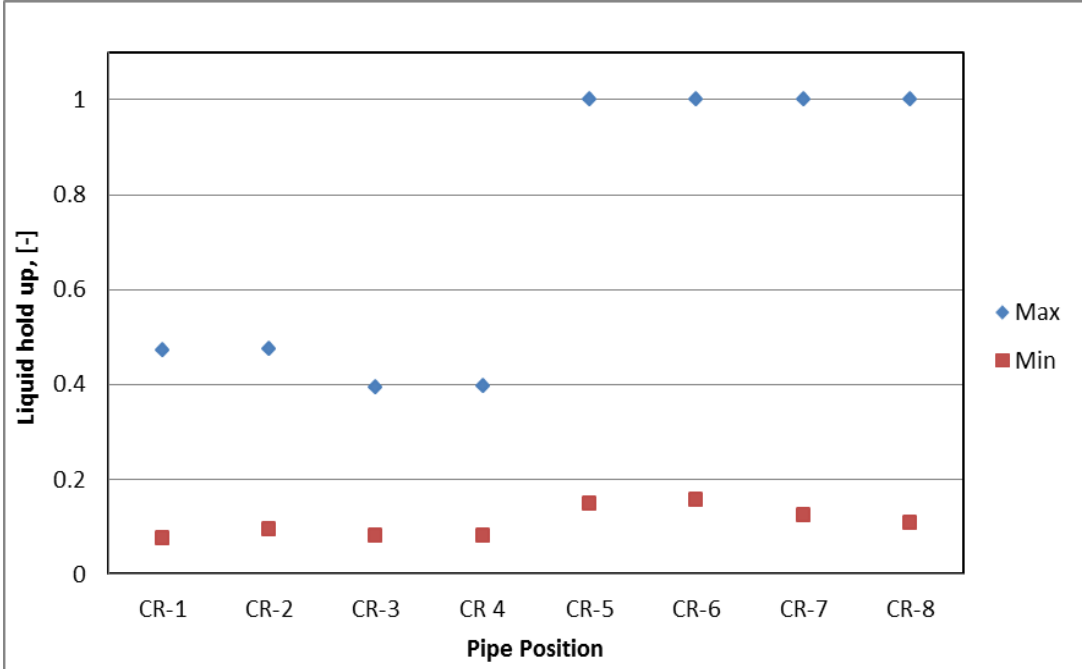


Figure 4-62: Bifurcation map across the 12° dip geometry pipe,  $V_{sl}=0.35\text{m/s}$  and  $V_{sg}=0.7\text{m/s}$

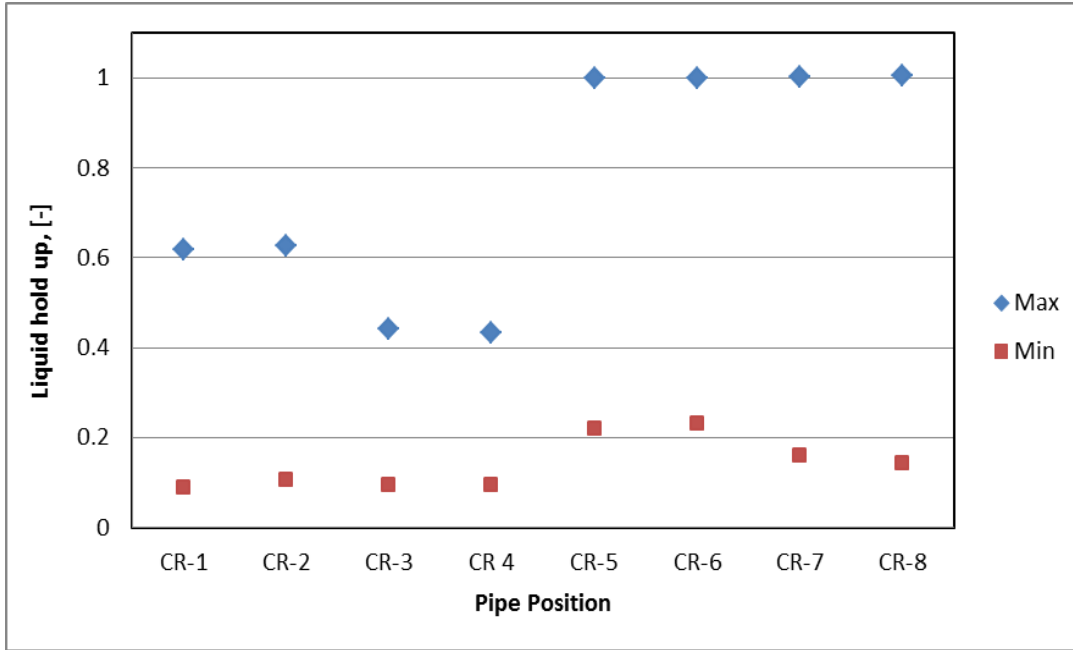


Figure 4-63: Bifurcation map across the 12° dip geometry pipe,  $V_{sl}=0.55\text{m/s}$  and  $V_{sg}=0.7\text{m/s}$

#### 4.2.4 Slug Flow Characteristics in 2-inch 12° Dip Pipeline

Based on typical time series of slugs from the conductivity rings and physical observation, two major types of slugs were similarly determined in 12° uphill sections.

The slug data were obtained based on similar approach used in section 4.1.6 to determine the slug parameters. In order to determine the slug parameters, a threshold value was considered in order to identify slug. For consistency with 24° test section result and to have basis for comparison, the same threshold value of 0.7 was also used to determine the slug parameters.

The overall slug results shows that there was no significant difference between the CR-5 and CR-6, similarly CR-7 and CR-8 have negligible deviation in their result due to their position on the pipe. Hence for convenience of discussion, CR-5 result is use to represent upward dip section while CR-7 is use to represent uphill section.

#### 4.2.4.1 Slug Liquid Holdup in 2-inch 12° Dip Pipeline

The slug liquid hold up is determined based on the threshold level with the time series. The variation of liquid hold up in the slug body with superficial gas velocity is given in Figure 4-64 and Figure 4-65 for two of conductivity at the uphill section for discussion. For all the results, liquid holdup approaches unity as the superficial gas velocity approaches zero.

The results showed that for a given  $V_{sl}$ , the slug liquid holdup decreases as  $V_{sg}$  increases for uphill section of the pipe. This phenomenon can be explained by the fact that; as the gas increase, it swept more liquid away and prevented the liquid to bridge up the pipe easily.

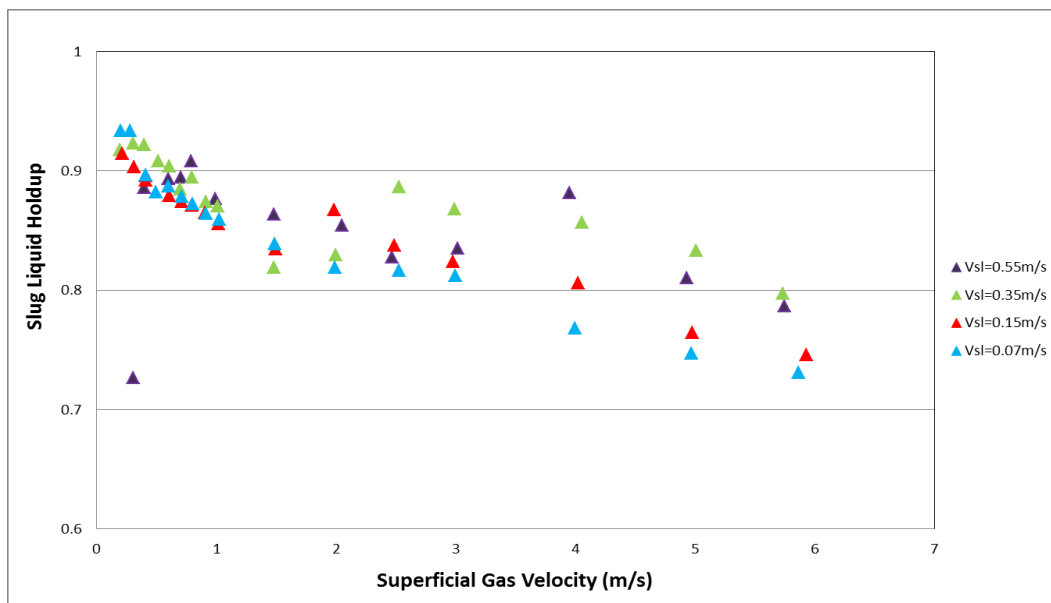


Figure 4-64: Slug liquid holdup in the slug body for uphill 12° test section (CR-5)

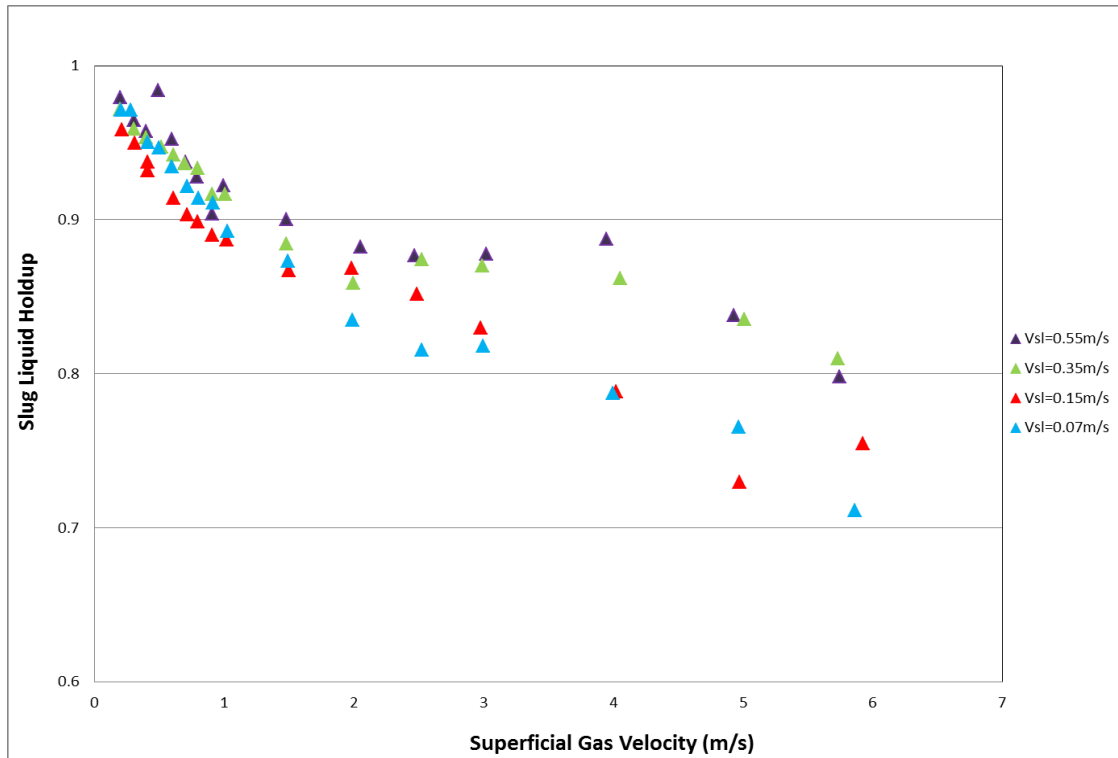


Figure 4-65: Slug liquid holdup in the slug body for uphill 12° test section (CR-7)

#### 4.2.4.2 Slug Frequency in 2-inch 12° Dip Pipeline

Slug frequency is the number of slug passing through per unit time at a specific location in the pipe. Figure 4-66 and Figure 4-67 presented the slug frequency results at various gas velocities and given superficial liquid velocity for upward dip section and uphill section respectively. The results showed that at a given superficial liquid velocity, the slug frequency decreases as the superficial gas increases. At a given gas velocity, the slug frequency decreases as the superficial liquid decreases.

Figure 4-66 and Figure 4-67 presented slug frequency upstream dip section (CR-5) and the downstream elbow (CR-8) respectively. The results showed that at low Vsl; the slug frequency is higher for CR-5/6 than CR-7/8 at low Vsg. This is because some of the slug decay along this section and only few of them survive through the entire pipe.

In addition, at very high Vsl of about 0.55m/s, and a lower Vsg of 0.5m/s to 1m/s, the slug frequency is very low at CR-5 because the slug initiation shifted away from the dip to the uphill section.

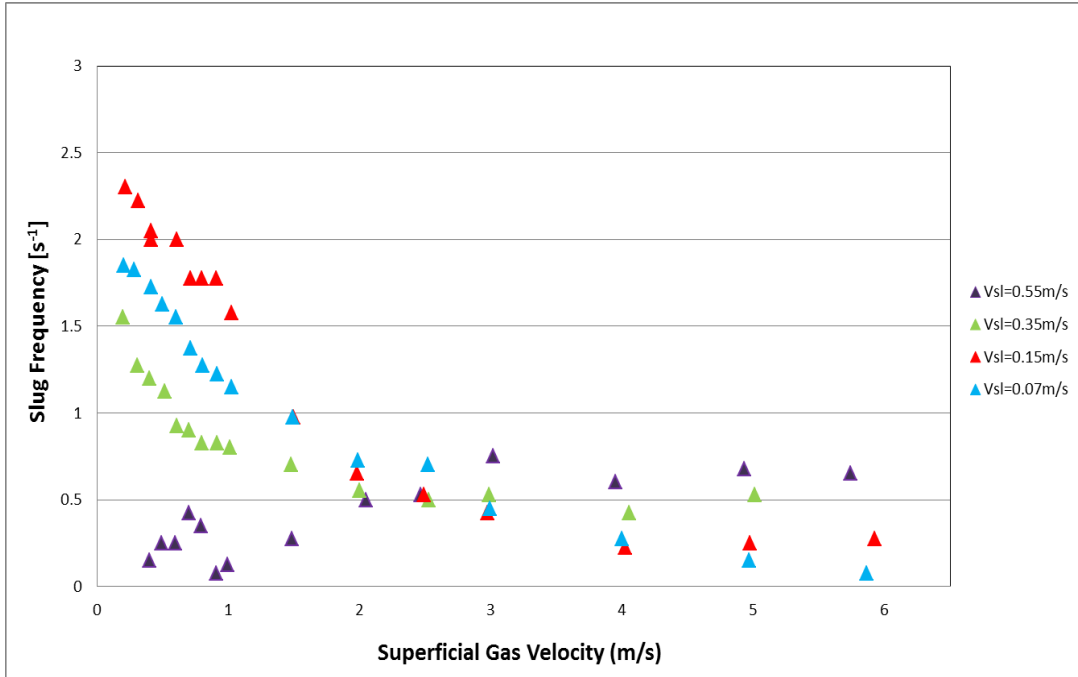


Figure 4-66: Slug frequency for uphill 12° test section (CR-5)

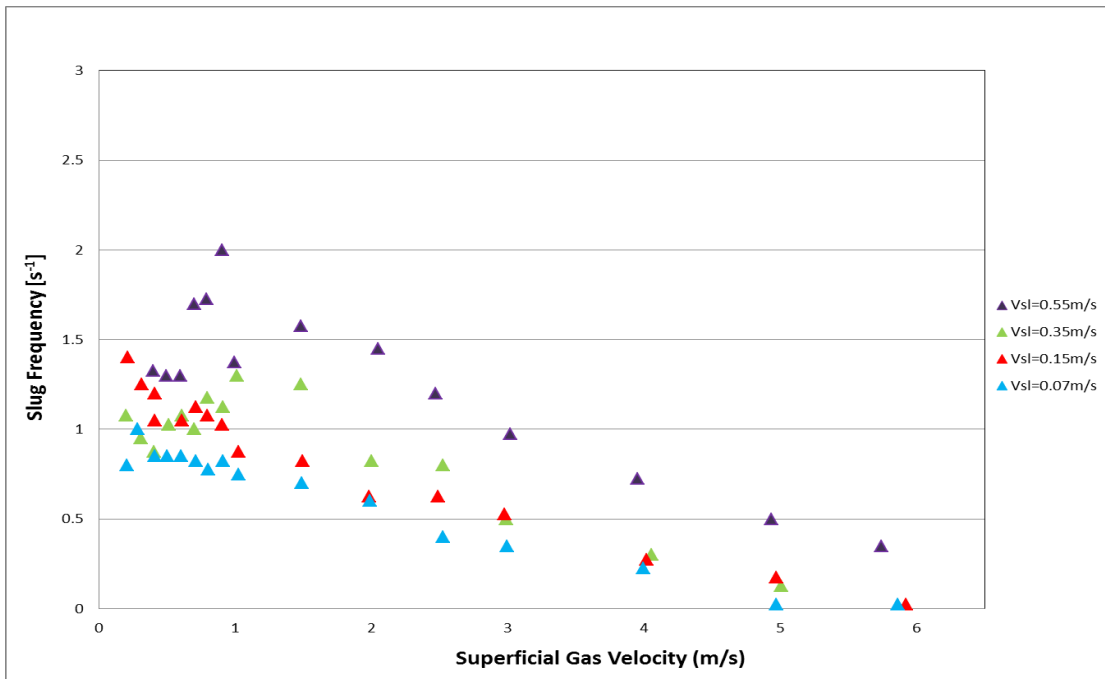


Figure 4-67: Slug frequency for uphill 12° test section (CR-7)

#### 4.2.4.3 Slug Translational Velocity in 2-inch 12° Dip Pipeline

The slug translational velocity is also calculated using the cross correlation technique of two signals from a pair of conductivity ring installed apart.

Figure 4-68 and Figure 4-69 showed that the slug translational velocity increases linearly with superficial velocity up to certain point and then remained relatively constant from  $V_{sg}=3\text{m/s}$ . The transition from linearity to a constant at  $V_{sg}=3\text{m/s}$  is due to the slug flow structure of the aerated slug present at this flow condition.

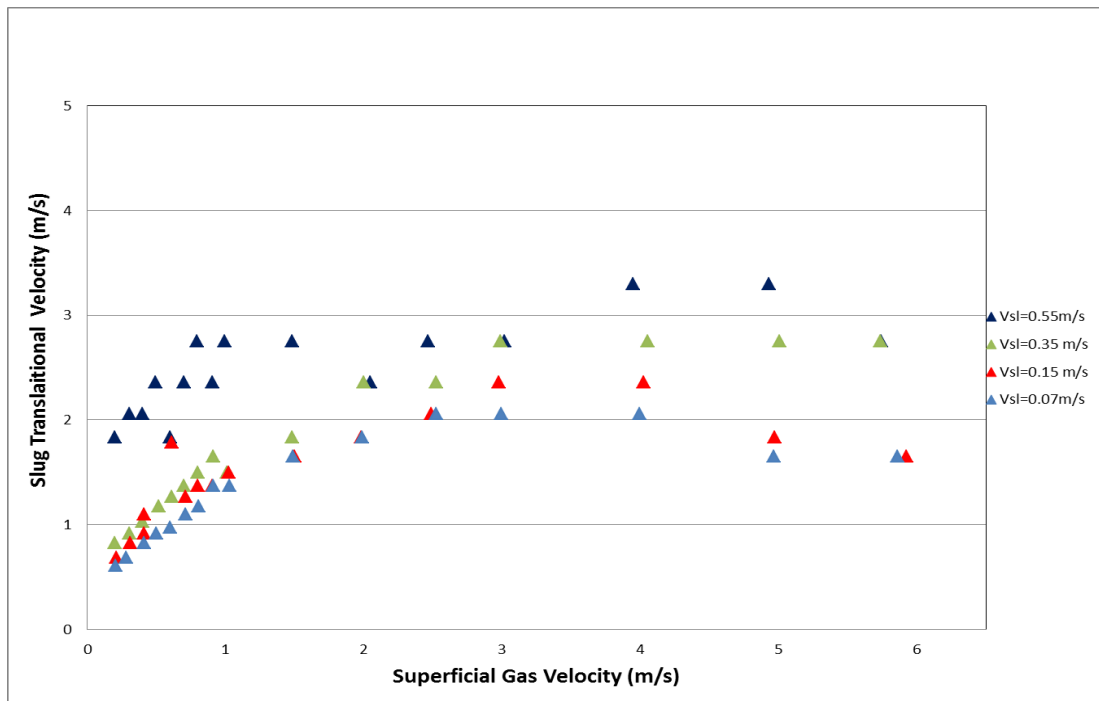


Figure 4-68: Slug translational velocity for upward-dip, 12° test section (CR-5 & CR-6)



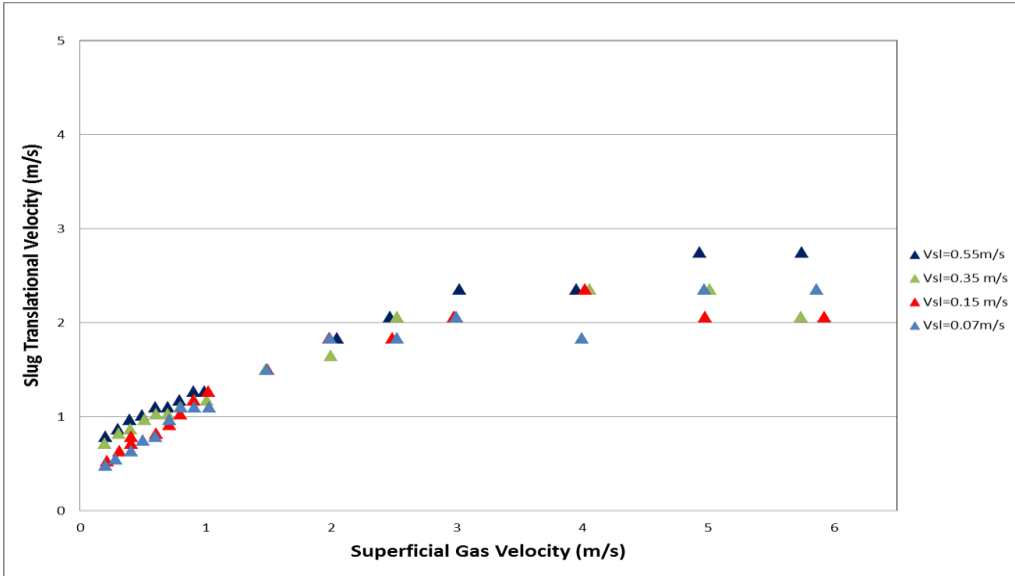


Figure 4-69: Slug translational velocity for uphill, 12° test section (CR-7 & CR-8)

#### 4.2.5 Criteria for Slug Flow Mechanism in 2-inch 12° Test Section

The criteria for slug flow initiation mechanisms in  $\pm 12^\circ$  test section as a function of dimensionless slug velocities against superficial gas velocities is presented in Figure 4-70 below.

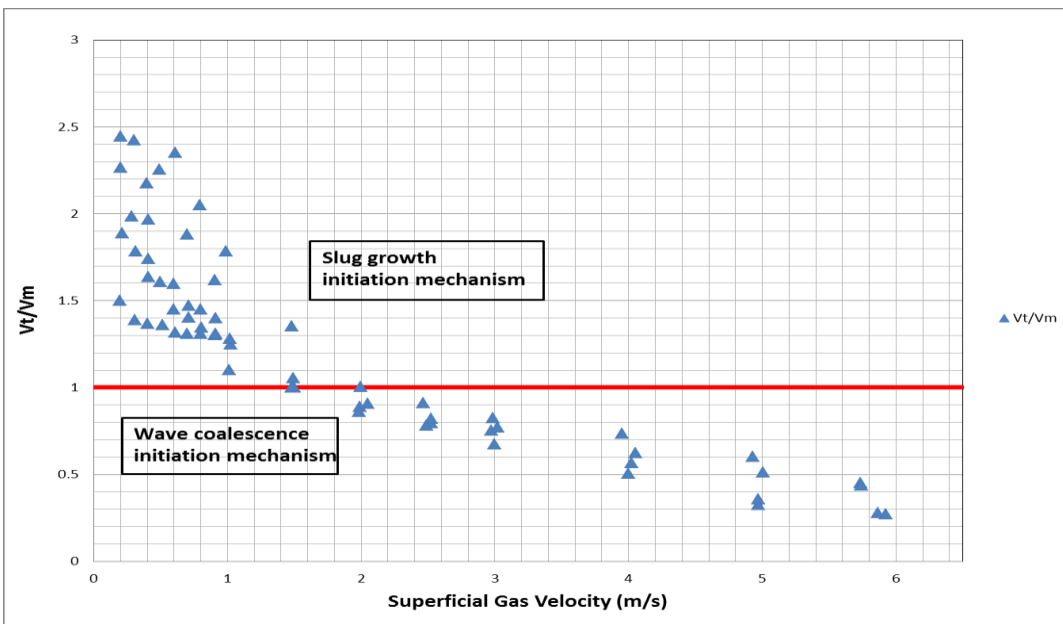


Figure 4-70: Initiation slugs translational to mixture velocities ratio for 12° test section

### 4.3 Chapter Summary

In this chapter, the experimental flow pattern maps were developed based on the range of superficial liquid velocities (0 - 0.55m/s) and superficial gas velocities (0 - 6m/s) for both  $\pm 24^\circ$  and  $\pm 12^\circ$  configurations.

In Section 4.1, air-water results were discussed for  $\pm 24^\circ$  configuration. In this section, various flow regimes were identified for different pipe section using both visual observation and time series analysis. The results showed that stratified flow mostly dominates the downhill pipe with other flow behaviour such as stratified flow with energetic ripples, stationary air pocket and aerated slug flow. Slug and aerated slugs dominate the uphill section. New flow regimes such as: wavy with aerated slug initiation and wavy with slug initiation were observed at the dip. Three slug behaviours were observed at the dip: complete stratified flow downhill with slug initiation at dip; stratified flow (with energetic ripple) downhill with slug initiation and slug growth upward dip; and aerated slug downhill and slug growth at the dip. This behaviour is different from existing work on this subject with low angle of inclination.

Slug parameters such as slug holdup, slug translational velocity, slug frequency and mean slug length were calculated. Average liquid holdup and slug parameters were compared with existing correlations. The result from the slug parameters coupled with visual observation were used to determine the two types of slug initiation mechanisms (wave growth and wave coalescence) which are geometry specific. Slug translational velocity was used as criterion to distinguish the flow condition for each slug initiation mechanism at the dip. The slug flow behaviour categories based on the pipe geometry ( $\pm 24^\circ$ ) showed that the slug flow structure of hilly terrain is pipe geometry specific.

Similarly in Section 4.2, air-water results were discussed for  $\pm 12^\circ$  configuration, most of the flow behaviour in  $\pm 24^\circ$  configuration is exhibited in  $\pm 12^\circ$  but at different flow conditions. The downhill section of  $12^\circ$  has no stationary air pocket in  $12^\circ$  dip pipe downhill test section. Unlike the  $24^\circ$  downward dip flow regime, there is no liquid accumulation at the dip in  $12^\circ$  configuration; this is due to the pipe geometry. The uphill section exhibited similar flow regime and slug initiation mechanism.

Bifurcation maps were developed to determine the flow behaviour along the pipeline using the maximum and minimum value of liquid holdup time series across the pipeline section. The results are in good agreement with visual observation.



## **5 RESULTS AND DISCUSION OF SAND–WATER TEST**

In this chapter, sand-water sand transport characteristics are discussed for  $\pm 24^\circ$  and  $\pm 12^\circ$  configurations from the settling and entrainment experimental results.

In order to investigate sand flow regime; visual observation and high speed cameras were used to record and identify the sand flow pattern developed during settling test at different sand concentration.

Results from conductivity rings data of sand-water settling test are also analysed for flow regime identification.

Furthermore, sand dune behaviour was investigated in dip pipeline from the entrainment test of sand-water and compared with existing work in horizontal pipes. Formation of dunes are characterised by measuring the sand dune geometry transporting inside the pipe.

In addition, comparison of results with literature is made on the relationship of sand dunes formation as a function of sand bed layer and flow rates. The statistical instability of sand dune and the condition of stability of sand dune geometry are discussed.

The minimum transport conditions for sand-water test are also discussed and the results are compared with literature.

### **5.1 Sand-Water Settling Test Result**

#### **5.1.1 Sand-Water Transport Characteristics**

When liquid and solid phase move together in a pipe, several flow regimes are possible and it is clearly important to recognise the behaviour and transition of these sand flow patterns. This task was carried out by visual observation according to sand concentration at various velocities.

In this section, sand settling test was carried out by slowly reducing the water superficial velocity until sand deposits were observed. The sand settling test in this work is under different sand conditions (50 lb/1000bbl, 100 lb/1000bbl, 200 lb/1000bbl, 500 lb/1000bbl) of average sand particle size of 270 microns as reported in chapter 3.

Both configurations ( $\pm 12^\circ$  and  $\pm 24^\circ$ ) exhibit similar observation and sand pattern. Hence,  $\pm 24^\circ$  configuration for sand concentration will be used to describe the sand characteristics for convenience of this discussion.

It was observed that sand transport characteristics for different sand concentrations in the dip configuration exhibit all the sand behaviour but at different flow conditions. The reason for various flow pattern is due to the inter play of different significant hydrodynamic forces involve in solid particles such as gravity, buoyancy, lift and drag forces.

Therefore, observations from experiments of sand concentration at 50 lb/1000bbl and 500 lb/1000bbl were described below for comparison. Specific illustrations are shown in Appendix E.

In general, the sand flow regimes observed for sand-water test based on visual observation and high speed camera video clips, can be classified into the following:

1. **Full suspension:** In this flow regime, sand particles are fully suspended and well dispersed in the flowing water. At high concentration, the sand particles are visibly observed to be transported at the middle of the pipe with velocity close to the velocity of the carrier fluid (water).
2. **Streak:** As the velocity of fluid reduces slightly from dispersed phase, the sand particles start forming a thin layer along the flow path but not settling at the bottom of the pipe.
3. **Saltation:** As the velocity further reduces, sand particle starts saltating and are continuously picked up and transported further in the pipe by the flowing water
4. **Sand dunes:** This is characterised by the formation of dunes as a result of the momentum of the sand being smaller than the fast moving water
5. **Sand bed:** This flow regime is observed at a very low velocity of water. Sand particles form a very slow moving bed at the bottom of the pipeline. Unlike saltation, there are no fast particles at the top of the bed.

### 5.1.2 Sand-Water Settling Test Result in $\pm 24^\circ$ Inclined Section

The results of various sand concentration shows that there are pronounced difference between horizontal (Yan, 2010) and inclined sand transport behaviour in  $\pm 24^\circ$  and  $\pm 12^\circ$  dip configuration. This is due to the influence of angle of repose formed by the sand for different pipe geometry coupled with gravity effect. Unlike horizontal pipeline, sand particles rolled and bounced along the inclined section.

Based on observations, sand transport characteristics in downhill and uphill pipe were similar but not exactly the same. Five different sand behaviours were identified within the range of flow condition (full suspension, streak, saltation, dunes, sand bed) as described above. At a very high water velocity above 1m/s, sand particles travelled very actively in both uphill and downhill pipe to form fully suspended flow for all the sand concentration ranges. At this flow condition, high water flow rate was sufficient to suspend the sand particles and prevent sand deposit. This may be as result of the sum of buoyant, lift forces and drag forces being greater than the gravity force, hence prevent sand settling at the bottom of the pipe at this flow condition. As the velocity reduces from 1m/s, the turbulent energy was not sufficient to keep the sand grains at full suspension, and gravity enhances the degree of sedimentation. The sand particles were therefore found transporting in form of streaks at water velocity of 0.9m/s for 50lb/100bbl while transition to streak begins from 1.0m/s for 500lb/1000bbl. It was also observed that sand streaks were denser towards the central line of pipe bottom in the downhill pipe than in uphill pipe, as shown in Figure 5-1.

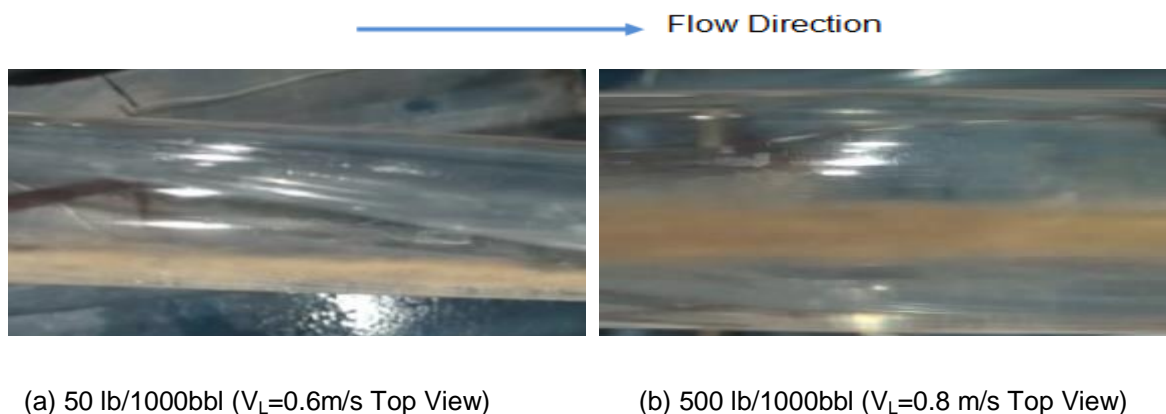


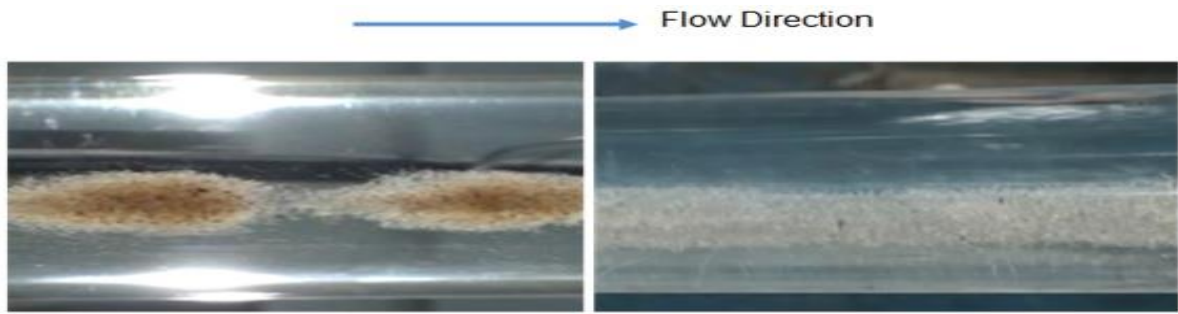
Figure 5-1: Sand streaks transition to saltation in downhill section

By further reducing the water velocity to 0.6m/s for 50lb/1000bbl, saltation of sand particles was observed; while transition to saltation occurred in 500lb/1000bbl at water velocity of 0.7m/s. It was observed that the sand grains moved by successive jumps at the bottom of the pipe.

By further reducing the water velocity,  $V_L$ , the particle grouped into clumps or islands within minutes after the flow rate was adjusted. At water velocity of 0.4m/s and 0.5m/s, sand dunes were formed for 50lb/1000bbl and 500lb/1000bbl respectively. Moving sand dunes were observed in the downhill pipe while a thin sand layer was found in the uphill pipe, as shown in Figure 5-2. Therefore, the sand concentration observed in downhill pipe was much higher than that in uphill pipe. In addition, at the uphill pipe section; a few sand particles were found tending to fall back due to the gravity effect. However, some of them stopped falling and balanced their position with other settled sand particles. The experimental results showed that the formation of sand dunes is possible at given sand concentration of sand particles at reduced stream velocity. The momentum that the sand particles obtained was not sufficient to keep them travelling, as a result the particles will accumulate at the downstream. At high sand concentration and relatively low velocity  $V_L$ , sand dunes were found travelling end to end; thus, high liquid velocity  $V_L$  will be required to entrain more sand particles. At lower concentration sand transport are narrowed and segregated at the bottom of the pipe section.

Further reducing the velocity below 0.3m/s, the sand dune disappeared and forming sand bed; there was a continuous formation of highly concentration of solid deposit on the bottom of the pipe. This could lead to partial or complete blockage and also reduce throughput. Such flow condition is always avoided in industrial application and pipeline design





(a) Downhill (Moving dunes, Bottom View)

(b) Uphill (Stationary, Top View)

Figure 5-2: Sand characteristics in downhill and uphill pipe (50lb/1000bbl,  $V_L=0.3\text{m/s}$ )

Table 5-1 and Table 5-2 presented below are the summary results of the flow conditions for various sand concentration for different flow downhill and uphill section for  $\pm 24^\circ$ . While Figure 5-3 and Figure 5-4 presented are the sand flow regime maps from Table 5-1 and Table 5-2 respectively.

Table 5-1: Velocity range of various sand flow regimes at  $24^\circ$  downhill

Sand Concentration (lb/1000bbl)	Water Velocity ( $V_L$ ) (m/s)				
	Full Suspension	Streak	Saltation	Sand Dune	Sand Bed
50	>0.9	0.8 – 0.6	0.5	0.4 – 0.3	0.2 – 0.1
100	>0.9	0.8 – 0.6	0.5	0.4 – 0.3	0.2 – 0.1
200	>1.0	0.9 – 0.8	0.7 – 0.5	0.4 – 0.3	0.2 – 0.1
500	>1.5	1.0 – 0.8	0.8 – 0.6	0.5	0.4 – 0.1

Table 5-2: Velocity range of various sand flow regimes at 24° uphill

Sand Concentration (lb/1000bbl)	Water Velocity ( $V_L$ ) (m/s)				
	Full Suspension	Streak	Saltation	Sand Dune	Sand Bed
50	>0.9	0.8 – 0.7	0.6	0.5 – 0.3	0.2 – 0.1
100	>0.9	0.8 – 0.7	0.6	0.5 – 0.3	0.2 – 0.1
200	>1.0	0.9 – 0.7	0.7	0.6 – 0.3	0.2 – 0.1
500	>1.5	1.0 – 0.9	0.8	0.7 – 0.5	0.4 – 0.1

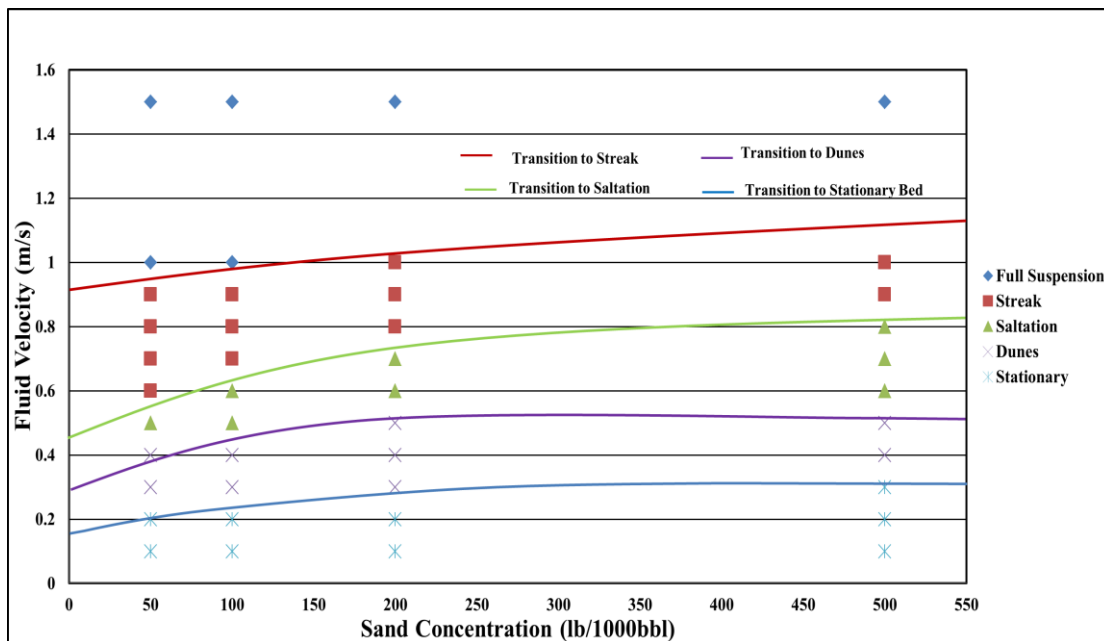


Figure 5-3: Downhill sand-water flow regime map for  $\pm 24^\circ$  inclined section

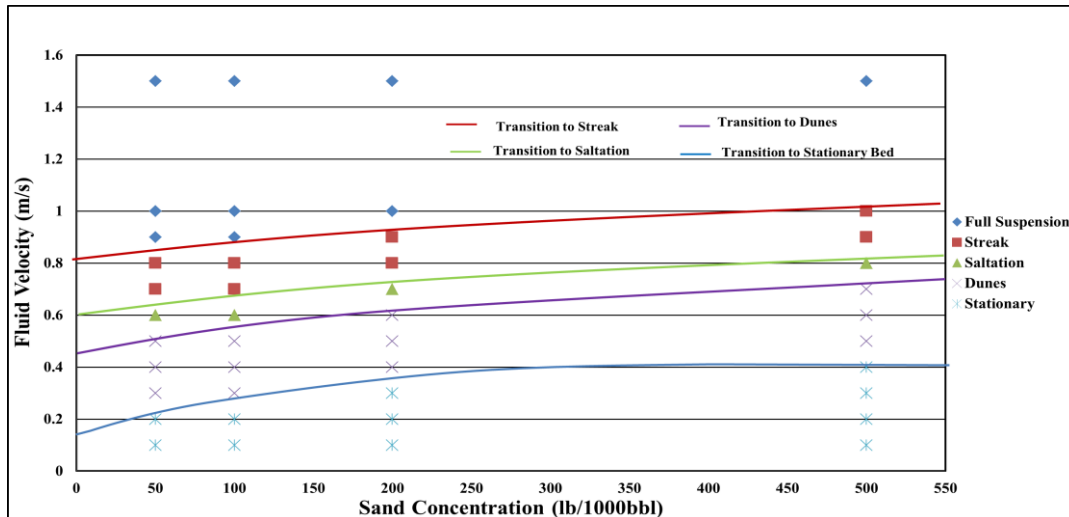


Figure 5-4: Uphill sand-water flow regime map for  $\pm 24^\circ$  inclined section

### 5.1.3 Sand-Water Settling Test Result in $\pm 24^\circ$ Dip Section

Similar observations were found at the dip section but slightly different from the downhill and uphill pipe section.

At a very high water velocity above 1m/s, sand particles travelled very actively at the dip (lower elbow) of the pipe to form fully suspended flow for all the sand concentration range.

The sand particles were found transporting in form of streaks at water 1.0m/s for all sand concentration shown in Figure 5-5.

By further reducing the water velocity to 0.6m/s for 50lb/1000bbl, saltation of sand particles was observed; while transition to saltation commenced at a higher water velocity of 0.8m/s in higher sand concentration like 500lb/1000bbl.

At water velocity of 0.5m/s and 0.7m/s, sand dunes were formed for 50lb/1000bbl and 500lb/1000bbl respectively. When sand dunes were generated at the dip, terrain influence could still be observed, especially at the upward of the dip section (Figure 5-7). At the bottom of the dip section, it was observed that sand dunes dissipated gradually until it transformed to sand streaks.

In contrast, sand dunes travelling in downhill section persist. The discrepancy may owe to the velocity profile changing because of the dip configuration and gravity effect. This phenomenon was observed obviously at the sand concentration of 50 lb/1000bbl and 200 lb/1000bbl.

As the water velocity was below 0.2m/s, the sand dune disappeared and forming a sand bed in 50lb/100bbl while sand bed starts to form at 0.3m/s for 500lb/1000bbl.

The velocities of the transition of flow regime for various sand concentrations were as a result of the internal flow structure observed at the dip. It was observed that when dense sand streak persist at the downhill section, sand particles appeared to be more dispersed at the entrance of the dip (upstream of the lowest point). When the water velocity was further lower, sand dunes were observed at the downhill pipe and at the entrance of the dip, whereas becoming dispersed when reaching the exit of the dip (immediate downstream of the lowest point). This condition was for a short period before sand dunes were observed at the uphill pipe. The reason for this phenomenon is due to the co-existence of gravity effect on the sand transport, and centrifugal force developed due to influence of secondary flow. This changes the flow behaviour at the dip.

Based on these observations, Table 5-3 below presents result obtained for various sand concentrations for 24 degrees bend. Figure 5-8 presents the sand flow regime from the plot of water velocity against sand concentration.

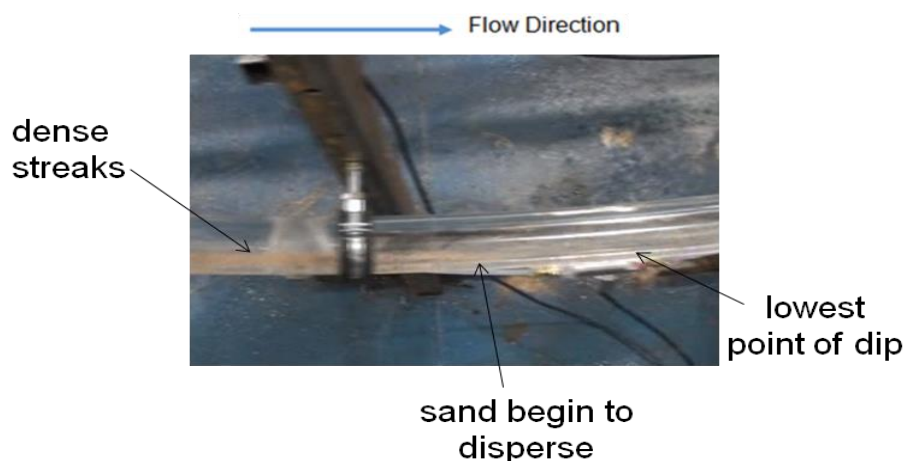


Figure 5-5: Terrain effect on sand characteristics at the dip ( $V_L=0.7\text{m/s}$ , 200lb/1000bbl)

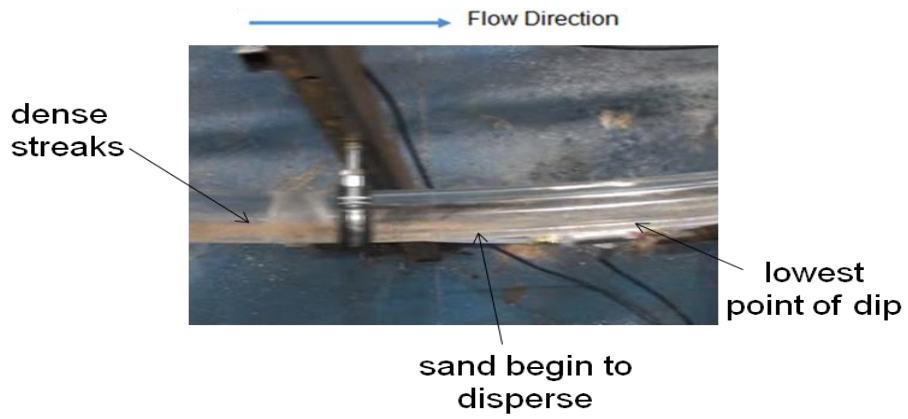
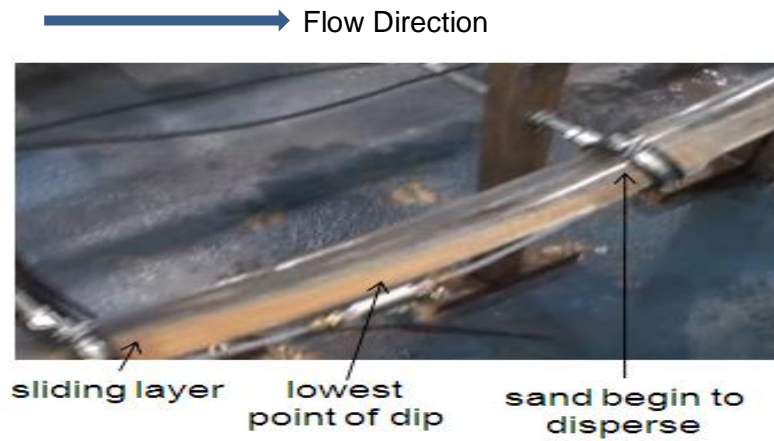


Figure 5-6: Terrain effect on sand characteristics at the dip ( $V_L=0.7\text{m/s}$ , 200lb/1000bbl)



(a) Dip section



(b) Uphill pipe

Figure 5-7: Terrain effect on sand characteristics at the dip ( $V_L=0.6\text{m/s}$ , 500lb/1000bbl)

Table 5-3: Velocity range for different flow regime of 24° downstream-dip section

Sand Concentration (lb/1000bbl)	Water Velocity ( $V_L$ ) (m/s)				
	Full Suspension	Streak	Saltation	Sand Dune	Sand Bed
50	>1.0	1.0 – 0.6	0.5	0.4 – 0.3	0.2 – 0.1
100	>1.0	1.0 – 0.6	0.5	0.4 – 0.3	0.2 – 0.1
200	>1.0	1.0 – 0.7	0.6	0.5 – 0.3	0.2 – 0.1
500	>1.0	1.0 – 0.8	0.7 – 0.6	0.5 – 0.4	0.3 – 0.1

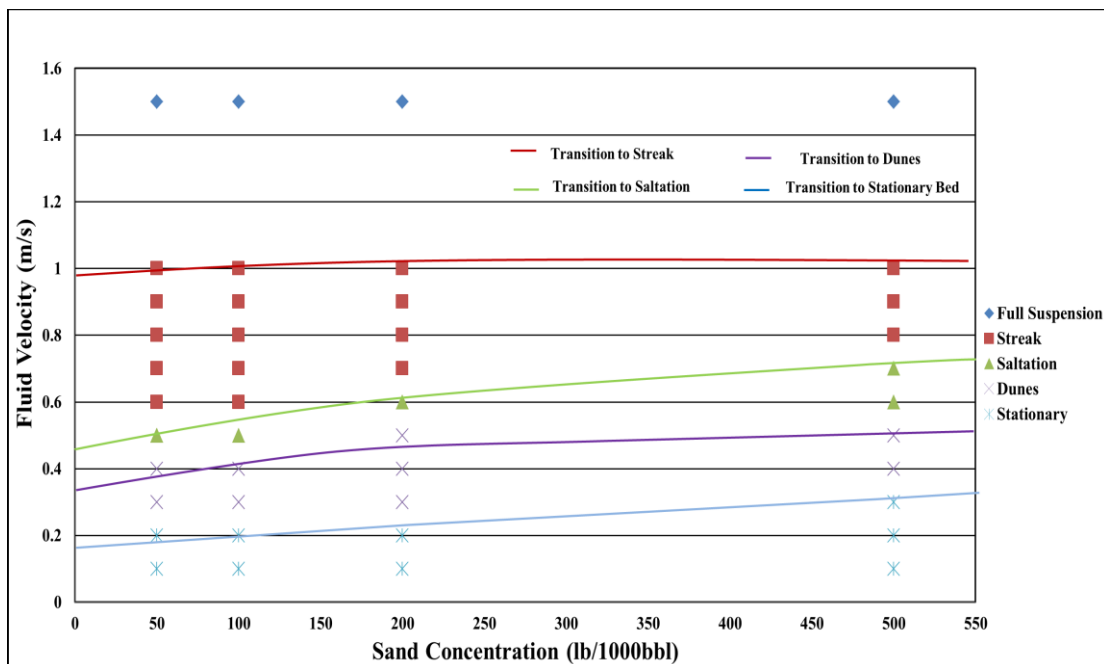


Figure 5-8: Dip section sand-water flow regime at the dip

### 5.1.4 Sand-Water Settling Test Result in $\pm 12^\circ$ Dip Configuration

Similar to the  $\pm 24^\circ$  configuration, sand settling test for sand–water experiment in  $\pm 12^\circ$  was carried out for various sand concentration. Flow regime maps for all sections (downhill, downstream-dip and uphill) in the  $\pm 12^\circ$  test were developed based on visual observation and re-examined by recorded video from high speed camera. The sand flow regime map for each section is shown below.

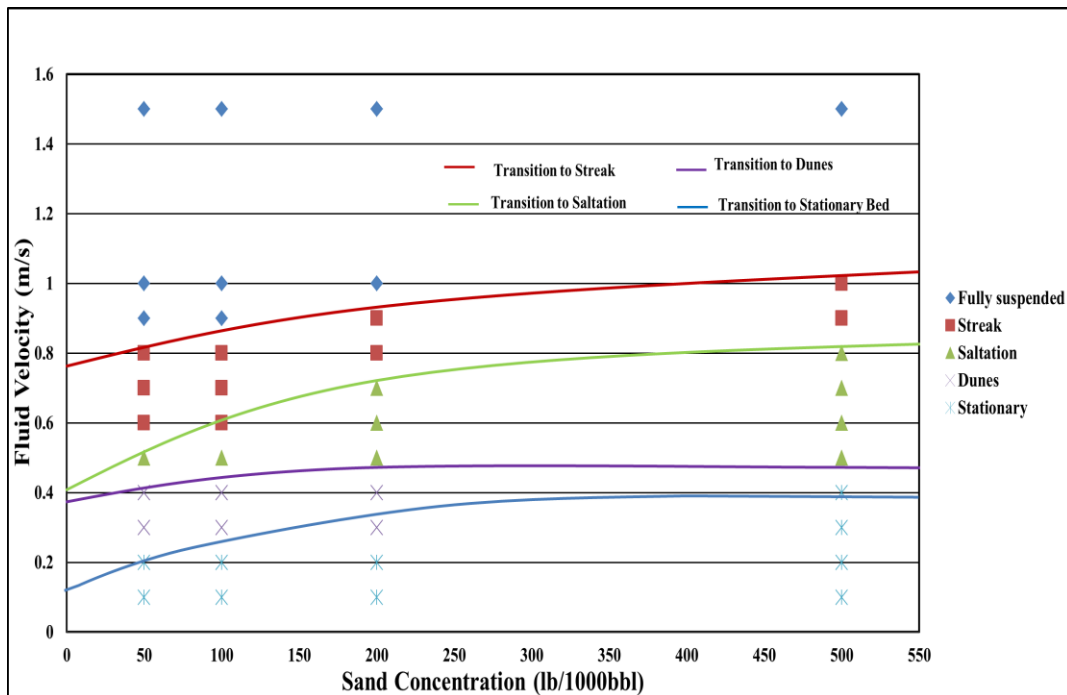


Figure 5-9: Downhill sand-water flow regime map for  $\pm 12^\circ$  dip pipeline

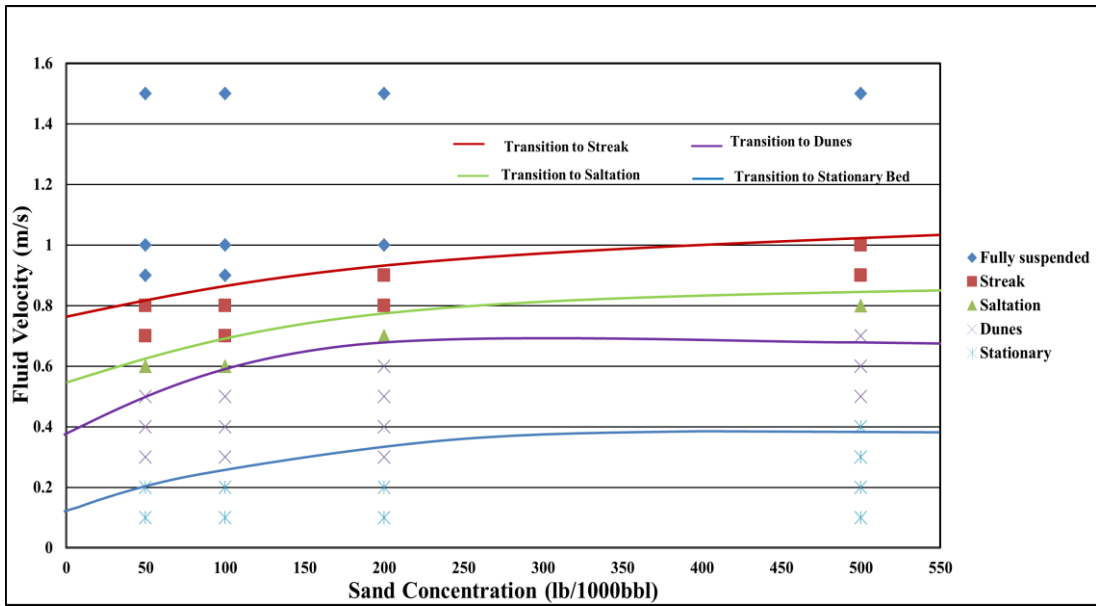


Figure 5-10: Uphill sand-water flow regime Map for  $\pm 12^\circ$  dip pipeline

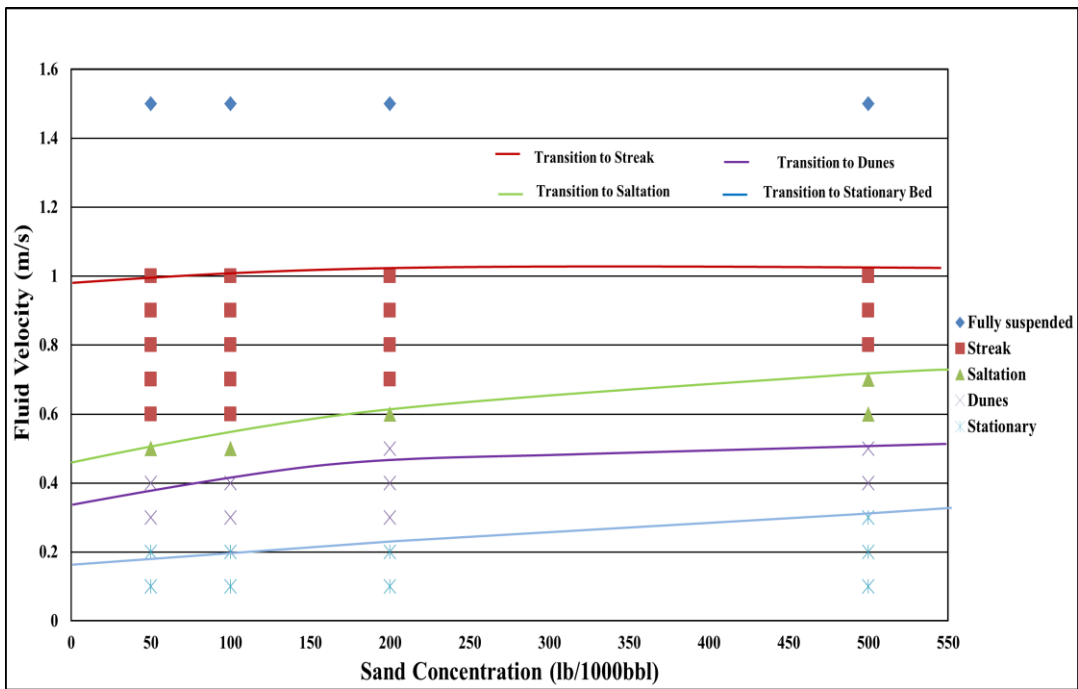


Figure 5-11: Dip section sand-water flow regime map for  $\pm 12^\circ$  dip pipeline



### 5.1.5 Comparison of Sand Flow Regime with Published Work

The results from the two configurations have their unique features which can be attributed to the orientation of the pipes. Figure 5-3 shows that the downhill section of the dip is mainly dominated by streak and the saltation flow regime. This is as a result of downward inclination acting downwards; which enhances the occurrence of sand saltation at slightly low velocity below dispersed phase. Also,  $\pm 24^\circ$  shows that uphill section is dominated by formation of sand dunes and sand bed due to upward flow direction against gravitational force; forming sand dune immediately the velocity reduces. There is slight difference result between  $\pm 12^\circ$  and  $\pm 24^\circ$  configuration.

Yan, 2010 carried out similar sand settling test in 2-inch (horizontal and  $5^\circ$  uphill section) within the same operating conditions (i.e. sand concentration and water velocity). In his work, he observed the same sand flow characteristics at sand concentration of 50lb/1000bbl.

Table 5-4: Comparison of measured velocity range for sand flow regime of inclined section and Yan, 2010 result

Sand Concentration (lb/1000bbl)	Water velocity ( $V_L$ )			
	Full Suspension (m/s)	Streak (m/s)	Saltation (m/s)	Sand Dune (m/s)
50 (Horizontal and $5^\circ$ ) (Yan, 2010)	1.0 -0.6	0.55-0.47	0.47-0.45	0.4
50 ( $+12^\circ$ )and ( $+24^\circ$ )	1.0 - 0.9	0.8 -0.7	0.6-0.5	0.5-0.3

Table 5-4 presents Yan, 2010 result with uphill section of  $12^\circ$  and  $24^\circ$  configurations, the result showed that the higher the inclined angle, the higher the velocity to settle at the bottom of the bed This is due to the rolling and falling back of sand particles and the dominating effect of gravity force over the net effect of lift, drag and buoyancy forces being experienced in inclined pipe.

## 5.2 Identification of Sand-Water Flow Regime Using Conductivity Ring Signals

The water-sand settling test experiment was also measured using the conductivity ring installed in all the sections (downhill and uphill). Each of the configurations has a total of four pairs of conductivity rings as previously discussed in chapter 3.

The conductivity ring data obtained were examined to determine the sand flow pattern from the conductivity signals. The time series obtained from conductivity ring signals were analysed by plotting the normalised voltage value for each pair of the rings. The normalised voltage value is defined as  $(\text{Voltage}_{(\text{water} + \text{sand})} / \text{Voltage}_{(\text{water only})})$ .

Each data point recorded from the conductivity sensor represents 0.02sec, a total of 15,000 data points (300s) were recorded as continuous sand injection persist. Normalised time series plots of conductivity rings signals for the  $\pm 24^\circ$  configuration were used to demonstrate the use of conductivity rings for flow identification of the five established sand characteristics already discussed in Section 5.1.1 (i.e. full suspension, streak, saltation, dunes and sand bed) for all sand concentration.

### 1. Full suspension

Figure 5-12 shows the flow regime of full suspension for 50lb/1000bbl for downhill section. Appendix E presents characteristic feature for full suspension flow rates for all pipe sections at various sand concentration. Full suspension depicts a narrow strip of normalised time series lines representing the respective pairs of conductivity rings. It is observed that the normalised voltage values are very close to value of 1.0; indicating that the sand particles are fast moving and suspended in the water and are not in contact to the internal walls of the conductivity rings. Hence this gives a reading close to one.

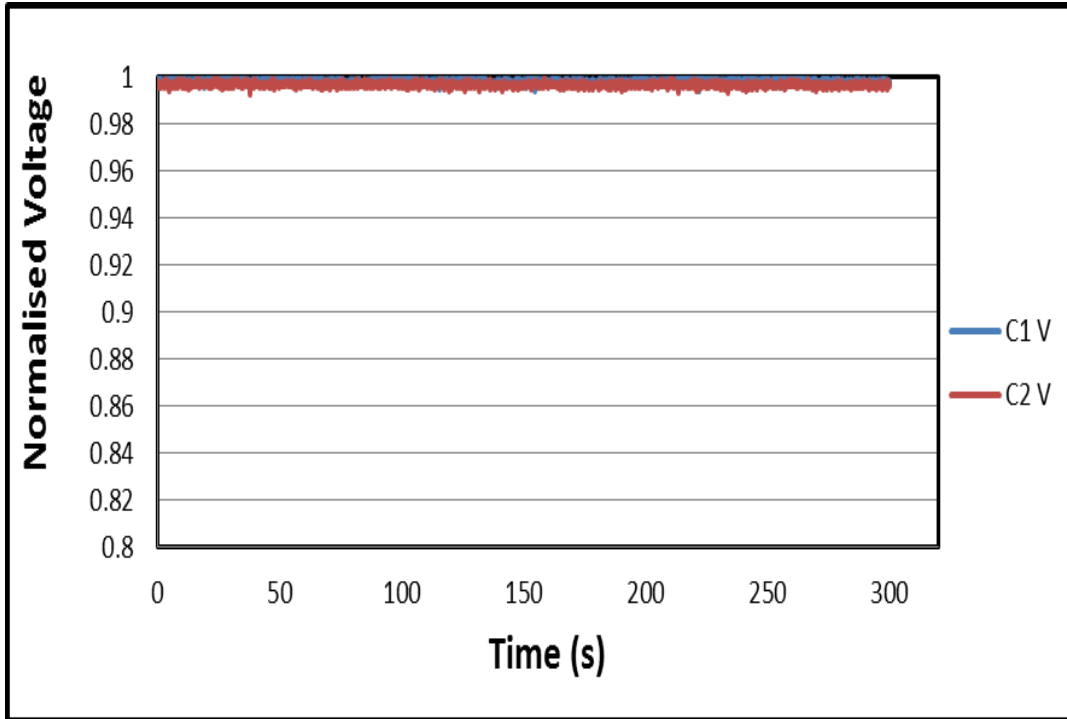


Figure 5-12: Full suspension from conductivity ring, (50lb/1000bbl,  $V_{sl}=1.0\text{m/s}$ )

## 2. Streak

Figure 5-13 shows the flow regime of streak for 100lb/1000bbl for all downhill sections. The characteristic feature for each plot in all pipe sections depicts a narrow strip of normalised time series lines representing the respective pairs of conductivity rings. From the plots for all pipe sections in Appendix E, the normalised voltage values reduced to range between 1 to 0.9 based on the sand concentration and the water flow rate. This indicates that the presence of more sand particles in the streak flow regime is more than the fully suspended flow regime. The voltage readings for all sections are almost of the same range.

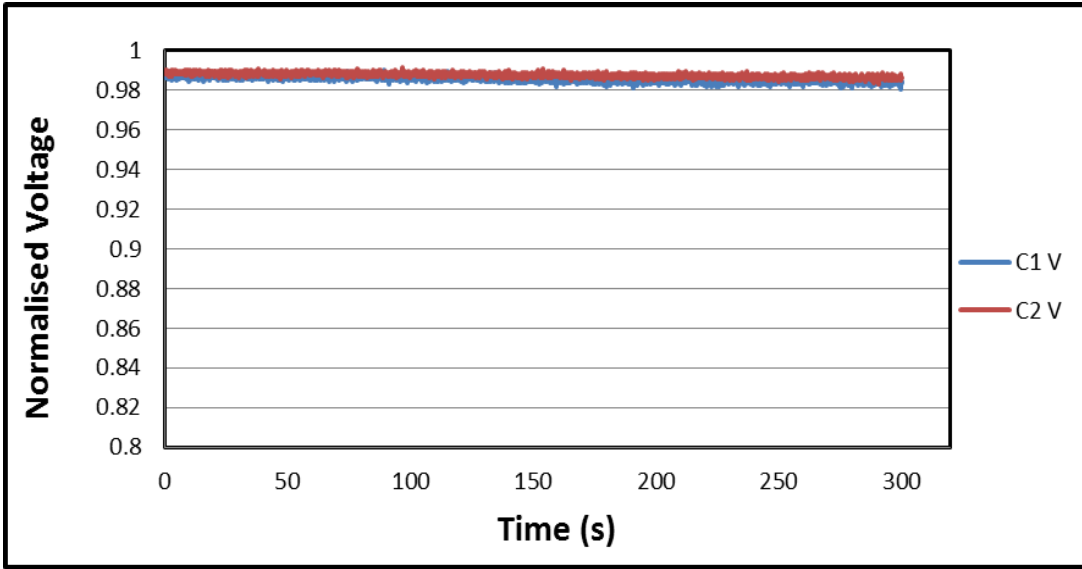


Figure 5-13: Streak regime from conductivity ring, (50lb/1000bbl,  $V_{sl}=0.8\text{m/s}$ )

**3. Saltation**

Figure 5-14 shows the flow regime of streak for 200lb/1000bbl for downhill section. The characteristic feature for each plot in all sections (in Appendix E) depicts a slightly curved strip of normalised time series lines with high and low spikes along the trend plot. The high and low spike indicates the saltation of sand particles further in the pipe.

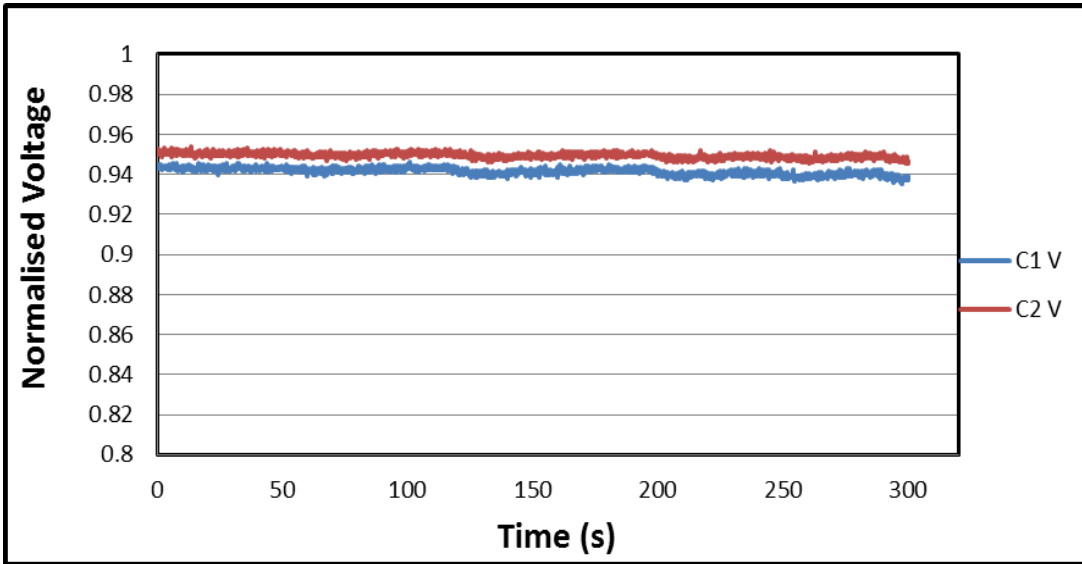


Figure 5-14: Saltation regime from conductivity ring, (50lb/1000bbl,  $V_{sl}=0.6\text{m/s}$ )

#### 4. Sand Dune

Figure 5-15 shows the flow regime of sand dune for 50lb/1000bbl for uphill-dip. The plots show a typical fluctuation of a sand dune. The lower spike or trough of the dune indicates the peak of the dune when the sand particles build up. The upper spike represents the region of low sand particle region (dune tail) i.e. more of water.

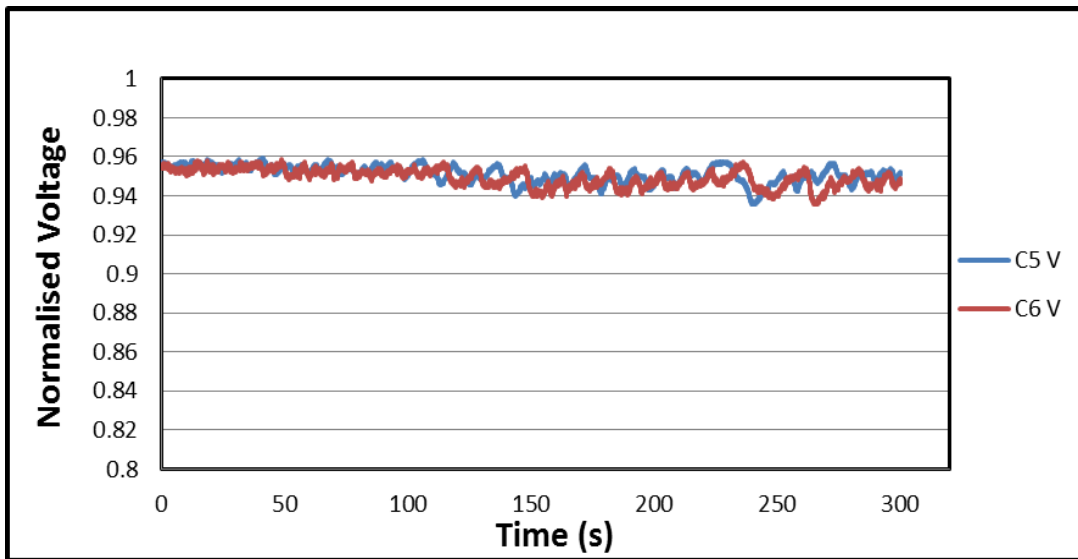


Figure 5-15: Sand dune regime from conductivity ring, (50lb/1000bbl,  $V_{sl}=0.4\text{m/s}$ )

#### 5. Sand Bed

Figure 5-16 shows the flow regime of sand bed for 200lb/1000bbl for all sections. The characteristic feature for each plot in all sections depicts a narrow strip of normalised time series lines representing the respective pairs of conductivity rings. From results for all sections, it was observed that the normalised voltage values have reduced to a range of 0.92 to 0.8 at the downhill section when compared to the full suspension regime, thus indicating the presence of more sand particles in the sand flow regime.

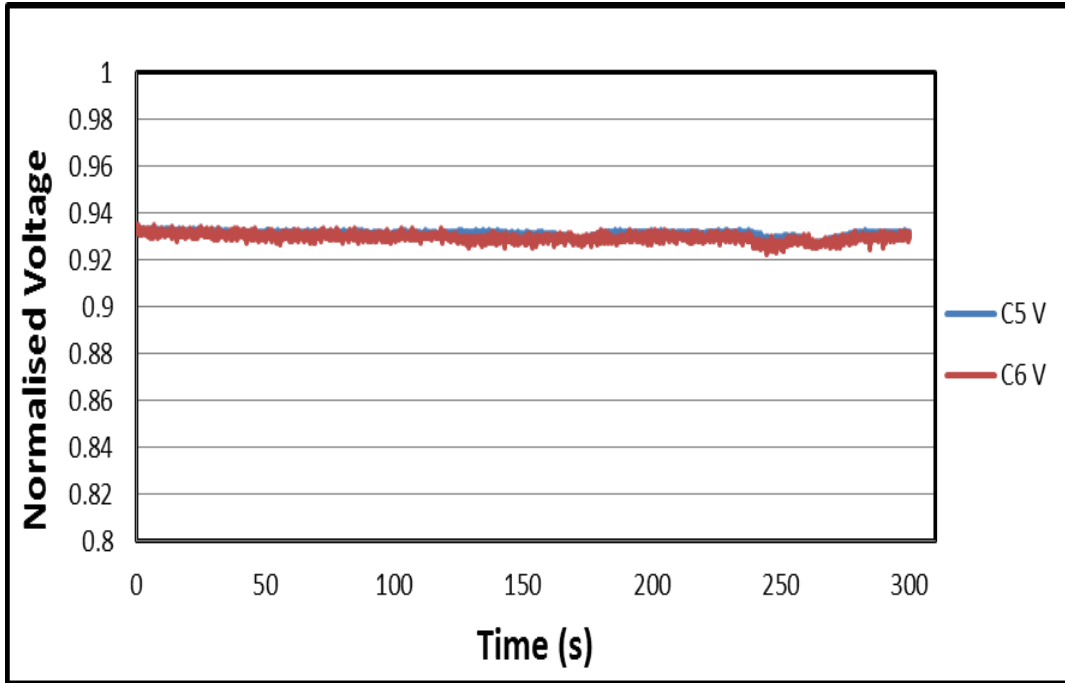


Figure 5-16: Sand bed regime from conductivity ring, (200lb/1000bbl,  $V_{sl}=0.3\text{m/s}$ )

Figure 5-17 to Figure 5-20 presented the average normalised voltage of various sand concentrations at various pipe sections. The result showed that as the velocity reduces the sand concentration settling in the pipe (being captured by the sensor) increases. At high velocity where it is full suspension, the average normalised voltage is about 0.98 for 50lb/1000bbl while it is about 0.90 for 500lb/1000bbl.

The normalised voltage result ranges from 0.8 -1 with the range of liquid velocity of 0.3-1m/s. The reason is due to low sand concentration (<1%) considered for this study.

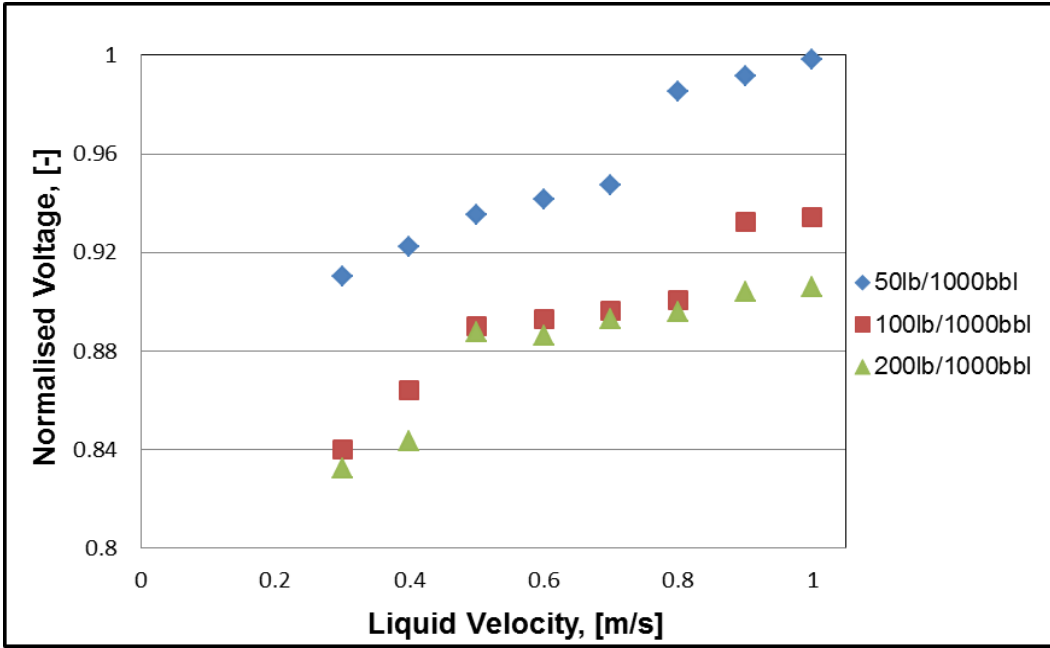


Figure 5-17: Average normalised voltage vs. liquid velocity (downhill, (CR-1))

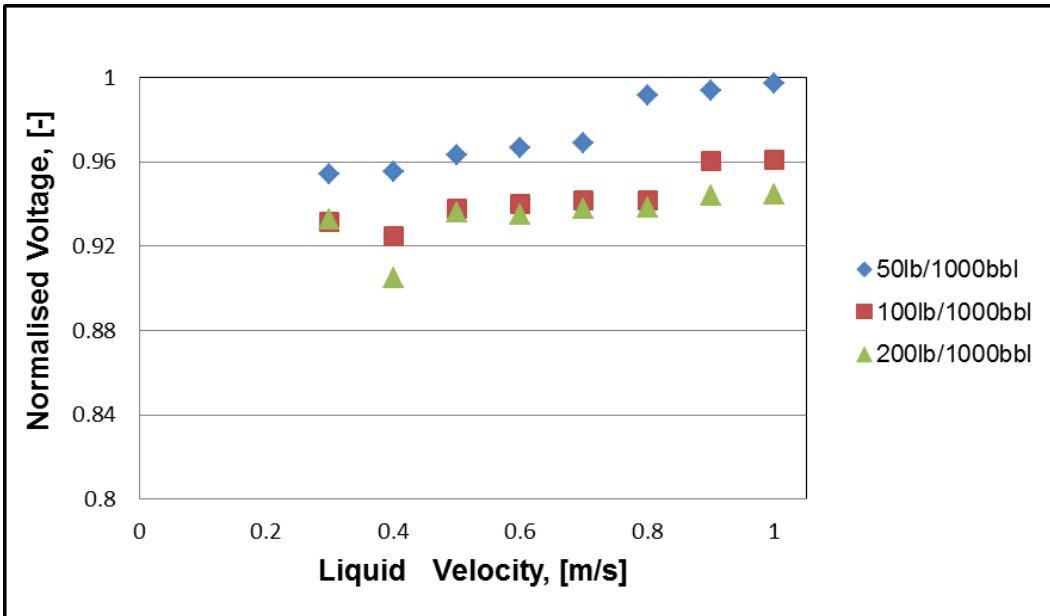


Figure 5-18: Average normalised voltage vs. liquid velocity (downward-dip, (CR-3))

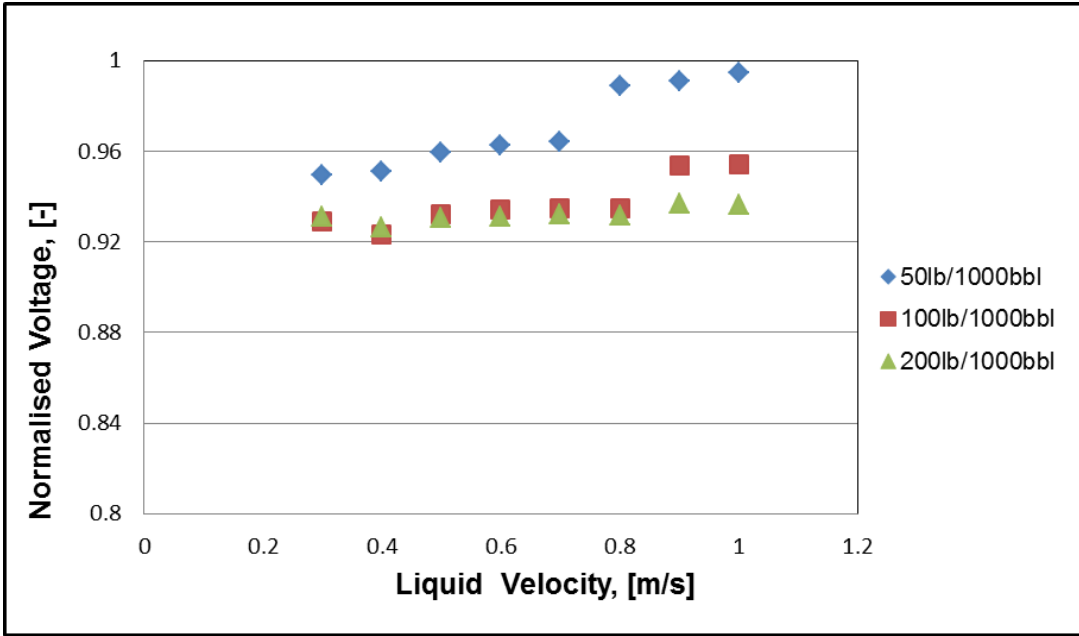


Figure 5-19: Average normalised voltage vs. liquid velocity (upward dip, (CR-5))

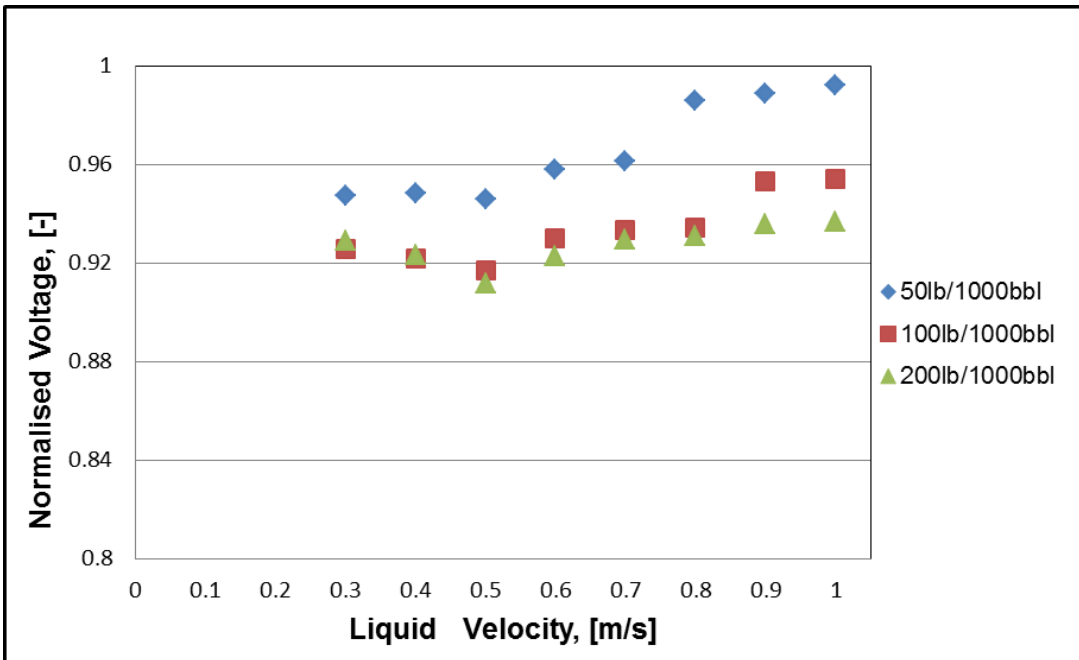


Figure 5-20: Average normalised voltage vs. liquid velocity (uphill section, (CR-7))



### **5.2.1 Limitation of Conductivity Ring in Sand Measurement**

The conductivity ring measurement has its own limitation in distinguishing certain categories of sand characteristics. From the conductivity ring signal results, there was no clear distinction between the full suspension, streak and sand bed flow regime. These sand characteristics can only be distinguished based on the relative values of the normalised voltage at a given sand concentration. However, the conductivity ring results clearly describe the sand dune flow regime by generating a typical fluctuating shape. Hence, it is deduced that the conductivity ring is best suitable for describing the sand dune and sand bed flow regimes. In addition, the sand fraction for each flow regime was cross examined below, based on the correlation obtained from the conductivity ring calibration.

### **5.2.2 Sand Holdup Measurement Conductivity Ring**

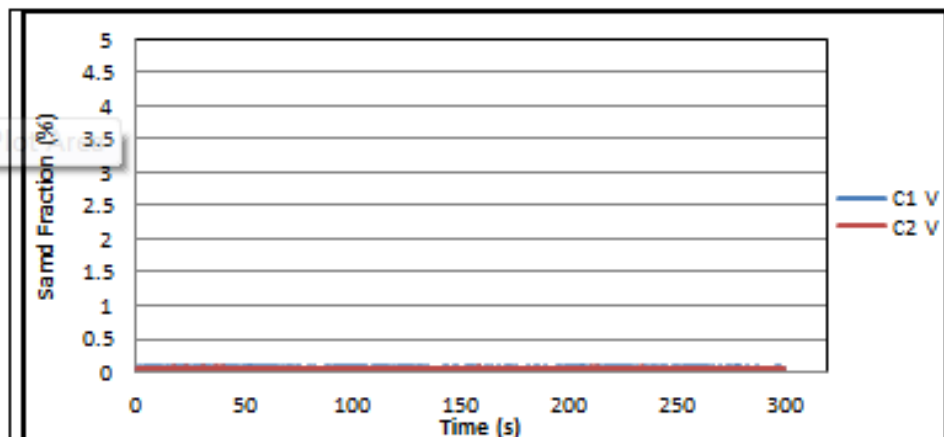
The instantaneous values of sand phase concentration can be obtained by means of the conductance technique. This work investigates the sand fraction time series in undulating pipe line using conductivity ring techniques.

The 2-inch conductivity ring calibration for sand-water raw data of the voltage was reported in chapter 3. In addition, sand normalised voltage value has been reported in section 5.2.

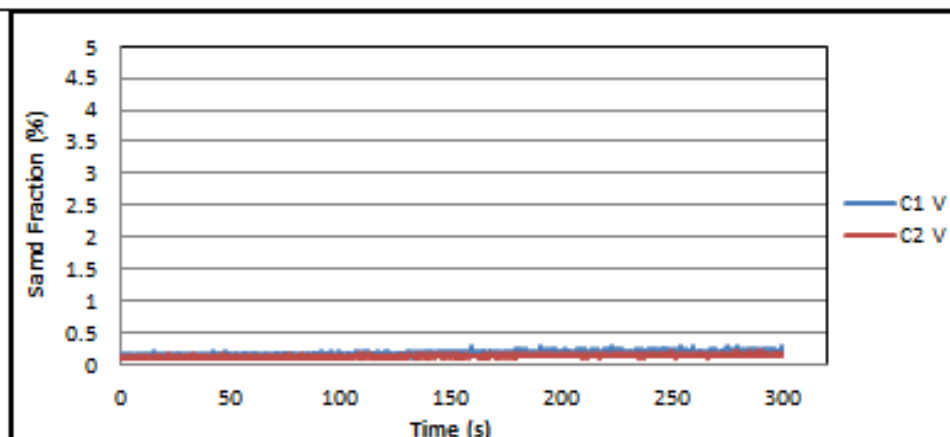
The response of conductivity rings output voltage signals were converted to sand fraction (%) using the normalized voltage and the calibrated curve of the individual signals of the conductivity rings.

The sand fraction (ordinate-axis) was not scale equally for all the plots because of the variation in sand concentration and sand deposit at the bottom of the pipe. Using full scale was not applied in order to clarify actual value of instantaneous sand fraction. Table 5-5 presents sand fraction for (50lb-1000bbl) indicating the same trend as normalised voltage. See Appendix E for full result of sand-water settling test.

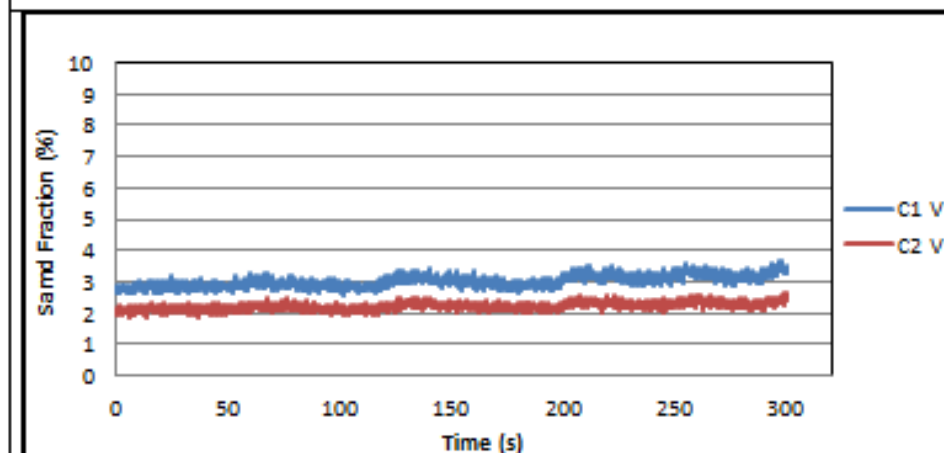
Table 5-5: Flow behaviour from conductivity ring sand hold up measurement



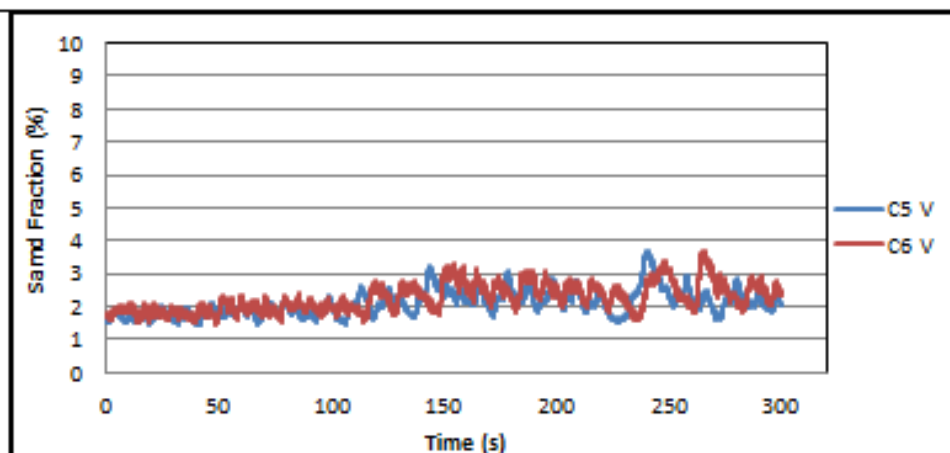
(a): Conductivity ring sand fraction for downhill section (50lb/1000bbl,  $V_{sl}=1.0\text{m/s}$ )



(b): Conductivity ring sand fraction for downhill section (50lb/1000bbl,  $V_{sl}=0.8\text{m/s}$ )



(c): Conductivity ring sand fraction for downhill section (50lb/1000bbl,  $V_{sl}=0.60\text{m/s}$ )



(d): Conductivity ring sand fraction for uphill-dip section (50lb/1000bbl,  $V_{sl}=0.40\text{m/s}$ )

### **5.3 Sand-Water Entrainment Test Result**

In this section, sand-water entrainment test was carried to study sand dunes behaviour at the dip and compared with published work in horizontal pipes. Saltation is characterised by the formation of dunes with specific length and velocity travelling inside the pipe. One of the typical characteristics of solid-liquid mixture at low velocity is to form dunes. The sand dune influences the dynamics of sand transportation and partial blockage in the pipeline which causes local velocity and pressure fluctuations due to sand dune movements. The sand dune is strongly dependent on the flow rate, height of the bed layer and the pipe diameter. In this section, the sand dune evolution is related to inertial phenomenon similar to Kelvin Helmholtz Instability (KHI). The condition of stability of sand dune geometry was examined.

### **5.4 Sand Dune Mechanism**

Sand-water entrainment experiment was carried out on sand bed deposited in  $\pm 24^\circ$  dip section. Different level of sand (0.26D, 0.29D, 0.37D, 0.44D and 0.53D) were systematically placed at the bottom of the dip as follows:

- a. Inject sand mixture at high sand concentration with high velocity of water
- b. Set the sand-water mixture flow condition at homogenous condition
- c. Switch of the water supply and sand injection pump at the same time and allow the sand to settle with a flat level of sand at the dip.

The level of settled sand increases as the sand concentration increases. While the sand settled at the dip section, the sand entrainment starts increasing with liquid flow rate from zero to a rate when the sand particles start to move.

Sand bed height of 0.29D will be used to describe the entrainment mechanism for convenience of discussion. At very low liquid velocity of 0.06m/s, few particles of smallest sand size starts moving, this is regarded as the sand bed threshold velocity for this sand bed height (0.29D). At this flow condition, the particles did not make any significant difference to the sand bed level. The sand bed level remains at 0.29D until the water flow rate was increased to a value slightly greater than this threshold velocity that kept the sand bed stationary (see Figure 5-21). As water velocity was increased up to 0.18m/s; the local velocity at the dip increases thereby initiate sand particles

movement. Within minutes, sand particles get initiated to form ripple at the top of the sand bed towards the exit of the dip section as shown in Figure 5-22. It was observed that the velocity of the liquid was fast enough to roll the static sand particles.

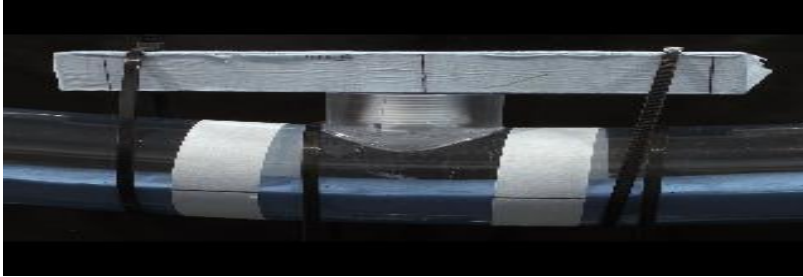


Figure 5-21: Static sand bed, sand bed layer =0.29D

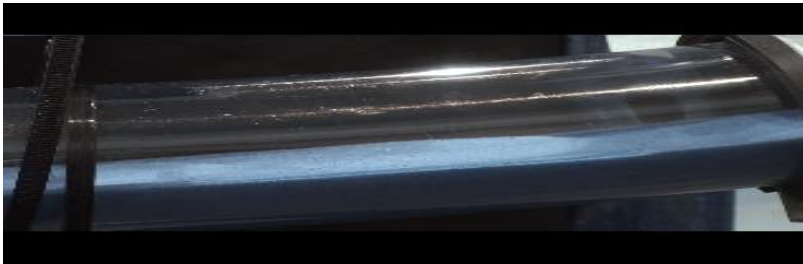


Figure 5-22: Sand dune Initiation at water velocity =0.18m/s



Figure 5-23: Sand bed forming Ripple at water velocity =0.18m/s

Sand dune is yet to be initiated at the upstream of the dip

Sand Particles experienced eddies that enhanced the picking of sand particles forward

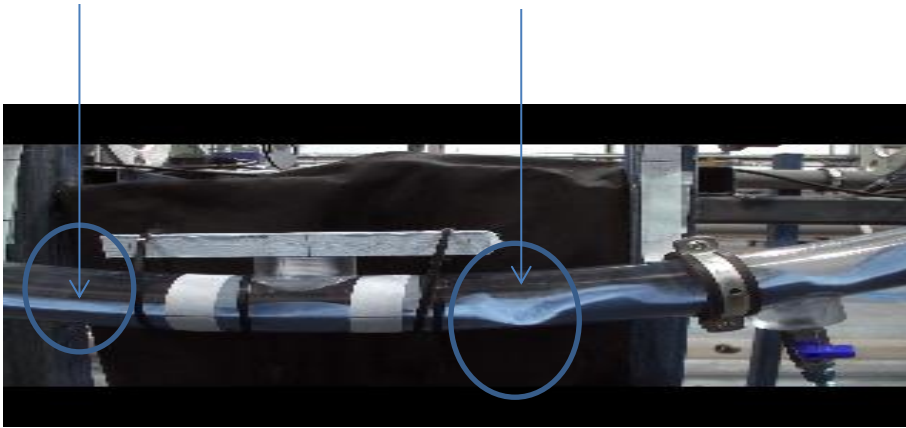


Figure 5-24: Unstable sand dune at water velocity =0.18m/s



Figure 5-25: Sand dune reach stability at water velocity =0.18m/s

As the velocity remains constant at 0.18m/s, the ripple on the sand bed extended to the whole section of the dip in form of sand wave. The amplitude of the crest increases with time with a short wave length. The sand wave structures create a local turbulence that enhances sand saltation and consequently forms sand dune. As the sand dunes are formed, the local velocity of water reduces at the trough and coupled with gravity effect leads to decrease in sand velocity.

After sand dune was observed, the sand dune geometry measured at a given position is relatively constant while moving. Although, unlike straight pipe, the amplitude of the sand dune geometry was not uniform throughout the dip section but the dune height at a given position remains constant. The stability condition is defined as the local velocity that sand dune is in equilibrium. This is when sand dune height at a given position is constant over a given time. This stability of sand dune (i.e. when the sand dune geometry is constant at a given condition) is a function of sand bed layer and the liquid velocity.

The stage of this phenomenon corresponding to the initiation of sediment transport; known as threshold velocity of sand entrainment (or critical stage of a moving bed). Table 5-6 below presents the threshold velocity stages of sand particle movement for +24° dip from the entrainment test carried out for various sand bed layers.

Table 5-6: Threshold velocity of sand entrainment

Sand Bed Level (m)	Water Velocity (m/s)
0.26D	0.1
0.29D	0.06
0.37D	0.05

Where D= Pipe Diameter (2-inch)

As water velocity increases to 0.21m/s, the wave amplitude increases, the local velocity changes which enhances sand dune movement. The particles began to break up into separate dunes along the bottom of the pipe based on flow condition and level of sand bed that initiate the sand dune. The sand dunes are spaced periodically, initially unstable but became stable after some time.

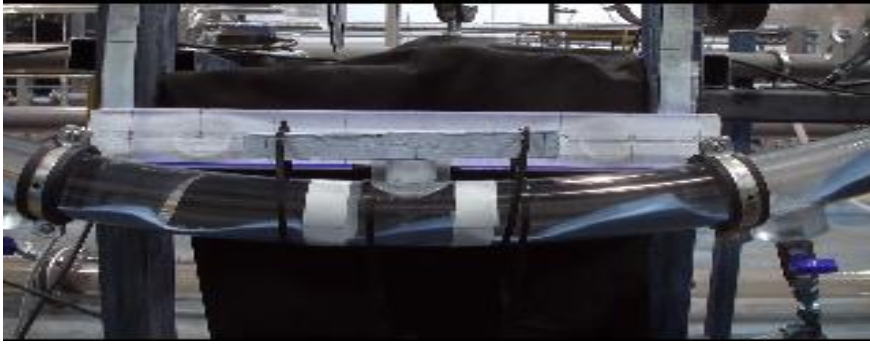


Figure 5-26: Sand dune evolution at water velocity =0.21 m/s

Once the stream velocity increases above critical velocity of single sand bed movement, wave like deformation on the surface of the sand bed appeared. Therefore, the critical condition for dune formation was examined in order to determine the critical condition to transport particles deposited in pipelines.

This formation of sand forming ripples and periodic sand dunes occurred in sediment transport and during start-up of a partially blocked pipeline.

The character of the fluid motion, local velocity and the motion of sand dune are interdependent and must be taken into consideration when describing sand dune characteristics. Therefore, the geometry and the velocity of the sand dunes were measured by high speed camera and image process techniques as described below.

## 5.5 Sand Dune Measurement

Sand dune geometrical parameter dimensions (Sand holdup, Height (h), Pitch (p) and Velocity) were measured using a high speed video camera.

However, the interface between the liquid and sand bed (and sand dune) is not well demarcated. This generates measurement uncertainty which was reported in appendix A as percentage error of 6.5% and standard deviation mean of  $\pm 0.008$  with 68% confidence limit.

### 1. Sand Dune Pitch (Wavelength)-Sand dune Length ( $l_s$ )

This is defined as the leading edge distance between the two dune fronts or the distance between two peaks or crests. The metering unit value is determined using the calibrated measurement resolution with the ruler placed at the dip.

### 2. Sand Dune Frequency ( $w_f$ )

This is the number of dunes passing a given point per second. The sand dune frequency for a given velocity can be determined by counting dune front/crest at a particular point on the pipe.

### 3. Sand Dune Height

This is the height of the amplitude of the crest of the sand dunes. It is defined as fraction of the pipe diameter.

### 4. Sand Dune Velocity ( $u_s$ )

The sand dune front velocity is defined as the distance moved by the dune per second. Sand dune front velocity is measured using video camera and calibrated scale of the distance. This is then determined using equation as follows:

$$\bar{u}_s = \overline{(l_s * w_f)} \quad \mathbf{5-1}$$

Where

$\bar{u}_s$  is the average sand dune velocity,  $l_s$  is the sand dune length and  $w_f$  is the sand dune frequency.

### 5. Local Mean Velocity ( $V_l$ )

The local velocity ( $V_l$ ) of the flow can be calculated as follows:

$$V_l = \frac{Q_l}{AH_s} \quad \mathbf{5-2}$$

Where: ( $Q_l$ ) and ( $A$ ) are Liquid flow rate and pipe area respectively

( $H_s$ ) is the holdup of the sand dune as calculated below in section 5.5.1



### **5.5.1 Sand Hold up Calculation**

The sand holdup was determined by simple geometry, assuming the sand bed is flat. For calibration purpose, a measured tape was also recorded with each video film of sand bed layer. This will enable the pixel coordinates to be converted to millimetres. As a result, all screen resolutions (magnification) in the video could be scaled to real unit values. Also, the porosity of sand was determined by filling a spool piece (of the same pipe diameter pipe) with given amount of sand. The sand porosity was found to be 0.36. The procedure of sand holdup calculation and calibration is in Chapter 3.

## **5.6 Sand Dune Analysis**

The sand dune wavelength and dune height metering unit value were determined using the calibrated measurement resolution recorded from high speed camera focused on the dip. The sand dune analysis are categorised into: (1) Sand dune evolution and (2) Stability of sand dunes.

### **1. Sand Dune Interfacial Wave Characteristics**

The observation of the sand dune shows that sand dune evolution was unstable which may result to local velocity fluctuation and other geometry characteristics variation. This unstable sand dune geometry is a consequence of sand bed sliding from the downhill section due to the influence of the flow rate and pipe geometry. This is a form of interfacial wave behaviour similar to Kelvin Helmholtz Instability (KHI) theory. To analyse this phenomenon, the sand dune parameters are based on average value.

The evolution of sand dune was studied using 0.44D and 0.53D sand bed layer at various stream velocities are shown in Figure 5-29. For 0.44D, sand dune evolution commenced at critical velocity of 0.25m/s and persist till  $V_L = 0.33\text{m/s}$ . The sand dune was flushed out completely between 0.36-0.4m/s. These sand bed layers represent a partially blocked pipe. However, at a given sand bed, increasing the mixture velocity reduces the sand dune height. This is due to additional turbulent energy from increased liquid velocity to transport the sand particle forward which reduces the sand dune height. Figure 5-30 showed the behaviour of the sand dune for a high level of sand bed (above 0.44D). The velocity ratio is almost constant at any given sand dune height. This implies that the velocity of the dunes increases as the mean stream velocity

increases. Another observation in the result is that the ratio of sand dune wavelength to the dune height at the dip is between 2- 6 while for horizontal pipe was 9 to 40 in Thomas (1964) work. Sand dune parameters obtained from dip was compared with Thomas' correlation of sand dune mechanism for closed pipe and open channel that was developed based on Kelvin Helmholtz instability theory presented as dimensionless number ( $Y$ ) and ( $Z$ ) in equation (5-3 and 5-4) below

$$Y = \frac{\left(\frac{u^2}{g\lambda}\right)}{\left(\frac{\rho_p - \rho}{\rho}\right)} \quad 5-3$$

$$Z = \frac{1}{2\pi} \left[ \frac{1}{4} \left(\frac{u_d^2}{gH}\right) \left(\frac{D}{H}\right)^{\frac{5}{3}} \left(\frac{D}{D_p}\right)^{\frac{2}{3}} \right] \quad 5-4$$

Where

$u$  = Fluid velocity,  $H$  = Sand Dune Height,  $D$  = Pipe Diameter,  $\rho$  = Water Density

$\rho_p$  = Sand density,  $\lambda$  = Sand dune wavelength,  $u_d$  = Sand dune velocity.

Figure 5-31 shows there is slight deviation from Thomas' correlation. This is may be due to different ratio of sand dune wavelength to the dune height used; and effect of the dip geometry.



Figure 5-27: 0.44D sand bed layer ( $V_L = 0$  to 0.20m/s)

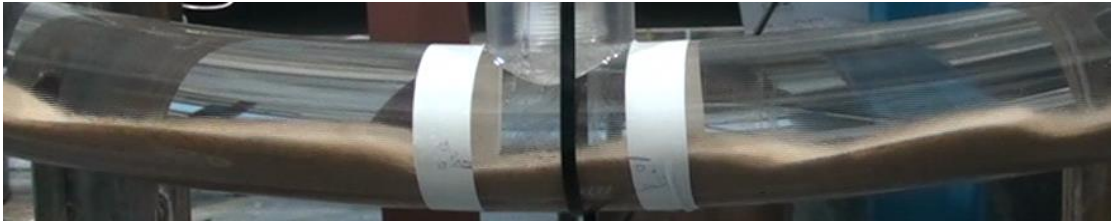


Figure 5-28: Sand dune formation at ( $V_L = 0.30\text{m/s}$ )

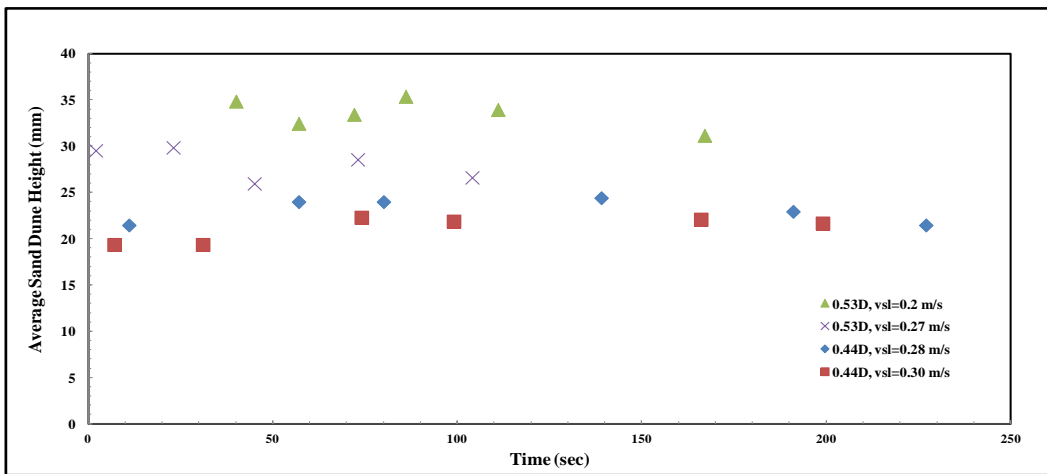


Figure 5-29: Sand dune development

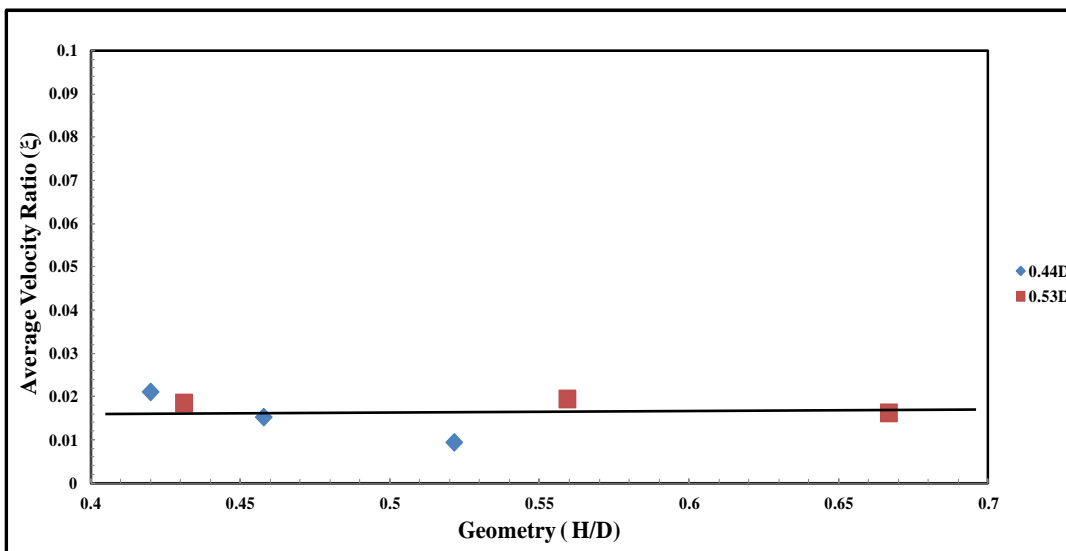


Figure 5-30: Average sand dune velocity with sand dune geometry

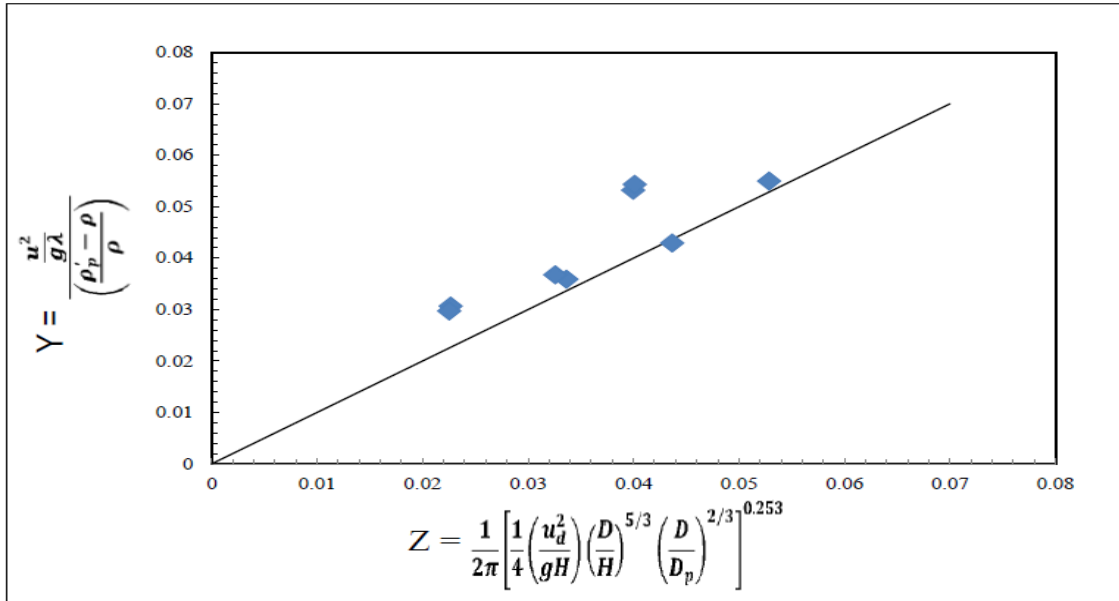


Figure 5-31: Comparison of sand dune parameter in this work and Thomas (1964) result

## 2. Stability of Sand Dune

In addition, stable sand dune could only be achieved at certain flow conditions and for a short period of time. This stability discontinue after sometime because there was no continuous sand injection from the sand hopper to keep the sand dune geometry constant. Time series of the sand dune geometry shows this stability. Sand bed of 0.29D and 0.37D were examined at water velocities of 0.18m/s, and 0.15m/s respectively. Figure 5-32 and Figure 5-33 showed stable sand dune height along the pipeline for over 10minutes. It implies that the higher the sand bed, the lower the velocity to reach stability. It was also observed the sand dune geometry at the downstream of the dip is greater than the upstream. This is because the sand dune initiation commenced at the downstream coupled with gravity as it ascends the upstream section.

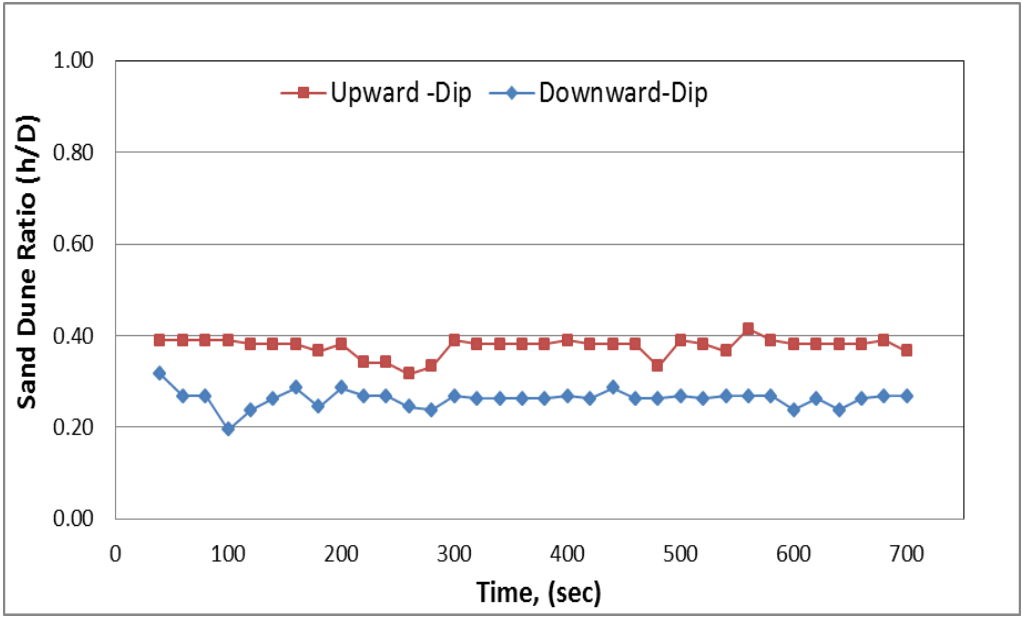


Figure 5-32: Stable sand dunes developed from sand bed height = 0.29D and water velocity = 0.18m/s

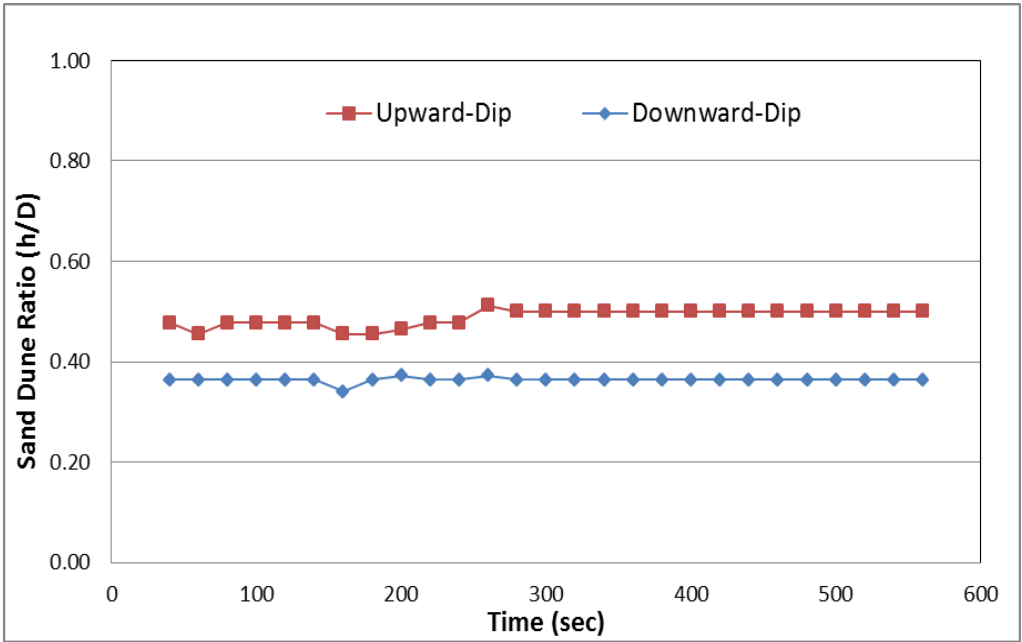


Figure 5-33: Stable sand dunes developed from sand bed height = 0.37D and water velocity = 0.15m/s

## 5.7 Sand Minimum Transport Condition in Dip Pipelines

Minimum sand transport condition in water flow was observed while slowly reducing the water velocity. In this work, Thomas (1962) definition of sand minimum transport velocity,  $V_{MTC}$ , under water flows was adopted, which was described as “*the mean stream velocity required preventing the accumulation of a layer of sliding sand particles on the bottom of horizontal pipe*”. This definition also had been used by Al-lababidi et al., 2012 and Yan, 2010. Based on the experimental observation and the definition of MTC, sand minimum transport condition (MTC) of single phase sand-water flow at the sand concentration of 50 lb/1000bbl, 100lb/1000bbl, 200 lb/1000bbl and 500 lb/1000bbl were reported for downhill and uphill followed by the dip result in this section.

### 5.7.1 Sand Minimum Transport Velocities in Sand-Water Flow in $\pm 24^\circ$ Dip Pipeline

#### 5.7.1.1 Downhill and Uphill ( $\pm 24^\circ$ Configuration)

Based on observations, it was found that there was no significant difference for minimum transport velocities in the downhill and uphill pipes. The sand particles were found transporting in form of streaks at minimum transport velocities  $V_{MTC}$  for 500lb/1000bbl as shown in Figure 5-34. The minimum transport condition (MTC) was observed between liquid velocity,  $V_L$  of 0.7m/s to 0.8m/s when the sand concentration was 500lb/1000bbl.

Mapping out the  $V_{MTC}$  result on the sand regime map shows that  $V_{MTC}$  correspond to the boundary between the sand streak and saltation regime.

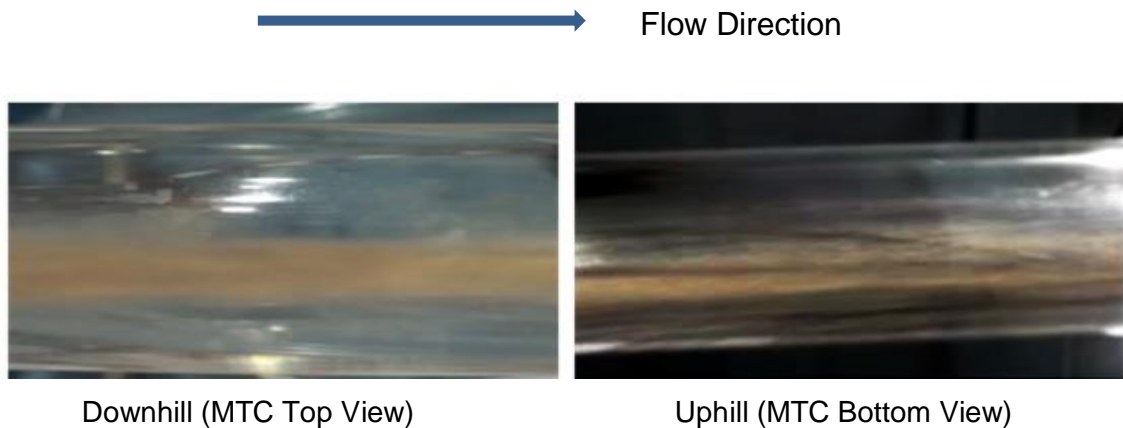


Figure 5-34: sand characteristics at MTC in downhill and uphill pipe, 500lb/1000bbl ( $V_{MTC}=0.8\text{m/s}$ )

#### 5.7.1.2 Dip Section of 24° Bend

The trend of sand transportation at the elbow was found similar to that in the downhill and uphill section. However at the elbow, sand particles were found to be scooped up from the bottom and transport dispersedly at the middle of the pipe. This phenomenon indicates the minimum transport condition (MTC) at the elbow shall be lower than that in the downhill section. This is due to changes in the velocity profile observed at the entrance of the dip and thereby enhances the sand transport. At low sand concentration of 50 lb/1000bbl, the terrain effect is not very obvious. The minimum transport condition (MTC) is observed when  $V_L$  is between 0.4 m/s to 0.5 m/s (Figure 5-35).

However, when the sand concentration was increased, the discrepancy was more obvious. Figure 5-35 illustrates the sand transport characteristics in downward and bottom sections of dip at MTC when sand concentration is 200 lb/1000bl and 500 lb/1000bbl respectively. Nonetheless,  $V_{MTC}$  in uphill/downhill pipe (i.e.  $> V_{MTC}$  in dip section) should be considered in pipeline design in order to be conservative.

Fixed quantity of sand was injected continuously at the entrance of the downhill pipe. Figure 5-35 shows the MTC result for sand water flow in  $\pm 24^\circ$  inclined section. At high  $V_L$ , there was no deposition occurring along the pipeline, all the sand particles are transported fluently which means, the amount of sand in uphill section is the same with that in the downhill and dip section. When the  $V_L$  was decreased close to the upper

limit of MTC, the sand movement in downhill and uphill sections are approximately the same. As a result, the deposition takes place in these two sections at the same time.

By further decreasing the  $V_L$ , sand particles began to settle at the bottom, and less sand particles were transported to the uphill pipeline. It explains the reason why at low  $V_L$  there are much less sand particles in the uphill section than those in the downhill and dip section.

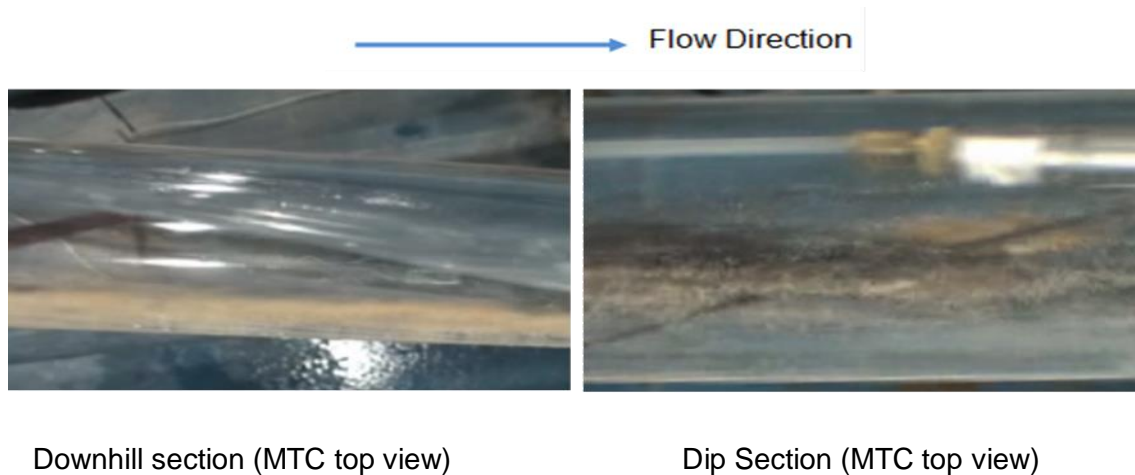


Figure 5-35: Comparison between downhill and dip section (50lb/1000bbl,  $V_L = 0.5$  m/s)

Table 5-7: Sand (MTC) in sand-water flow for  $\pm 24^\circ$  dip pipeline

Sand Concentration lb/1000bbl	$\pm 24^\circ$ Configuration, $V_{TMC}$			
	Downhill (m/s)	Downward of dip (m/s)	Upward of dip (m/s)	Uphill (m/s)
50	0.4-0.5	0.4-0.5	0.5-0.6	0.5-0.6
100	0.4-0.5	0.5-0.6	0.5-0.6	0.5-0.6
200	0.5-0.6	0.6-0.7	0.6-0.7	0.6-0.7
500	0.6-0.7	0.6-0.7	0.7-0.8	0.7-0.8



### 5.7.2 Sand Minimum Transport Velocities in Sand-Water Flow in $\pm 12^\circ$ Dip Pipeline

The minimum transport velocity for sand-water test in the  $\pm 12^\circ$  dip pipeline is outlined in Table 5-8. The result shows there was no significant difference in the MTC for the downhill and uphill sections. However, the MTC for the downstream of the dip was much lower compared to other sections. This is due to secondary flow of sand particles through the curved pipe. In conclusion, the uphill section MTC has a higher tendency for sand particles to settle at a much higher velocity than the dip section. Such upper limit is conservatively recommended for pipeline design and operability.

Table 5-8: Sand-water MTC for  $\pm 12^\circ$  dip pipeline

Sand Concentration lb/1000bbl	$\pm 12^\circ$ Configuration, $V_{TMC}$			
	Downhill (m/s)	Downward of dip (m/s)	Upward of dip (m/s)	Uphill (m/s)
50	0.4-0.5	0.4-0.5	0.4-0.5	0.5-0.6
100	0.4-0.5	0.4-0.5	0.5-0.6	0.5-0.6
200	0.5-0.6	0.5-0.6	0.6-0.7	0.6-0.7
500	0.6-0.7	0.6-0.7	0.7-0.8	0.7-0.8

### 5.7.3 Comparison of Sand Minimum Transport Condition with Published Work

Table 5-9 and Table 5-10 show the comparisons of MTC in sand-water flow between the results obtained in  $\pm 24^\circ$  and  $+12^\circ$  respectively with those horizontal and inclined systems of previous work.

Durand (1953) in one of its early work on slurry studies established the concept of “sand limit deposition velocity”,  $V_D$  which he defined as the velocity below which bed deposition occur. The sand limit deposition velocity is synonymous with the minimum transport velocity. Though their interpretations are different, they both represent the

threshold conditions before deposition. Therefore, the comparison will be between the MTC in this work and other published correlations for 50lb/1000bbl, 2000lb/1000bbl and 500lb/1000bbl.

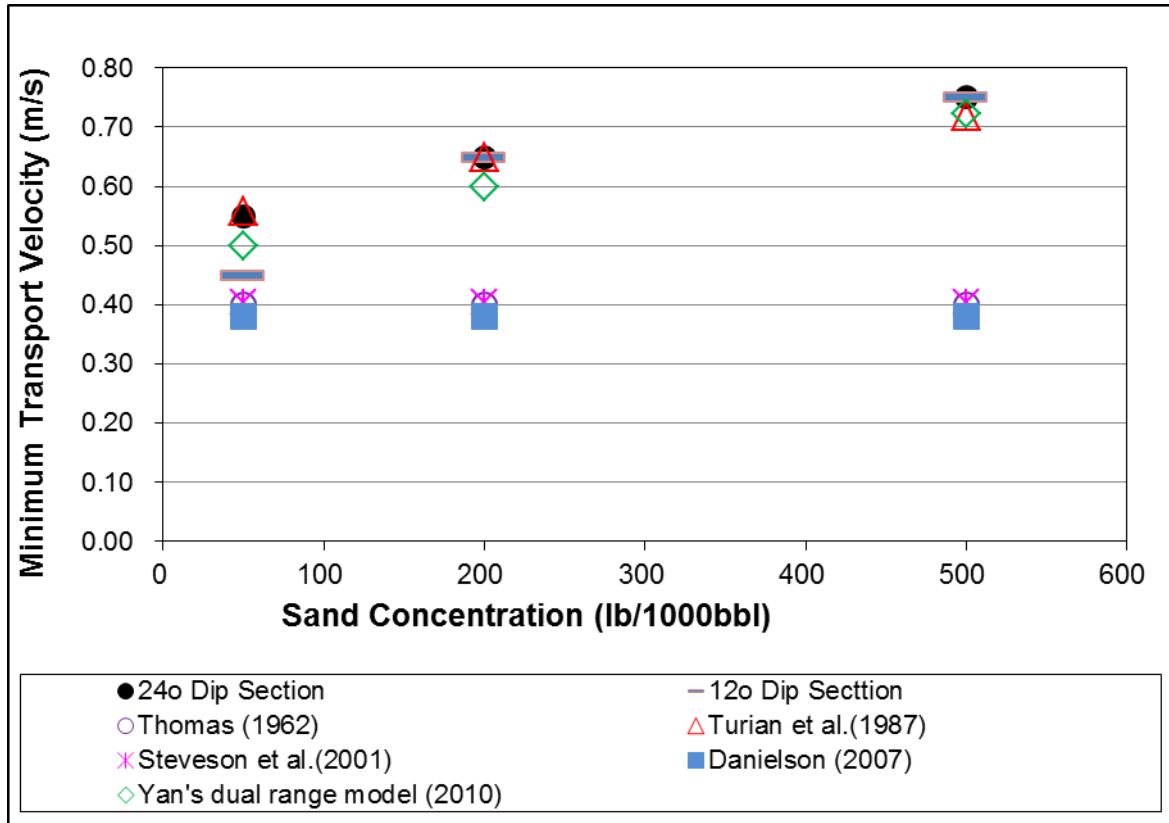


Figure 5-36 MTC comparison with other published correlations for 12° and 24° configuration bend

Figure 5-36 shows the comparison of minimum transport velocity for the 12° dip test section with the MTC for 24° dip pipeline and deposition velocity from previous studies. The  $V_{MTC}$  is for upward dip section of 12° and 24° while the other studies are for horizontal pipelines.

It was observed that the  $V_{MTC}$  for 24° upward dip test section was slightly higher than that of the 12°. This indicates that the higher the angle of uphill inclination, the higher the  $V_{MTC}$ . This is as a result of the influence of gravity effect on the sand particles as the pipe inclination increases. As the inclination increases, the gravity will contribute to the retarding motion of the suspended sand particles and easily fall backward (or saltating) on the bottom of the pipe. However, the discrepancies between the present

work and other published prediction could be due to the different assumptions and their concept of minimum transport velocity.

Table 5-9: Comparison of MTC in single phase flow between  $\pm 24^\circ$  and previous work

Sand Concentration (lb/1000bbl)	This Work		(Yan, 2010)	
	2inch $\pm 24^\circ$ Downhill $V_{MTC}$ (m/s)	2inch $+24^\circ$ Uphill $V_{MTC}$ (m/s)	2 inch $+5^\circ$ inclined $V_{MTC}$ (m/s)	4-inch $+20^\circ$ inclined $V_{MTC}$ (m/s)
50	0.4-0.5	0.5-0.6	0.50-0.55	0.50-0.60
200	0.5-0.6	0.6-0.7	0.60-0.70	0.65-0.75
500	0.6-0.7	0.7-0.8	0.65-0.75	0.75-0.85

Table 5-10: Comparison of MTC in single phase flow between  $\pm 12^\circ$  and previous work

Sand Concentration (lb/1000bbl)	This Work		(Yan, 2010)	
	2inch $\pm 12^\circ$ Downhill $V_{MTC}$ (m/s)	2inch $+12^\circ$ Uphill $V_{MTC}$ (m/s)	2 inch $+5^\circ$ inclined $V_{MTC}$ (m/s)	4-inch $+20^\circ$ inclined $V_{MTC}$ (m/s)
50	0.4-0.5	0.5-0.6	0.50-0.55	0.50-0.60
200	0.5-0.6	0.6-0.7	0.60-0.70	0.65-0.75
500	0.6-0.7	0.7-0.8	0.65-0.75	0.75-0.85

According to the data indicated above, it was observed that increasing the sand concentration will require higher liquid velocities to transport sand particles. Moreover, increasing the pipe diameter,  $V_{MTC}$  increases the minimum sand transport. In addition, it can be found that the MTC obtained in this study is a little lower than those in 2 inch and 4 inch horizontal pipeline under whole range of sand concentrations. This may be due to the gravity effect dominating the sand particle movement as the angle of inclination increases upward dip.

## 5.8 Chapter Summary

In this chapter, the experimental sand flow regime for sand-water test for  $\pm 12^\circ$  and  $\pm 24^\circ$  were developed. It was observed that the sand behaviour are similar in water flow tests for downhill and uphill pipes under different sand concentrations (50lb/1000bbl, 100lb/1000bbl, 200lb/1000bbl, 500lb/1000bbl; while relatively low at the dip. Five sand-water flow regimes (full suspension, streak, saltation, sand dune, and sand bed) were observed for the downhill, uphill and dip section). It was also observed that sand streaks were denser towards the central line of pipe bottom in the downhill pipe than that in uphill pipe. At downhill pipe section, there were sand gathering toward the central line of the pipe bottom. The characteristics of sand transportation at the dip section were found slightly different from downhill and uphill pipe for higher sand concentrations. When dense streak occurred at the downhill, the sand particles become dispersed at the dip. This interesting phenomenon is due to the co-existence effect of sand gravity and change in velocity profile at the bend. The local velocity profile at the dip changes due to centrifugal effect and local sand holdup at the dip. This dispersed flow does not survive at the uphill section and thereby settles at the uphill section of the pipe. This implies that the critical point of the dip is the upward dip section

In order to avoid being subjective in identification of sand pattern in this study, the sand dune regime is identified distinctively using conductivity ring time series. Identification of sand dune would assist in determine the operating conditions that allow sand dune formation

In engineering application, all erosion rate correlation available in the open literature required the critical (or minimum) velocity when sand is in full suspension but not above this condition. The knowledge of flow condition at full suspension is an important parameter to determine the erosion rate over the life span of the pipeline. Also, the quantity of sand bed and flow condition of sand settling at the bend is useful information for production chemist in order to determine the effectiveness of corrosion inhibitor at the bottom of the pipe.

The sand-water entrainment test result shows that the entrainment of sand particles is initiated at lower velocity. The higher the sand bed, the lower the sand transport initiation velocity. The local velocity has greater effect to create local turbulent in the direction of flow. As the velocity increases within certain intervals of flow condition, the surface of a sand bed develops statistically periodic irregularities commonly known as sand dunes. It was established that sand dunes evolution is an inertial phenomenon similar to Kelvin Helmholtz instability based on the assumption that surface tension effect can be neglected. Also, stability of sand dunes was observed at velocity of 0.18m/s and 0.15m/s for 0.29D and 0.37D respectively for  $\pm 24^\circ$ .

The minimum transport condition in single phase water flow were determined under different sand concentrations (50 lb/1000bbl, 200 lb/1000bbl and 500 lb/1000bbl) for  $\pm 12^\circ$  and  $\pm 24^\circ$  configurations. The sand minimum transport condition in the dip section was found to be slight lower than those in the downhill and uphill section. This may due to the variation of velocity profile at the bend configuration.

The minimum transport condition for a single phase water flow for the  $24^\circ$  dip test section was slightly higher (with difference of about 0.1m/s) than that of the  $12^\circ$  at the downward and upward of the dip section with sand concentration of 50lb /1000bbl and 100lb/1000bbl This indicates that the higher the angle of inclination, the higher the minimum transport condition. This is as a result of the influence of gravity effect on the sand particles as the pipe inclination increases.



## **6 RESULTS AND DISCUSSION OF SAND-AIR-WATER TEST**

In this chapter, sand-air-water test result was discussed to gain better understanding of sand behaviours based on different flow regimes for  $\pm 12^\circ$  and  $\pm 24^\circ$  configurations; while sand entrainment test at the dip for sand-air-water test was also investigated. In addition, minimum transport conditions for sand-air-water test were discussed.

Prior to sand transport tests, two phase air-water flow regime maps were developed and reported in chapter 4, which gave an insight and understanding of flow patterns in 2 inch dip test facilities ( $\pm 12^\circ$  and  $\pm 24^\circ$  configuration). The minimum transport condition results at various superficial gas and liquid velocities are function of multiphase flow and thus were mapped on the flow regime.

Similar to previous discussion, pipe geometry is in four parts: (1) downhill section, (2) upstream-dip section (i.e. entrance to the dip), (3) downstream-dip section (i.e. exit from the dip section) and (4) upstream section.

### **6.1 Sand Transport Characteristics in Air-Water Flow Regime**

Sand transport characteristics along the whole dip test section especially in the dip and uphill sections is introduced to provide a better understanding of sand transport behaviour in different air-water flow multiphase flow regimes such as segregated and intermittent flow.

In order to emphasize the sand concentration influence on the sand behaviour, low concentration of 50lb/1000bbl and high concentration of 500lb/1000bbl for  $\pm 24^\circ$  were described below. The specific illustrations of all the test points were listed in Appendix F.

#### **6.1.1 Sand Transport Characteristics in Segregated Flow**

In this experiment, it was observed that the dominant segregated flow was stratified flow in downhill section, where sand particles were transporting at the bottom of the stratified liquid film as a thin sand streak. Similar phenomenon was observed during the whole test with different sand concentrations. Figure 6-1 below illustrates the sand transportation as a thin sand layer that was observed on the bottom of the downhill pipe.

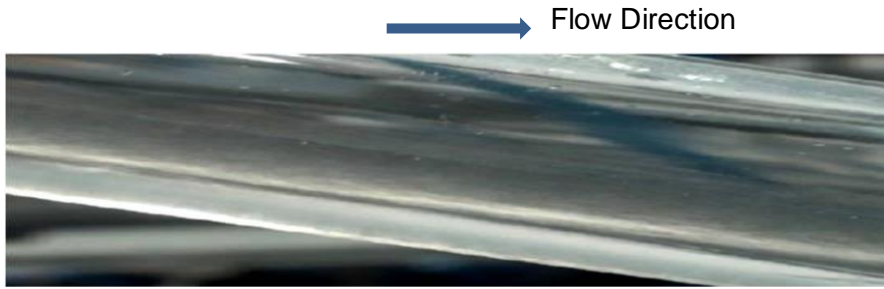


Figure 6-1: Sand streaks transporting on the bottom of the pipe  
 sand concentration = 200 lb/1000bbl,  $V_L = 0.35$  m/s

### 6.1.2 Sand Transport Characteristics in Intermittent Flow

In this flow regime, three flow patterns were observed (plug flow, slug flow and aerated slug flow) in the downstream of dip section and uphill section. Sand transportation in different flow regimes revealed diverse characteristics, which also owned an enormous effect on sand minimum transport condition in those regions.

#### 6.1.2.1 Plug flow

It was observed that in plug flow, sand particles settled at the bottom of the pipe and formed a stationary sand layer. The gas bubble travelling at the top of the pipe was not able to shatter the sand bed even with large bubble size. The same phenomenon was observed under higher sand concentration (Figure 6-2).

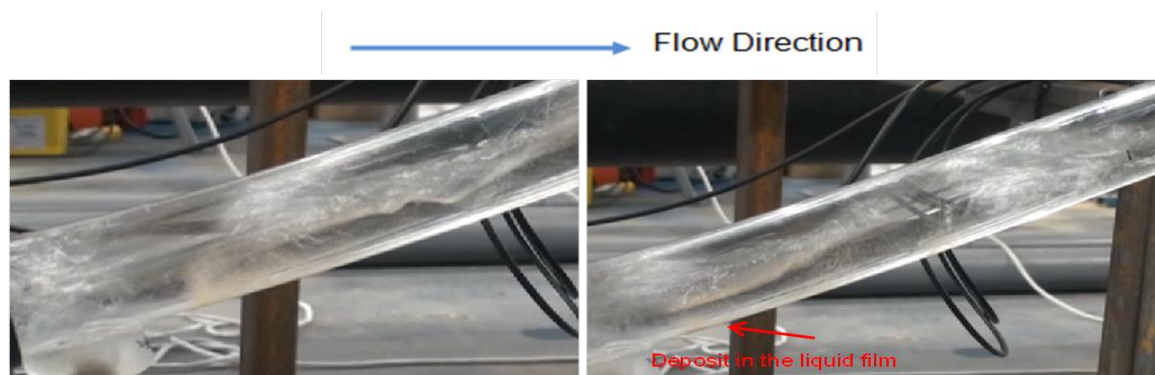


Figure 6-2: sand transport characteristics in plug flow ( $V_{sl}=0.55$ m/s,  $V_{sg}=0.2$  for 500lb/1000bbl)



### 6.1.2.2 Slug flow

By increasing gas velocity, slug was found to be generated at the upward of the dip. The compressed air on the liquid film region penetrates into the slug body, turbulent was generated. The turbulent diffused at the slug front reaches the sand particles that have settled at the bottom of the pipe, and lift some sand particles and travel forward in the slug body. As they start to move, they became energetic due to the kinetic energy impacted by the turbulence of the slug front. At the slug tail, velocity begins to decelerate; the rest of the sand particles crept back on the bottom of the pipe into the film zone; and are kept rolling or salting along the upward pipe (Figure 6-3).



Slug body pick up some particles

Part of the sand left in the liquid film

Figure 6-3: Sand transport characteristics in slug flow, (50/1000bbl,  $V_{sl}= 0.15\text{m/s}$ ,  $V_{sg}= 0.3\text{m/s}$ )

### 6.1.2.3 Aerated slug flow

The mechanism of aerated slug is distinct against slug initiation, which has been described in air-water two-phase flow in Chapter 4. The sand particles travelling on the bottom were picked up by the dispersed gas bubble. Some of the particles were scooped up and transporting along with the aerated slug. The rest of the sand particles fell back. The returned liquid film with sand particles in the liquid body was picked up by the next slug. A typical process is illustrated in Figure 6-4.

At higher sand concentration with constant superficial gas velocity of 2.0 m/s, aerated slug was observed to entrain limited quantity of sand. Thus, more sand particles settled as shown in the Figure 6-5 of 500lb/1000bbl of sand concentration.

In sand-air-water multi-phase flow, the major discrepancy of sand transport between slug flow and aerated slug flow is that; in slug flow, the turbulence diffusion generated at the slug body picks up sand particles; while in aerated slug flow, the dispersed bubble gas enhances the chaotic behaviour that scoops the sand up and entrains them upward.

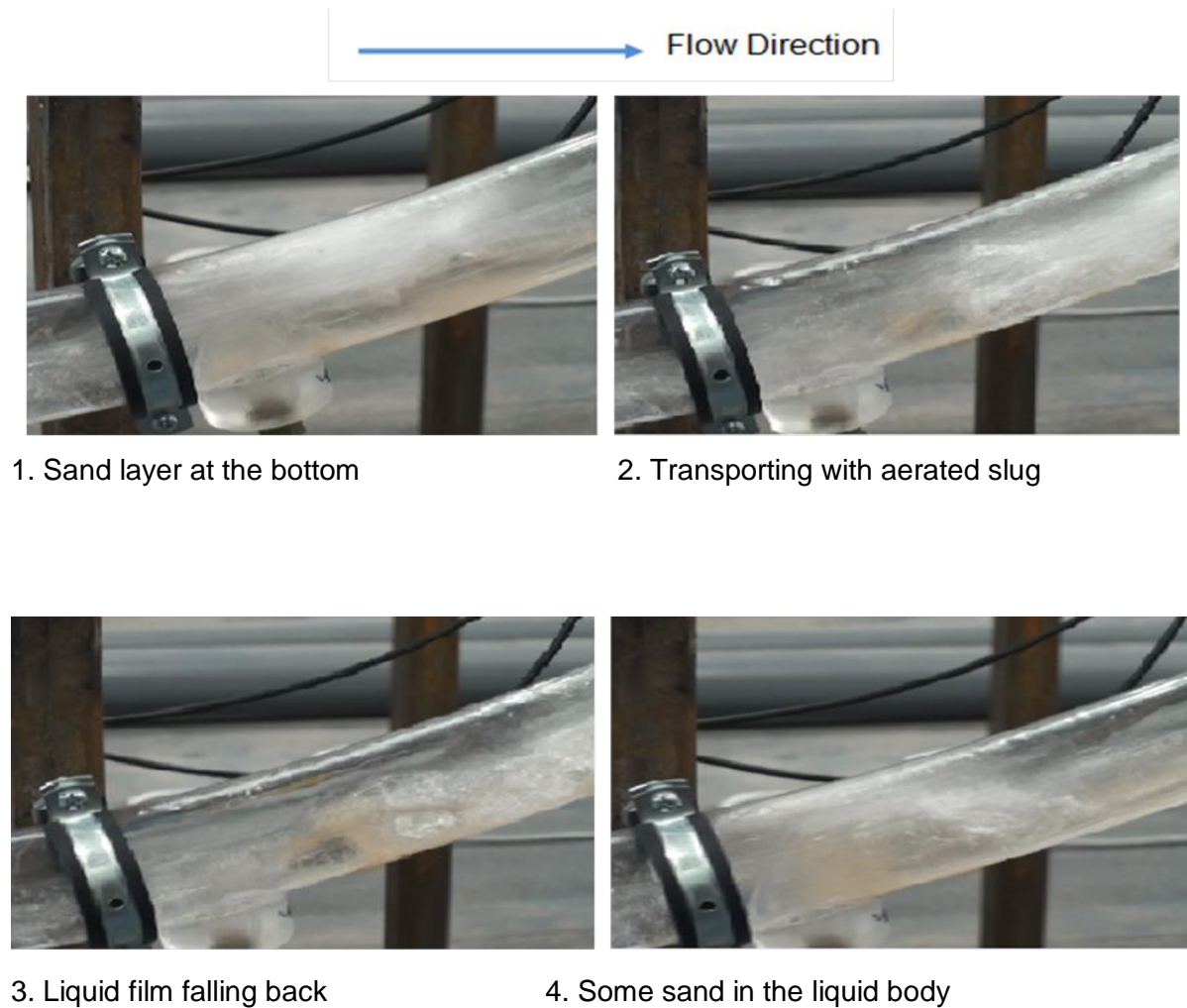
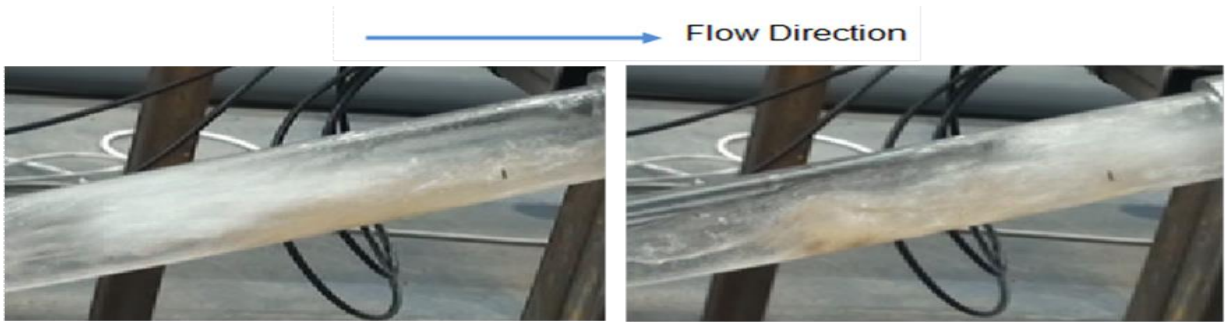


Figure 6-4: Sand transports in aerated slug (50 lb/1000bbl,  $V_{sl} = 0.08$  m/s  $V_{sg} = 2.0$  m/s)



1. Aerated slug body pick up some particles

2. More sand particles left

Figure 6-5: Sand transports in aerated slug (500lb/1000bbl,  $V_{sl} = 0.15 \text{ m/s}$ ,  $V_{sg} = 2.0 \text{ m/s}$ )

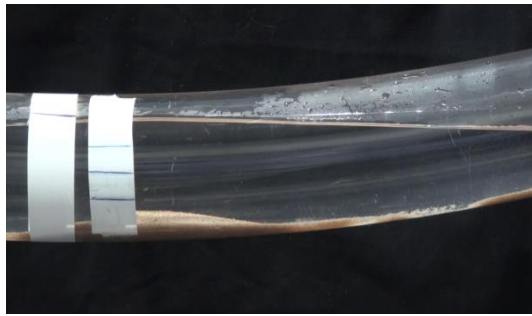
## 6.2 Sand-Air-Water Entrainment Test Result

Sand transport characteristics are strongly dependent on air-water flow regime. In this work, the sand entrainment test with air-water was carried out in order to understand the effect of multiphase flow on sand bed at the dip section. The water level at the dip section was almost filled to the top of pipe with 50g of sand bed placed at the bottom of the dip of  $24^\circ$  configuration. At low superficial gas velocity up to  $0.2 \text{ m/s}$ , there was no movement of sand and the water interface was smooth. As the superficial velocity increases to  $0.3 \text{ m/s}$ , the interface becomes wavy with occurrence of eddies with slug being initiated. The sand bed thickness reduces at the centre of the dip and sand moved to the upward dip section. At this velocity ( $0.3 \text{ m/s}$ ), there was fall back of sand due to insufficient kinetic energy impacting on the sand particles. The sand bed particles were not evenly distributed along the dip and they could not move upward. The reason is because the rate of forward movement (picking process) is almost equal to the rate of falling back with long film section. Increasing the gas velocity further than  $0.5 \text{ m/s}$ ; slug is initiated whereby the slug body picks up the sand particles upward while the sand bed slip backward in the film body as shown in Figure 6-8.

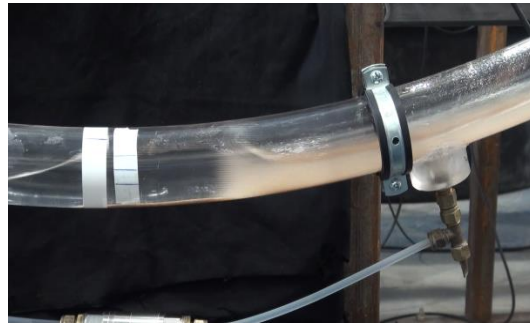
Further increasing the  $V_{sg}=1.0 \text{ m/s}$  there was no complete flushing of the sand from the dip. This implies that the sand bed cannot be completely flushed along the dip with air. This experiment is similar to the multiphase flow test (Air/static water /sand) by King et al., 2000. They reported that with gas superficial velocity of  $0.85 \text{ m/s}$ , the sand was stationary at the dip and when sand moved  $5 \text{ m}$  downstream the dip, the slug was capable of transporting the sand. It

was observed with the series of experiments carried out that the sand transport is a function of the turbulent energy at the slug front that consequently affect the sand picking and shedding process of the sand particles.

The observation of entrainment test of static water at the dip is compared with continuous flow of air-water experiment (i.e. flowing water). Majority of sand particles for continuous flowing of air-water experiment were observed to be entrained in the slug body once slug gets initiated and travelled upward, it was observed that the sand was more likely to settle in downstream of the dip (uphill) rather than at the exact location of dip. This is due to either the active mixing region at the dip (wave growth mechanism, Figure 6-7 (a)) or enough momentum gained while travelling from the upstream downhill pipe (wave coalescence mechanism, which preventing sand settlement at the dip, Figure 6-7(b)). It was observed that the type of slug initiation mechanism (wave growth mechanism and wave coalescence mechanism) by continuous air-water flow was a major influence on the sand bed behaviour.



a.)  $V_{sg} = 0.2\text{m/s}$



b)  $V_{sg} = 0.3\text{m/s}$



c.).  $V_{sg} = 0.4\text{m/s}$



d)  $V_{sg} = 0.5\text{m/s}$

Figure 6-6: Sand transport characteristics in air/water flow in dip pipeline

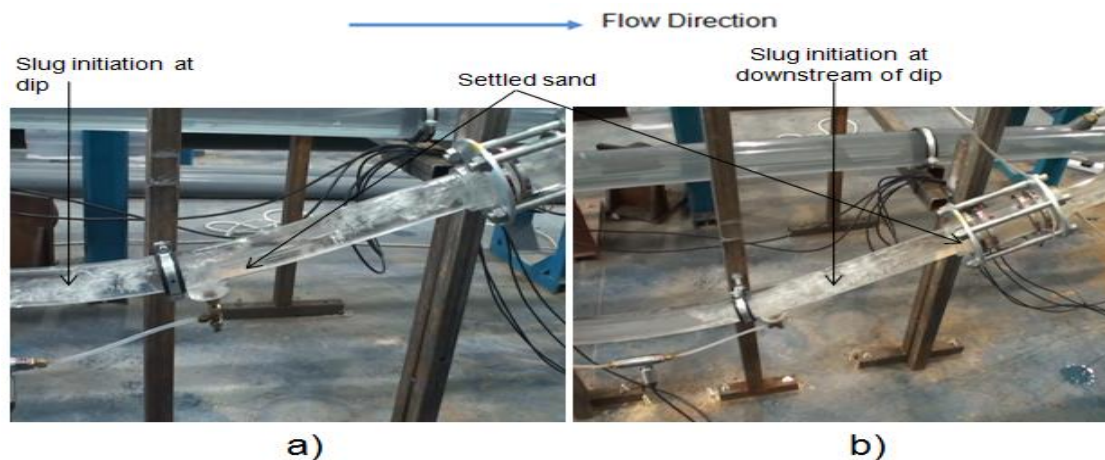


Figure 6-7: Sand streaks transporting on the bottom of the pipe

(a: 200 lb/1000bbl,  $V_{SL} = 0.35$  m/s,  $V_{SG} = 0.2$  m/s; b: 50lb/1000bbl,  $V_{SL} = 0.15$  m/s,  $V_{SG} = 0.2$  m/s )

### 6.3 Sand Minimum Transport Condition in Sand-Air-Water Flow in $\pm 24^\circ$ and $\pm 12^\circ$ Dip Pipeline

Comparing the sand transportation in air-water multiphase flow with single phase water, it was observed that once gas phase was introduced into the system, the sand particles were more transported. In the dip section, the sand layer coming from the downhill section at MTC were transported due to the motion of slug initiated at the dip. Then the sand particles were picked up (or scooped up) by the slug body and transported further upward.

In this study, the sand minimum transport condition in air-water multiphase flow is redefined as: **“the condition at which the sand particles are active enough to keep travelling, instead of accumulating in the liquid film.”**

Comparing to Yan, 2010 definition, “the condition at which the sand particles will continue to be energetic enough to keep moving and not deposit in the slug body”.

According to the definition in this study, sand particles at the bottom of the pipe were not totally constant, they kept transporting forward. As long as the coming sand particles from upstream

are less than those entrained, it was not able to form a sedimentary sand bed at the bottom of the pipe.

To better distinguish the discrepancies, the MTC of sand concentration 50lb/1000bbl and 500 lb/1000bbl for  $\pm 24^\circ$  are illustrated in this section to emphasize on sand concentration influence on the multiphase flow. Result for  $\pm 24^\circ$  and  $\pm 12^\circ$  configurations are discussed in the Section 6.3.1.1 and section 6.3.1.2 respectively.

**At  $V_{sl} = 0.08$  m/s:**

To prevent the deposition at this low liquid velocity; the gas velocity should be sufficient enough to entrain sand out (Figure 6-8).

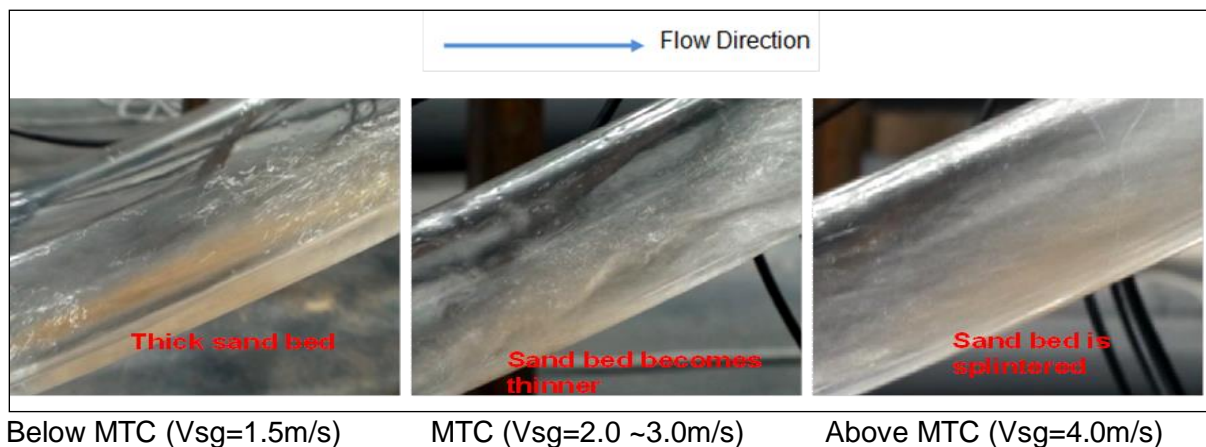


Figure 6-8: Sand behaviour around MTC (50 lb/1000bbl,  $V_{sl} = 0.08$  m/s)

According to the comparison introduced above, the sand behaviour around minimum transport condition is distinct. At very low liquid flow rate and low gas flow rate, a thick sand layer was observed which implies the condition was below MTC. As gas velocity increases, more sand particles were entrained by the aerated slug flow. The sand bed became thinner and shorter and would be occasionally shattered but still at the bottom of the pipe. By further increasing the  $V_{sg}$ , the sand bed was totally shattered and most of the sand particles were transported along with the aerated slug flow.

At higher sand concentration 500 lb/1000bbl, when  $V_{sl}$  was at 0.08 m/s, a quite high gas velocity was required to flush all the sand particles out. In this test, the upper limit of the  $V_{sg}$  was 6.0 m/s. Even with this velocity, sand particles still deposited at the elbow (Figure 6-9). Thus, within the limit of  $V_{sg}$  in this work (0-6m/s) and  $V_{sl}$  of 0.08m/s; the MTC cannot be reached.



Figure 6-9: Sand transport behaviour before MTC (500lb/1000bbl,  $V_{sl}$ =0.08 m/s,  $V_{sg}$ = 6.0 m/s)

**$V_{sl} = 0.15$  m/s:**

At low sand concentration, sand particles were found to be transported in plug and slug flow rather than aerated slug flow. It was also observed that once the flow regime began to transform, the MTC changed with it (Figure 6-10).

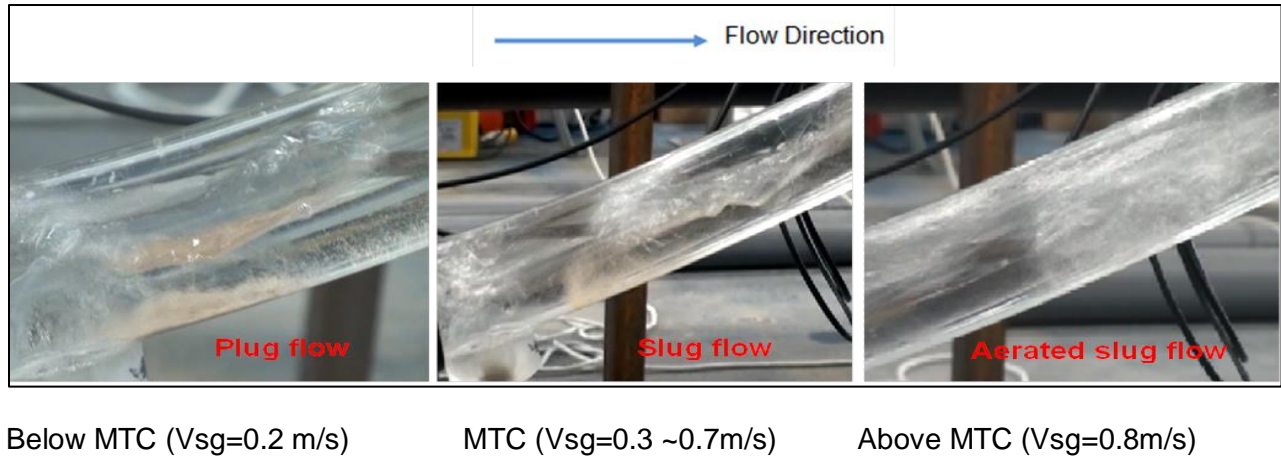


Figure 6-10: Sand behaviour around MTC (50 lb/1000bbl,  $V_{sl} = 0.15$  m/s)

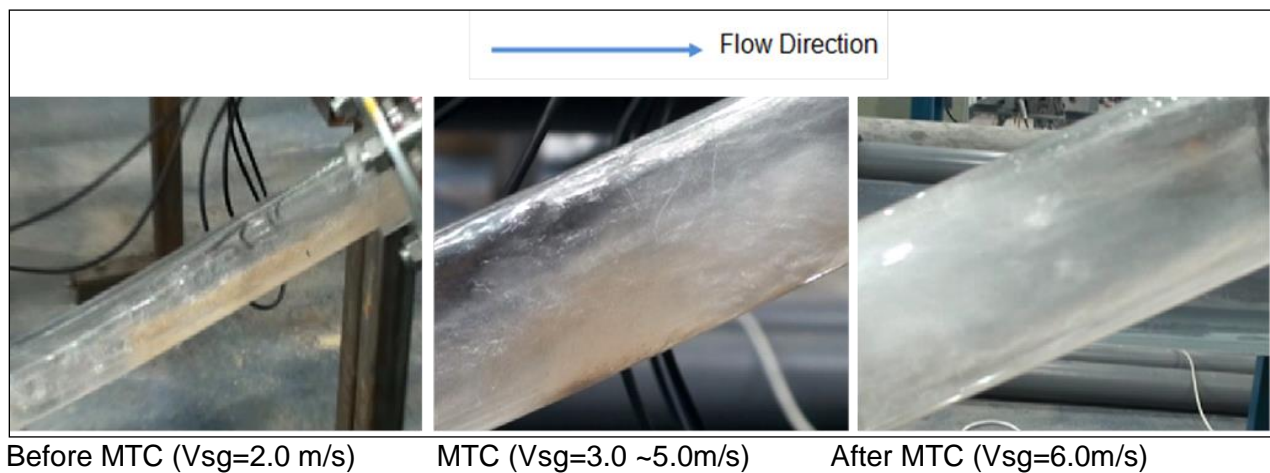


Figure 6-11: Sand behaviour around MTC (500lb/1000bbl,  $V_{sl} = 0.15$  m/s)

Under sand concentration of 500 lb/1000bbl, high gas velocity is still required to approach the minimum transport condition (Figure 6-11). Another phenomenon observed during the test was the effect of energetic ripples, which was specified in the air-water two-phase flow section. The slug flow coming from the horizontal line dissipated in the downhill section and transformed to stratified flow with long ripple. This energetic ripple flushed all the sand particles out of the elbow effectively (Figure 6-12).



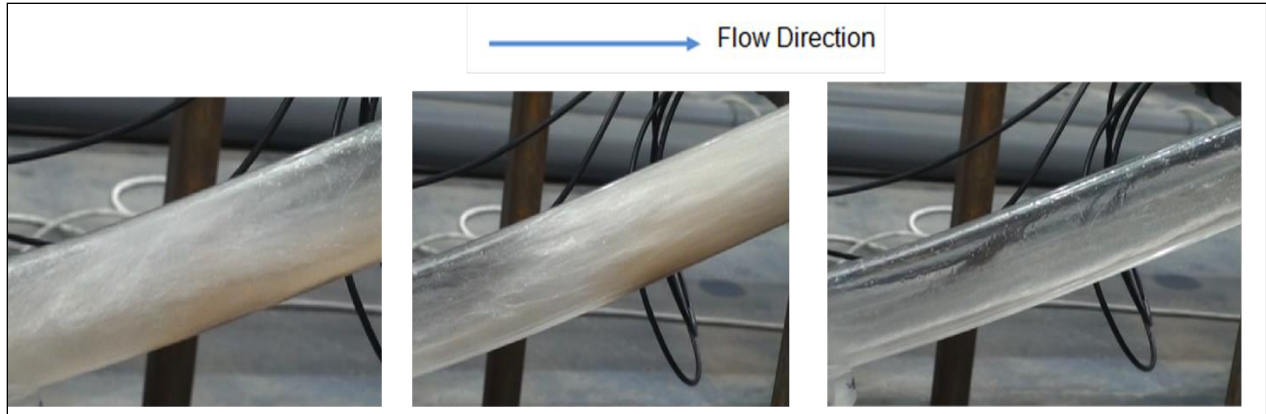


Figure 6-12: Illustration of energetic ripples' effect (500lb/1000bbl,  $V_{sl} = 0.15$  m/s,  $V_{sg} \geq 3.0$  m/s)

**$V_{sl} = 0.35$  m/s**

In this experiment, the flow regimes were observed to be plug and slug flow with a transitional regime of plug to slug flow. The MTC is shown in Figure 6-13.

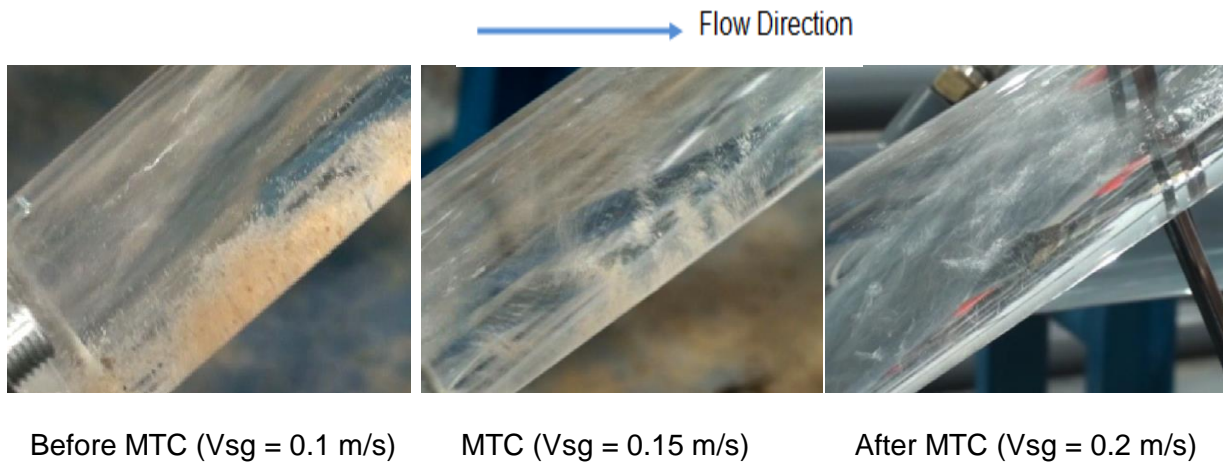


Figure 6-13: Sand behaviour around MTC (50lb/1000bbl,  $V_{sl} = 0.35$  m/s)

Similarly when sand concentration increased to 500 lb/1000bbl, Figure 6-14 presents the sand transport characteristics around MTC.

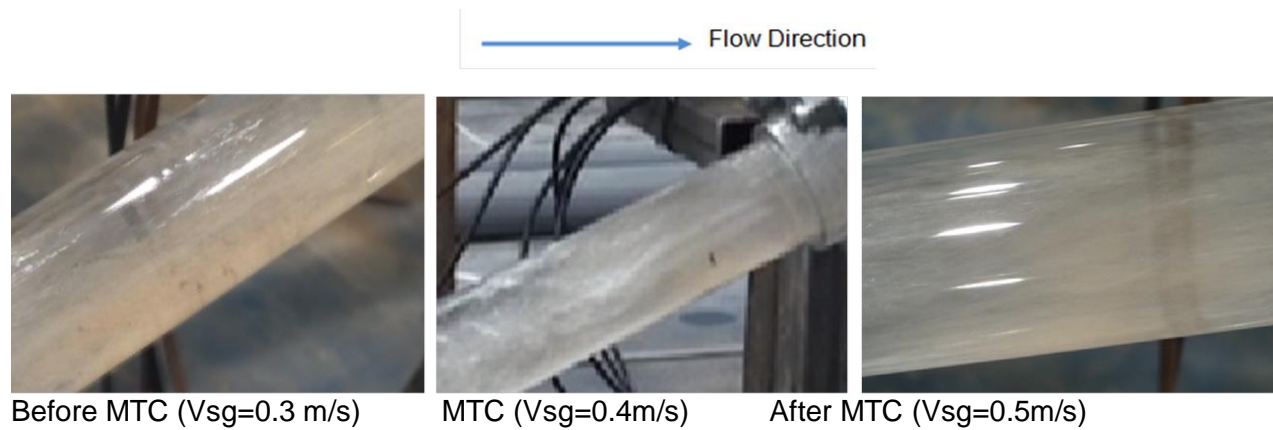


Figure 6-14: Sand behaviour around MTC (500 lb/1000bbl,  $V_{sl} = 0.35$  m/s)

### **$V_{sl} = 0.55$ m/s**

At low sand concentration when superficial liquid velocity reaches 0.55 m/s, there was no sand particles settling observed at the bottom, even at zero gas velocity. Therefore, reference is thereby made to the MTC in single phase water flow in the dip section when  $V_L = 0.4\text{--}0.5$ m/s

At high sand concentration, sand particles tended to deposit in the uphill section because of the high flush energy provided by the liquid flow at the downhill through the bend. The trend of the MTC was similar to that under the flow condition of 50 lb/1000bbl,  $V_{sl}$  at 0.35 m/s as illustrated in Figure 6-15.

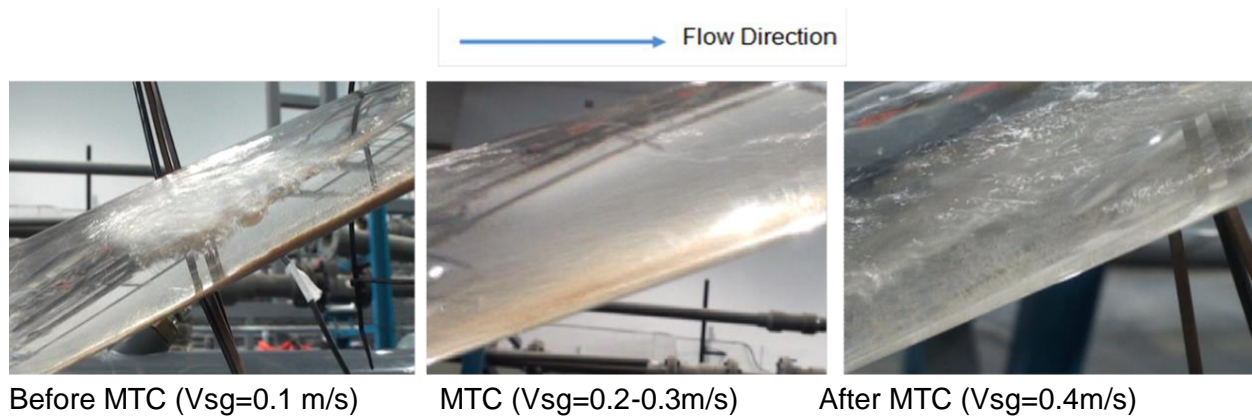


Figure 6-15: Sand behaviour around MTC, 500 lb/1000bbl  $V_{sl} = 0.55$  m/s)

### 6.3.1.1 Summary of Sand MTC in Sand-Air-Water Multiphase Flow $\pm 24^\circ$

Based on the experimental investigation, it was found that the sand transport characteristics were highly related to the flow regimes. Within the flow regimes (slug flow and aerated slug flow), MTC was clearly observed. Sand bed layer was observed to be in the uphill section at higher  $V_{sg}$ . In this region, the dominant flow regime was aerated slug flow.

Figure 6-16 and Table 6-1 presented the summary of uphill sand minimum transport condition (MTC) in sand-air-water multiphase flow under the sand concentration of 50 lb/1000bbl, 200 lb/1000bbl and 500 lb/1000bbl.

Figure 6-17 presented the mapping of sand MTC in sand-air-water multiphase flow on flow regime for uphill section  $\pm 24^\circ$  dip pipeline configuration reported in Section 4.1.1.3. The result shows that the MTC is dominated at slug and aerated slug flow regime.

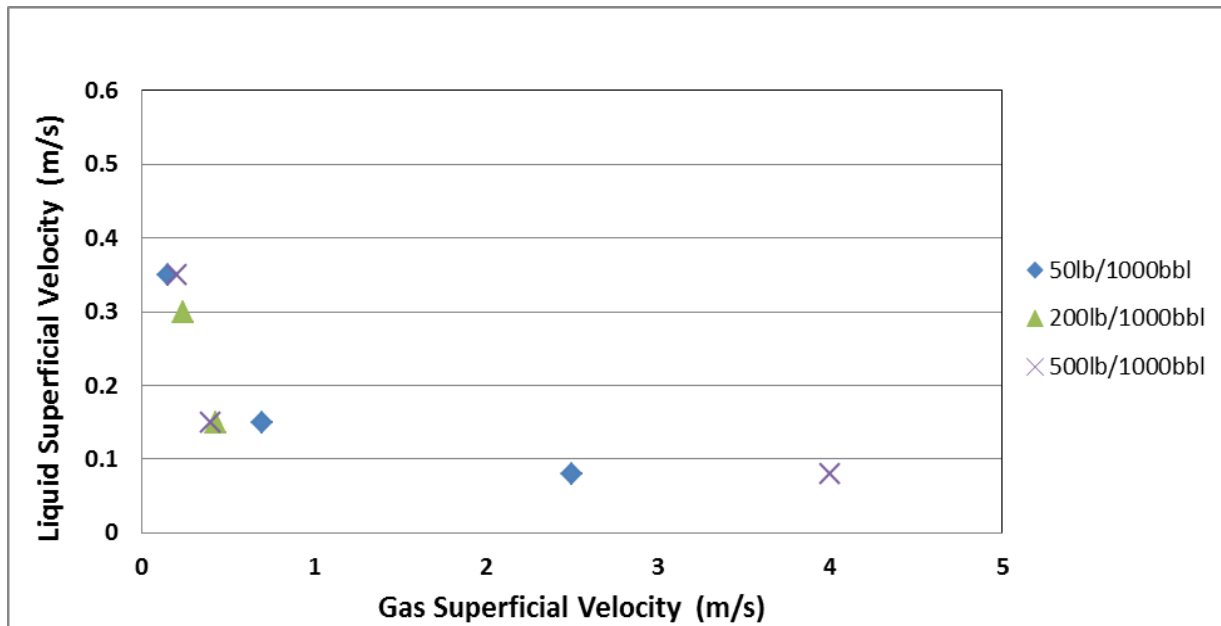


Figure 6-16: MTC for sand-air-water on  $\pm 24^\circ$  dip (uphill section)

Table 6-1: Sand MTC in Sand-air-water multiphase flow for  $\pm 24^\circ$  dip (uphill section)

Sand Concentration (lb/1000bbl)	Superficial Liquid Velocity (m/s)	Superficial Gas Velocity (m/s)	Flow Regime
50	0.08	2.5	Aerated slug
	0.15	0.7	Slug
	0.35	0.15	Slug
200	0.15	2.5	Aerated slug
	0.35	0.3	Slug
	0.55	0.15	Slug
500	0.08	6.0	Aerated slug
	0.15	4.0	Aerated slug
	0.35	0.4	Slug
	0.55	0.2	Slug

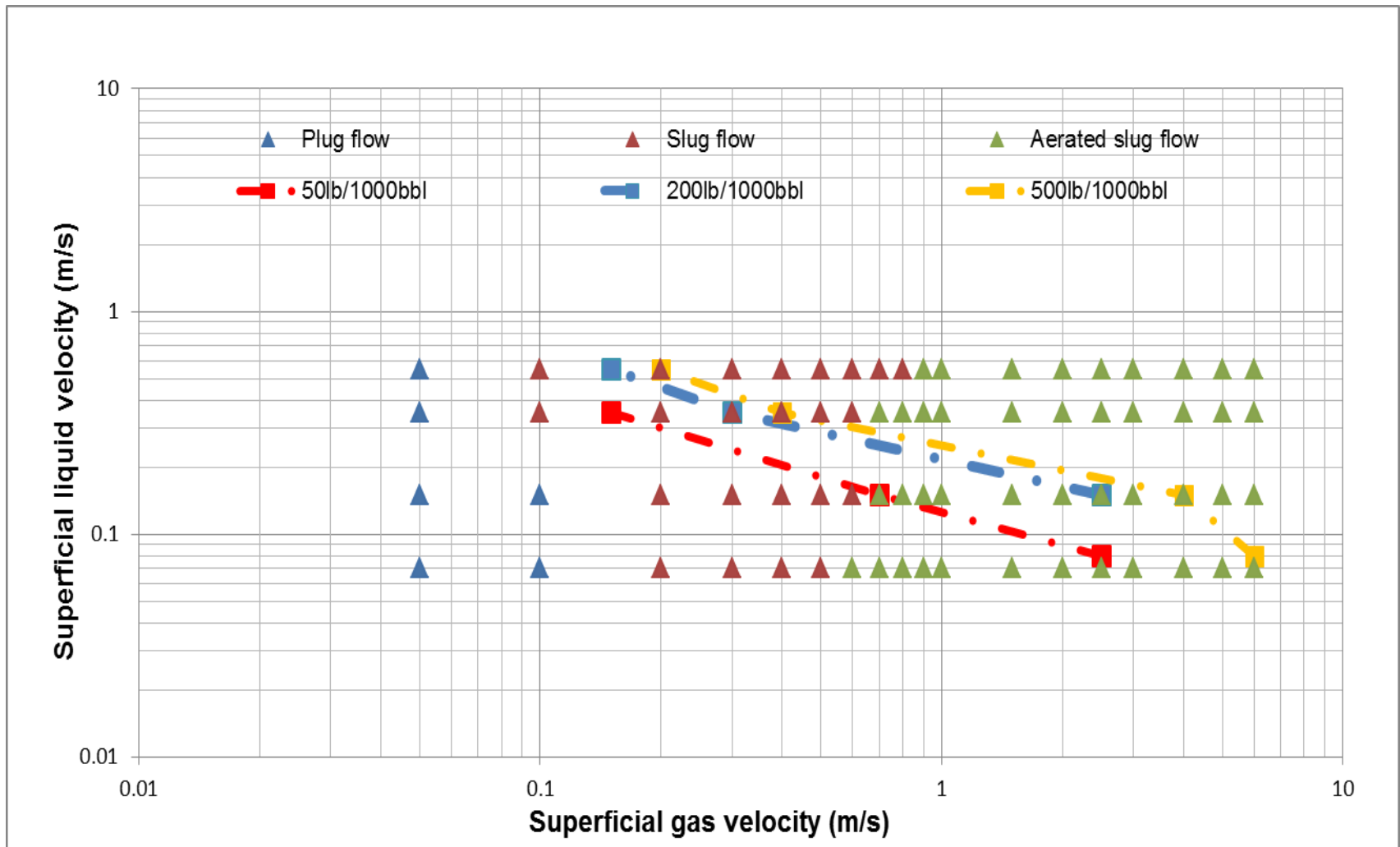


Figure 6-17: Sand MTC in sand-air-water multiphase flow on flow regime map ( $\pm 24^\circ$  dip, uphill section)

### 6.3.1.2 Summary of Sand MTC in Sand-Air-Water Multiphase Flow $\pm 12^\circ$ Configuration

Table 6-2 and Figure 6-18 presented the minimum transport velocities for air-water sand experiment for sand concentration of 50,100, 200 and 500 lb/1000bbl of water. The sand-air-water experiment was carried out by varying the gas velocity at different fixed liquid velocity in order to observe the condition below which sand particles starts to settle at the bottom of the pipe while recording the liquid and gas superficial velocities as the minimum transport velocities.

The liquid velocity was fixed for all sand concentration while the gas velocity was varied to achieve the MTC. As the liquid velocity is reduced for all sand concentration, the minimum transport condition is attained at higher gas velocity i.e. at a reduced liquid velocity the sand particles can only be transported at higher gas velocity. At a fixed liquid velocity, the higher the sand concentration, the higher the gas velocity required to attain MTC.

Table 6-2: Sand MTC in sand-air-water multiphase flow for  $\pm 12^\circ$  dip (uphill section)

Sand Concentration (lb/1000bbl)	Superficial Liquid Velocity (m/s)	Superficial Gas Velocity (m/s)	Flow Regime
50	0.15	0.3	Slug
	0.24	0.25	Slug
	0.43	0.15	Slug
	0.63	0.10	Plug
100	0.15	0.36	Slug
	0.24	0.28	Slug
	0.43	0.19	Slug
	0.63	0.13	Slug
200	0.15	0.50	Slug
	0.24	0.30	Slug
	0.43	0.20	Slug
	0.63	0.15	Slug
500	0.15	1.00	Slug
	0.24	0.70	Slug
	0.43	0.30	Slug
	0.63	0.18	Slug

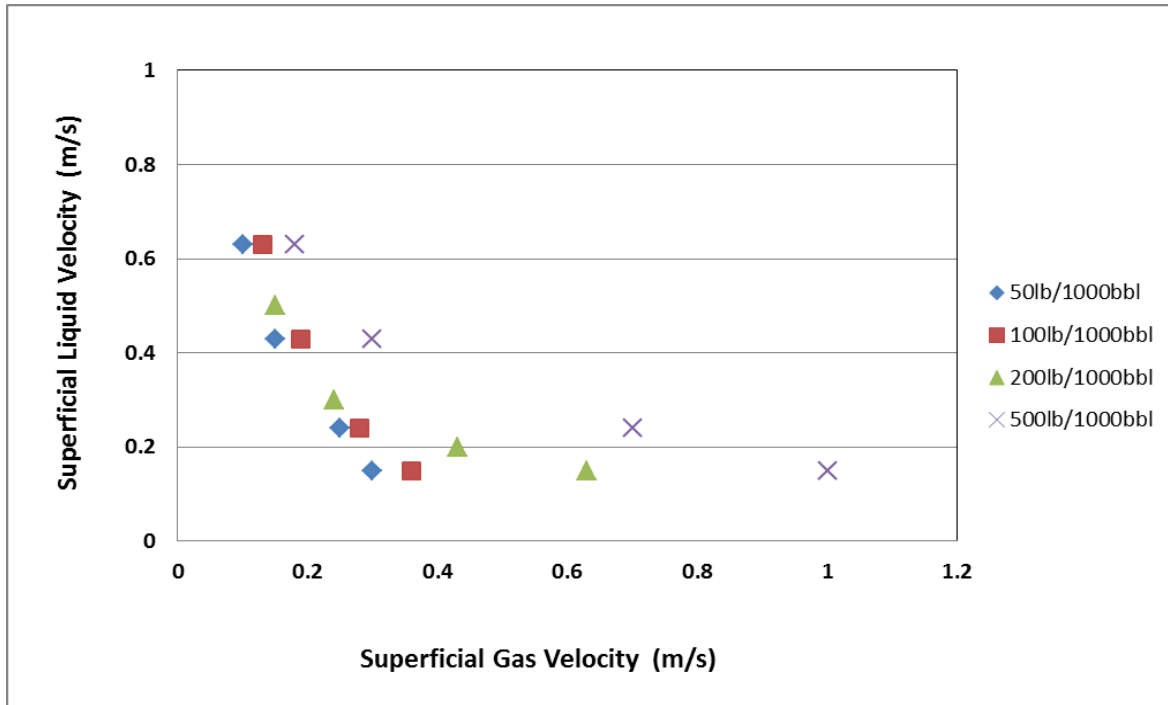


Figure 6-18 MTC for Sand-Air-Water on  $\pm 12^\circ$  dip (uphill section)

Similarly, Figure 6-19 presented the mapping of sand MTC in sand-air-water multiphase flow on flow regime for uphill section  $\pm 12^\circ$  dip pipeline configuration reported in Section 4.1.1.3. The result shows that the MTC is dominated at slug and aerated slug regime.

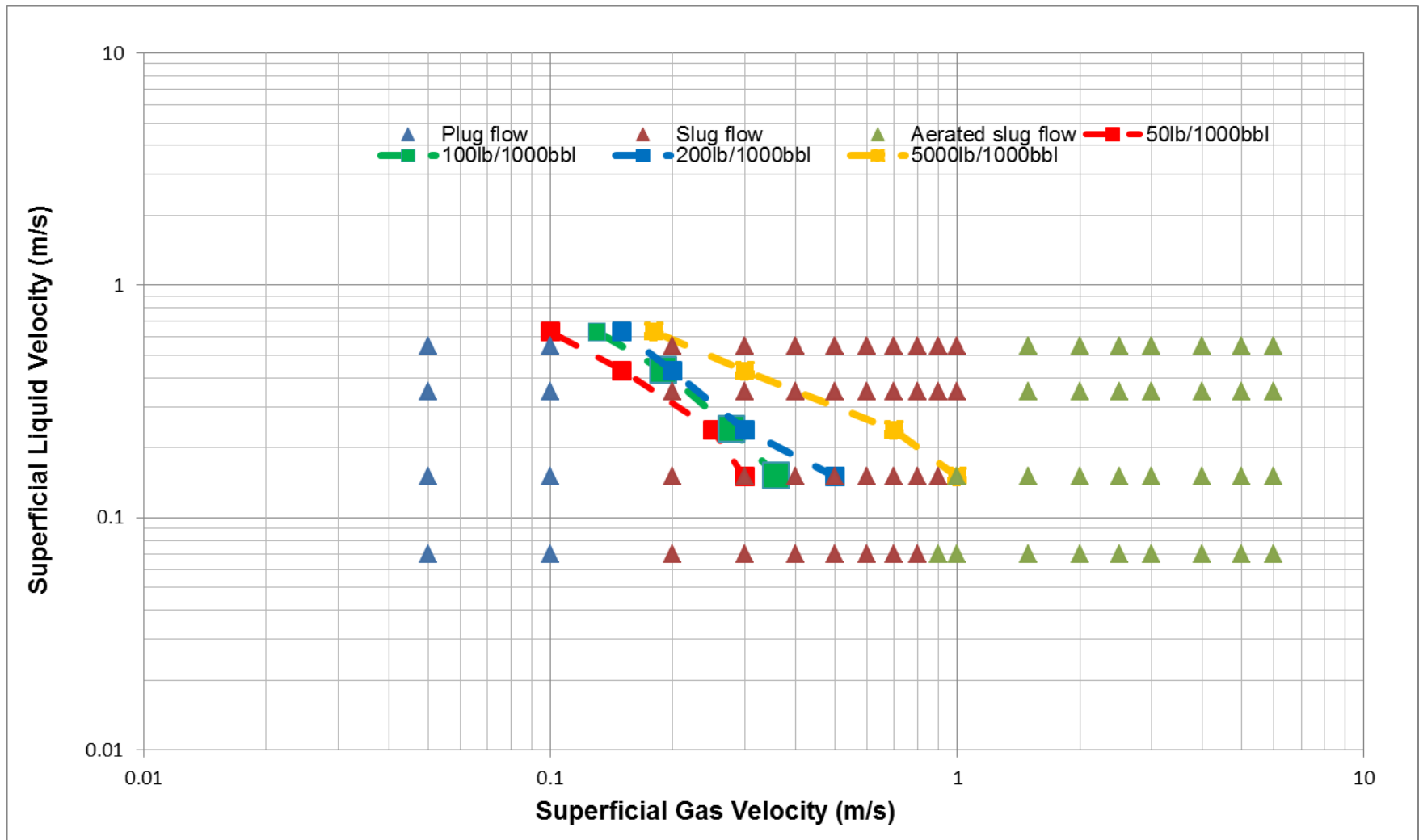


Figure 6-19: Sand MTC in sand-air-water multiphase flow on flow regime map ( $\pm 12^\circ$  dip, uphill section)



### 6.3.2 Comparison of MTC in Sand-Air-Water Flow

Comparisons between the MTC obtained in the dip section during this work and the results in 4 inch horizontal and +5° inclined pipeline in Yan, 2010 are presented below (Figure 6-20 and Figure 6-21).

The results presented in Figure 6-20 and Figure 6-21 showed similar trend of MTC for various sand concentration as the superficial gas velocity increases and superficial liquid velocity decreases; this is due to sand transporting in slug flow regime. Moreover, the MTC in horizontal flow reported in Yan, 2010 is higher than the uphill inclined geometry as result of the strong effect of slug initiation mechanism and the dominating effect of slug behaviour at the dip which enhances the sand transport inclined section. The results also showed that MTC in +24° pipe inclination in slug flow regime (at high  $V_{sg}$ ) is higher than other (+12° and +5°) due to of gravitational force enhancing the liquid fall back. There is interplay of flow regime dependence and effect of gravity at high inclination. However, as superficial gas velocity reduces less than 0.15m/s, the +12° had MTC higher than +24°. This is as result of different slug initiation mechanism behaviour observed at the dip (Waver coalescence and Wave growth).

According to Figure 6-20 and Figure 6-21 below, the result shows that the MTC is not directly dependent on the flow rate. However, mapping the MTC on the flow regime maps as shown in previous section (Figure 6-17 and Figure 6-19) gave better understanding of the flow regime that the MTC can be established at different sand concentration. Therefore, MTC is more understood as a function of the flow regime exhibited in the flowline. In addition, since the pipeline flow regime is geometry specifics, minimum transport condition at various inclinations will be different.

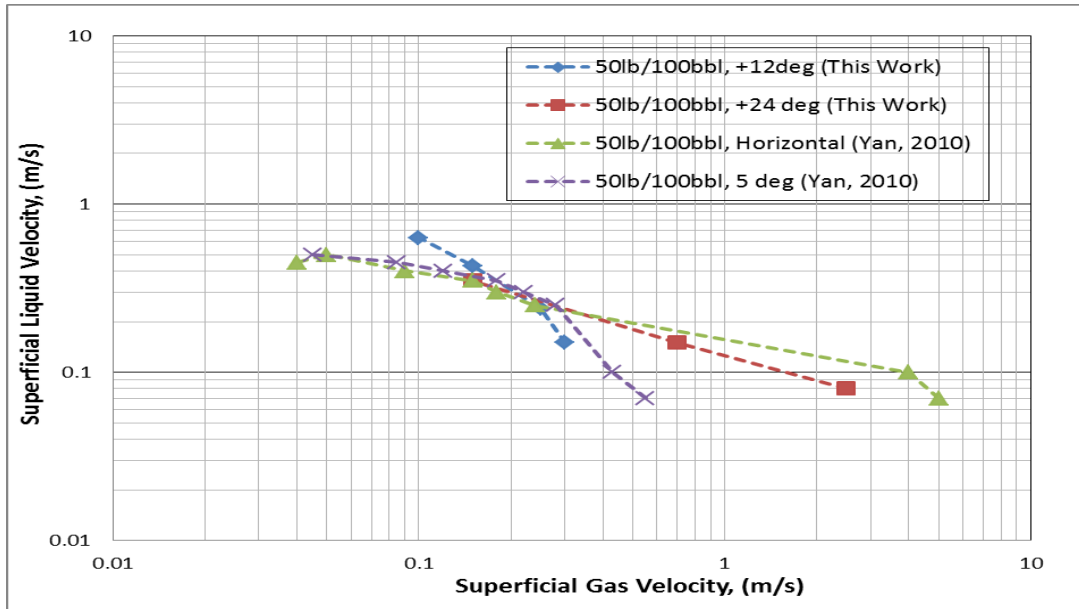


Figure 6-20: Comparison of MTC in sand-air-water flow between + 24° and +12° dip section, and Yan, 2010 work, sand concentration 50 lb/1000bbl

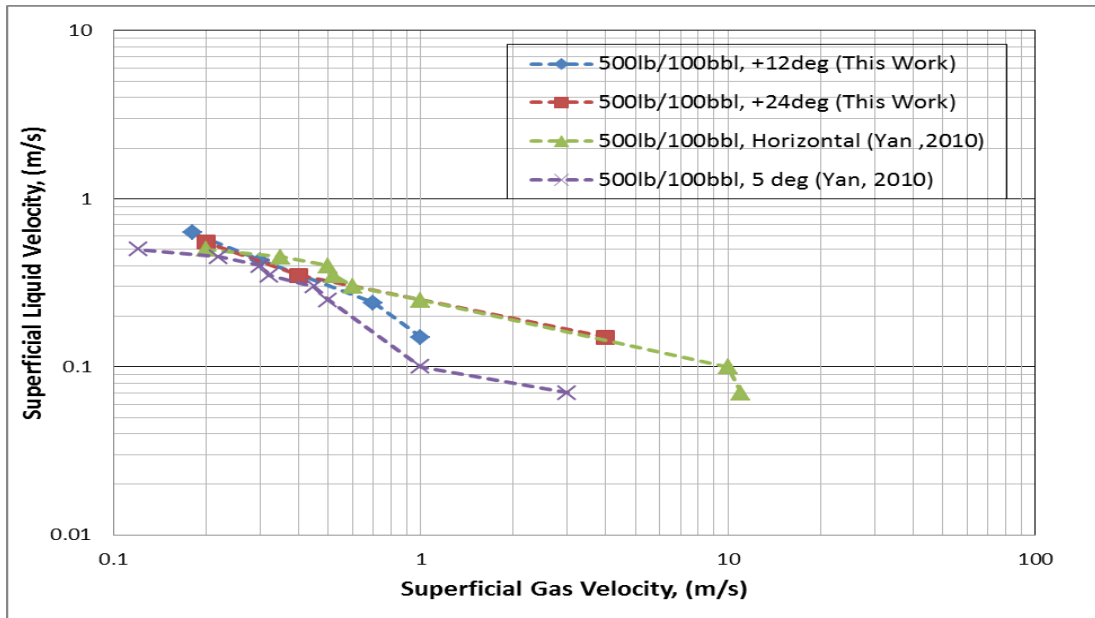


Figure 6-21: Comparison of MTC in sand-air-water flow between + 24° and +12° dip section, and Yan, 2010, sand concentration 500 lb/1000bbl

## 6.4 Chapter Summary

Sand transport characteristics in multiphase flow have been experimentally observed during the tests carried out in 2 inch Perspex dip facility for  $\pm 12^\circ$  and  $\pm 24^\circ$  configurations. In multiphase air-water flow, it was found that the sand particles are normally transported in slug and aerated slug flow, while it does not get transported in the plug flow.

Sand entrainment was carried out for multiphase flow to study the influence of slug flow in sand transport. The result shows that sand deposited at the dip cannot be completely flushed out. This is in agreement with King et al, 2000.

However, dip section has higher tendency of erosion due to increase in local velocity of fluid flow due to change in the velocity profile at the entrance of the bend. This could enhance the continuous impingement of sand at the dip (bend).

Also, minimum transport condition in multiphase flow air-water-sand were observed under different sand concentrations (50 lb/1000bbl, 200 lb/1000bbl and 500 lb/1000bbl) for  $\pm 12^\circ$  and  $\pm 24^\circ$  configurations. In sand-air-water flow, the sand transport characteristics and MTC are strongly dependent on the air-water flow regime and pipe geometry; and cannot be generalised on the superficial liquid and gas velocities of the transport fluid.



## 7 Conclusions and Recommendation for Future Work

This chapter presents the summary of the research work concerning the effect of dip pipeline in sand transportation of multiphase flow with recommendations for future research.

### 7.1 Conclusions

The literature review confirms there is significant effect of undulating pipe geometry on slug flow characteristics. The lack of understanding of how flow characteristics change when these sections are interconnected in hilly-terrain pipelines may lead to inaccurate pipeline and downstream facility design. Thus, the basis of this research work is to understand the different physical phenomenon that inter play at the bottom of the dip during sand transportation at the dip where gravity and pipe geometry play important role in determining minimum sand transport condition.

The behaviour of sand in multiphase depends on the flow pattern existing in the flow line, while the flow regime is strongly dependent on the pipe orientation. Therefore, to shed more light on the understanding of the behaviour of sand in multiphase flow, series of experiments were conducted in this study and the outcomes of the investigation are:

- The experimental studies of air-water, sand-water and air-water-sand were conducted using 2-inch (ID=50.24 mm) dip facility which consists of a downhill , a dip (lower elbow) and an uphill pipeline of  $\pm 24^\circ$  and  $\pm 12^\circ$  configuration test rigs respectively. The experiments were conducted with sand particles of an average diameter of 270 microns. The sand concentration tested in this work ranged from 50lb/1000bbl to 500lb/1000bbl.
- Prior to sand transport tests, the air-water experiment was conducted based on the range of superficial liquid velocities (0 - 0.55m/s) and superficial gas velocities (0 - 6m/s) for both  $\pm 24^\circ$  and  $\pm 12^\circ$  configurations. While various flow regimes were identified; stratified flow was mostly dominated at the downhill pipe with other flow behaviour such as stratified flow with energetic ripples, stationary air pocket and aerated slug flow. Slug and aerated slugs dominate the uphill section. New flow regimes such as: wavy with aerated slug initiation and wavy with slug initiation were observed at the dip. Three slug behaviours were observed at the dip: Complete stratified flow downhill with slug initiation at dip; stratified

flow (with energetic ripple) downhill with slug initiation and slug growth upward dip; and aerated slug downhill and slug growth at the elbow. This behaviour is different from existing work on this subject with low angle of inclination. Two types of slug initiation mechanisms (wave growth and wave coalescence) which are geometry specific were identified. The slug flow behaviour categories based on the pipe geometry shows that the slug flow structure is pipe geometry specific.

- Air-water results for  $12^\circ$  configuration showed that most of the flow behaviour in  $\pm 24^\circ$  configuration are exhibited in  $\pm 12^\circ$  but at different flowing conditions. The downhill section of  $\pm 12^\circ$  had no stationary air pocket in  $\pm 12^\circ$  dip pipe downhill test section. Unlike the  $\pm 24^\circ$  downward dip flow regime, there was no liquid accumulation at the dip in  $\pm 12^\circ$  configuration. This is due to change in pipe inclination. The uphill section exhibited similar flow regime and slug initiation mechanism.
- Bifurcation maps were developed to determine the flow behaviour along the pipeline at a given position using the maximum and minimum value from the instantaneous liquid holdup across the pipeline section. The results were in good agreement with visual observation. Therefore, bifurcation maps can be used to determine the flow regime along the pipeline.
- The experimental sand flow regime for sand-water test for  $\pm 12^\circ$  and  $\pm 24^\circ$  observed that the sand behaviour are similar in water flow tests for downhill and uphill pipes under different sand concentrations (50lb/1000bbl, 100lb/1000bbl, 200lb/1000bbl, 500lb/1000bbl). Five flow regimes (Full suspension, Streak, Saltation, Sand dune, and Sand bed) were observed for the downhill, uphill and dip section. It was also observed that sand streaks were denser towards the central line of pipe bottom in the downhill pipe than in the uphill pipe. The characteristics of sand transportation at the dip section were found slightly different from downhill and uphill pipe for higher sand concentrations. When dense streak occurred at the downhill, the sand particles become dispersed at the dip.
- Sand dune behaviour was investigated in undulating pipe line and compared with existing work in horizontal pipes. The result shows that sand dune is strongly dependent on the flow rate, height of the bed layer and the pipe diameter. The statistical instability of sand dune

was related to Kelvin Helmholtz Instability. The stability of sand dunes was observed at velocity of 0.18m/s and 0.15m/s for 0.29D and 0.37D respectively for  $\pm 24^\circ$ .

- Also, minimum transport condition in single phase water flow and multiphase flow air-water-sand were observed under different sand concentrations (50 lb/1000bbl, 200 lb/1000bbl and 500 lb/1000bbl) for  $\pm 12^\circ$  and  $\pm 24^\circ$  configurations .
- In single phase water flow, sand minimum transport condition in the dip section was found to be slightly lower than that in downhill and uphill section. This may due to the variation of velocity profile at the bend configuration. The minimum transport condition for a single phase water flow for the  $24^\circ$  upward dip test section was slightly higher than that of the  $12^\circ$  for various sand concentrations. This indicates that the higher the angle of uphill inclination, the higher the minimum transport condition which is as a result of gravity effect dominating the hydrodynamic forces.
- Experimental Investigation on sand entrainment was carried out for multiphase flow to study the influence of slug flow in sand transport. The result shows that sand deposited at the dip cannot be completely flushed out.
- In multiphase air-water flow, it was observed that the sand particles were normally transported in slug flow and aerated slug flow, while it was deposited in plug flow. Thus, sand transport characteristics and MTC in sand-air-water flow are strongly dependent on air-water flow regime; which depend on not only velocities of the transport fluid but also the pipe geometries.

## **7.2 Recommendation for Future Work**

The following tasks are recommended for future work.

- This study has developed flow regime and determined slug parameters and sand measurement using conductivity rings. However, pressure gradient measurements across the whole dip section will provide useful information and compliment this study, and should

be investigated. Also, effects of sand particle sizes have not been implemented in this work. These factors are required to be considered as future work. This will enable comparison to be made with studies undertaken with respect to pressure gradient measurement. The pressure drop across the pipe due to sand transport is important for design and operating condition.

- It was observed that in stratified flow, the liquid can be transported as a thin film or streak which can adversely affect the effectiveness of corrosion inhibitor and also increase the effect of corrosion at the bottom of the pipe. Thus, the study of sand transportation should not be limited to minimum transport condition.
- Once sand settle at the dip, it is difficult to flush out, this could lead to erosion–corrosion problem at the bend. In addition, dip section has higher tendency of erosion due to increase in velocity profile as a result of secondary flow at the entrance of the bend. This could enhance the continuous impingement of sand at the dip (bend) and it is a great concern in the design and operability of well head and riser base in particular. There is limited data regarding erosion rate in sand transportation in single phase and multiphase in pipe bend. More work is required to develop models that will provide engineers the operating conditions and design of pipelines at the bend.
- This work is limited to air-water-sand flow which has limited application in the oil and gas industry. There is still limited research work into the transportation of solids in multiphase systems when properties deviate from air-water. More work should be done on effect of viscosity by using oil as liquid phase in the test loop for multiphase flow and sand transport characteristics.
- On a wider consideration of this study for industrial application in oil and gas industry. Further work should be carried out on the use of other transient commercial simulator codes for slug capturing of terrain slugging at the dip and coupling of sand phase in the model.
- Computer simulation of the effect of undulating pipeline in sand transportation and compared with experimental result should be carried out. Computational fluid dynamics (CFD) of the fluid flow coupled with sand phase at the bend to determine minimum sand



transport and sand transport characteristics at the bend. The result should be compared with the experimental results.

- Quantitative measurement of sand particle velocity at the bend that provides detail understanding of the influence of the velocity profile at the bend on sand transportation should be carried out.
- Modelling of hydrodynamic forces of sand transport in single and multiphase flow; in order to determine the velocity required to lift sand particles and transport it through an undulating pipeline will provide better understanding on the interplay of the various forces involve in sand transport.



## REFERENCES

- Abdul-Majeed, G.H. (2000), Liquid slug holdup in horizontal and slightly inclined two-phase slug flow. *Journal of Petroleum Science and Engineering* 27 (2000), pp. 27–32
- Abduvayt, P., Manabe, R. and Arihara, N., (2003), *Effects of Pressure and Pipe Diameter on Gas-Liquid Two-Phase Flow Behavior in Pipelines*, Denver, Colorado.
- Dukler, A .E., and Hubbard, M. G., (1975), "A Model for Gas-Liquid Slug Flow in Horizontal and Near Horizontal Tubes", *International Journal of Multiphase Flow*, vol. 14, no. 4, pp. 337-347.
- Al-lababidi, S., Yan, W. and and Yeung, H. (2012), "Sand transportation and deposition characterization in multiphase flow in pipelines", *Journal of Energy Resources Technology, transactions of ASME*, vol. 134, no. 034501, pp. 1-13.
- Al-lababidi, S., Yan, W. and and Yeung, H. (2008), "Sand transport charactersitics in water and two phase flows in pipes", *6th North American conference on multiphase technology*, 4-6 June, 2008, Banff, Canada, BHR group, UK, .
- Al-Mutahar, Faisal, (2006), "Modeling of critical deposition velocity of sand in horizontal and inclined pipes", MSc Thesis, Department of Mechanical Engineering, The University of Tulsa, Tulsa.
- Al-Safran, E., (2008), Slug frequency in Gas/Liquid horizontal flow. BHR Group 2008 Multiphase Technology – 6<sup>th</sup> North American Conference on Multiphase Technology, Banff, AB, Canada: 4-6 June 2008, pp 271-240.
- Al-Safran, E., Sarica, C., Zhang, H. -. and Brill, J. (2005), "Investigation of slug flow characteristics in the valley of a hilly-terrain pipeline", *International Journal of Multiphase Flow*, vol. 31, no. 3, pp. 337-357.
- Al-safran, E. M., Taitel, Y. and Brill, J. P. (2004), "Prediction of slug length distribution along a hilly terrain pipeline using slug tracking model", *Journal of Energy Resources Technology*, vol. 126, no. 1, pp. 54-62.
- Alvarez C.J.; Al-Awwami, M.H., (1999), Wet Crude Transport Through a Complex Hilly Terrain Pipeline Network. SPE 56463
- Andreussi, P. and Bendiksen, K. (1989), "An investigation of void fraction in liquid slugs for horizontal and inclined gas—liquid pipe flow", *International Journal of Multiphase Flow*, vol. 15, no. 6, pp. 937-946.
- Andreussi, P., Di Donfrancesco, A. and Messia, M. (1988), "An impedance method for the measurement of liquid hold-up in two-phase flow", *International Journal of Multiphase Flow*, vol. 14, no. 6, pp. 777-785.

- Angelsen, S., Kvernfold, O., Lingelem, M., Olsen, S., (1989), "Long-distance transport of unprocess HC sand settling in multiphase pipelines", *Proceedings of The Fourth International Conference on Multiphase Flow*, Nice, France, June, pp.1 9-21.
- Baker, O., (1954), "Simultaneous flow of oil and gas", *Oil and Gas J.* Vol. 53, No. 12, pp. 185-195.
- Baker, O., (1957), "Discussion on how uphill and downhill flow affect pressure drop in two-phase pipelines in hilly country", *Oil and Gas J.*, pp. 150-152.
- Barnea, D., (1987), "A unified model for prediction flow pattern transitions in the whole range of pipe inclination", *International Journal of Multiphase Flow*, Vol. 13, pp. 1-12.
- Barnea, D. and Brauner, N. (1985), "Holdup of the liquid slug in two phase intermittent flow", *International Journal of Multiphase Flow*, vol. 11, no. 1, pp. 43-49.
- Barnea, D., Shoham, O. and Taitel, Y. (1982), "Flow pattern transition for downward inclined two phase flow; horizontal to vertical", *Chemical Engineering Science*, vol. 37, no. 5, pp. 735-740.
- Barnea, D., Shoham, O., Taitel, Y., and Dukler, A. E., (1985), " Gas-liquid flow in inclined tubes: Flow pattern transitions for upward flow", *Chemical Engineering Science*, Vol. 40, No. 5, pp. 131-136.
- Beck MS, Plaskowski A. Cross correlation flowmeters. Their design and application. Bristol: Adam Hilger, IOP Publishing Ltd; 1987.
- Barnea, D., Shoham, O., Taitel, Y. and Dukler, A. E. (1980a), "Flow pattern transition for gas-liquid flow in horizontal and inclined pipes. Comparison of experimental data with theory", *International Journal of Multiphase Flow*, vol. 6, no. 3, pp. 217-225.
- Barnea, D., Shoham, O., Taitel, Y. and Dukler, A. E. (1980b), "Flow pattern transition for gas-liquid flow in horizontal and inclined pipes. Comparison of experimental data with theory", *International Journal of Multiphase Flow*, vol. 6, no. 3, pp. 217-225.
- Beggs, D. H. and Brill, J. P. (1973), "A Study of Two-Phase Flow in Inclined Pipes", *SPE Journal of Petroleum Technology*, vol. 25, no. 5.
- Bello, O. O. (2008), Modeling particle transport in gas-oil-sand multiphase flows and its applications to production operations, Ph.D Thesis, Clausthal University of Technology, Germany.
- Bello O.O, Reincke K.M and Teodoriu C., (2005). Measurement of sand velocity and hold up distributions in multiphase slug using digital image analysis techniques. 12th international conference on multiphase production technology '05 BHR group multiphase flow.
- Bendiksen, K. H. and Malnes, D. (1987), "Experimental data on inlet and outlet effects on the transition from stratified to slug flow in horizontal tubes", *International Journal of Multiphase Flow*, vol. 13, no. 1, pp. 131-135.

- Bendiksen, K. H. (1984), "An experimental investigation of the motion of long bubbles in inclined tubes", *International Journal of Multiphase Flow*, vol. 10, no. 4, pp. 467-483.
- Bonnecaze, R. H., Erskine, W., and Grescovich, E. J., (1971), "Holdup and pressure drop for two-phase slug flow in inclined pipelines", *AIChE Journal*, Vol. 17, No. 5, pp. 1109-1113.
- Brill, J.P., (1981). Analysis of two-phase tests in large-diameter flow lines in Prudhoe Bay field, *SPEJ* (June 1981), pp. 363–378
- Caicedo, G. R., Marqués, J. J. P., Ruíz, M. G. and Soler, J. G. (2003), "A study on the behaviour of bubbles of a 2D gas–solid fluidized bed using digital image analysis", *Chemical Engineering and Processing*, vol. 42, no. 1, pp. 9-14.
- Cairns, R. C., Lawther, K. R. and Turner, K. S., (1960), "Flow characteristics of dilute small particle suspensions", *Brit. Chem. Eng.*, Vol. 5, pp. 849-856.
- Charles, M. E., (1970), "Transport of solids by pipelines", *Hydrotransport 1*, pp. A3-A25.
- Chen, N.H., (1979), "An Explicit equation for friction factor in pipe", *Ind. Eng. Chem. Fund.*, 18, 296.
- Chien, S.F., (1993), "Critical velocity of sand-fluid mixtures in horizontal pipe flow", *FED*, Vol. 189, 23 1-247.
- Condolios, E. and Chapus, E. E., (1963), "Transporting solid materials in pipelines", *Chem. Eng.*, Vol. 24, pp. 93-98.
- Cook, M., Behnia, M., (2000). Slug length prediction in near horizontal gas-liquid intermittent flows. *Chemical Engineering Science* 55 (2000), pp. 2009-2018.
- Cowe, T. C., (2005), "*Multiphase Flow Handbook*". 1 edition. CRS Press, USA.
- Coney, M. W. E. (1973), "The theory and application of conductance probes for the measurement of liquid film thickness in two-phase flow", *Journal of Physics E: Scientific Instruments*, vol. 6, no. 9, pp. 903.
- Danielson, T. J., (2007), "Sand transport modeling in multiphase pipelines", *Offshore Technology Conference*, OTC paper 18691.
- Davies, J. T. (1987), "Calculation of critical velocities to maintain solids in suspension in horizontal pipes", *Chemical Engineering Science*, vol. 42, no. 7, pp. 1667-1670.
- De Henau, V. and Raithby, G. D. (1995), "A transient two-fluid model for the simulation of slug flow in pipelines—II. Validation", *International Journal of Multiphase Flow*, vol. 21, no. 3, pp. 351-363.
- Doron, P. and Barnea, D., (1993 A), Three Layer Model for Solid – Liquid flow in Horizontal Pipes. *International Journal of Multiphase Flow*, 19 (6), 1029 – 1043.

- Doron, P. and Barnea, D. (1996), Flow Pattern Maps for Solid – Liquid Flow in Pipe, *International Journal of Multiphase Flow*, 22 (2), 273 – 283.
- Doron, P., Garnica, D. and Barnea, D., (1987), Slurry Flow in Horizontal Pipes: Experimental and Modeling, *International Journal of Multiphase Flow*, 13 (4), 535 – 547.
- Duckler, A., and Hubbard, M.G., (1975), A model for gas-liquid slug flow in horizontal and near horizontal tubes, *Ind. Eng. Chem. Fundam.* 14, pp. 337-347.
- Durand, R., (1953), “Basic relationships of the transportation of solids in Pipes experimental Research”, *Proceedings Minnesota International Hydraulics Convention*, pp. 89-103.
- Durand, R and Condolios, E., (1952), “The Hydraulic transportation of coal and solid material in pipes”, *Processing of Colloquium on Hransport of Coal*, National Coal Board, November 5, London, UK.
- Fairhurst, C. P. & Baker, P. J., (1983), “*Multiphase sand transport in oil production flowlines*”, Draft report on BHRA Project RP D00935, bHRA, Cranfield, Bedfordshire, UK.
- Fairhurst, C.P. and Barrett, N., ( 1997), *Oil/Water/Gas transport in undulating pipelines - Field Observations, Experimental Data, and Hydraulic Model Comparisons*, San Antonio, Texas.
- Fossa, M. (1998), "Design and performance of a conductance probe for measuring the liquid fraction in two-phase gas-liquid flows", *Flow Measurement and Instrumentation*, vol. 9, no. 2, pp. 103-109.
- Fossa, M., Guglielmini, G. and Marchitto, A. (2003), "Intermittent flow parameters from void fraction analysis", *Flow Measurement and Instrumentation*, vol. 14, no. 4-5, pp. 161-168.
- Gillies, R. G., Shook, C., Kristoff, B. & Parker, P., (1994), “Sand transport in horizontal wells”, *11<sup>th</sup> Annual Calgary University Heavy Oils and Oil Sands Technology Symposium*, March 2<sup>nd</sup>.
- Gillies, R.G., McKibben, M.J. and Shook, C.A. (1997), “Pipeline flow of gas, liquid and sand mixtures at low velocities”, *J.Can.Pet.Tech*, Vol. 36, pp. 36-42.
- Gomez, L. E., Shoham, O. and Taitel, Y. (2000), "Prediction of slug liquid holdup: horizontal to upward vertical flow", *International Journal of Multiphase Flow*, vol. 26, no. 3, pp. 517-521.
- Gould, T. L., Tek, M. R., and Katz, D. L., (1974), “Two-phase flow through vertical, inclined or curved pipes”, *J. Pet. Tech.*, Vol. 19, pp. 815-828.
- Gregory, G. A., Nicholson, M. K. and Aziz, K. (1978), "Correlation of the liquid volume fraction in the slug for horizontal gas-liquid slug flow", *International Journal of Multiphase Flow*, vol. 4, no. 1, pp. 33-39.
- Gregory, G.A., and Scott, D.S., (1969). Correlation of liquid slug velocity and frequency in horizontal cocurrent gas-liquid slug flow, *AIChE J.* 15 (1969), pp. 833–835.

- Greskovich, E.J., and Shrier., A.L, (1972). Slug frequency in horizontal gas-liquid slug flow, *Ind. & Eng. Chem. Proc. Design Dev.* (1972) 11, No. 2, pp. 317-318.
- Greskovich, E. J. (1972), "Holdup Predictions for Stratified downflow of gas-liquid mixtures", *Industrial & Engineering Chemistry Process Design and Development*, vol. 11, no. 1, pp. 81-85.
- Guzhov, A. I., Mamayev, A. A., and Odishariya G.E., (1967), "A study of transportation in gas-liquid systems", *10<sup>th</sup> Intern. Gas Conf. Hamburg Germany*.
- Hanyang, G. U. and Liejin, G. (2008), "Experimental investigation of slug development on horizontal two-phase flow", *Chinese Journal of Chemical Engineering*, vol. 16, no. 2, pp. 171-177.
- Heywood, N.I., and Richardson, J.F. (1979). Slug flow of air-water in a horizontal pipe: Determination of liquid holdup by  $\gamma$ -ray absorption, *Chemical Engineering Science*, Vol 34, pp. 17–30.
- Hill, T.J., and Wood, D.G., (1994). Slug flow: Occurrence, consequences, and prediction. SPE 27960.
- Hill, T.J.; Fairhurst, C. P; and Nelson C. J., (1996). Multiphase Production Through Hilly Terrain Pipelines in Cusiana Oilfield, Colombia. SPE 36606
- Hubbard, M. G. and Dukler, A. E., (1966), "The characterization of flow regimes for horizontal two-phase flow I. Statistical Analysis of Wall Pressure Fluctuations", *Proceedings Heat transfer and fluid mechanics Institute. Stanford University Press*, pp. 385-400.
- Hughmark, G. A. (1961), "Aqueous transport of settling slurry", *Industrial and Engrg. Chem*, Vol. 55, pp. 3 89-390.
- Hyllestad, E.L.(2010), *Stabilization of two phase flow in risers from reservoirs - anti-slug control*, M.Sc Thesis, Norwegian University of Science and Technology, Norway.
- Karima, H., Cao, Y., and Lao, L. (2012), Gas Injection for Hydrodynamic Slug Control, Proceedings of the 2012 IFAC workshop on Automatic control in offshore oil and gas production. Norwegian University of science and Technology, Norway,
- King, M. J. S., Fairhurst, C. P. and Hill, T. J. (2000), "Solids transport in multiphase flows-application to high-viscosity systems", *Journal of Energy Resources Technology*, vol. 123, no. 3, pp. 200-204.
- Kokal, S. L. and Stanislav, J. F. (1989a), "An experimental study of two-phase flow in slightly inclined pipes—I. Flow patterns", *Chemical Engineering Science*, vol. 44, no. 3, pp. 665-679.
- Kokal, S. L. and Stanislav, J. F. (1989b), "An experimental study of two-phase flow in slightly inclined pipes—II. Liquid holdup and pressure drop", *Chemical Engineering Science*, vol. 44, no. 3, pp. 681-693.

- Kokpinar, M.A., and Gogus, M., (2001), "Critical flow velocity in slurry transporting horizontal pipelines", *Journal of Hydraulic engineering*, Vol. 127, pp. 763-771.
- Lee, J. Y., Ishii, M. and Kim, N.S. (2008). "Instantaneous and Objective Flow Regime Identification Method for the Vertical Upward and Downward Co-current Two Phase Flow", *International Journal of Heat and Mass Transfer*, vol. 51, pp. 3442 – 3459.
- Malnes, D., (1983). Slug flow in vertical, horizontal and inclined pipes. Inst. for Energy. Tech., Kjeller, Norway. Report IFE/KR/E-83/002.
- Mandhane, J. M., Gregory, G. A. and Aziz, K. (1974), "A flow pattern map for gas—liquid flow in horizontal pipes", *International Journal of Multiphase Flow*, vol. 1, no. 4, pp. 537-553.
- Mattar, L. and Gregory, G. A. (1974), "Air-Oil slug flow In an upward-inclined pipe - I: Slug velocity, holdup and pressure gradient", vol. 13, no. 1.
- Marsden J. E., and McCracken, M. (1976), The HOPF bifurcation and its applications. Applied Mathematical Sciences,19, Springer-Verlag, New York, USA
- Merilo M, Dechene R.L and Cichowlas W.M (1977), "Void fraction measurements with a rotating electric field conductance gauge.", *J. Heat transfer*, vol. 99, pp. 330-332.
- Minami, K. and Brill, J. P. (1987), "Liquid holdup in wet-gas pipelines", *SPE Production Engineering*, vol. 2, no. 1.
- Mukherjee, H. and Brill, J. P. (1983), "Liquid holdup correlations for inclined two-phase flow", *SPE Journal of Petroleum Technology*, vol. 35, no. 5.
- Newitt, D. M., Richardson, J. F., Abbott, M. and Turtle, R. B., (1955), "Hydraulic conveying of solids in horizontal pipes", *Trans. Inst. Chem. Eng.*, Vol. 33, 2, pp. 93- 113.
- Nicholson, M. K., Aziz, K. and Gregory, G. A. (1978), "Intermittent two-phase flow in horizontal pipes: Predictive models", *The Canadian Journal of Chemical Engineering*, vol. 56, pp. 653-663.
- Nicklin, O. J., Wilkies, J. O. and Davison, J. F. (1962), "Two phase flow in vertical tubes", *Transaction of the institute of Chemical Engineers*, vol. 40, pp. 61-68.
- Nydal, O. J., Pintus, S. and Andreussi, P. (1992), "Statistical characterization of slug flow in horizontal pipes", *International Journal of Multiphase Flow*, vol. 18, no. 3, pp. 439-453.
- Oddie, G., *et al.* (2003). "Experimental Study of Two and Three Phase Flows in Large Diameter Inclined Pipes", *International Journal of Multiphase Flow*, vol. 29, pp. 527 – 558.
- Oroskar, A. R. and Turian, R. M. (1980), "The critical velocity in pipeline flow of slurries", *AIChE Journal*, vol. 26, no. 4, pp. 550-558.
- Oudemans, P. (1993), "Sand transport and deposition in horizontal multiphase trunklines of subsea satellite developments", *SPE Production & Operations*, vol. 8, no. 4.



- Peker, S., and Helvacı.,(2008), *Solid-Liquid Two Phase Flow*, Elsevier, Oxford, UK
- Salama, M. M. (2000), "Sand production management", *Journal of Energy Resources Technology*, vol. 122, no. 1, pp. 29-33.
- Scott, D. S. and Rao, P. K. (1971), "Transport of solids by gas-liquid mixtures in horizontal pipes", *The Canadian Journal of Chemical Engineering*, vol. 49, pp. 302-309.
- Scott, S.L. and Kouba, G.E., ( 1990), *Advances in slug flow characterization for horizontal and slightly inclined pipelines*, New Orleans, Louisiana.
- Scott, S.L., Shoham., O., Brill, J.P., (1989). Prediction of slug length in horizontal, large-diameter pipes, *SPE Production Engineering*, August 1989, pp. 335–340.
- Shen, L., Johnsson, F. and Leckner, B. (2004), "Digital image analysis of hydrodynamics two-dimensional bubbling fluidized beds", *Chemical Engineering Science*, vol. 59, no. 13, pp. 2607-2617.
- Shook, C. A. and Roco, M. C. (1991), *Slurry Flow: Principles and Practices*, Butterworth-Heinemann series in Chemical engineering.
- Sinclair, C.G., (1962), "The limit deposit-velocity of heterogeneous suspension", *Proceeding of the Symposium on Interaction between Fluids and Particles*, European Federation of Chemical Engineers, London, England, June, pp.26-29.
- Singh, G. and Griffith, P., (1970), "Determination of pressure drop optimum pipe size for Two-phase slug flow in an inclined pipe", *J. Eng. Ind., Trans. ASME*, pp. 92.
- Smart S. J. (2009), Flow velocity required for solid particle movement in oil and gas pipelines, NACE International, Paper No. 09469.
- Spedding, P. L., Spence, D. R., (1993), "Flow regimes in two-phase gas-liquid Flow", *Int. J. Multiphase Flow*, Vol. 19, 2, pp. 245-280.
- Stevenson, P. and Preston, A.P., (1996), "*Sand transport in pipes in inclined slug flow - Pt. II Project Report*", Dept. Chem. Eng., University of Cambridge.
- Stevenson, P., Thorpe, R.B., Kennedy, J.E. and McDermott C., (2001), "The similarity of sand transport by slug flow and hydraulic conveying", *Proc. 10<sup>th</sup> Int. Conf. On Multiphase Flow*, B.H.R. Group, Cannes, France, pp. 13-15
- Stevenson, P., (2001), "*Particle transport in pipes by two-phase flows*", Ph.D. Thesis, University of Cambridge, Cambridge UK.
- Stevenson, P., Thorpe, R.B., Kennedy, J.E. and McDermott, C., (2001a), "The similarity of sand transport by slug flow and hydraulic conveying", *Proceedings of 10<sup>th</sup> Int. Conf. on Multiphase Flow*, bHRA, France, pp. 249-260.
- Stevenson, P., Thorpe, R.B., Kennedy, J.E. and McDermott, C., (2001b), "The transport of

- particles at low loading in near-horizontal pipes by intermittent Flow”, *Chem. Eng. Sci.*, Vol. 56, pp. 2149-59.
- Stevenson, P., Thorpe, R.B., (2002), “Velocity of isolated particles along a Pipe in Smooth Stratified Gas Liquid Flow”, *AIChEJ.*, Vol. 48, 5, pp. 963-969.
- Stevenson, P., Thorpe, R.B., (2003), “Energy dissipation at the slug nose and the modeling of Solids transport in intermittent flow”, *J. Can. Chem. Eng.*, Vol. 81, pp. 271-278.
- Stevenson, P., Thorpe, R. B., Kennedy, J. E. and and McDermott, C. (2001), "The transport of particles at low loading in horizontal pipes by intermittent flow", *Chemical Engineering Science*, vol. 56, pp. 2149-2159.
- Taitel, Y., Shoham, O. and Brill, J. P. (1990), "Transient two-phase flow in low velocity hilly terrain pipelines", *International Journal of Multiphase Flow*, vol. 16, no. 1, pp. 69-77.
- Taitel, Y. and Barnea, D. (1990), "Two-Phase slug flow", in James P. Hartnett and Thomas F. Irvine, Jr. (ed.) *Advances in Heat Transfer*, Elsevier, , pp. 83-132.
- Taitel, Y. and Barnea, D. (2000), "Slug-tracking model for hilly terrain pipelines", *SPE Journal*, vol. 5, no. 1.
- Taitel, Y. and Dukler, A. E. (1976), "A model for predicting flow regime transitions in horizontal and near horizontal gas-liquid flow", *AIChE Journal*, vol. 22, no. 1, pp. 47-55.
- Taitel, Y., Barnea, D., and Dukler, A. E., (1980), “Modelling flow pattern transitions for steady upward gas-liquid flow in vertical tubes”, *AIChE Journal*, Vol. 26 , No. 3, pp. 345-354.
- Taitel, Y. and Dukler, A. E., (1977), “A model for slug frequency during gas-liquid flow in horizontal and near horizontal pipes”, *International Journal of Multiphase Flow*, Vol. 3, No. 6, pp. 585-596.
- Taitel, Y., Lee, N., and Dukler, A. E., (1978), “Transient Gas-Liquid flow in horizontal pipes: Modelling the flow pattern transitions”, *AIChE Journal*, pp. 920.
- Thomas, D.G. (1961), “Transport Characteristics of suspensions Part I. Minimum transport velocity of flocculated suspensions in horizontal pipes”, *AIChE J.*, Vol. 7, 3, 423-430.
- Thomas, D.G. (1962), “Transport Characteristics of suspensions Part VI. Minimum transport velocity of large particle size suspensions in round horizontal pipes”, *AIChEJ.*, Vol. 8, 3, 373-377.
- Thomas, D.G. (1964), “Transport Characteristics of suspensions Part IX. The representation of Periodic Phenomena on a Flow Regime Diagram for Dilute Suspension Transport”, *AIChEJ.*, Vol. 10, 3, pp 303-308.
- Thomas, D. G. (1964), "Periodic Phenomena Observed with spherical particles in horizontal pipes", *Science*, vol. 144, no. 534, pp. 536.

- Tippetts, J. R. and Priestman, G. H. (1997), "Mobility of solids in multiphase undulating pipeline", BHR Group Conference Series Publication.
- Turian, R. M., Hsu, F. L., and Ma, T. W., (1987), "Estimation of Critical Velocity in Pipeline Flow of Slurries," *Powder Technol.*, 51, pp. 35–47.
- Ujang, P.M., Lawrence, C.J., Hale, C.P., Hewitt, G.F. (2006). Slug initiation and evolution in two phase horizontal flow. *International Journal of Multiphase Flow* 34 32 (2006), pp. 527-552.
- Valle A.; Utvik O.H.,(2005). Field tests and analysis of hydrodynamic slugging in multiphase crude oil flow lines", BHR Group 2005 Multiphase Production Technology 12, Barcelona.
- Wani, G. A., Sarkar, M. K. and Mani, B. P., (1982), "Critical Velocity in Multisize Particle Transportation through Horizontal Pipes", *Journal of Pipelines*, Vol. 2, 1, pp. 57-62.
- Wang, X., Guo, L., Zhang, X. (2007). An experimental study of the statistical parameters of gas-liquid two phase slug flow in horizontal pipeline, *International Journal of Heat and Mass Transfer* 50 (2007), pp. 2439–2443.
- Wasp, E.J., Aude,T.C., Kenny, J.P., Seiter, R.H., Jacques, R.B., (1970) "Deposition velocities, transition velocities and spatial distribution of solids in slurry pipelines", *Proceedings of Hydrotransport 1*, bHRA Fluid Engineering, Cranfield, Bedford, England, Paper H4.
- Wicks, M., (1971), "Transport of Solids at Low Concentrations in Horizontal Pipes", In Zandi, I (Ed.), *Advances in Solid-Liquid Flow in Pipes and its Applications*, Pergamon Press, pp.101-123.
- Wilson, K.C., (1970). Slip points of the beds in solid–liquid pipeline flow. *Proceedings ASCE, Journal of Hydraulics Division*, 96, 1–12.
- Woldesemayat, M. A., Ghajar, A.J. (2007). Comparison of void fraction correlations for different flow patterns in horizontal and upward inclined pipes. *International Journal of Multiphase Flow* 33 (2007) 347-370.
- Woods, B.D., Fan, Z., Hanratty, T.J. (2006). *Frequency and development of slugs in a horizontal pipe at large liquid flows*. *International Journal of Multiphase Flow* 32 (2006) 902-925.
- Yan, W. (2010), *Sand Transport in Multiphase pipeline*, Ph.D Thesis, Cranfield University, Cranfield, UK.
- Zabaras, G.J. (2000). Prediction of slug frequency for gas/liquid flows. SPE 65093
- Zandi, I., Haydon, J. A., (1971), "A Pneumo Slurry System of Collecting and Removing Solids Waste", In Zandi, I (Ed.), *Advances in Solid-Liquid Flow in Pipes and its Applications*, Pergamon Press.
- Zandi, I., and Govatos, G., (1967), "Heterogeneous Flow of Solids in Pipelines," *Journal of the Hydraulics Division, ASCE*, Vol.93, No.HY3, Proc.Paper 5244, May, pp. 145-159

- Zhang, H., Jayawardena, S. S., Redus, C. L. and Brill, J. P. (2000), "Slug Dynamics in Gas-Liquid Pipe Flow", *Journal of Energy Resources Technology*, vol. 122, no. 1, pp. 14-21.
- Zhang, H.Q., Wang, Q., Sarica, C., Brill, J.P., (2003). *A unified mechanistic model for slug liquid holdup and transition between slug and dispersed bubble flows*. *International Journal of Multiphase Flow* 29 (2003) pp 97–107
- Zheng, G., Brill, J. P. and Taitel, Y. (1994), "Slug flow behavior in a hilly terrain pipeline", *International Journal of Multiphase Flow*, vol. 20, no. 1, pp. 63-79.
- Zheng, G. H., Brill, J. P. and Shoham, O. (1995), "An Experimental Study of Two-Phase Slug Flow in Hilly Terrain Pipelines", *SPE Production & Operations*, vol. 10, no. 4.
- Zheng, G., Brill, J.P. and Shoham, O., (1993), *Hilly terrain effects on slug flow characteristics*, Houston, Texas.

# APPENDICES

## Appendix A : Conductivity Calibration

### A.1 Conductivity Sensors Calibration

#### Principle of Operation

The conductivity sensors are designed to measure hold up (sand or liquid) and slug characteristics in the pipe. Conductivity is a measure of the ability of a liquid to conduct electricity. It is measured in Siemens (S or  $\text{ohm}^{-1}$ ). It is directly proportional to the concentration of free ions in the liquid and is inversely proportional to the electrical resistance.

The principle of conductivity sensors is based on the high conductivity of a liquid (water for example) that provide a voltage output proportional to the liquid holdup.

#### Description of the Conductivity sensor

The conductivity sensor is made of two pairs of 2-inch stainless steel rings (electrodes) built with the same geometric area coupled into a 2-inch pipe spool section without restriction to flow. The electrodes are placed in parallel position to each other and separated by a determined and fixed distance apart.

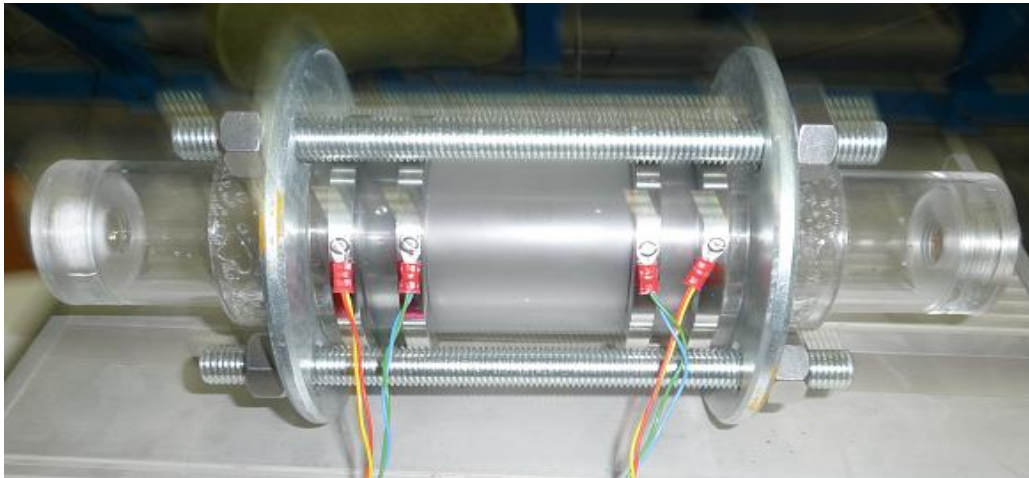


Figure A 1: Conductivity Ring

The conductivity rings function as a pair, in this present work, there are sixteen conductivity rings, making up eight sensors; two of these spools unit is installed in the downhill and uphill section.

The conductivity sensor is connected to a conductivity box which process the sensor input into a readable output. A signal with a current source output is transmitted to the conductivity sensors and apply a small current to the liquid. The sensor built up an output voltage through the resistivity of the liquid according to different liquid holdups.

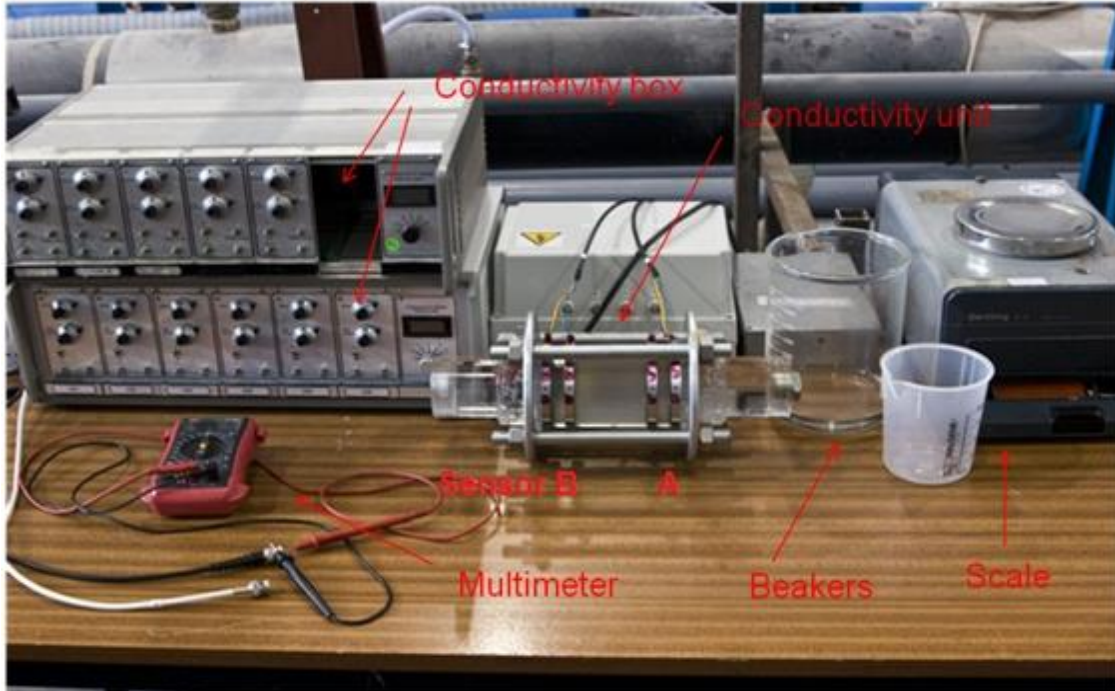
A conductivity unit and a voltmeter are linked to two channels of the conductivity box. The voltmeter reads instantaneous output voltage of its corresponding sensor. The conductivity box is tuned so as to adjust the outputs displayed on the voltmeter. These settings are unique for each channel and pair of sensors and depend also on the fluid tested.

Calibration is important to make sure the output signal from the conductivity sensors remains within a fixed voltage range. The calibration will be carried out using tap water, the same liquid used in the experiment.

## **A.2 Air-Water Conductivity Ring Calibration**

As seen in Figure A 2, two pairs of rings are marked as sensor A and sensor B; where sensor A is the one that close to the open end (use a screw cap to seal). Two cables are coupled to the sensors respectively and connect to the curtain channel of the conductivity box. There are four conductivity sensors asking for calibration, which means 8 channels are required. Hence an extra conductivity box is collected. Once the in-situ setting and corresponding channels are fixed, it should not be changed anymore.

When the conductivity sensor is empty, it measures the conductivity of air which may not be noticeable due to high resistance caused by air. This is taken as the lowest range value of the sensor. As liquid is introduced into the sensor a conducting path is created across the electrodes. The volume of liquid in the pipe determines the resistance to the induced current in the sensor rings. As the amount (volume) of the liquid in the pipe increases the resistance reduces and this translates to increase in the conductivity of the liquid.



**Figure A 2: Calibration of the conductivity sensor**

**Result of Conductivity Ring Calibration for Air-Water Experiment:**

The following aforementioned procedure was followed during the calibration of each conductivity ring. Total of 8 pairs of conductivity rings, two pairs on a spool piece. Each pair of ring has two channels. There are 8 channels in total.

The calibration experiment was repeated 3 times for each calibration (conductivity ring) process and the graph of liquid fraction is plotted to ensure a good repeatability. The result shows a good fit as shown in Figure A 3 to Figure A 10.

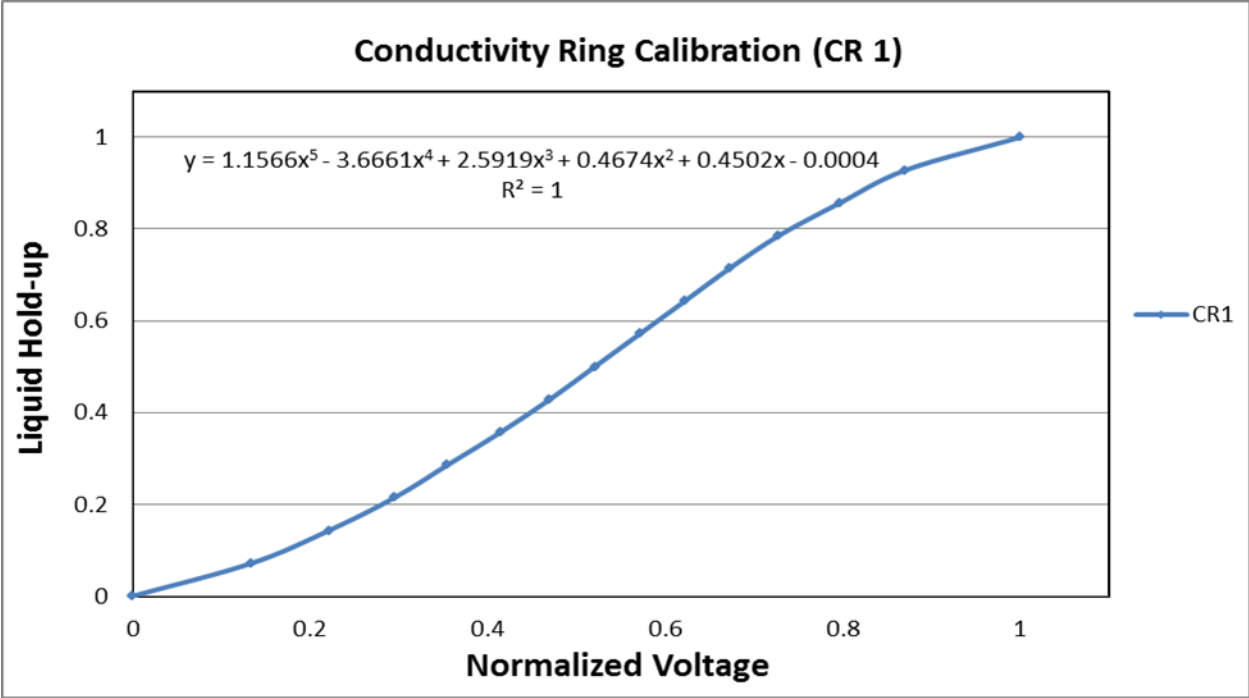


Figure A 3: Conductivity ring-1

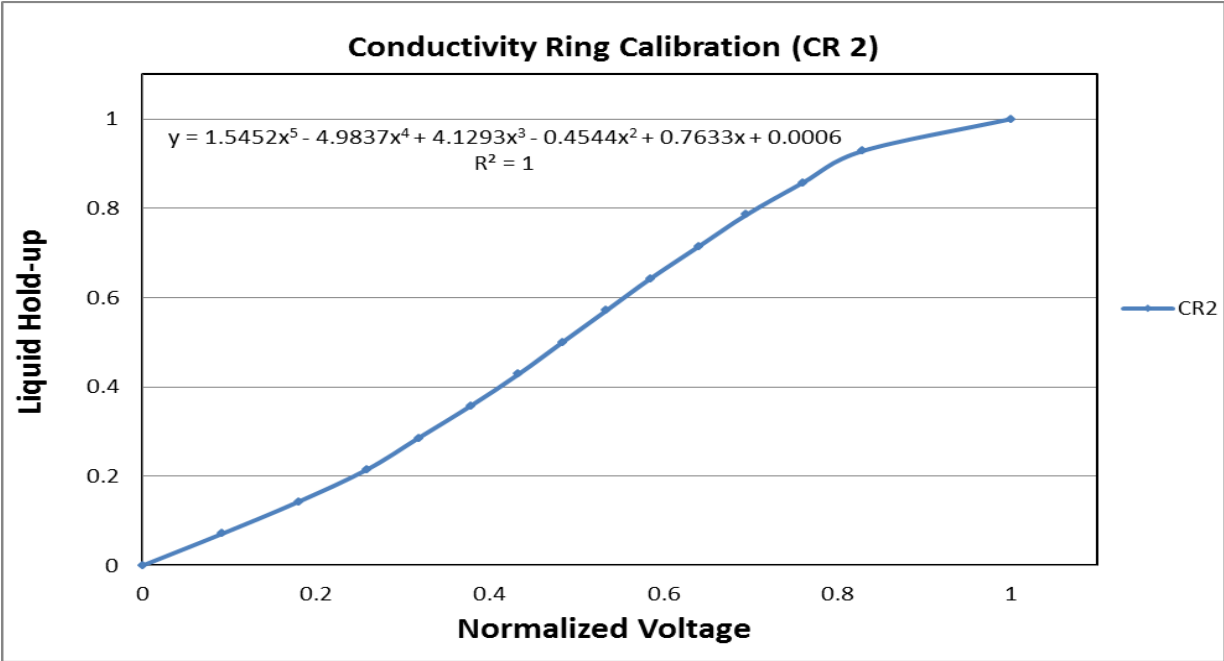


Figure A 4: Conductivity ring-2



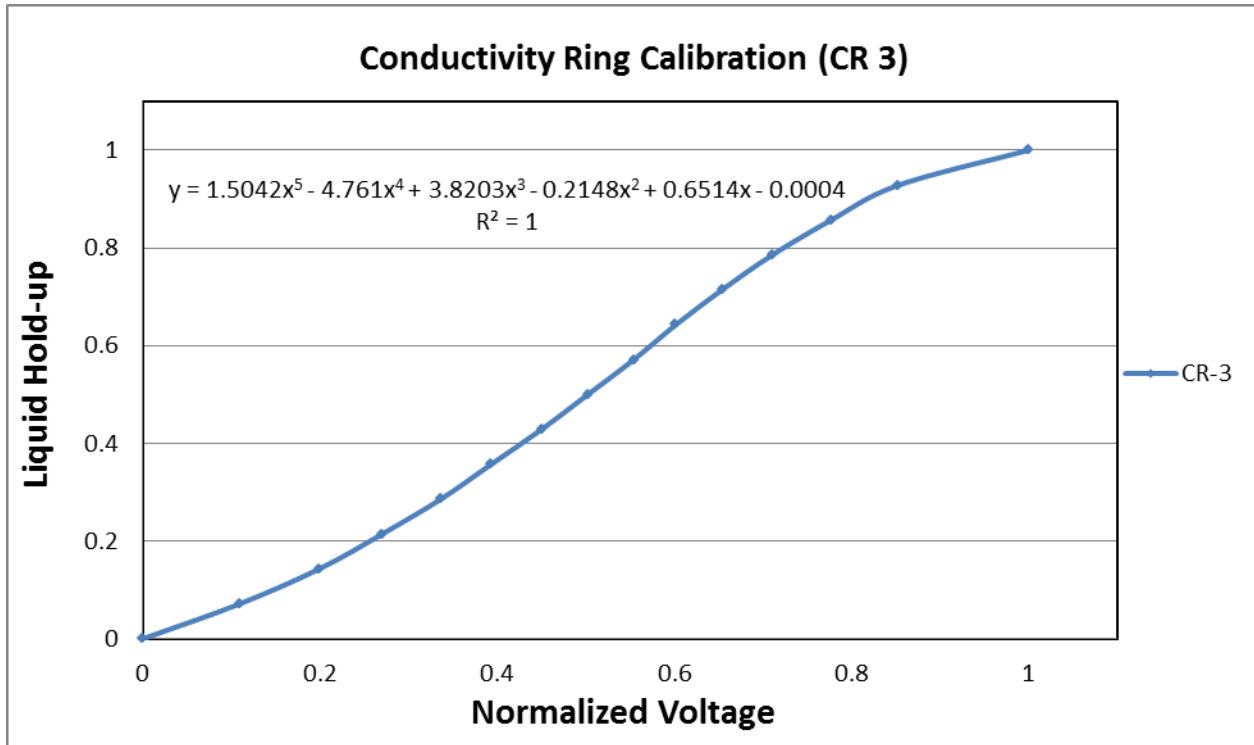


Figure A 5: Conductivity ring-3

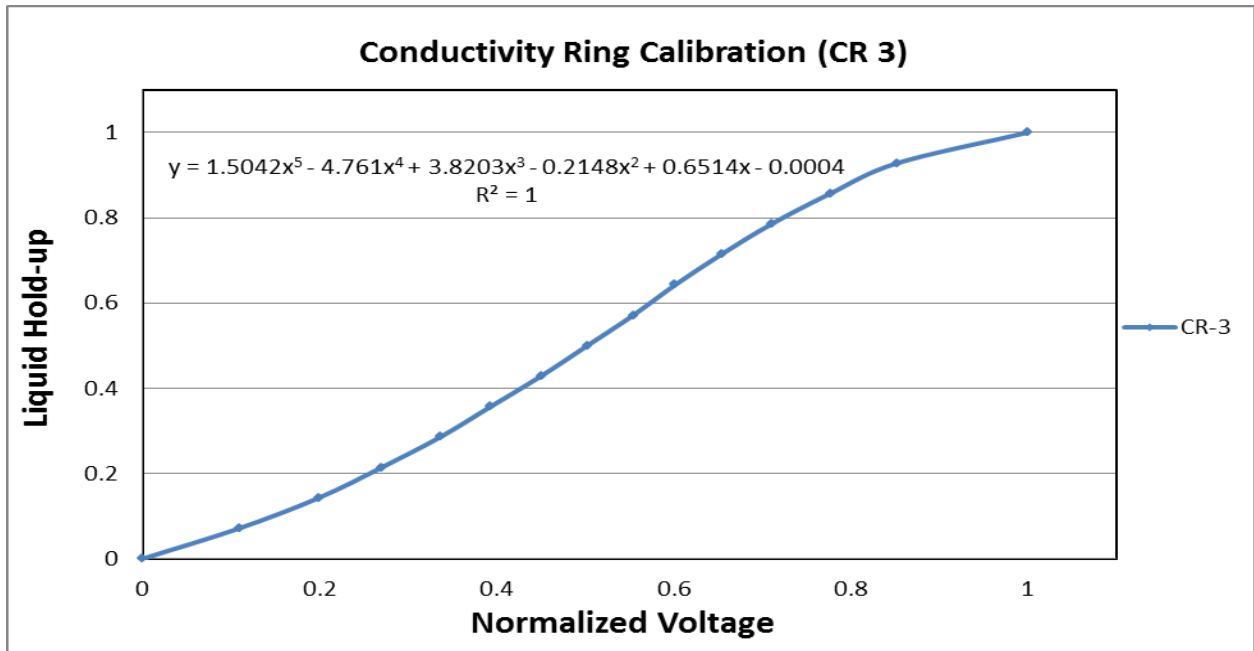


Figure A 6: Conductivity ring-4

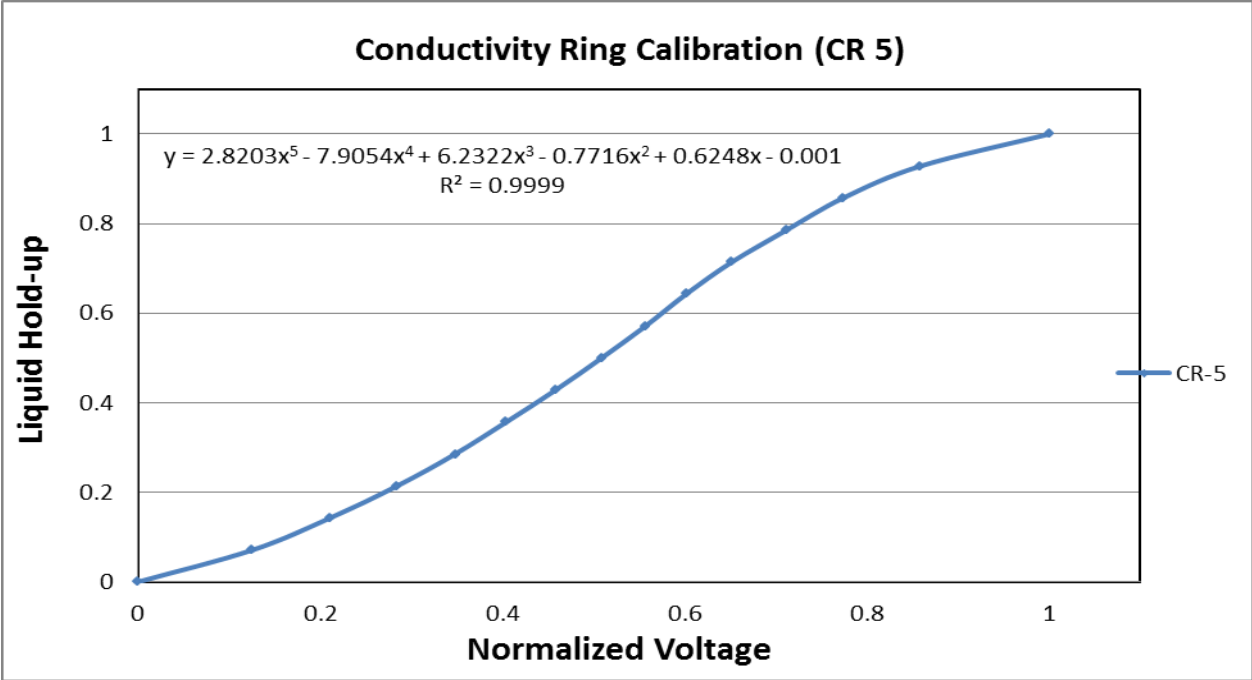


Figure A 7: Conductivity ring-5

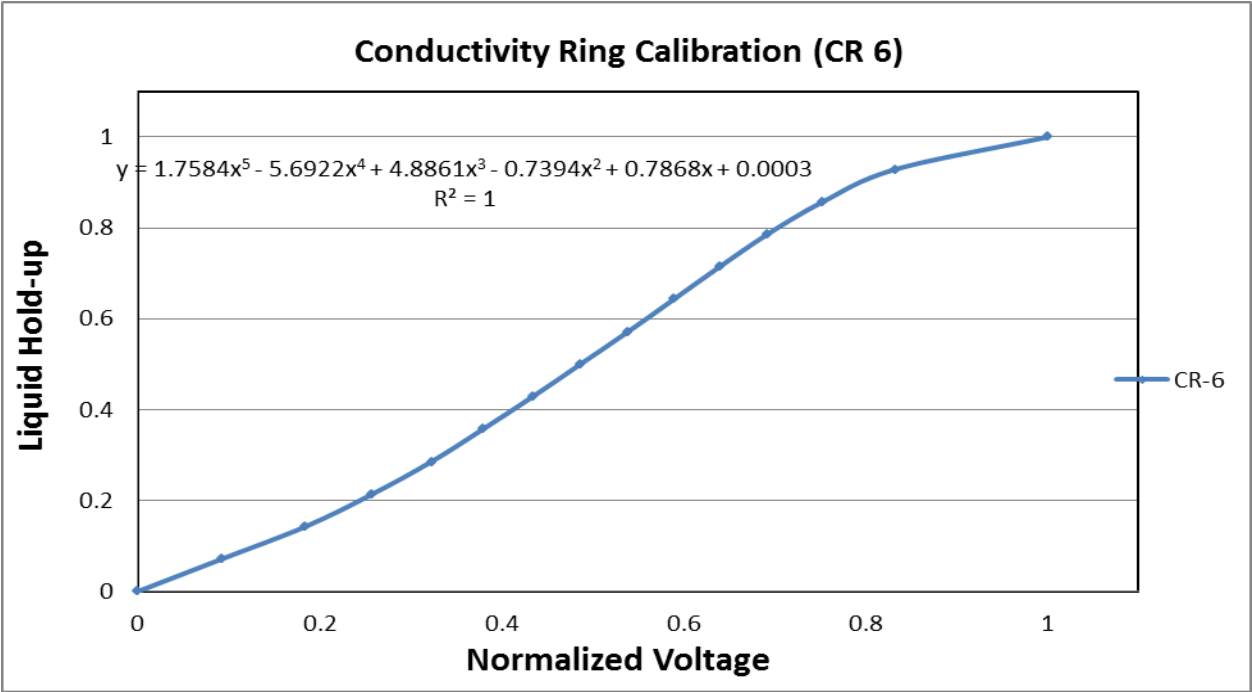


Figure A 8: Conductivity ring-6

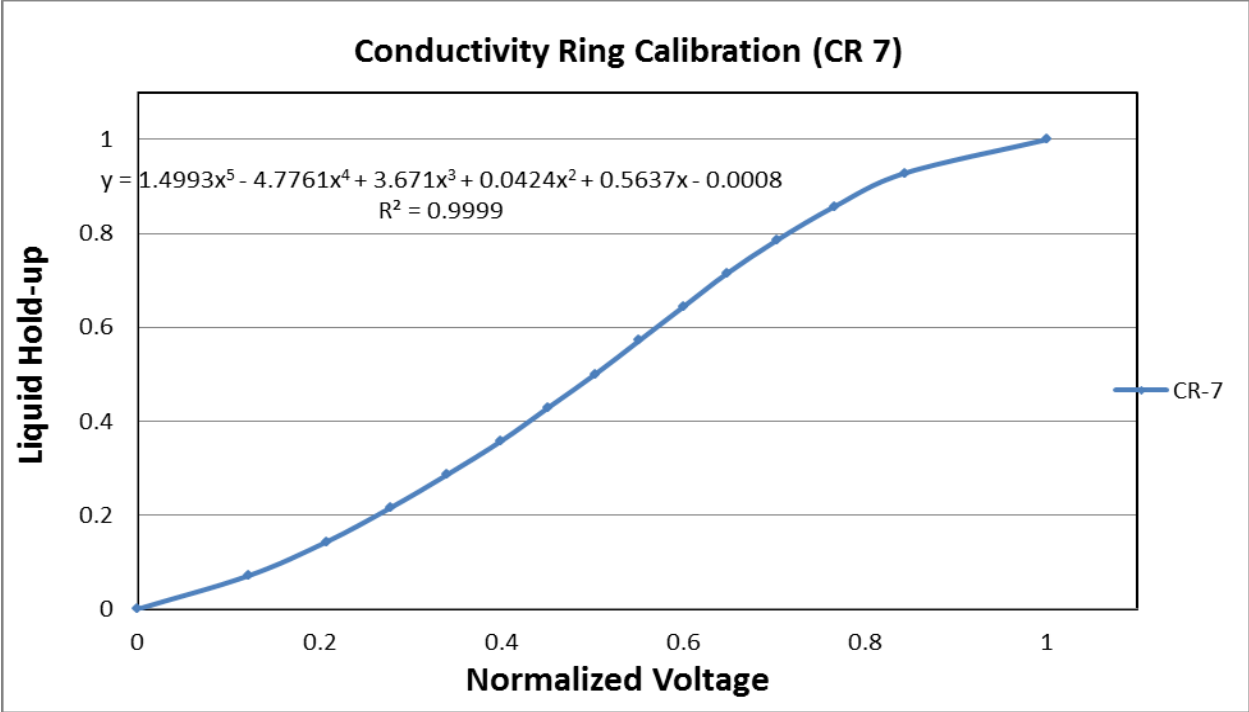


Figure A 9: Conductivity ring-7

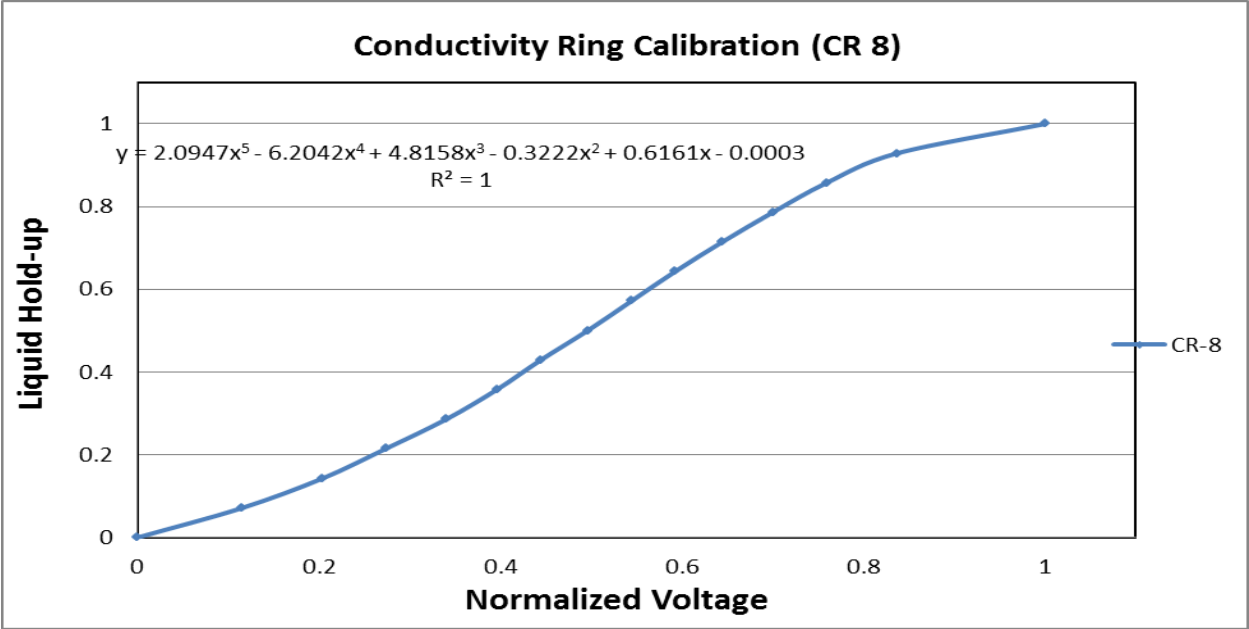


Figure A 10: Conductivity ring-8

### A.3 Sand-Water Conductivity Ring Calibration

The aim of this section is to provide calibration procedure for conductivity ring in order to develop techniques to measure the solid holdup at low sand concentration from conductivity rings.

The technique is based on the relationship between the electrical properties of the liquid composition (i.e. water) and the amount (and composition) of sand present (i.e. sand fraction) in the pipe. The electrical impedance of the medium (water) is used to study the phase distribution and also determine sand hold up.

The sand-water test calibration was carried out in homogenous and sand bed layer distribution for the same various sand fractions.

#### Test Matrix

The test matrix in the dynamic experiment is basically of very low sand concentration 50lb/100bbl -500lb/1000bbl(=0.0005% -0.05% v/v). Therefore the concentration of the sand focused on sand concentration less than 6% sand concentration (v/v). Table A-1 presents the following parameters used in calculating the sand concentration and mass of sand presented in Table A-2.

Table A- 1: Test parameters

Parameters	Quantity
Density of sand (kg/m <sup>3</sup> )	2650
Pipe diameter (m)	0.05024
Volume of empty Pipe (ml)	380

The static test was carried in two categories of sand distribution in the pipe: sand bed layer and homogenous phase distribution using the test matrix in Table A-2. The definition of sand concentration is the percentage ratio of volume of sand in the pipe to the pipe volume (%v/v).

The normalised voltage determined from the conductivity ring signal is defined as  
 (Voltage<sub>(sand and water)</sub> / Voltage<sub>(water only)</sub>)

Table A- 2: 2-inch Conductivity ring sand matrix for low sand concentration (sand-water test)

Mass of sand (g)	Volume of sand (ml)	Volume of water in the sand (ml)	Sand fraction in pipe ( $V_{sand}/V_{total}$ )	% Sand fraction	Liquid holdup [-]	Sand Concentration (lb/1000bbl)
Full water	0.00	380.00	0.00000	0.000	1.000	0
1	0.37	379.63	0.00098	0.098	0.999	915
2	0.75	379.25	0.00197	0.197	0.998	1830
4	1.50	378.50	0.00394	0.394	0.996	3659
6	2.25	377.75	0.00591	0.591	0.994	5489
8	2.99	377.01	0.00788	0.788	0.992	7318
10	3.74	376.26	0.00985	0.985	0.990	9148
12	4.49	375.51	0.01182	1.182	0.988	10977
14	5.24	374.76	0.01379	1.379	0.986	12807
16	5.99	374.01	0.01576	1.576	0.984	14636
18	6.74	373.26	0.01773	1.773	0.982	16466
20	7.48	372.52	0.01970	1.970	0.980	18295
25	9.36	370.64	0.02462	2.462	0.975	22869
30	11.23	368.77	0.02954	2.954	0.970	27443
35	13.10	366.90	0.03447	3.447	0.966	32017
40	14.97	365.03	0.03939	3.939	0.961	36590
45	16.84	363.16	0.04431	4.431	0.956	41164
50	18.71	361.29	0.04924	4.924	0.951	45738
55	20.58	359.42	0.05416	5.416	0.946	50312
60	22.45	357.55	0.05909	5.909	0.941	54885
636	240.00	140.00	0.63158	63.158	0.368	586675

### Conductivity Calibration Result:

The tests were carried out for sand bed layer and homogenous phase distribution. The raw data of the voltage was normalised and plotted for sand bed layer and homogenous phase distribution as shown in Figure A 11 and Figure A 12 below respectively. Figure A11 and Figure A 12 presented below shows that increasing sand concentration generally decreases the voltage signal.

Considering the scattered data around its average, the random error by nature of experiment is calculated using standard deviation from the mean value of 3 repeated runs of test used to determine the calibration curve.

Figure A15 and Figure A 16 presented the comparison of estimated sand fraction against the actual sand fraction for homogenous and sand bed layer distribution respectively. The average percentage error and standard deviation at 68% confidence limit are presented in Table A-3.

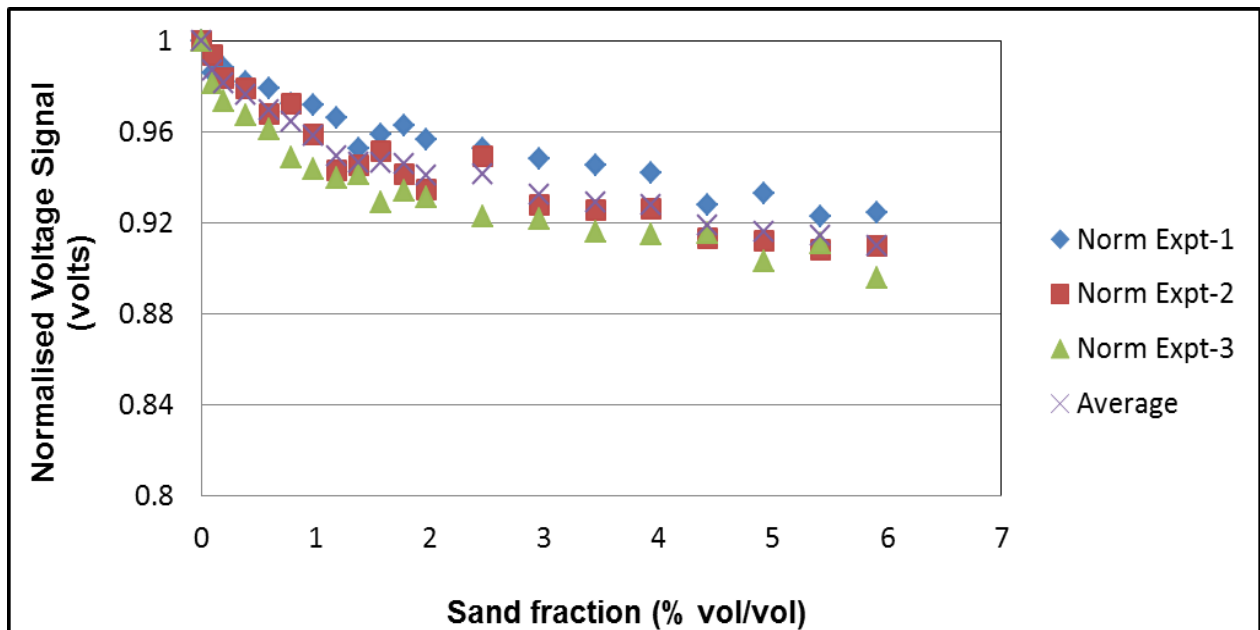


Figure A 11: Normalised voltage signal from sand-water calibration (Sand bed)

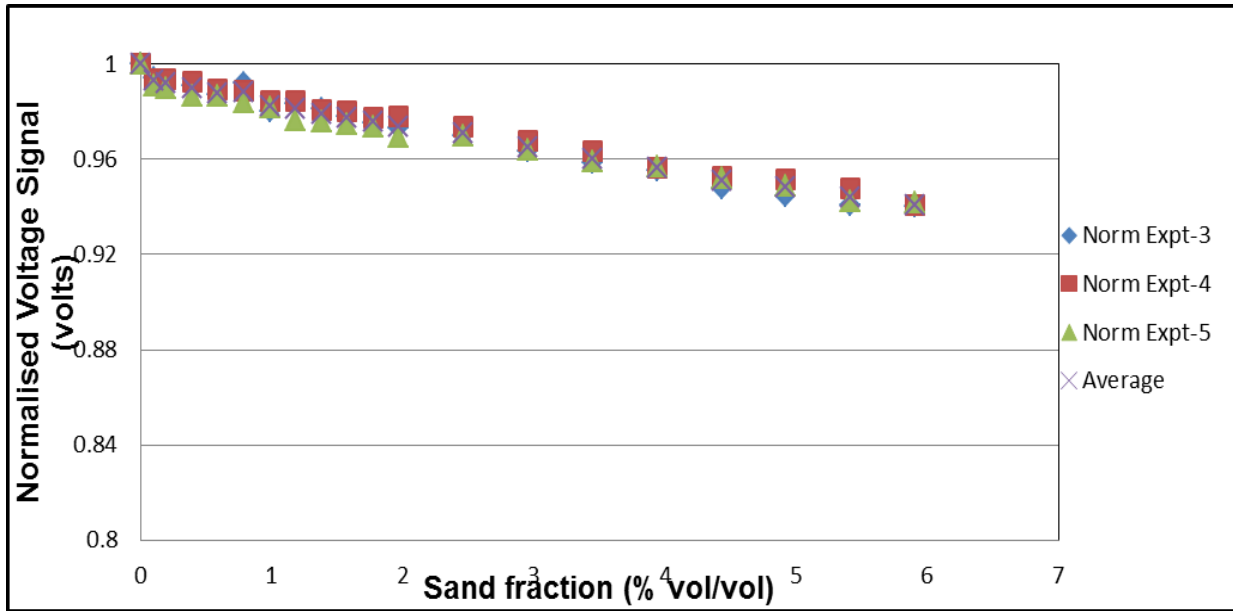


Figure A 12: Normalised voltage signal from sand-water calibration (Homogenous)

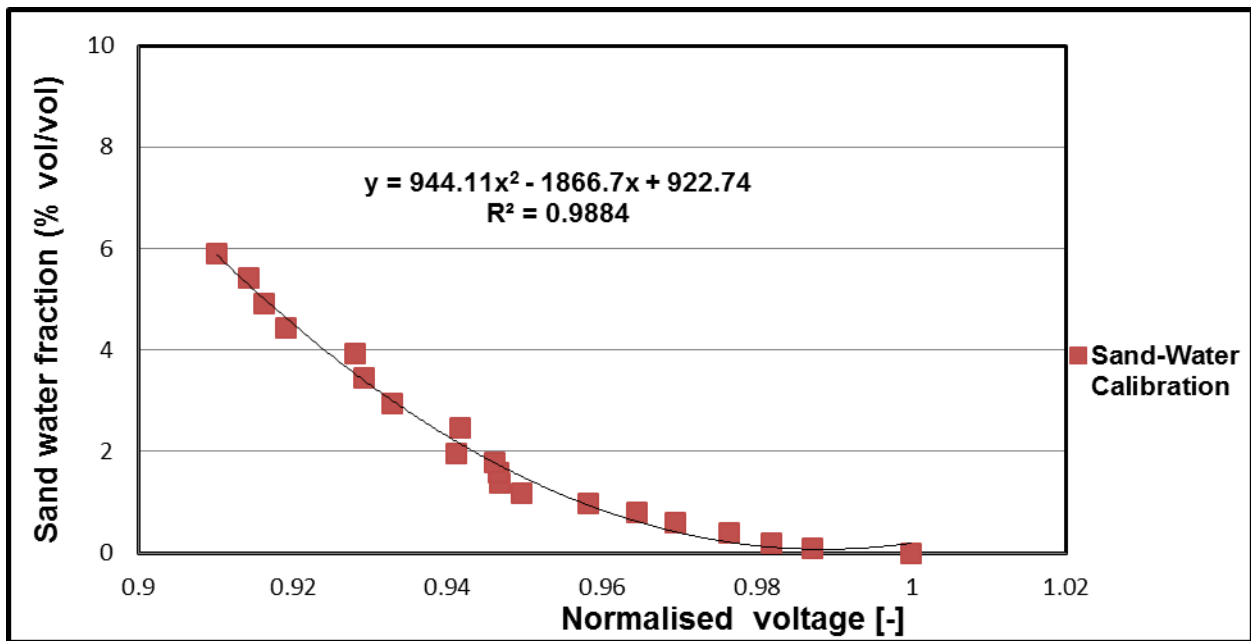


Figure A 13: Calibration curve of sand-water for low concentration (<6%, sand bed)

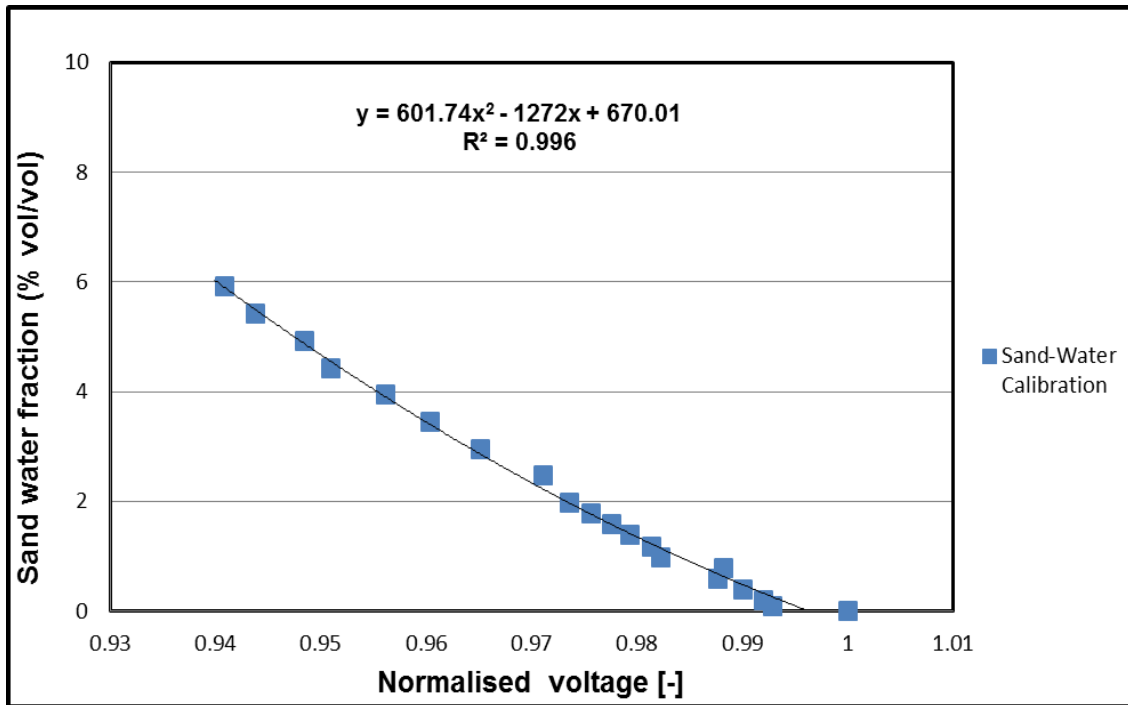


Figure A 14: Calibration curve of sand-water for low concentration (<6%, Homogenous)

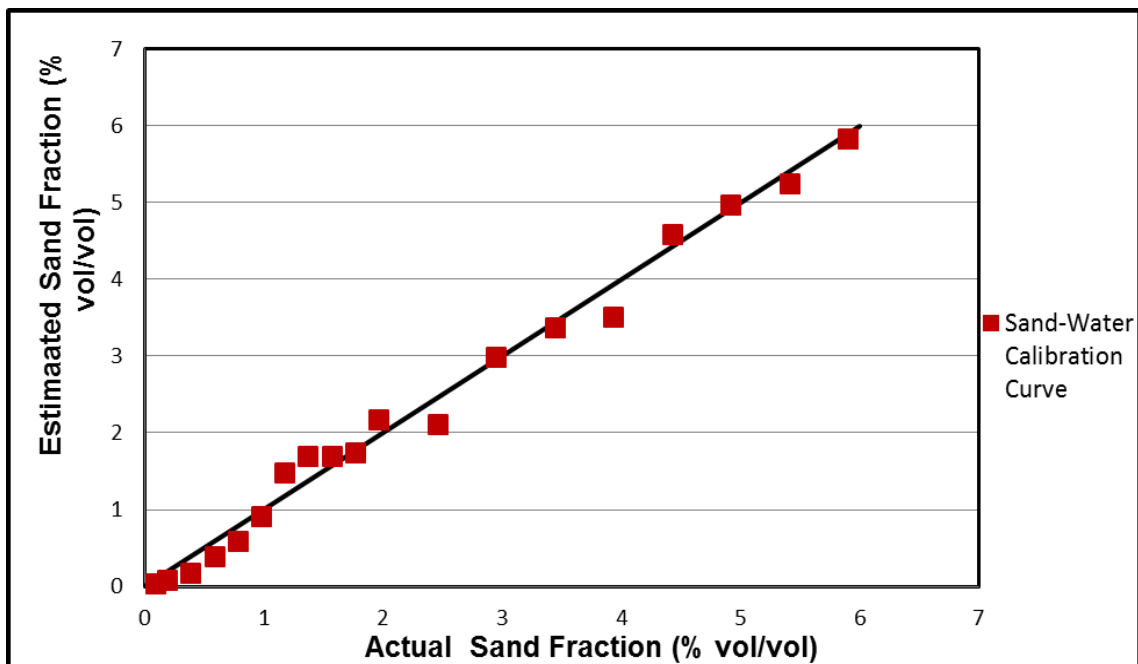


Figure A 15: Estimated sand concentration against actual sand concentration (sand bed)



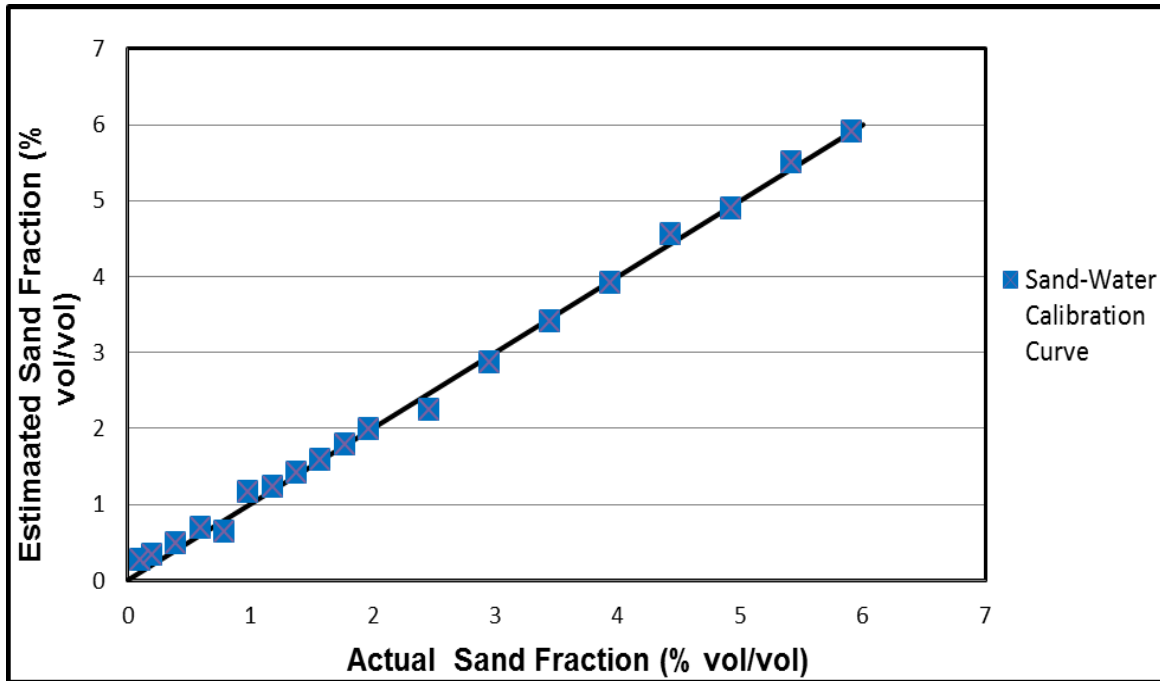


Figure A 16: Estimated sand concentration against actual sand concentration (Homogenous)

Table A- 3: Measurement error

Sand Concentration (%v/v)	Average Relative Percentage Error [%]	Standard Deviation Mean (68% Confidence limit)
Sand Bed Layer Distribution	12.18	0.048
Homogenous Layer	14.83	0.025

#### A.4 Sand Holdup Calculation

In this present work, the sand holdup is determined by simple geometry as shown below by assuming the sand bed is flat. For calibration purpose, a measured tape was also recorded with

each video film. This will enable the pixel coordinates to be converted to millimetres. As a result, all screen resolutions (magnification) in the video could be scaled to real unit values.

Also, the porosity of this particular pipe was determined by filling a spool piece (of the same pipe diameter pipe) with given amount of sand. The sand porosity is found to be 0.36.

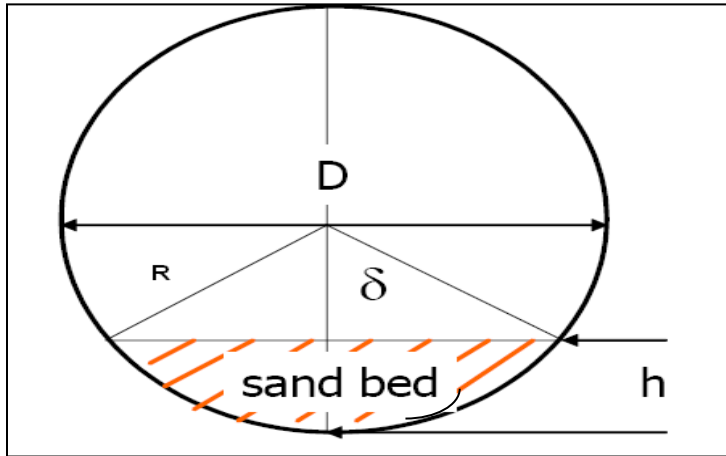


Figure A 17: Sand bed in pipe

A rough estimate of the sand holdup will be considered by assuming the interface is flat; the holdup can be calculated from the geometry as follows.

From Figure A 17 where  $\theta = 2\delta$

$$\cos \delta = \frac{R-h}{R} = 1 - \frac{h}{R} = \left(1 - 2\frac{h}{D}\right)$$

$$\theta = 2\delta = 2\cos^{-1}\left(1 - 2\frac{h}{D}\right) \quad (\text{A-1})$$

Where ( $\theta$  and  $\delta$ ) are in radian

Area of the circular segment is the area of the circular sector minus the area of the triangular portion

$$\text{Area of the sand bed} = \frac{1}{2} R^2 (\theta - \sin\theta) = \frac{1}{2} \left(\frac{D}{2}\right)^2 (\theta - \sin\theta)$$

$$\text{Area of the whole pipe} = \frac{\pi D^2}{4}$$

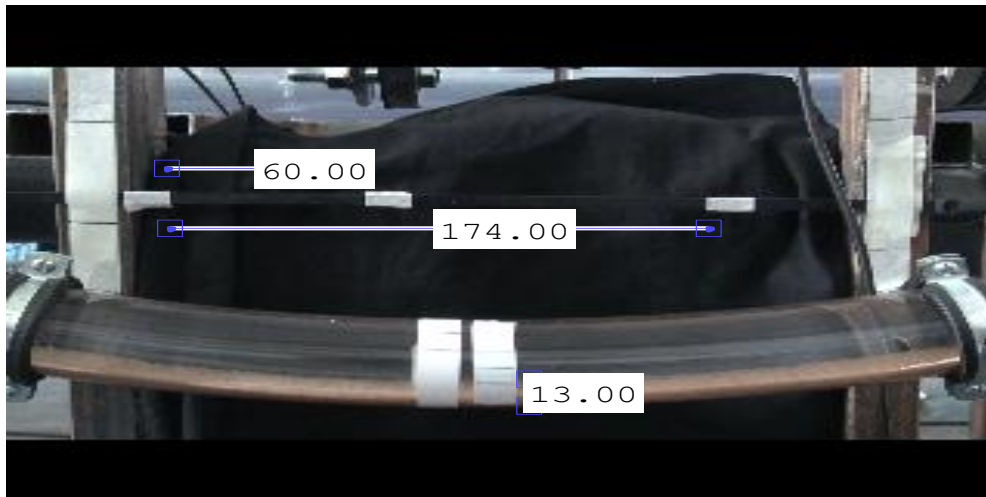
$$\text{Sand Holdup } (H_s) = \frac{\text{Area of sand bed}}{\text{Area of whole pipe}} = \frac{\frac{1}{2} \left(\frac{D}{2}\right)^2 (\theta - \sin\theta)}{\frac{\pi D^2}{4}} = \frac{(\theta - \sin\theta)}{2\pi} \quad (\text{A-2})$$

Using the image technique, the bed height can be determined at the dip by calibration.

Pipe Diameter = 50.24mm

Using equation (1)

$$\text{Where } \beta = \left(1 - 2 \frac{h}{D}\right)$$



**Figure A 18: Sand Holdup Measurement of 400g sand injection**

Table A- 4: Result of Sand Holdup Calculation

Mass	h(mm)	$\beta$	$\text{Cos}^{-1}\beta$	Angle ( in radian)	Sand Hold up( $H_s$ )	( $H_s$ )using Porosity
20g	10.3	0.589968	0.939777	1.879553859	0.147511486	0.094407351
100g	10.6	0.578025	0.954489	1.908978836	0.153683135	0.098357207
200g	19.2	0.235669	1.33289	2.665779286	0.35136918	0.224876275
400g	20.7	0.175955	1.39392	2.787840172	0.388564031	0.24868098

However, this is a rough estimate. In order to rely on this method of calculating sand hold up, a short spool piece will be used with a known sand fraction for calibration and image process techniques will then be used to obtain the holdup. The result will then be compared.

### Camera Resolution

In order to rely on this method of calculating sand hold up, a short spool piece was used with a known sand fraction for calibration and image process techniques to obtain the holdup.

In order to validate this method, a calibration was carried out with a short spool piece of 2 inch pipe as shown in Figure A 19 for various amount of sand.

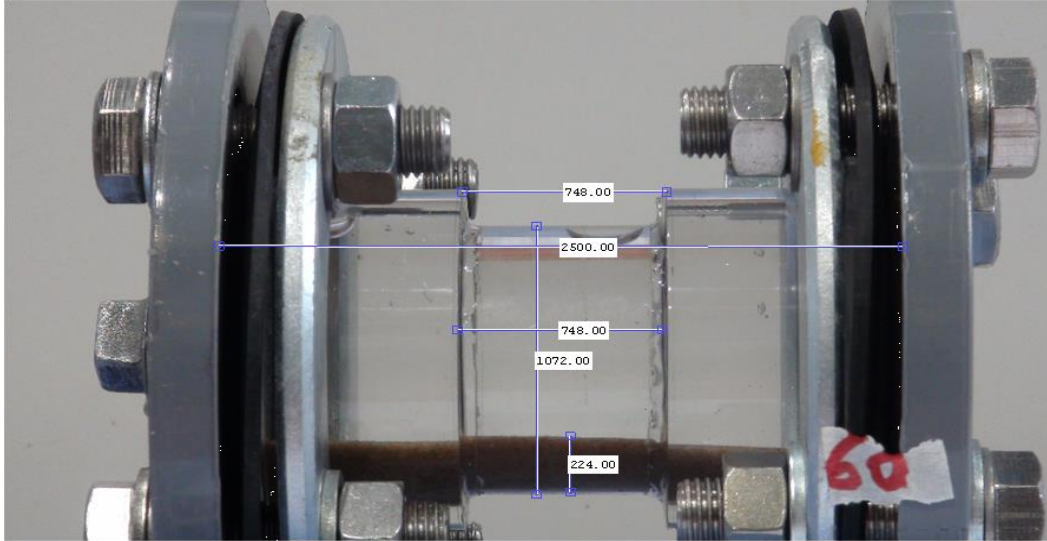


Figure A 19: Sand Calibration

Table A- 5: Sand holdup Calibration

Pipe Diameter = 49.6mm						By geometry	By volume
Mass (g)	H(mm)	$\beta$	$\text{Cos}^{-1}\beta$	$2 \text{Cos}^{-1}\beta$	Sand Hold up( $H_s$ )	Holdup with porosity	Actual(v/v)
0	0	0	-	-	0	0	0
20	5.01	0.80	0.64	1.29	0.05	0.03	0.03
40	8.17	0.67	0.83	1.66	0.11	0.07	0.06
60	10.36	0.59	0.94	1.89	0.15	0.10	0.09
80	15.25	0.39	1.17	2.33	0.26	0.16	0.12
100	16.35	0.35	1.21	2.43	0.28	0.18	0.16
120	17.47	0.30	1.26	2.52	0.31	0.20	0.20
140	18.75	0.25	1.31	2.63	0.34	0.22	0.24
160	23.06	0.08	1.49	2.98	0.45	0.29	0.28
180	22.81	0.09	1.48	2.96	0.44	0.28	0.33

Height of the series of sand bed was measured using the image technique as shown above in Figure A 19 . The height from image technique is used to calculate the sand hold using equation (A-2).

The actual sand hold up in the pipe is compared with the holdup obtained using the calculated sand holdup as shown in Table 2. The result from this analysis is presented in Figure A 20. The percentage error is 6.5% with standard deviation mean of  $\pm 0.008$  with 68% confidence limit.

The result showed a fair agreement between the actual sand holdup and the calculated sand hold up based on the image height. The height of the sand bed must be below the middle section of the pipe (i.e. half or less than half full (  $< 180^\circ$ )) otherwise equation (A-1 & A-2) will change slightly. Several reasons could cause slight deviation from the actual sand holdup such (1) getting the actual image height by using high speed camera and lightning (2). How evenly the sand bed is distributed. (3) The compartment of the sand particle varies as the sand bed increases.

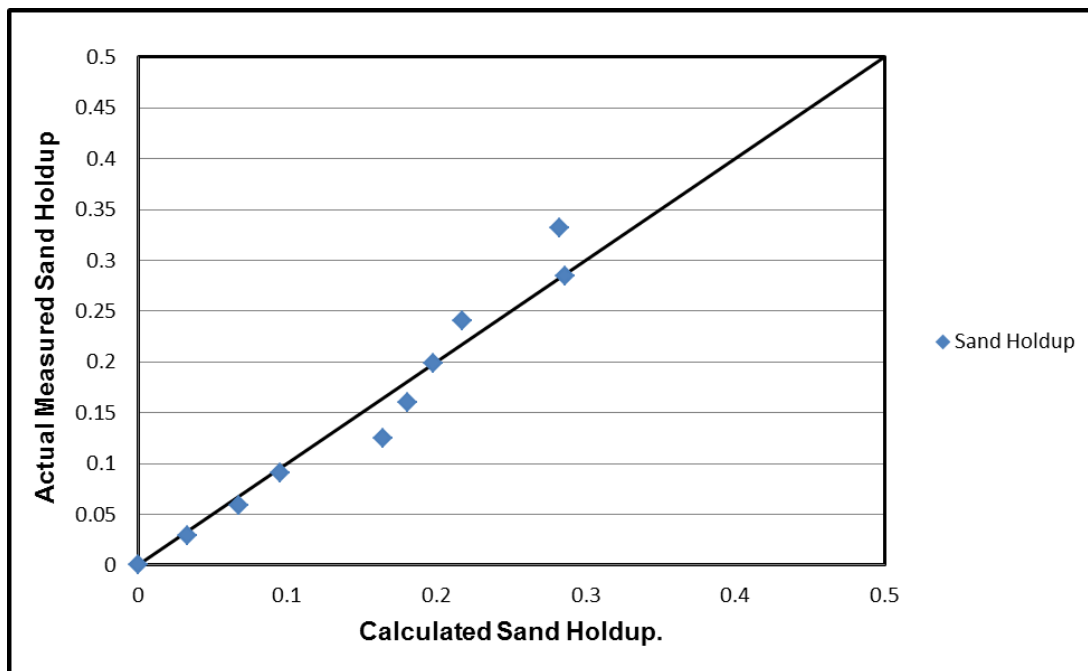


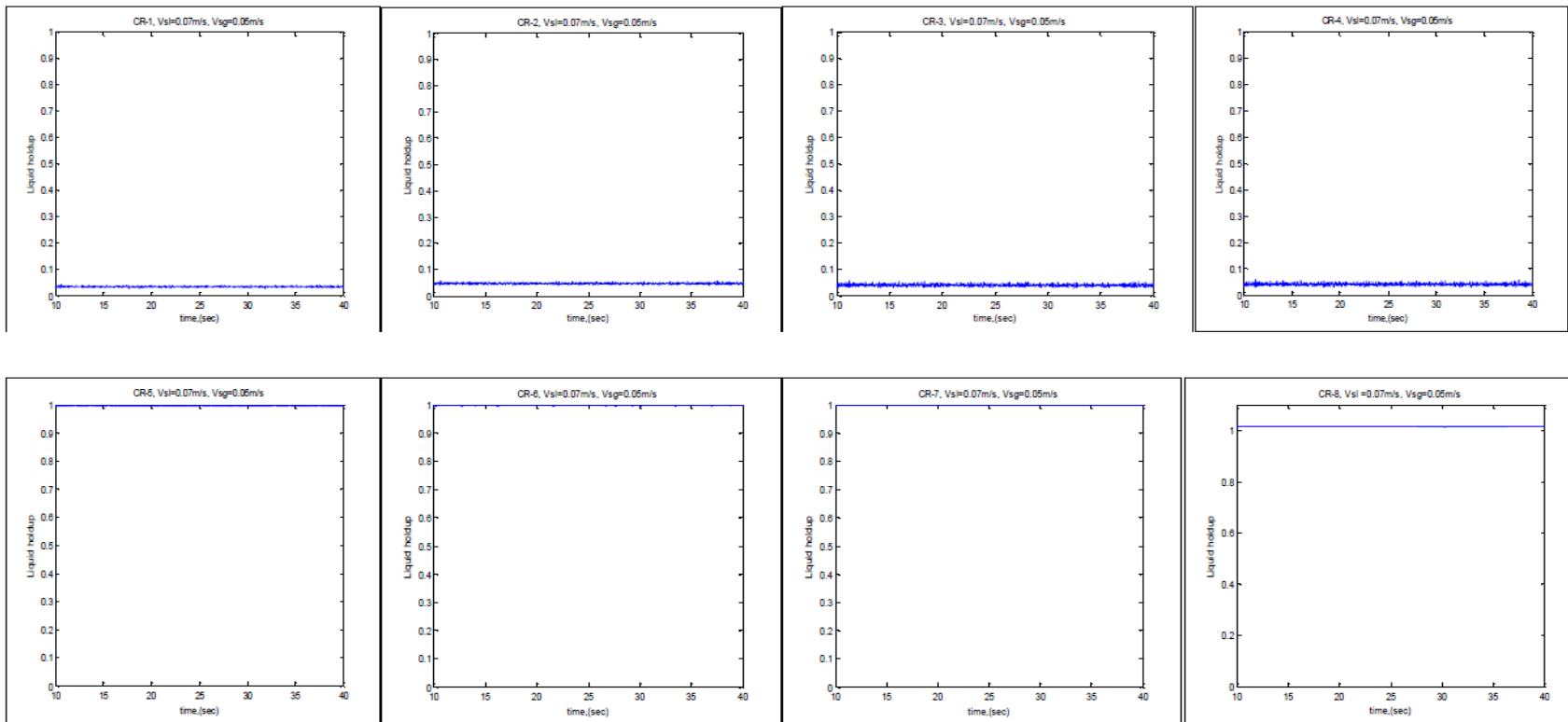
Figure A 20: Sand holdup calibration comparison

# Appendix B : Air-Water Flow Regime Using Time Series

B.1 :  $V_{sl} = 0.07\text{m/s}$

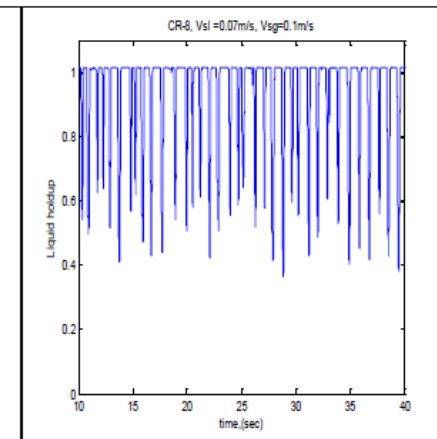
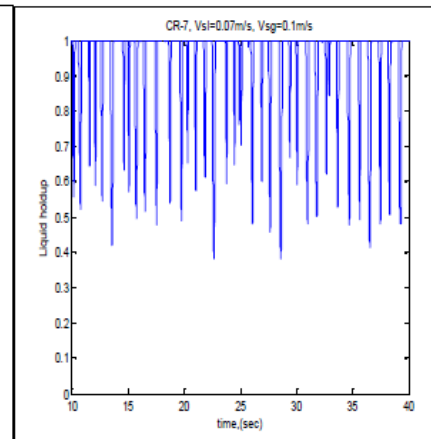
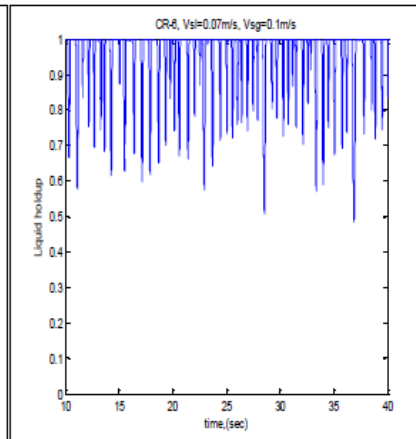
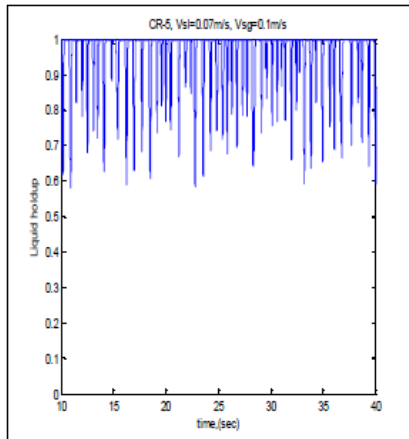
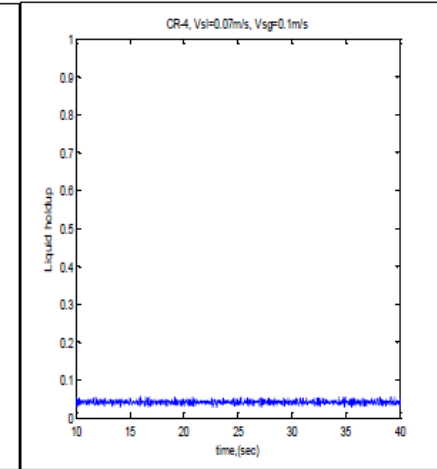
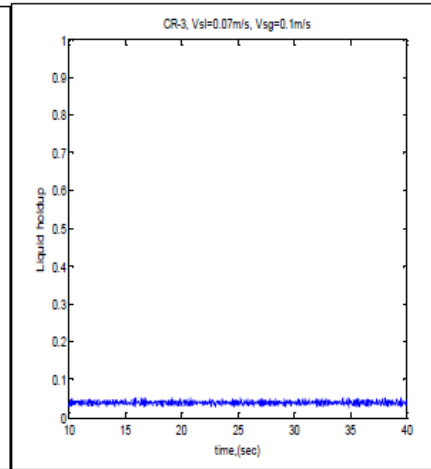
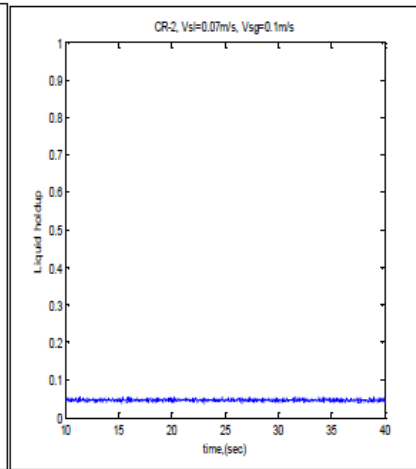
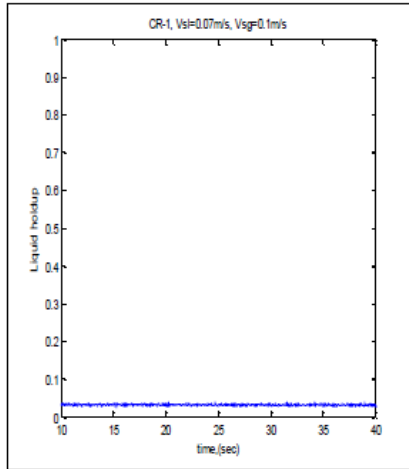
$V_{sg} = 0.05\text{m/s}$

$V_{sl} = 0.07\text{m/s}$ ,  $V_{sg} = 0.05\text{m/s}$



Vsg=0.1m/s

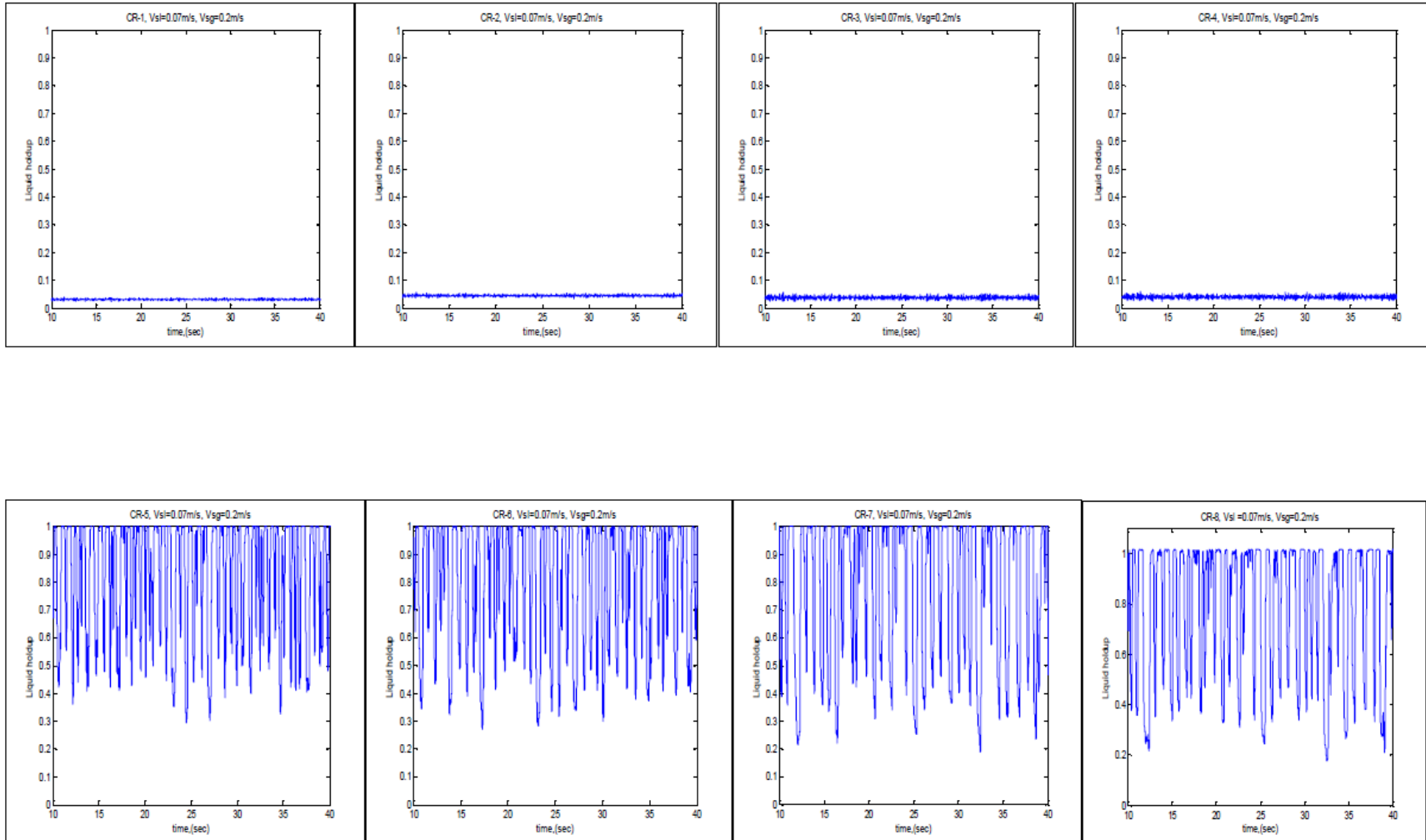
Vsl=0.07m/s, Vsg=0.1m/s





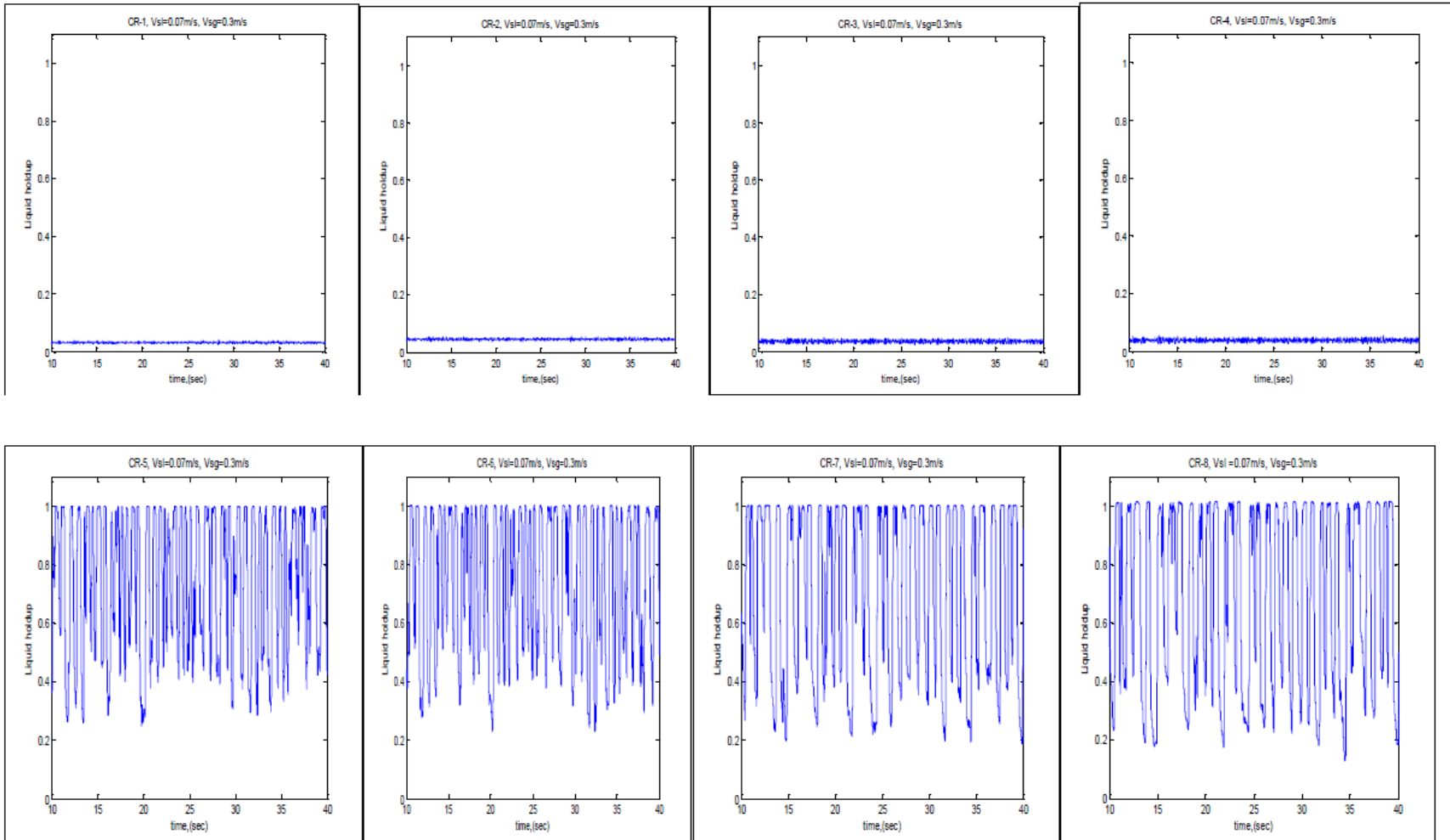
Vsg=0.2m/s

Vsl=0.07m/s, Vsg=0.2m/s



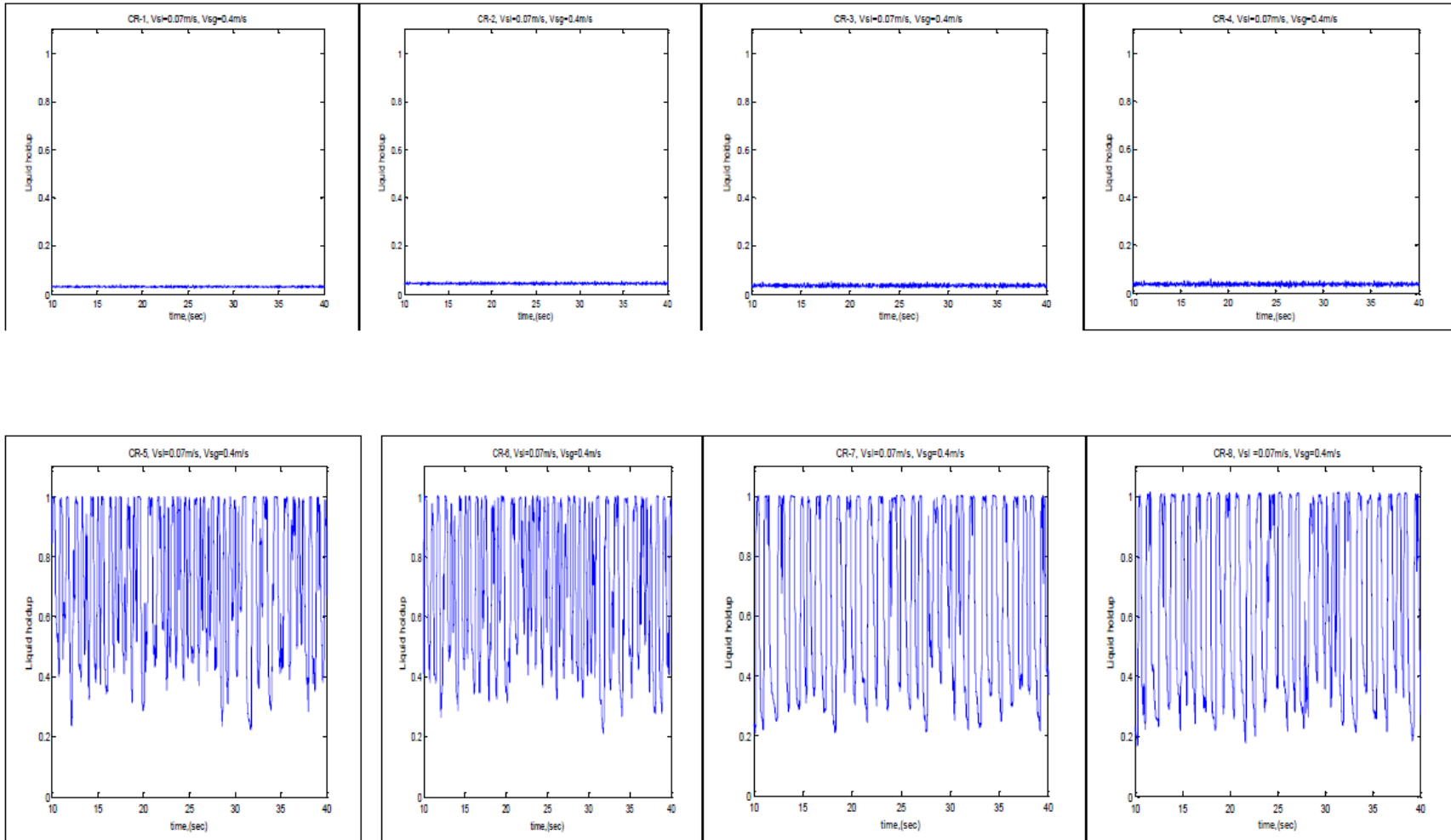
**Vsg=0.30m/s**

**Vsl=0.07m/s, Vsg=0.3m/s**



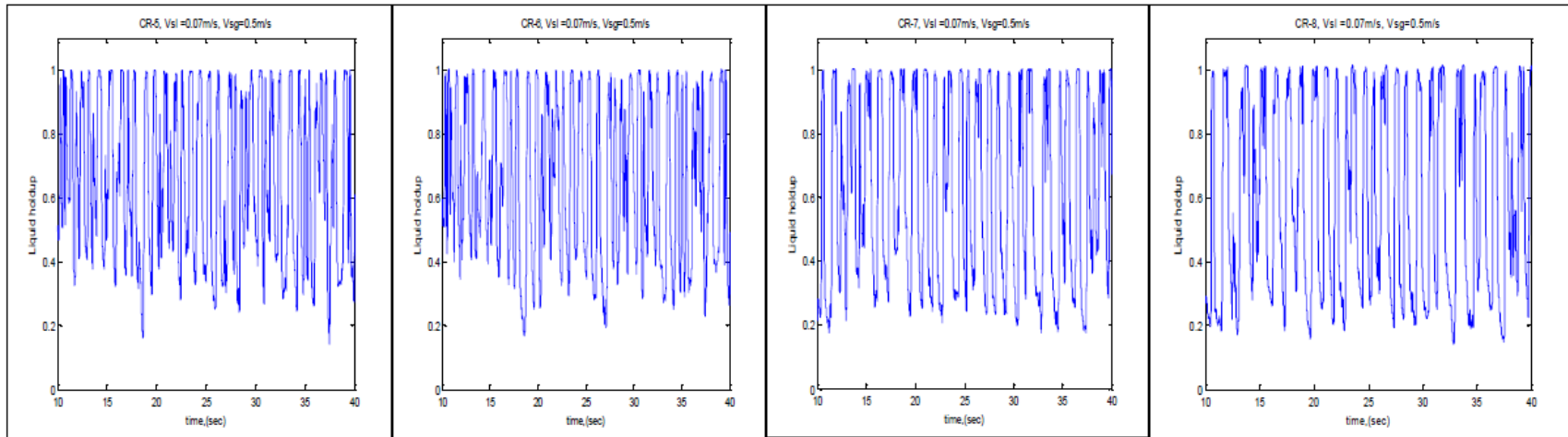
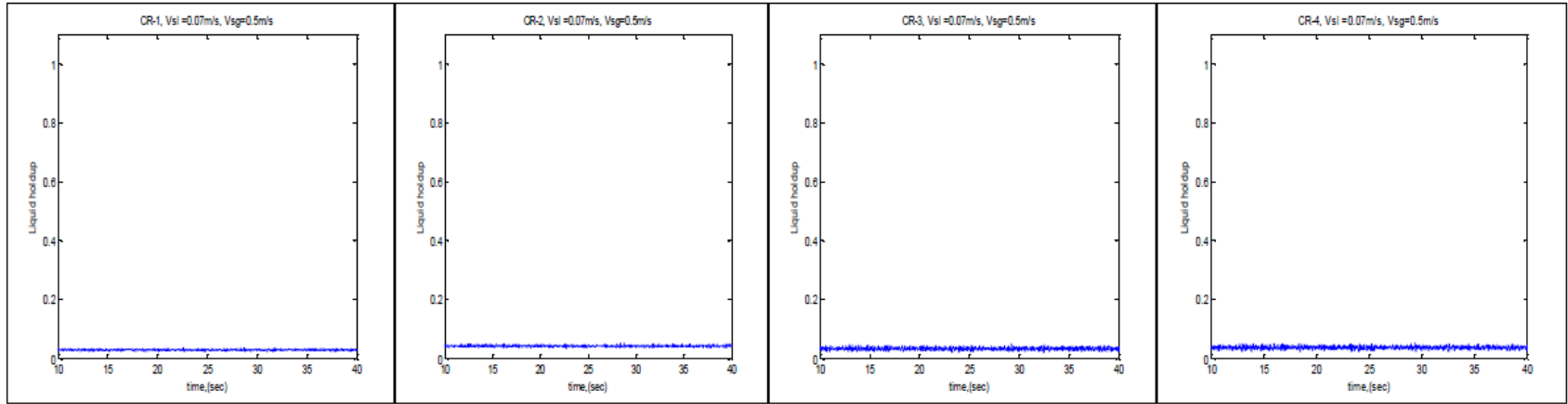
Vsg=0.40m/s

Vsl=0.07m/s, Vsg=0.4m/s



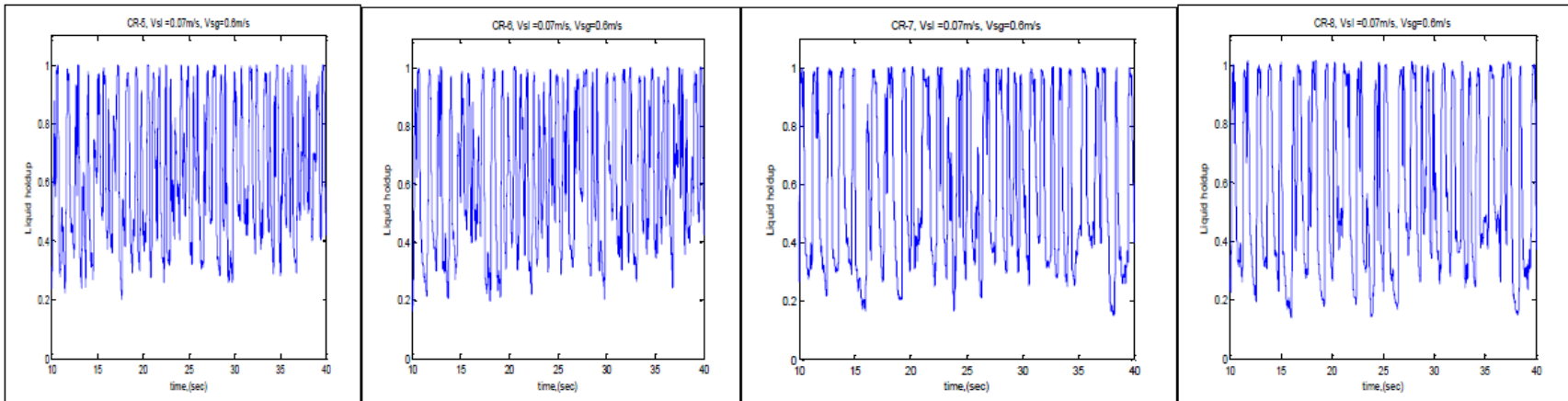
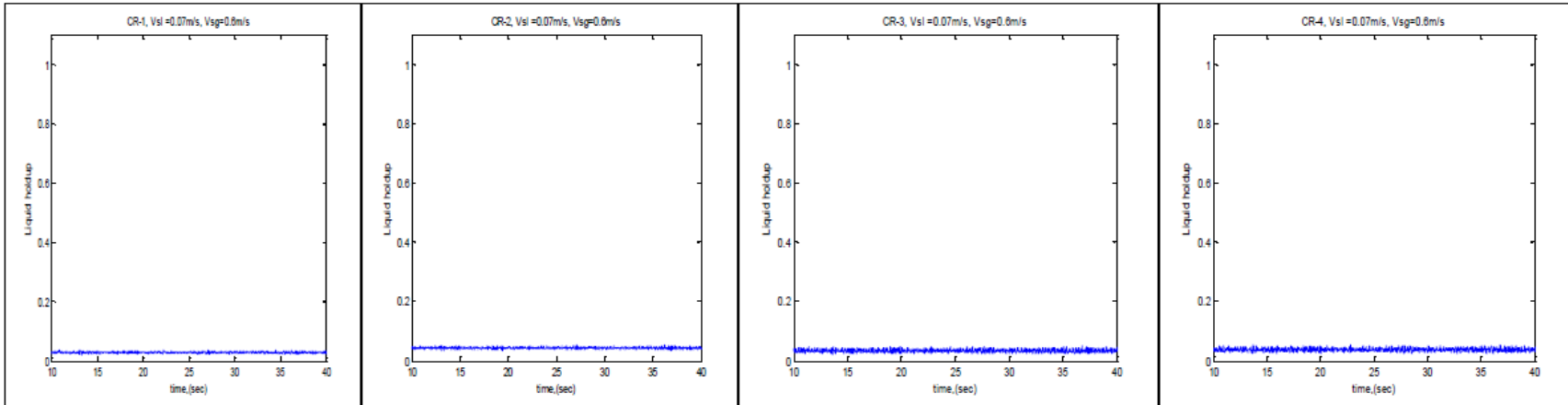
Vsg=0.50m/s

Vsl=0.07m/s, Vsg=0.5m/s



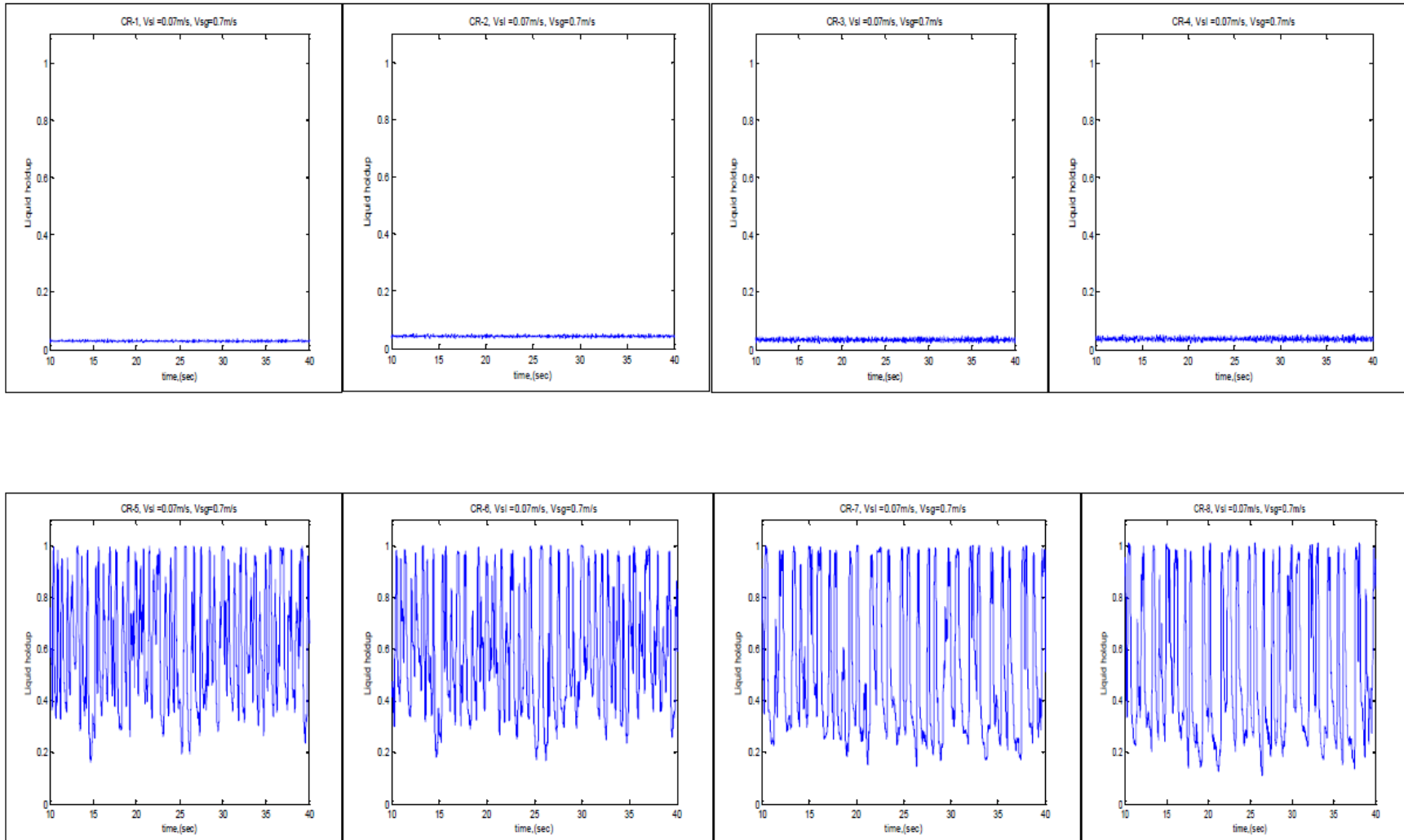
Vsg=0.60m/s

Vsl=0.07m/s, Vsg=0.6m/s



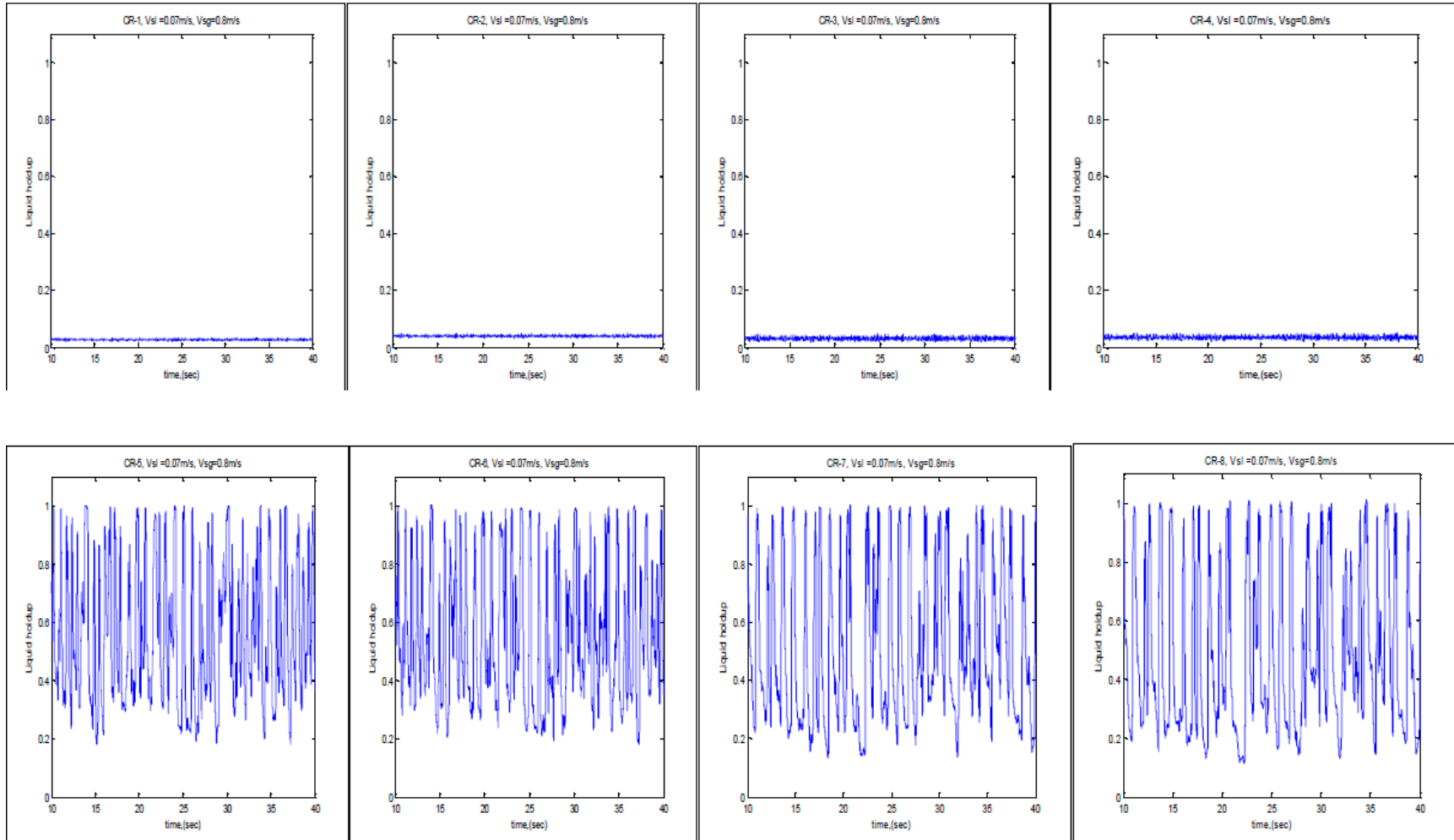
Vsg=0.7m/s

Vsl=0.07m/s, Vsg=0.7m/s



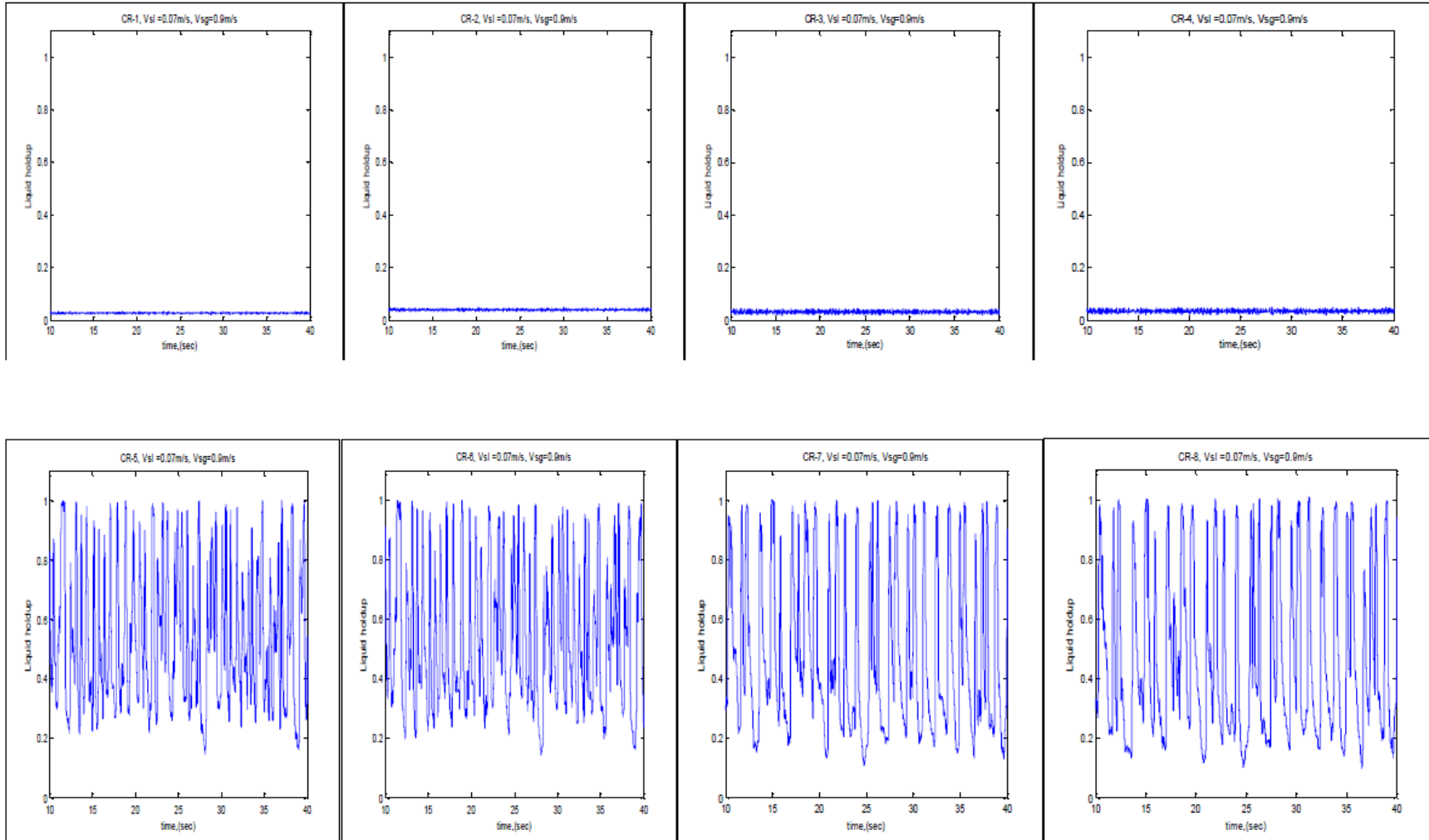
Vsg=0.80m/s

Vsl=0.07m/s, Vsg=0.8m/s



$V_{sg}=0.90\text{m/s}$

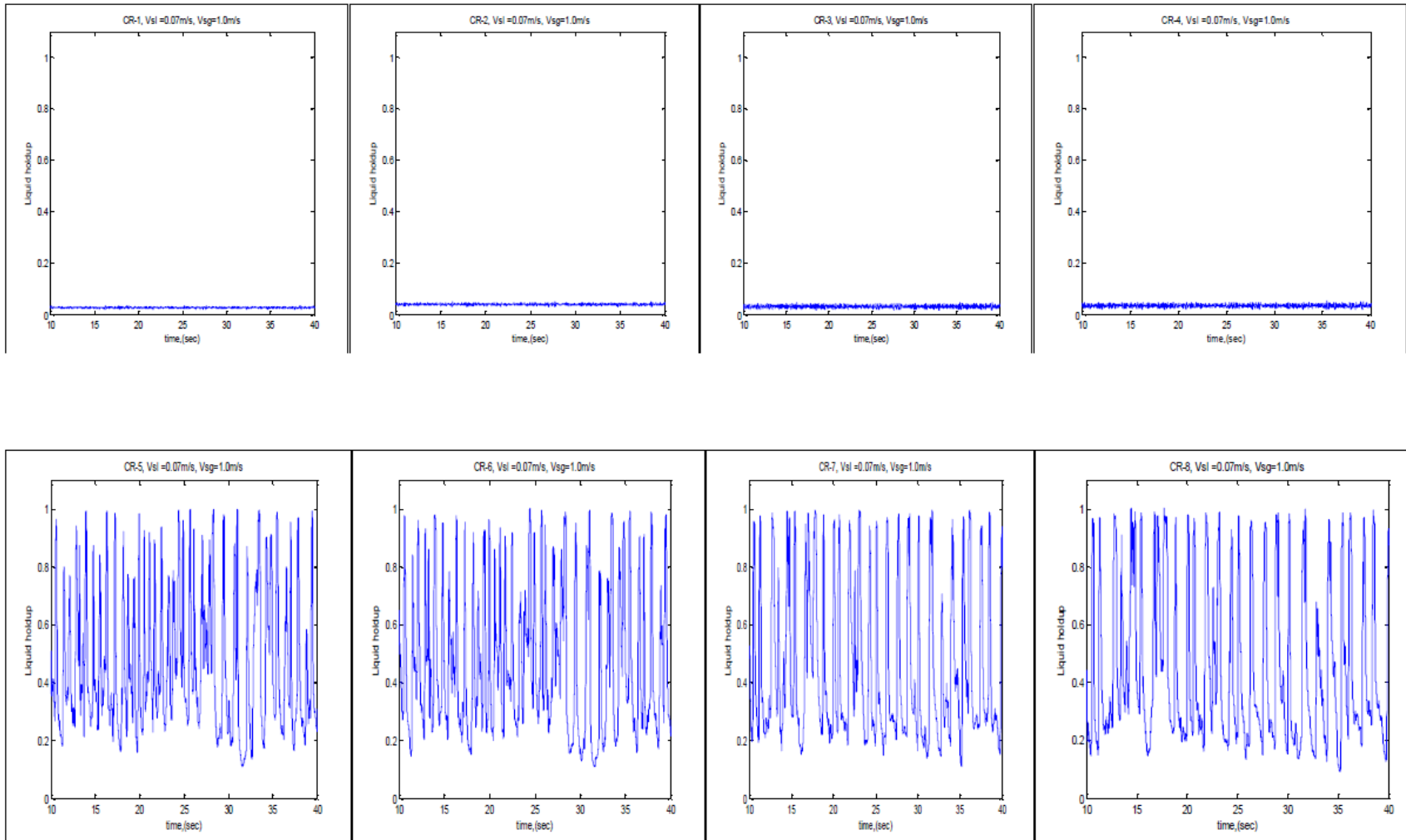
$V_{sl}=0.07\text{m/s}$ ,  $V_{sg}=0.9\text{m/s}$





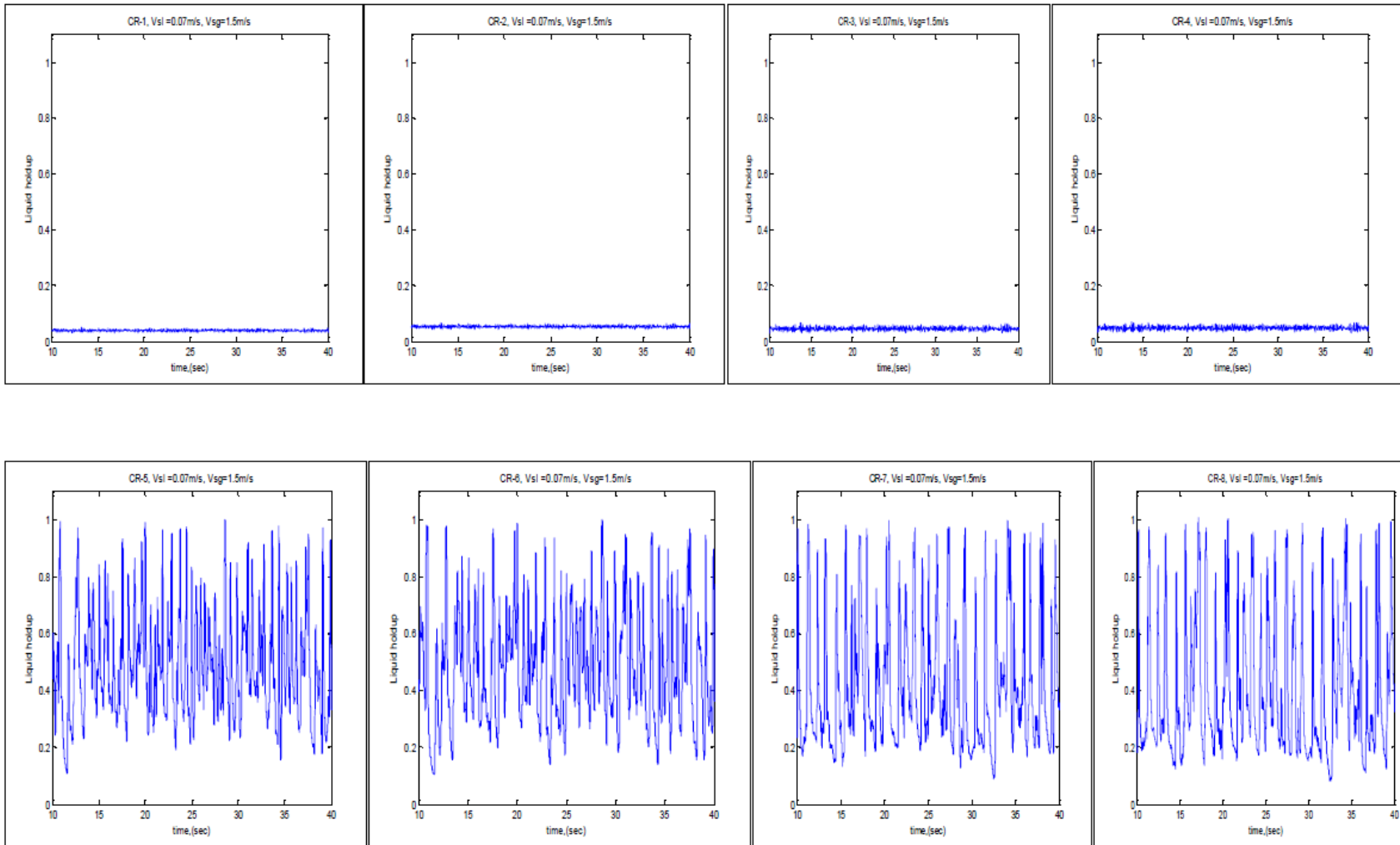
**Vsg=1.0m/s**

**Vsl=0.07m/s, Vsg=1.0/s**



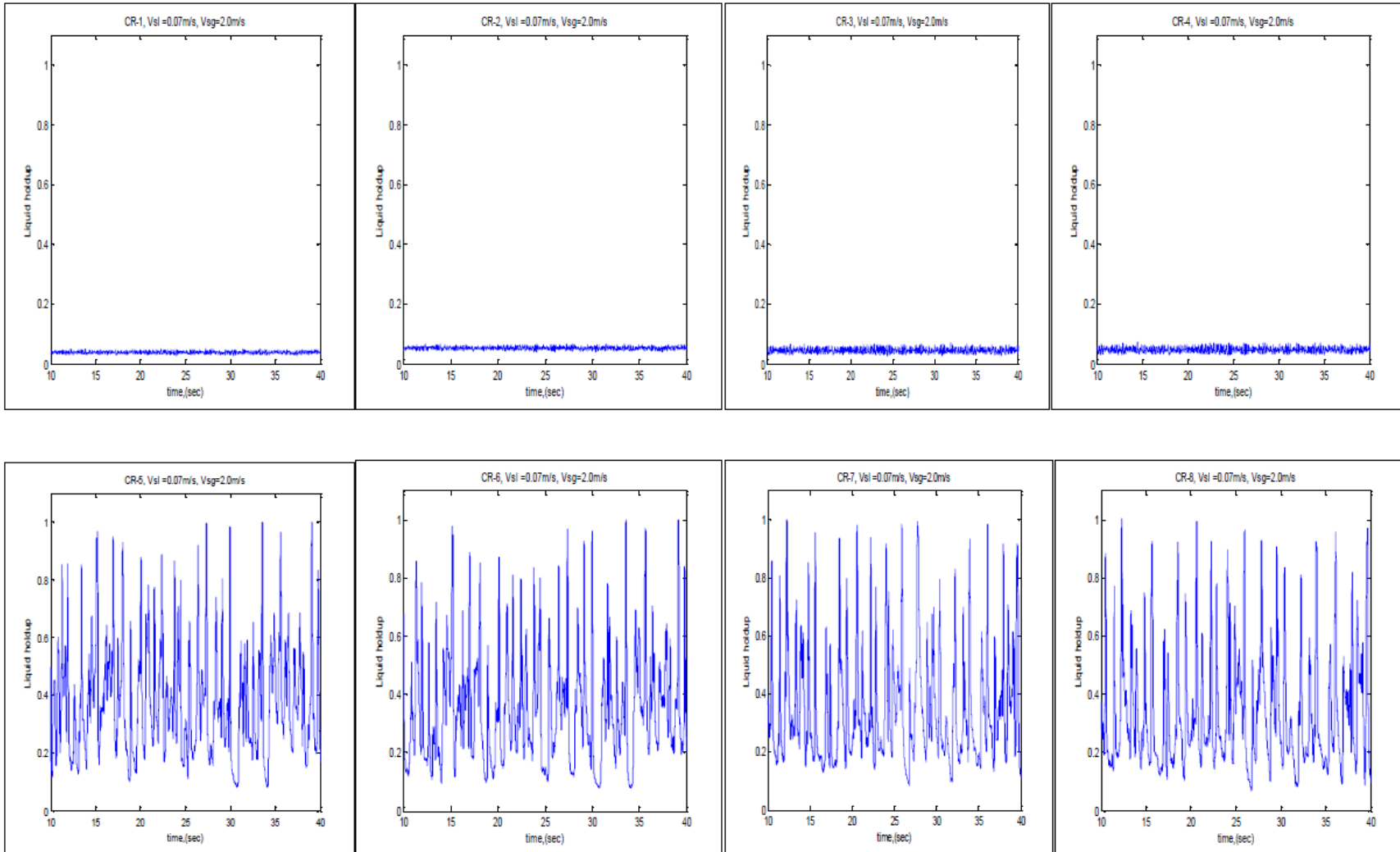
Vsg=1.5m/s

Vsl=0.07m/s, Vsg=1.5m/s



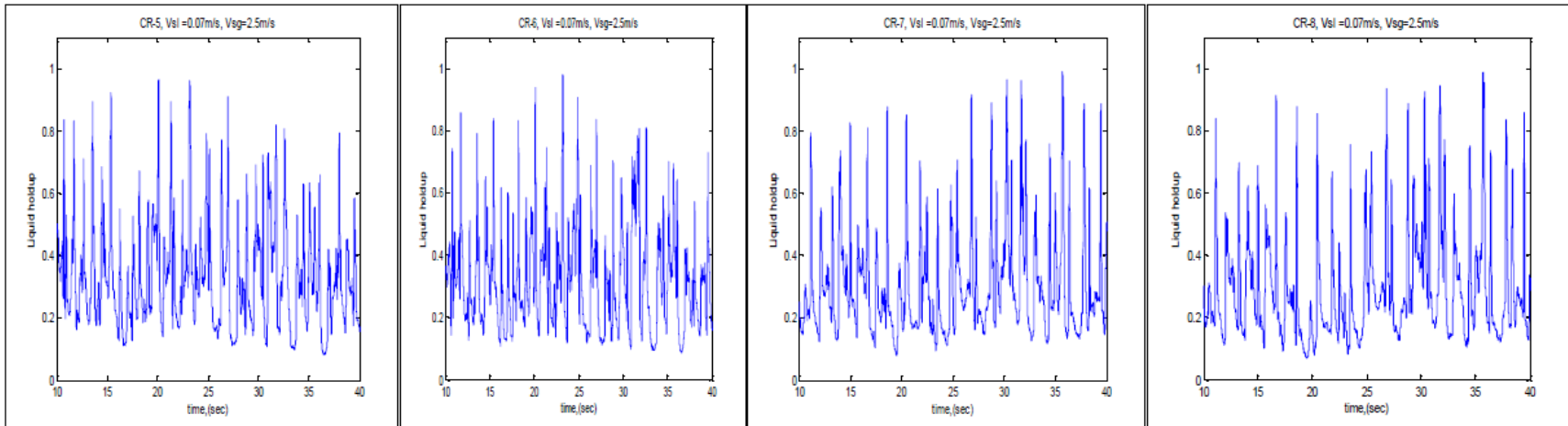
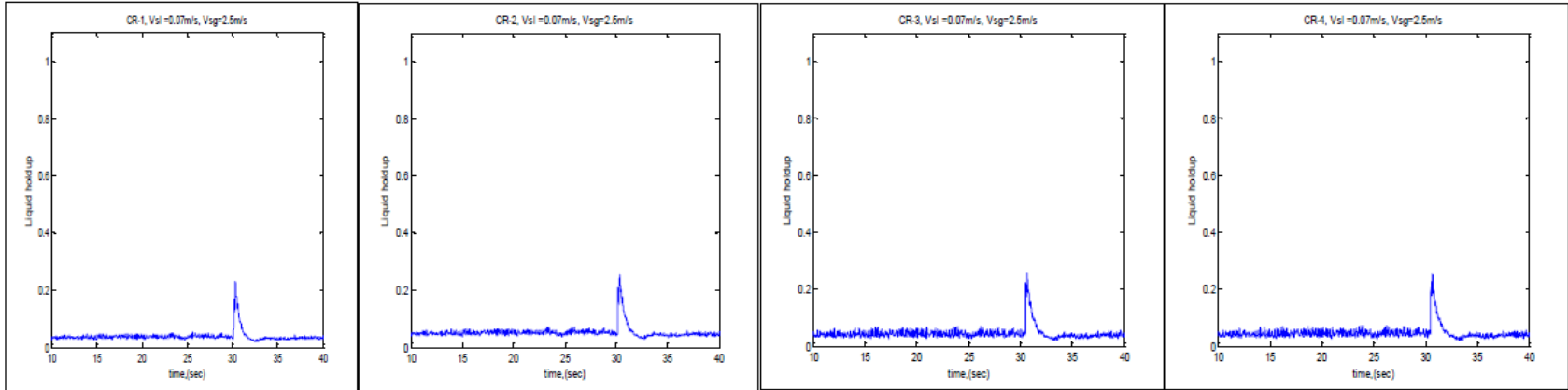
Vsg=2.0m/s

Vsl=0.07m/s, Vsg=2.0m/s



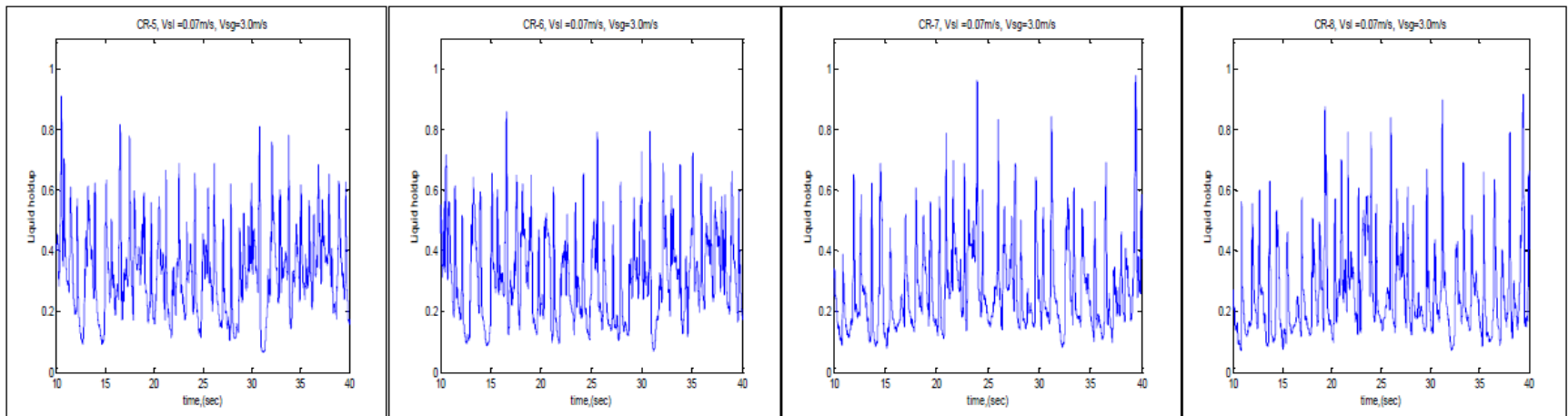
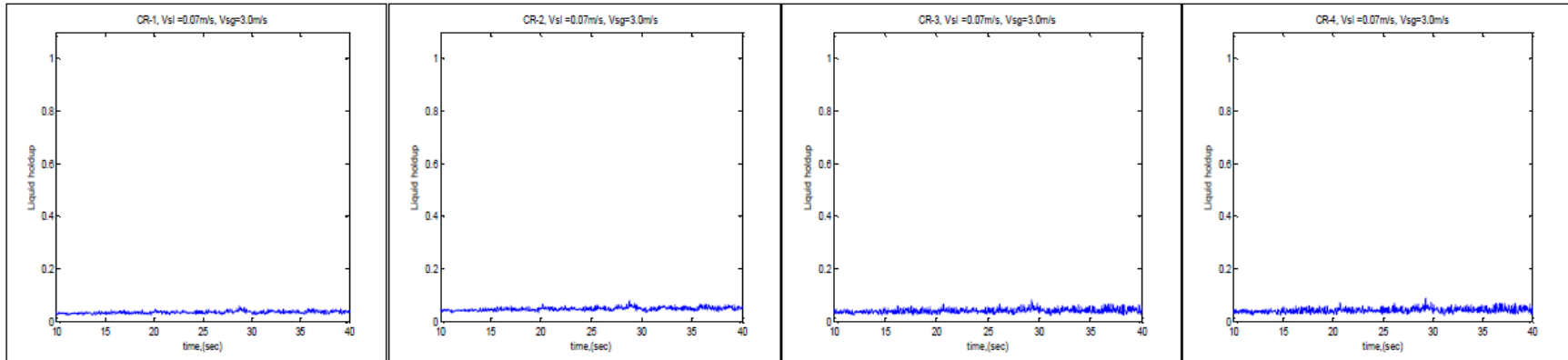
Vsg=2.5m/s

Vsl=0.07m/s, Vsg=2.5m/s



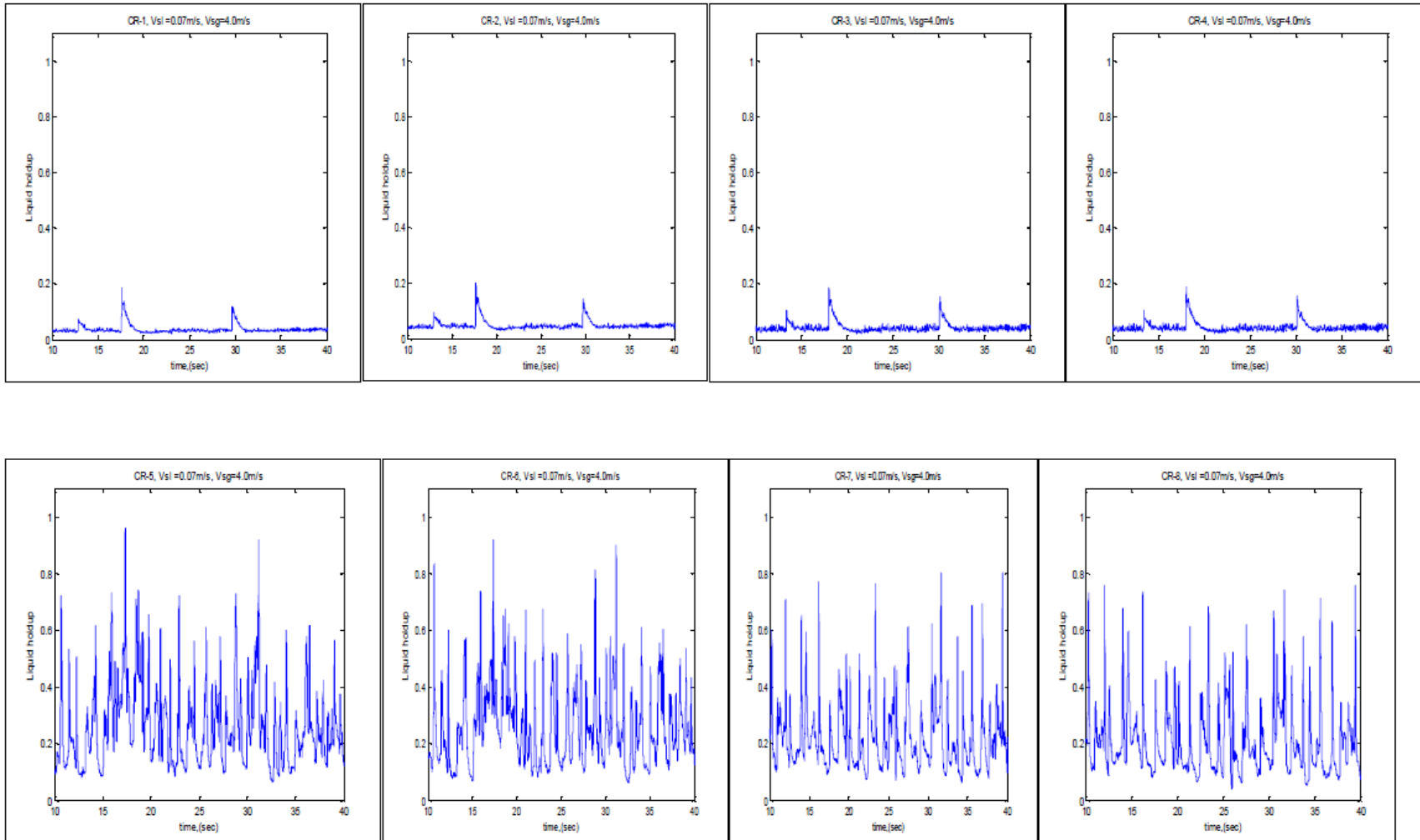
Vsg=3.00m/s

Vsl=0.07m/s, Vsg=3.0m/s



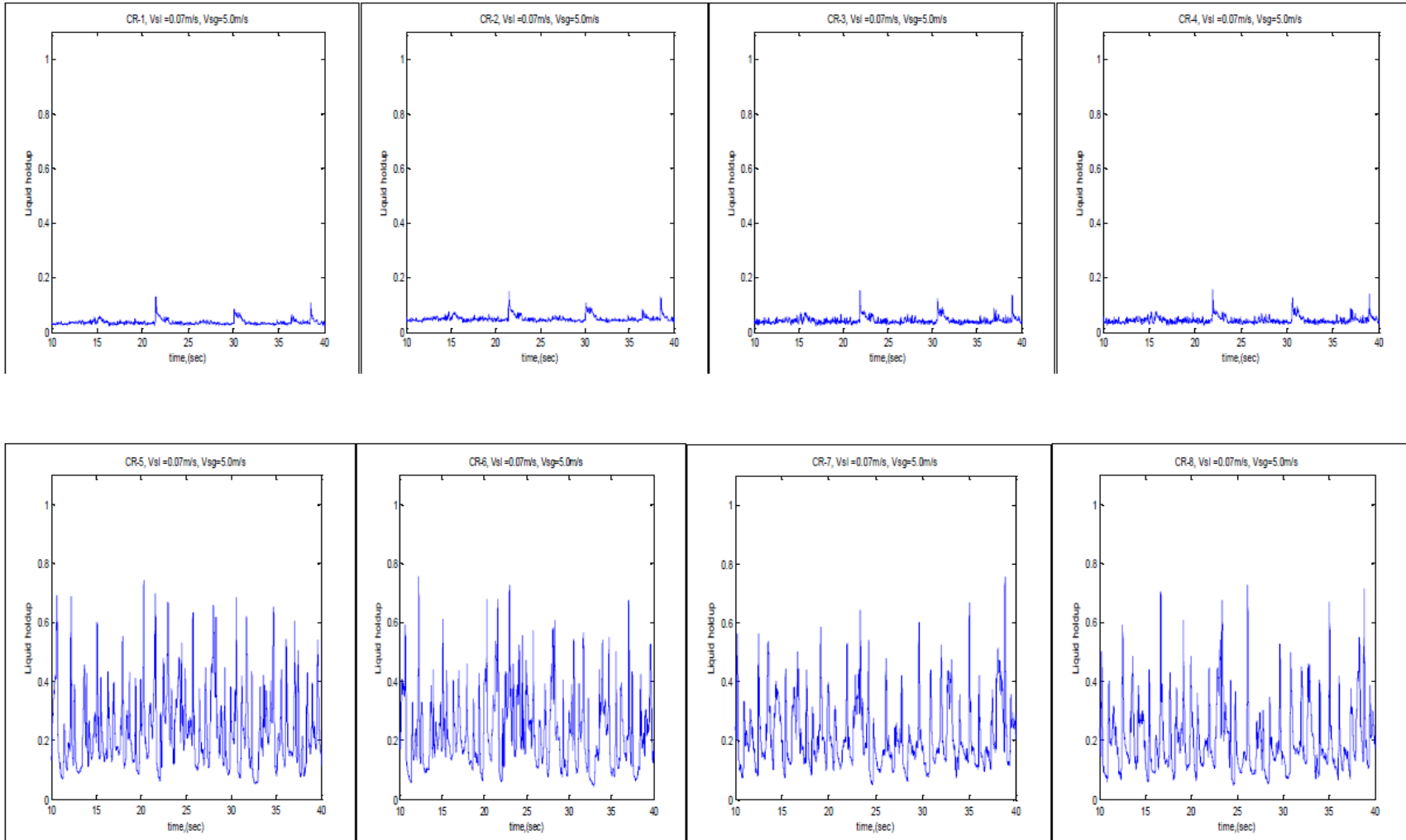
Vsg=4.0m/s

Vsl=0.07m/s, Vsg=4.0m/s



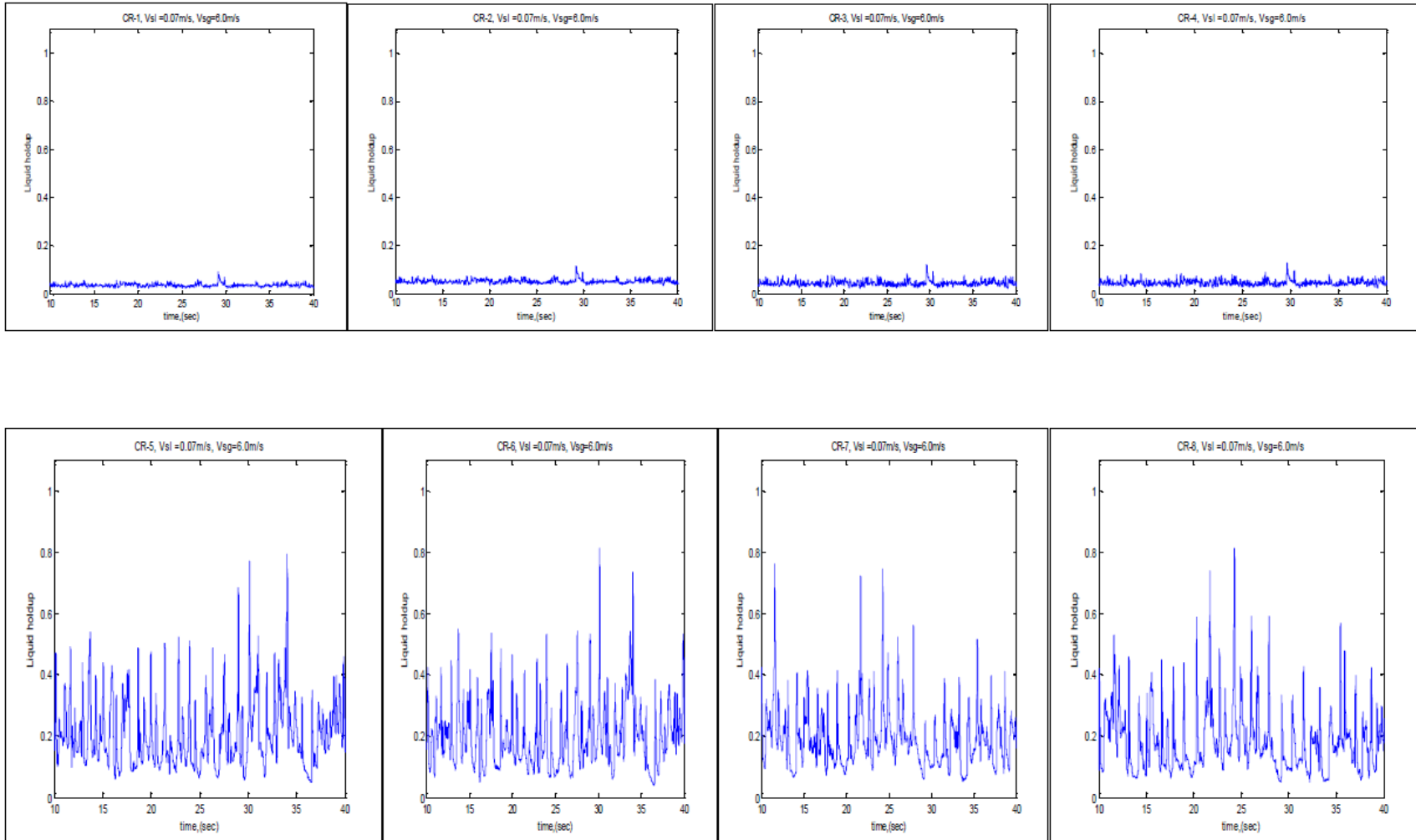
Vsg=5.0m/s

Vsl=0.07m/s, Vsg=5.0m/s



Vsg=6.0m/s

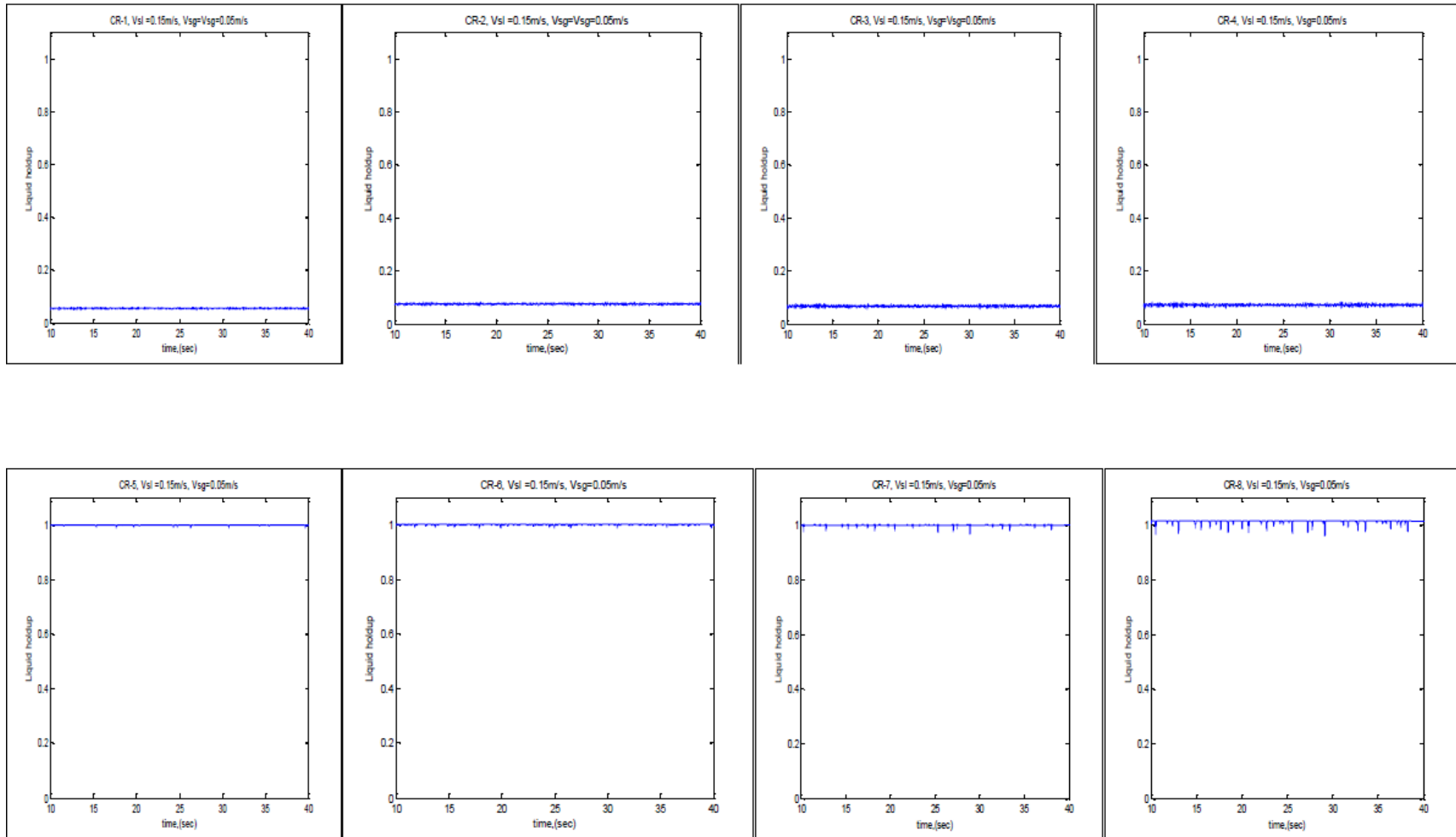
Vsl=0.07m/s, Vsg=6.0m/s





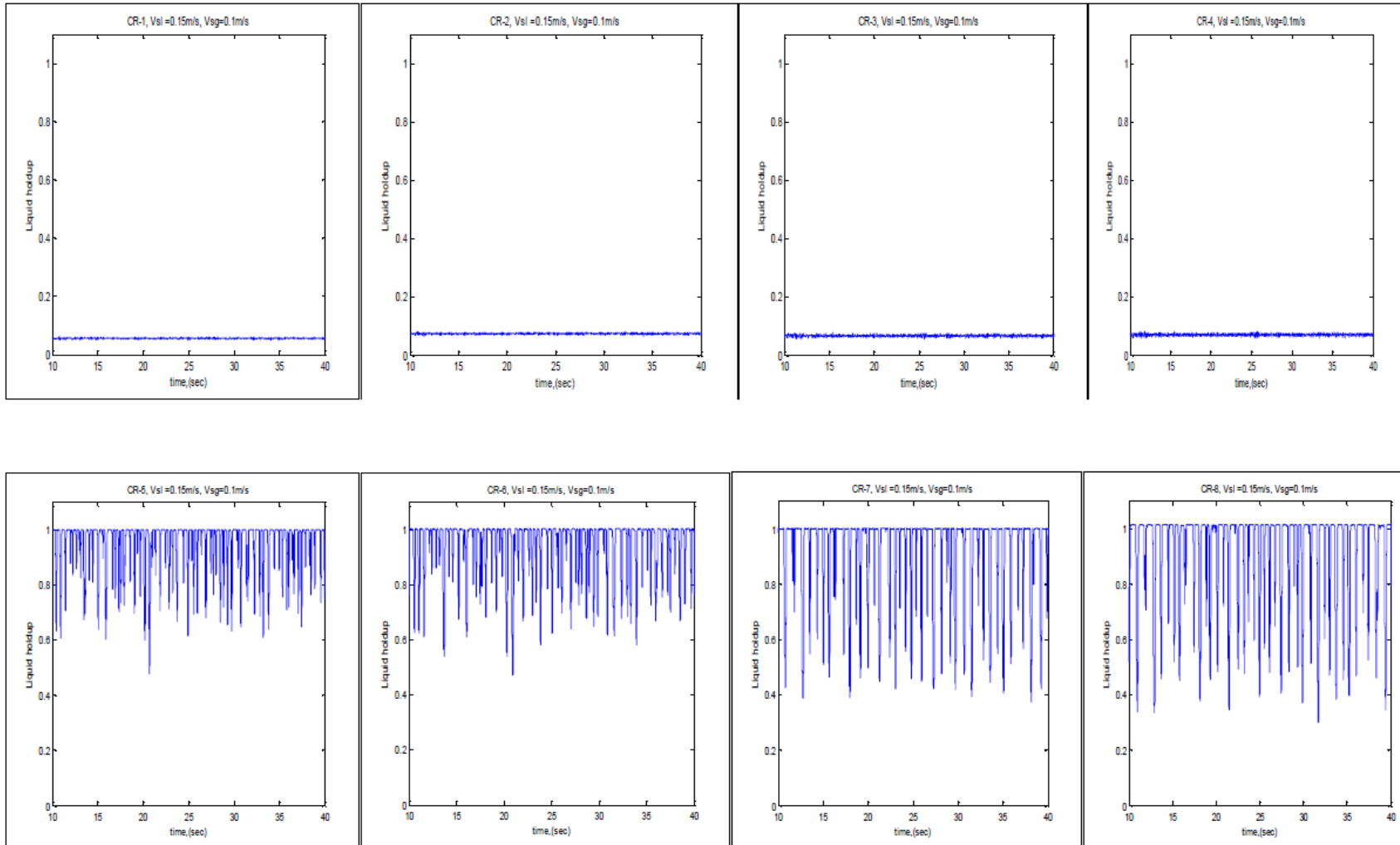
**Vsl=0.15**  
**Vsg=0.05m/s**

**Vsl=0.15m/s, Vsg=0.05m/s**



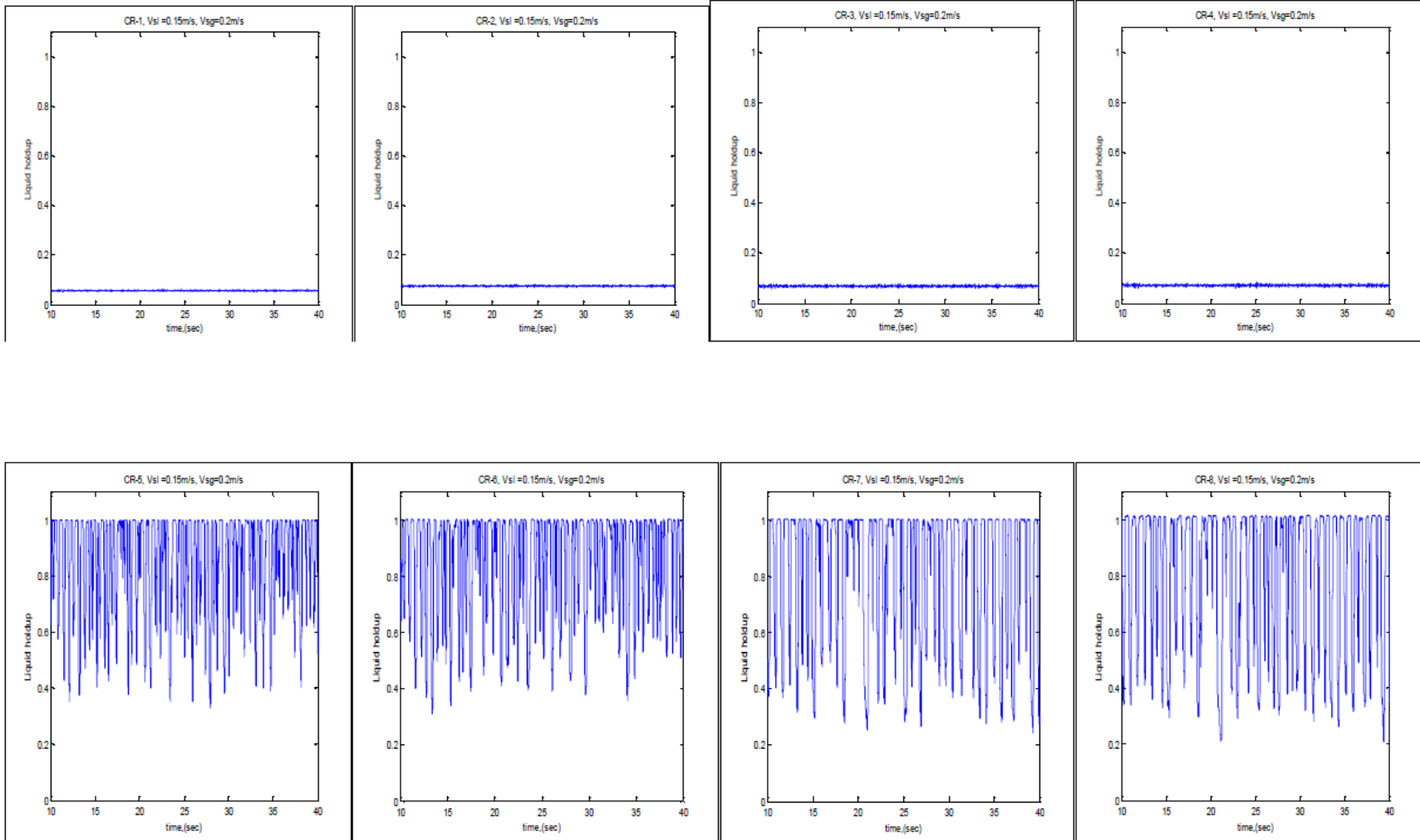
Vsg=0.1m/s

Vsl=0.15m/s, Vsg=0.1m/s



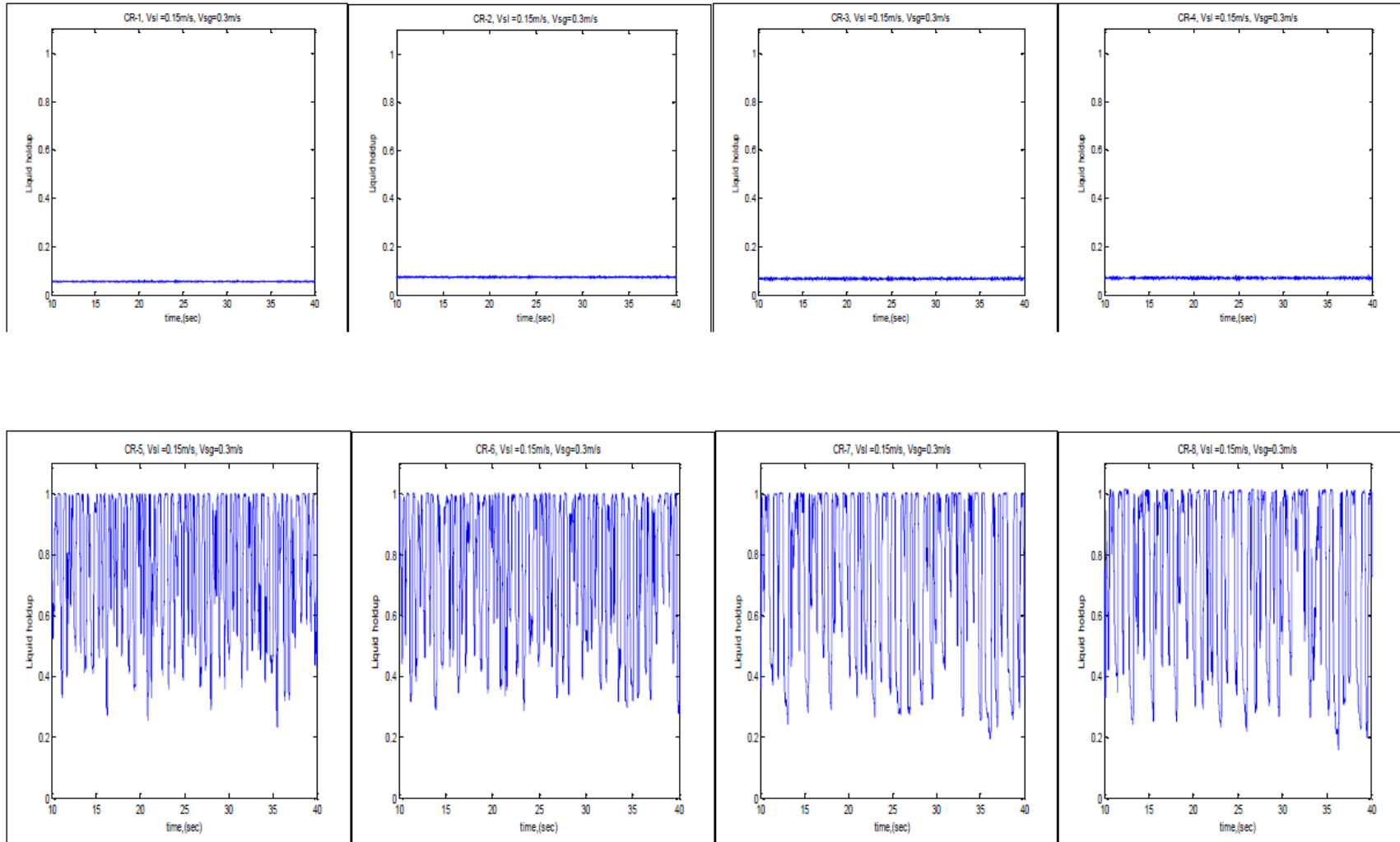
Vsg=0.2m/s

Vsl=0.15m/s, Vsg=0.2m/s



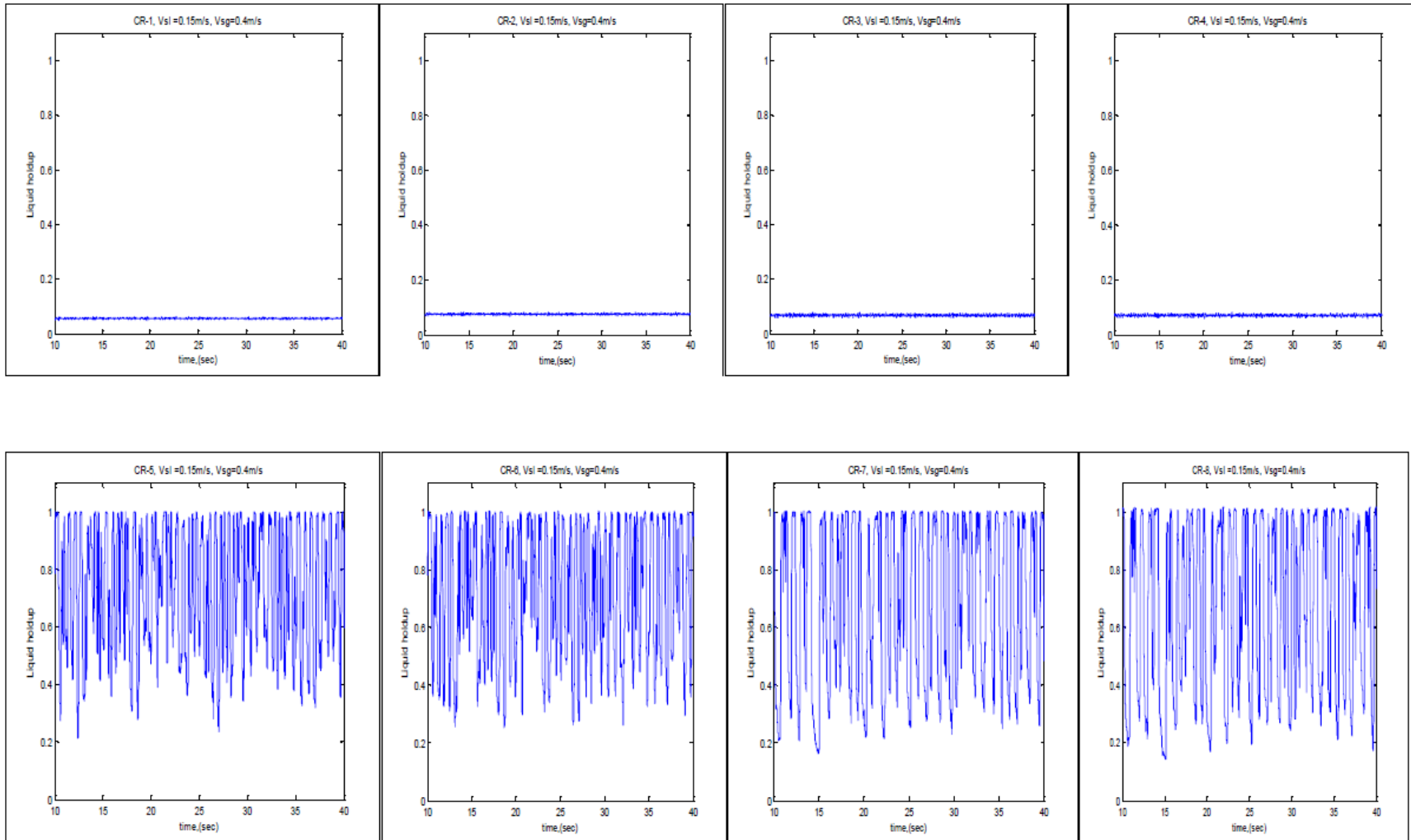
Vsg=0.3m/s

Vsl=0.15m/s, Vsg=0.3m/s



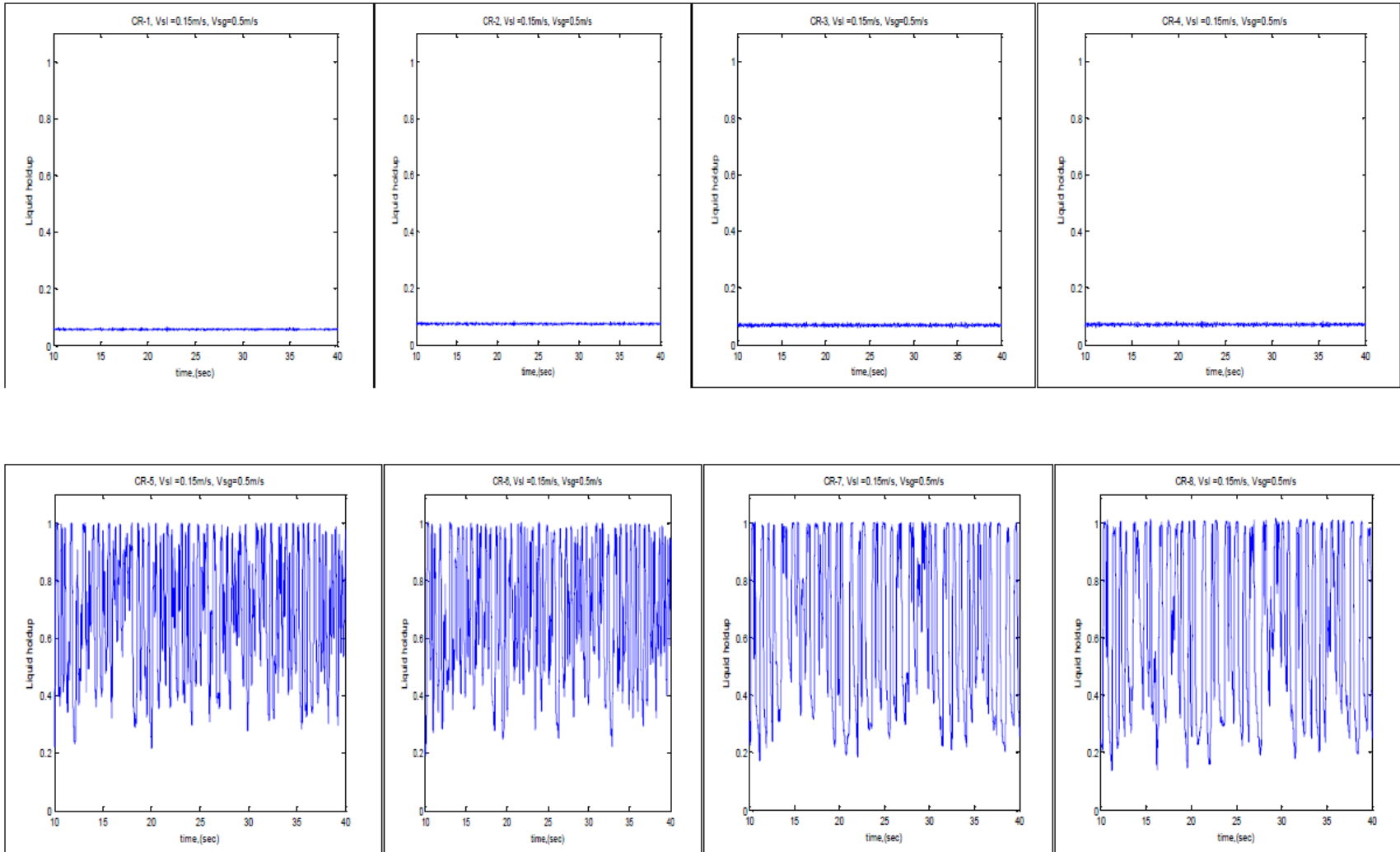
Vsg=0.4m/s

Vsl=0.15m/s, Vsg=0.4m/s



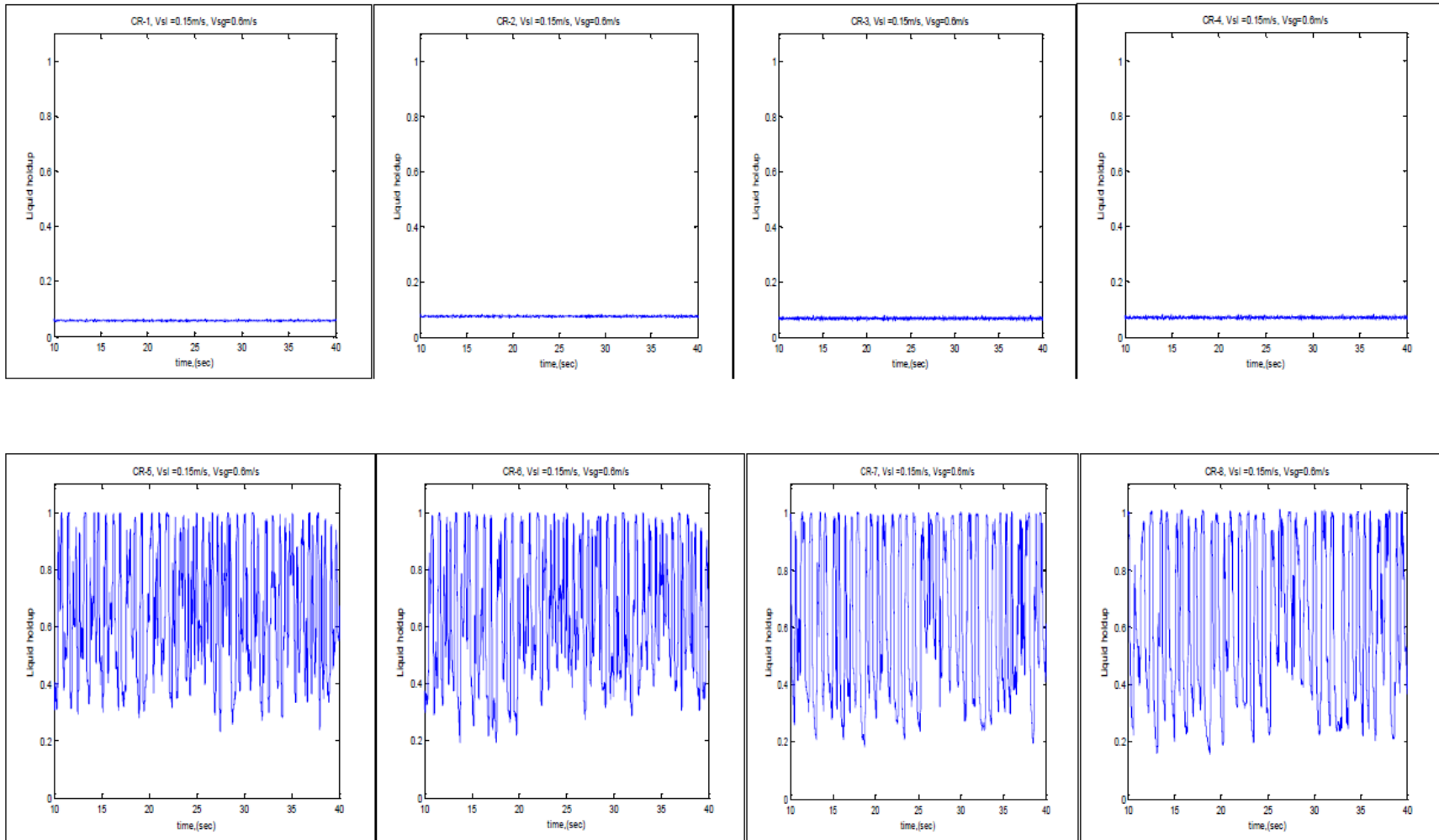
Vsg=0.5m/s

Vsl=0.15m/s, Vsg=0.5m/s



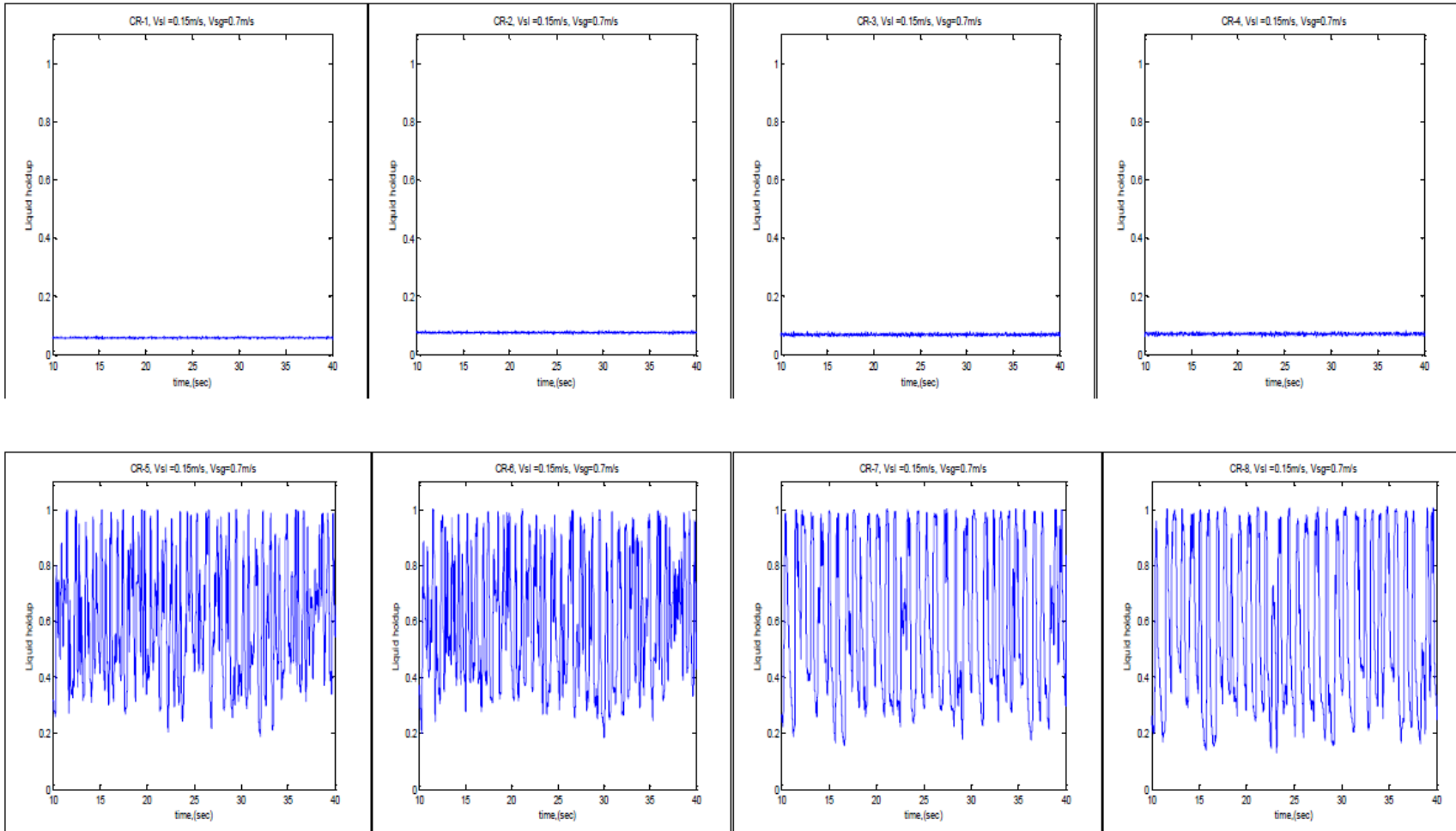
Vsg=0.6m/s

Vsl=0.15m/s, Vsg=0.6m/s



Vsg=0.7m/s

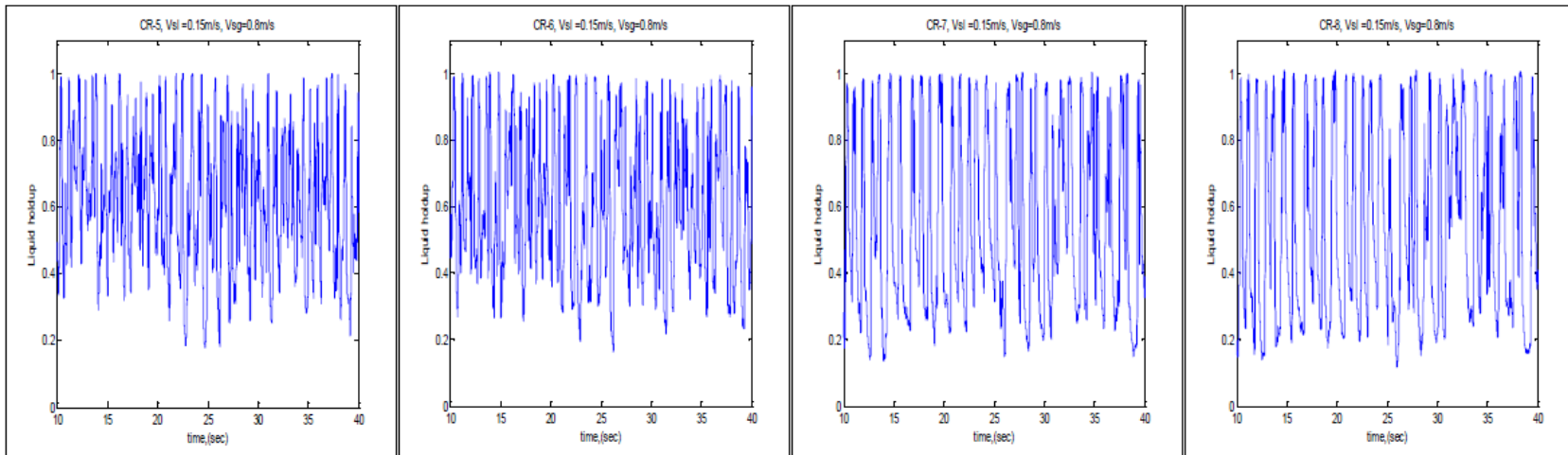
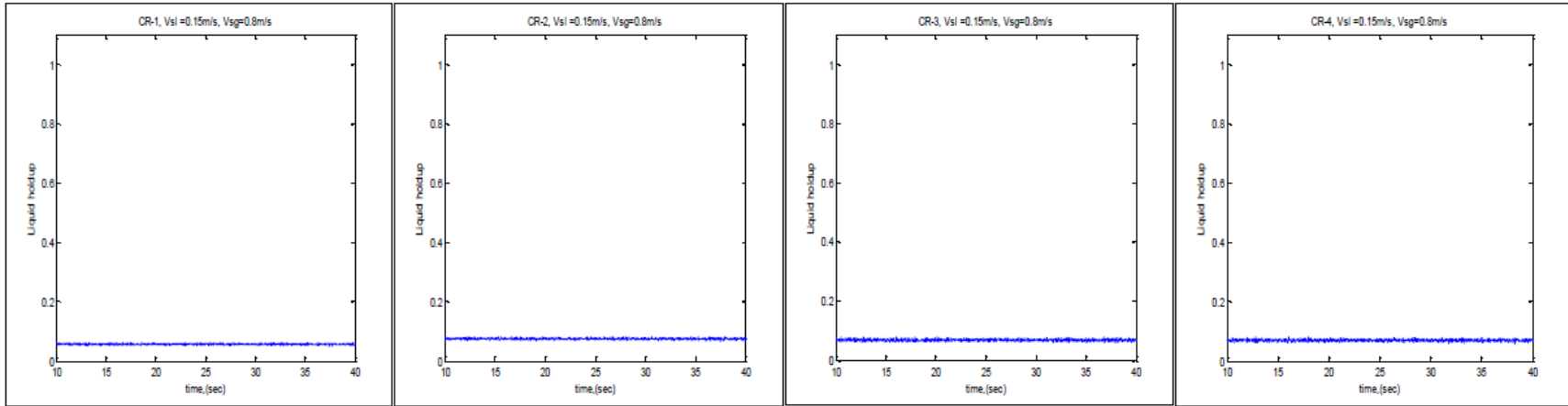
Vsl=0.15m/s, Vsg=0.7m/s





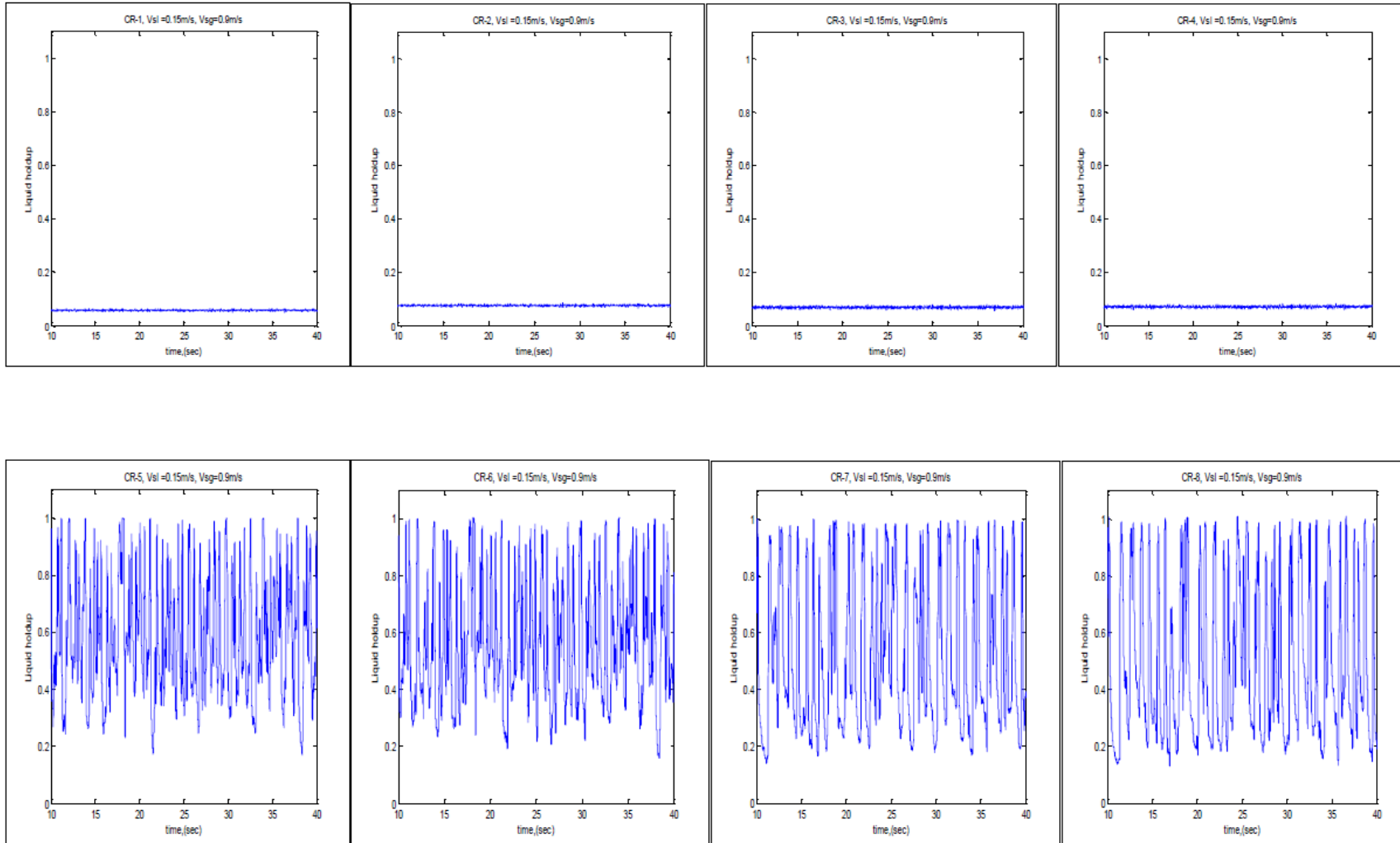
Vsg=0.8m/s

Vsl=0.15m/s, Vsg=0.8m/s



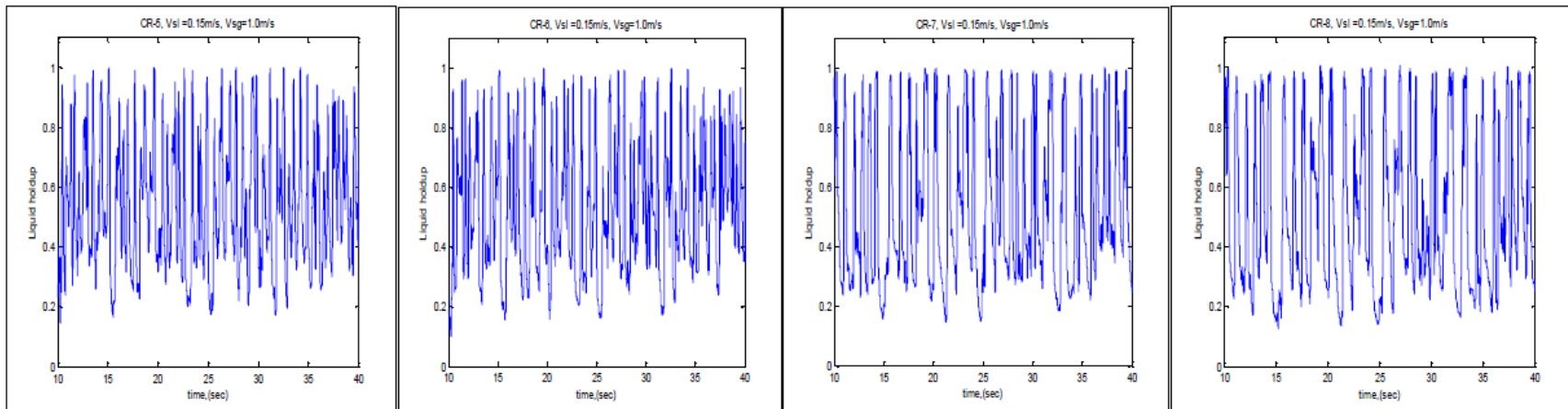
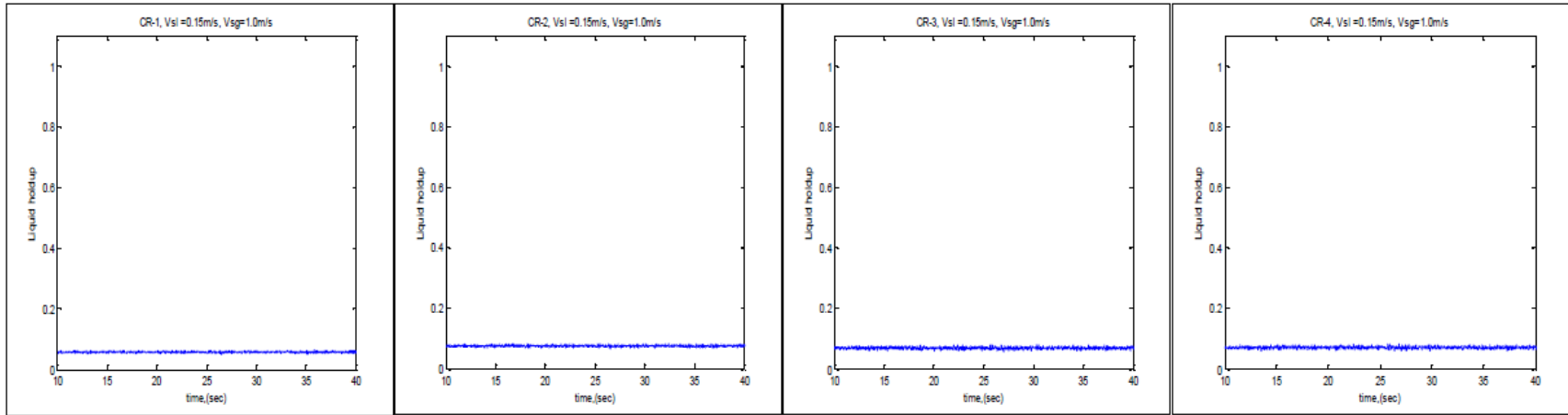
Vsg=0.9m/s

Vsl=0.15m/s, Vsg=0.9m/s



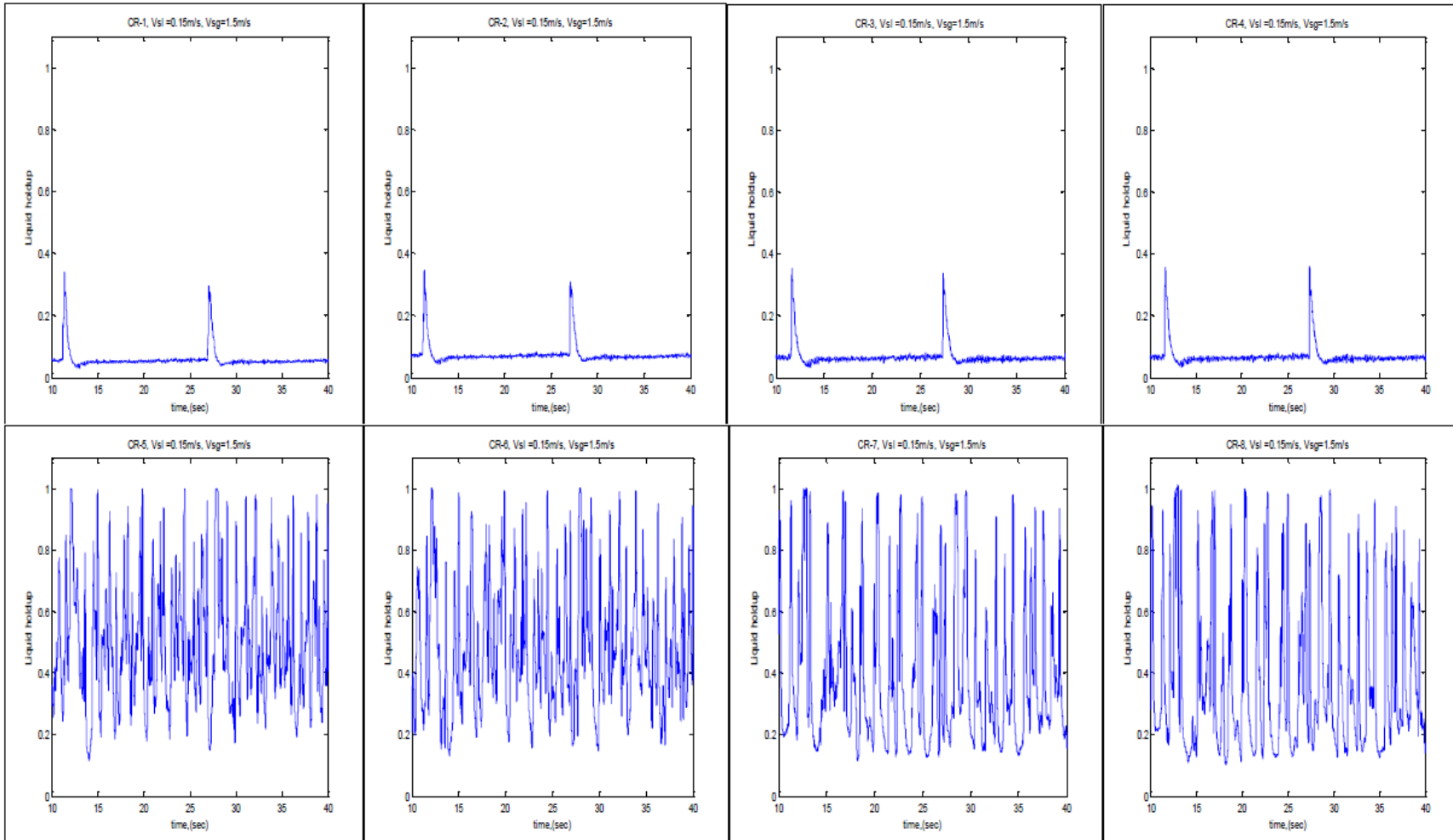
Vsg=1.0m/s

Vsl=0.15m/s, Vsg=1.0m/s



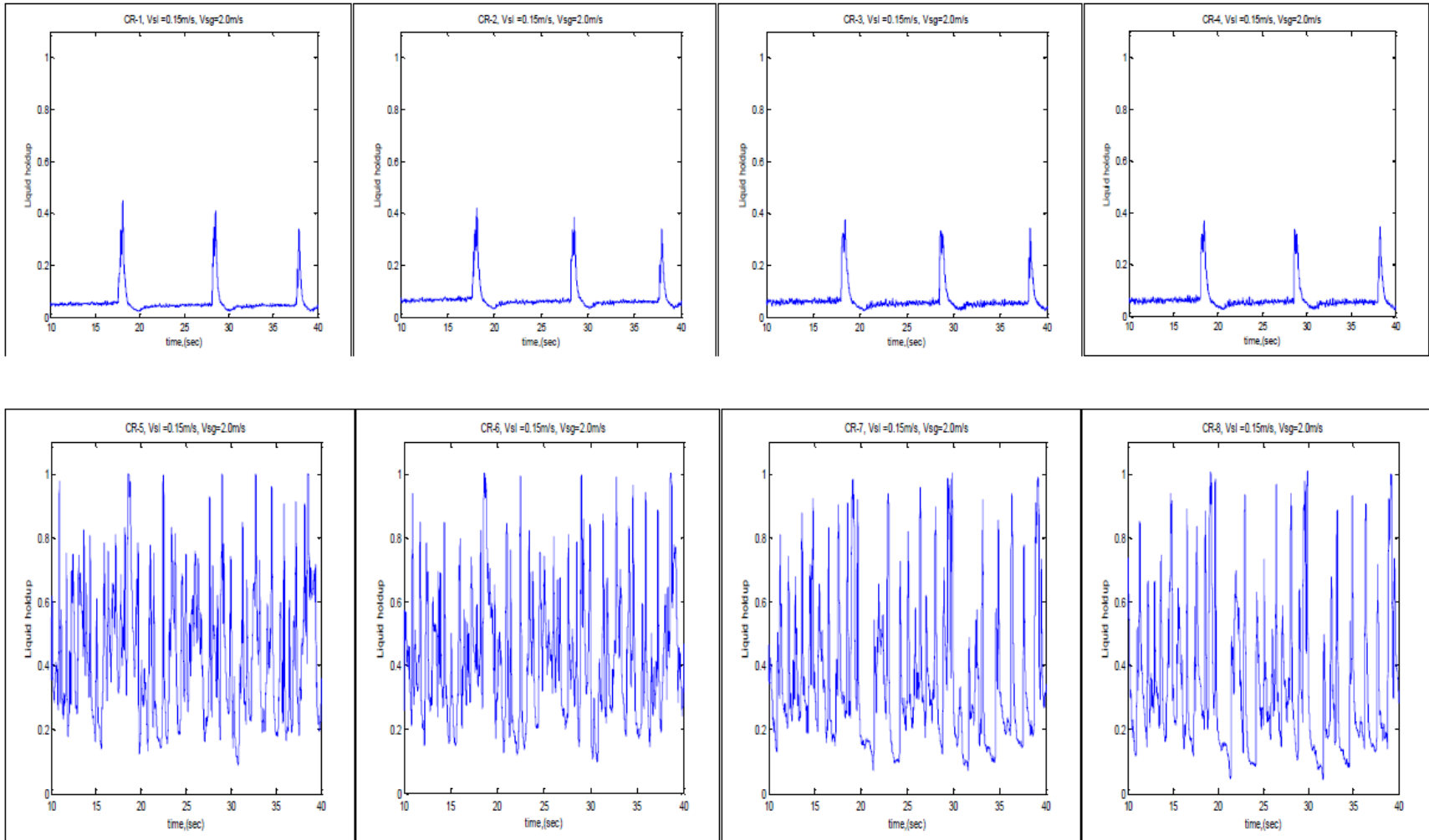
Vsg=1.5m/s

Vsl=0.15m/s, Vsg=1.5m/s



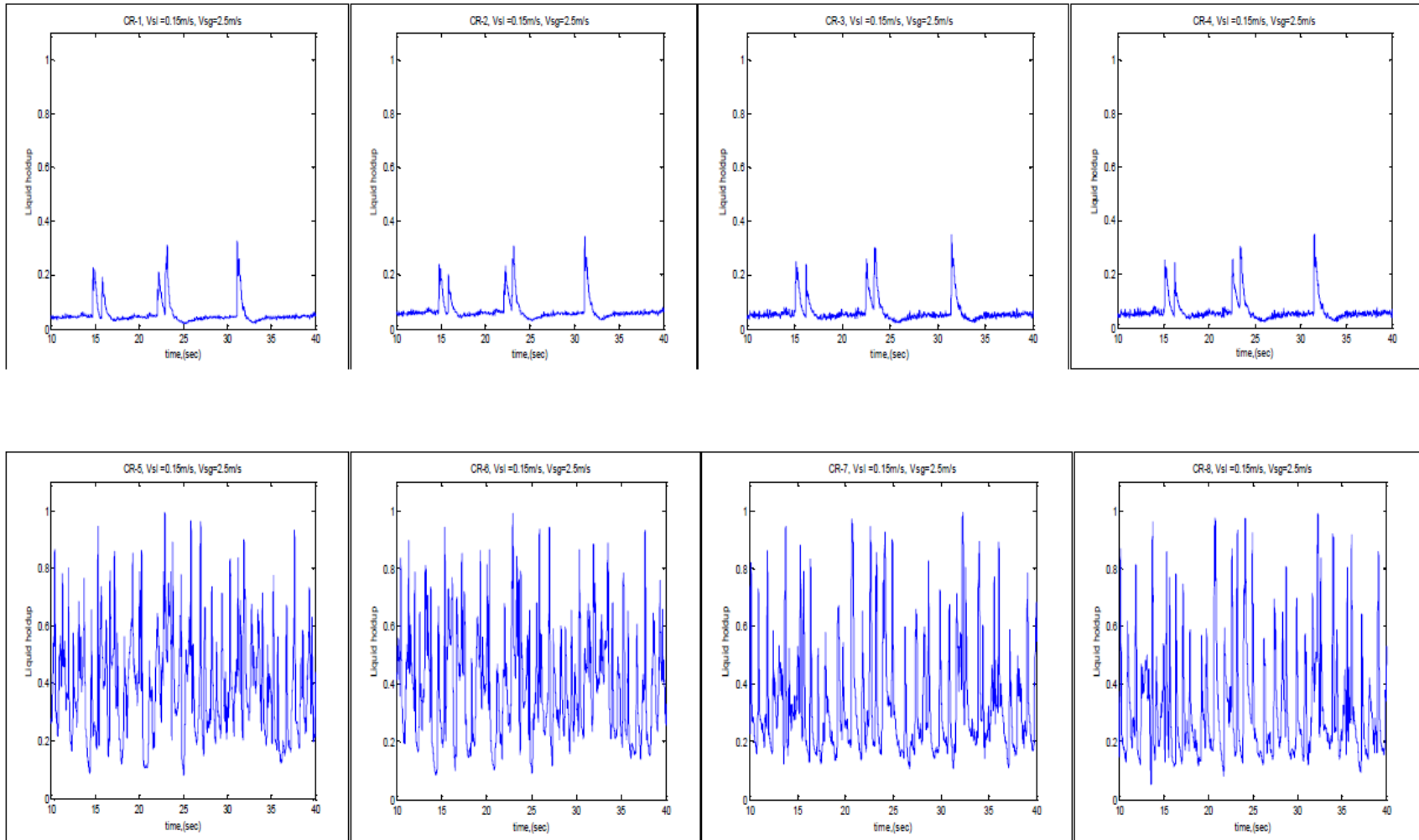
Vsg=2.0m/s

Vsl=0.15m/s, Vsg=2.0m/s



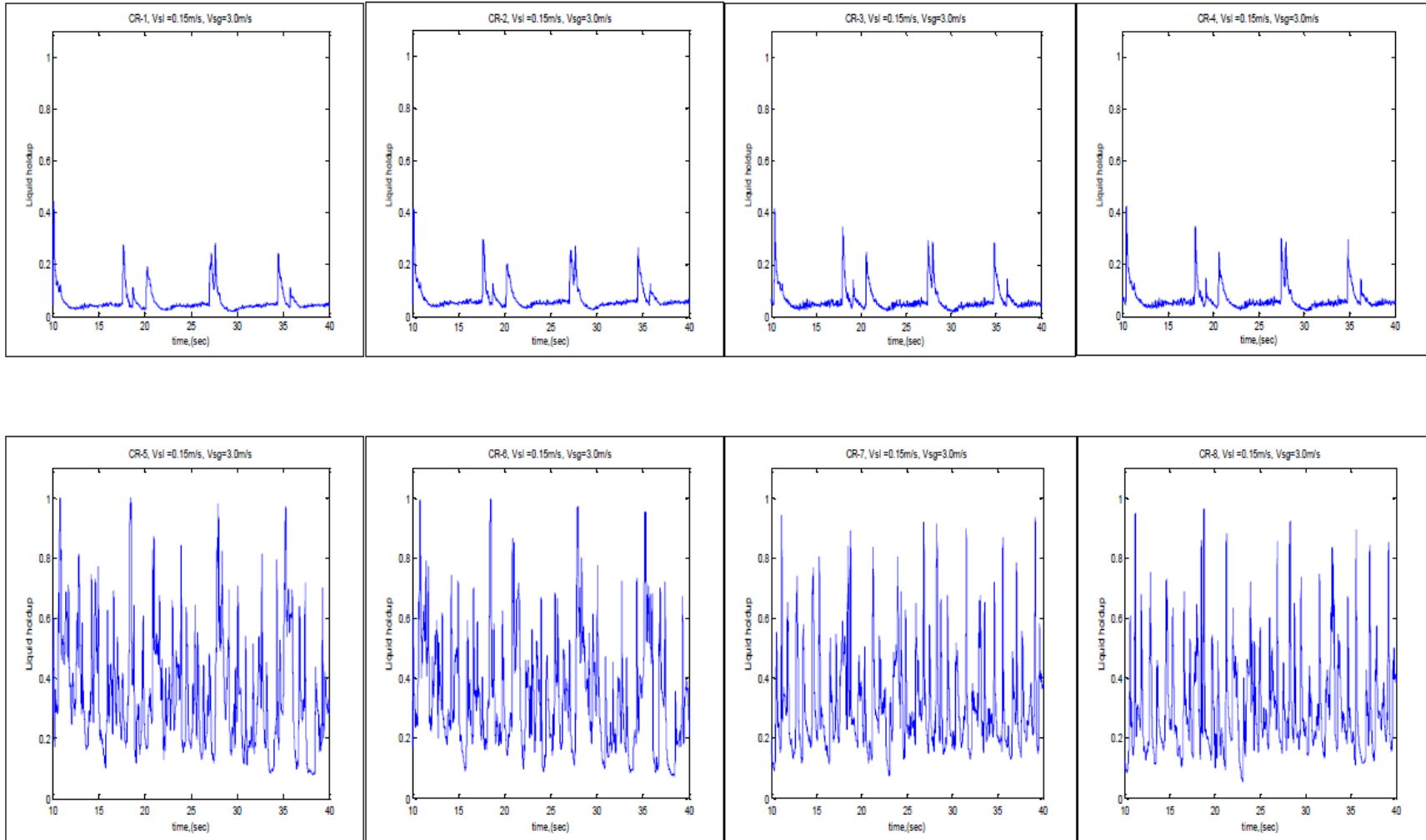
Vsg=2.5m/s

Vsl=0.15m/s, Vsg=2.5m/s



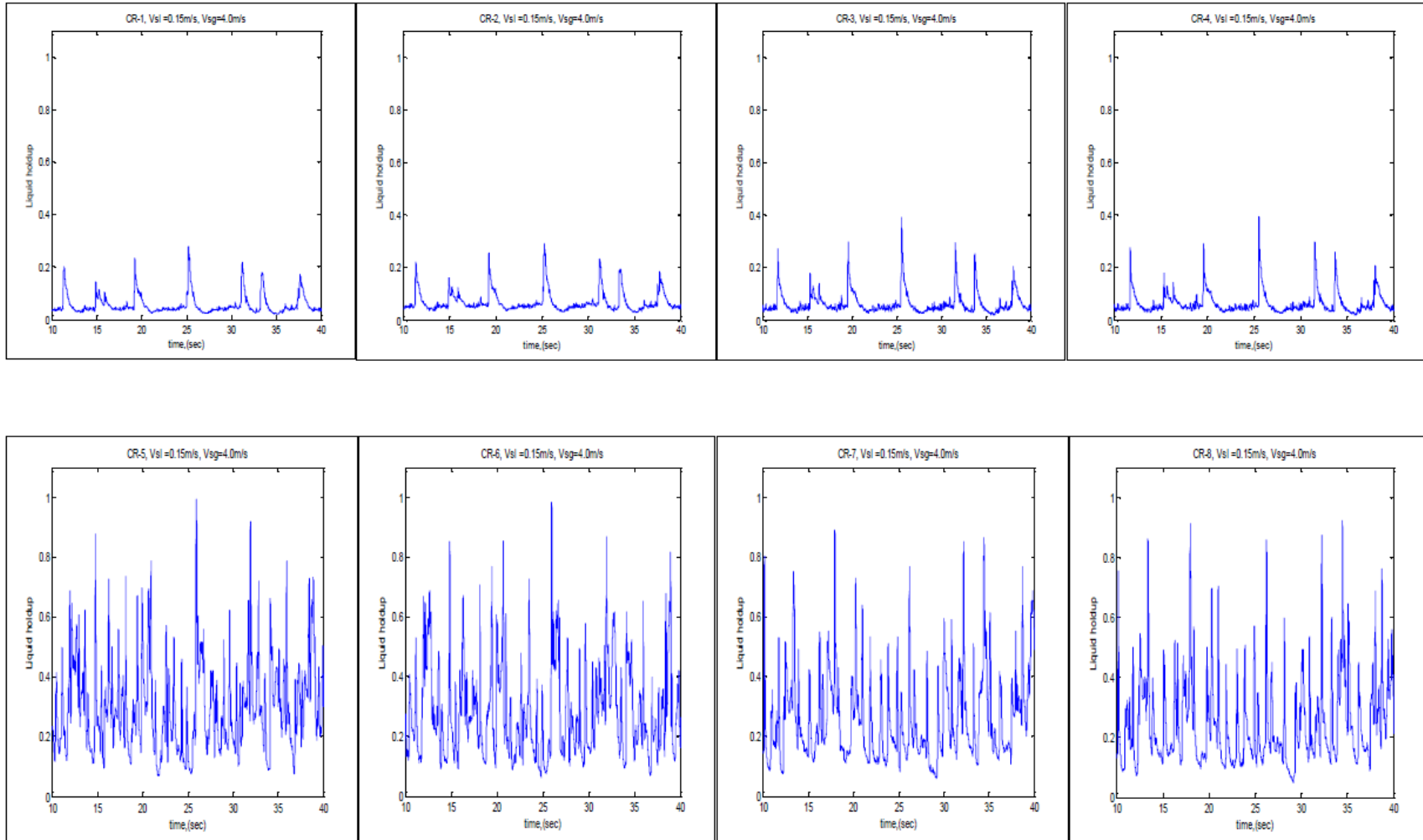
Vsg=3.0m/s

Vsl=0.15m/s, Vsg=3.0m/s



Vsg=4.0m/s

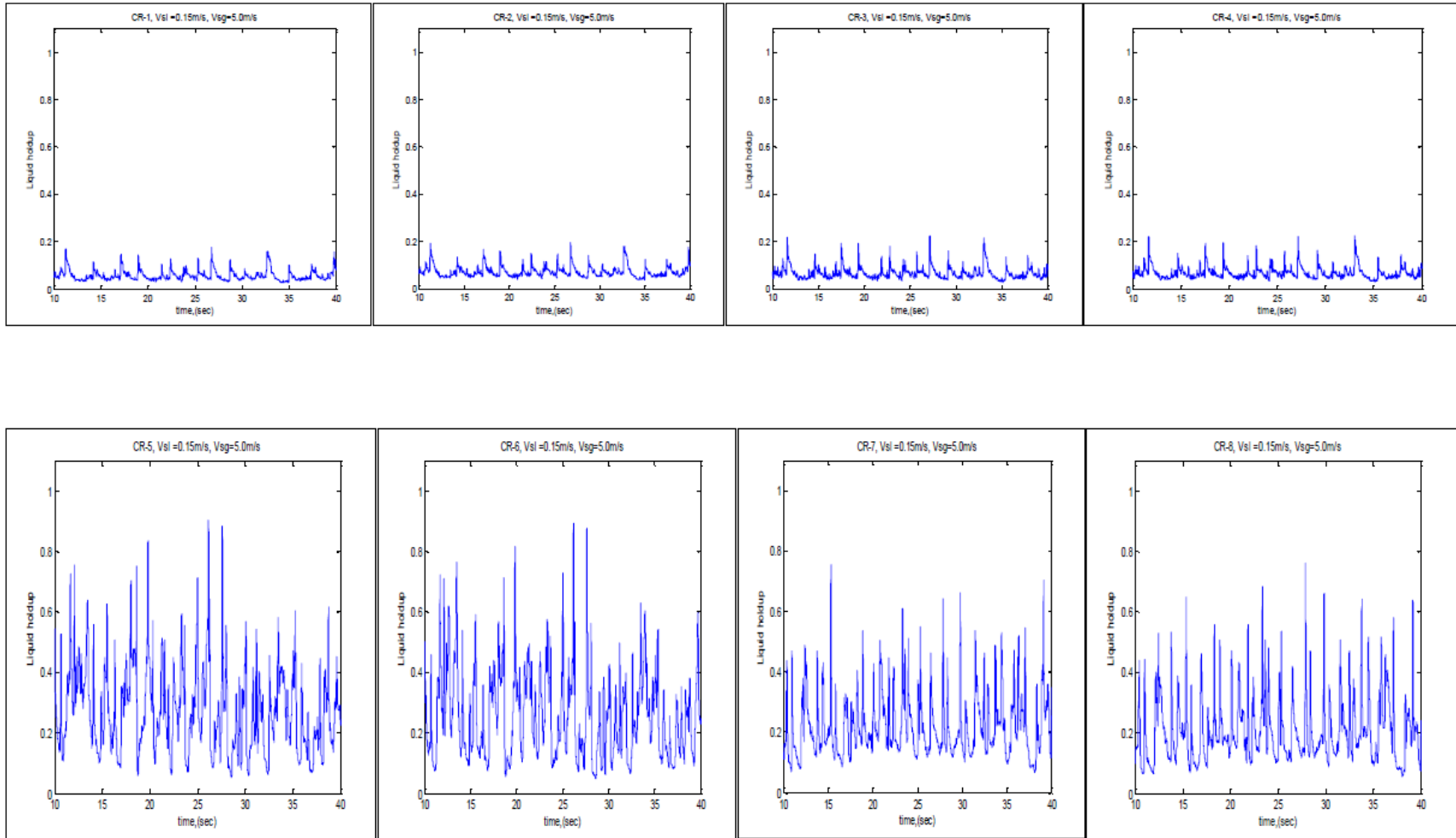
Vsl=0.15m/s, Vsg=4.0m/s





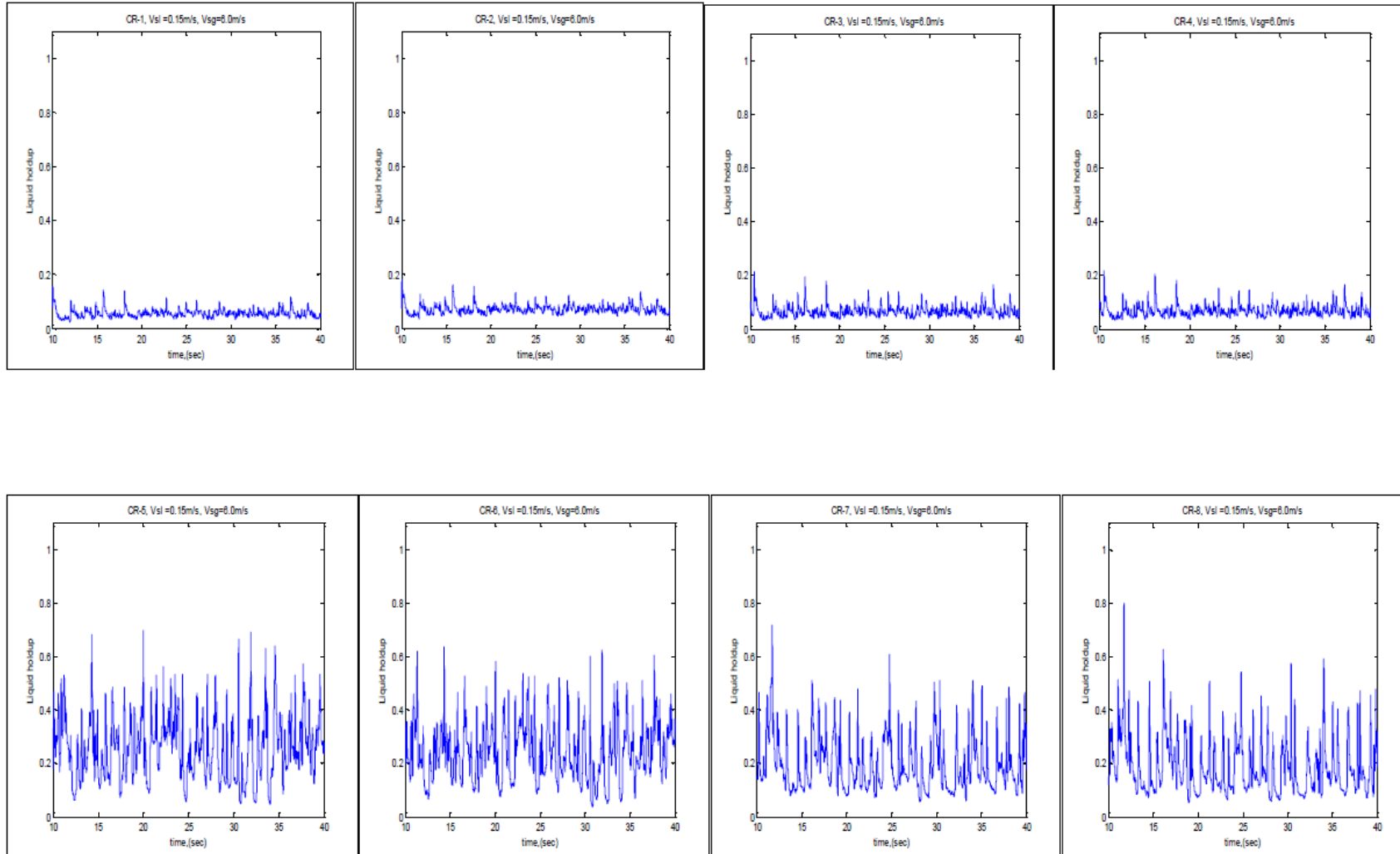
Vsg=5.0m/s

Vsl=0.15m/s, Vsg=5.0m/s



Vsg=6.0m/s

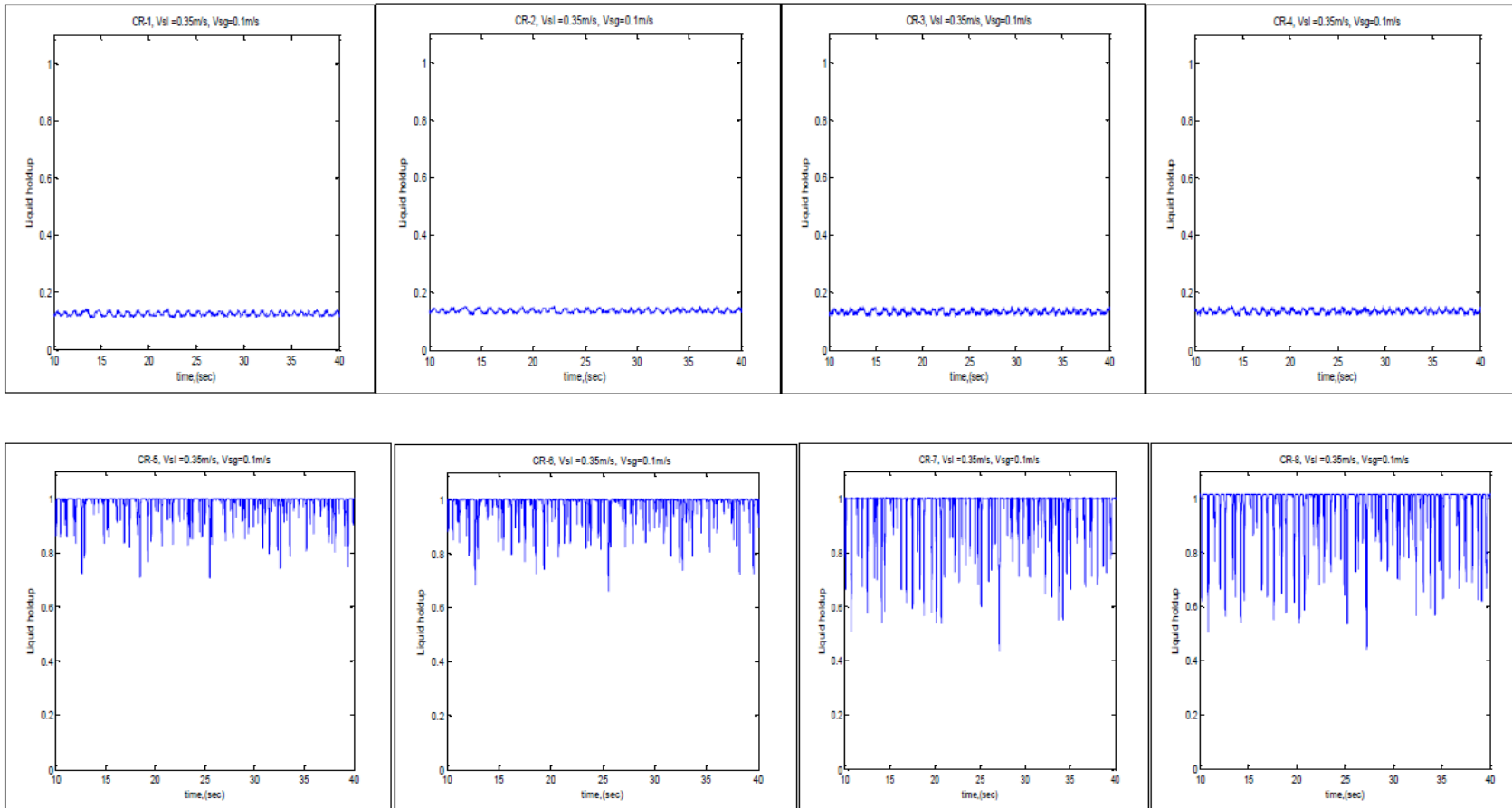
Vsl=0.15m/s, Vsg=6.0m/s



**Vsl= 0.35m/s**

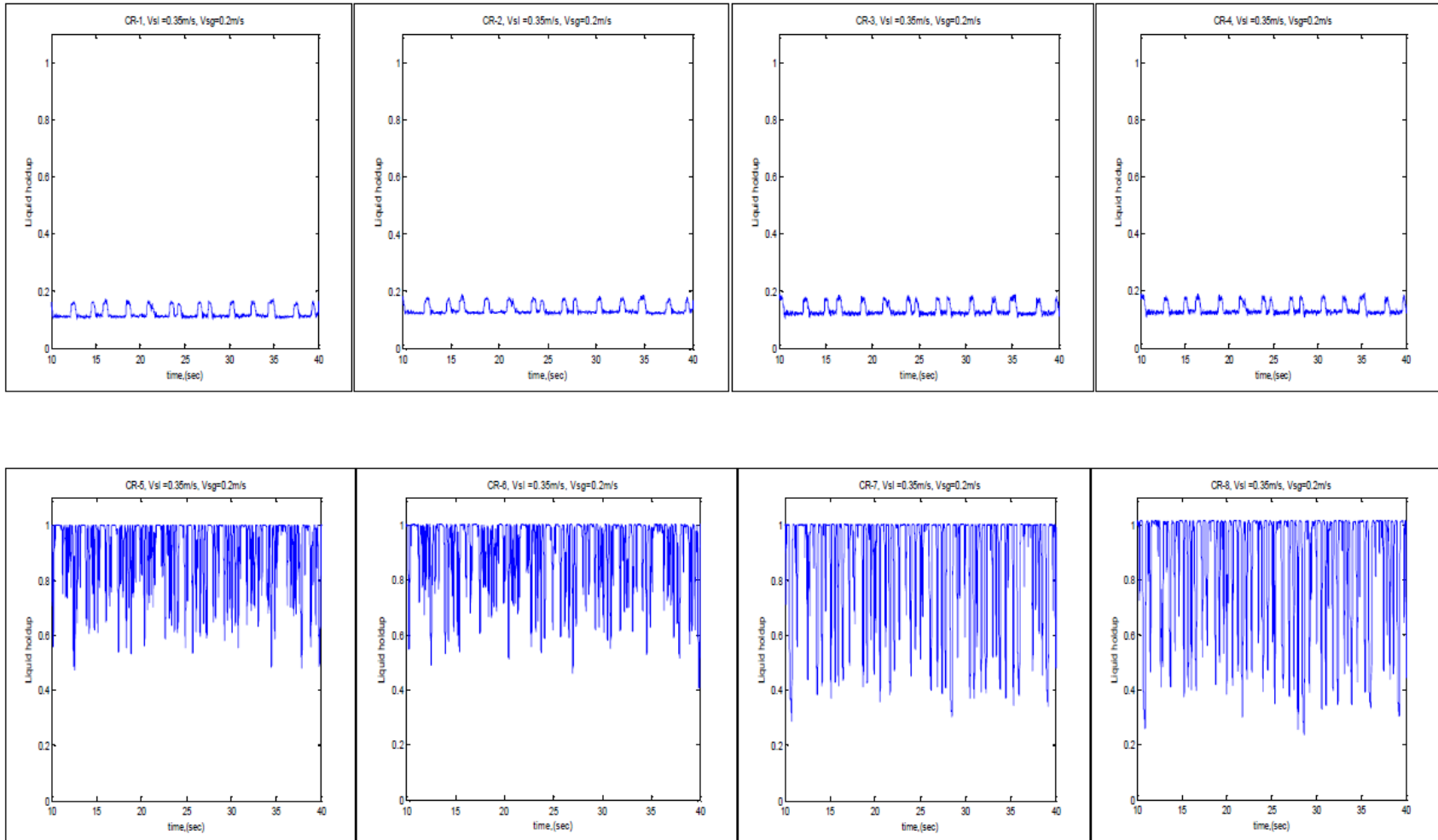
Vsg=0.1m/s

**Vsl=0.35m/s, Vsg=0.1m/s**



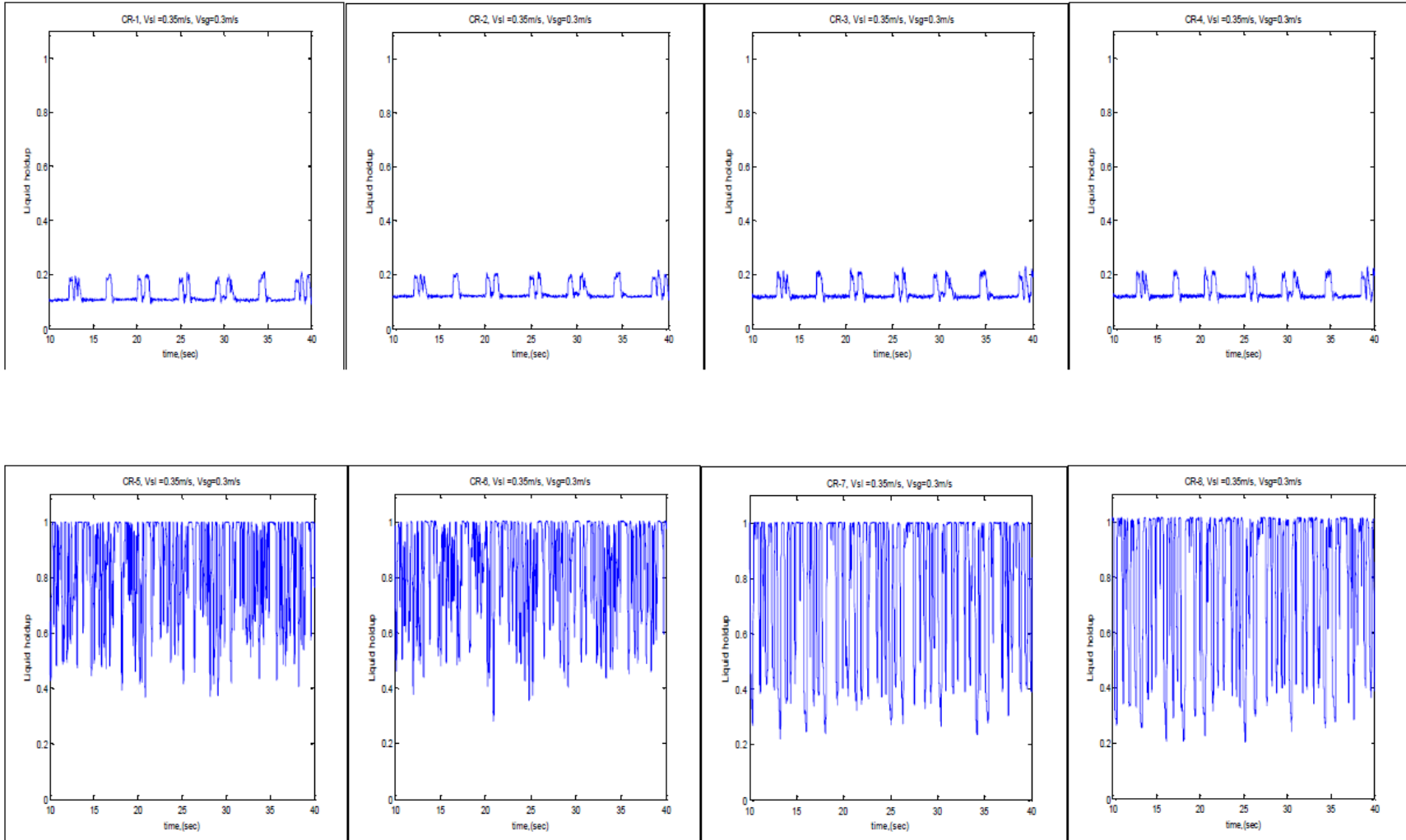
Vsg=0.2m/s

Vsl=0.35m/s, Vsg=0.2m/s



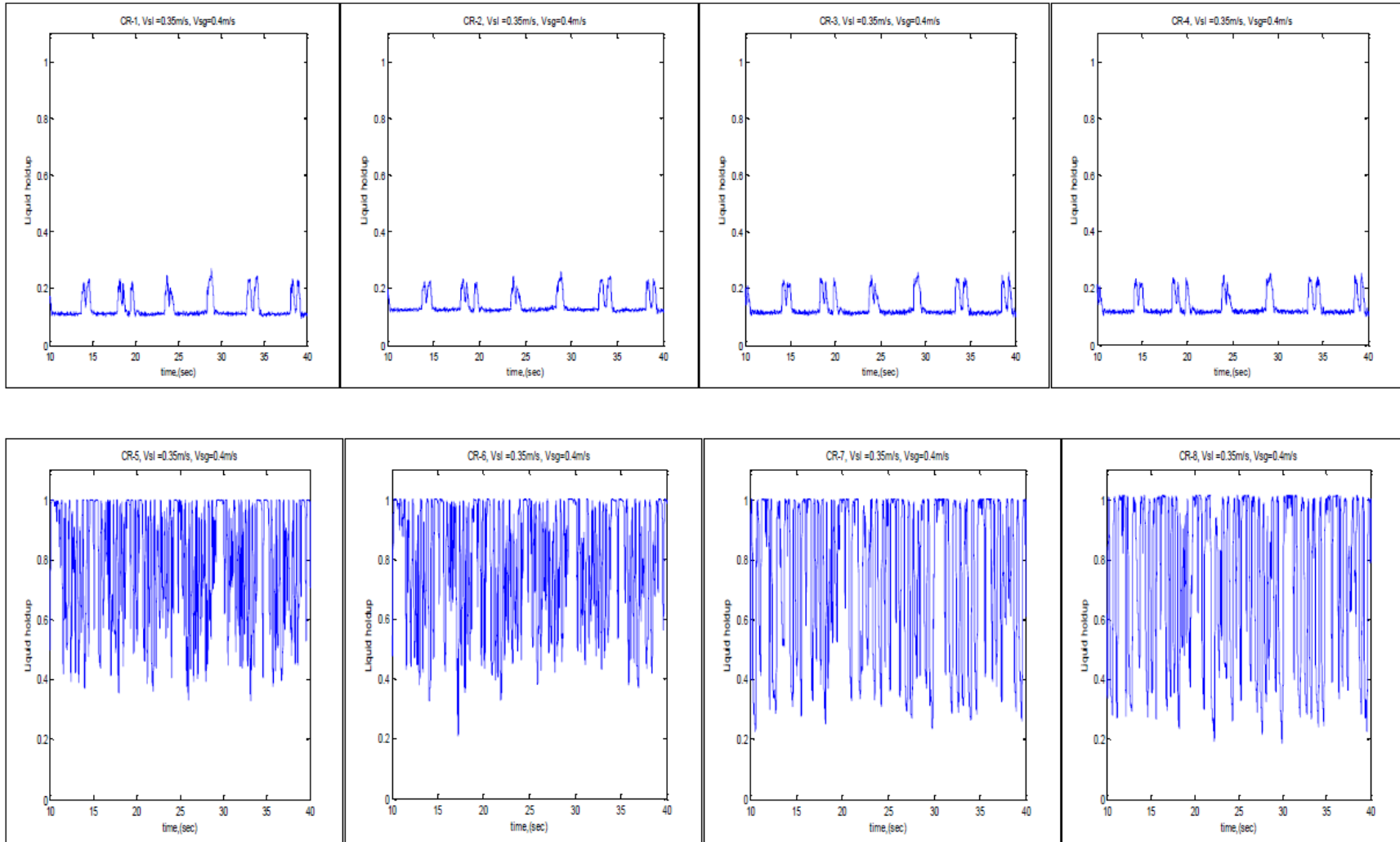
Vsg=0.3m/s

Vsl=0.35m/s, Vsg=0.3m/s



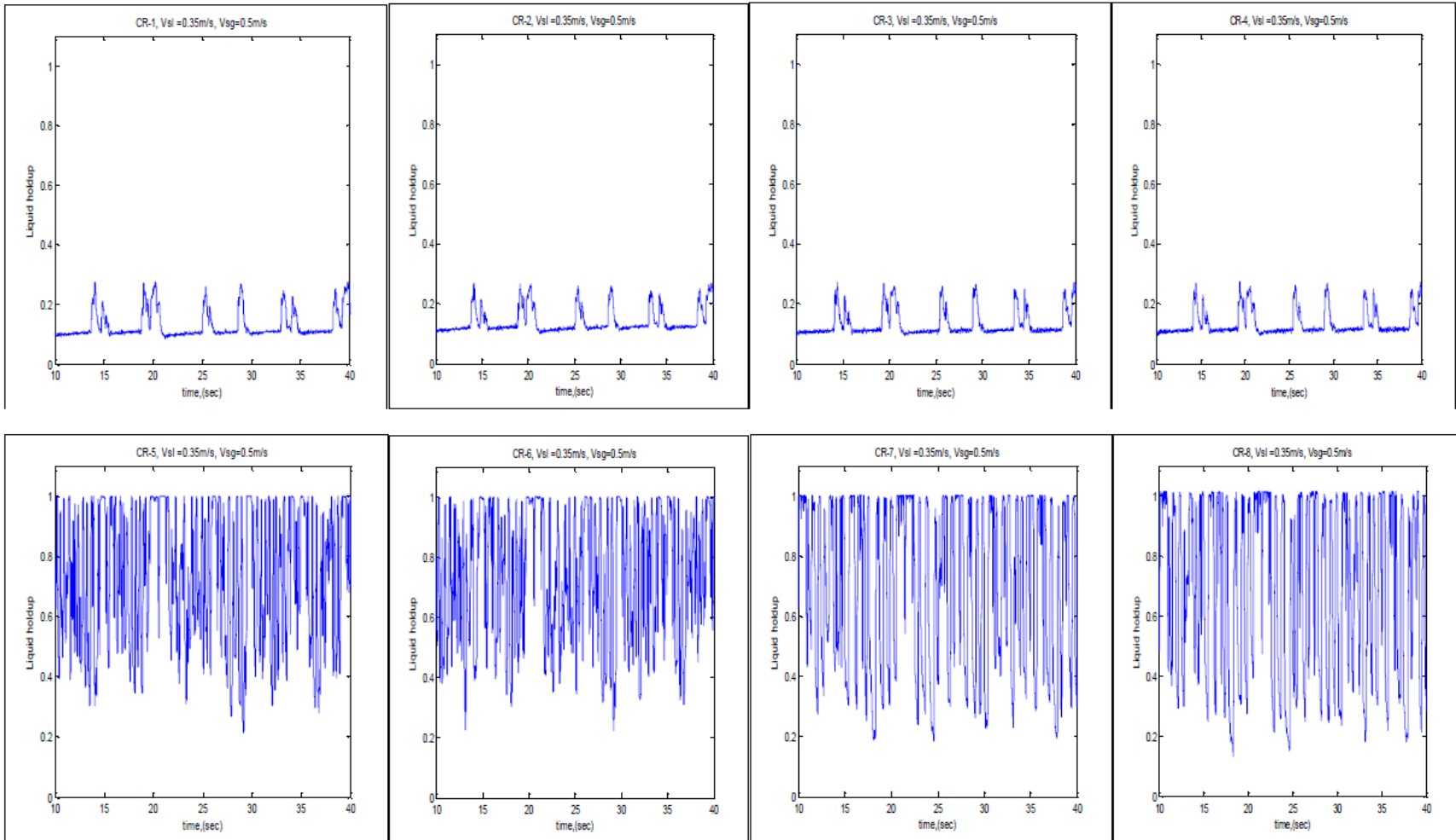
Vsg=0.4m/s

Vsl=0.35m/s, Vsg=0.4m/s



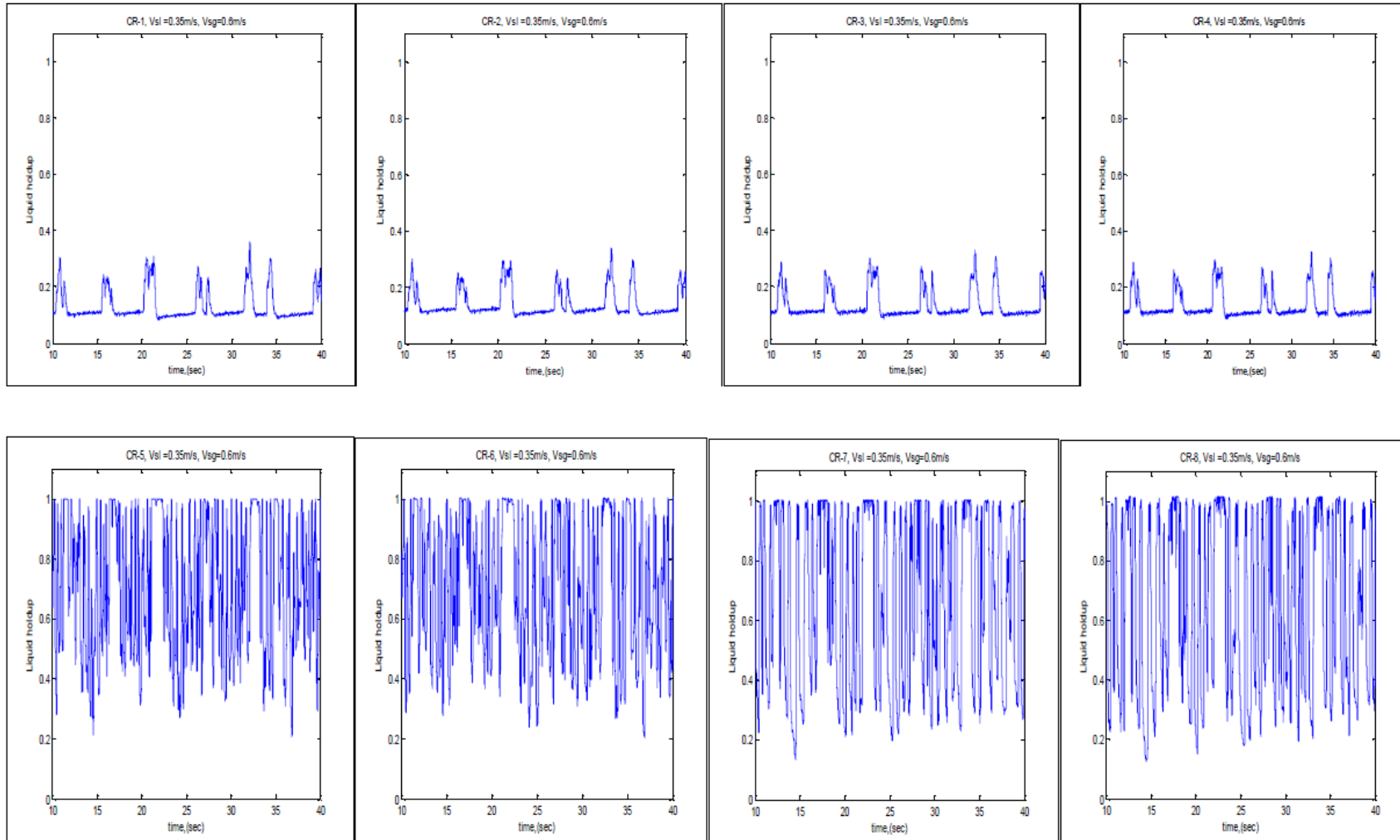
Vsg=0.5m/s

Vsl=0.35m/s, Vsg=0.5m/s



Vsg=0.6m/s

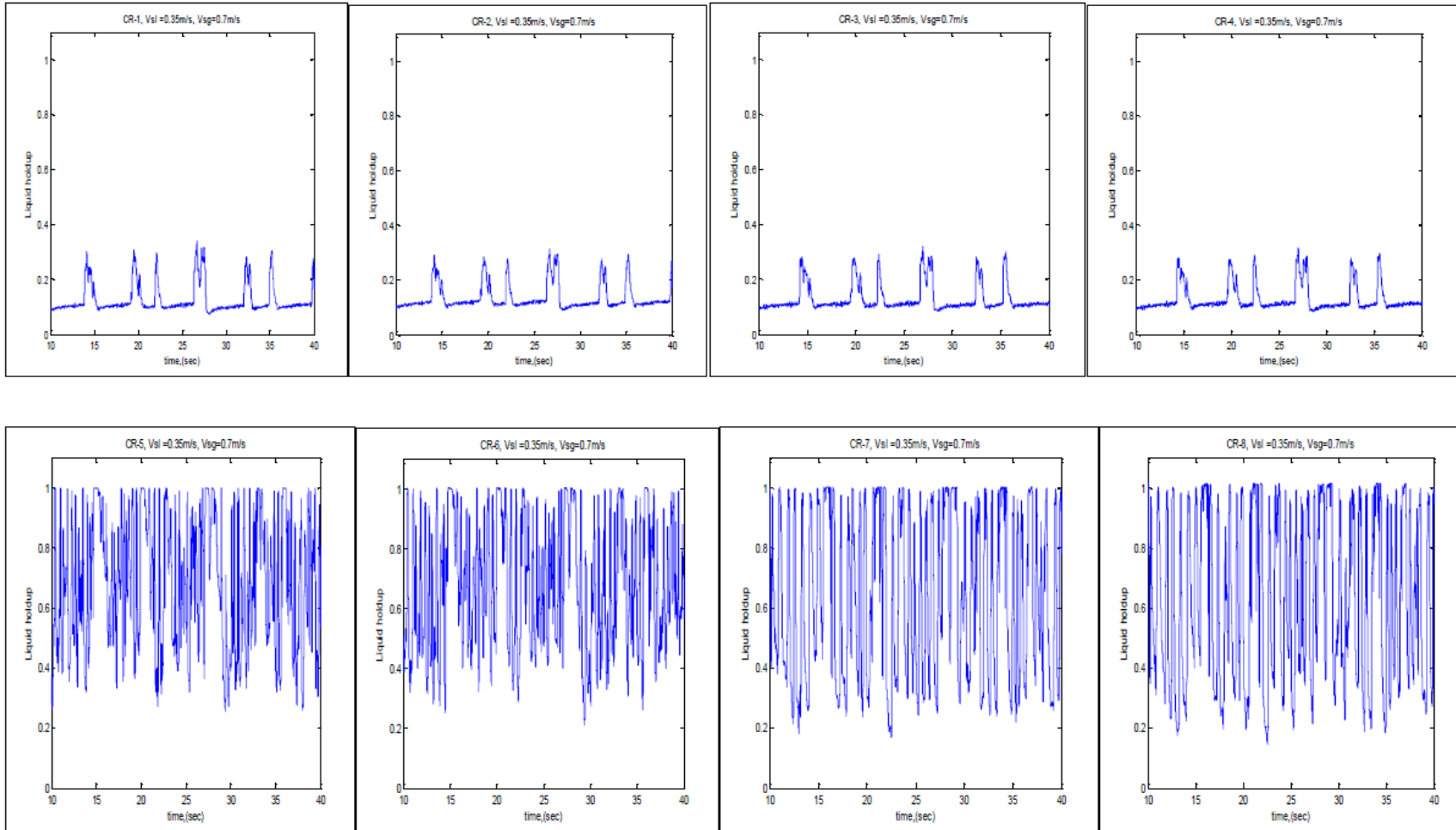
Vsl=0.35m/s, Vsg=0.6m/s





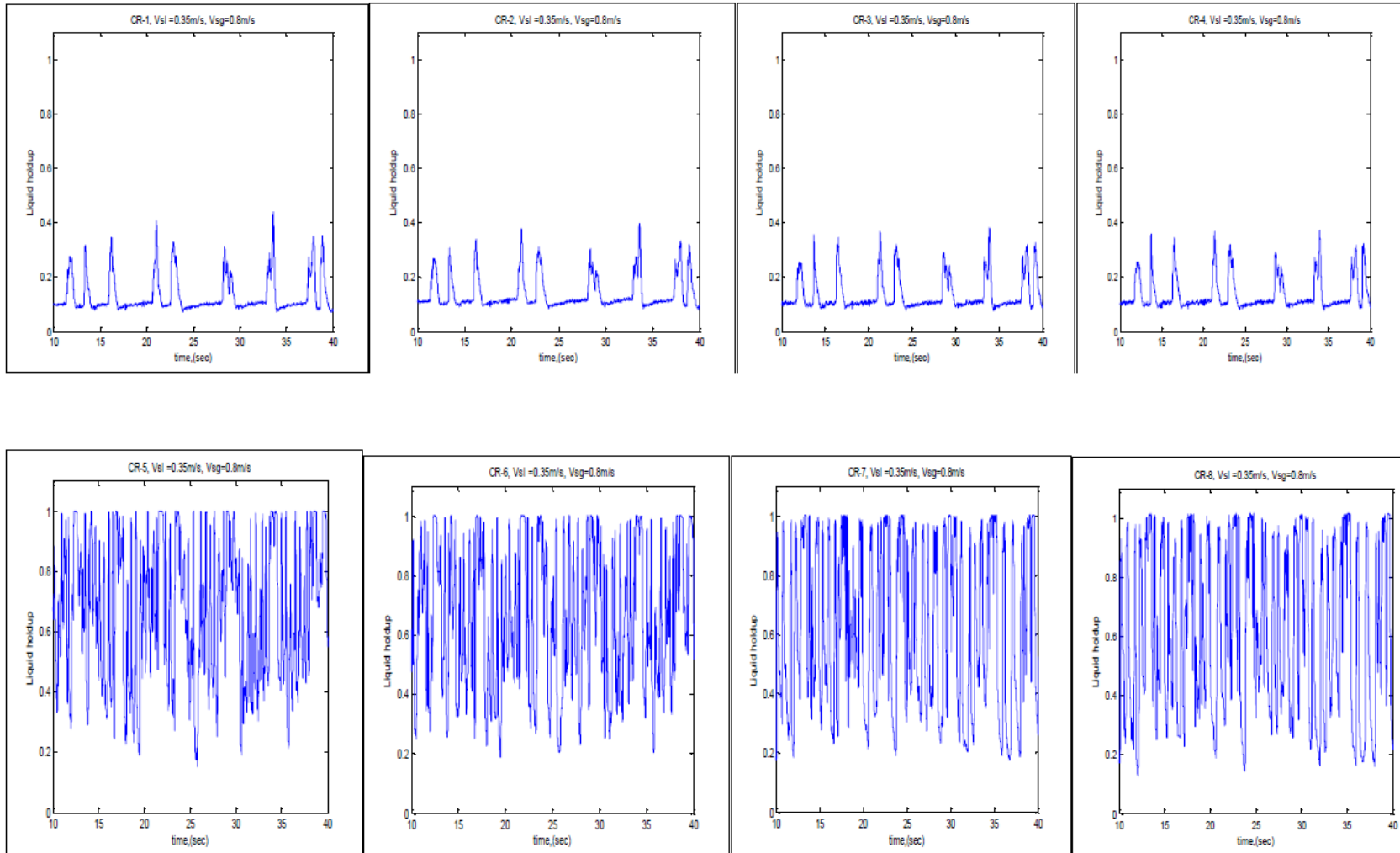
Vsg=0.7m/s

Vsl=0.35m/s, Vsg=0.7m/s



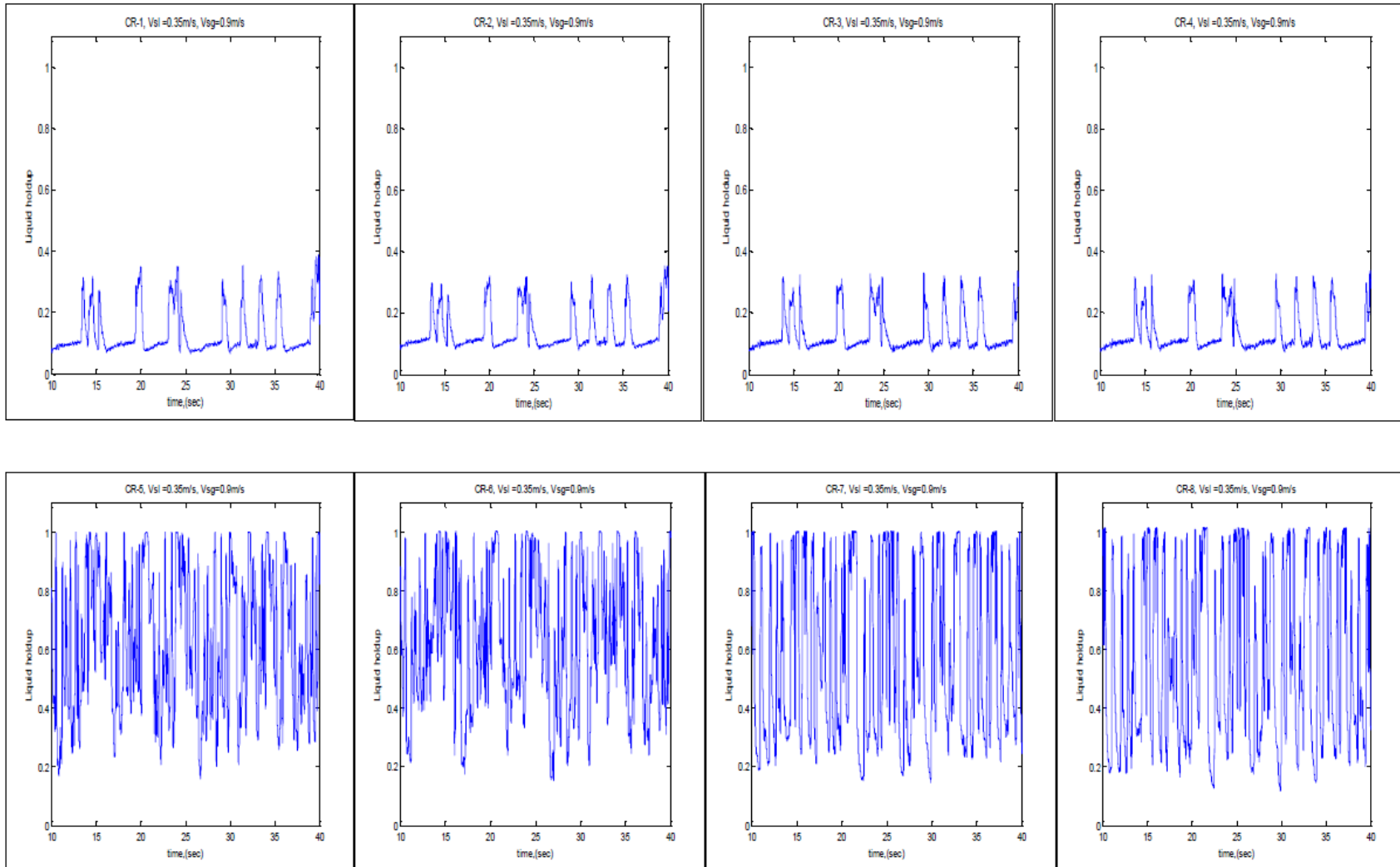
Vsg=0.8m/s

Vsl=0.35m/s, Vsg=0.8m/s



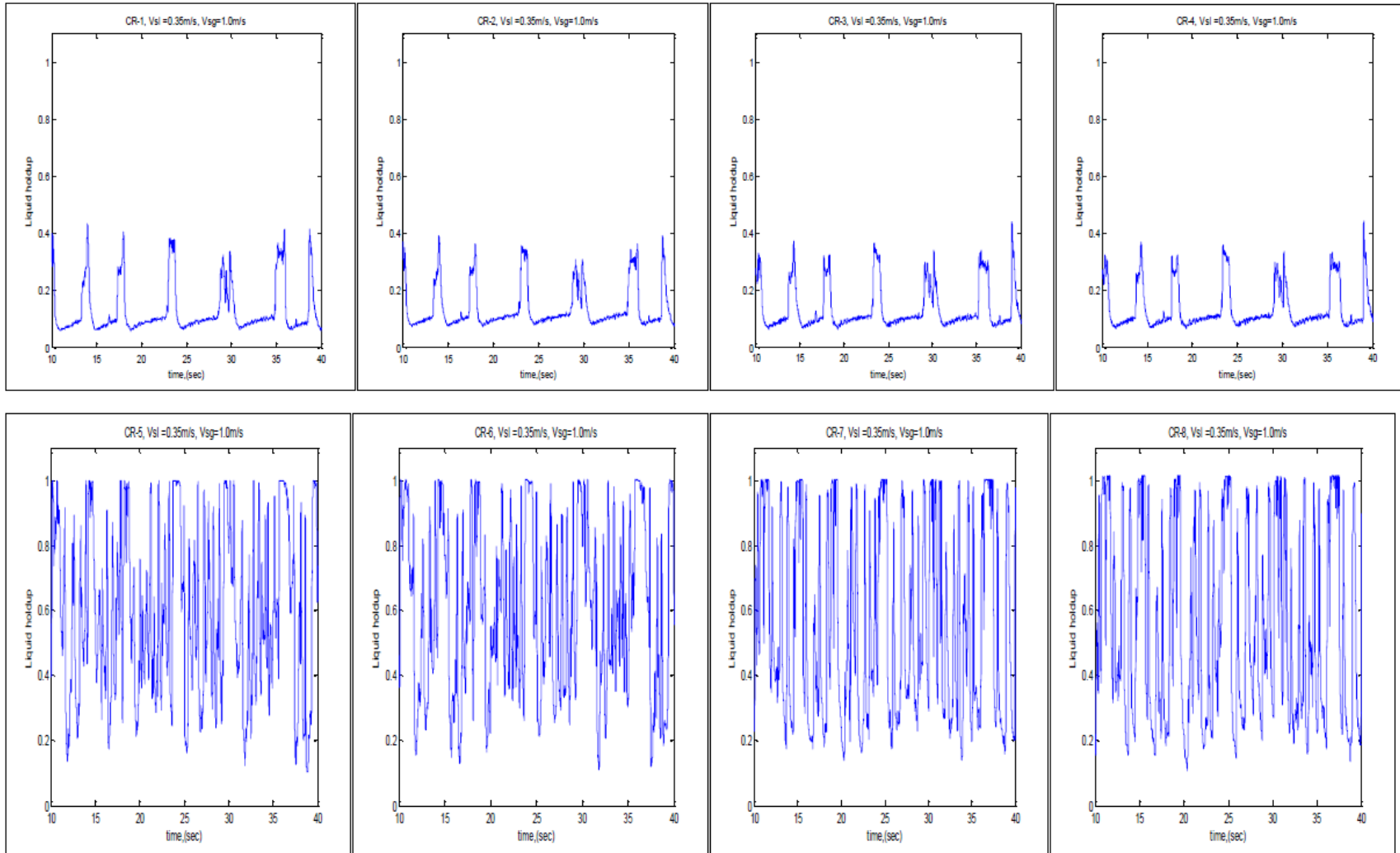
Vsg=0.9m/s

Vsl=0.35m/s, Vsg=0.9m/s



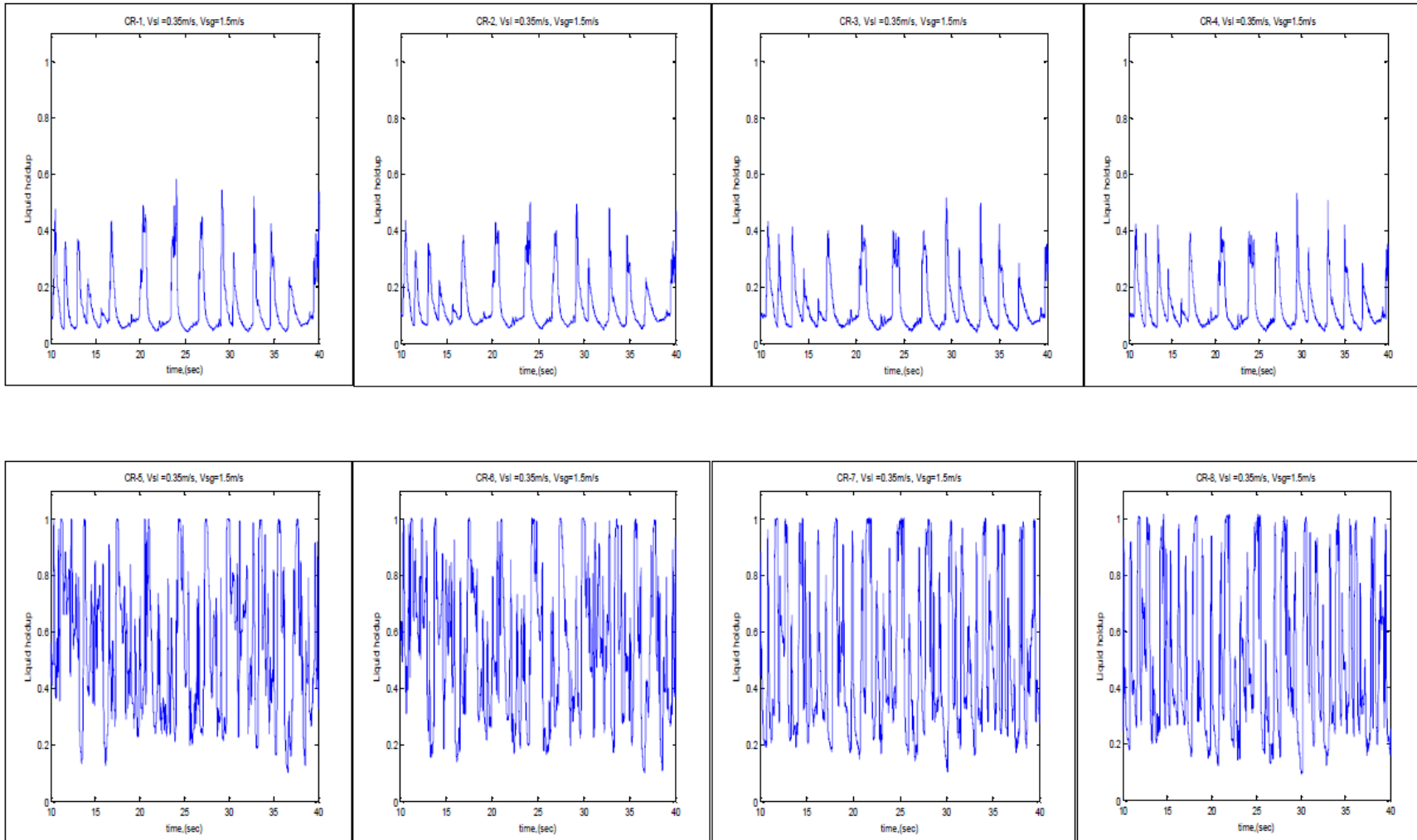
Vsg=1.0m/s

Vsl=0.35m/s, Vsg=1.0/s



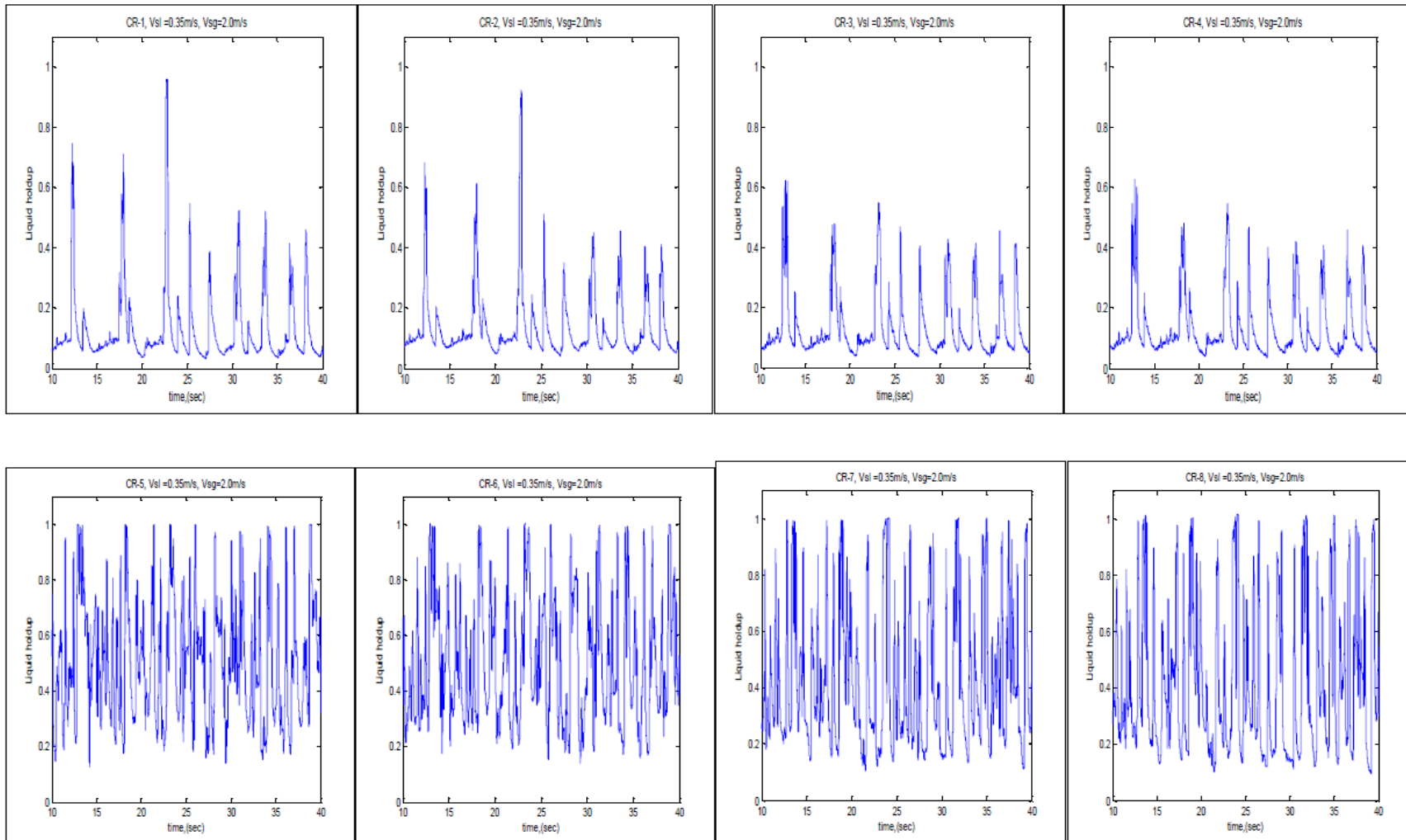
Vsg=1.5m/s

Vsl=0.35m/s, Vsg=1.5m/s



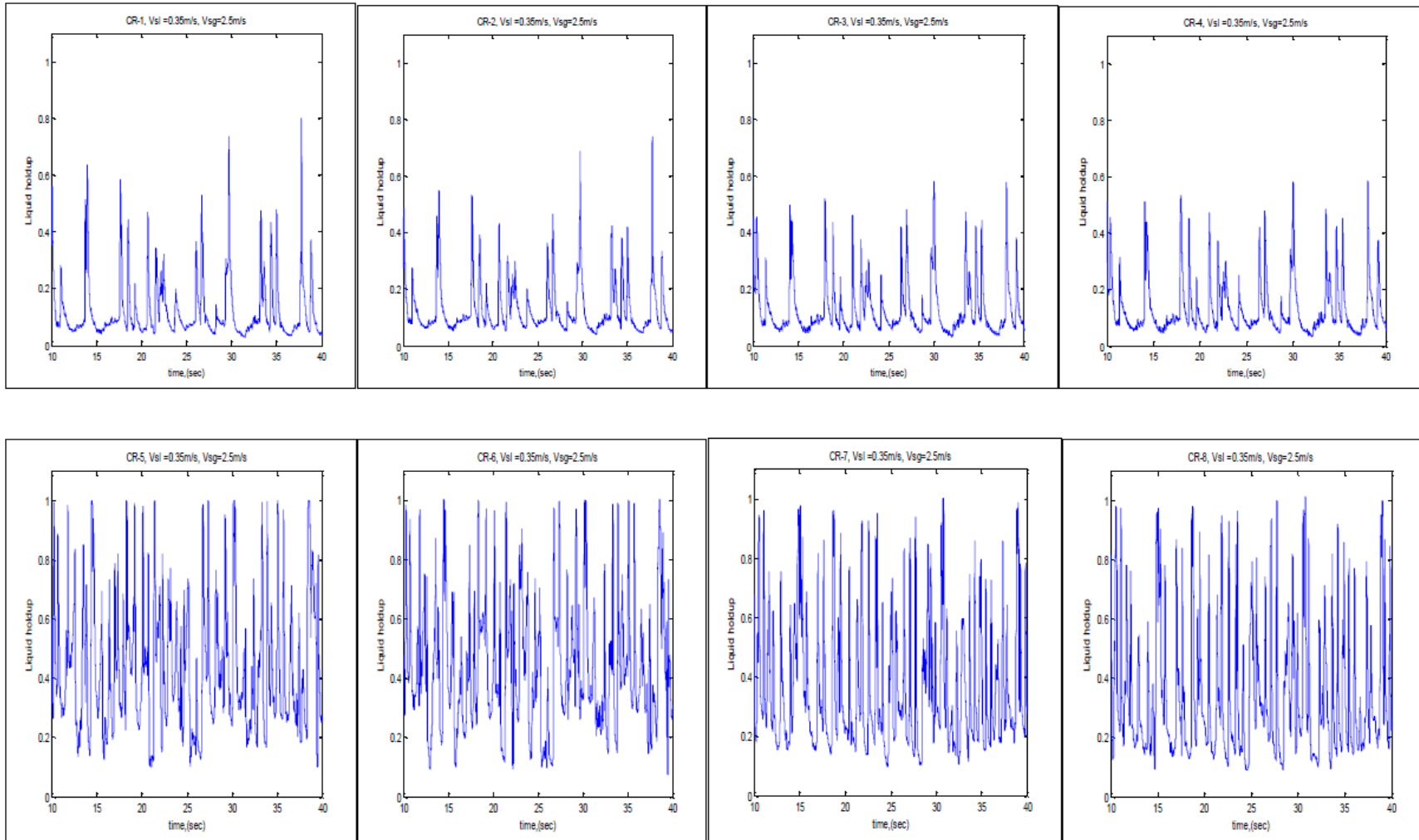
Vsg=2.0m/s

Vsl=0.35m/s, Vsg=2.0m/s



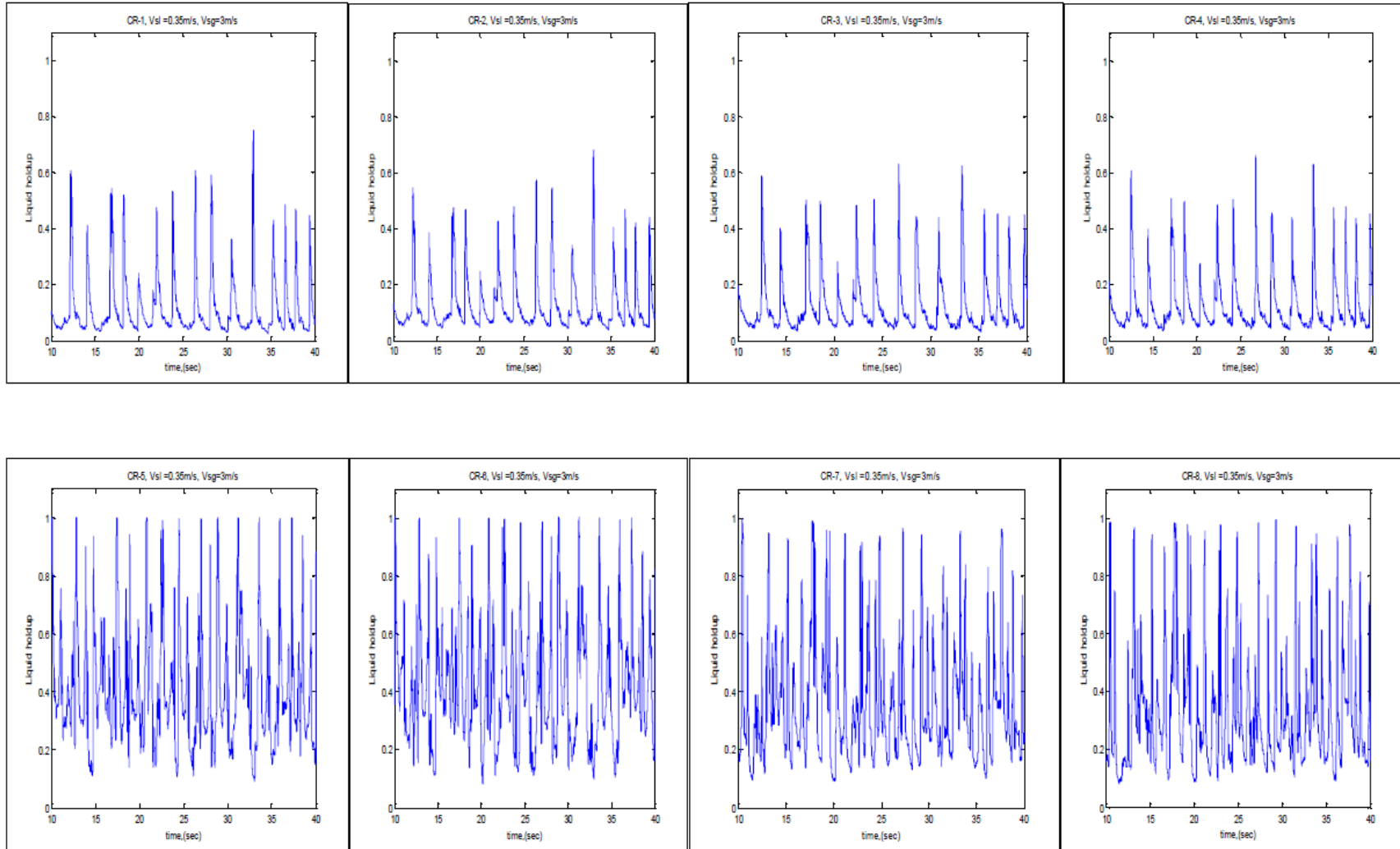
Vsg=2.5m/s

Vsl=0.35m/s, Vsg=2.5m/s



Vsg=3.0m/s

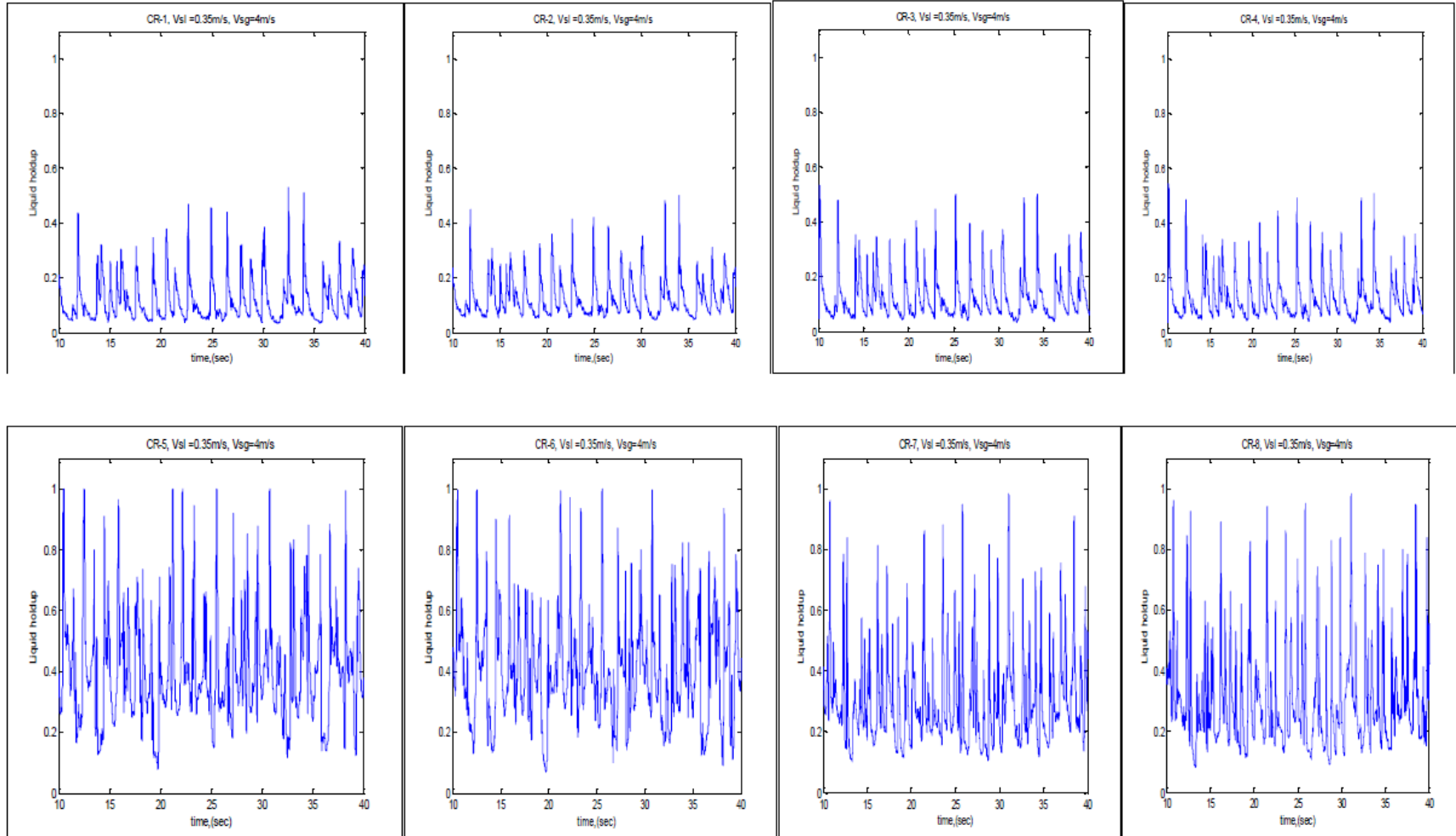
Vsl=0.35m/s, Vsg=3.0m/s





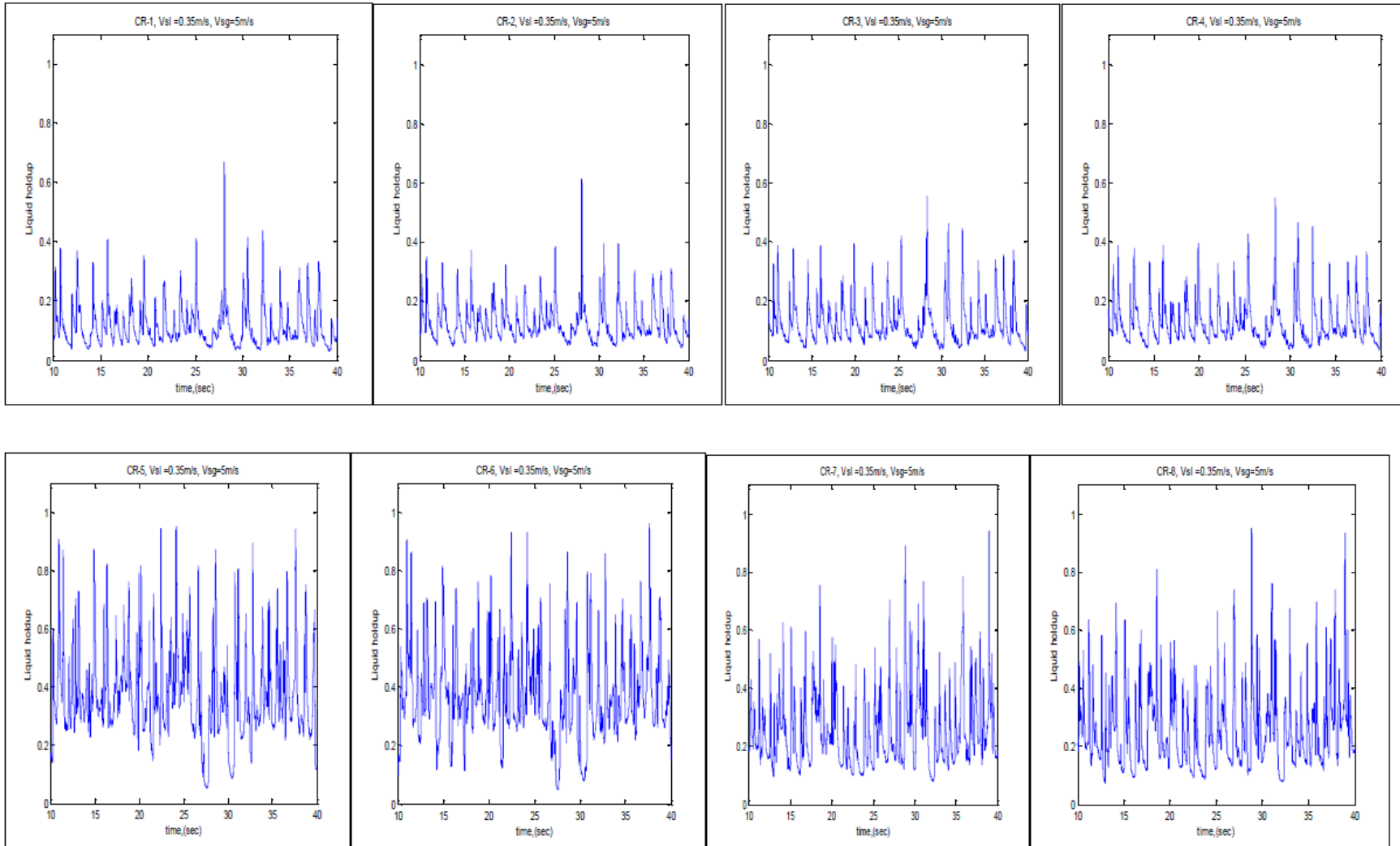
Vsg=4.0m/s

Vsl=0.35m/s, Vsg=4.0m/s



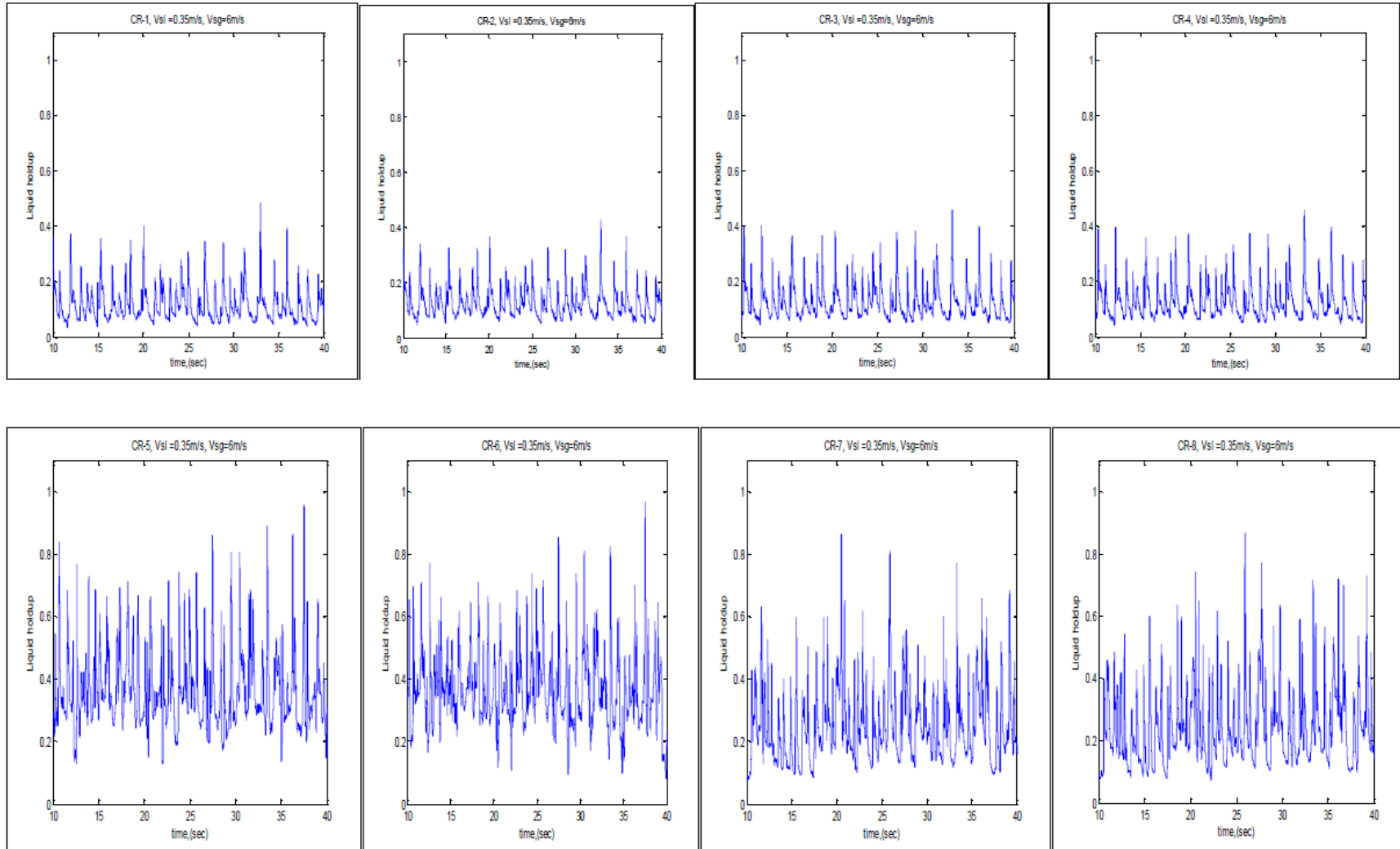
Vsg=5.0m/s

Vsl=0.35m/s, Vsg=5.0m/s



Vsg=6.0m/s

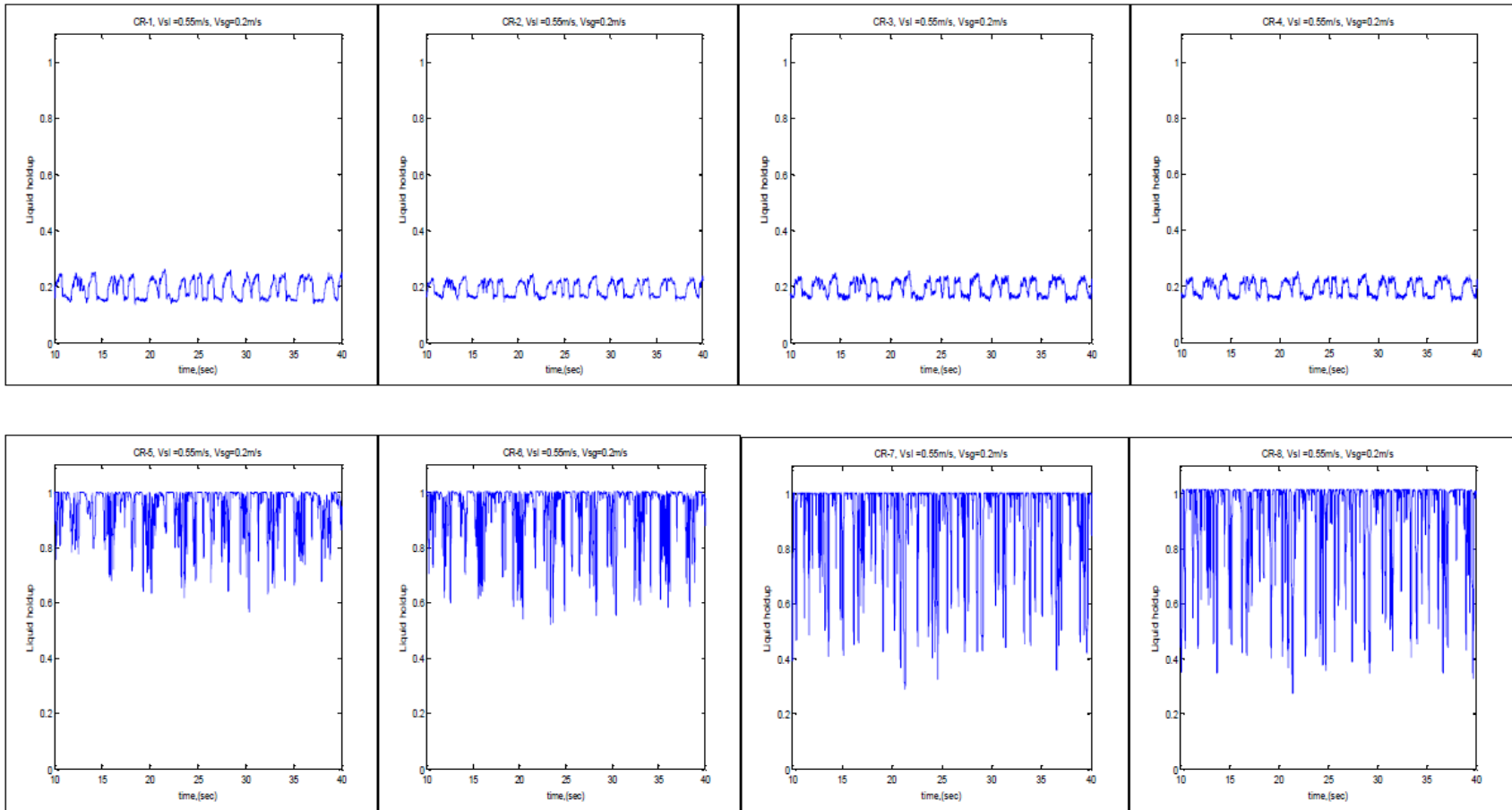
Vsl=0.35m/s, Vsg=6.0m/s



$V_{sl}=0.55\text{m/s}$

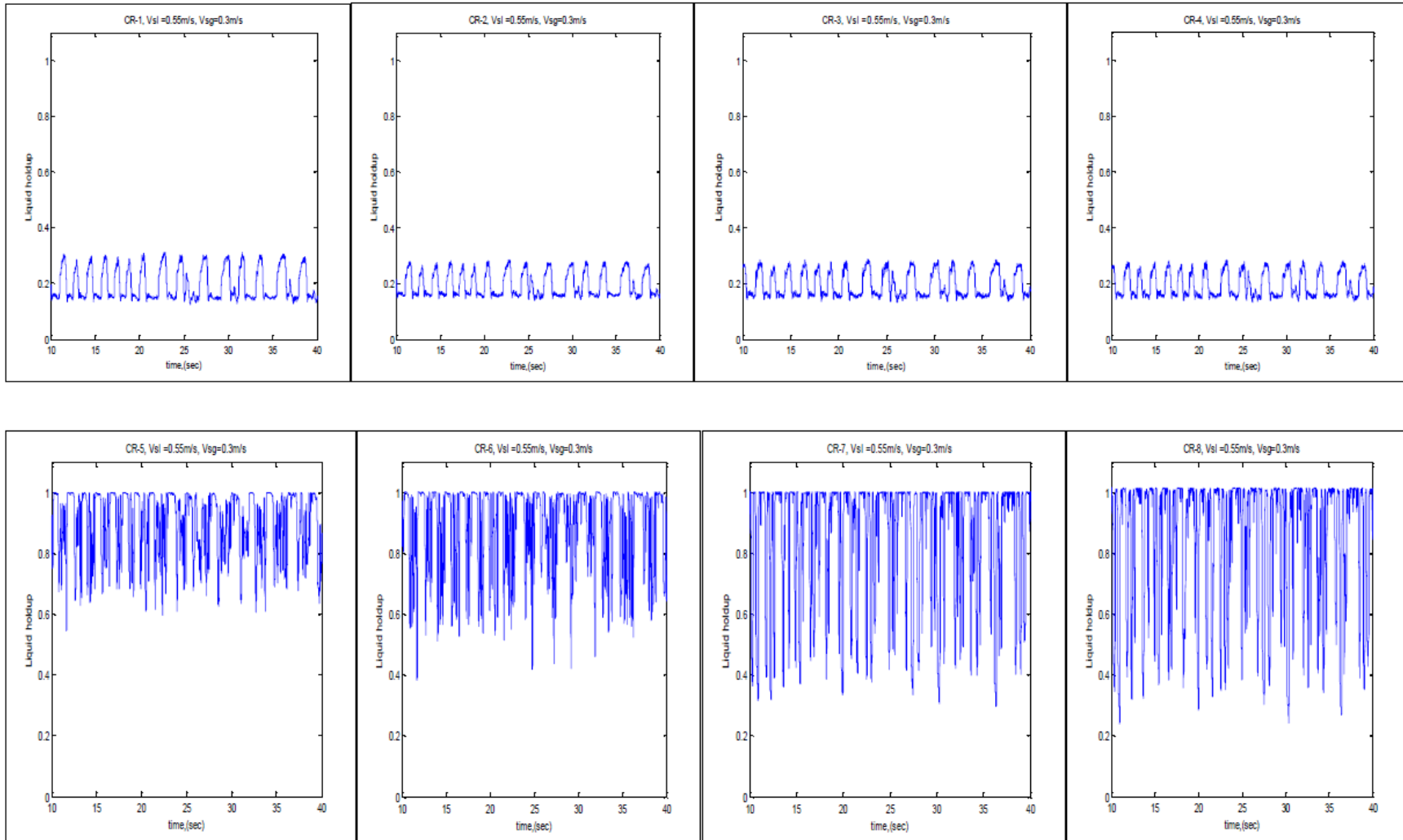
$V_{sg}=0.2\text{m/s}$

$V_{sl}=0.55\text{m/s}, V_{sg}=0.2\text{m/s}$



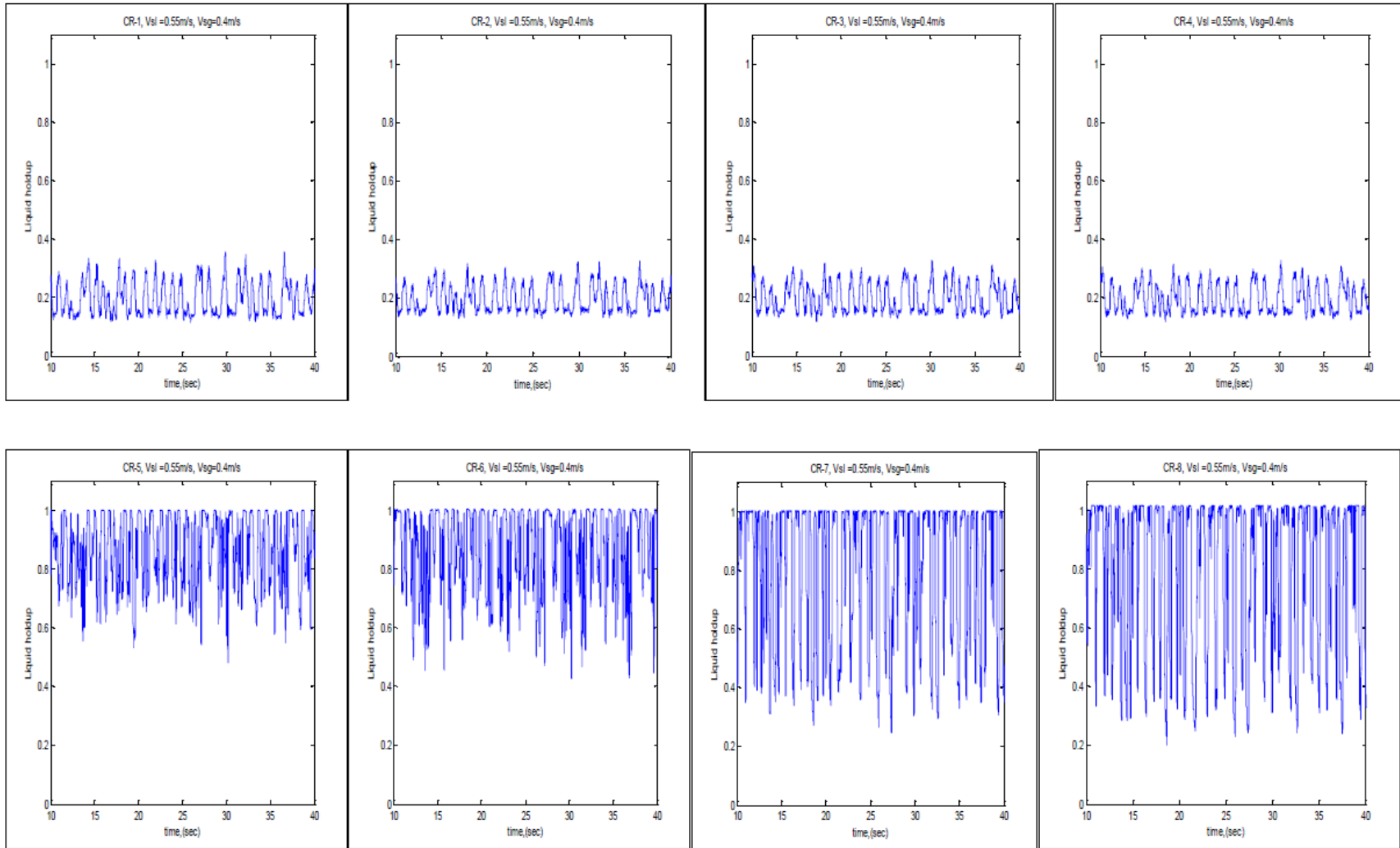
Vsg=0.3m/s

Vsl=0.55m/s, Vsg=0.3m/s



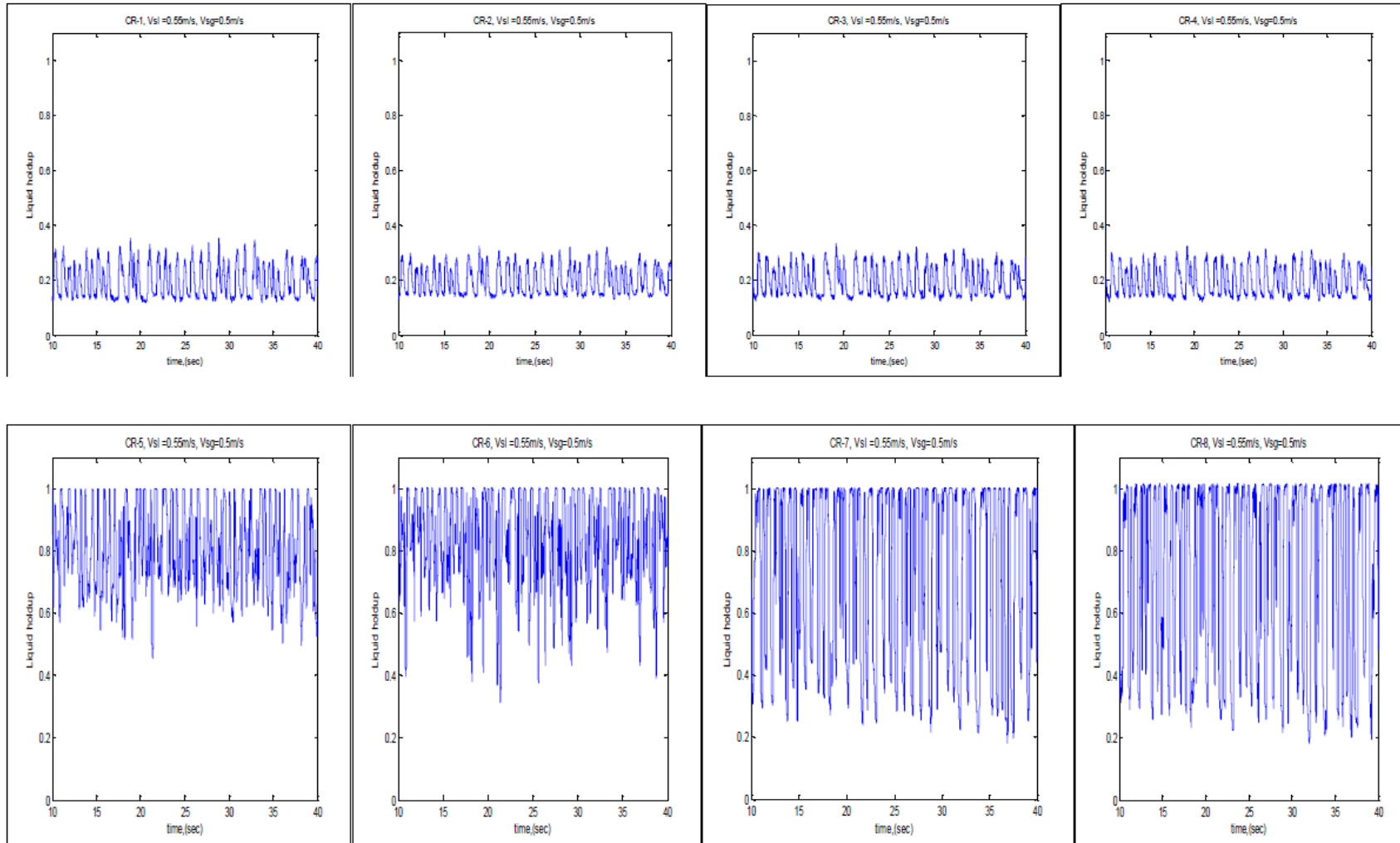
Vsg=0.4m/s

Vsl=0.55m/s, Vsg=0.4m/s



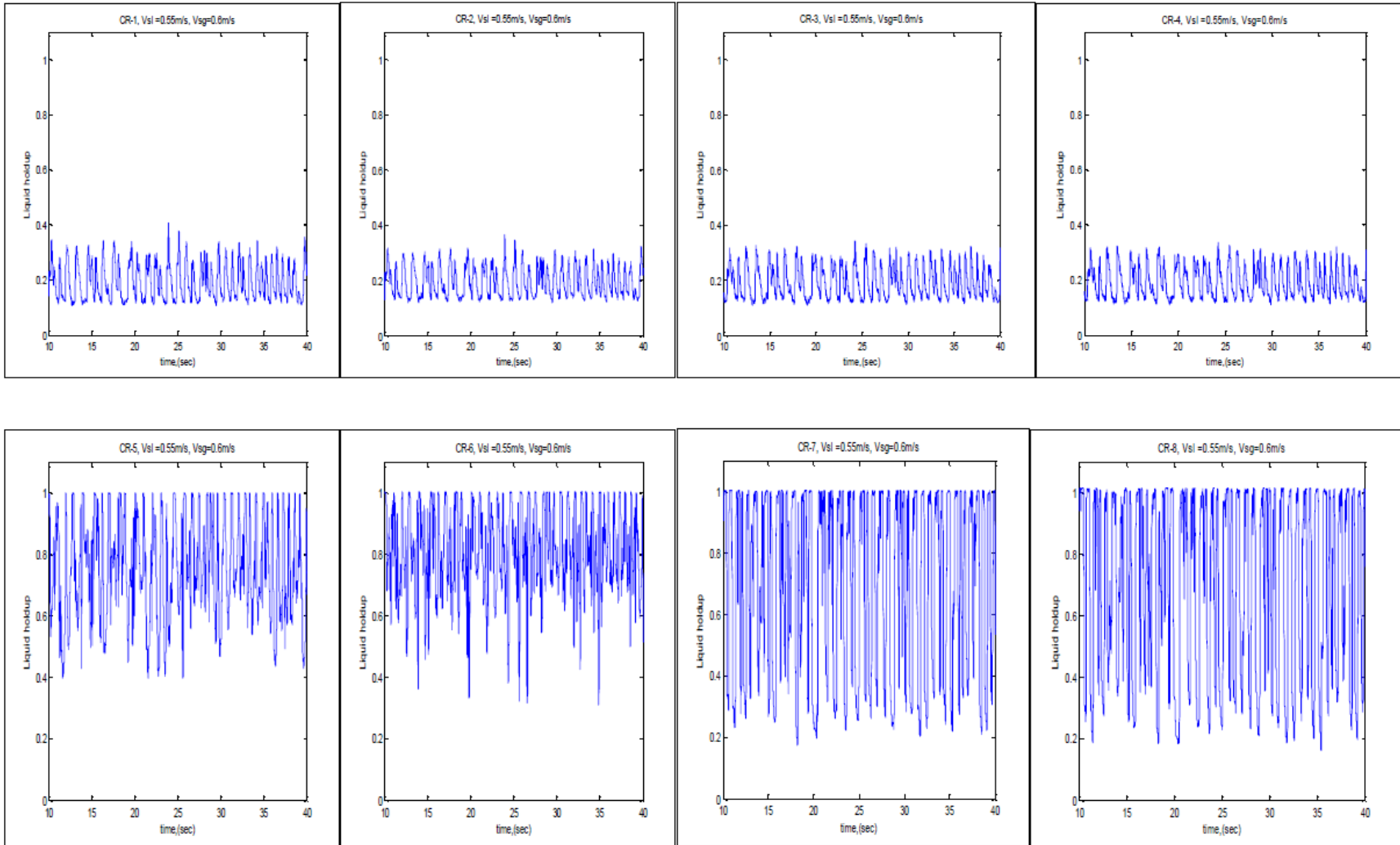
Vsg=0.5m/s

Vsl=0.55m/s, Vsg=0.5m/s



Vsg=0.6m/s

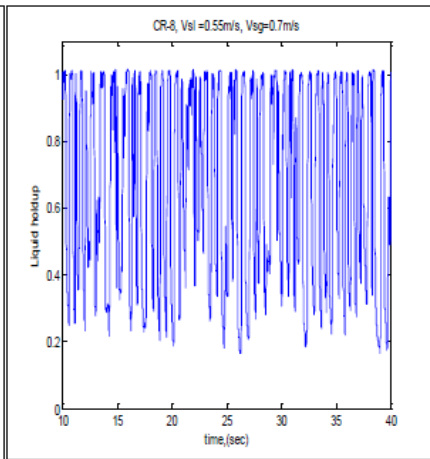
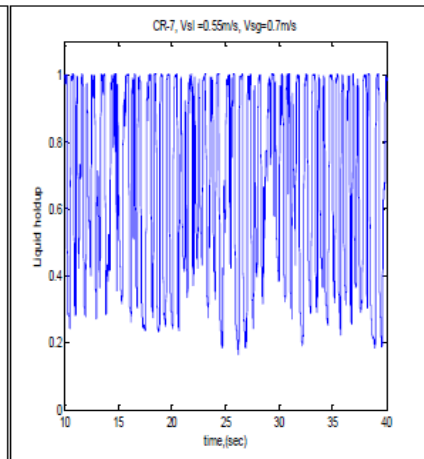
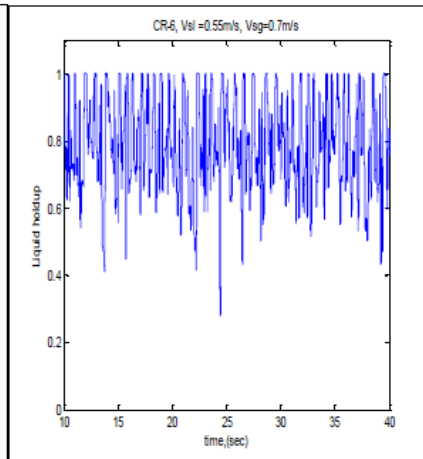
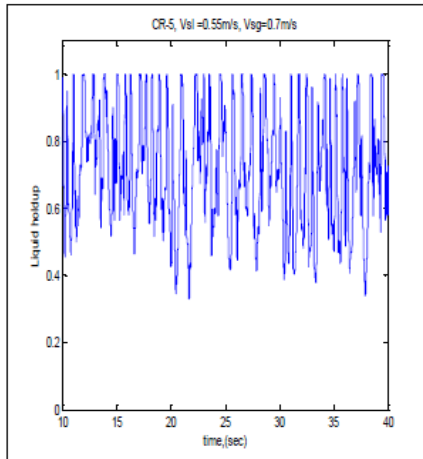
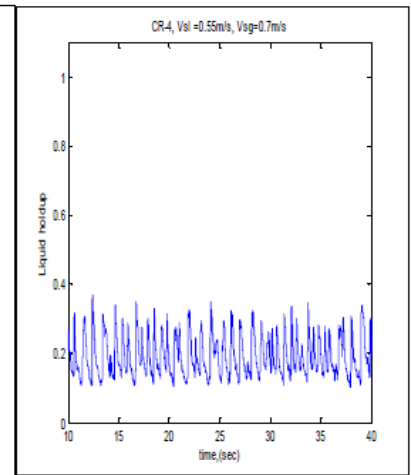
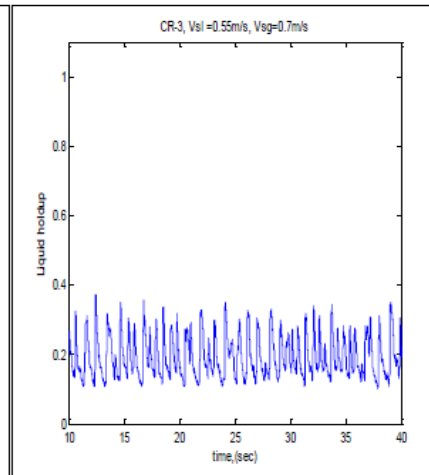
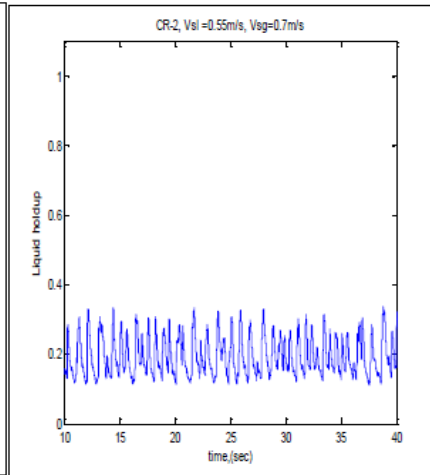
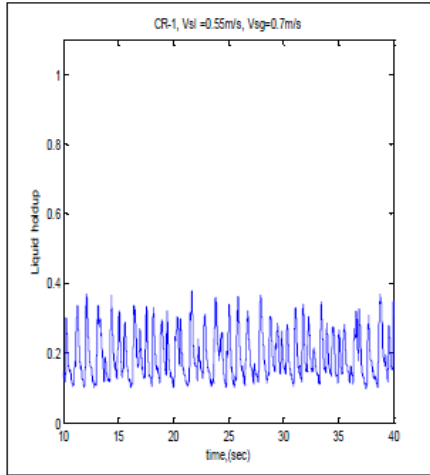
Vsl=0.55m/s, Vsg=0.6m/s





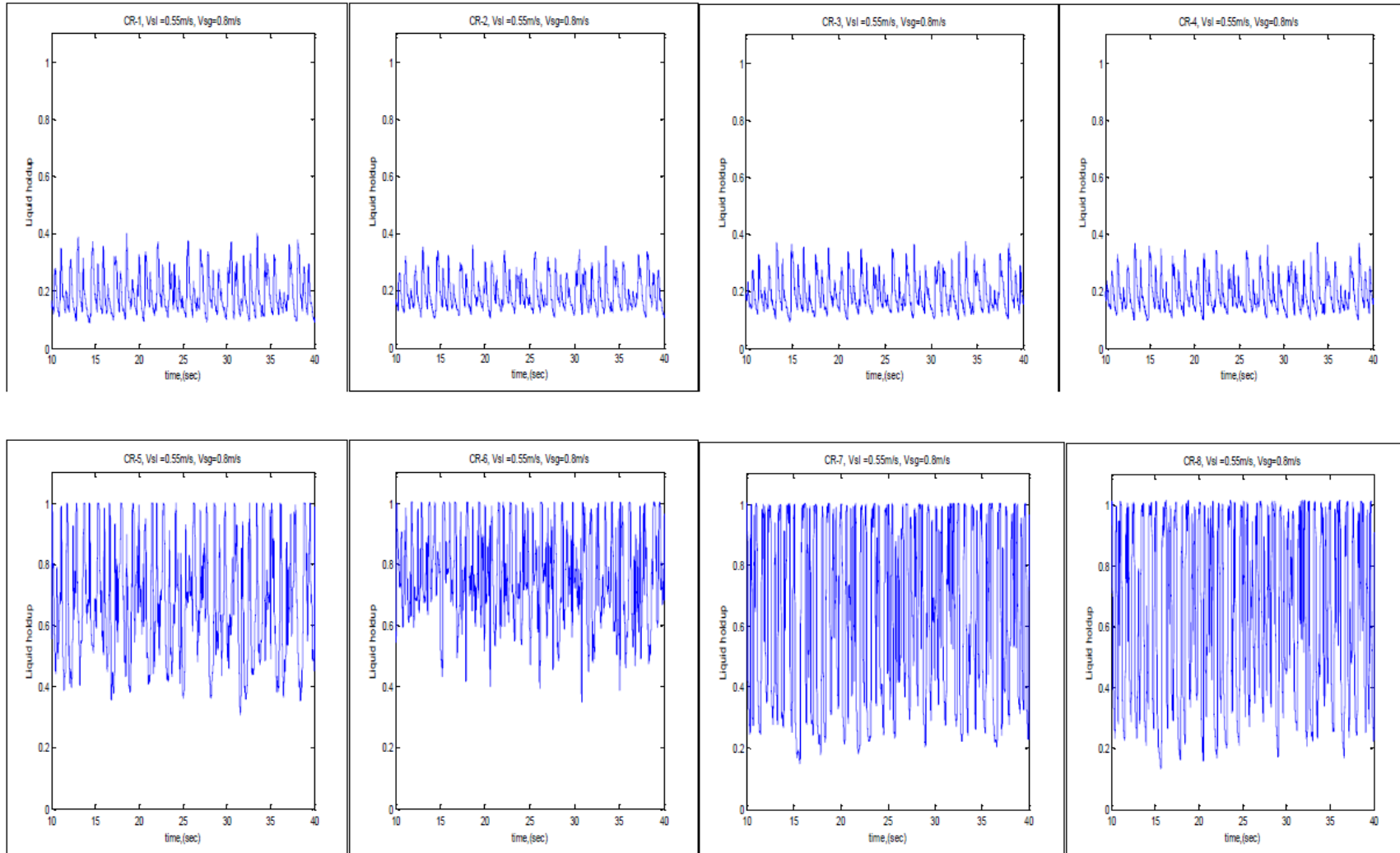
Vsg=0.7m/s

Vsl=0.55m/s, Vsg=0.7m/s



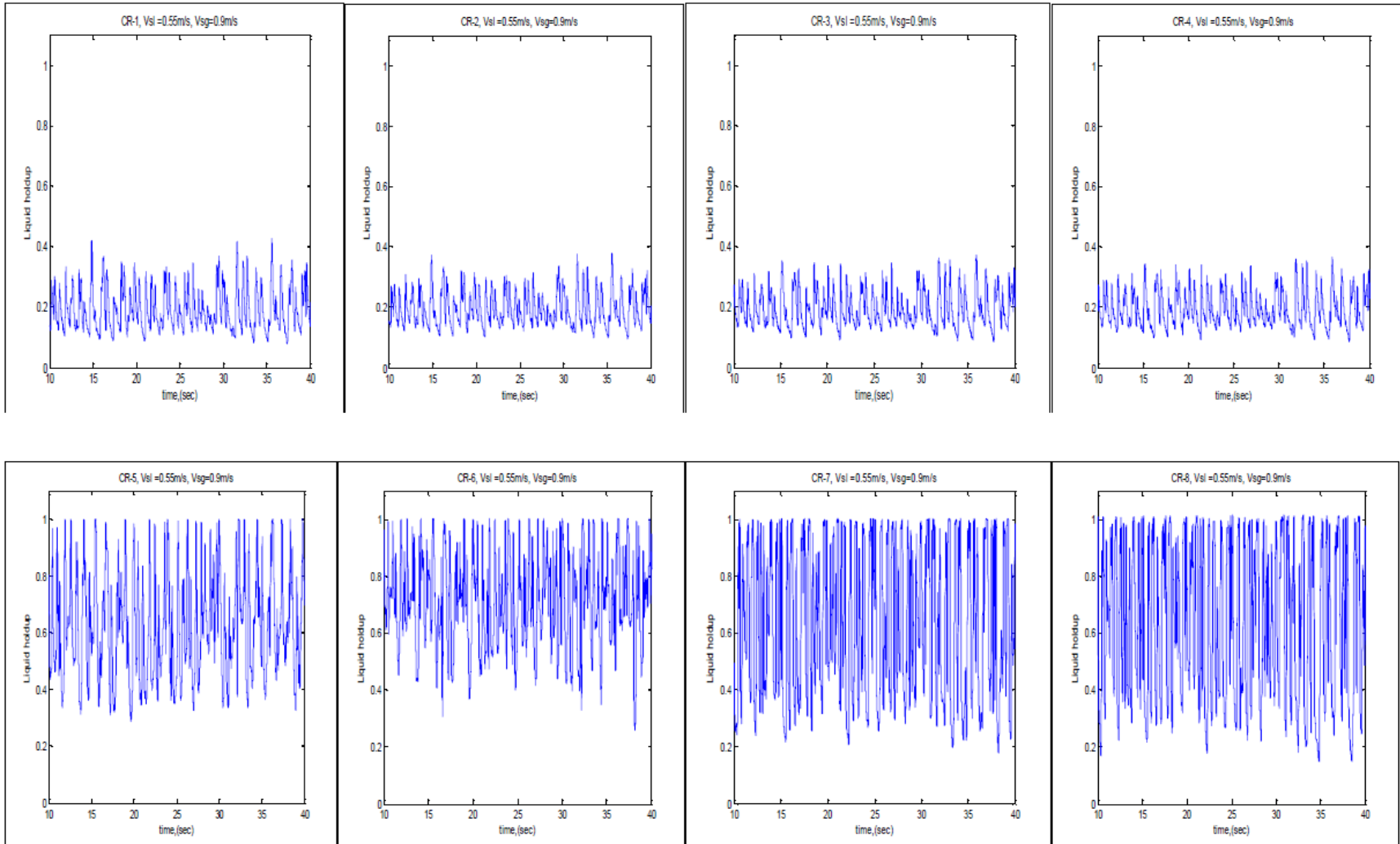
Vsg=0.8m/s

Vsl=0.55m/s, Vsg=0.8m/s



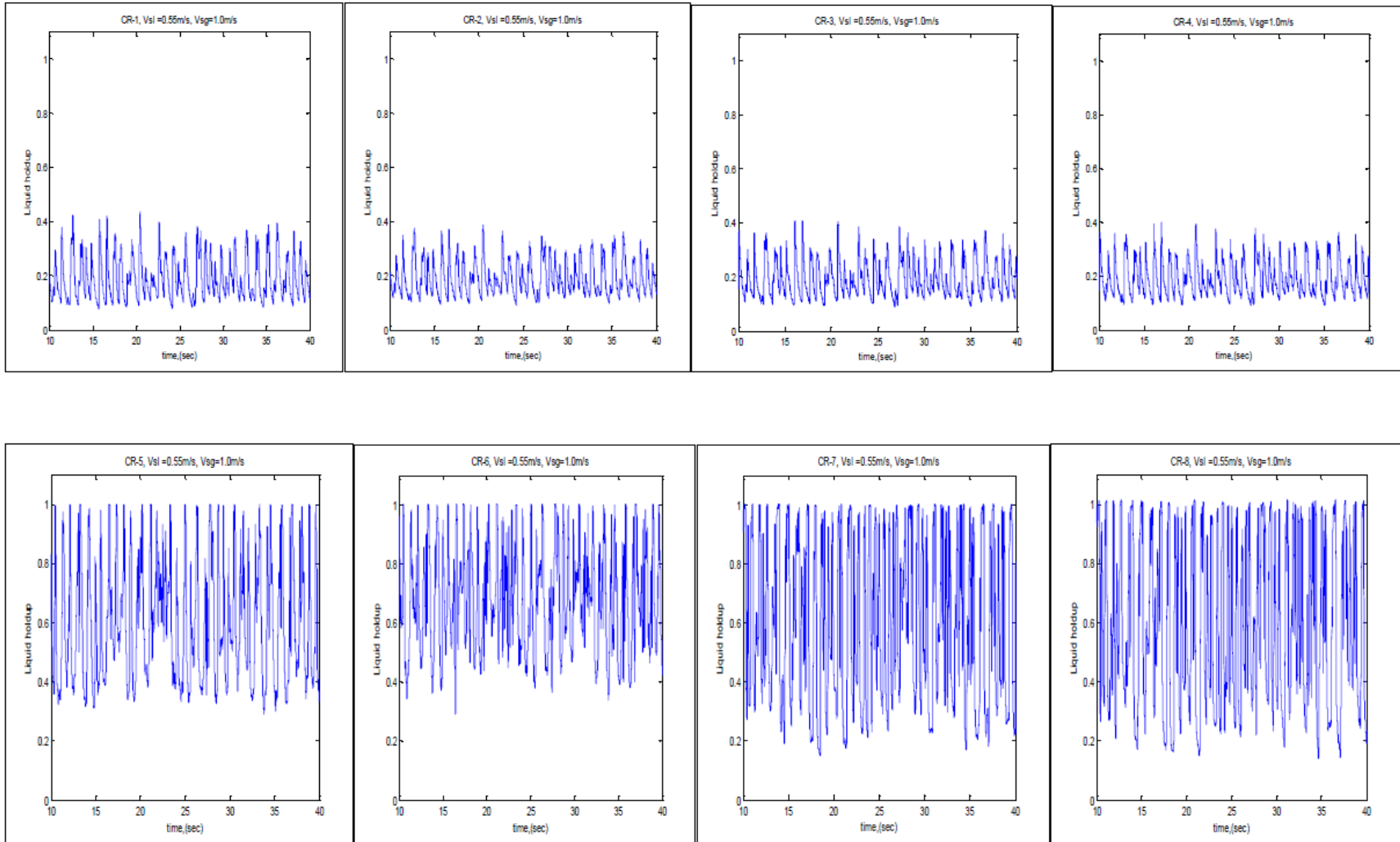
Vsg=0.9m/s

Vsl=0.55m/s, Vsg=0.9m/s



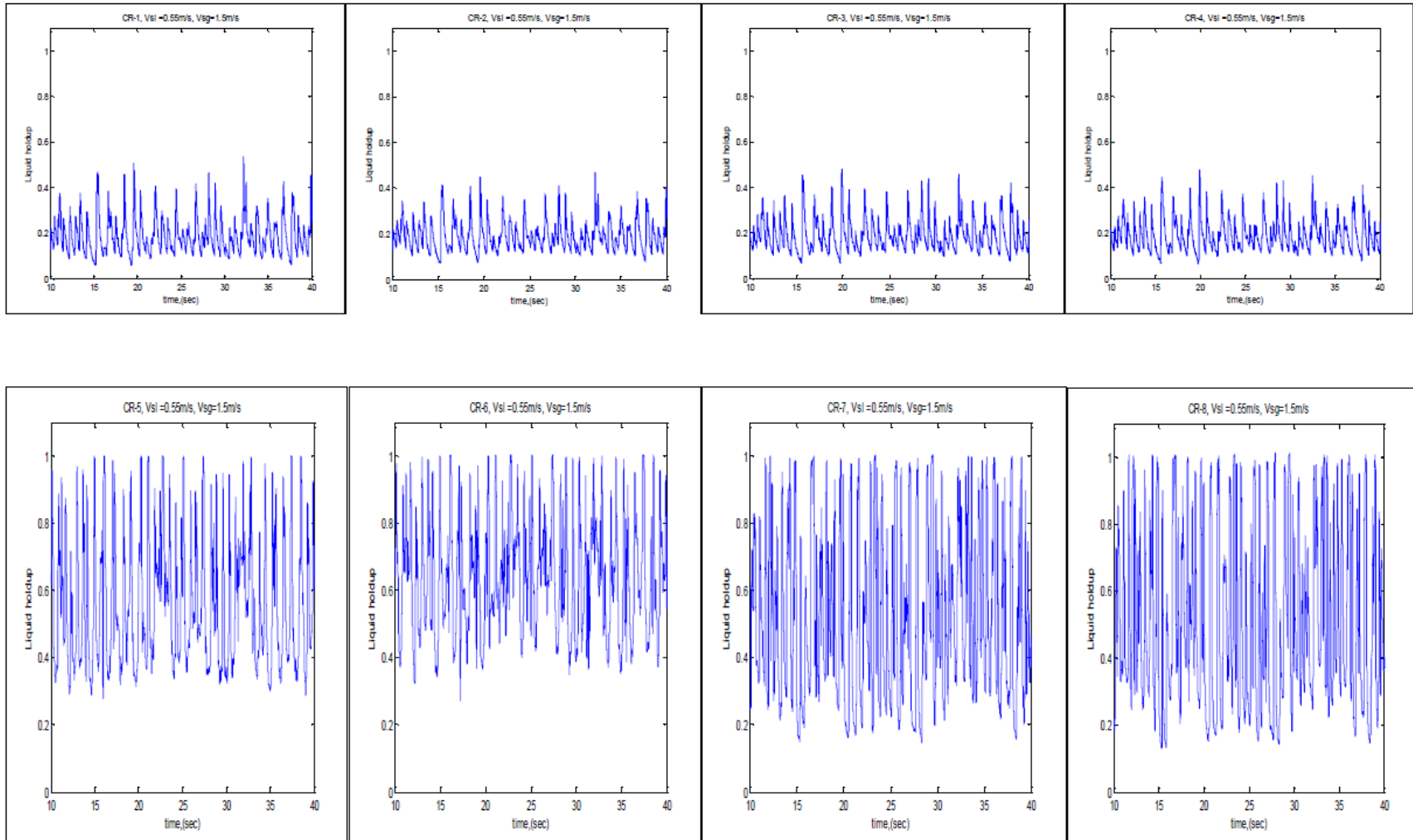
Vsg=1.0m/s

Vsl=0.55m/s, Vsg=1.0m/s



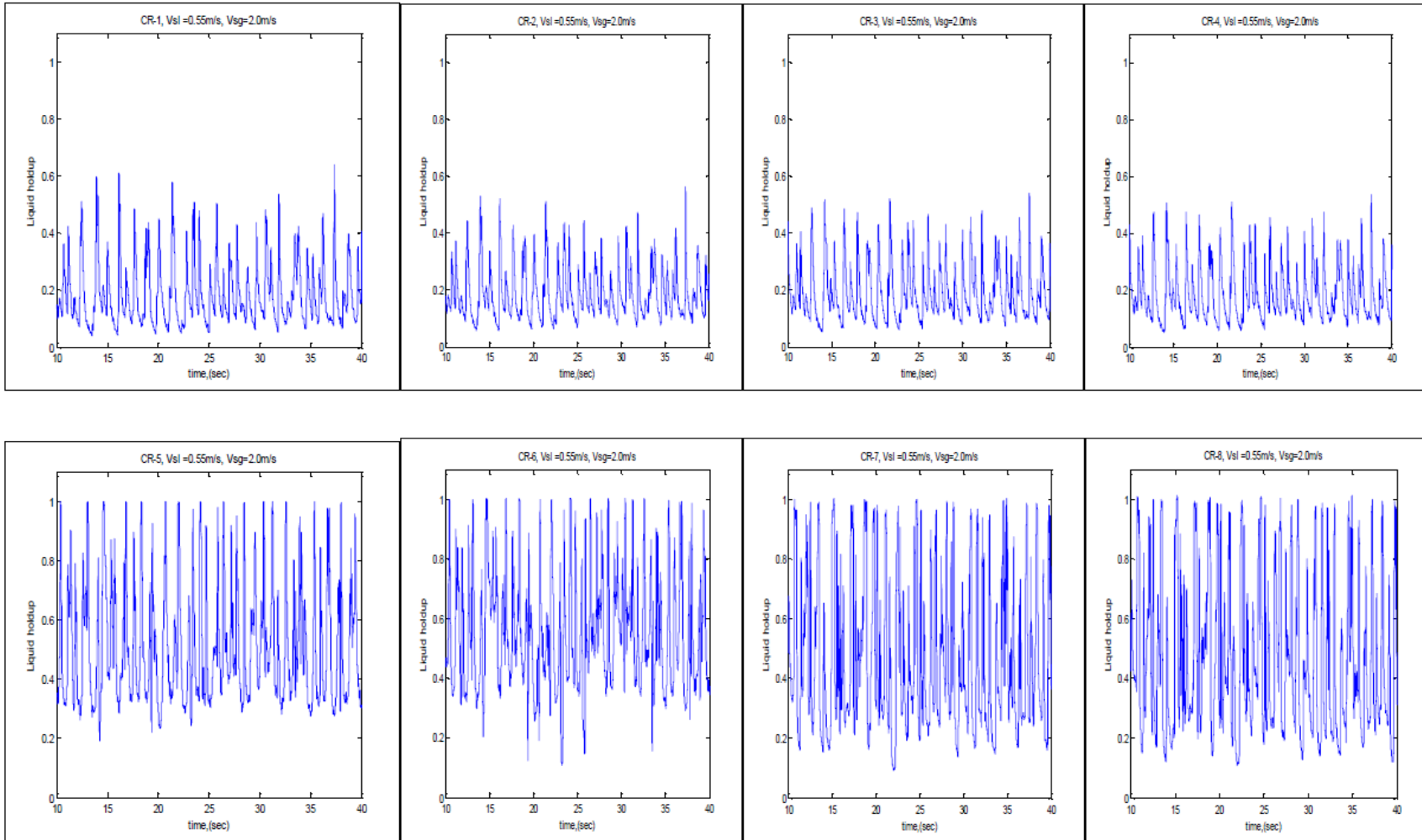
Vsg=1.5m/s

Vsl=0.55m/s, Vsg=1.5m/s



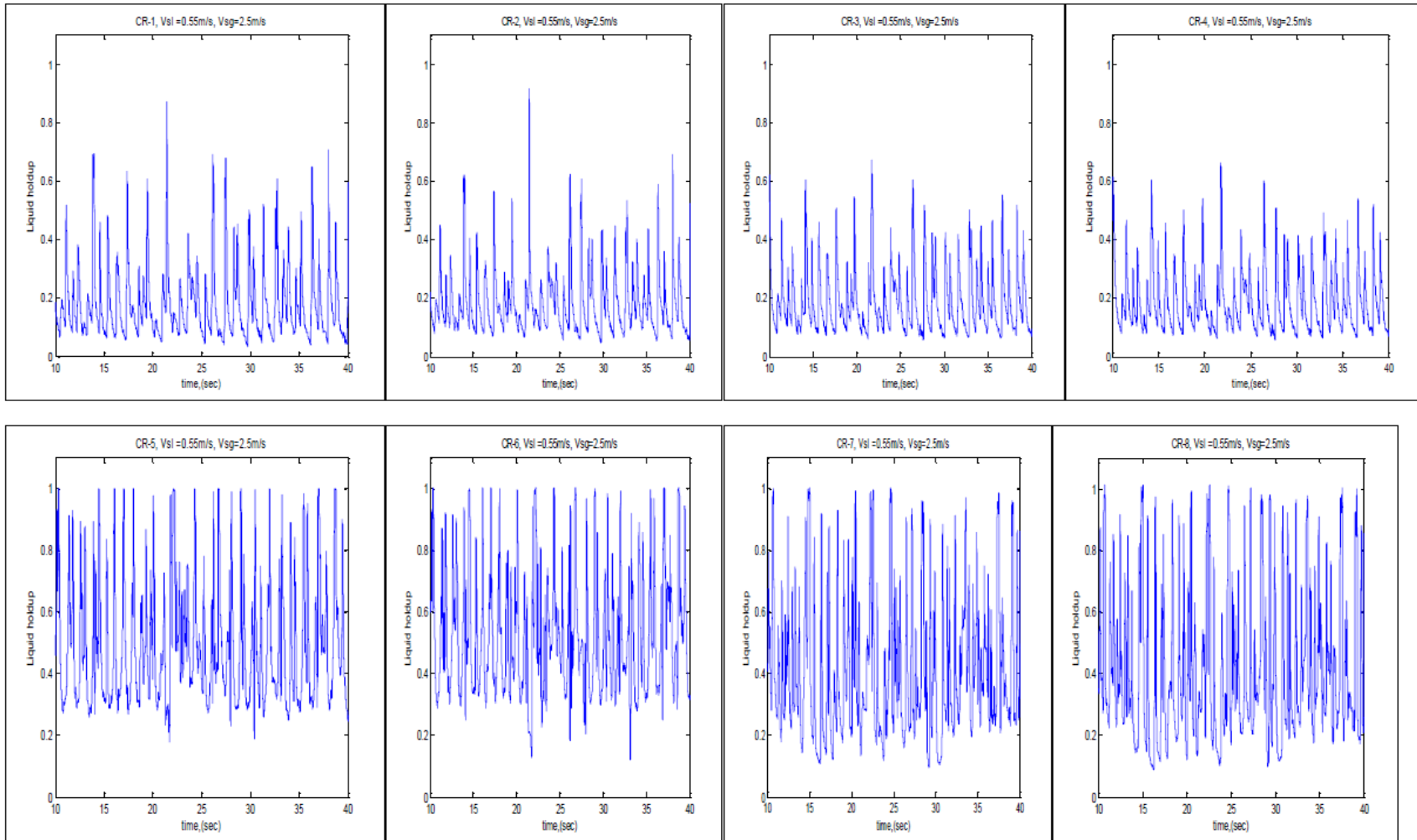
Vsg=2.0m/s

Vsl=0.55m/s, Vsg=2.0m/s



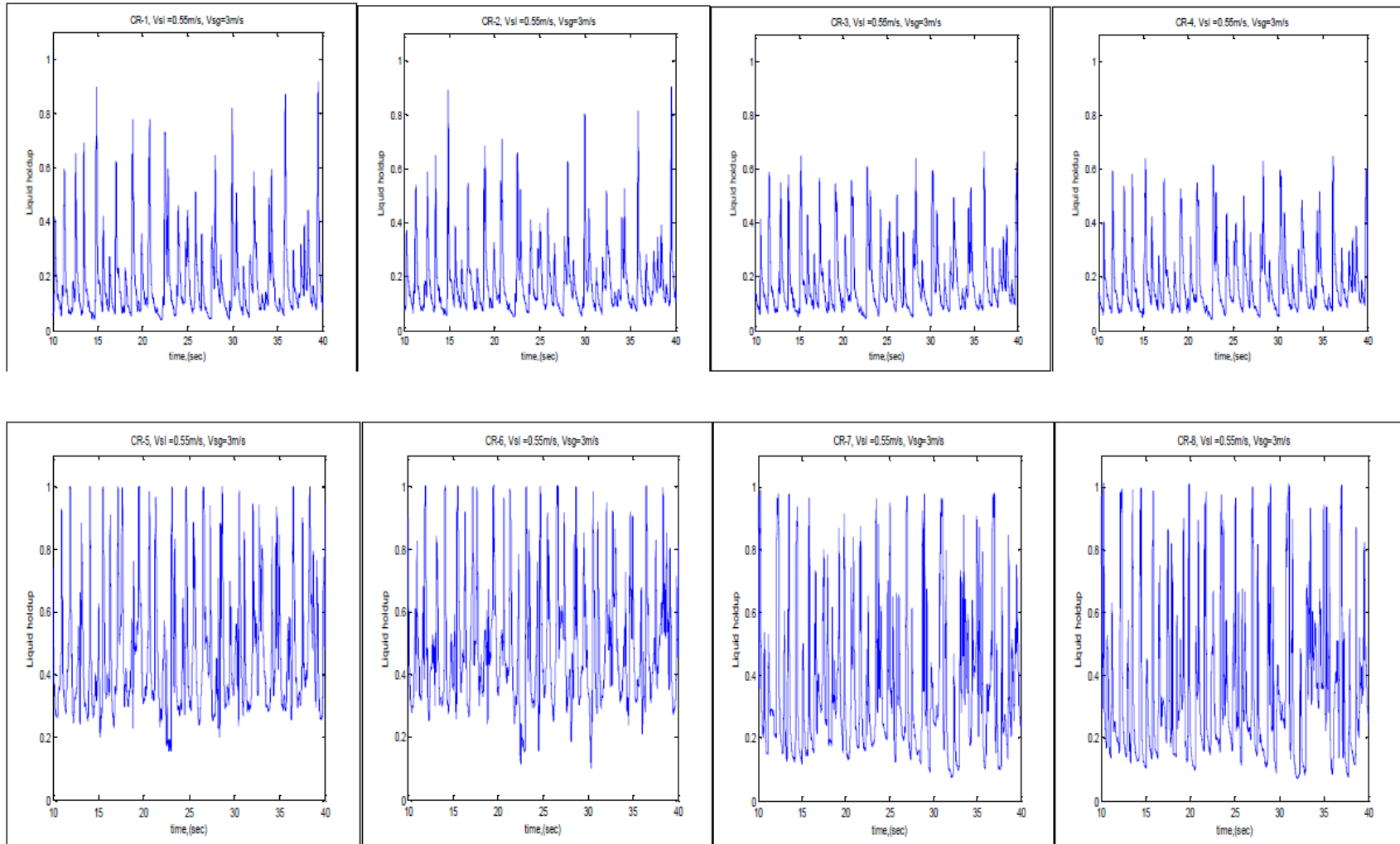
Vsg=2.5m/s

Vsl=0.55m/s, Vsg=2.5m/s



Vsg=3.0m/s

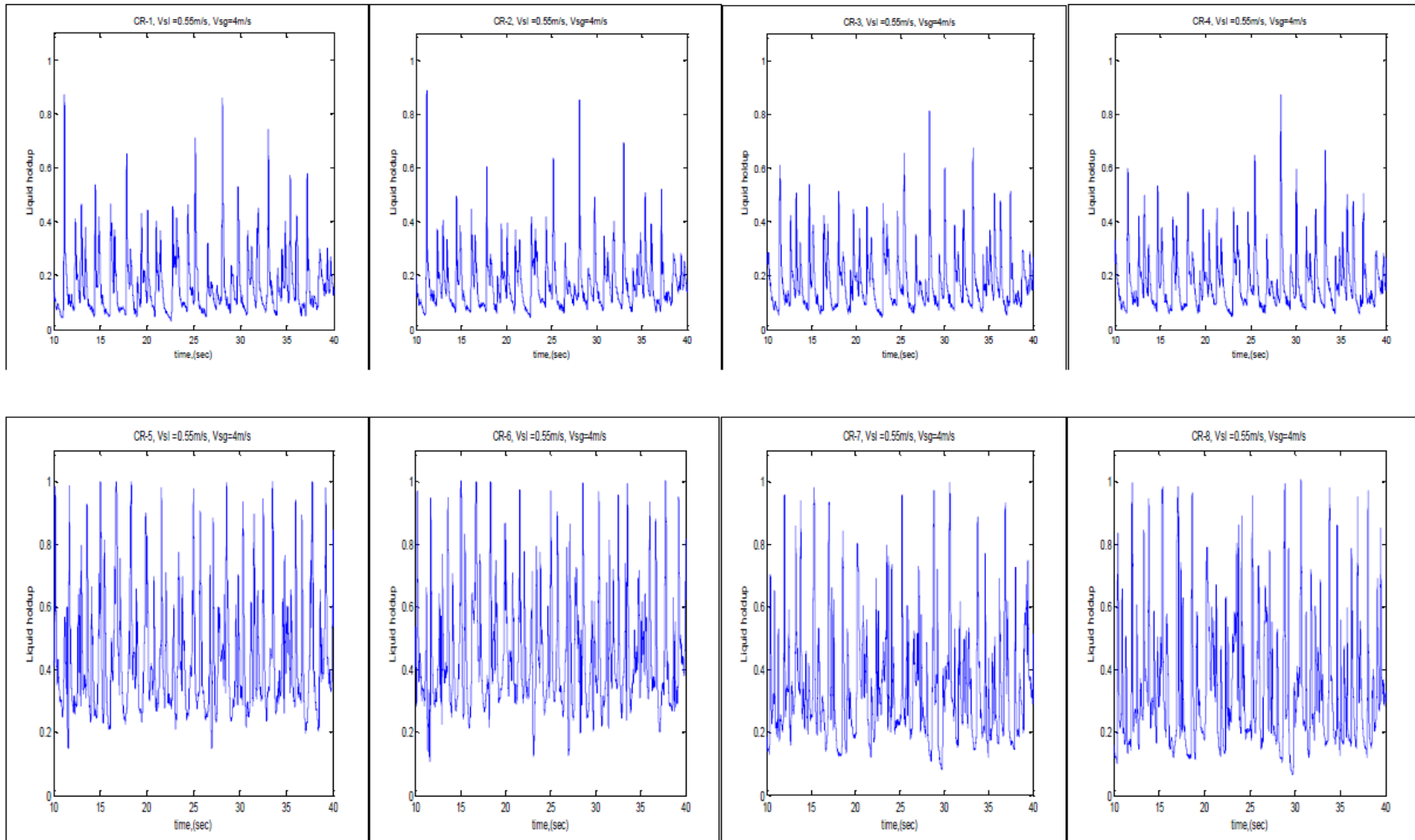
Vsl=0.55m/s, Vsg=3.0m/s





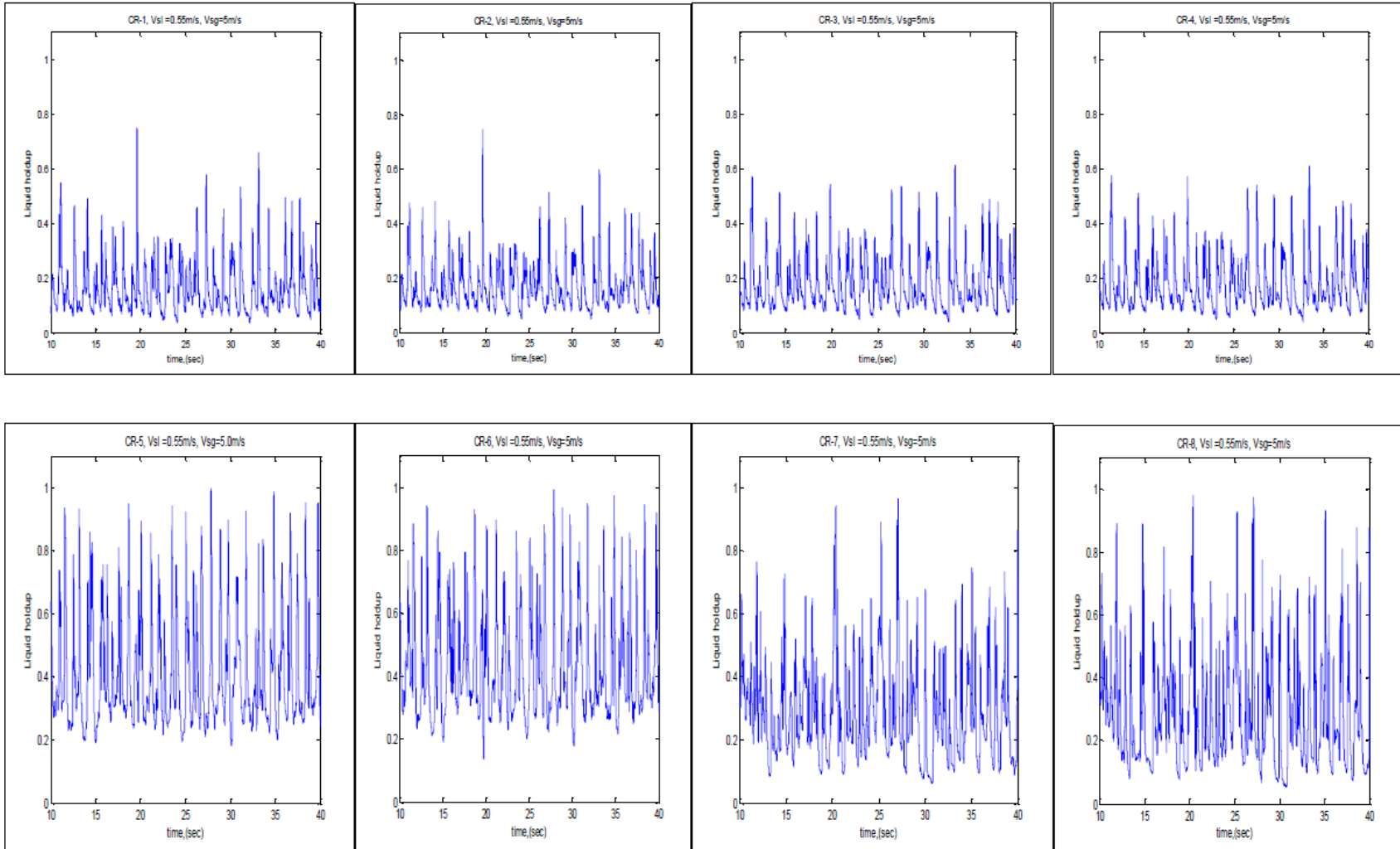
Vsg=4.0m/s

Vsl=0.55m/s, Vsg=4.0m/s



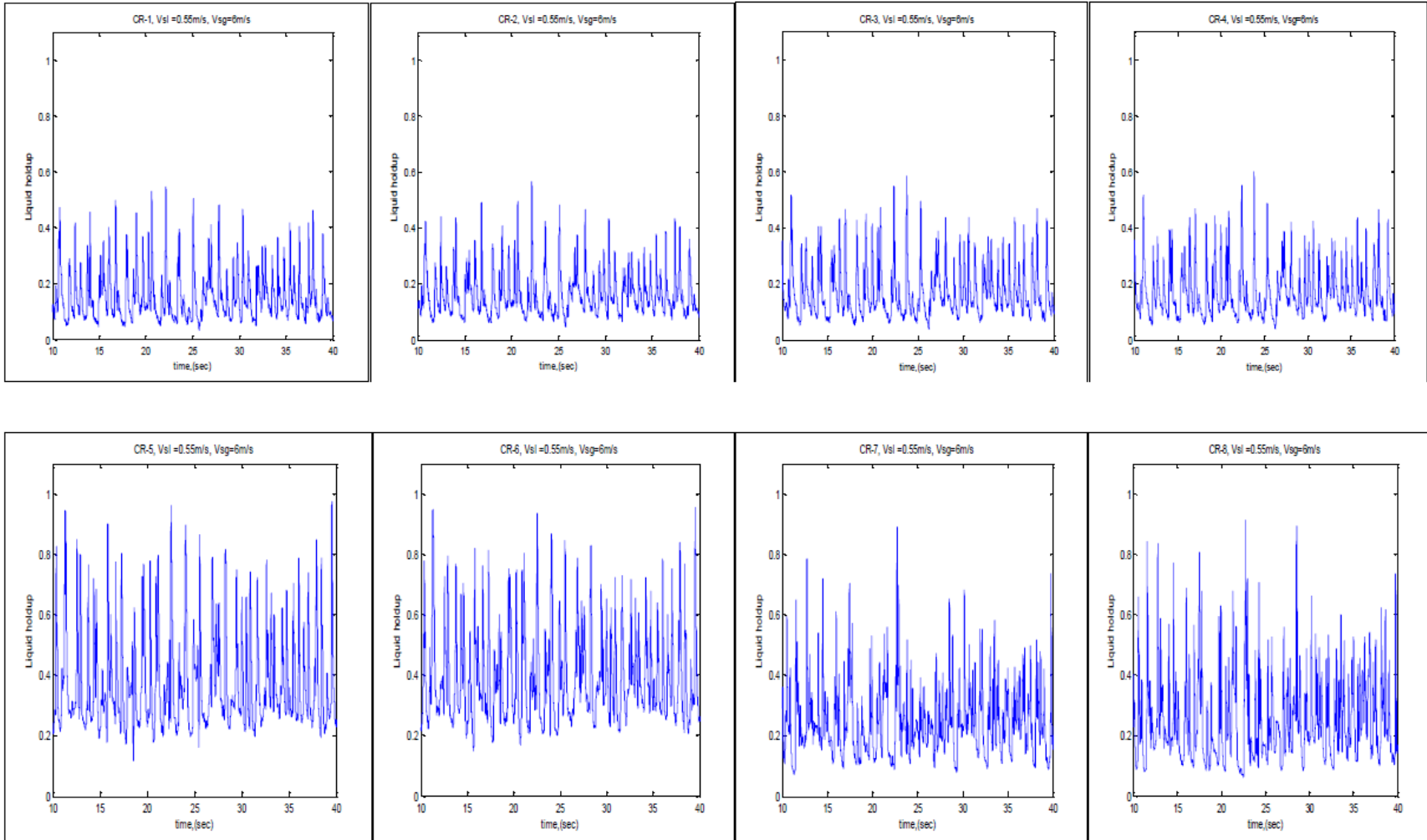
Vsg=5.0m/s

Vsl=0.55m/s, Vsg=5.0m/s



Vsg=6.0m/s

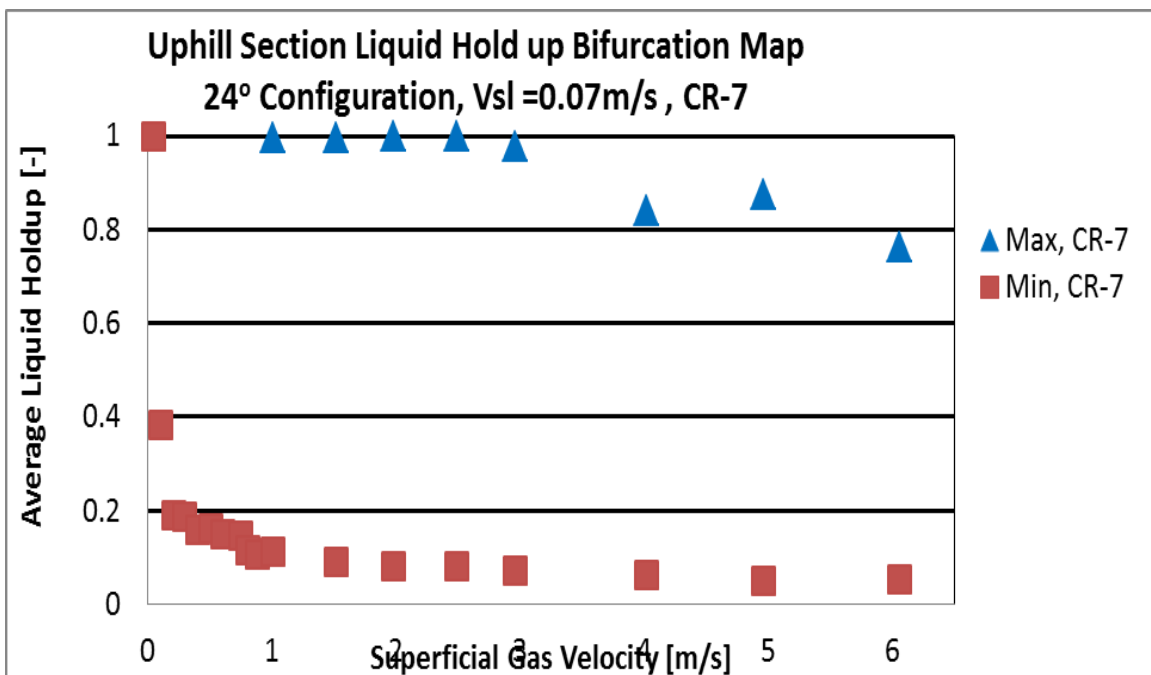
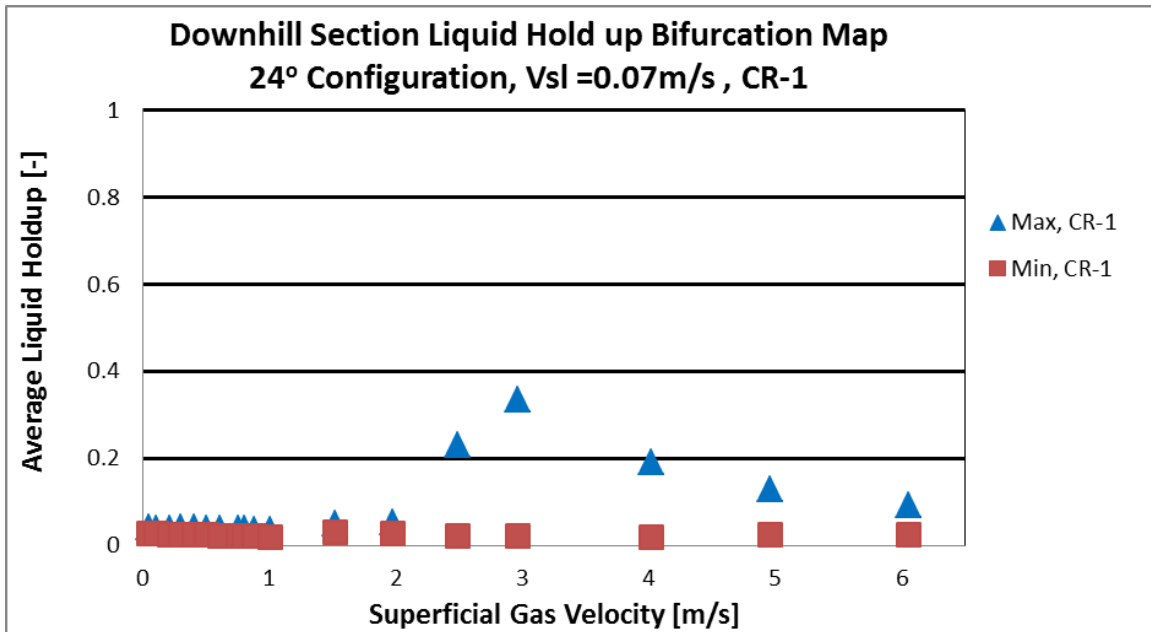
Vsl=0.55m/s, Vsg=6.0m/s

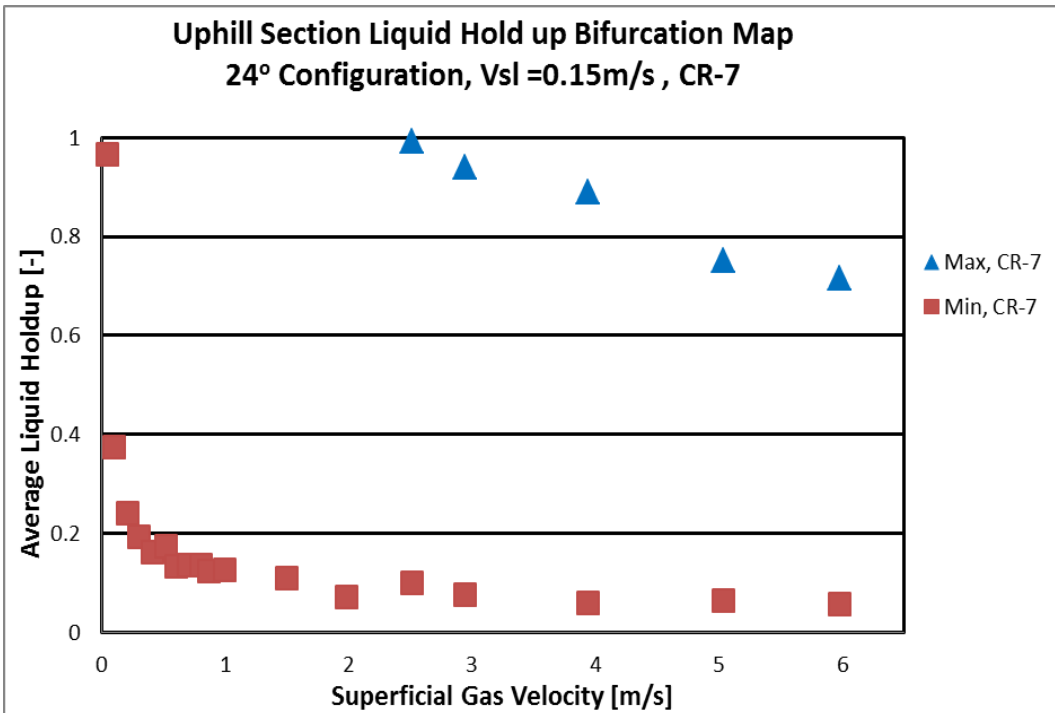
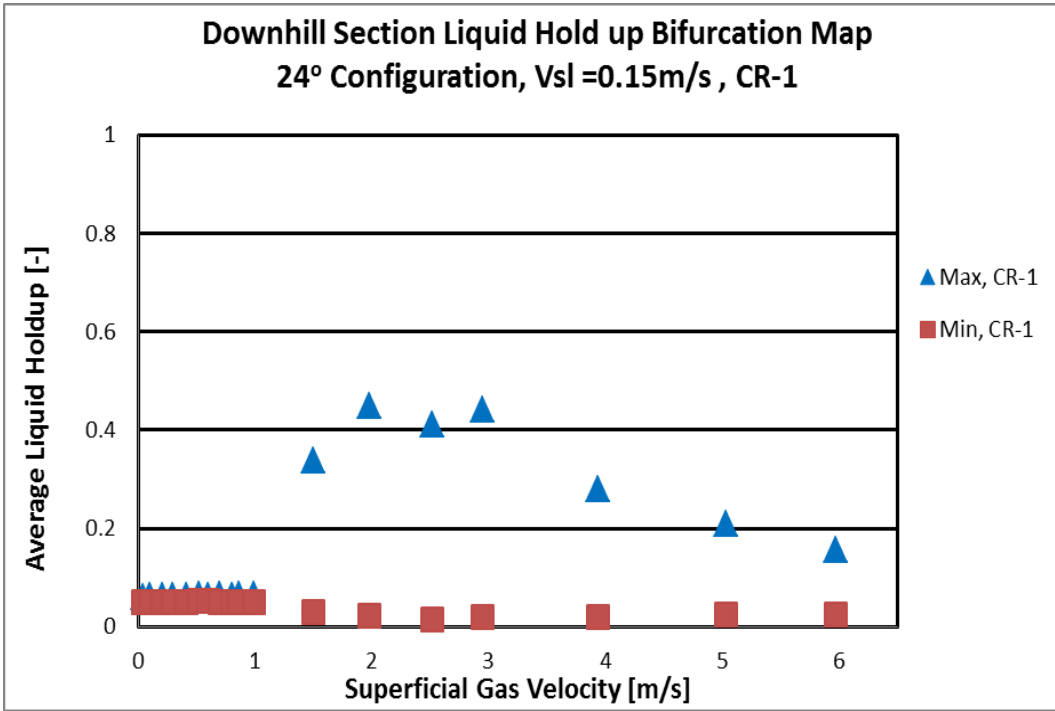


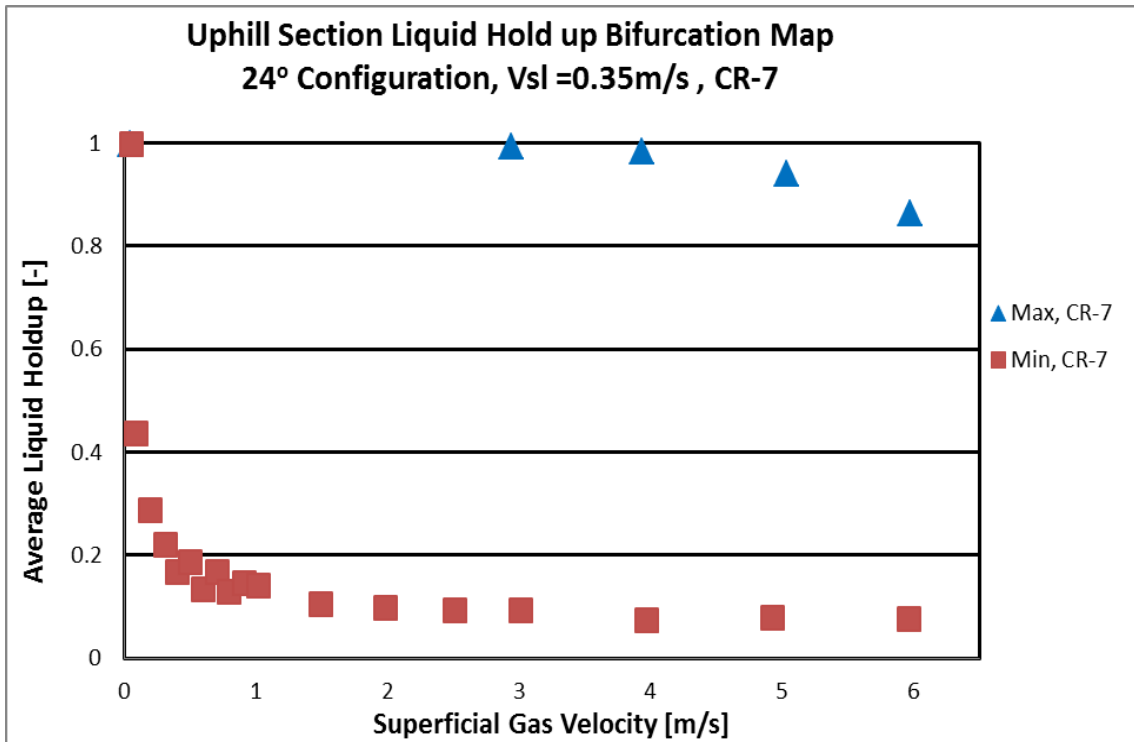
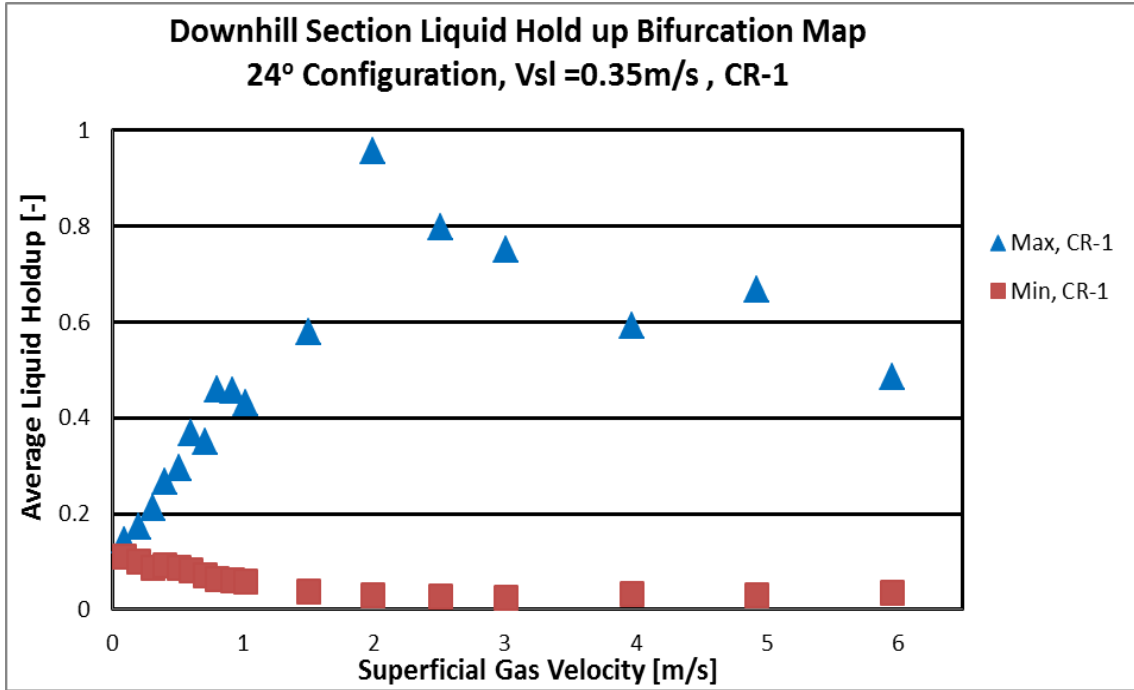


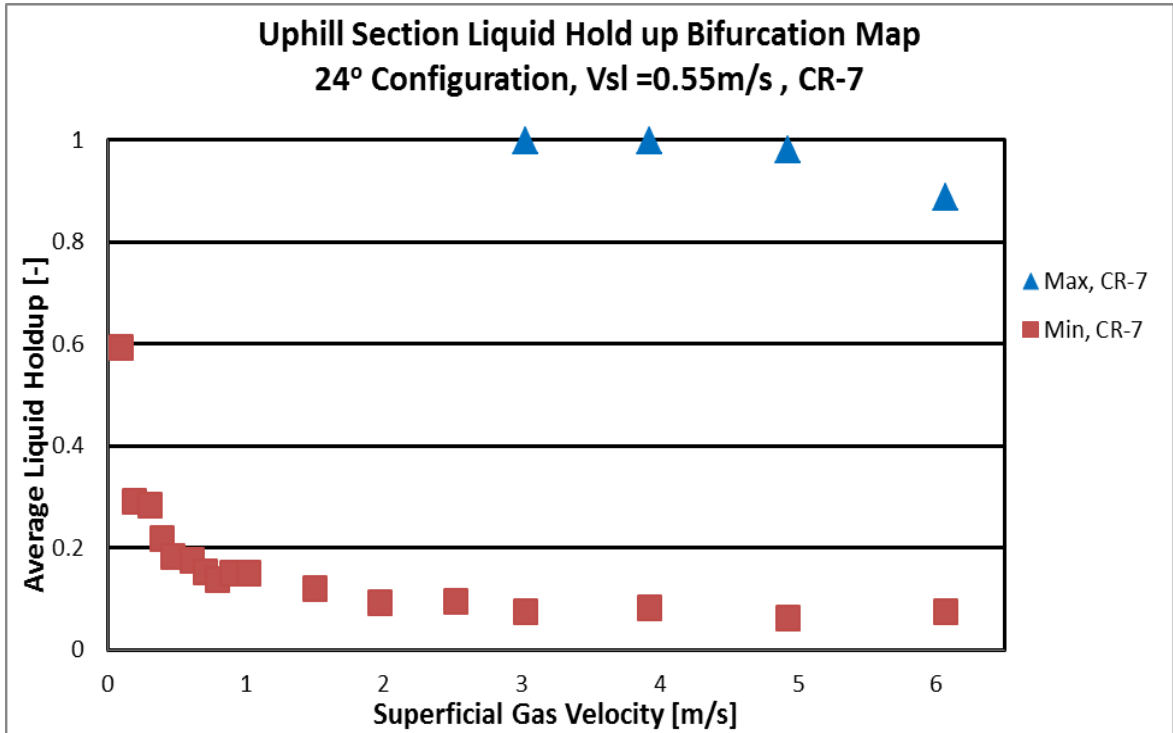
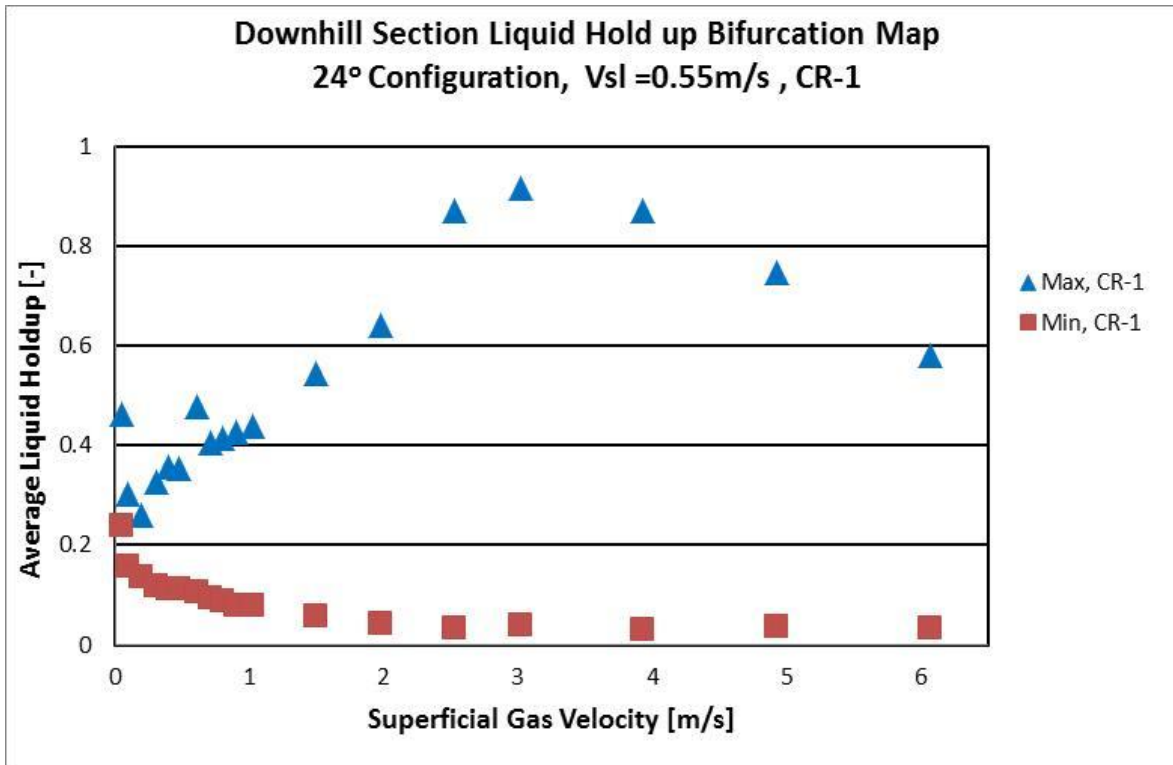
## Appendix C : Air-Water Flow Behaviour Analysis

### C.1 : Bifurcation Map of Air-water flow in 2-inch 24° Configuration



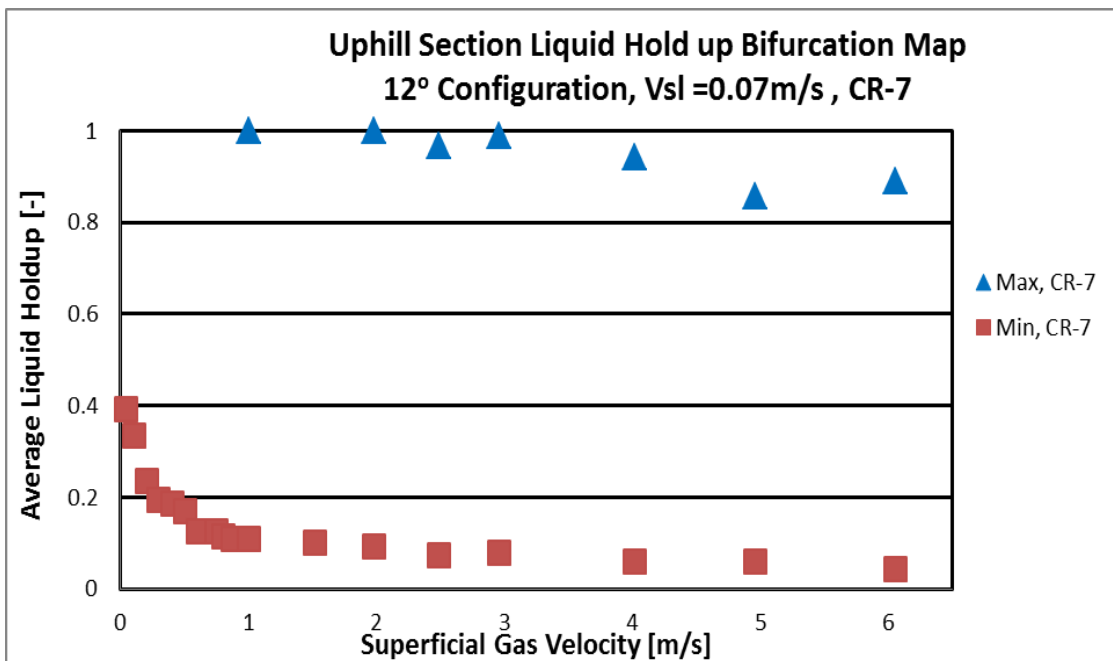
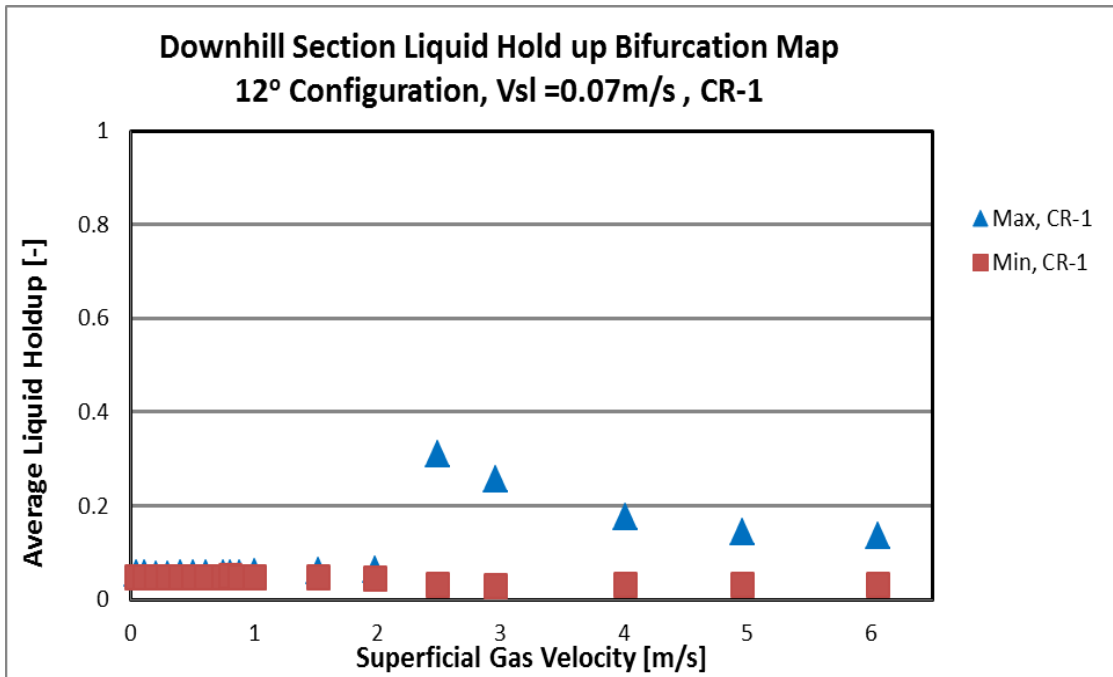


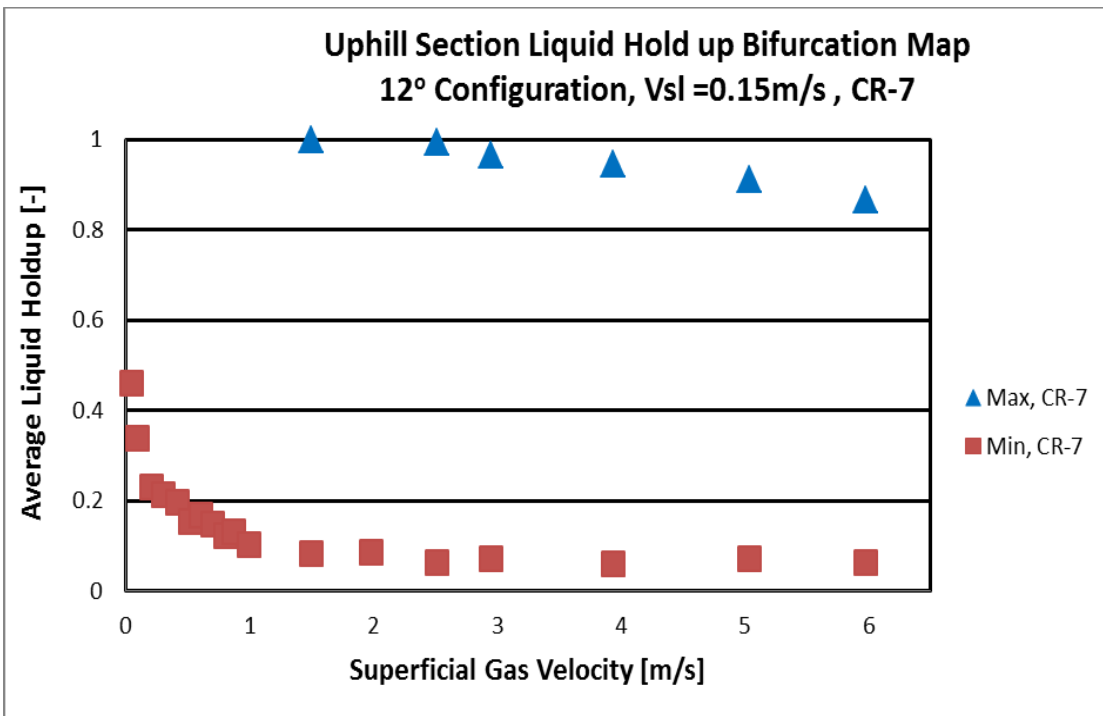
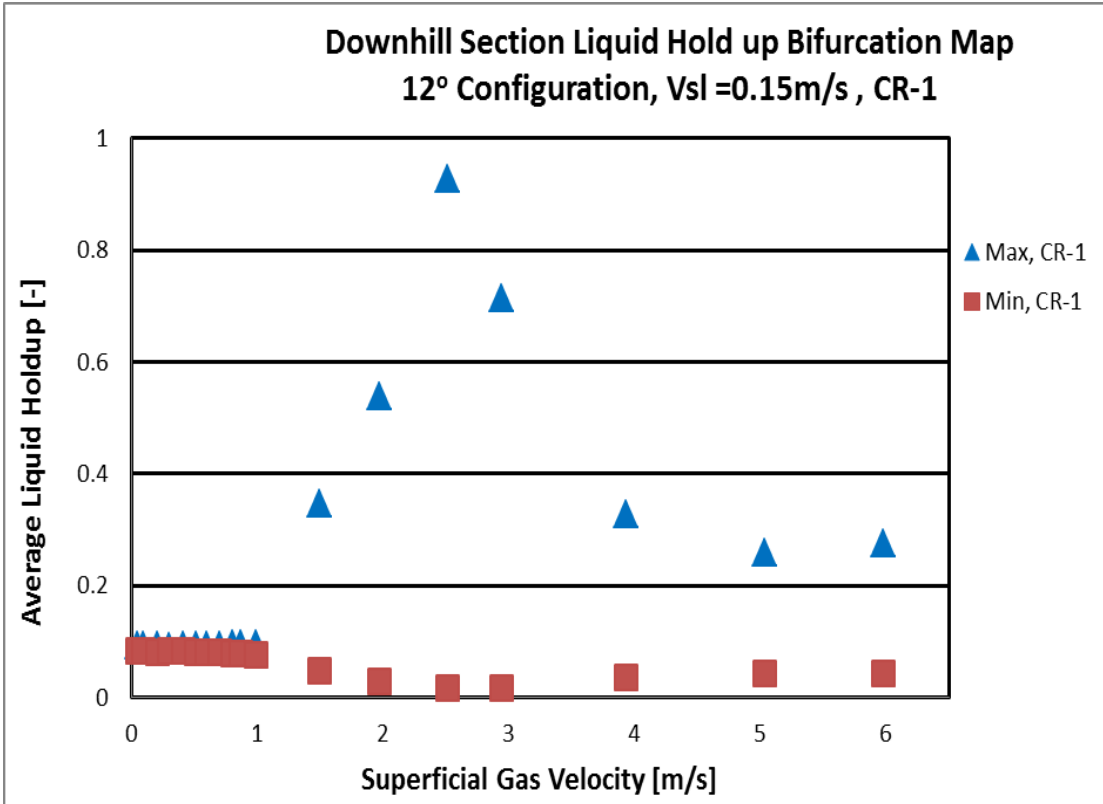


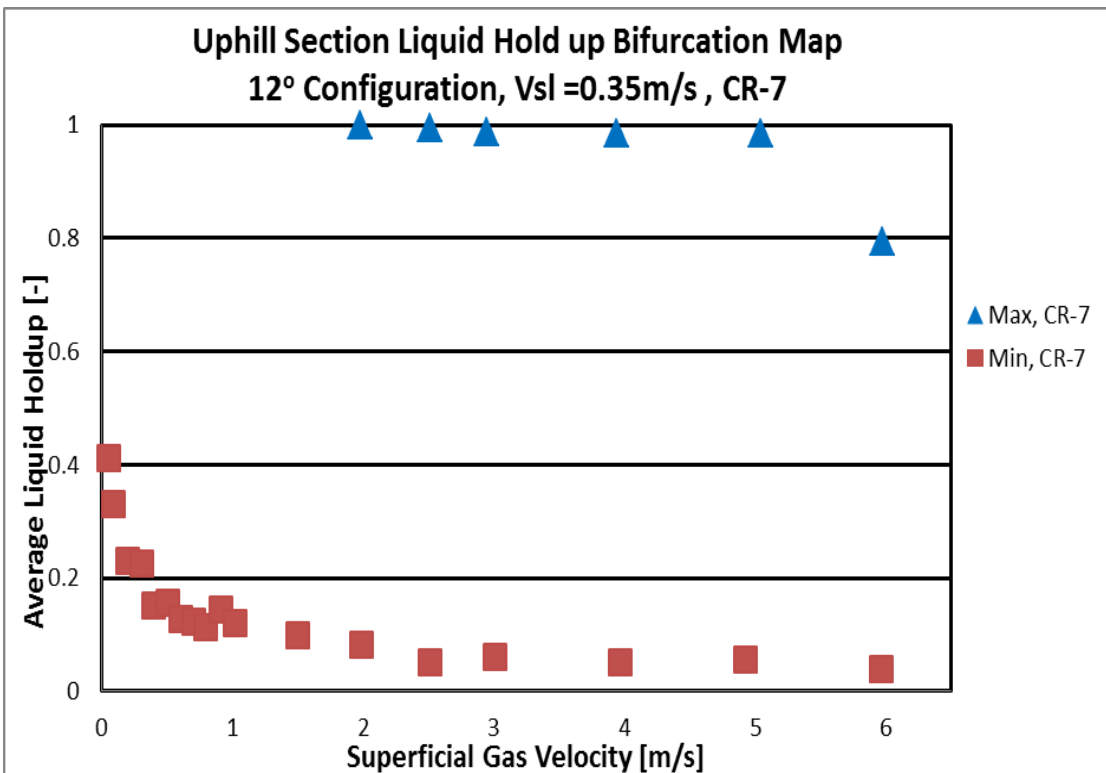
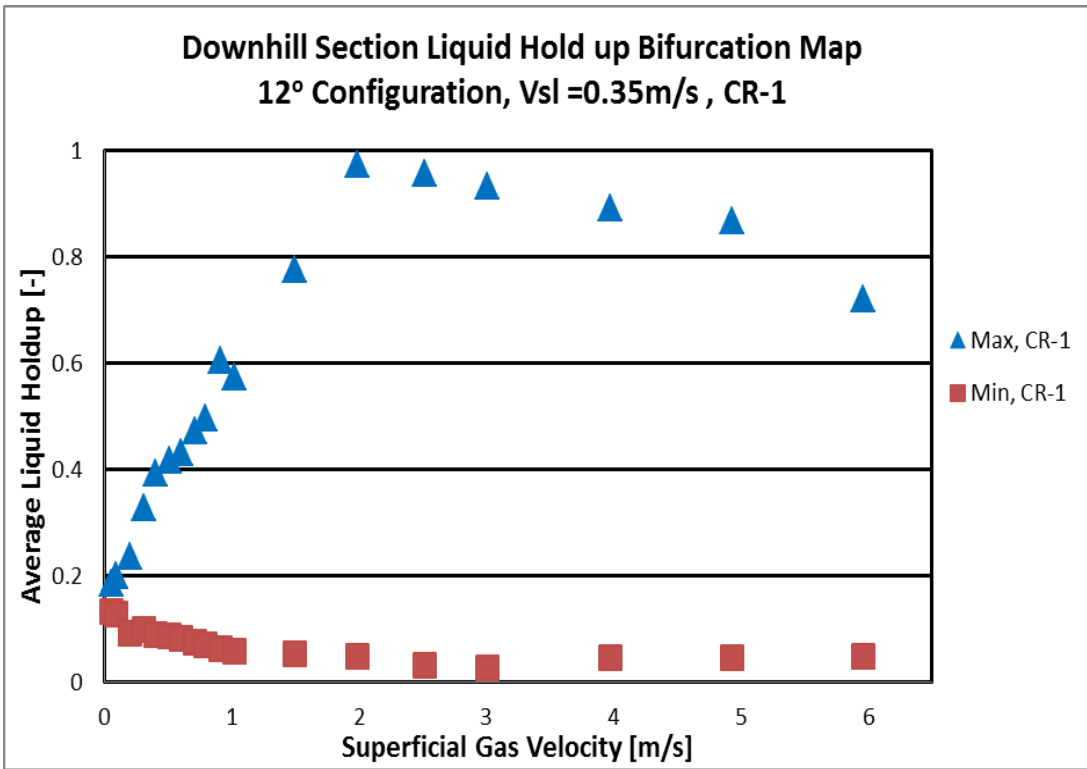




## C.2 : Bifurcation Map of Air-water flow in 2-inch 12° Configuration







### **C.3 Statistical Analysis of Slug Flow in 2-inch 24° Test Section**

Figure C1- 1 and Figure C1- 2 present the threshold profile for the conductivity ring at the dip (CR-5) and downstream uphill section (CR-8). The results showed that there are deviations as the superficial gas velocity increases. This is due to the presence of energetic wave being discriminated as slug at lower threshold

Therefore, a sensitivity test is performed for various thresholds in order to determine the optimal threshold. Standard deviation was carried out at different flow conditions to measure the variation or spread from the mean slug holdup distribution. This approach has been used by (Nydal et al., 1992) to discriminate between the developed and non-developed slug.

The result of the standard deviation of slug hold up data for CR-8 is used because waves in uphill flow regime are easily discriminated compared to dip section.

Figure C1- 3 shows that the standard deviation increases as the threshold level decreases for all flow conditions because the low threshold will consist of low liquid holdup and resulted to a wider spread.

From the result, standard deviation increases as gas velocities increase and later decreases. The decrease in standard deviation at a given threshold is as a result of the slug becoming aerated due to increase in gas flow rates.

Moreover, there is a trade off in the selection of threshold level between having the lowest standard deviation and being able to account for the slug in the pipe. The threshold ( $=0.7$ ) is considered here because it fairly accounts for slug occurrence more relatively than threshold ( $=0.8$ ) at high flow rate.

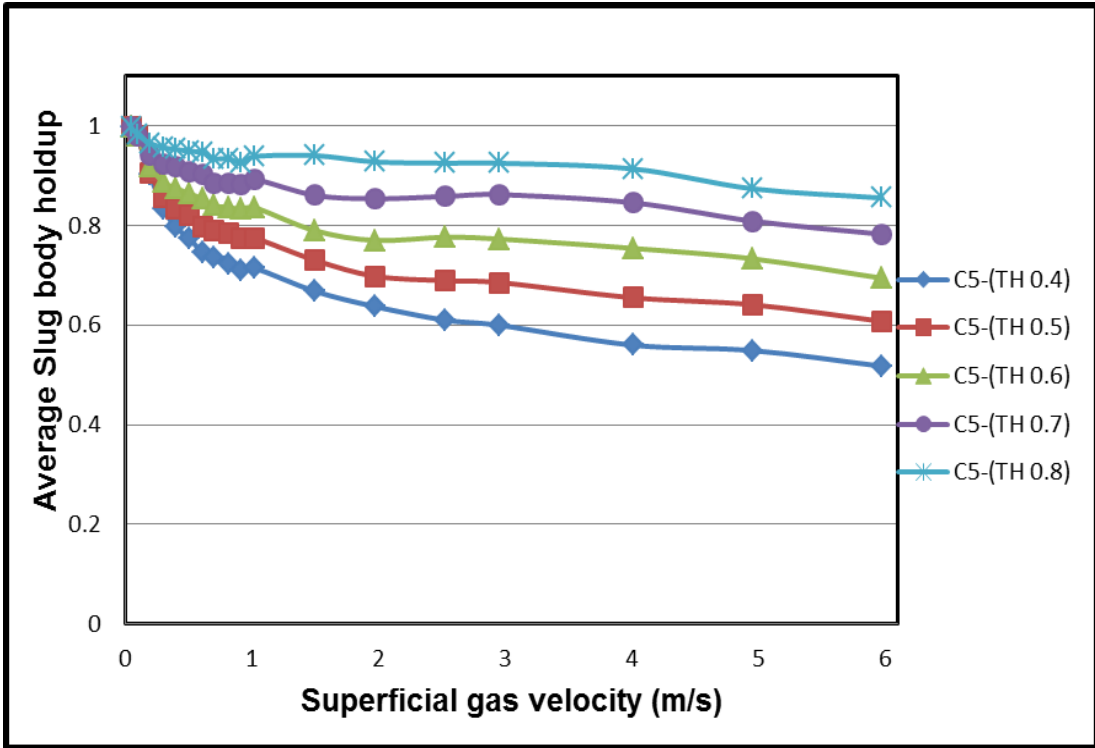


Figure C1- 1: Threshold profile for CR-5 at Vsl=0.35m/s

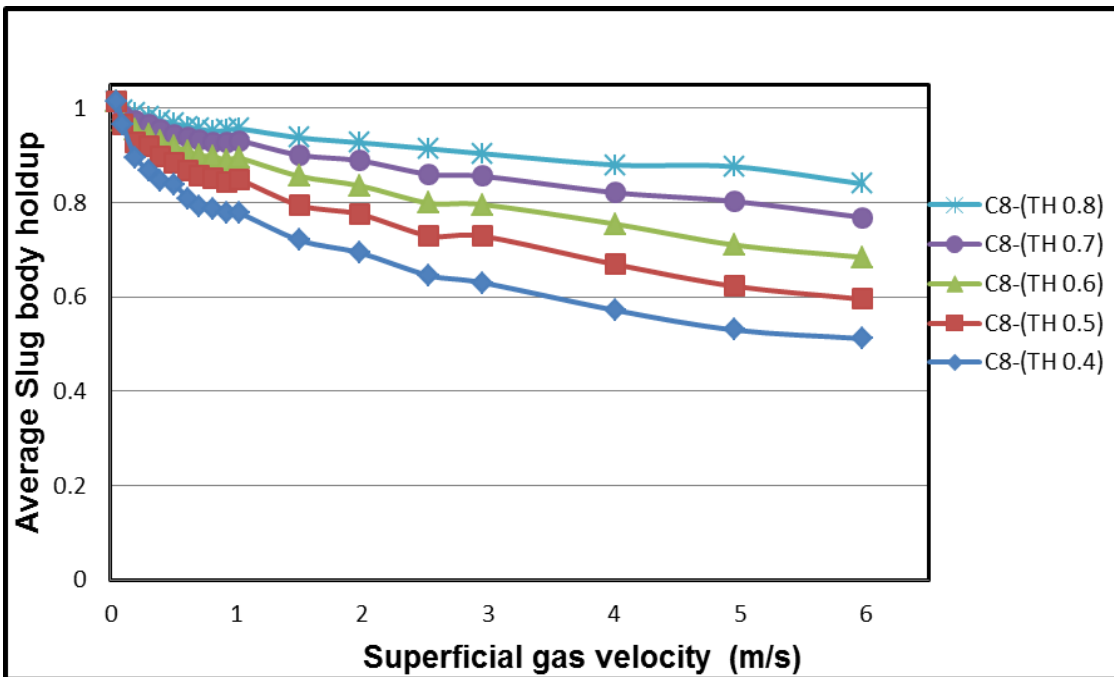


Figure C1- 2: Threshold profile for CR-8 at Vsl=0.35m/s

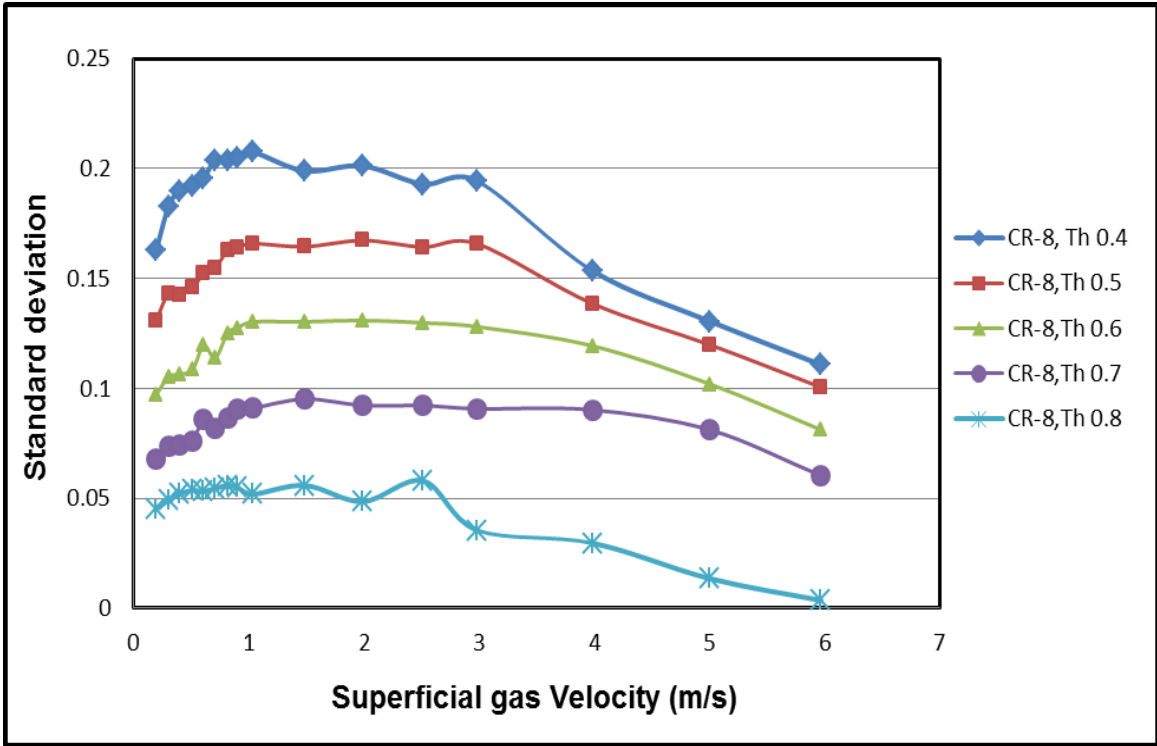
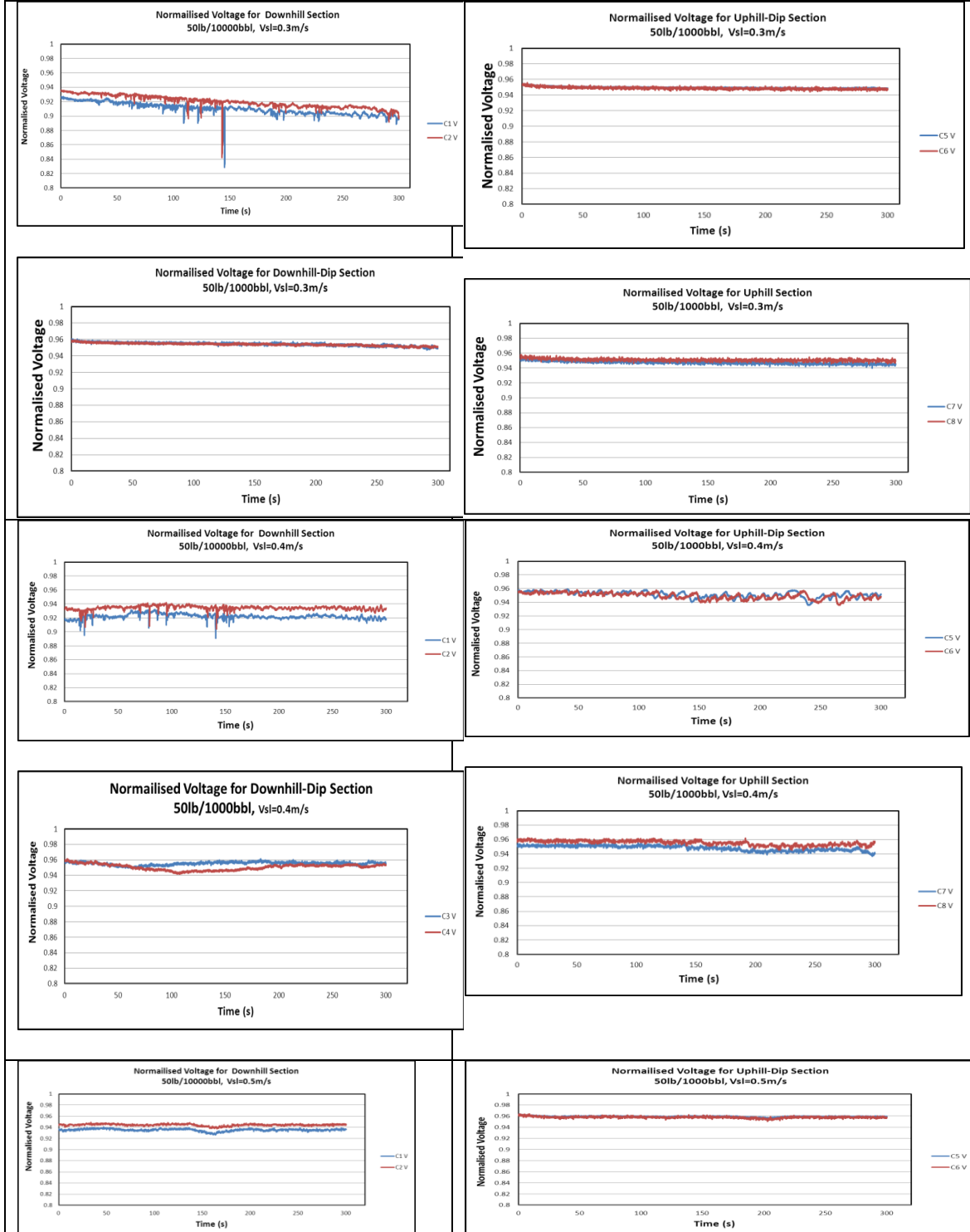
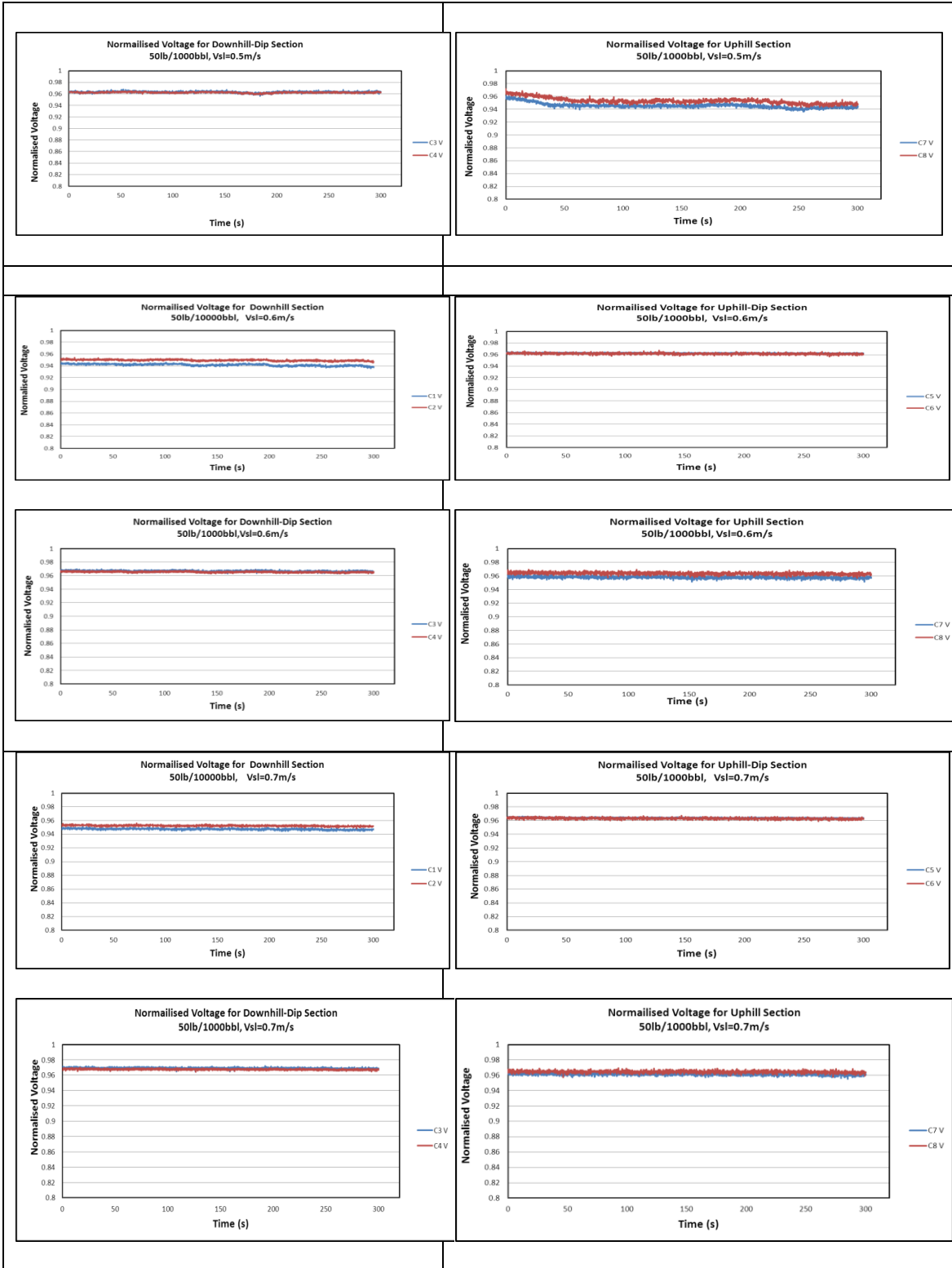


Figure C1- 3: Standard deviation of slug holdup at different thresholds

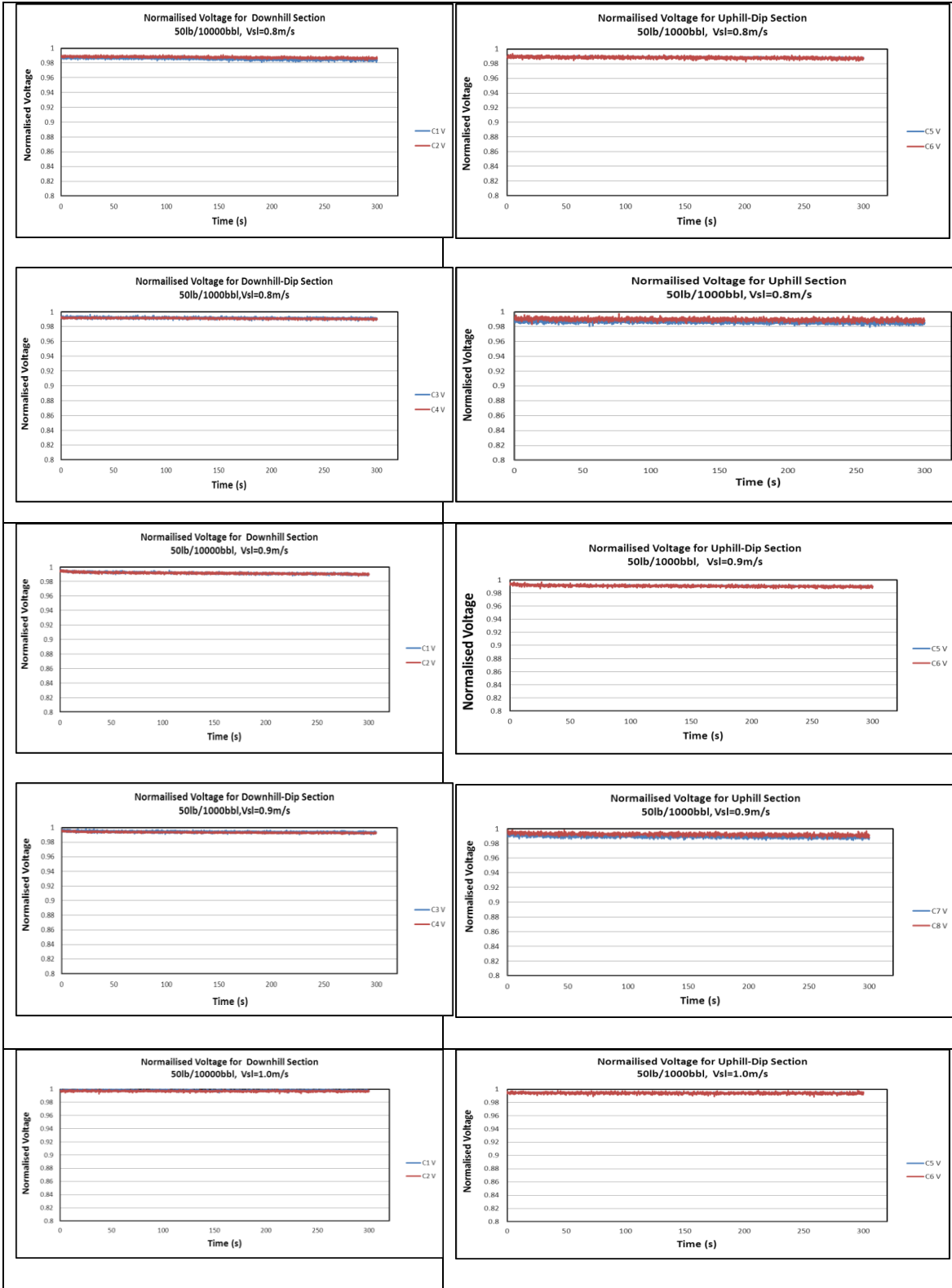
# Appendix D : Conductivity Measurement

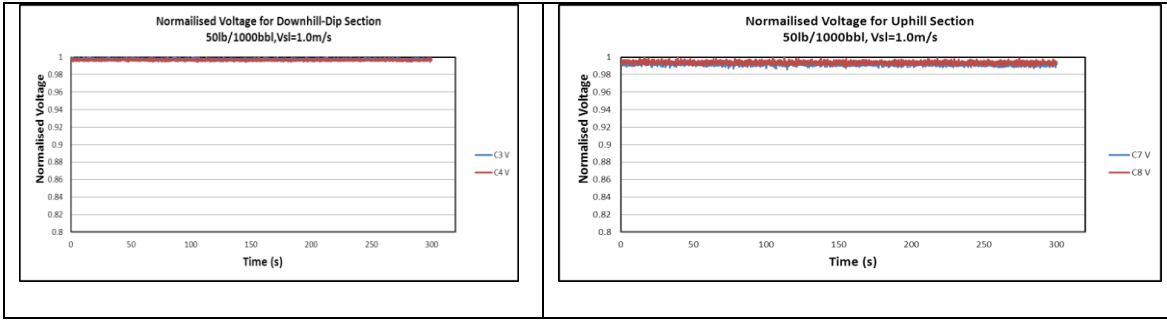
## D.1 : Normalised Voltage for 50lb/1000bbl



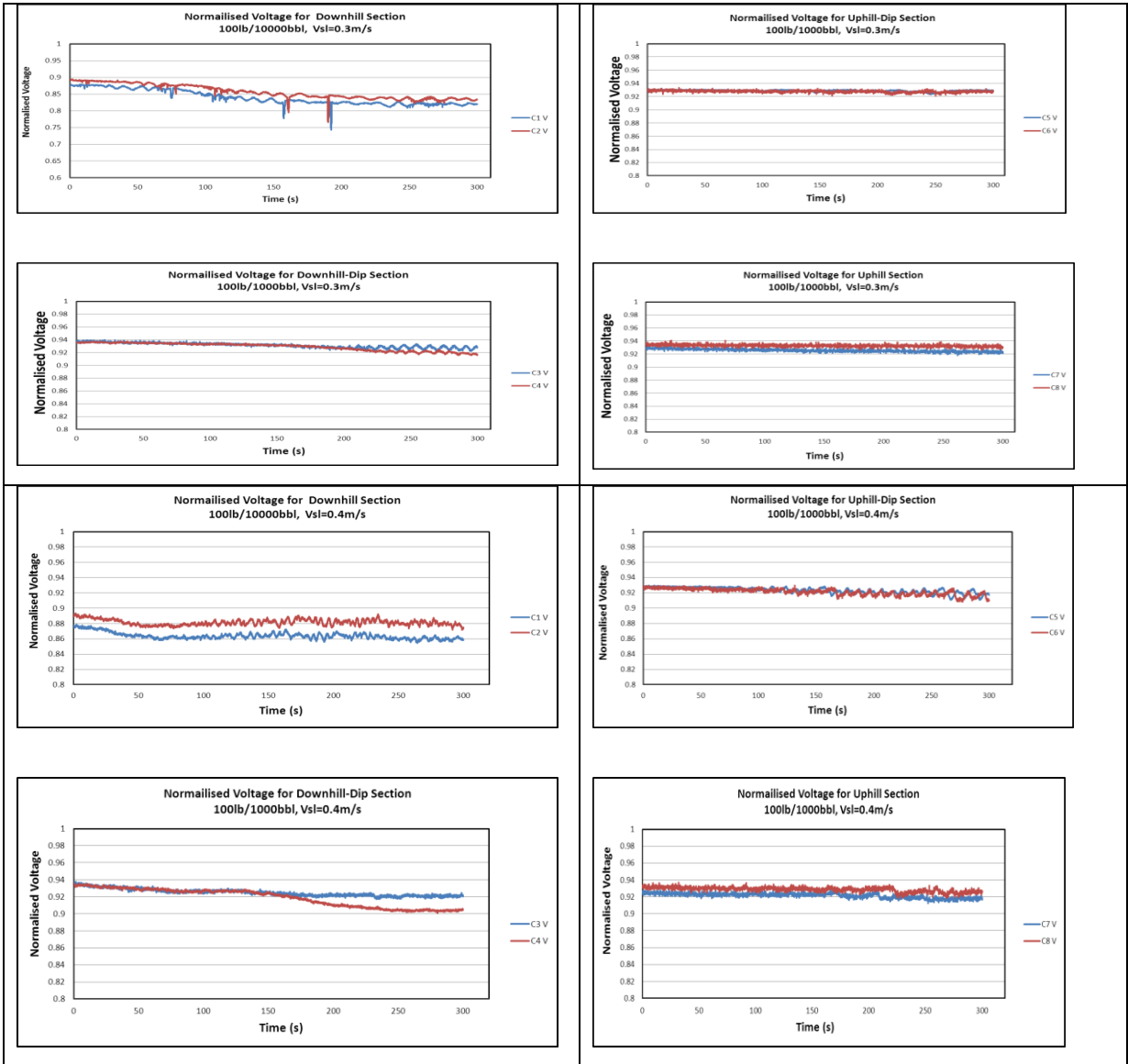


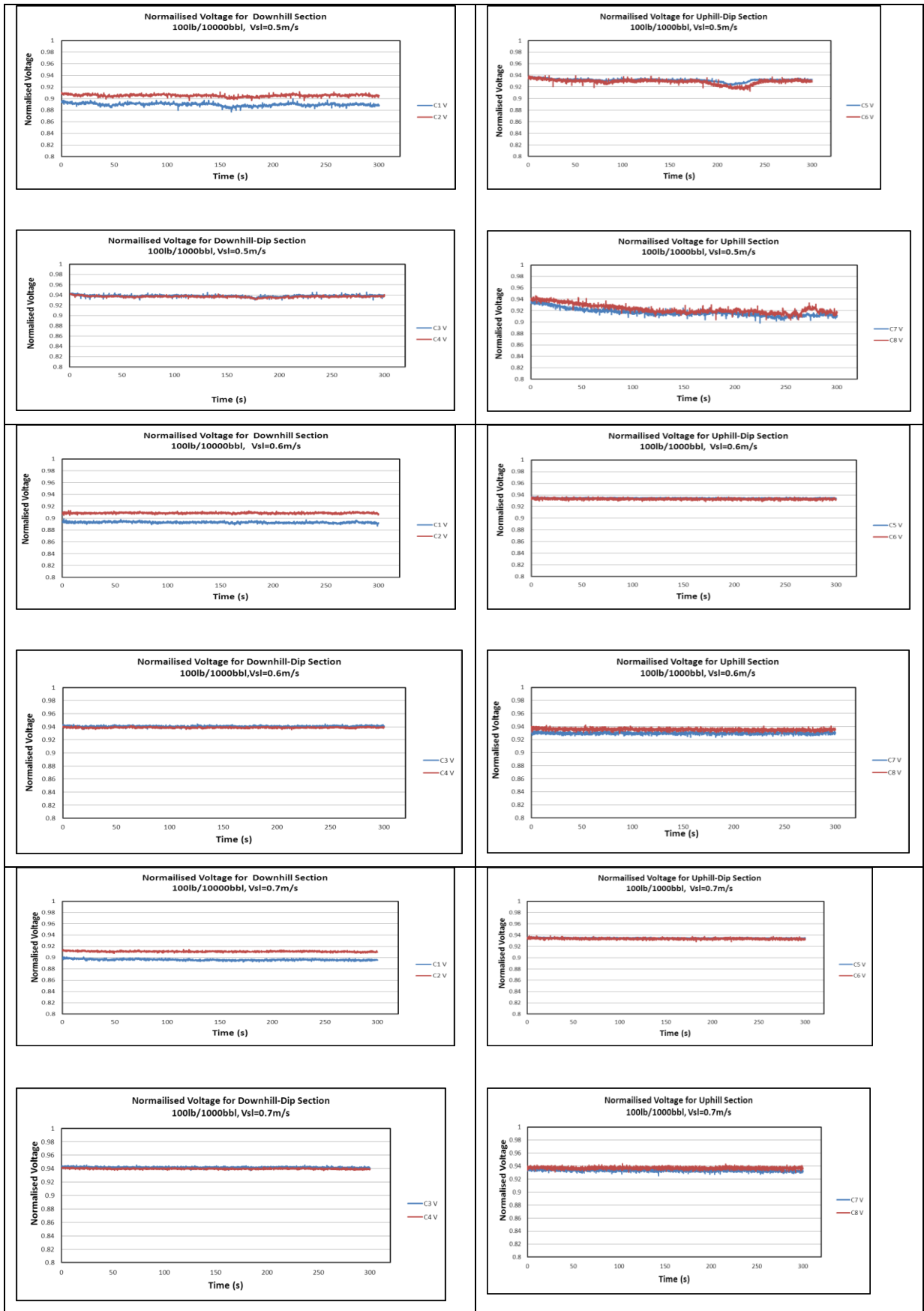


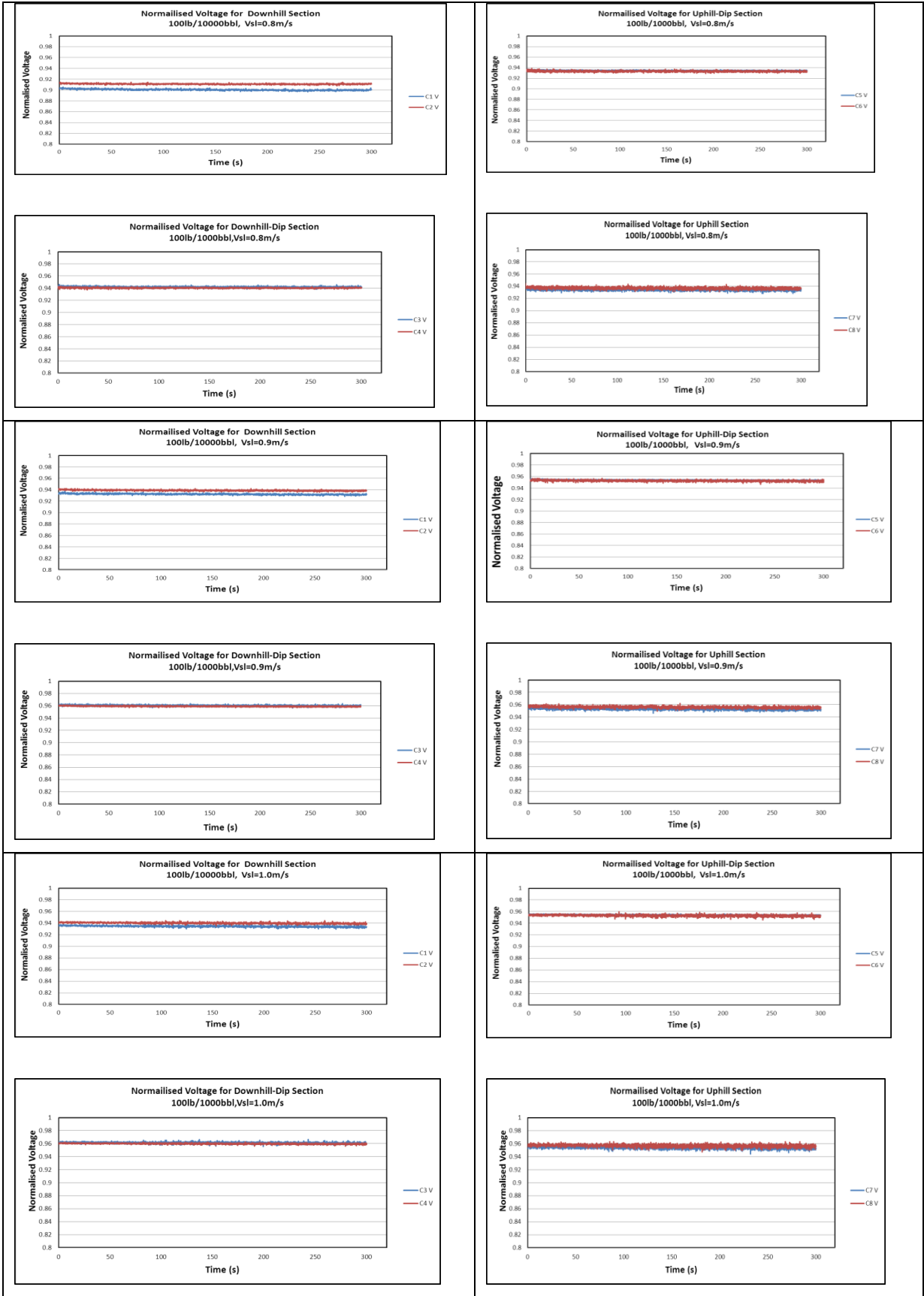




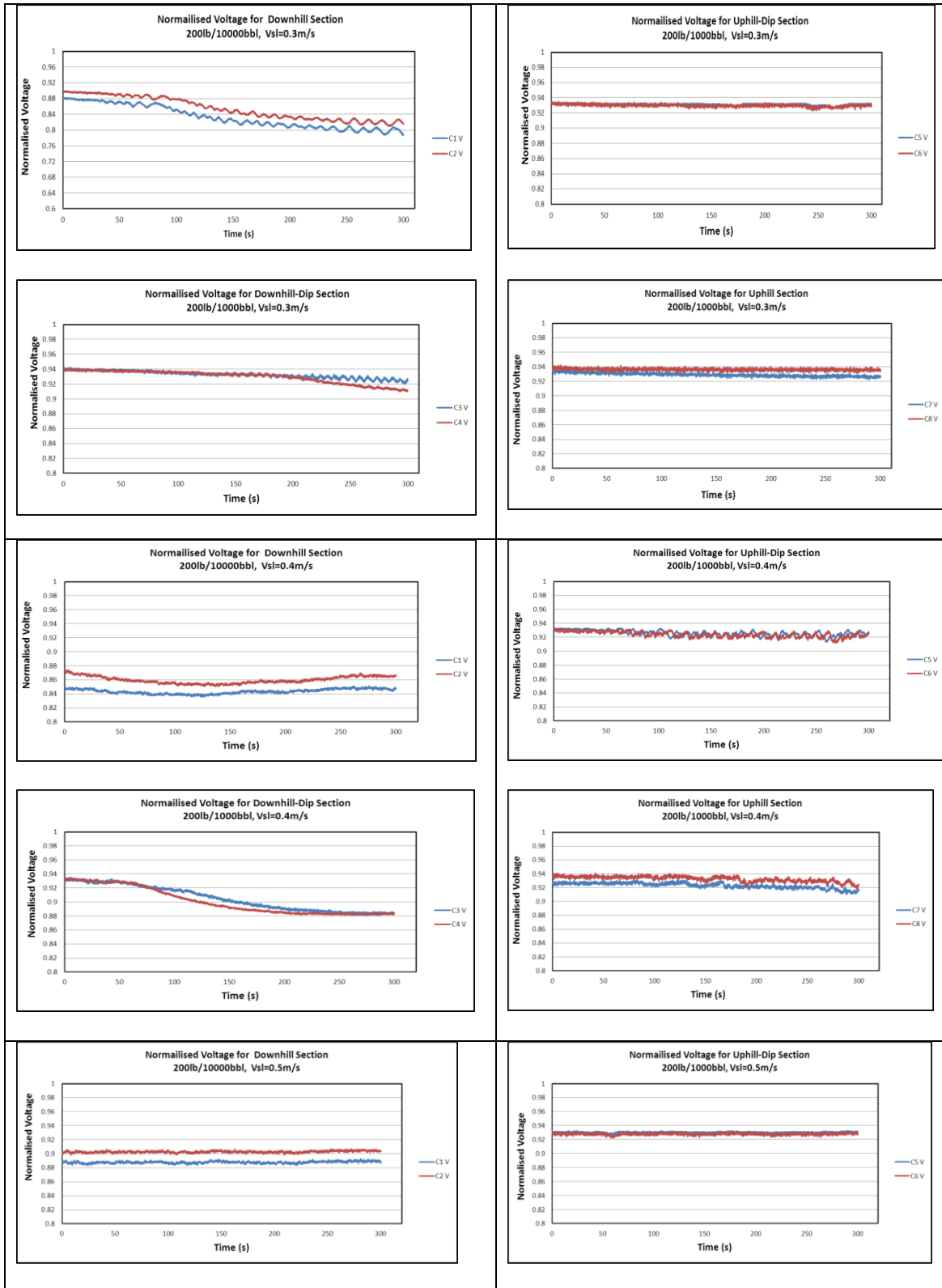
## D.2 : Normalised Voltage for 1000lb/1000bbl

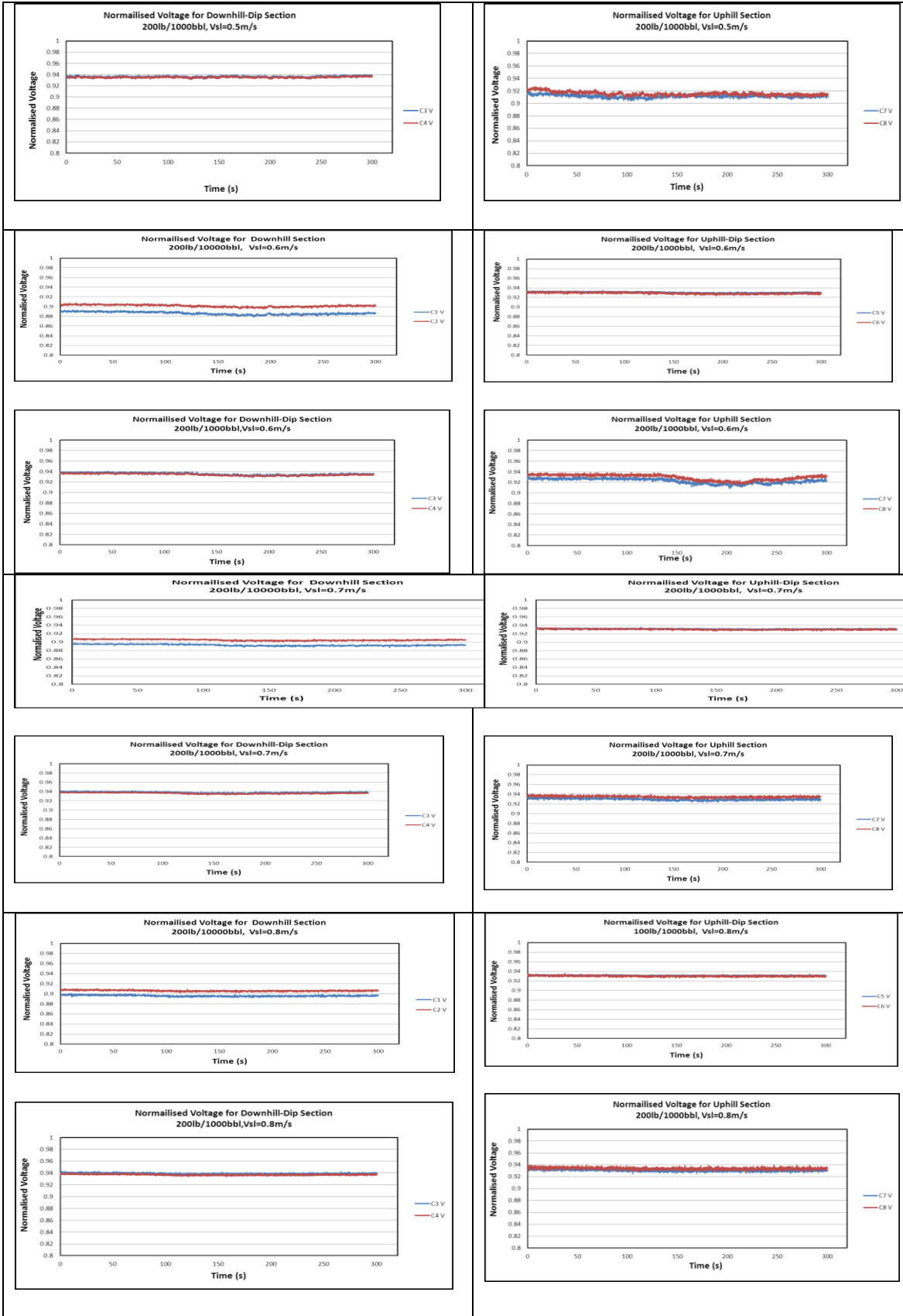


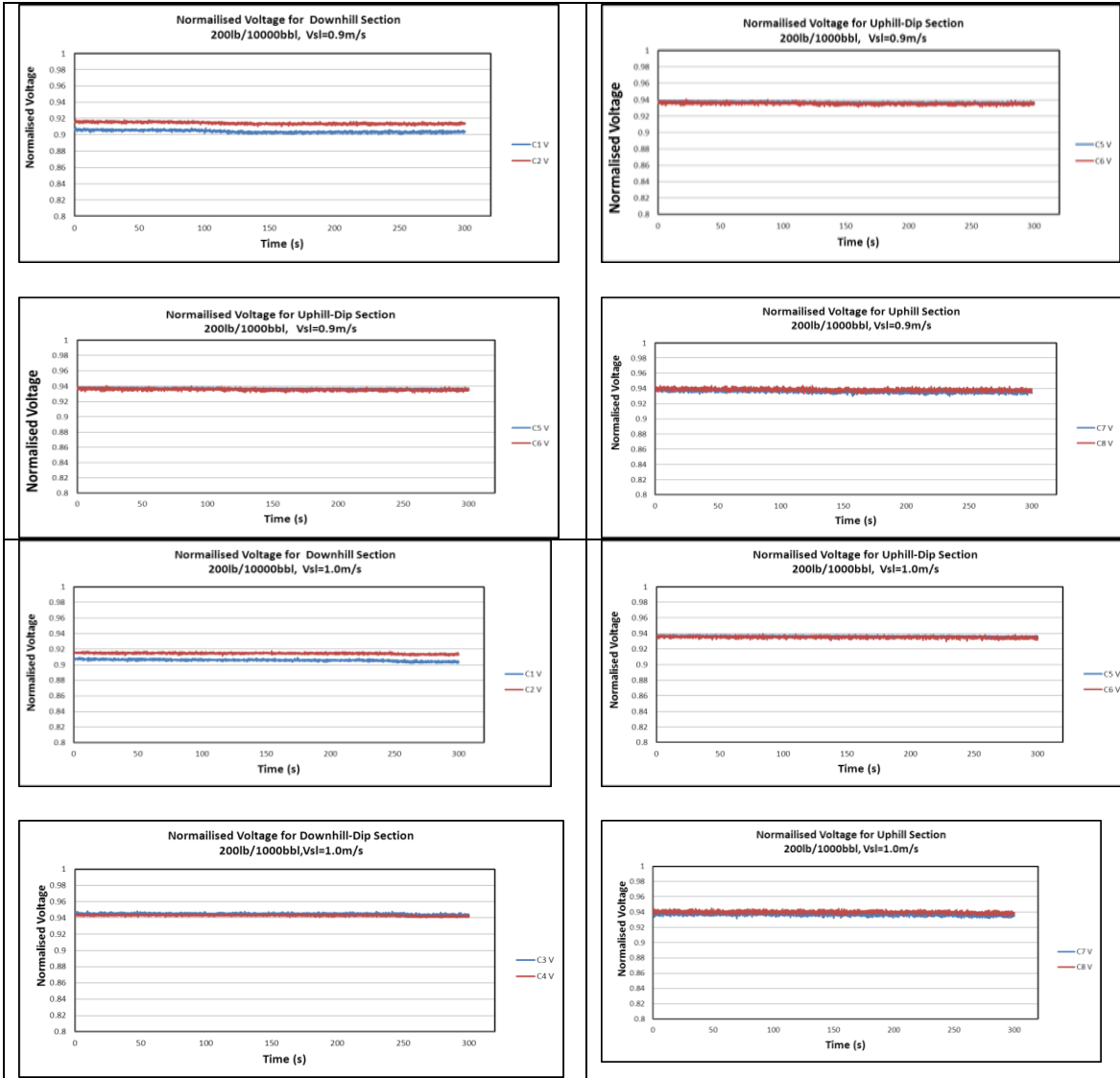




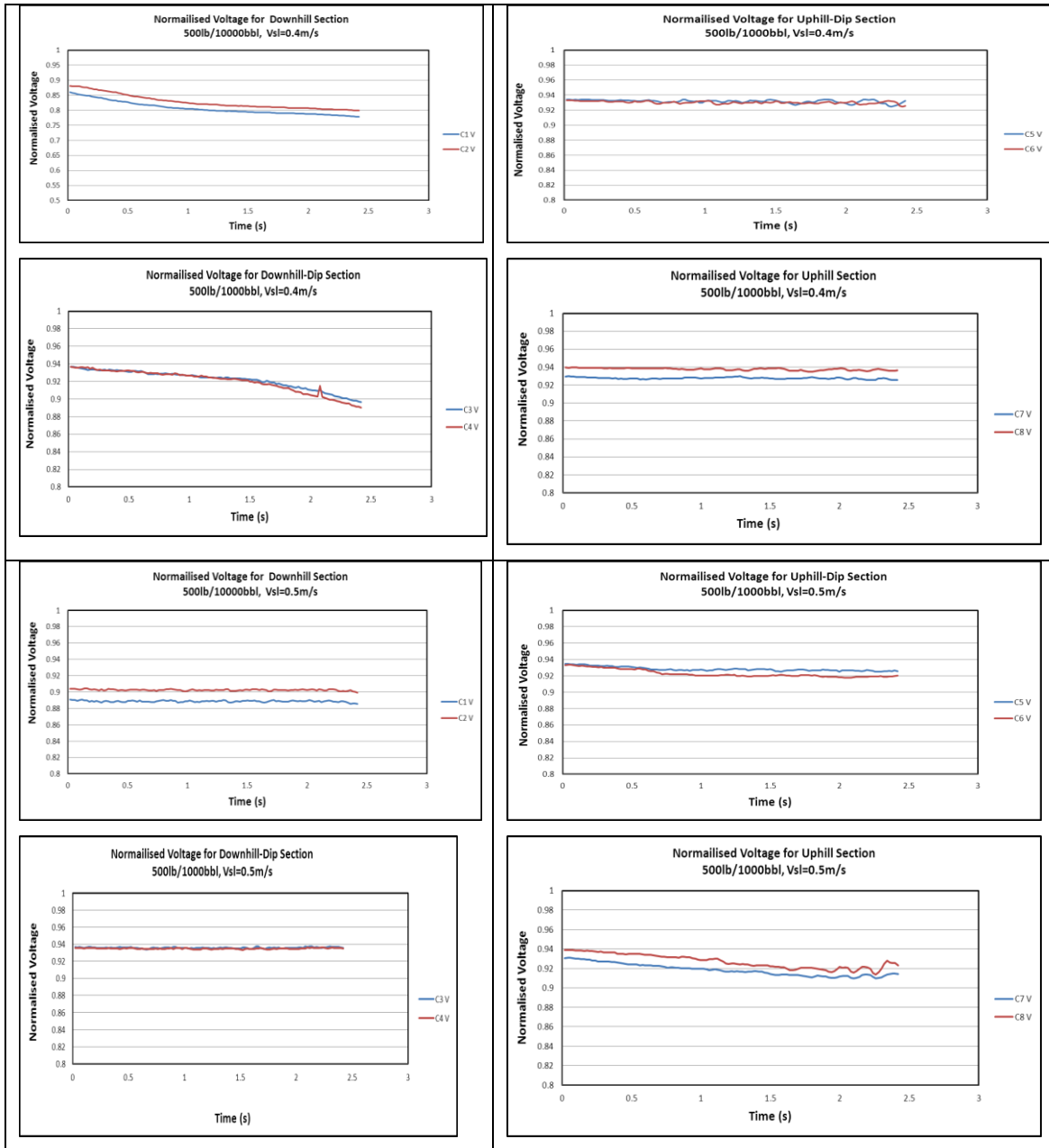
## D.3 : Normalised Voltage for 200lb/1000bbl





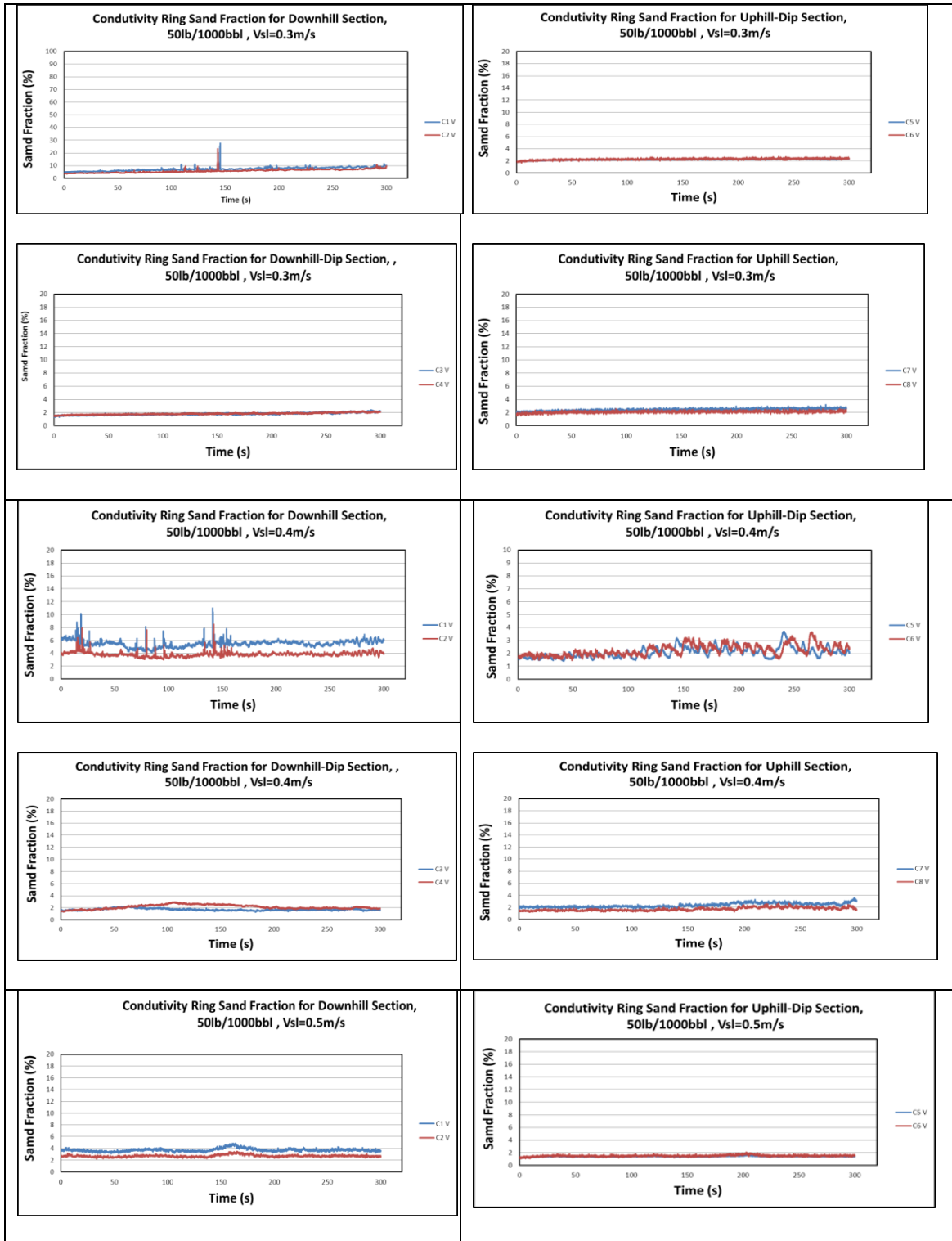


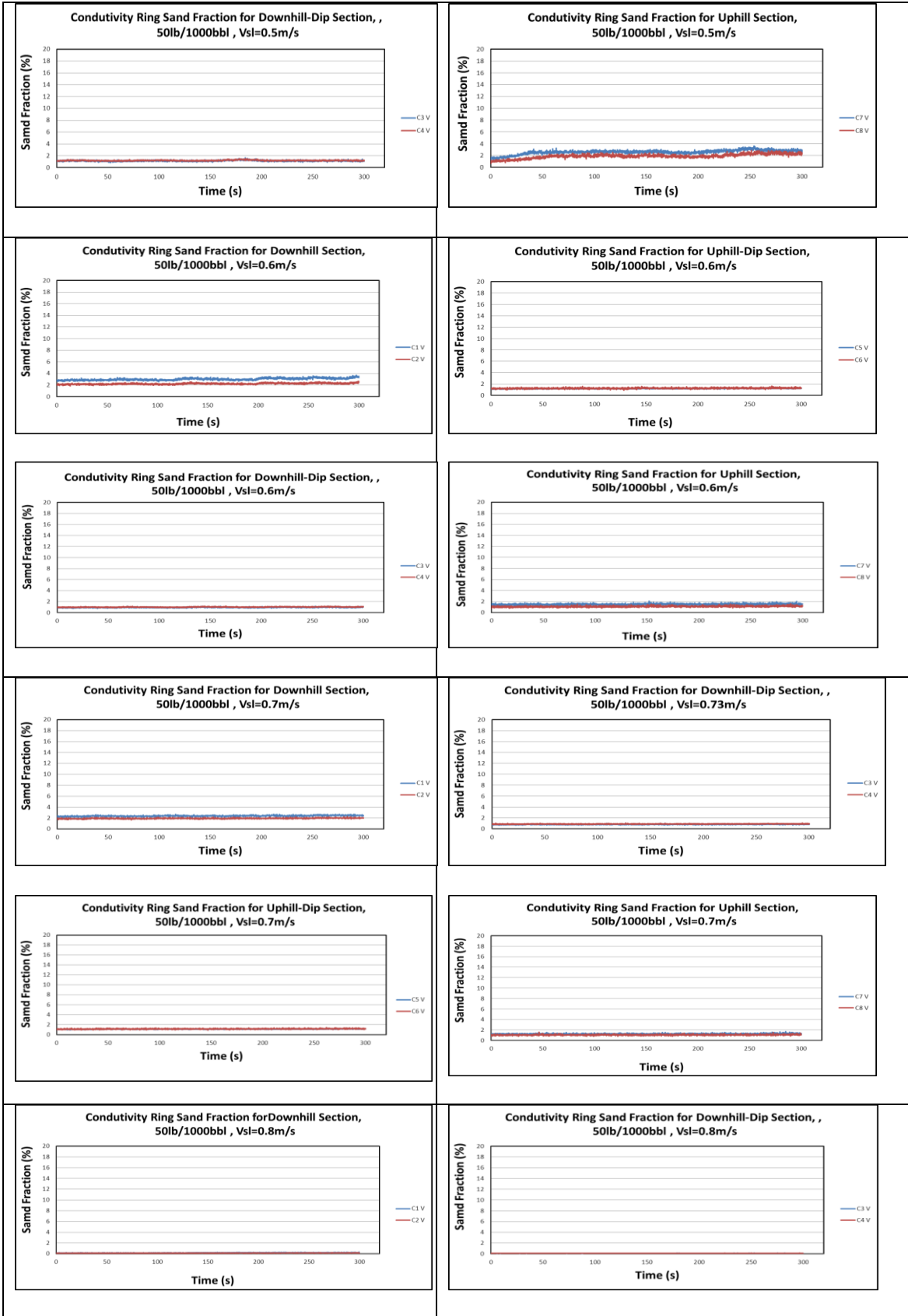
## D.4 : Normalised Voltage for 500lb/1000bbi

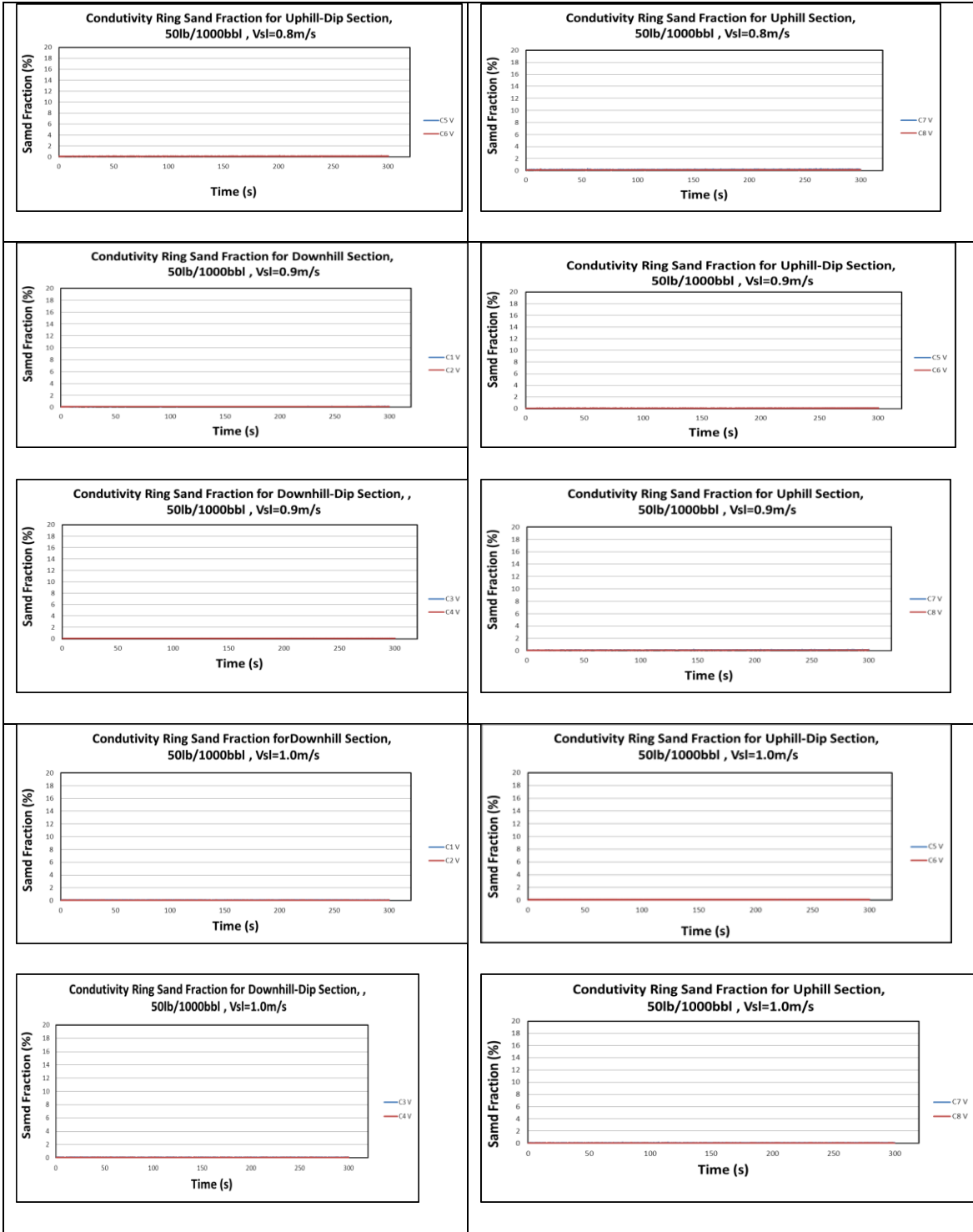




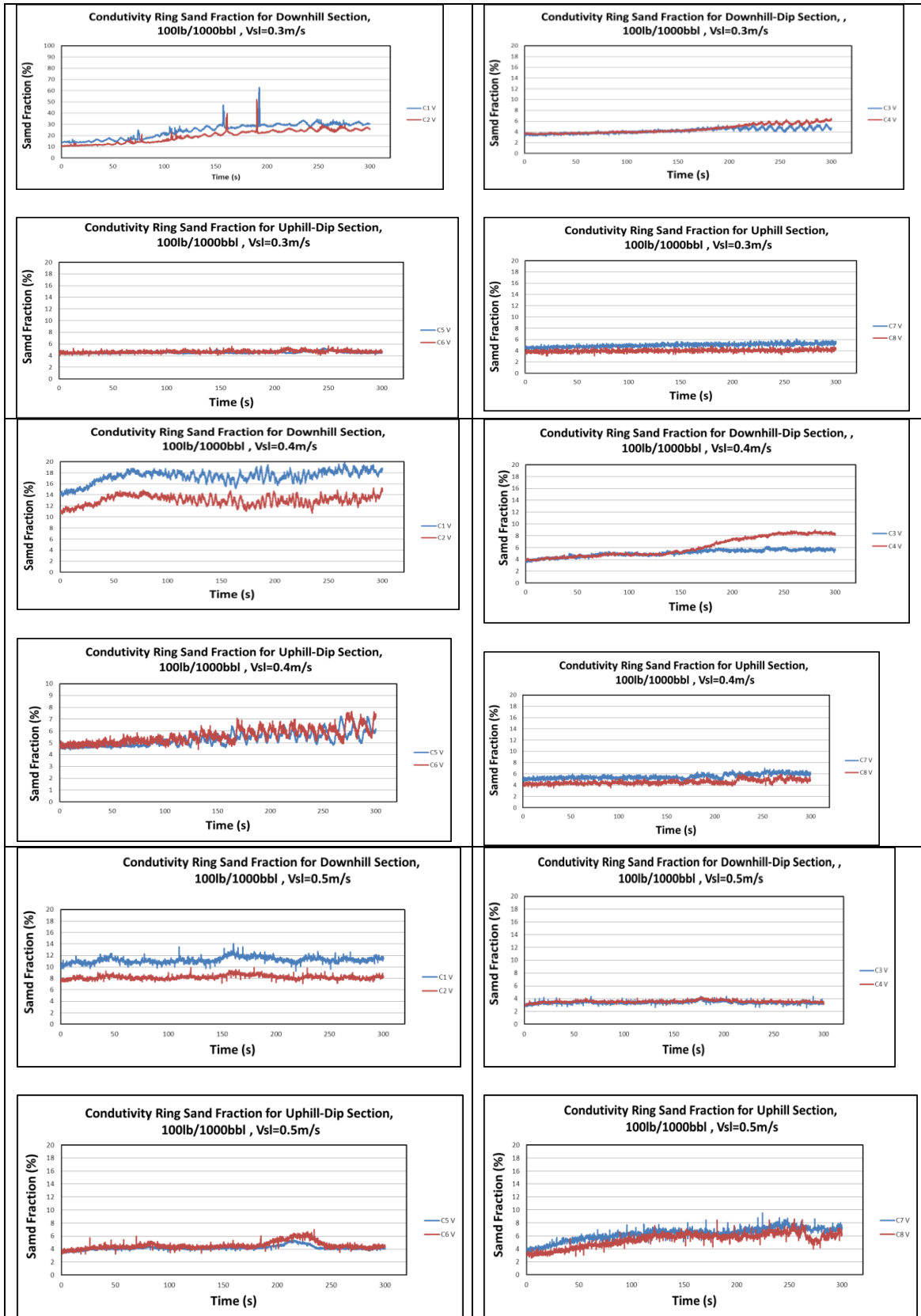
## D.5 : 50lb/1000bbl Conductivity Ring Sand Fraction

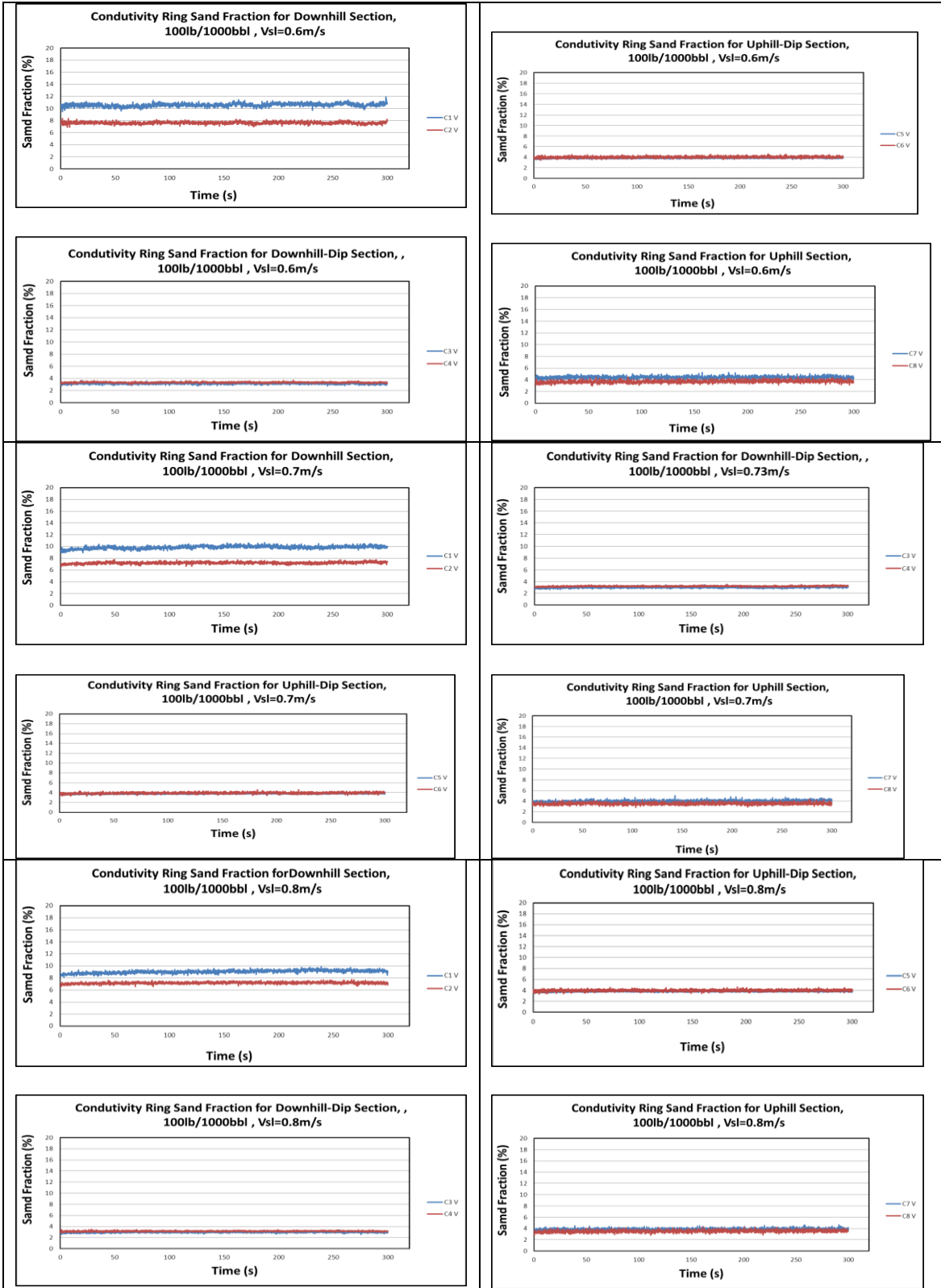


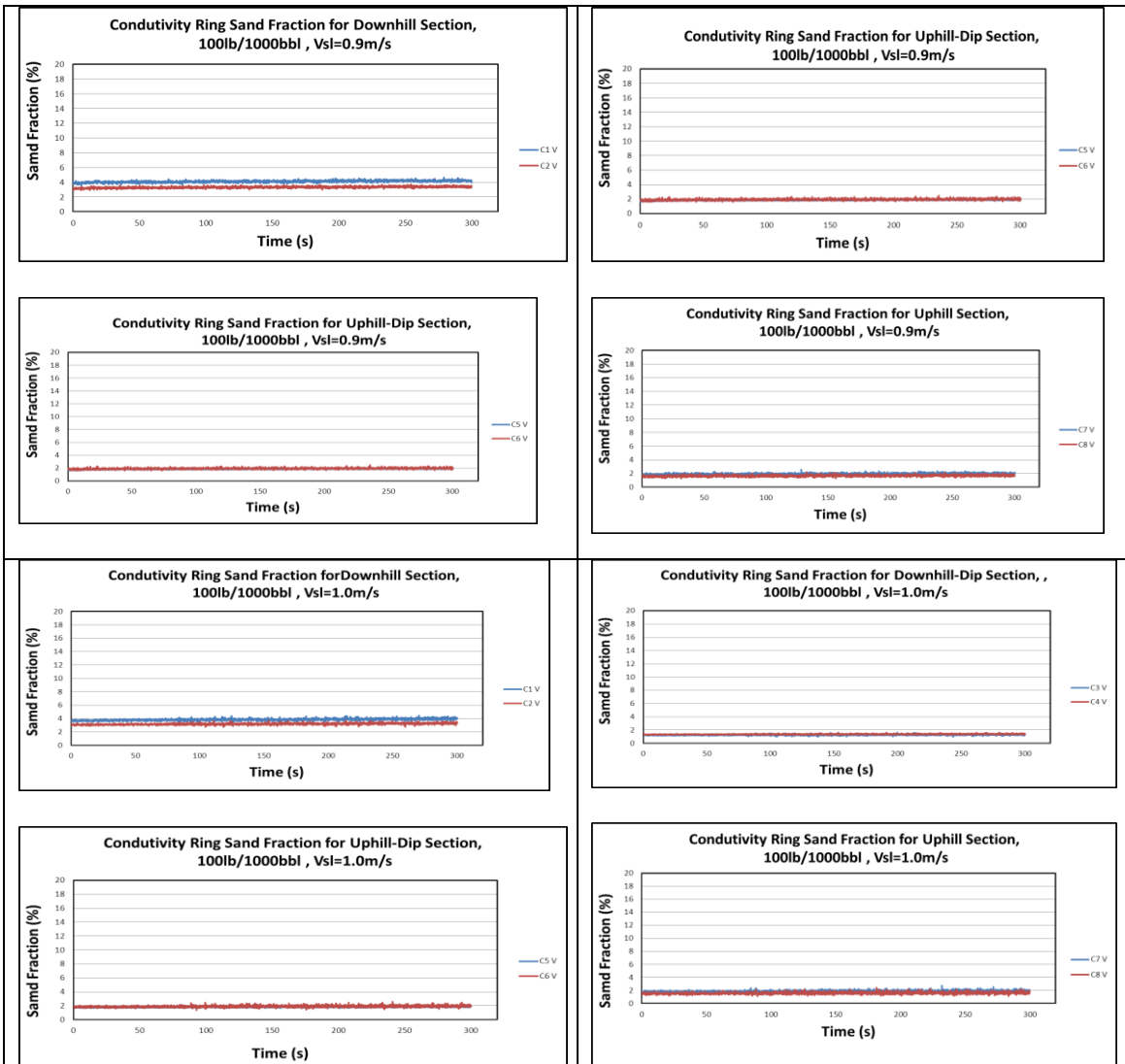




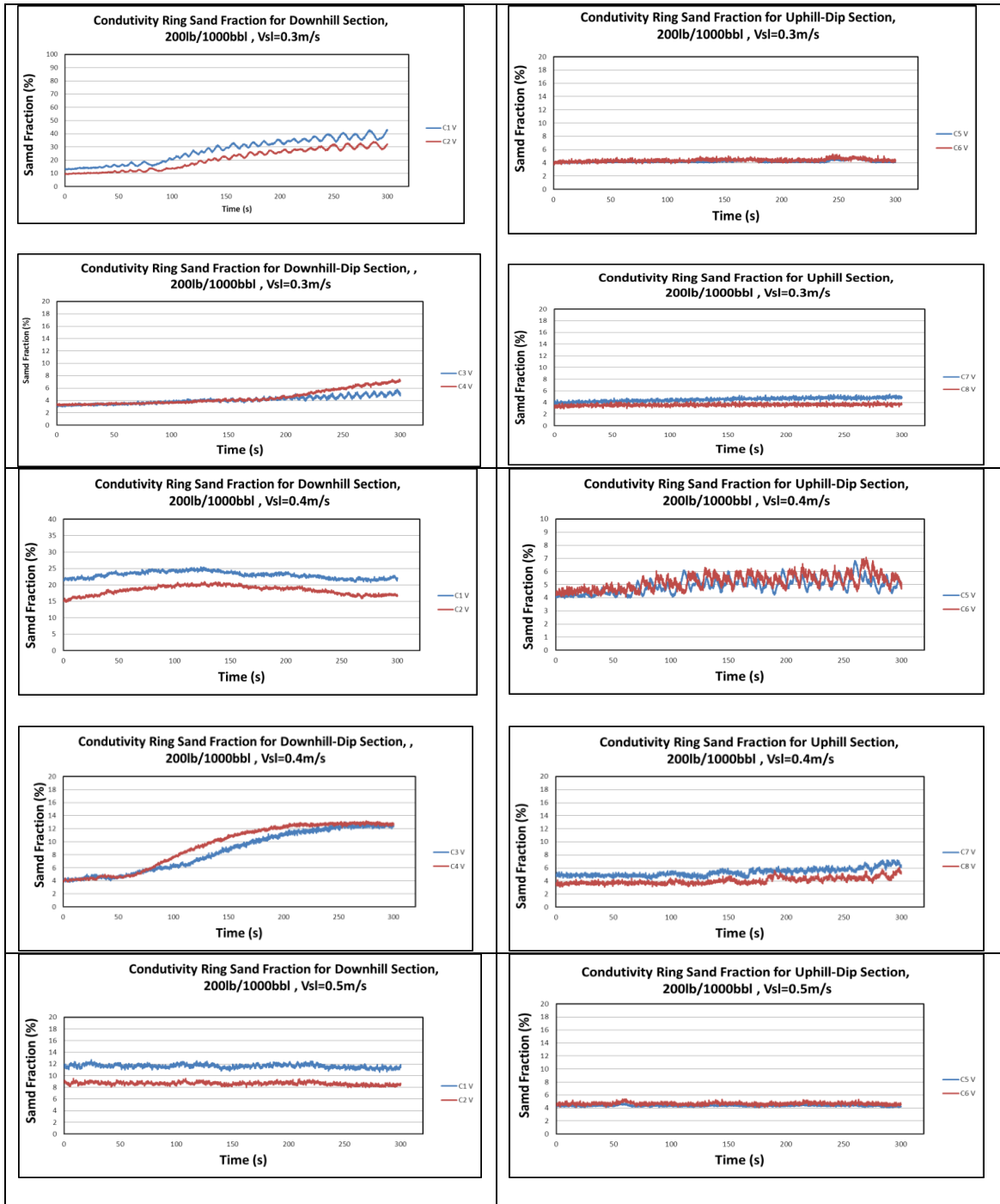
## D.6 : 100lb/1000bbl Conductivity Ring Sand Fraction

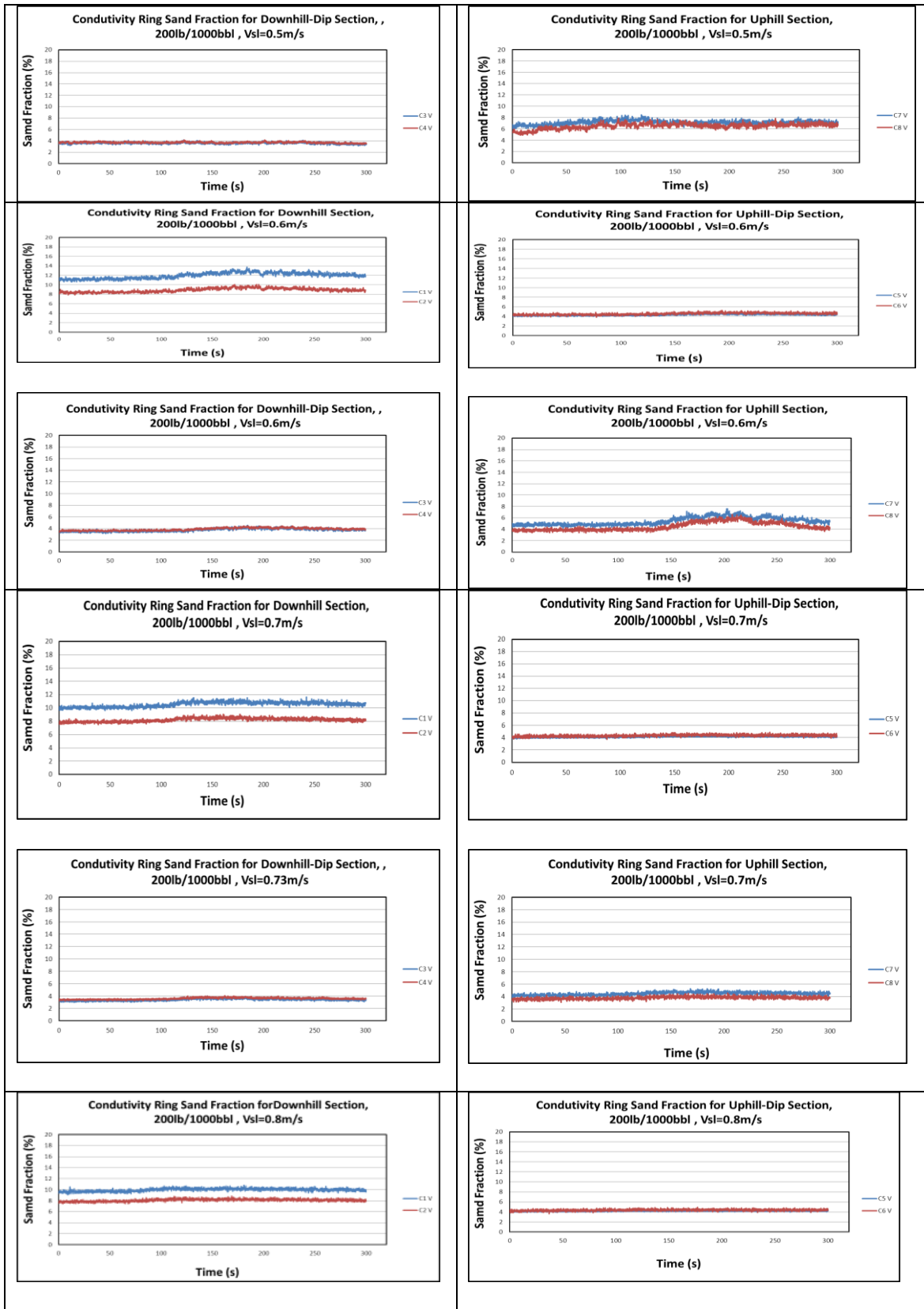




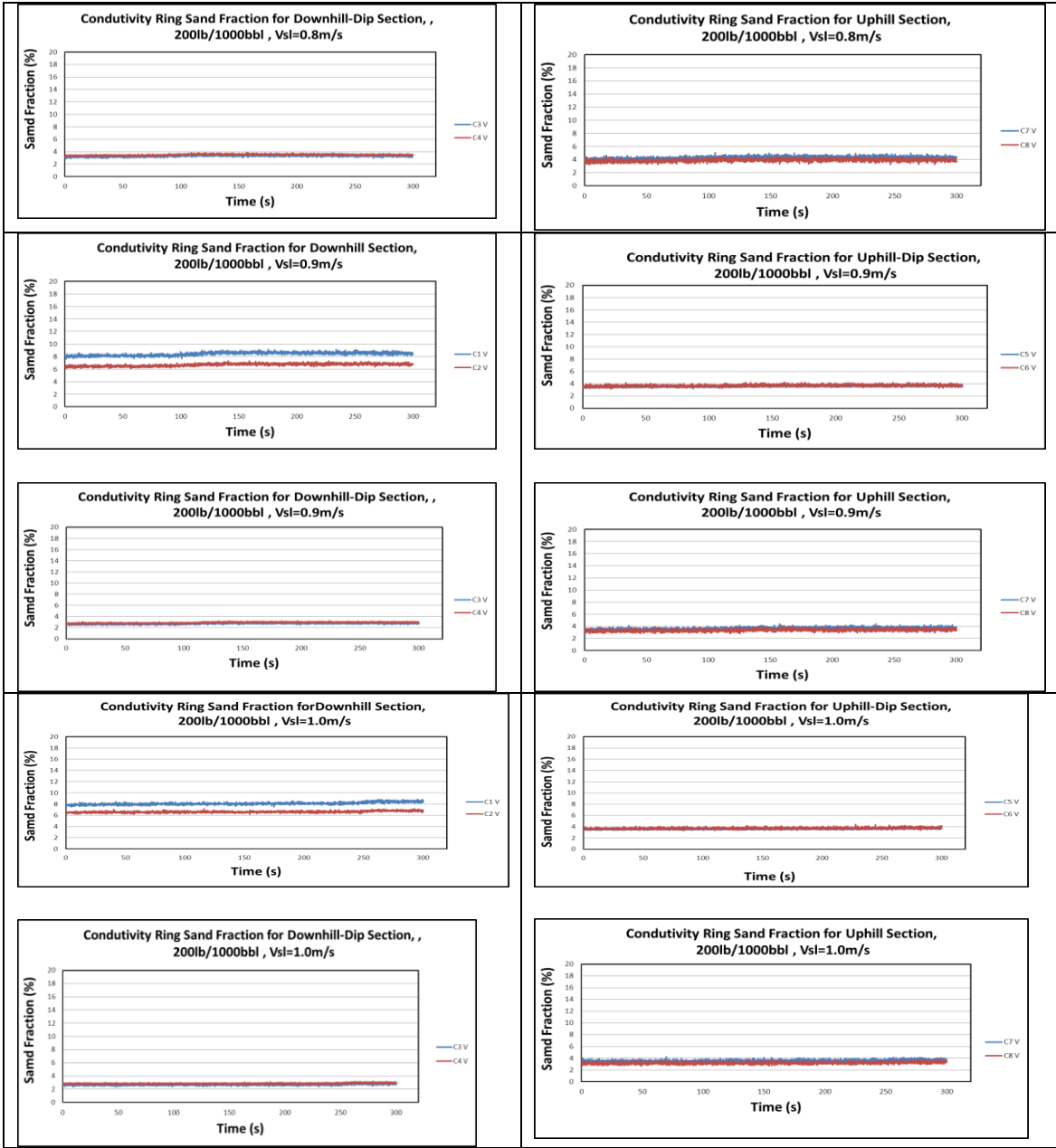


## D.7 : 200lb/1000bbl Conductivity Ring Sand Fraction

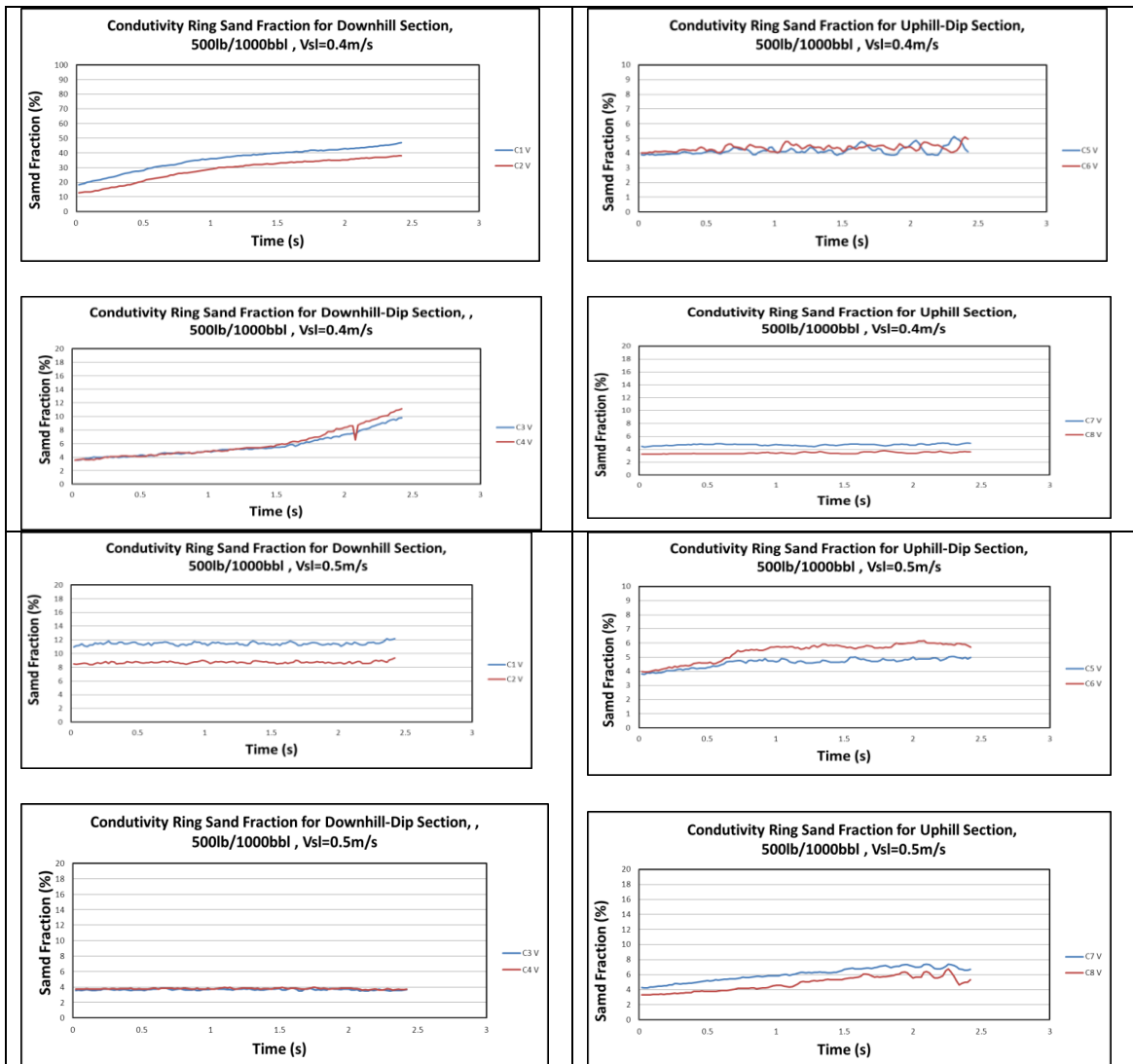















## D.8 : 500lb/1000bbl Conductivity Ring Sand Fraction







## Appendix E : Description of Sand Minimum Transport Condition in Single Phase Water Flow




**Table F- 1: Sand behaviour in water with the sand concentration of 50lb/1000bbl  
in the downhill section**

V <sub>L</sub> [m/s]	Sand Concentration 50 lb/1000bbl		
	Sand Particle size 270 micron		
	Downhill Section		
	MTC	Sand Behavior	Description
0.8	No		Active Sand Streaks
0.7	No		Active Sand Streaks
0.6	No		Active Sand Streaks



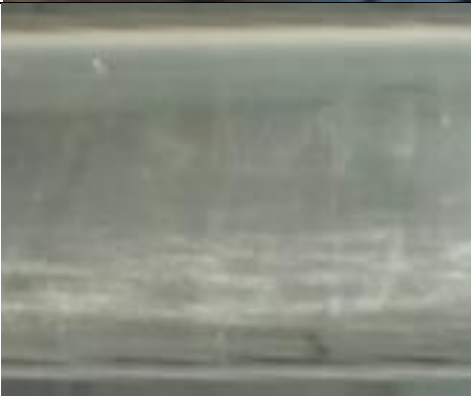
0.5	Yes		Sand particle starts settling
0.4	Yes		Scouring
0.3	No		Moving Dunes
0.2	No		Stationary Bed is formed close the injection point





**Table F- 2: Sand behaviour in water with the sand concentration of 50lb/1000bbl in the dip section**

V <sub>L</sub> [m/s]	Sand Concentration 50 lb/1000bbl		
	Sand particle size 270 micron		
	Dip Section		
	MTC	Sand Behavior	Description
0.8	No		Active Sand Streaks
0.7	No		Active Sand Streaks
0.6	No		Active Sand Streaks
0.5	Yes		Active Sand Streaks and sand particle is about to settle

0.4	Yes		Moving Dunes
0.3	No		Sand dunes moves slowly
0.2	No		Most of the sand particle is trapped near the injection position, just a little sand stays stable at the dip





**Table F- 3: Sand behaviour in water with the sand concentration of 50lb/1000bbl in the uphill section**





V <sub>L</sub> [m/s]	Sand Concentration 50 lb/1000bbl		
	Sand particle size 270 micron		
	Uphill Section		
	MTC	Sand Behavior	Description
0.8	No		Active Sand Streaks
0.7	No		Active Sand Streaks
0.6	No		Active Sand Streaks (bottom view)

0.5	Yes		Scouring with sliding layer at the bottom (bottom view)
0.4	Yes		Moving Dunes
0.3	No		Sand bed stays stable at the uphill section
0.2	No		No sand in the uphill section











**Table F- 4: Sand behaviour in water with the sand concentration of 200lb/1000bbl in the downhill section**

V <sub>L</sub> [m/s]	Sand Concentration 200 lb/1000bbl		
	Sand Particle size 270 micron		
	Downhill Section		
	MTC	Sand Behavior	Description
0.9	No		Active Sand Streaks
0.8	No		Active Sand Streaks
0.7	Yes		Active Sand Streaks and sand particle is going to settle
0.6	Yes		Sand layer is forming at the bottom


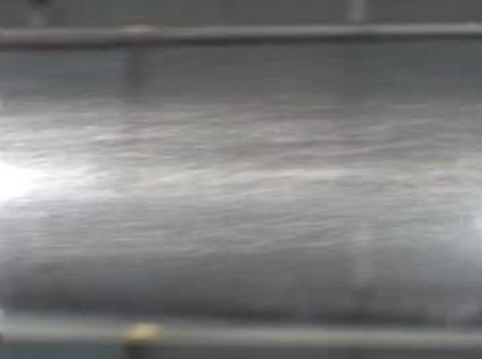

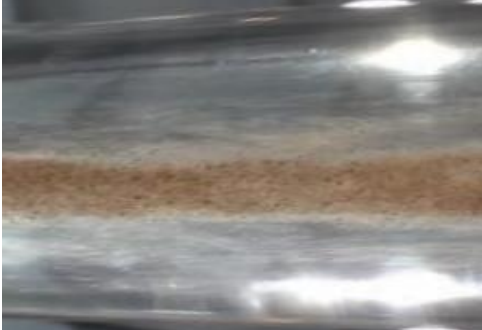
0.5	No		<p>Still sand layer is observed at the bottom while sand particle transporting at the top</p>
0.4	No		<p>Moving Dunes</p>
0.3	No		<p>Sand dunes moves slowly (viewing from bottom)</p>
0.2	No		<p>Sand bed stays stationary near the injection point</p>





**Table F- 5: Sand behaviour in water with the sand concentration of 200lb/1000bbl in the dip section**

$V_L$ [m/s]	Sand Concentration 200 lb/1000bbl		
	Sand Particle size 270 micron		
	Dip Section		
	MTC	Sand Behavior	Description
0.9	No		Active Sand Streaks
0.8	No		Active Sand Streaks
0.7	No		Active Sand Streaks
0.6	Yes		Sliding layer transporting near the bottom





0.5	Yes		<p>Still sand layer is observed at the bottom while sand particle transporting at the top</p>
0.4	No		<p>Moving Dunes</p>
0.3	No		<p>Sand dunes moves slowly</p>
0.2	No		<p>Sand bed stays stationary near the injection point, nearly no sand at the dip</p>





**Table F- 6: Sand behaviour in water with the sand concentration of 200lb/1000bbl in the uphill section**

$V_L$ [m/s]	Sand Concentration 200 lb/1000bbl		
	Sand Particle size 270 micron		
	uphill Section		
	MTC	Sand Behavior	Description
0.9	No		Active Sand Streaks
0.8	No		Active Sand Streaks (viewing from bottom)
0.7	Yes		Active Sand Streaks (viewing from bottom)
0.6	Yes		A stationary sand layer at the bottom, as sand particle transporting above it (viewing from bottom)

0.5	No		Moving Dunes
0.4	No		Sand dunes moves slowly
0.3	No		Stationary Bed is formed
0.2	No		No sand at the uphill section because sand bed stays stationary near the injection point





**Table F- 7: Sand behaviour in water with the sand concentration of 500lb/1000bbl in the downhill section**





$V_L$ [m/s]	Sand Concentration 500 lb/1000bbl		
	Sand Particle size 270 micron		
	Downhill Section		
	MTC	Sand Behavior	Description
0.9	No		Active Sand Streaks
0.8	Yes		Active Sand Streaks and sand particle is going to settle
0.7	Yes		Moving sand layer at the bottom of the pipe (viewing from the bottom)
0.6	No		Sand layer at the bottom of the pipe getting thicker

0.5	No		<p>Sand layer is transforming to sand dunes, the sand particle above the layer moves slower</p>
0.4	No		<p>Moving Dunes</p>
0.3	No		<p>Sand dunes merge together and the particle at the top of the dunes moves slowly</p>
0.2	No		<p>Sand bed stays stationary near the injection point</p>











**Table F- 8: Sand behaviour in water with the sand concentration of 500lb/1000bbbl in the dip section**

$V_L$ [m/s]	Sand Concentration 500 lb/1000bbbl		
	Sand Particle size 270 micron		
	Dip Section		
	MTC	Sand Behavior	Description
0.9	No		Active Sand Streaks (side View)
0.8	No		Active Sand Streaks (side view)
0.7	Yes		Active Sand Streaks
0.6	Yes		Sliding layer transporting at the bottom

0.5	No		<p>Sand layer is observed at the bottom while sand particle transporting at the top (side view)</p>
0.4	No		<p>Sand dunes is forming</p>
0.3	No		<p>Moving dunes</p>
0.2	No		<p>Sand bed stays stationary near the injection point, nearly no sand at the dip (side view)</p>




**Table F- 9: Sand behaviour in water with the sand concentration of 500lb/1000bbl in the uphill section**





$V_L$ [m/s]	Sand Concentration 500 lb/1000bbl		
	Sand Particle size 270 micron		
	uphill Section		
	MTC	Sand Behavior	Description
0.9	No		Active Sand Streaks (bottom view)
0.8	Yes		Active Sand Streaks and sand particle is moving near the bottom (bottom view)
0.7	Yes		Sand layer is observed at the bottom while sand particle transporting at the top (bottom view)
0.6	No		A thicker sand layer is generated at the bottom and transporting forward with sand particle above it (bottom view)


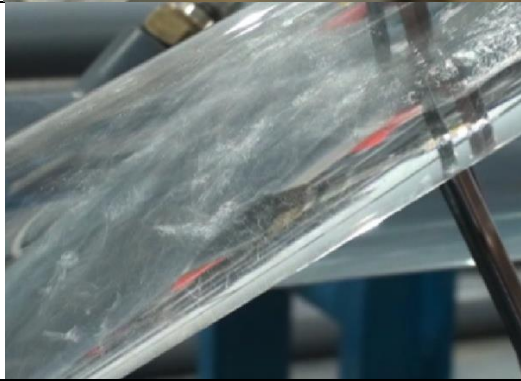
0.5	No		Moving Dunes
0.4	No		Sand dunes moves slowly
0.3	No		Stationary Bed is formed
0.2	No		No sand at the uphill section because sand bed stays stationary near the injection point

## Appendix F : Specification of Sand Minimum Transport Condition in Sand-Air-Water Flow




**Table G- 1: Illustration of sand behaviour around the minimum transport condition when sand concentration of 50 lb/1000bbl**

Liquid superficial velocity (m/s)	Gas superficial velocity (m/s)	Sand concentration 50 lb/1000bbl		
		Sand particle size 270 micron		
		MTC	Sand behavior	Description
0.08	1.5	before		A thick sand bed is formed at the bottom of the pipe.
0.08	2.0~3.0	MTC		Sand bed becomes much thinner, and will be shattered by the following aerate slug.
0.08	4.0	after		The sand particles that fell back from the upward pipe will be flushed away soon, and there is insufficient time for them to form a sand bed.





0.15	0.2	before		Sand settles constantly at the bottom of the pipe while gas bubble travelling above it as plug flow.
0.15	0.3~0.5	MTC		Slug flow picks up some sand particles, while rest of them settling at the bottom.
0.15	0.6	after		Most of the sand particles are entrained forward, and Barely can fall back.
0.35	0.1	before		Sand particles deposit in uphill section



0.35	0.15	MTC		<p>Sand particles are picked up by the slug flow and sand bed is splintered.</p>
0.35	0.2	after		<p>Barely no sand particles left in the pipe</p>

**Table G- 2: Illustration of sand behaviour around the minimum transport condition when sand concentration of 200 lb/1000bbl**




Liquid superficial velocity (m/s)	Gas superficial velocity (m/s)	Sand concentration 200 lb/1000bbl		
		Sand particle size 270 micron		
		MTC	Sand behavior	Description
0.15	2.0	before		A thick sand bed is formed at the bottom of the pipe.
0.15	2.5~3.0	MTC		Sand bed becomes much thinner, and will be shattered by the following aerate slug.
0.15	4.0	after		The sand particles that fell back from the upward pipe will be flushed away soon, and there is insufficient time for them to form a sand bed.








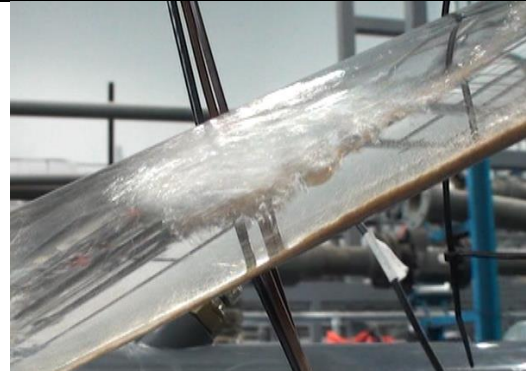


0.35	0.2	before		Sand settles constantly at the bottom of the pipe while gas bubble travelling above it as plug flow.
0.35	0.3	MTC		Slug flow picks up some sand particles, while rest of them settling at the bottom as a thin sand layer.
0.35	0.4	after		Most of the sand particles are entrained forward, and there are almost no particles left.
0.55	0.1	before		Sand particles deposit in uphill section, and the entire sand bend moves forward slowly.

0.55	0.15~0.2	MTC		<p>Sand particles form a thin sand layer at bottom of the pipe and will be soon dispersed.</p>
0.55	0.3	after		<p>A little segregated sand particles travels at the bottom</p>

**Table G- 3: Illustration of sand behaviour around the minimum transport condition when sand concentration of 500 lb/1000bbl**

Liquid superficial velocity (m/s)	Gas superficial velocity (m/s)	Sand concentration 500 lb/1000bbl		
		Sand particle size 270 micron		
		MTC	Sand behavior	Description
0.08	3	before		A thick layer of sand particles are deposited at the bottom of the pipe
0.08	6	before		It is unable to flush the sand bed, even at the upper limit of gas superficial velocity.
0.15	2.0	before		A sand bed is observed at the bottom of the pipe.

0.15	3.0~5.0	MTC		Sand bed becomes much thinner, and will be shattered by the following aerate slug.
0.15	6.0	after		The sand particles that fell back from the upward pipe will be flushed away soon, and there is insufficient time for them to form a sand bed.
0.35	0.3	before		Sand settles constantly at the bottom of the pipe.
0.35	0.4	MTC		Slug flow picks up some sand particles, while rest of them settling at the bottom as a thin sand layer.

0.35	0.5	after		Sand particles are entrained forward by the aerated slug flow (Top view).
0.55	0.1	before		Sand particles deposit in uphill section as a stationary bed.
0.55	0.2~0.3	MTC		Sand particles form a thin sand layer at bottom of the pipe and will be soon picked up by the following slug flow.
0.55	0.4	after		A little segregated sand particles travels at the bottom

## Appendix G : Statistical Calculation Error

Measurement is known to have a degree of exactness which is referred to as error. Error is defined as the difference between the measurement and true value or accepted value. The uncertainty of a measured value is an interval around that value such that any repetition of the measurement will produce a new result that lies within this interval

Throughout the present work, the relative error,  $E$  between an experimental measurement and the value predicted using a model or correlation is given by:

$$E = \frac{P - M}{M} \quad \text{G-1}$$

Where  $P$  and  $M$  are the predicted and measured values, respectively.

The mean, or average error,  $\bar{E}$ , is given by:

$$\bar{E} = \frac{\sum_{i=1}^N E_i}{N} \quad \text{G-2}$$

Where  $N$  is the number of data points in the sample

The standard deviation,  $\sigma$ , is obtained from

$$\sigma = \sqrt{\frac{\sum_{i=1}^N (E_i - \bar{E})^2}{(N - 1)}} \quad \text{G-3}$$

The standard error of the mean ( $\sigma_{mean}$ ) also defined as the 68% confidence limit is defined as:

$$\sigma_{mean} = \frac{\sigma}{\sqrt{N}} \quad \text{G-4}$$

## Appendix H : Publications

The following publications have resulted from this work

- Yan, W., Hu, X., Osho, A.J., and Yeung, H. (2011), "Experimental study on sand transport characteristics in water and air-water flow in dip pipeline", 15-17 June, 2011, Cannes, France, BHR group, UK
- Osho, A.J., Yan, W., and Yeung, H. (2012). Experimental study of air-water flow in undulating pipeline and implication on sand transported. OTC (2012), Houston, USA